DURABILITY OF CEMENT-BASED MATERIALS IN AGGRESSIVE ACIDIC ENVIRONMENTS

A THESIS

Submitted by

RAMASWAMY K. P.

for the award of the degree

of

DOCTOR OF PHILOSOPHY

DEPARTMENT OF CIVIL ENGINEERING
INDIAN INSTITUTE OF TECHNOLOGY MADRAS

JULY 2018

THESIS CERTIFICATE

This is to certify that the thesis entitled “**DURABILITY OF CEMENT-BASED MATERIALS IN AGGRESSIVE ACIDIC ENVIRONMENTS**", submitted by **Ramaswamy K. P.**, to the Indian Institute of Technology Madras, for the award of the degree of **Doctor of Philosophy** is a bona fide record of the research work done by him under my supervision. The contents of this thesis, in full or in parts, have not been submitted to any other Institute or University for the award of any degree or diploma.

Chennai – 600 036
Date: 13th July 2018

Dr. Manu Santhanam
Research Guide
Professor
Department of Civil Engineering
IIT Madras, Chennai - 600 036

ACKNOWLEDGEMENTS

I express my profound thanks and deep sense of gratitude to my research guide, Dr. Manu Santhanam, Professor, Dept. of Civil Engineering, IIT Madras for his constant inspiration, support and encouragement to me throughout the course of the research. His expertise in the subject, the utmost care, brotherly affection and kindness he has shown is beyond my words to express and thank. I am deeply indebted to him for the knowledge and wisdom he has imbibed on me.

I would like to express my heartfelt thanks to Prof. Alexandra Bertron, Professor in Civil Engineering, Laboratoire Matériaux et Durabilité des Constructions (LMDC), INSA Toulouse, France for her encouragement, motivation, and for providing valuable suggestions during my research.

I express my sincere thanks to Prof. Ravindra Gettu, Professor, Dept. of Civil Engineering, IIT Madras for his thought provoking discussions and constructive comments at every stage of my research. I also extend my sincere gratitude and thanks to Prof. Radhakrishna G. Pillai, Associate Professor, Dept. of Civil Engineering, IIT Madras who is also one of my doctoral committee members, for his valuable motivation and suggestions during the course of my study. He has always been a source of encouragement to me.

My sincere thanks to Prof. K. Ramamurthy, Professor and Head, Dept. of Civil Engineering and my doctoral committee chairman for his constant encouragement and motivation during my stay at IIT Madras. I also extend my thanks to Prof. Meher Prasad, Former Head, Dept. of Civil Engineering for providing excellent laboratory facilities in the Department.

I express my sincere thanks to my doctoral committee members, Prof. B. S. Murty, Professor, Department of Metallurgical and Materials Engineering, IIT Madras and Prof. Amlan K. Sengupta, Professor, Dept. of Civil Engineering, IIT Madras for their constant encouragement and suggestions during my research work. My special thanks to Prof. B. S. Murty for permitting me to avail the X-ray diffraction testing facility in the nano-technology laboratory at IIT Madras.

I am grateful to Sri. T. K. Shahal Hassan Musaliar, Chairman, Governing Body, TKM College of Engineering, Kollam and Principal, TKM College of Engineering, Kollam for permitting me to do research at IIT Madras. I also extend my thanks to Directorate of Technical Education, Kerala for sponsoring me to do Ph.D. at IIT Madras under the Quality Improvement Programme scheme.

I convey my deep sense of gratitude to Prof. K. N. Satyanarayana, Director, IIT Tirupati for being a constant source of motivation and inspiration, which prompted me to take up the research work at IIT Madras.

I extend my sincere thanks to Prof. Krishnan Balasubramanian, Institute Chair Professor and Former Dean (IC & SR), IIT Madras for extending the X-ray tomography facility in Centre for Non Destructive Evaluation for my research work.

I convey my special thanks to Sri. Raguvarun Kannaiyan, Former Project Officer, Centre for Non Destructive Evaluation, IIT Madras and to Sri. Harikrishnan Ravichandran, Project Officer, Centre for Non Destructive Evaluation, IIT Madras for their immense help in X-ray tomography imaging during my research. The support and the encouragement they have shown is beyond my words to express.

I would like to express my sincere thanks to Prof. Koshy Varghese, Prof. K. Ananthanarayanan, Prof. Ashwin Mahalingam, Prof. Benny Raphael, Prof. Sivakumar Palaniappan, Faculty members of Building Technology and Construction Management Division, Dept. of Civil Engineering, IIT Madras for the help and encouragement they offered me in each and every stage of my research work.

I extend my heartfelt thanks to Prof. Mark. G. Alexander, Professor Emeritus, Department of Civil Engineering, University of Cape Town for his valuable suggestions and comments during my research work. My sincere thanks to Prof. Jose Duchesne (Professor, Dept. of Geology and Geological Engineering, University of Laval, Canada), Prof. Prasad Rao Rangaraju, (Professor in Civil Engineering, Clemson University, USA) and Prof. Frank Dehn (Faculty of Chemistry and Mineralogy, Leipzig University, Germany) for their suggestions and valuable comments during various stages of my research.

I convey my special thanks to Sri. N. Sivaramakrishnan, Sri. N. K. Gopinath, Ms. K. P. Kalpana, and Sri. G. Sundaraman for providing the various testing facilities at Sophisticated Analytical Instrument Facility (SAIF) at IIT Madras. My sincere thanks to staff of Sophisticated Test & Instrumentation Centre (STIC), Cochin University of Science and Technology, Kerala, especially to Dr. Shibu M. Eappen, Scientific Staff for the help provided with the material analysis during my research. My special thanks to Sreejith Krishnan, Doctoral Research Scholar, IIT Delhi for helping me with the X-ray diffraction testing during my research.

I express heartfelt sense of gratitude to all the staff in the BTCM laboratory, especially to Ms. A Malarvizhi, Mr. R. Muthusamy, Mr. G. Subramanian, Mr. B. Krishnan, Mr. Siva for their help and support given to me in the successful completion of my research. I also thank Mr. R. Murali, Mr. Prince Anantharaj and other staff in Civil Engineering Department Workshop facility for their help rendered in the fabrication of moulds and test setups.

I extend sincere thanks to my friends, Anto Vibin Marckson, Poornima Rao, Jaikiran, Gunjan, Pritesh and summer internship students from IIT Tirupati for helping me during casting and testing. My special thanks to all my BTCM friends and researchers especially Sivakumar, Satyanarayana, Yuvaraj, Divya Rani, Fathima, Priyadarshini and Sujatha. My special thanks to Padmanabhan Krishnaswamy for helping me in arranging a field investigation in connection with my research.

I would also like to thank the BTCM office staff Ms. Ramya and Ms. Lakshmi Priya. The support from the Office of Dept. of Civil Engineering, especially Mr. Balakrishnan, Ms. Rani, Ms. Geetha. Mr. Subramani, Ms. Padmini, Mr. Ramaswamy are gratefully acknowledged. The support from the Chairman and office staff of the Centre for Continuing Education, IIT Madras is also thankfully acknowledged.

This research work is dedicated to my loving family. The work would not have been materialised without the meticulous support, care and prayers from my wife Hema V. and from my father Mr. Santhanam Parasuraman K. R., my mother Ms. A. V. Visalakshy and my sister Bhageerathy K. P. The support from my father-in-law Mr. K. Padmanabha Iyer and my mother-in-law K. Vijayalekshmi are also gratefully acknowledged.

The love and support given by my wife, parents and my guide throughout my study period have given me the motivation and confidence to complete the research successfully. I am deeply indebted to all who helped me during my stay at IIT Madras. Above all I thank the God Almighty for giving me enough strength and patience to complete my research work and for making my stay at IIT Madras, a memorable one in my life.

Ramaswamy K. P.

ABSTRACT

KEYWORDS: acid attack, leaching, characterisation, degradation kinetics, deterioration, durability, mechanism, microstructure, supplementary cementitious material, tomography.

Concrete structures are susceptible to attack by various aggressive acidic solutions present in industrial effluents. Cement hydrates are unstable in such low pH environments; these leach out to the solution and form salts, and this process results in the rapid deterioration of microstructure, affecting the concrete durability. This phenomenon is influenced by multitude of factors and there are hardly any codes or standards available, which holistically address the durability testing of cement-based materials exposed to acids.

Hence, the current study deals with the evaluation of kinetics and the understanding of mechanism of degradation of cementitious materials caused by various acids present in industrial effluents. Accelerated leaching tests were developed to evaluate the performance of various cementitious systems, without changing the mechanism of degradation. The influence of various factors like type of binder, type of acid, type of aggregate, concentration of acid solution, pH and water to binder ratio (w/b) on the performance of cementitious paste and mortar specimens was investigated.

To achieve these objectives, preliminary case study investigations (at a sewage treatment plant and a molasses based distillery plant) were carried out in order to understand the nature and severity of the problem. This was followed by laboratory investigations on paste and mortar. Accelerated immersion tests were done on paste and mortar specimens made with commonly used and special binders, with and without the abrasive action, to investigate the degradation kinetics. The degradation kinetics was studied using parameters such as mass change, change in pH of the acid solution, altered depth and thickness change. In the case of mortar, the alterations in the physico-mechanical properties were studied based on change in strength and dynamic modulus of elasticity. Micro-analytical studies including X-ray diffraction (XRD), X-ray tomography (CT), scanning electron microscopy (SEM), mercury intrusion porosimetry (MIP), and thermogravimetric analysis (TGA) were done on the attacked paste and mortar samples to understand the mechanism of degradation and the role of interfacial transition zone (ITZ) in mortar. Based on the kinetics data, a non-linear model was developed for predicting the kinetics in terms of mass changes in the case of exposure to acetic acid. Further, the effect of mineralogical nature of aggregate on the kinetics of degradation was also investigated.

The micro-analytical characterisation on samples collected from sewage treatment plant and molasses based distillery plant indicated intense decalcification of the hydrated phases, exhibiting degradation. This necessitated the importance of developing laboratory based accelerated test methods to test alternative binders for their acid resistance. The study on degradation kinetics in paste showed that the acid attack is primarily influenced by the solubility of salt and its properties such as molar volume, and its affinity with the inner cement matrix. Among the acids tested, citric acid was found to be aggressive, and its action resulted in severe mass and thickness loss in specimens. Acetic acid, although considered as a weak organic acid, was found to be aggressive to the cementitious medium due to strong calcium leaching, as the degradation led to considerable mass loss and alteration depth. The salts being soluble in the case of acetic acid, the final end product in the matrix was a weak amorphous silica gel. The major reaction product in the case of sulphuric acid attack was gypsum and the deterioration is ascribed to the expansion associated with its formation. The attack by acids resulted in substantial increase in capillary porosity, thus enhancing the ingress of acid further, by diffusion.

The periodic abrasive action was found to accelerate the degradation kinetics in the case of attack by sulphuric acid. The use of smaller sized specimens with higher surface area to volume ratio along with frequent replenishment of acid enabled accelerated attack to aid in the performance evaluation of various binder systems. The performances of supplementary cementitious materials (SCMs) and special binders were found to be satisfactory only on exposure to lower concentrations of acids. The use of lower w/b (0.40) in the mortar resulted in more damage on exposure to sulphuric acid when compared to a w/b of 0.55. However, in the case of acetic acid, lowering the water to binder ratio enhanced the acid resistance. The mortar made with limestone aggregates performed better on exposure to sulphuric acid and was inferior on exposure to acetic acid when compared to the mortar with siliceous aggregates. Among the binders tested, slag incorporated mixes performed well in sulphuric and acetic acids. The performance of fly ash (Type F) was found to be inadequate, especially in the case of organic acids. In general, the alteration depths of SCM incorporated mixes were found to be higher compared to the control mix containing Ordinary Portland Cement (OPC). The presence of ITZ in mortar was found to accelerate the rate of attack.

Accelerated test methods were used in the study to examine the degradation kinetics in paste and mortar. In addition to the regular choice of test parameters such as changes in mass and strength, new test parameters such as altered area/depth and relative dynamic modulus of elasticity are proposed as additional measures of degradation, which are related to the alterations in the microstructure. A non-invasive imaging technique known as X-ray computed tomography was comprehensively used to characterise the acid attack phenomenon. The mineralogical zonation and associated microstructural changes due to acid attack was well captured using this technique. Further, based on these images, image analysis was used to extract parameters related to the decalcification such as altered depth/area. A single test parameter called Performance Ranking factor (PRF) is formulated as a performance indicator which combines the kinetics parameters related to changes in mass, alterations in microstructure and physico-mechanical properties. The choice of these test methods and parameters further helped to get a better understanding of the performance of various common and advanced binder systems in varied acidic solutions. A detailed micro-analytical characterization study was carried out on paste and mortar, which helped in understanding the mechanism of degradation and the various reaction products formed and its impact on the deterioration process. Additionally, recommendations for the development of a sound test method to assess the material resistance to acid attack were formulated. The kinetics and the microstructure studies on paste and mortar specimens thus helped to understand the acid attack phenomenon and the issues and challenges to ponder with, in the development of a test method to evaluate the performance of various binders.

TABLE OF CONTENTS

LIST OF TABLES

LIST OF FIGURES

ABBREVIATIONS

ASP	Activated Sludge Process
BFS	Blast Furnace Slag
BOD	Biochemical Oxygen Demand
BSE	Back Scattered Electron
CAC	Calcium Aluminate Cement
CASH	Calcium Alumino Silicate Hydrate
CH	Calcium Hydroxide
COD	Chemical Oxygen Demand
CSH	Calcium Silicate Hydrate
CT	X-ray Computed Micro-tomography
DA	Depth of alteration (or altered depth)
DD	Depth of degraded layer
DM	Depth of middle layer
DR	Depth removed due to reactions/brushing
DTG	Differential Thermogravimetry
EDS	Energy Dispersive Spectroscopy
EPMA	Electron Probe Micro-Analysis
FA	Fly Ash
GGBFS	Ground Granulated Blast Furnace Slag
GSV	Grayscale Value
HAC	High Alumina Cement
HCP	Hydrated Cement Paste
HSR	High Sulphate Resistant Portland cement
ICSD	Inorganic Crystal Structure Database
ITZ	Interfacial Transition Zone
LAC	Linear Attenuation Coefficient
LC2	Limestone Calcined Clay
LC3	Limestone Calcined Clay Cement
LOI	Loss on Ignition
LS	Limestone Sand
MIP	Mercury Intrusion Porosimetry

MLD	Million Litres per Day
NMR	Nuclear Magnetic Resonance
OM	Optical Microscopy
OPC	Ordinary Portland Cement
PC	Primary Clarifier
PCE	Polycarboxylic Ether
PRF	Performance Ranking Factor
RS	River Sand
S/GC	Screen and Grit Chamber
SCM	Supplementary Cementing Material
SE	Secondary Electron
SEM	Scanning Electron Microscopy
SF	Silica Fume
SLM	Synthetic Liquid Manure
SOM	Sulphur-Oxidising Microorganisms
STP	Sewage Treatment Plant
TG	Thermogravimetric
TGA	Thermo-gravimetric Analysis
UPV	Ultrasonic Pulse Velocity
XRD	X-Ray Diffraction
XRF	X-Ray Fluorescence

NOTATIONS

˚C	Degree Celsius
Δm	Mass change
Δm_B	Mass changes with abrasion
μ	Poisson’s ratio of the mortar
A_c	Area of the core layer
A_f	Final area of the specimen after the acid exposure
AF_m	Monosulphate
AF_t	Ettringite
AH_3	Gibbsite
A_i	Initial area of the specimen before the acid exposure
A_m	Area of the middle layer
A_o	Area of the outer layer
B	Brushing factor
B28	With brushing
$\underline{C}$	CO_2 (carbon dioxide)
c	Concentration of acid
C_2S	Dicalcium silicate
C_3A	Tricalcium aluminate
C_3AH_6	Hydrogarnet (or katoite)
C_3S	Tricalcium silicate
C_4AF	Tetracalcium alumino-ferrite
Cc	Calcite (calcium carbonate)
CH	Portlandite (calcium hydroxide)
CO_2	Carbon dioxide
d	lattice inter-planar spacing of the crystal
D	Total altered depth of the specimen
D_{50}	Average particle size
E	Dynamic modulus of elasticity
E_0	Dynamic modulus of elasticity before the acid exposure
E_t	Dynamic modulus of elasticity at age of acid exposure ‘t’
H_2S	Hydrogen sulphide

Hc	Hemi carbo-aluminate
HCl	Hydrochloric acid
HF	Hydrofluoric acid
K_a	Dissociation constant
M	Molarity
M_0	Average mass of the specimen before the acid exposure
M_{105}	Mass of the sample after heating to 105 °C
M_{1050}	Mass of the sample after ignition at a temperature of 1050 °C
Mc	Mono carbo-aluminate
M_t	Average mass of the specimen at age of exposure ‘t’
n	Order of diffraction
P	Pressure
r	Radius of pore
S/V	Surface area to volume ratio
$\underline{S}$	SO_3 (sulphur trioxide)
t	Age of acid exposure
T_0	Average thickness of the specimen before the acid exposure
T_t	Average thickness of the specimen at age of exposure ‘t’
V	Ultrasonic pulse velocity
w/b	Water to binder ratio
WB28	Without brushing
γ	Surface tension of mercury
θ	X-ray incidence angle
θ_c	Contact angle
λ	Wavelength of characteristic X-rays
ρ	Average bulk density of the specimen

CHAPTER 1

INTRODUCTION

1.1 PROBLEM STATEMENT

Concrete structures can come into contact with aggressive acidic environments in many situations and the understanding of the alteration kinetics and mechanisms of degradation of concrete by these acidic media is a fundamental step towards making a durable concrete which will then increase the service life of the concrete structures. Many industries still rely on the processes that produce effluents or wastewater. Such effluents contain a wide range of both organic and/or inorganic acids whose action may lead to severe and rapid degradation of concrete structures (Bertron, 2014; Aiken et al., 2017).

Industrial manufacturing plants use various processes that either consume or produce various types of chemical acids such as sulphuric, hydrochloric and nitric acids. Spillage and accidental leakage of these acids can severely and rapidly deteriorate the adjoining concrete structures, as the concentration of acid, which comes in the direct contact with concrete, may reach alarmingly high values in these places (Harrison, 1987; Fattuhi and Hughes, 1988; Allahverdi and Skavara, 2000a, b). Sewage is capable, under the ideal conditions, of producing sulphuric/organic acids leading to severe degradation of concrete sewer pipes (Hudon et al., 2011; Scrivener and De Belie, 2013). This is a biogenic process (produced by bacteria) and the favourable temperature for this process is approximately 30 °C, which means that it could be more commonly encountered in hotter countries like India. Biogenically-induced attacks involving various types of acids (sulphuric acid, organic acids) can be seen in concrete septic tanks, biogas reactors, sewage treatment plants etc. High Biochemical Oxygen Demand (BOD) and Chemical Oxygen Demand (COD) of the sewage effluent could mean that the dissolved oxygen content is very low. This would help anaerobic microorganisms to thrive in these effluents; these microbes consume the organic matter for their metabolism and in turn produce a mixture of organic acids, among other aggressive chemical species, whose effects can be detrimental to concrete as well.

The attack due to organic acids can also arise in industrial applications, but predominantly from the effluents generated in the agricultural and agro-food industry. Such effluents can contain organic acids such as acetic, propionic, tartaric, oxalic, lactic, citric acids etc. depending on the type of the effluent (Bertron and Duchesne, 2013; Larreur-Cayol et al., 2011a). The concrete inside biogas reactor digesters is also prone to deterioration due to the production of organic acids and ammonium in the liquid phase and H_2S and CO_2 in the gas phase (Voegel et al., 2016).

The attack by acidic waters thus represents a topic of growing significance due to increasing damages to concrete structures globally, demanding frequent repair and maintenance of structures, and inducing huge costs notably linked with the interruption of production processes during repair works. This undesirable situation is a consequence of increased consumption and production of acidic media due to rapid industrialisation, especially in developing countries.

Cementitious materials being highly alkaline in nature are easily attacked by acidic solutions. This disturbs the equilibrium of the cement matrix causing calcium leaching and associated degradation (Zivica and Bajza, 2001; Duchesne and Bertron, 2013; Gutberlet et al., 2015). Degradation of cement-based materials due to acids is a complex phenomenon influenced by many factors related to acid, binders, aggregates as well as the test method (Dyer, 2014). This complicated mechanism of degradation is still not properly understood. The response of given cementitious materials to acid attack clearly depends on architecture of tests as well as various other parameters. Moreover, the assessment of cementitious materials is still hindered by the lack of standardised test or at least reference test methods. This absence is also a major obstacle to the evaluation of alternative binders in terms of performance and deterioration mechanisms and thus to their commercial development.

Nowadays, the use of Supplementary Cementing Materials (SCMs) in concrete is on the rise; their use as cement replacement leads to a reduction of the CO_2 emissions and thus makes the concrete more sustainable. However, the results depicting the performance of SCMs in aggressive acidic environments are, in general, inconclusive. Contradictory results were obtained, especially for silica fume, fly ash and slag incorporated mixes (Monteny et al., 2003; O'Connell et al., 2012; De Belie et al., 2004; Roy et al., 2001; Chang et al., 2005; Saricimen et al., 2003; Fattuhi and Hughes, 1988; Attiogbe and

Rizkalla, 1988; Alexander and Fourie, 2011) and more detailed investigation must be conducted to validate the same. There are hardly any microstructural characterisation studies carried out to conclude the role of SCMs in resisting the damage due to acid attack.

A review of literature of acid attack on concrete reinforces the fact that even though considerable research has been done on effect of inorganic acids on concrete, only very few studies have focused on the effect of organic acids such as acetic and citric acids which can be equally aggressive and detrimental to the cementitious matrix. Majority of the studies in organic acids were on paste specimens and the study needs to be extended to mortar so as to investigate the role of Interfacial Transition Zone (ITZ), besides evaluating the influence of SCMs. Further detailed studies are essential to investigate the mechanisms of degradation and alteration kinetics in these conditions by developing new laboratory based accelerated test methods and to design materials and mixtures that perform well in these aggressive environments.

In this context, the present work deals with understanding the degradation kinetics and the mechanism of degradation of cement-based materials exposed to various acidic solutions. The terms ‘degradation kinetics’ and ‘alteration kinetics’ are commonly used in the acid attack/leaching studies to describe the variation of degradation related parameters (mass change, thickness change, altered depth etc.) with the age of acid exposure (Bertron et al., 2005; Larreur-Cayol et al., 2011a), and hence, widely used throughout the work.

Field investigations were conducted in order to understand the severity of the problem. The influence of SCMs and the various factors that could affect the acid attack were studied by conducting accelerated immersion based leaching test on paste specimens. In order to understand the mechanism of degradation, micro-analytical characterisation tests were carried out on the degraded samples. The paste study was extended to mortar to evaluate the role of SCMs and the effect of ITZ in resisting acid attack. The effect of mineralogical nature of aggregate on influencing the kinetics of degradation was also studied. Further attempts were made to develop models for predicting the deterioration due to acid attack.

1.2 OBJECTIVES

This research study is focused to achieve the following objectives:

1. To evaluate the alteration kinetics and to understand the basic mechanism of degradation of cementitious materials caused by acids present in industrial effluents by characterising chemical, physical and mineralogical alterations of cementitious materials.
2. To develop accelerated test methods that better reflect the deterioration mechanism of cementitious materials due to acid attack in real conditions.
3. To evaluate the effect of various parameters like type of binder, type of aggregate, type of acid, concentration of acid solution, pH and water to binder ratio on the performance of cementitious paste and mortar specimens exposed to acids.

1.3 SCOPE

1. The laboratory study is limited to tests on paste and mortar specimens. The corrosion of steel in concrete due to acid attack and the degradation of concrete are excluded from the current study.
2. Ordinary Portland cement of grade 53 conforming to IS 12269 (2013) is used throughout the study. The common binders considered for the study are limited to Class F fly ash, ground granulated blast furnace slag and silica fume.
3. Special binders that are evaluated for acid resistance include high alumina cement and limestone calcined clay cement.
4. The paste study is carried out at water to binder ratio of 0.40. The mortar study is restricted to a binder aggregate proportion of 1:3, and two different water to binder ratios of 0.40 and 0.55.
5. Only graded sand conforming to IS 650 (2008) is used for the mortar study. Further, graded limestone aggregates are also tested to evaluate the effect of mineralogical nature of aggregate on the acid resistance.
6. While the paste study incorporates acetic, citric, hydrochloric and sulphuric acids, the mortar study is restricted to the attack of cement-based materials by sulphuric

acid and acetic acid only. The alteration kinetics and degradation mechanisms are assessed for three levels of concentrations and one elevated pH for each of the acids in the mortar study.

7. The maximum acid exposure period is limited to 6 weeks for the paste study and 4 months in the case of static immersion tests for mortar specimens.

1.4 METHODOLOGY

As there is no specific standard existing for the testing of cementitious specimens in acids, research-based specially designed test set-ups in addition to existing test facilities were used in this study. According to De Belie et al. (2002), the resistance of concrete to acid solutions can be tested in laboratory experiments in various ways: (1) realistic concentrations of the aggressive acid solutions can be used in combination with a sensitive method to detect the deterioration; (2) accelerated tests can be performed, in which the degradation rate can be increased in different ways (e.g. by means of higher concentrations of the acid solution, higher ratio of volume of acids to volume of specimens, higher temperatures, increasing the surface area to volume ratio of specimen, smaller sized specimen or alternate wetting and drying cycles etc.). Test methods using realistic acid composition may not be an ideal option because extremely sensitive methods are needed to detect the deterioration, or more importantly to detect the differences in degradation between various test specimens, within a reasonable time period. Furthermore, the use of an extrapolation method to predict the future degradation in this method envisages the risk that new mechanisms, which are not perceived during the time of measurement, arise in a later period of the deterioration process. Hence, in general, to study deterioration of concrete in acids, accelerated test methods are preferred and therefore, adopted in this study. The study has been subdivided into four phases and the methodology followed in each phase is explained in the section below.

1.4.1 Phase I: Field investigations

The objective of the field investigation was to study the extent of decalcification that has happened to the concrete structures due to attack by acid solutions. In this context, a site visit to Nesapakkam sewage treatment plant, Chennai was conducted to investigate the possible areas where acid attack can occur. Concrete samples were collected from various locations (screening and grit chamber and primary clarifier) affected by biogenic sulphuric acid attack, and stored in desiccators for further characterisation tests.

Another case study was done where the concrete underwent deterioration due to spent wash in a molasses based distillery in Erode district of Tamil Nadu, India. The concrete tank which is used to store the distillery spent wash was seen to be experiencing premature deterioration; the resultant frequent repairs had huge cost implications for the plant. Concrete samples were collected from the deteriorated locations, just below the water level where the spent wash is stored, and characterisation techniques were used to investigate the deterioration further.

The micro-analytical characterisation studies carried out on the samples include X-ray diffraction, X-ray micro-tomography, scanning electron microscopy and mercury intrusion porosimetry. X-ray micro-tomography and scanning electron microscopy (secondary imaging mode coupled with energy dispersive spectroscopy) were done to study the microstructural changes due to the deterioration by acids in real life conditions. The mineralogical changes were investigated using X-ray diffraction. The changes in the porosity and the pore structure of the matrix were investigated by using mercury intrusion porosimetry for the selected samples.

1.4.2 Phase II: Laboratory investigations on paste

The methodology used for Phase II is depicted in Figure 1.1, which is further subdivided into characterisation of binders and accelerated leaching test on cement paste. The various binders used for the laboratory investigations were characterised for their physical and chemical properties. Particle size distribution of binders was studied using laser diffraction technique. The mineralogical phases present in the binders and oxide composition were obtained from X-ray diffraction studies and X-ray fluorescence technique respectively.

A static immersion based accelerated leaching test was conducted on prismatic cement paste specimens of size 10 × 10 × 60 mm. The different types of acids used in the study were sulphuric acid (1% and 3%), hydrochloric acid (1%), acetic acid (0.25M and 0.5M) and citric acid (0.5M). These acids were selected so as to investigate the effect of type of acid, concentration of acid, the solubility and kinetics of salt formation on acid attack. In order to study the role of binders in influencing the alteration kinetics, common binders such as Class F fly ash (30% replacement), blast furnace slag (50% replacement), and silica fume (10% replacement) were considered as mass replacements to cement in addition to the control mix containing Ordinary Portland Cement (OPC) only. Additionally, special binders such as High Alumina Cement (HAC) and Limestone Calcined Clay (LC2, at 45% replacement of cement) were also investigated.

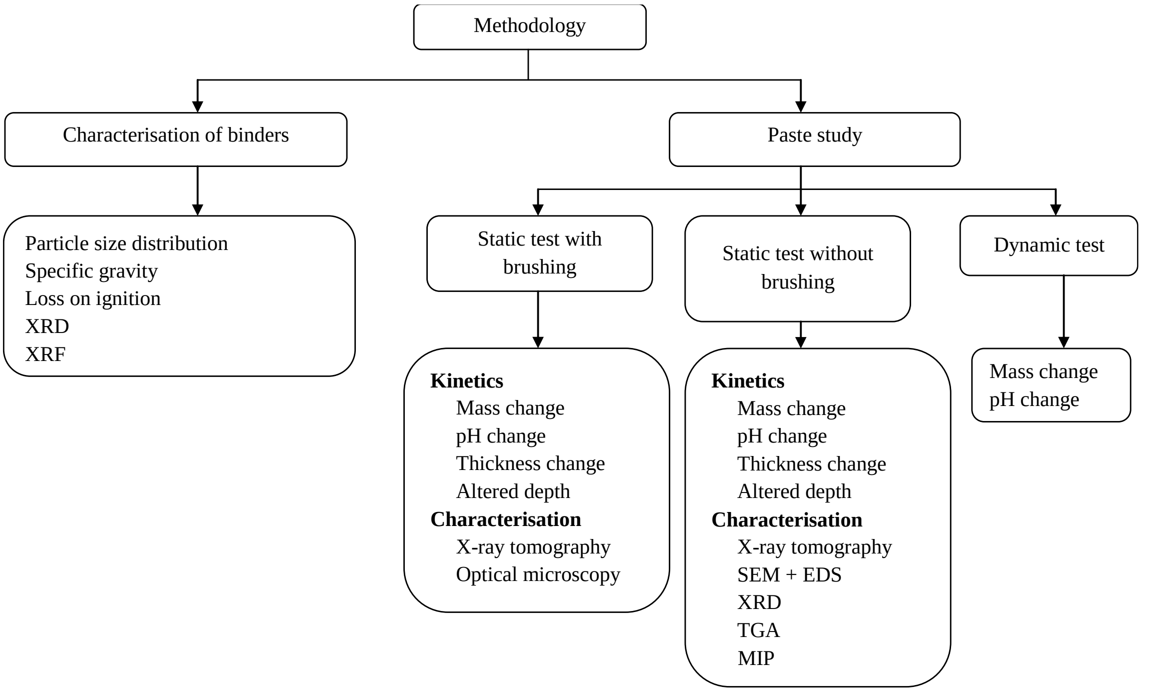

Figure 1.1 Methodology for paste study

Two types of static immersion tests were done on prismatic specimens: with and without brushing to simulate various real life conditions. Brushing of specimens (with soft nylon brush) was done to remove the loosely held corroded particles and also to accelerate the testing besides simulating the action of flowing effluents on the cementitious surface. Test with brushing is useful in studying alteration kinetics while the study without brushing is essential to preserve the corroded layers so as to investigate the mechanism of degradation. The alteration kinetics were studied by measuring parameters such as mass change, change in thickness, change in pH of the acid solution and altered depth (quantified based on X-ray tomography slice images) along with continuous visual observations.

Micro-analytical characterisation studies were carried out to understand the mechanism of degradation. The techniques used include X-ray Computed Micro-tomography (CT), Optical Microscopy (OM), X-ray Diffraction (XRD), Scanning Electron Microscopy (SEM), Mercury Intrusion Porosimetry (MIP) and Thermogravimetric Analysis (TGA). An attempt was made to study the microstructural zonation using optical microscopy for the selected samples. Later, X-ray tomography was explored to investigate the deterioration in detail. The objective of using X-ray tomography was to visualise the microstructural deterioration and to study the extent of degradation. The specimens with and without brushing were scanned to investigate the same. Mineralogical zonation, altered depth/area and other degradation related parameters were studied using tomography. The mineralogical changes in the various cementitious phases were studied using XRD. The variation in porosity and the pore structure due to acid attack was evaluated using MIP. SEM (secondary electron mode coupled with energy dispersive spectroscopy) was used to study the morphology and chemical composition of the attacked layers. Energy Dispersive Spectroscopy (EDS) was used to identify the reaction products. TGA was also carried out on selected samples before and after the degradation, so as to understand the chemical alterations that occur due to degradation of the cement matrix.

Another test method known as dynamic test for accelerated degradation was developed, based on the existing slake durability test (IS 10050, 1996; ASTM D4644, 2008). Alteration kinetics in this test was evaluated based on visual observations, mass changes of specimens and changes in pH of the acid solution.

1.4.3 Phase III: Laboratory investigations on mortar

The test methods applied to prismatic specimens as discussed in the paste study were extended in Phase III of the study to investigate the changes due to acid attack in mortar of proportion 1:3 made with siliceous standard sand as fine aggregate. The objective of the mortar study is to throw light on the role of various common binders, special binders and ITZ in acid attack. Figure 1.2 shows the methodology followed in the mortar study. Based on the results obtained in the paste study, the mortar study was limited to exposure in sulphuric (with and without brushing) and acetic acid (without brushing only). The study was done on mortars with two water to binder ratios: 0.40 and 0.55. Mortar specimens of size 10 × 10 × 60 mm (surface area to volume, S/V = 0.433) and 25 × 25 × 35 mm (S/V = 0.217) were prepared to study the size effect, i.e. the effect of surface area to volume ratio of specimens. To study the effect of concentration and pH levels, tests were done with 0.5%, 1%, 3% and pH of 2 (with 1% acid and sodium hydroxide pellets) and 0.125M, 0.25M, 0.5M and pH of 4 (with 0.25M acid and sodium hydroxide pellets) for sulphuric and acetic acids respectively. In the paste study, it was noticed that the edges of the specimen had undergone severe deterioration compared to surfaces and hence, to study this edge effect further, mortar study was also carried out in cylindrical specimens of size 25 mm diameter and height of 35 mm. This study however was restricted to exposure in 3% sulphuric acid.

Mass changes, pH changes and thickness changes were monitored regularly to investigate alteration kinetics, and the detailed characterisation study was limited to mortar specimens of size 10 × 10 × 60 mm exposed to 1% sulphuric and 0.25M acetic acid. Tests such as compressive strength and ultrasonic pulse velocity were carried out on cylindrical specimens to study the changes in strength and dynamic modulus of elasticity respectively. The characterisation tests were limited to X-ray diffraction, X-ray tomography, scanning electron microscopy and thermogravimetric analysis for the selected samples.

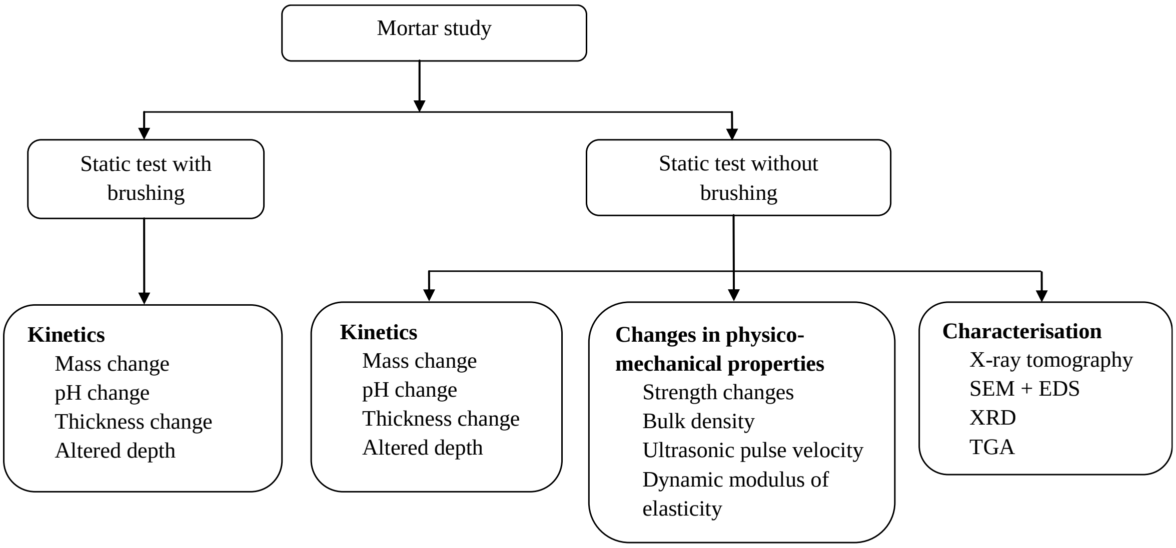

Figure 1.2 Methodology for mortar study

1.4.4 Phase IV: Effect of mineralogy of aggregate

In this phase, the effect of mineralogical nature of aggregate on degradation kinetics was investigated. Two types of aggregates were used to prepare mortar with OPC as the binder; limestone aggregates (calcareous) and graded river sand (siliceous). The investigation was limited to exposure to various concentrations of sulphuric and acetic acid. Alteration kinetics was studied through mass change, change in thickness, change in pH of the acid solution along with continuous visual observations. The microstructural studies were limited to imaging using X-ray tomography.

1.5 OUTLINE OF THESIS

The thesis is organised into ten chapters. The present chapter discusses the problem in general, followed by research objectives, scope and the methodology followed in the study. The second chapter gives a detailed review of literature covering various facets of acid attack in cement-based materials. The research gaps arrived at based on the review and the need for the present study are also detailed in the second chapter. The third chapter deals with the materials and methods which include the description of the materials used, mix proportions, test methods and parameters used for studying the degradation kinetics and mechanism. The details of field investigations and the micro-analytical characterisation studies on the samples carried out to understand the problem of acid attack are presented in the fourth chapter. The fifth chapter deals with the laboratory studies carried out on paste specimens to evaluate the degradation kinetics. The various micro-analytical characterisation tests conducted on degraded paste samples to investigate the mechanism of degradation are presented in the sixth chapter. The seventh chapter describes the studies carried out on mortar specimens to study the role of various binders and the effect of ITZ. The influence of mineralogical nature of aggregate in degradation kinetics of mortar is discussed in the eighth chapter. The ninth chapter provides insight on the analysis of results and recommendations proposed based on the study. The tenth chapter deals with the conclusions drawn from the current study and the scope for further research.

CHAPTER 2

LITERATURE REVIEW

2.1 INTRODUCTION

This chapter focuses on the critical review of literature compiling the research studies on the interaction of cementitious materials with acidic environments. The opening section explains the microstructure of concrete with various cementitious systems, which consists of the paste phase, aggregate phase and the interfacial transition zone, and its influence on the durability properties. A general discussion on concrete durability is also provided in this section in which the various factors affecting the durability, general mechanisms of deterioration, and various durability problems are briefly explained. The subsequent section provides an in-depth review of the acid attack in cement-based materials. The various acidic media that could come into contact with cementitious materials, the general mechanism of reactions, the various factors that affect the degradation kinetics, the mechanism of attack by specific acids, developments in the test methods to assess the resistance to acid attack, the various ways to achieve acid resistance by following standard guidelines, use of SCMs and special cement composites, effect of mix design, influence of protective coatings are critically reviewed and discussed in this section. Finally, a summary of literature review is presented along with the needs identified for the research.

2.2 REVIEW OF CONCRETE MICROSTRUCTURE AND DURABILITY

2.2.1 Concrete microstructure

Cement concrete is a versatile material of choice for building various constructed facilities. Concrete is a heterogeneous multiphase material, composed of three phases namely the hardened cement paste phase (HCP), aggregate phase and the interfacial transition zone (Alexander and Beushausen, 2009; Mehta and Monteiro, 2006). In general, the properties of concrete are governed by the properties of its ingredients, mix design and the method of production. Microscopically, the properties of concrete depend on the properties of these three phases; and the microstructure details of each phase along with its influence on durability of concrete are explained in the following sections.

2.2.1.1 Paste phase

Hydrated cement paste (HCP) is comprised of capillary pores and the products of hydration. (Mehta and Monteiro, 2006). The hydration product of typical cementitious system includes calcium silicate hydrate gel (CSH), Portlandite (CH), ettringite (AF_t), monosulphate (AF_m) etc. (Young et al., 1998). The hydration process and the microstructure vary based on the type of cement and SCM used. The hydration process of some of the common and advanced binder systems considered in the study is briefly explained in the sections below.

a) Hydration of OPC

Bogue’s compounds (anhydrous phases such as alite, belite, celite and felite) present in OPC react with water to form the hydrated products. This reaction is exothermic. The presence of soluble alkali oxides such as Na_2O and K_2O makes the pore solution more alkaline (pH 12 – 13). The calcium silicates (C_3S and C_2S) react with water to form CSH gel and calcium hydroxide (CH). CSH gel occupies nearly 60% of the volume of the solids in HCP, possesses very high surface area, and hence is an important phase in influencing the strength and durability properties of concrete**.** CH deposits as hexagonal crystals, occupies nearly 20% of the volume of the solids in HCP and the strength contribution is limited due to its considerably lower surface area compared to CSH (Mehta and Monteiro, 2013). In the presence of gypsum, tricalcium aluminate (C_3A) reacts with gypsum and water to form ettringite (AF_t), which gets crystallised as acicular, columnar, hexagonal crystals. The excess C_3A which is still unreacted could react with ettringite forming monosulphate (AF_m), with a composition of $C_4A\underline{S}H_{12-18}$. These calcium sulphoaluminate hydrates (ettringite and monosulphate) occupy 15 – 20% of the volume of the solids in HCP and hence play a secondary role in the microstructure – property relationships. Tetracalcium alumino-ferrite (C_4AF) undergoes similar reactions as C_3A, with the Al^{3+} in the hydration products being partly replaced by Fe^{3+}.

b) Blended OPC based binder systems

Cement hydration forms Portlandite ($Ca(OH)_2$ or CH), which is readily attacked by chemicals. Also, Portlandite does not provide as efficient space-filling characteristics as CSH. Also, the inefficient filling of void spaces in OPC systems leads to interconnected porosity, especially in the ITZ between paste and aggregate phase. These factors could contribute to enhance the permeability, paving the way to poor durability eventually. Mineral admixtures (or supplementary cementing materials) are a solution to this issue to a certain extent as their reactions consume lime ($Ca(OH)_2$) producing more CSH (through hydraulic or pozzolanic activity or both), and strengthening the ITZ, thus enhancing the strength and durability properties of concrete (Thomas, 2013). Also, fine mineral admixtures impart a filler effect, filling the void spaces effectively and reducing the permeability of concrete.

The commonly used SCMs to make concrete include fly ash, ground granulated blast furnace slag (or slag), silica fume, volcanic ashes, calcined clay, diatomaceous earth etc. The usage of SCMs also makes the concrete more sustainable. The use of right quality SCMs in concrete could result in increase in later age strength, lowering of water demand, reduction in permeability, reduced heat of hydration (reduced potential for cracking), enhanced durability, and correcting the deficiencies in aggregate gradation (by acting as fillers) etc. Most of the SCMs are either waste or by-products of industry. As SCMs are used commonly as mass replacement to OPC, the concrete becomes more economical. Also, the processing of these SCMs needs less energy when compared to cement. Along with reduced clinker usage, this leads to considerable reduction in the greenhouse gas emissions and helps to minimise the pollution.

The reactivity of SCMs depends primarily on their chemical composition in addition to the fineness. Figure 2.1 shows the ternary diagram showing the chemical composition (major oxides: lime, silica and alumina) of some of the commonly available SCMs like silica fume, Class C fly ash, Class F fly ash, slag, and metakaolin, along with Portland cement.

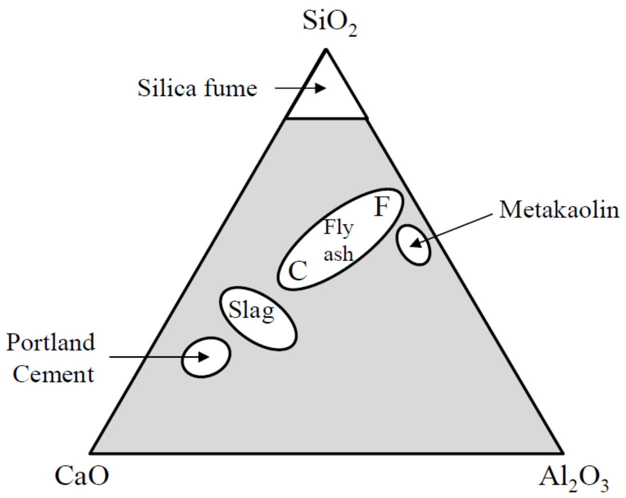

Figure 2.1 Ternary diagram showing the chemical composition of some commonly used SCMs (Dhanya, 2015)

Hydration of OPC + fly ash

In OPC – fly ash (FA) systems, a pozzolanic reaction occurs between the amorphous silica present in the fly ash and the CH from the OPC hydration in the presence of water. The pozzolanic reaction can be represented (Eq. 2.1) as follows.

$$x\ CH + yS + zH \rightarrow C_xS_yH_z\ (CSH\ gel) \tag{2.1}$$

The alumina phases present in the pozzolan and cement react with CH to form many phases, the major ones being stratlingite (C_2ASH_8), hydrogarnet (C_3AH_6), calcium aluminate hydrate (C_4AH_{13}), ettringite ($C_6A\underline{S}_3H_{32}$), calcium monosulphoaluminate ($C_4A\underline{S}H_{12-18}$), and calcium carboaluminate ($C_4A\underline{C}H_{11}$). Even though early age strength is less, the consumption of CH and more production of pozzolanic CSH, along with pore refinement, result in increased strength and enhanced durability at later ages when compared to OPC system (Lewis et al., 2003; Siddique and Khan, 2011; Taylor, 1997; Papadakis, 2000; Lane and Best, 1982).

Hydration of OPC + slag

Ground granulated blast furnace slag (GGBFS) is a processed by-product of the extraction of iron from iron ore in the blast furnace. By blending slag with OPC, and in the presence of water, the hydration process involves the activation of slag by the alkalis and sulphates in OPC to form hydration products (Lewis et al., 2003; Taylor, 1997; De Schutter, 1999). In the case of alkali activation, the products formed are CSH, C_4AH_{13} and C_2ASH_8 (Gehlenite). If the activation is by sulphates, the products formed are CSH, ettringite and aluminium hydroxide (AH_3).

The OPC – GGBFS hydrated cement paste has more number of smaller gel pores and fewer number of large capillary pores in comparison to the hydrated cement paste of OPC system. This finer pore structure gives OPC – GGBFS binder systems lower permeability than plain OPC systems (Siddique and Khan, 2011). Also, the aluminate present in slag has the potential to bind the free chlorides and hence, GGBFS is the ideal mineral admixture in the concrete for marine environment (Dhir et al., 1996). Moreover, slag admixed concrete exhibits excellent resistance to chemical attack and corrosion. Slag blended cement concrete is reported to be better when tested for chloride penetration, water sorptivity and gas permeability but with higher carbonation rates compared to OPC concrete (Dhanya, 2015).

Hydration of OPC + silica fume

Silica fume (SF) contains high amount of fine amorphous silica. On blending SF with OPC and water, the amorphous silica in SF reacts with CH from OPC hydration and water to form the pozzolanic CSH. The improved microstructure and durability properties are attributed to its pozzolanic property and high reactivity (due to higher surface area of SF particles), consuming the lime in producing additional CSH and due to the filler effect imparted by the fine SF particles. As a result, the ITZ also get strengthened (Taylor, 1997; Siddique and Khan, 2011). Thus, OPC – SF binder systems have increased strength and lower permeability (chloride permeability and diffusion) than plain OPC systems (Gjrov, 1993; Perraton et al., 1988; Cong et al., 1992).

Hydration of OPC + limestone calcined clay

Recent literature shows that limestone calcined clay cement (called as LC3) can be effectively used to achieve ternary blended cements with good performance even at very low (50%) levels of cement clinker (Scrivener et al., 2017). Such LC3 blends are produced by grinding limestone and calcined clay along with OPC clinker in the ball mill. Alternatively, limestone can be ground with calcined clay and this blend (limestone calcined clay, named LC2) may be used as a mineral admixture (partial replacement of cement) in concreting applications similar to slag.

The hydration mechanism remains the same for LC3 blend and OPC + LC2 systems. The kaolinitic clay on calcination forms metakaolin, which consists of reactive amorphous alumina-silicate ($Al_2Si_2O_7$). This further reacts with calcium hydroxide liberated due to OPC hydration (similar to pozzolanic materials) to form C(A)SH and aluminate hydrates. Additionally, the aluminate component of the calcined clay (especially of the kaolinitic type) can react with calcium carbonate (limestone, denoted as Cc) and calcium hydroxide (from OPC hydration) to produce space filling carbo-aluminate hydrates (mono carbo-aluminates (Mc) and hemi carbo-aluminates (Hc)) (Eq. 2.2).

$$\text{A (calcined clay)} + \text{Cc} + 3\ \text{CH} \rightarrow \text{C}_3\text{A Cc H}_{11} \qquad (2.2)$$

The formation of carbo-aluminates can improve the filling efficiency of the system as these additional hydrates are less dense (more voluminous) compared to the primary hydrates such as CSH and Portlandite (Balonis, 2009). These hydrates thus fill the space and continue to reduce the porosity as they are formed. This results in the enhancement of the strength and durability of the system (Antoni et al., 2012; Scrivener, 2014; Lopez, 2009; Puerta-Falla et al., 2015). The improved performance is also in part due to the filler effect of fine limestone (Puerta-Falla et al., 2015; Berodier and Scrivener, 2014; Bentz et al., 2012). The concrete made with LC3 ((50% clinker, 30% calcined clay, 15% limestone and 5% gypsum) was reported to be stronger and durable compared to OPC concrete and fly ash based concrete (Dhandapani and Santhanam, 2017). The microstructure of LC3 concrete is less porous compared to other binder systems.

Hydration of high alumina cement

Calcium aluminate cements (sometimes also known as high alumina cement, referred as HAC hereafter), has distinct chemical composition (Figure 2.2) when compared to OPC (Gosselin, 2009). Aluminous (bauxite) and calcareous components are sintered and ground fine to produce this type of cement. Figure 2.2 shows the ternary diagram indicating the approximate zone of calcium aluminate cements along with the zones of OPC and slag.

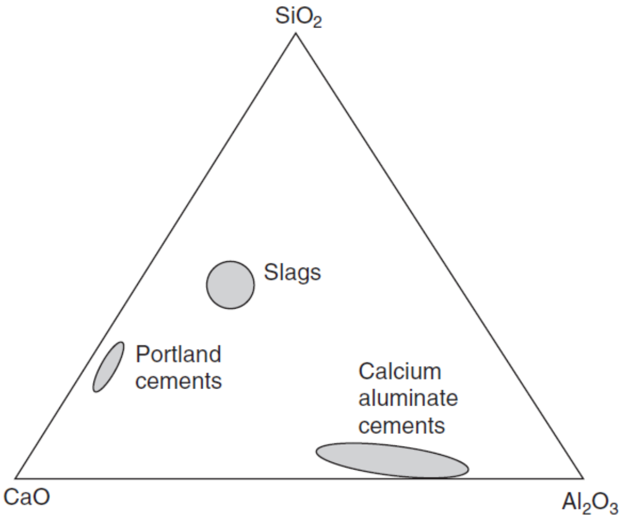

Figure 2.2 Composition range of calcium aluminate cement
(Newmann and Choo, 2003)

Generally, HAC has significant differences in its mineralogical composition mainly due to the varying iron content. The dark iron-rich cement typically contains 32 - 45% Al_2O_3, 15% Fe_2O_3, and 5% SiO_2, with the remainder comprising of CaO. The type used in this study is white low-iron (< 2% Fe_2O_3) designed primarily for the refractory lining applications. The principal phases present in the binder are calcium mono-aluminate ($CaAl_2O_4$, referred as CA) and calcium-di-aluminate ($CaAl_4O_7$) (referred as CA_2, also known as grossite). CA is the primary reactive phase responsible for properties of the material and typically constitutes up to 40 – 60% of the HAC. The hydraulic reactivity of calcium aluminate phases increases with the calcium content of the phase, and therefore CA shows higher reactivity than CA_2 (considered as weakly hydraulic).

The hydration products that are formed are dependent on the temperature of the system. When the temperature is less than 10 ˚C, CAH_{10} is the main hydration product, while between 10 and 27 ˚C, CAH_{10} and C_2AH_8 could form. However, both these phases are unstable and get converted to a stable phase C_3AH_6, when the temperature is higher than 27 ˚C (Fryda et al., 2001). In the long term, gibbsite (AH_3) also forms. The conversion to C_3AH_6 is often accompanied by loss in strength due to increase in the porosity of the system (due to loss of water). Moreover, the durability also could be compromised as C_3AH_6 can combine with SO_4^{2-} in the presence of calcium hydroxide to form ettringite, which causes expansion. The later age strength is due to C_3AH_6 and AH_3. However, HAC is widely used for refractory lining applications because the ceramic bond developed between hydration products and fine aggregate at very high temperature leads to enhanced durability at high temperatures. The hydration reactions of HAC are given below.

$$CA + 10H \rightarrow CAH_{10} \tag{2.3}$$

$$2CA + 16H \rightarrow C_2AH_8 + AH_3 \tag{2.4}$$

$$2CA_2 + 17H \rightarrow C_2AH_8 + 3AH_3 \tag{2.5}$$

At all temperatures, the final stable hydrated phases of CA are C_3AH_6 (a form of hydrogarnet) and AH_3 (gibbsite) which are formed as per the following equation.

$$3CA + 12H \rightarrow C_3AH_6 + 2AH_3 \tag{2.6}$$

C_3AH_6 has cubic crystal structure, while AH_3 is poorly crystalline which gets deposited as shapeless masses (Newmann and Choo, 2003).

The alkalinity of the HAC binder system is less compared to OPC system (pH of around 12.4 in comparison to > 13 for OPC) (Gosselin, 2009). The less alkalinity of the pore solution and the absence of Portlandite in the hydrated cement paste could have an impact on exposure to aggressive environments, which needs further study.

Interim summary

Based on the detailed review of hydration and microstructure of various cementitious systems, it is shown that the use of SCMs (fly ash, slag, silica fume and LC2 binder) as replacement of OPC results in long term benefits. In the case of SCM based binder systems, the consumption of lime and subsequent formation of further secondary hydration products result in the strengthening of ITZ, densified and finer pore structure within the hydrated cement paste, lowering the permeability, and leads to increased strength development on prolonged curing. It is also interesting to explore the potential of advanced binder systems like LC2 and HAC in resisting acidic media. Hence, more detailed investigation should be carried out in order to know the role of these binders when exposed to aggressive acidic environments.

2.2.1.2 Aggregate phase

The aggregate phase is largely responsible for contributing to the density, modulus of elasticity and dimensional stability of concrete. The above mentioned properties depend to a significant extent on the physical characteristics of the aggregate such as bulk density and strength of the aggregate, and the chemical characteristics offer only a secondary role (Alexander and Mindess, 2005). Even though physical characteristics of aggregates are considered important for the hardened properties of concrete, the mineralogical nature of the aggregate may be more important from durability considerations, especially on exposure to chemically aggressive environments. The behaviour of calcareous and siliceous aggregates in concrete may be different in acidic environments due to the difference in their neutralisation capacity and this should be investigated further (Dyer, 2014).

2.2.1.3 Interfacial transition zone

The microstructure and properties of the interfacial transition zone that exists between aggregate and the HCP are different from the bulk HCP (Mehta and Monteiro, 2006). Due to the higher water to cement ratio near to the aggregate surface, hydration products such as ettringite and Portlandite (CH) form as large crystals and this results in a porous microstructure of ITZ compared to the bulk HCP (Figure 2.3). In addition, the presence of microcracks in the ITZ limits the strength and contributes to increased permeability, thus reducing the concrete durability (Mehta and Monteiro, 2006). The usage of SCMs in the concrete strengthens the ITZ due to consumption of Portlandite present in the ITZ and improved packing in ITZ due to the formation of pozzolanic CSH with higher surface area in the expense of Portlandite.

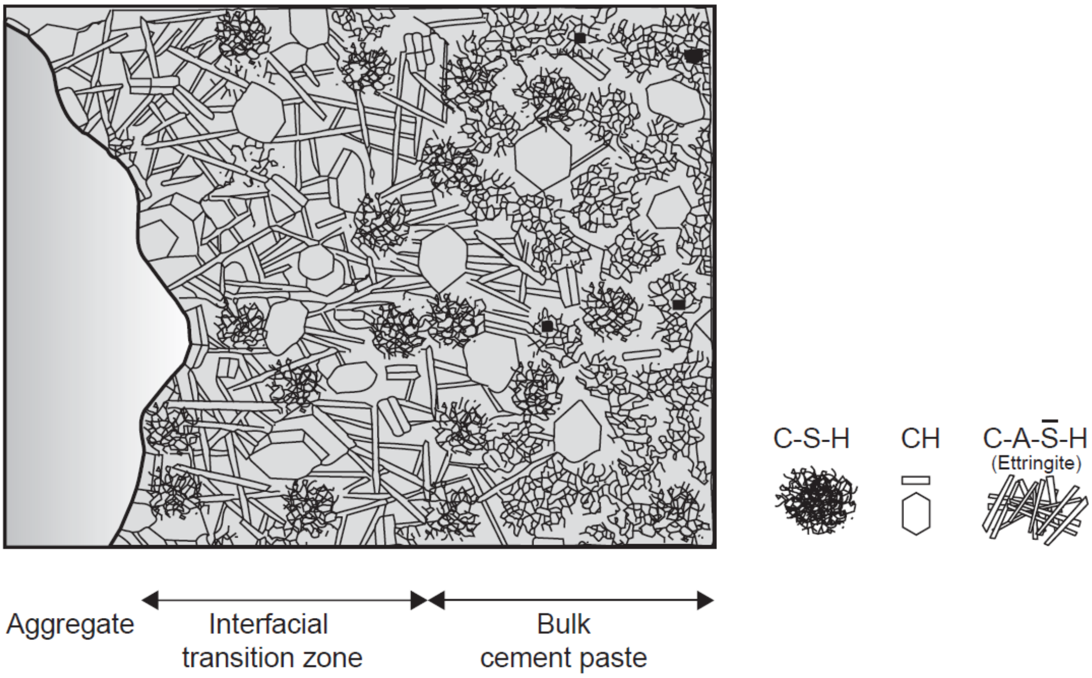

Figure 2.3 Schematic representation of the microstructure of ITZ and bulk cement paste in concrete (Mehta and Monteiro, 2006)

2.2.2 Concrete durability

Over the years, there has been a shift from the conventional prescriptive approaches towards performance based approaches in achieving the concrete durability. Concrete needs to be designed not only to meet the strength requirements but also for durability to withstand a specific environment (Richardson, 2002; Dhanya, 2015). Durability of concrete is defined as its ability to resist weathering action, chemical attack, abrasion, or any other processes of deterioration. According to ACI 201-2R (2008), durable concrete retains its original form, quality and serviceability, when exposed to its intended service environment.

The conventional wisdom that durability is a function of strength may not hold true always, especially in chemically aggressive environments. In the case of reinforced concrete structures, the durability of the structure is largely governed by the quality and transport properties of the cover-crete. As per ASTM E632-82 (2008), durability is associated with the deterioration of the material over the intended service life of the structure in a given environment. A concrete durable in one environment may not be durable in another, and it is important to understand the various factors that affect the concrete durability, as discussed in the subsequent sections.

2.2.2.1 Factors affecting durability

As shown in Figure 2.4, the concrete durability must be seen as the interaction between concrete system and its service environment (Ballim et al., 2009). Both these factors need to be considered while assessing the durability of concrete. Factors associated with the concrete system influence the ability of the concrete to resist deterioration, while environmental factors influence the level of aggressiveness that the concrete has to withstand. The concrete system related factors can be further subdivided into intrinsic and extrinsic factors. The intrinsic factors are related to the materials used, their properties and the mix design adopted, while the extrinsic factors are related to the various processes involved in the manufacturing of concrete, including workmanship.

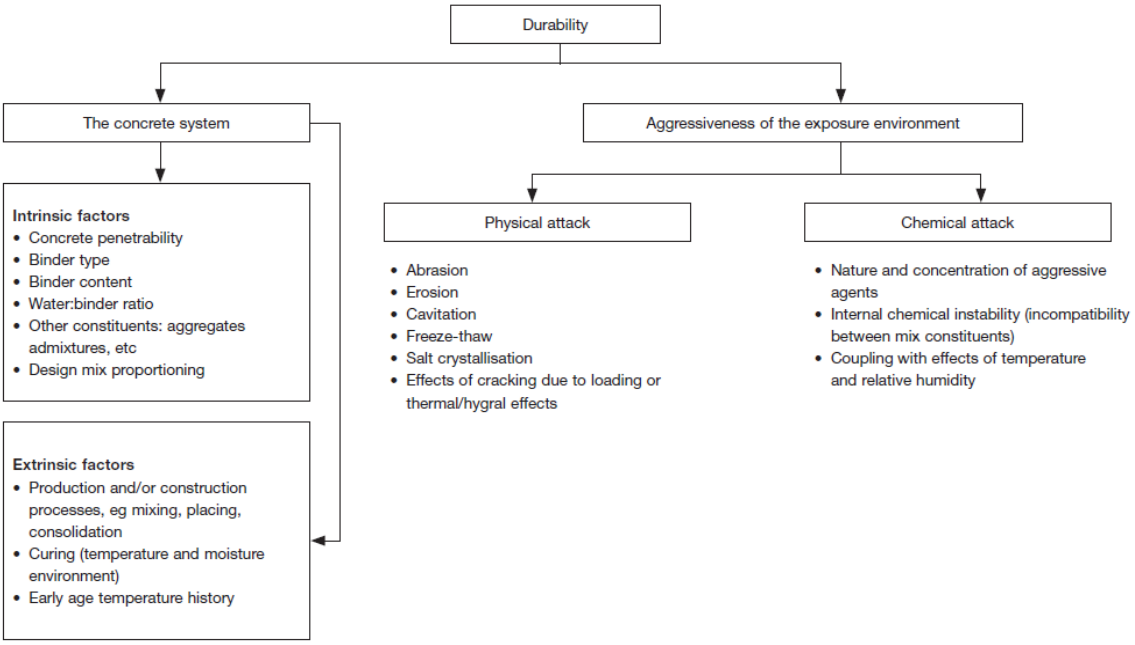

Figure 2.4 Factors influencing the durability of concrete (Ballim et al., 2009)

Damage of reinforced concrete structures occur either due to the deterioration of concrete or due to corrosion of reinforcement. The causes of concrete deterioration can be of two types, viz., physical and chemical. The major physical factors that deteriorate the concrete include abrasion, erosion, cavitation, freeze-thaw cycles, salt crystallisation, effects of cracking due to loading or thermal effects etc. The chemical attack in concrete depends essentially on the nature and concentration of the aggressive agents that attack the concrete, internal chemical instability (incompatibility between the mix ingredients), along with effects of temperature and relative humidity.

Concrete has to withstand various types of service environments; few of them are aggressive or deteriorating to the concrete. Such aggressive environments include seawater and coastal water containing sulphates and chlorides, acidic water (industrial effluents, agricultural and agro-food effluents, waste water, acidic soil, concrete sewers), freezing and thawing conditions etc. The concrete for these conditions should be designed taking into consideration the changes that the concrete microstructure will undergo upon interaction with these environments. The exposure to the above-said aggressive environments results in durability issues such as corrosion of steel, sulphate attack, acid attack, leaching, alkali aggregate reaction, alkali carbonate reaction, carbonation etc. and the deterioration eventually manifests in the form of mass loss, strength loss, volume changes, loss of alkalinity etc. In most of these durability issues, the presence of water or its involvement in the reactions is necessary. This implies that the durability of concrete is related to its permeability.

The permeability of concrete depends on the permeability of the HCP, of the aggregate, and of the ITZ. The permeability of these phases is further related to the interconnected porosity. The capillary porosity of paste is typically 30 – 40%, while normal aggregates have a porosity of 2 – 3%. The ITZ is also porous to a large extent owing to the presence of microcracks and bleed-channels in addition to the inefficient filling of spaces by large crystals of ettringite and Portlandite. The processes involved in fluid and ion movement through the concrete is influenced by the concrete permeability, which include the distinct transport mechanisms of capillary action, flow under pressure and flow under a concentration gradient. These mechanisms are characterised by the material properties of sorptivity, permeability and diffusivity respectively (Richardson, 2002; Alexander and Mindess, 2005). The above-mentioned transport mechanisms and the properties of ITZ govern the rate of most of the deterioration processes in concrete.

Both porosity and permeability also depend on the mix characteristics. The permeability of the paste increases with an increase in water to binder ratio of the mix. Both the threshold diameter and cumulative intruded volume (as measured by mercury intrusion porosimetry) increase with the water to binder ratio. The permeability also depends on the method and extent of curing, and the usage of mineral admixtures. As already discussed, the incorporation of SCMs could lead to strengthening of ITZ, besides the pore refinement and physical filler effect. These lead to reduction in the permeability.

The durability also depends on the type of cement and aggregate. Blended cements are generally expected to perform well in service environments such as marine environment, sulphate environment etc. As far as aggregates are concerned, the mineralogical nature and the porosity could affect the durability of concrete. The bond of the aggregate with cement paste dictates the quality of ITZ, which in turn depends on the texture of the aggregate. The presence of non-structural cracks could also accelerate the deterioration, as the aggressive agents may find an easy way to ingress into the concrete through these cracks.

2.2.2.2 Chemical deterioration

As chemical attack is the area of the study, this section aims to summarise the chemical mechanisms of concrete deterioration. The primary transport mechanism in the chemical deterioration is diffusion (based on Fick’s second law). Diffusion of ions or salts occurs in partially or fully saturated concrete. On exposure to chemically aggressive environment, high ionic concentrations are developed at the surface of the matrix. As a result, concentration gradient develops and ions or salts migrate by diffusion from high concentration to low concentrations of the matrix (Richardson, 2002). The diffusion rate depends on the temperature, moisture content of the concrete, type of diffusing agent, inherent chemical stability of the hydrates present in the matrix etc.

As deterioration of cement-based materials by acids is the topic of research, a summary of the deterioration of concrete by chemical reactions are shown in Figure 2.5.

Figure 2.5 also shows the various types of chemical reactions along with their outcomes; these are detailed in the subsequent sections. These reactions eventually manifest in the form of reduction in alkalinity, changes in mass, strength and rigidity, cracking, spalling and deformation.

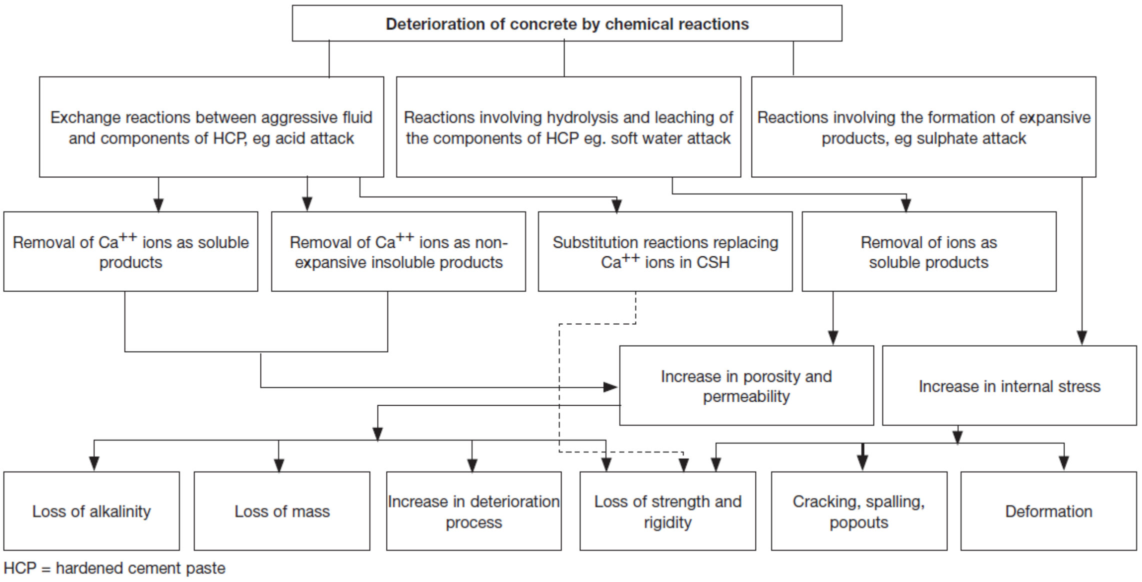

Figure 2.5 Summary of some of the chemical reactions and their effects in concrete deterioration (Ballim et al., 2009)

Exchange reactions between acids and components of HCP (ion exchange or substitution)

Because of the generally alkaline nature of the pore solution of hydrated cement paste, the products of hydration as well as unhydrated cement react with acids; the ionic chemical equilibrium is disturbed resulting in deterioration of the cement matrix. This form of deterioration starts from the surface and continues into the concrete until all the acid or the cement paste has been consumed.

Dissolution of the products of cement hydration (ion removal)

The products of cement hydration are dissolved in the aggressive solution due to their chemical instability in low pH environments, and leached out of the concrete causing the destruction of CSH gel, thus affecting the integrity of the matrix and the concrete strength.

Dissolution of $Ca(OH)_2$ from concrete by pure water is typical of this form of deterioration.

Expansive stresses caused by conversion of the products of hydration by external agents (ion addition)

External aggressive agents such as acids or salts diffuse into the pore structure of the concrete, react with the products of hydration, and create expansive forces within the matrix. This causes cracking and mechanical degradation of the concrete. The effect of sulphates on concrete is an example of this form of deterioration, causing expansion due to the formation of gypsum and ettringite. In the case of acids, the salts may form with a higher molar volume when compared to the original hydrates and this could lead to build-up of expansive stresses causing rapid deterioration.

2.3 ACID ATTACK IN CONCRETE

Concrete structures are vulnerable to the attack by aggressive aqueous environments in many situations, resulting in deterioration. The understanding of the alteration kinetics and mechanism of degradation of concrete by these aggressive aqueous media is a fundamental step towards the development of a durable concrete which will increase the service life or the safety of the structures. As far as India is concerned, many industries still remain dependent on processes that produce effluents or wastewater. Such effluents contain a wide range of both organic and/or inorganic acids whose action may lead to severe degradation of concrete structures.

Cementitious materials being highly alkaline in nature are easily attacked by acidic solutions. This disturbs the equilibrium of the cement matrix causing leaching and associated degradation. Degradation of cement-based materials due to acids is a complex phenomenon influenced by many factors related to both acid and cement. This intricate mechanism of degradation is still not well understood. Further detailed studies are needed to study and elucidate the mechanisms of degradation and kinetics in these conditions by developing new test methods and to formulate materials and mixtures that could withstand these aggressive environments. The following section explains in detail, the various acidic media that could attack the concrete, the basic mechanism of attack, various factors influencing the degradation kinetics, mechanism of attack by specific acids (inorganic and organic), and a critical review of various test methods developed to evaluate the acid resistance of materials. An insight is also given on achieving the acid resistance which includes the approach followed by various international standards, the role of SCMs and special cement composites, the effect of mix design and the role of protective coatings to mitigate the effects of acid attack.

2.3.1 Acidic environments

Concrete structures can be attacked by acidic solutions in various situations. The range of aggressive species that attack the concrete is wide. Industrial manufacturing plants and factories utilise various processes that use or produce a variety of synthetic acids. Spillage and accidental leakage of these acids can severely deteriorate the concrete structures, as the concentration of acid, which attacks the concrete, may reach alarmingly high values (Harrison, 1987; Fattuhi and Hughes, 1988; Allahverdi and Skvara, 2000a, Ramaswamy and Santhanam, 2017). Aside from the actual production of such acids, fertiliser industry uses nitric acid (HNO_3) and sulphuric acid (H_2SO_4) or phosphoric acid (H_3PO_4) in the production of ammonium nitrate (NH_4NO_3) and superphosphate ($Ca(H_2PO_4)_2$), respectively. Glass industry uses hydrofluoric acid (HF) as an etchant. Similarly, lots of acids are involved in the metal processing units. Particularly, hydrochloric acid (HCl) is used widely in the pickling process in steel industry in removing the rust layers on the steel surface. Superphosphate fertiliser used in the agriculture industry could have presence of free sulphuric and phosphoric acids.

Sewage, under the ideal conditions, could deteriorate the concrete sewer pipes due to the attack by sulphuric acid. This is a biogenic process and the optimal temperature for this process is approximately 30 °C, which means that it can be more frequently encountered in tropical hot countries like India. Also, domestic and industrial waste water generates lot of acids, predominantly sulphuric and acetic acid in waste water treatment plants, and concrete structures in these areas are vulnerable to get attacked by these acids generated due to the microbial action (Ramaswamy et al., 2017a). The nature of the biogenic process implies that the acid generation is limited by the bacterial activity and hence the deterioration phenomenon may only be inadequately modelled by the laboratory tests using synthetic acids where the volume of acid is large in comparison with the volume of cementitious materials (Scrivener and De Belie, 2013). Consequently, Alexander and De Belie (2013) opine that this process is not easy to simulate in the laboratory tests, especially using test methods with mineral acids. However, test methods utilising mineral acids can be developed to study the interaction between acid and the cement based materials to arrive at the mixture formulations.

The air pollution caused by the presence of atmospheric carbon dioxide, sulphur dioxide, and nitrogen oxides could result in the production of acidic media (Zivica and Bajza, 2001). Industrial emissions of sulphur and nitrogen compounds can be oxidised and converted further to sulphuric and nitric acids. The precipitation of rain containing these acids could be detrimental to cementitious materials as the pH value is low (pH about 3-5) (Pavlik, 1994a; Sersale et al., 1998). Thus, acid rain could be an additional aggressive media for the concrete structures.

Organic acids could be either present inherently in the agricultural products (i.e. plants or fruit) and/or are formed during the metabolism of microbes thriving in the effluents (Bertron and Duchesne, 2013; Bertron et al., 2017). Organic acids could also be present in industrial applications, mostly from the food and drink industry. Sour alcoholic beverages and vinegar contain acetic acid. Alcoholic beverages also contain lactic acid, while pharmaceutical industry uses citric acid. Agricultural activities such as the production of silage generate effluents containing acetic and lactic acid. Concrete structures in cattle milk sheds degrade because of lactic acid attack combined with abrasive action of animals. Liquid manure contains a mixture of organic acids, including acetic, butyric, propionic, iso-butyric acids etc. and concrete structures used to store manure are prone to attack by these acids. Among agro-food effluents, whey water produced by the dairy industry contains lactic, acetic and citric acids. Sugar industry produces molasses which has lactic, malic, acetic, oxalic, citric and succinic acids. The fermenting industry effluents mainly contain tartaric, succinic and acetic acid. The composition of the various aggressive media that could produce a wide range of organic acids is given in Table 2.1. Furthermore, the concrete inside biogas reactor digesters are also prone to deterioration due to the production of organic acids and ammonium in the liquid phase and H_2S and CO_2 in the gas phase (Voegel et al., 2016).

Table 2.1 Organic acids present in some agro-food industries (Larreur-Cayol et al., 2011a)

Industry	Waste waters	Acids	Concentration (mmol/L)	pH
Wine industries	Vinasses	Tartaric	3.2–8.7	4-6
		Acetic	3.1–5.0	
		Lactic	2.2–5.6	
		Succinic	0.3–6.8	
		Malic	0.5–0.8	
		Total (max.)	26.9	
Sugar industries	Sugar cane vinasses	Lactic	18–80.4	4-7
		Glycolic	12–25	
		Citric	1.7–10.4	
		Trans-aconitic	0.2–4.8	
		Cis-aconitic	0.1–2.8	
		Oxalic	0.08–0.8	
		Fumaric	0.1–0.4	
		Total (max.)	124.2	
Dairy industries	Whey	Acetic	14.0	4-6
		Citric	9.2–9.6	
		Lactic	3.4–5.7	
		Propionic	1.0	
		Butyric	0.6	
		Total (max.)	30.9	
Animal rearing	Silage juice	Lactic	55.3–63.7	4-5
		Acetic	25.3–28.3	
		Butyric	4 3.4	
		Propionic	3.1	
		Total (max.)	99.1	
	Liquid manure	Acetic	31.7–213	5-8
		Butyric	1.1–28.8	
		Propionic	5.4–37.8	
		Total (max.)	279.6	

According to Rodhe et al. (2002), the average pH levels of rainwater in highly industrialised areas are below 4.5. Moreover, the modelling of wet acid deposition indicates that the quantities of acids are alarmingly high. The production and deposition of acids of high magnitude could be detrimental to the durability of concrete, especially in those areas where rainwater gets accumulated. Thus, the attack of concrete by acidic waters is a topic of emerging importance owing to escalating damages to reinforced concrete structures around the world. This adverse situation could be attributed to the end result of rapid urbanisation and industrialisation, generating increased sources of acidic media that could come into contact and attack the concrete which are already vulnerable to the degradation due to their high alkalinity of the pore solution and chemical composition (Zivica and Bajza, 2001; Pavlik, 1994a; Allahverdi and Skvara, 2000a, b).

2.3.2 General mechanism of attack

Concrete is multiphase material which is porous. The pore solution is alkaline (pH around 13) and hydration takes place in this pore solution. Thus, owing to its high alkalinity, the natural equilibrium of concrete is disturbed when it reacts with acids. Compounds present in the binders as well as acid-soluble aggregates (e.g. dolomite or limestone) are unstable in a solution containing an excess of hydrogen ions (acids). The attack is a classic acid (HA) – base (BOH) type of reaction to form a salt (BA) and water (Eq. 2.7).

$$HA_{(aq)} + BOH_{(aq)} \rightarrow B^{+}_{(aq)} + A^{-}_{(aq)} + H_2O_{(aq)} \qquad (2.7)$$

Portland cement hydration products are reactive in acids to a great extent. The chemical stability of the material is governed by the chemical composition of the components of the hydrated cement paste and their relative proportions inside the matrix. A schematic depiction of the solid (phases such as $Ca(OH)_2$ and CSH) - liquid equilibrium in relation to the concentration of calcium ions in the pore solution is given in Figure 2.6.

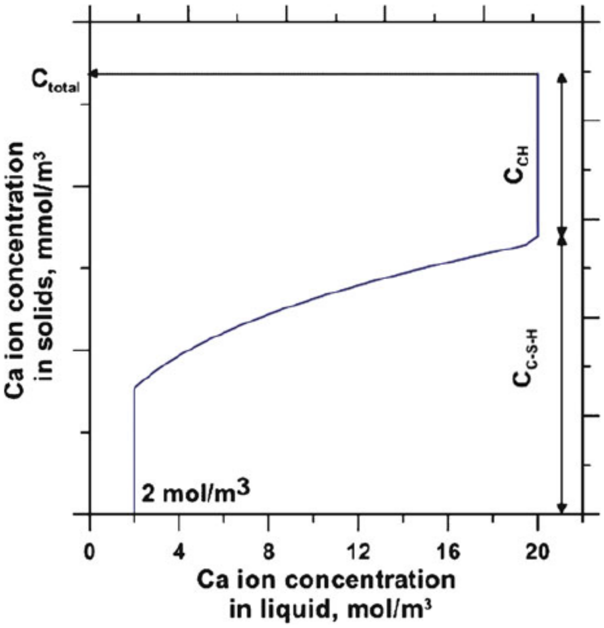

Figure 2.6 Pore solution – hydrated phases equilibrium curve for calcium (Jain and Neithalath, 2009)

Portlandite is the least stable among the cement hydrates; its dissolution happens when the concentration of calcium ions in the pore solution reduces below 22 mmol/L. CSH gels are more stable when the calcium ion concentration in the pore solution is between 22 and 2 mmol/L, which further depends on the Ca/Si molar ratio of the CSH gel.

When the calcium ion concentration in the pore solution drops below 2 mmol/L, CSH gel also becomes unstable; it undergoes decalcification to form eventually silica gel, which is stable at low concentrations of calcium in the pore solution.

Ingress of acid ions into the cement matrix by diffusion disturbs the chemical equilibrium and the phenomenon is schematically depicted in Figure 2.7. The cations dissociated from the hydrates such as Ca^{2+}, Al^{3+} leach out to the acid solution along with alkali ions in order to maintain the chemical equilibrium. In the process, these cations such as Ca^{2+} and Al^{3+} could react with the anions of the acids forming salts of varying solubility depending on the acid characteristics. The kinetics of degradation essentially depends on the various properties of the salts thus formed.

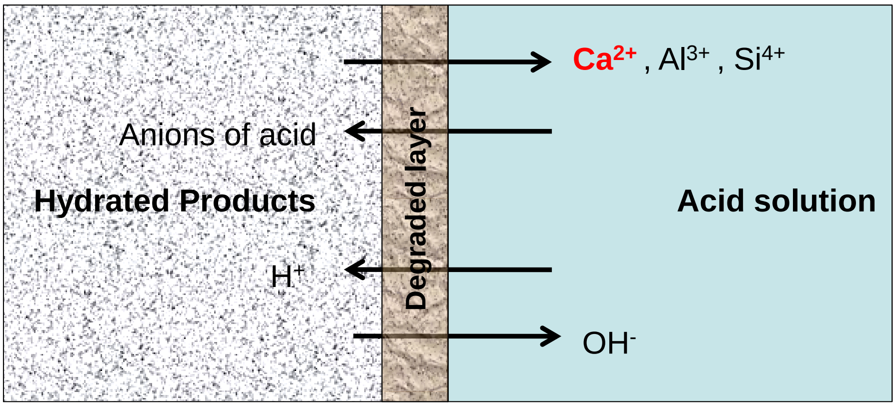

Figure 2.7 Acid attack phenomenon

The chemical reactions in the paste are basically of two types; the dissolution of hydrated and anhydrous phases in the binder system and the precipitation/leaching of new reaction products that are formed (Bertron, 2013). These reactions proceed from outside to the interior, forming a degraded layer in the process. The physico-mechanical properties of the degraded layer are weaker compared to the sound zone. If the products formed are soluble, they leach out into the solution increasing the porosity of the matrix. Sometimes, if products formed are less soluble, these may precipitate within the matrix, exerting crystallisation pressure resulting in the formation of cracks. These cracks further reduce the mechanical strength and enhance the diffusion of acid to the inside. Eventually, the aggressive agents reach the reinforcement resulting in the corrosion of reinforced structures. However, these are basic mechanisms of degradation; the degradation is specifically dependent on the type of acid and the properties of the products formed.

According to Alexander and Fourie (2011), Portlandite ($Ca(OH)_2$) is the most reactive of the hydrates and completely dissociates, while calcium silicates are less reactive followed by calcium aluminates and calcium alumino-ferrites. The elements such as Ca, Na, K, Mg leave the matrix whereas Si, Al and Fe remain, the stability of their bearing phases notably depending on the pH. A gel layer of mainly acid-insoluble silica (SiO_2) remains on the surface of the cement after the dissociation of calcium silicates. Aluminium hydroxide ($Al(OH)_3$) and iron hydroxide ($Fe(OH)_3$) precipitate in the layer after dissolution of the aluminates and alumino-ferrites depending on the hydrogen ion concentration of the solution; iron hydroxide precipitates at a pH greater than 1.0 and aluminium hydroxide precipitates at a pH greater than 3.0. More specifically, calcium hydroxide undergoes dissolution at a pore solution pH of 12.5, followed by ettringite at pH value of 10.7. CSH gel becomes unstable and undergoes dissolution at pH between ~10.5 and 8.8 (according to different authors) followed by calcium aluminate and ferrite hydrate phases. Eventually, the CASH gel is obtained, if the pH is above 7. If the pH is between 1 and 6, an amorphous silica gel containing Al and Fe ($SiO_2 . nH_2O$) is obtained as the end product (Duchesne and Bertron, 2013). These microstructural changes due to the decalcification of hydrates result in the formation of mineralogical zonation; these manifest in the form of changes in mass, strength, elastic modulus etc. and the integrity of the matrix is affected. The loss of alkalinity of the matrix and subsequently increased porosity due to the attack (due to decalcification of hydrates) result eventually in the corrosion of reinforcement when the entire concrete cover depth is attacked. However, the phenomenon is not simple, as the alteration kinetics and degradation mechanisms are influenced by various factors related to the material, attacking solution and the test method, and hence it is imperative to understand the various factors affecting the process of deterioration in detail. These influencing factors are critically reviewed and presented below.

2.3.3 Factors influencing degradation kinetics

Acid attack is a dissolution cum precipitation/leaching process influenced by many factors. The factors can be broadly classified into two groups; material (both acid solution, aggregate and cementitious medium) and the factors related to test method. Besides these factors, actions of microbes also influence the phenomenon to a great extent. A detailed list of factors is compiled from the literature and presented in Figure 2.8. The factors are discussed in the subsequent sections.

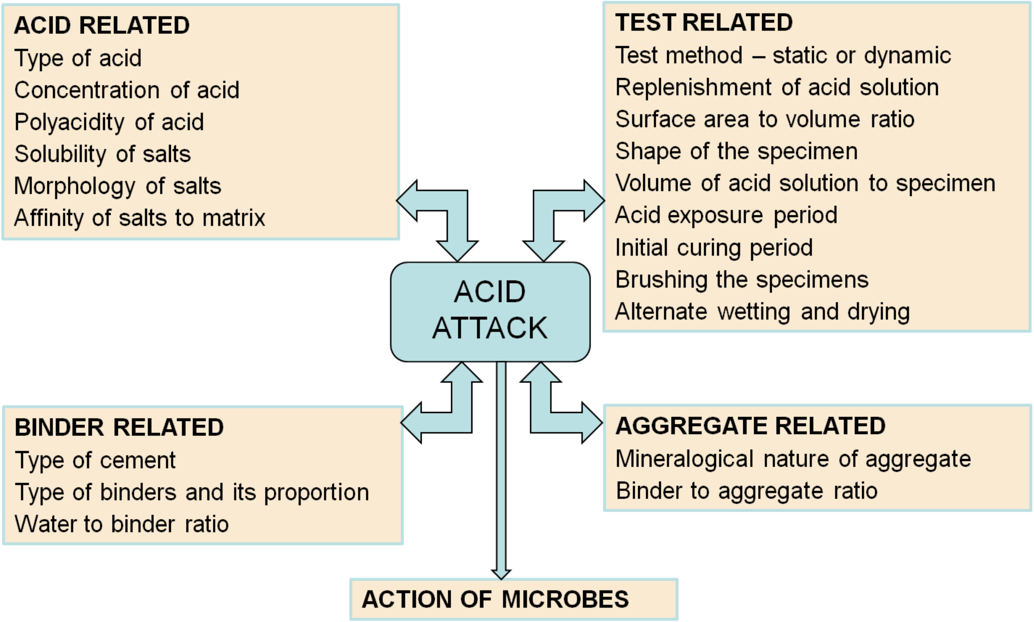

Figure 2.8 Factors influencing the degradation kinetics

2.3.3.1 Acid related factors

The aggressiveness of an acid is essentially related to its hydrogen ion concentration, with the amount of hydrogen ions liberated in an aqueous solution depending on acid type and concentration. Acid attack in concrete may also be broadly classified into two based on the type of acid; attack by inorganic acids such as hydrochloric acid, sulphuric acid and attack by organic acids such as acetic acid, citric acid etc. This is because the mechanism and kinetics depend on the salt characteristics, which in turn depend on the type of acid. At similar concentrations, a solution of a strong acid (e.g. hydrochloric, sulphuric acid or nitric acid) contains substantially more hydrogen ions than a weak acid, since strong acids completely dissociate in solution. Weak acids such as hydrogen sulphide and organic acids (acetic, lactic, citric acids etc.) dissociate only partially. In an ideal case, the dissociation of acid (HA) would be complete; the solution would then contain only H^+ (proton) and A^- (conjugate base) ions and no HA. But, in actuality, the acid and its conjugate base co-exist in equilibrium, and the extent to which dissociation occurs is determined by the acid dissociation constant, K_a, defined by the Eq. 2.8, where the terms in parentheses are concentrations.

$$K_a = \frac{[A^-][H^+]}{[HA]} \tag{2.8}$$

Acid dissociation constants are commonly expressed as pK_a (Eq. 2.9), where

$$pK_a = -\log_{10}(K_a) \tag{2.9}$$

The more negative the pK_a value of an acid, the greater the strength of acid. In other words, a higher positive value of pK_a means that the acid is weak and less dissociative. The pK_a values for the various commonly encountered acids are given in Table 2.2. Oxalic, tartaric and citric acids are polyacidic in nature, as they dissociate to give multiple protons, with each value in the table representing the pK_a for successive release of acid protons.

Table 2.2 pK_a values of acids (Dyer, 2014)

Acid	pK_a	Acid	pK_a
Hydrochloric	−8	Formic	3.77
Sulphuric	−3	Lactic	3.86
Nitric	−1.3	Acetic	4.76
Oxalic	1.25, 4.14	Butyric	4.83
Tartaric	2.99, 4.40	Iso-butyric	4.86
Citric	3.09, 4.75, 5.41	Propionic	4.87
Hydrofluoric	3.17	Carbonic	6.35

Degradation kinetics of cementitious materials due to acid attack to a large extent depends upon the type of acid and the salts formed (calcium/aluminium/iron etc.). Salts formed from acid reactions with concrete may precipitate as a layer on the original substrate, depending on their solubility. This in turn depends on acid type, with a readily soluble salt such as calcium chloride ($CaCl_2$) forming in hydrochloric acid. In addition, a porous silica gel layer and Friedel's salt (due to the reaction of chlorides with aluminates) that forms in a hydrochloric acid solution offer little protection against further attack. On the other hand, a sparingly soluble salt such as calcium sulphate forms in a sulphuric acid solution. This usually precipitates as a gypsum layer ($CaSO_4.2H_2O$), which binds together the insoluble residue in the gel layer, creating a physical barrier on the surface of the concrete, thus hindering the diffusion of ions involved in the reactions and slowing the attack rate (Gutberlet et al., 2015). The thickness of the gypsum layer increases until, at a certain thickness, the attack depends on the diffusion rate of the ions through this layer.

When the acids form soluble salts, these are leached away into the solution. The degraded layer then comprises only of a weaker and permeable silica gel. But, when the salts are less soluble, they precipitate within the matrix. This precipitation could be protective or detrimental depending on the molar volume of the salt that is formed. If the molar volume is less, they could seal the porosity and act as a protective barrier to the penetration of acid. However, if the molar volume is very high, the precipitation could lead to crystallisation pressure that could cause expansion and cracking. Table 2.3 gives the solubility data of calcium and aluminium salts that may be formed when acid reacts with cement paste (Bertron and Duchesne, 2013; Dyer, 2014).

Table 2.3 Solubility of calcium and aluminium salts of various acids
(Bertron and Duchesne, 2013; Dyer, 2014)

Acid	Calcium salt	Solubility at 20 °C (g/L)	Aluminium salt	Solubility at 20 °C (g/L)
Sulphuric	$CaSO_4\cdot 2H_2O$	2.4	$Al_2(SO_4)_3$	364
Hydrochloric	$CaCl_2$	745	$AlCl_3$	458
Nitric	$Ca(NO_3)_2\cdot 4H_2O$	1290	$Al(NO_3)_3\cdot 9H_2O$	673
Acetic	$Ca(CH_3COO)_2\cdot H_2O$	347	$Al(CH_3COO)_3$	Sparingly soluble
Citric	$Ca_3(C_6H_5O_7)_2.4\ H_2O$	0.95 (25°C)	$Al(C_6H_5O_7)_3$	2.3
Oxalic	$CaC_2O_4/CaC_2O.\ H_2O$	0.0067 (18 °C)/insoluble	$Al_2(C_2O_4)_3.4H_2O$	insoluble
Tartaric	$CaC_4H_4O_6.4H_2O$	insoluble	-	-

The kinetics of degradation is highly influenced by the concentration of the acid solution. The higher the concentration of the acid, the higher the kinetics in terms of mass changes, strength changes, altered depth etc. In addition to these factors, other factors such as pK_a, polyacidity, formation of organometallic complexes could also influence the aggressiveness of organic acids and hence the kinetics, although the influence of complex formation seems limited (De Windt et al., 2015).

Among the organic acids that form soluble salts, aggressiveness is primarily influenced by their pK_a. For example, lactic acid was found to be more aggressive because it has lower pK_a value when compared to other organic acids that form soluble salts (Bertron et al., 2005). However, when the salt is slightly soluble, the pK_a is no longer the first order influencing parameter and the salt characteristics such as molar volume, and its affinity to the cement matrix becomes important (Bertron and Duchesne, 2013; Larreur-Cayol et al., 2011a). Moreover, in the case of organic acids, cations coming from the dissolution of cement paste and anions from acids could form organometallic complexes which may have a minor influence on the aggressiveness depending on the value of complexation constants.

2.3.3.2 Binder related factors

The material related factors can be categorised further to cementitious medium related factors and aggregate related factors. The primary factors related to cementitious medium include the chemical and mineralogical nature of the matrix and its transfer properties which in turn will depend on the type of cement, type of binders used and its proportion. The water to binder ratio is not an intrinsic influencing parameter but the consequences of this ratio such as transfer properties, degree of hydration etc. are influencing parameters.

The cement paste which has high Portlandite (i.e. $Ca(OH)_2$) content is more vulnerable to attack as this phase dissolves first, leading to mass loss, substantial increase in the porosity and weakening of mechanical properties. Use of supplementary cementing materials (SCM) like fly ash, slag, silica fume etc. leads to dilution of ordinary Portland cement (OPC), and consumption of calcium hydroxide due to pozzolanic/hydraulic reactions, thus lowering the level of $Ca(OH)_2$. SCMs with right degree of fineness and prolonged curing may help in enhancing the acid resistance. Studies have found that silica fume does not improve the behaviour of cement paste to acid attack. On the other hand, SCMs such as slag and metakaolin are reported to enhance the resistance to acid attack (Oueslati and Duchesne, 2012). This could be attributed to the aluminium content. Aluminium is preserved in the degraded layer of pastes attacked by acids, thus imparting stability to the altered layer. The results pertaining to effectiveness of SCMs are still not conclusive enough and further research needs to be done to investigate the role of aluminium in enhancing the acid resistance (Monteny et al., 2003; O’Connell et al., 2012; De Belie et al., 2004; Roy et al., 2001; Chang et al., 2005; Saricimen et al., 2003; Fattuhi and Hughes, 1988; Attiogbe and Rizkalla, 1988; Alexander and Fourie, 2011).

Higher OPC contents (less replacement by SCMs) could enhance the neutralisation capacity of the system due to increased Portlandite content, which may protect the concrete when the acid is in limited quantities. However, when the volume of acid is very large compared to cementitious materials, increased Portlandite content could lead to more degradation. Also, Beddoe and Dorner (2005) opine that lower cement content may cause the concrete to be more susceptible to the abrasion and loss of the degraded layer.

Another important parameter governing the acid resistance is the water to cement ratio of the mix. As explained earlier, the diffusion of acid is controlled by the capillary porosity, which in turn is determined by the water to cement ratio (w/c). For most of the acids, it is expected that the use of a lower w/c ratio enhances the acid resistance, mainly because of the reduced permeability and hence reduced rate of diffusion of aggressive agents through the corroded layer, and a higher strength in this layer, which will lower the mass loss as a result of abrasive action. However, in the case of concrete exposed to sulphuric acid, contradictory observations are reported. Hewayde et al. (2007) and Roy et al. (2001) observed that the loss of mass was reduced as w/c ratio of the mix is increased when the concrete was exposed to sulphuric acid. This controversial result was not however justified by proper scientific explanations.

2.3.3.3 Aggregate related factors

The mineralogy of the aggregate (calcareous or siliceous) and the binder to aggregate ratio also influence the kinetics of degradation (Dyer, 2014; Hughes and Guest, 1978). Aggregates containing carbonates such as limestone are more prone to the attack by acids. Limestone aggregate reacts with acids (HA) forming calcium salt and CO_2 (Eq. 2.10).

$$CaCO_3 + 2HA \rightarrow CaA_2 + 2CO_2 \qquad (2.10)$$

Limestone aggregates neutralise acids as they dissolve. This will enhance the neutralisation capacity of the concrete compared to siliceous aggregates which are considered as inert. The use of calcareous aggregates such as limestone could lead to sacrificial protection as the attack on cement hydrates are shared also with the attack on calcium bearing aggregates. On the other hand, siliceous aggregates being inert, the paste is directly attacked resulting in the decalcification of hydrates leading to mass loss, exposing the aggregates further. However, the effect could be dependent on the type of acid, the salts that are formed and their properties. Dyer (2014) also highlights that the corroded layer of specimens exposed to few acids undergoes shrinkage. This could lead to formation of cracks, which further enhances the rate of ingress of acid and hence the deterioration. The binder to aggregate ratio of the mix also influences the kinetics and needs further study. At less pH of the solution, cement matrix could be easily attacked by acid and if coarse aggregate content is high (low binder to aggregate ratio), it would result in fall out of aggregates from specimen, indicating higher mass loss (Hewayde et al., 2007).

2.3.3.4 Action of microbes

Wherever the deterioration is due to acids produced by microbes, there could be subtle differences when synthetic acids are used for study. Also, the effect of microbes, the relationship between the microbes and the substratum is important. In such cases, the detrimental impact of microbes caused by biofilm formation must be considered when developing test methods for evaluating the material durability. The test method should be specific to the environment and new standards have to be developed which will consider the type and characteristics of acids and the effect of biofilm formation so as to formulate performance specifications to arrive at concrete mixture formulations (Bertron, 2014).

2.3.3.5 Test related factors

There exist a variety of test related factors which could influence the degradation. The selection of test variables should be such that it simulates the real environment to the closest extent possible. A more detailed investigation on test related factors is essential so as to propose a standard testing method to evaluate the acid attack phenomenon.

As mentioned earlier, the architecture of the test method and the test related factors will influence the results. Although the test procedure itself may be similar, the differences in the nature of specimen, the attack cycle (length of immersion and drying intervals), the way of maintaining the pH of the acid solution within certain limits, the choice of degradation measure, the fact whether loose material is abraded or not before measuring, etc. may result in different or even contradictory results (De Belie, 2013). No specific codes and standards are available that address test methods for acid attack. Hence, development of a sound and reliable test method is the pressing demand of today.

Several studies are conducted without the periodic renewal of acid solution. As a result of neutralisation, pH of the solution increases and the aggressiveness of the solution declines rapidly, and hence reducing the rate of attack. Smaller sized specimens with high surface area to volume ratio are widely used in tests to accelerate the attack. However, it would be interesting to study the effect of surface area to volume ratio of specimens in alteration kinetics to understand size effects. Specimens such as prisms and cubes having sharp edges are liable to experience more mass loss as edges are weak locations permitting more acid ions to penetrate from multiple directions. Volume of acid solution relative to the volume of specimen dictates the changes in pH and hence the rate of attack. The degradation process is enhanced when subjected to alternate wet dry cycles. This could be due to the increased capillary suction forces during wetting by suction which leads to more penetration of acid and microcracking due to shrinkage on drying. Oueslati and Duchesne (2012) showed experimentally, the beneficial effect of the initial curing before acid exposure when SCMs were used. The use of mechanical action on the specimens could affect the kinetics of degradation. When the aggregates are inert and insoluble in acid solution, the use of abrasive action could result in the preferential and faster removal of cement paste. This in turn will expose the aggregates on prolonged exposure to acids. Eventually, the bond between the aggregate and matrix will be lost resulting in the loss of aggregates from the matrix, leading to higher mass loss. The above-mentioned test related factors should be considered into account while developing a proper test method.

2.3.4 Mechanism of attack by specific acids

The mechanism of attack by acids to a large extent depends on the solubility of salts, which in turn is based on the anion of the acid and hence, the mechanism varies with the type of acid that attacks the matrix. Concrete could be attacked by strong and weak acids whose solubility can differ and hence the mechanism. Strong inorganic acids such as sulphuric acid and weak organic acids such as citric, succinic, malic, tartaric and oxalic acids form salts which are not highly soluble (slightly soluble to insoluble). At the same time, strong inorganic acids such as hydrochloric acid, nitric acid and weak organic acids such as acetic acid form salts which are highly soluble in acid solutions. The mechanisms of attack by these acids are explained in two sections based on the solubility of salts: acids forming soluble salts and acids forming less soluble salts. Also, sewage networks offer a very aggressive environment for cement-based materials causing sulphuric acid attack. As the attack here is caused by the microbial production of acid, the mechanism is treated separately and discussed in detail in the later subsections.

2.3.4.1 Attack by strong and weak acids forming less soluble salts

When the acids form less soluble salts, they precipitate inside the matrix. The deterioration depends upon the molar volume, morphology and affinity of the salts with the matrix. The cases of strong and weak acids forming less soluble salts are discussed below.

Strong (inorganic) acids forming less soluble salts

The attack by sulphuric acid leads to the formation of gypsum whose solubility is low. The gypsum is formed due to the reaction of calcium hydroxide and CSH with the acid anions (sulphate ion). CSH decalcifies to form amorphous silica gel. The formation of gypsum and decalcification of CSH is accompanied by expansion and softening of the degraded layer along with the loss in the integrity of the matrix.

Weak (organic) acids forming less soluble salts

Among the organic acids, salts formed by citric, succinic, malic, tartaric and oxalic acids are not highly soluble (Bertron et al., 2009; Larreur-Cayol et al., 2011a, b, c). According to Bertron and Duchesne (2013), these five acids can be grouped into two categories based on the protectiveness of the salt; acids forming calcium salts which are protective to the matrix and acids forming salts which are not protective to the matrix. The protectiveness of the salt could be assessed based on the kinetics measurements (mass changes/altered depth measurements). According to Bertron and Duchesne (2013), the salts are termed as protective if the degradation kinetics with these acids are lower than the acids that form soluble salts (acetic acid). The mechanisms of action of these acids are detailed below.

Mechanism of degradation by oxalic, malic and tartaric acids

Among the organic acids, oxalic, malic and tartaric acid form calcium salts whose molar volume is less when compared to that of the original hydrates; $Ca(OH)_2$ and CSH. The lower molar volume of the salt implies that the salt could at least partially fill the capillary porosity created by the dissolution of the hydrates. The sealing of porosity by salts takes place without creating the crystallisation pressures and hence no visible cracks are formed in the matrix. Also, the salts appear to adhere to the matrix well and hence contribute to lower kinetics of degradation compared to acetic acid, which forms soluble salts (Figure 2.9).

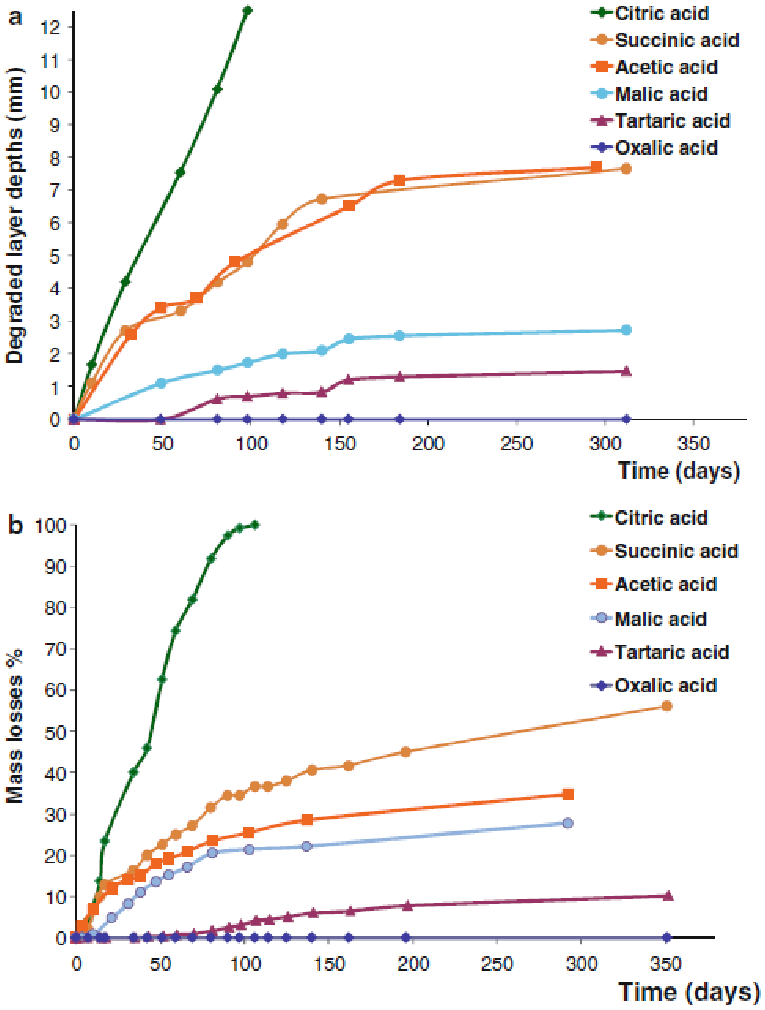

Figure 2.9 Alteration kinetics of Portland cement paste specimens immersed in organic acids (Bertron et al., 2011) – (a) degraded layer depths and (b) mass losses

Oxalic acid

The exposure of cement paste to oxalic acid results in the precipitation of calcium oxalate mono-hydrate salts ($CaC_2O_4.H_2O$), or Whewellite, on the surface of specimens. This has a protective effect to the matrix limiting the further kinetics (Larreur-Cayol et al., 2011a) as the molar volume of the salt is less. It is hypothesised that calcium oxalate salt is primarily formed from the hydrolysis of Portlandite and, apparently, at least partially due to the decalcification of CSH. The precipitation of this salt plugs the capillary porosity, thus preventing the ingress of the aggressive species further into the matrix. This results in reduced (negligible) mass loss/degraded depth as evident from Figure 2.9(a) and 2.9(b).

Research has shown that cement pastes made with slag have excellent resistance on exposure to acetic acid when compared to OPC paste (Oueslati and Duchesne 2011a, b, 2012). Nevertheless, the performance of slag was found to be inferior on exposure to oxalic acid. This could be ascribed to the limited availability of Portlandite in the slag system. The consumption of lime for the slag reactions might have led to the attack on CSH. Hence, the absence of Portlandite was found to be deleterious on exposure to oxalic acid. Despite the low pH of the oxalic acid solution, the kinetics was found to be limited for OPC paste and this could be ascribed to the protective effect and low solubility of calcium oxalate salt.

Tartaric acid

In the early ages of exposure, the attack by tartaric acid led to the precipitation of calcium tartrate tetrahydrate ($CaC_4H_4O_6.4H_2O$) on the periphery of the specimen, which was found to have a protective effect limiting the kinetics. However, on prolonged exposure, this outer layer was found to defragment. This could be due to high molar volume of the salt (143 cm^3/mol vs. 66 cm^3/mol), inducing expansion and exfoliation of the outer layer. The kinetics was found to be moderate (Figure 2.9) and less protective compared to oxalic acid (Larreur-Cayol et al., 2011a; Bertron et al., 2011).

Malic acid

The deterioration mechanism by malic acid was found to be similar to that by tartaric acid. The salt, calcium malate, was precipitated on the surface of the specimens (Bertron and Duchesne, 2013). However, the attack by malic acid led to increased kinetics (higher mass losses and degraded depths) compared to tartaric acid (Figure 2.9).

Citric acid

Citric acid has been found to be the most aggressive to the cement matrix. The exposure to citric acid resulted in the precipitation of calcium citrate tetrahydrate salt, $Ca_3(C_6H_5O_7)_2.4H_2O$ (Bertron et al., 2009; Larreur-Cayol et al., 2011a). The molar volume of this salt being very high (518.4 cm^3/mol) compared to the molar volume of the original hydrates, resulted in the complete defragmentation of the outer degraded layer (Bertron and Duchesne, 2013). This in turn led to the very high alteration kinetics of the specimens (Figure 2.9) when compared to all the other acids. The thickness of the outer layer was found to be less as the calcium citrate salt was non-protective in nature. It is loosely attached to the inner matrix; it exfoliates from the specimen and gets deposited in substantial quantities at the bottom of the beaker. The aggressiveness of citric acid could also be attributed to the poly-acidity of the acid as suggested by Larreur-Cayol et al. (2011a). At a pH around 4, one mole of citric acid releases two moles of H^+ ions while mono-acids such as acetic or propionic acid releases only one mole of H^+ ions.

Succinic acid

The attack by succinic acid led to increased kinetics when compared to oxalic, tartaric and malic acids (as shown in Figure 2.9). Similar to the other organic acids, the outer zone was found to be deficient in calcium and sulphur. Notably, the middle layer was only partially decalcified. In this zone, calcium succinate mono-or tri-hydrate salt is precipitated (Bertron, 2013). This salt is found to be not protective (unlike the case of tartaric or malic acid). This could be due to the slightly increased solubility of the calcium salt compared to the protective salts. However, even though not protective, the salt does not seem to be destructive either as the molar volume is moderate (Bertron et al., 2009; Bertron, 2013). Unlike the case of acetic acid, the exposure to succinic acid resulted in the dissolution of the outer degraded layer of the specimens, causing increased mass loss. Bertron et al. (2009) ascribed the slightly higher aggressiveness of succinic acid also to the poly-acidic behaviour of succinic acid.

2.3.4.2 Strong and weak acids forming soluble salts

Strong inorganic acids such as hydrochloric acid, nitric acid and weak acids such as acetic acid, lactic acid are highly aggressive to cementitious media. Acids such as hydrochloric, nitric and acetic acid form Ca salts which are soluble and leach out to the solution making the outer degraded layer porous offering less resistance to diffusion of acids. CSH also decomposes to form salts and an amorphous Al and Fe-bearing silica gel. Calcium aluminate hydrates produces salts along with $Al(OH)_3$, which is stable above pH of 4. $Al(OH)_3$ may also be attacked to release Al^{3+} ions, if the pH falls below a value of 4. As the salts are soluble, they do not form expansive precipitates (as in the case with sulphuric and citric acid). Hence, the deterioration may be less on visual observations. However, the leaching of calcium and the formation of silica-alumina gel results in high porosity. Decalcification associated shrinkage cracks could be seen in the outer layer which may enhance the ingress of acid further.

On exposure to nitric acid, the attack led to the formation of an outer corroded layer which is relatively white, and a thin brown region adjoining the corroded layer. Pavlik (1994b) analysed and found that the white layer was composed of amorphous silica. The brown zone was composed of increased amount of ferric hydroxide besides silica. Calcium nitrate, being highly soluble (1290 g/L), leaches out to the solution. This causes substantial reduction in the volume of the outer degraded layer, which manifests in the formation of visible cracks. The above mentioned mechanism and mineralogical zonation can be illustrated using X-ray micro-tomography (CT). Figure 2.10(a) shows the X-ray tomography image of OPC paste (made with w/c ratio of 0.40) exposed to 0.2M nitric acid for a period of 12 weeks. The outer layer is seen as a thin dark layer. Brown zone identified by Pavlik (1994b) is seen as a thin bright layer just inside to the outer layer. In addition, a thick dark layer is observed wherein the amount of Ca was found to be less when compared to the sound zone (unattacked). This could mean that the decalcification is ongoing and is partially complete in this zone.

Similar mineralogical zonation was observed in the case of OPC paste exposed to 0.5M acetic acid for a period of 6 weeks and the corresponding CT slice image is shown in Figure 2.10(b). The outer layer was observed to be thicker and this higher depth may be attributed to the higher concentration of acid and its aggressiveness. The outer and the middle layer were devoid of calcium and highly porous. This implies that the volume of the sound zone was less and is illustrated in the 3D rendered image (Figure 2.10(c)) obtained by performing suitable thresholding operations. The higher alteration depth and the high porosity of this layer results in very low mechanical properties. The attack by acetic acid and HCl results in the formation of an outer degraded layer which is orange brown in colour depending on the concentration. The salts of both the acids are soluble and the mechanisms are identical. Additionally, in the case of HCl, chlorides can further react with aluminates to form chloroaluminates (Friedel's salt) and upon crystallisation, they can form expansive products leading to the formation of microcracks, especially in higher water to binder ratio mixtures (Duchesne and Bertron, 2013).

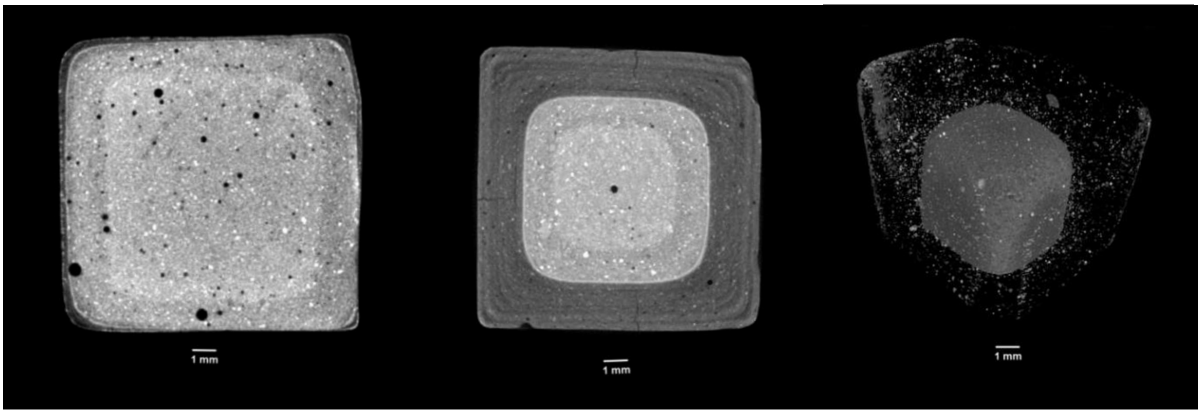

a) CT image of OPC paste immersed in 0.2M nitric acid showing zonation

b) CT image of OPC paste immersed in 0.5M acetic acid showing zonation

c) 3-D rendered CT image of OPC paste exposed to 0.5M acetic acid

Figure 2.10 X-ray microtomography images of OPC paste exposed to various acids (Ramaswamy et al., 2017b)

Liquid manure contains a mixture of organic acids (acetic, butyric and propionic acids) which are detrimental to the cementitious matrix, acetic acid being the predominant component. Figure 2.11 presents the oxide composition of OPC paste immersed in the synthetic liquid manure (SLM) with respect to the distance to the surface of the specimen in contact with the SLM solution. The same graph also shows the results of the control specimen without the acid exposure. The curves were corrected in the altered zone by means of the amount of titanium in the paste (Bertron et al., 2007). Zones 1, 2 and 3 marked on the curve correspond to the core layer, middle layer and the outer degraded layer of the specimen respectively. It can be seen that the curves of the inner layer of attacked paste (zone 1) and control specimen were identical. A high proportion of Ca was lost from zone 3, while zone 2 appears to be slightly decalcified. In the altered zone

(zone 3), the amount of SiO_2 was constant. Al_2O_3 and Fe_2O_3 oxides were well preserved in the inside part of zone 3, whereas the amounts decreased slightly next to the surface.

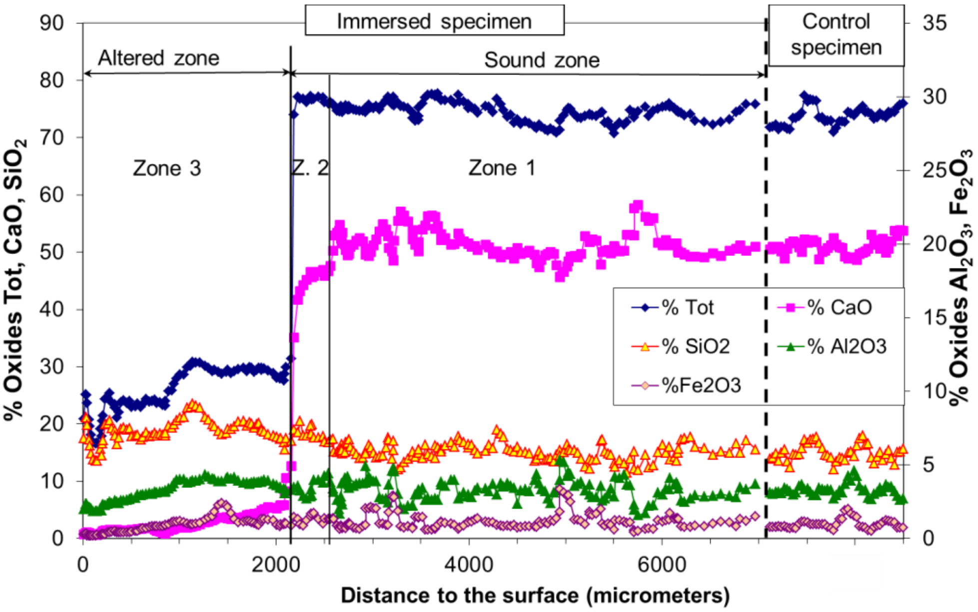

Figure 2.11 Chemical analysis with EPMA according to depth of OPC paste immersed in SLM1 (pH 4) 4 weeks of immersion – Absolute amounts of oxides (Bertron et al., 2007)

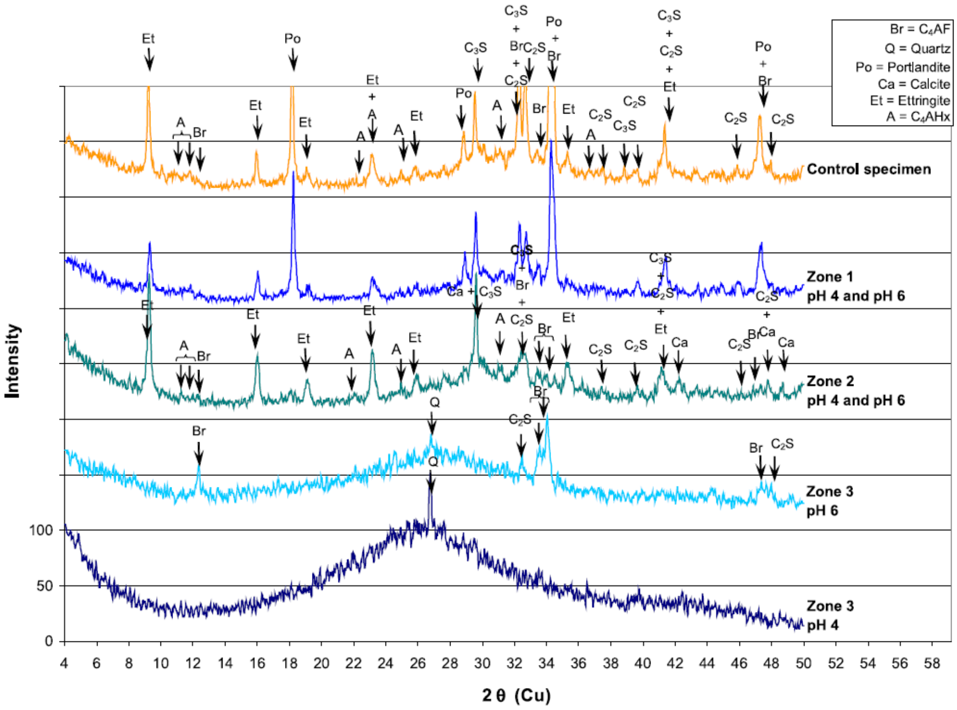

Figure 2.12 X-ray patterns of the 3 zones of the OPC paste specimen immersed in organic acid solutions at pH 4 (SLM1) and pH 6 (SLM2) after 9 weeks of immersion and of the control specimen – CEM I paste (Bertron et al., 2005)

Figure 2.12 shows the X-ray diffractograms of samples collected from various layers of OPC paste exposed to aggressive organic acid solutions, SLM1 and SLM2 (Bertron et al., 2005). The aggressive solutions were prepared using a mix of five organic acids found in liquid manure: acetic, propionic, butyric, isobutyric and valeric acids. This SLM solution was then added with 2 g/L NaOH in order to raise the pH up to 4 for the SLM1, and 9.6 g/L NaOH to bring the pH up to 6 for the SLM2. It can be seen that the X-ray patterns of specimens immersed in SLM1 and SLM2 are identical except for zone 3 (outer degraded layer). The zone 1 (inner unattacked layer) comprised of normal hydrates such as Portlandite, ettringite, C_4AF along with anhydrous phases and CSH halo. For both the cases (SLM1 and SLM2), Portlandite peaks are absent in zone 2 (middle layer), whereas the peaks of the C_2S and C_4AF grains as well as ettringite are still present, and the peak intensity for C_3S is reduced. The XRD pattern also shows that some calcite has also been formed in this zone. This confirms the decalcification in zone 2. Zone 3 was totally decalcified leaving only silica gel which is amorphous. The halo of silica gel with quartz peaks centered around 27° 2θ confirms the formation of this amorphous structure.

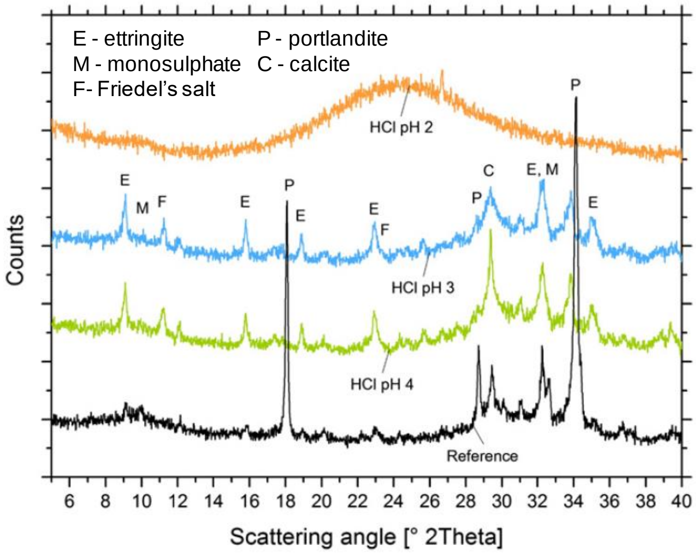

Figure 2.13 XRD patterns for OPC samples before and after immersion in HCl for 28 days (Gutberlet et al., 2015)

The mineralogical phase changes occurring in OPC paste after exposure to various pH solutions of HCl are illustrated by the X-ray patterns presented in Figure 2.13 (Gutberlet et al., 2015). It was found that the hydrated and anhydrous phases underwent dissolution on exposure to the acid solution. On exposure to pH 3 and pH 4, Portlandite was totally consumed, and intensity of anhydrous phases were reduced; ettringite and Friedel's salt were formed as the main reaction products. This formation could be attributed to the conversion of most of the monosulphate due to chloride ion penetration. Calcium chlorides being soluble leach out and hence could not be detected. Calcite was also formed as the secondary product. The pH 2 solution being more aggressive, the entire specimen got degraded and was found to be totally amorphous owing to the formation of silica-alumina gel skeleton. Ettringite, Friedel's salt, calcite peaks were not observed as they are unstable in very low pH.

2.3.4.3 Comparison of strong and weak acids

Pavlik (1994a) found that nitric acid (HNO_3) and HCl were more aggressive compared to formic (HCOOH), acetic (marked as HAc) and sulphuric acid (H_2SO_4) in terms of altered depth (Figure 2.14) for the same concentration (Pavlik, 1994a). When the acids form soluble salts, strong inorganic acids are found to be more aggressive than weak organic acids for a particular concentration of acid. This may be due to less pH and greater dissociation of inorganic acids compared to organic acids. However, organic acids which form soluble salts such as acetic acid can be equally detrimental to the matrix (as evident from higher corrosion depths at increasing concentrations shown in Figure 2.15) and the aggressiveness could be contributed by other factors which are detailed below.

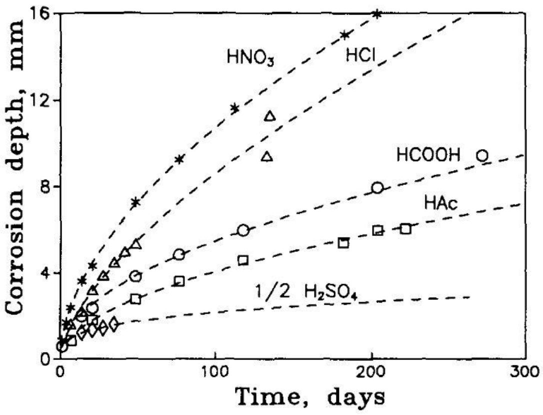

Figure 2.14 A comparison of the aggressiveness of strong and weak acids (Pavlik, 1994a)

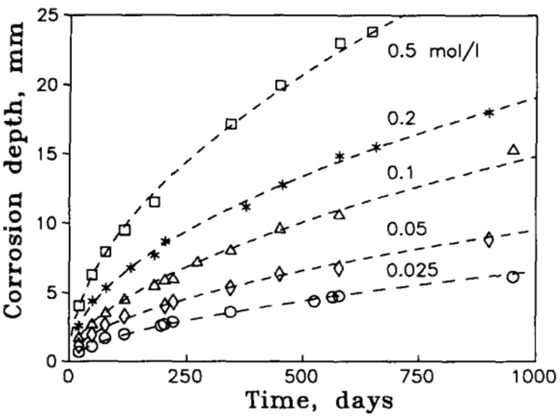

Figure 2.15 Variation of altered depth for various concentrations of acetic acid (Pavlik, 1994a)

Organic acids are regarded as weak acids which dissociate only partially depending on the dissociation constants (K_a). A weak acid is also characterised by the presence of a buffer zone, when the pH of the solution is close to the value of pK_a. In such pH values, release of large quantity of hydroxyl ions results only in a slight variation of the pH (Koenig and Dehn, 2016). The buffer action capacity of organic acids can have an influence on the kinetics. Acids such as acetic, propionic, butyric, iso-butyric, lactic acids are mono acids. Malic, tartaric, oxalic and succinic acids are bi-acids whereas citric acid is a tri-acid. On reaction with the cement matrix, the bi-acids and tri-acids release twice and thrice the hydronium ions when compared to mono-acid, for the same concentration of acid. It is also important to note that the pH value may not serve as a reliable indicator to know about the actual concentration of acid present in the solution and its aggressiveness. This is because, a strong acid which is present in small quantities in solution results in significantly lower pH values than a weak acid present in large quantities in the solution, due to its low dissociation. The above factors can influence the kinetics of degradation and have to be considered while designing a test method.

There is almost no difference between weak and strong acids that forms soluble salts in terms of the deterioration mechanisms. Certain organic acids despite its partial dissociation are equally aggressive to inorganic acids and could lead to higher alteration depths and associated degradation. Calcium salts of organic acids such as acetic, propionic, butyric, iso-butyric and lactic acids are highly soluble in water and hence leach out to the surrounding acid solution, causing substantial degradation of the cement matrix.

Interim summary

The mechanism of attack by various acids was discussed. As the mechanism of attack is affected to a significant extent by the solubility of salts, the review was intended to bring out the differences in the mechanism of attack due to the acids (strong and weak) which form soluble salts and the acids (strong and weak) which form insoluble salts. The test results show that the attack by weak organic acids such as acetic acid is comparable to the action of strong acids such as hydrochloric and nitric acids. There is almost no difference between weak and strong acids that forms soluble salts in terms of deterioration mechanisms. In these cases, acidolysis and leaching are the predominant factors leading to higher alteration depths. The attack due to acids forming soluble salts results in the formation of an undissolved altered zone with very low mechanical properties comprising of silica-alumina skeleton gel of high porosity.

In can be inferred that the organic acids which produce soluble calcium salts such as acetic acid can be highly detrimental to cementitious matrix wherein the aggressiveness could be attributed to a variety of factors such as concentration, specificity, buffer action and complexation properties of acid. Wherever the deterioration is due to acids produced by microbes, the differences could exist when synthetic acids are tested. In such cases, the megative impact of microbes caused by the biofilm formation must be considered into account when developing test methods for evaluating the material durability. The test method should be specific to the environment and new standards have to be developed which will consider the type and characteristics of acids and the effect of biofilm formation so as to formulate performance specifications to arrive at concrete mixture formulations. The deterioration of concrete sewer pipe is one such environment wherein the degradation mechanism is affected by the action of microbes and this is explained in the following section.

2.3.4.4 Mechanism of concrete deterioration in concrete sewers

Sewer corrosion due to biogenic acid attack on concrete pipes is a serious durability concern faced worldwide. The difficulty in accessing these sewage networks poses a major limitation in the timely maintenance and repair. Premature failure of sewer pipes could result in significant repair and maintenance costs. Consequently, there is a need to understand better the mechanisms of acid attack and deterioration of concrete sewer pipes and the specific causative conditions, so as to improve upon the material selection and mixture formulations for making durable concrete sewers. The primary cause of degradation is the deterioration of concrete due to sulphuric acid produced by bacteria, resulting in rapid degradation of the concrete sewers, as shown in Figure 2.16.

Figure 2.17 shows the various steps involved in the biological deterioration. Sulphuric acid is produced only in the final step in a sequence of processes leading to the deterioration of concrete sewers (Grengg et al., 2015). As the process is driven by the microbial activity, it is difficult to simulate the real sewer environment in a laboratory based testing with mineral acids (Scrivener and De Belie, 2013; Alexander and De Belie, 2013). However, a recent study done by Huber et al. (2017) points out that there are no major differences between the tests done using biogenic and synthetic acids, as the reaction products were found to be of similar chemical composition. Hence, it may be safe to say that the test methods utilising mineral acids can be developed to study the interaction between acid and the cement based materials to arrive at the preliminary mixture formulations. Additionally, there could also be attack due to organic acids produced by the microbes inside the sewers. The combined attack due to sulphuric and organic acids leads to premature deterioration of sewer pipes.

Figure 2.16 Disintegration of sewer pipe in Los Angeles sanitary sewer system by chemical attack (Source: ACI 210.1R-94)

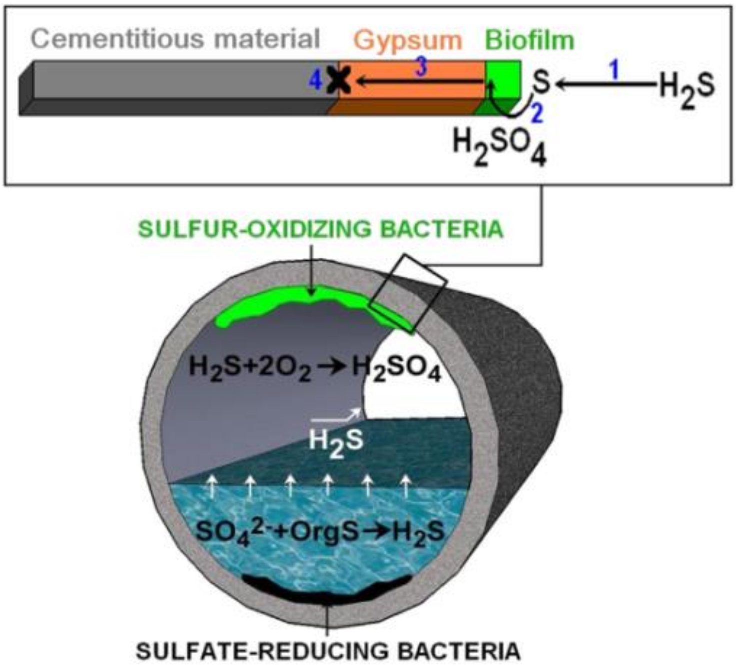

Figure 2.17 Bio-deterioration of sewer pipes (Herisson et al., 2013)

Acid generation and corrosion in sewers

This section discusses the mechanisms behind the biogenic degradation of concrete in sewer pipe environment. Sewage consists of organic matter and is rich in sulphates. When sewage flow is obstructed, and when the availability of oxygen is limited, anaerobic bacteria consume this organic matter producing hydrogen sulphide (H_2S) during the process. Another group of aerobic bacteria uses this gas as food breaking down hydrogen sulphide to generate sulphuric acid, which then deteriorates the concrete. These aerobic bacteria usually colonises the walls and crown region of the sewer pipes above the water line. Hence, the damage is usually seen at the crown and water line portions of the sewer pipes.

According to Wells and Melchers (2014), increased microbiologically induced corrosion (MIC) in recent times is essentially related to various factors such as the larger release of sulphate containing detergents to concrete sewers, increase in protein consumption rate, higher sewage temperatures as well as increased length of sewer lines (and hence increased residence times for sewage) caused by increasing suburban areas and population.

Wells and Melchers (2014) reported that the acids produced by the bacteria attack the calcium bearing hydrates to form gypsum and ettringite. The accompanying expansion (124% and 227% increase in volume respectively when compared to the volume of original hydrates) results in the formation of cracks, which further reduces the structural integrity of the pipe wall and which in turn permits the entry of moisture, acids and bacteria into the concrete microstructure, thereby continuing the deterioration cycle.

Mechanism of deterioration

The deterioration of concrete sewer pipes is a two stage process: initiation and chemical pH reduction stage followed by the active bio-deterioration and these stages are illustrated in Figure 2.18 and explained in the sub-sections.

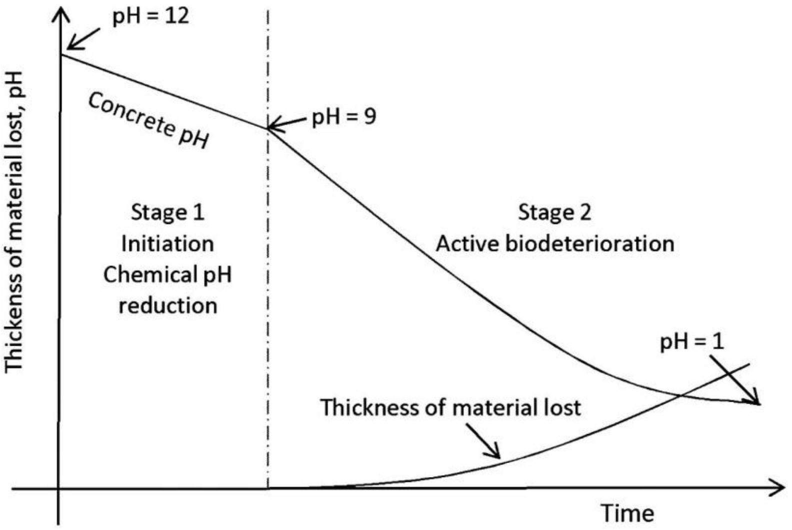

Figure 2.18 Stages of bio-deterioration in concrete sewers (Hudon et al., 2011)

Stage 1: Initiation, chemical pH reduction

This stage is completely physical rather than biological. The inherent alkalinity of the concrete (due to Portlandite and alkaline hydroxides in pore solution, formed due to cement hydration) protects it from the growth of microbes, and therefore from the deterioration. Weak acids such as carbonic acid (formed from CO_2) and hydrogen sulphide (from H_2S gas) are formed in this stage. When these acids react with the concrete, the alkalinity is reduced further. This stage ends, when the pH of the pore solution drops from 12 to about 9.

Stage 2: Active bio-deterioration

This stage is completely biological, marked by the commencement of formation of biofilms on the concrete surface. Hydrogen sulphide gas is oxidised both chemically (auto-oxidation) and by the action of sulphur-oxidising microorganisms (SOM). A group of SOM, Acidithiobacillus thiooxydans bacteria grows in the biofilm secreting sulphuric acid which reduces the pH of the pore solution and degrades the concrete. At pH less than 1, the growth of thiooxydans starts to decline by itself and the production of sulphuric acid ceases.

According to Hudon et al. (2011), the bacteriologically produced sulphuric acid reacts with cement matrix in concrete and the cement matrix is converted to gypsum and silica gel as it reacts with the acid. The matrix loses its binding ability, aggregates are exposed, and the sewer pipes experience reduction in thickness (Figure 2.18), eventually affecting the service life of the sewer pipe.

This bio-deterioration normally takes place in the unsubmerged areas of pipes, and is common in the crown portion of the pipe and along the water line. The fully submerged pressure pipes are typically unaffected as the SOM cannot grow in such conditions. Long sewer lines with a shallow slope followed by a section generating high turbulence form the ideal conditions for the deterioration.

Chemical reactions with concrete

In the initiation stage, carbon dioxide and hydrogen sulphide gas ingress into the concrete, reducing the pH. This stage is followed by the active bio-deterioration stage wherein the concrete is attacked by sulphuric acid along with various other organic acids produced by the microbes. The various chemical reactions that take place in these two stages are summarised in Figure 2.19 and explained below.

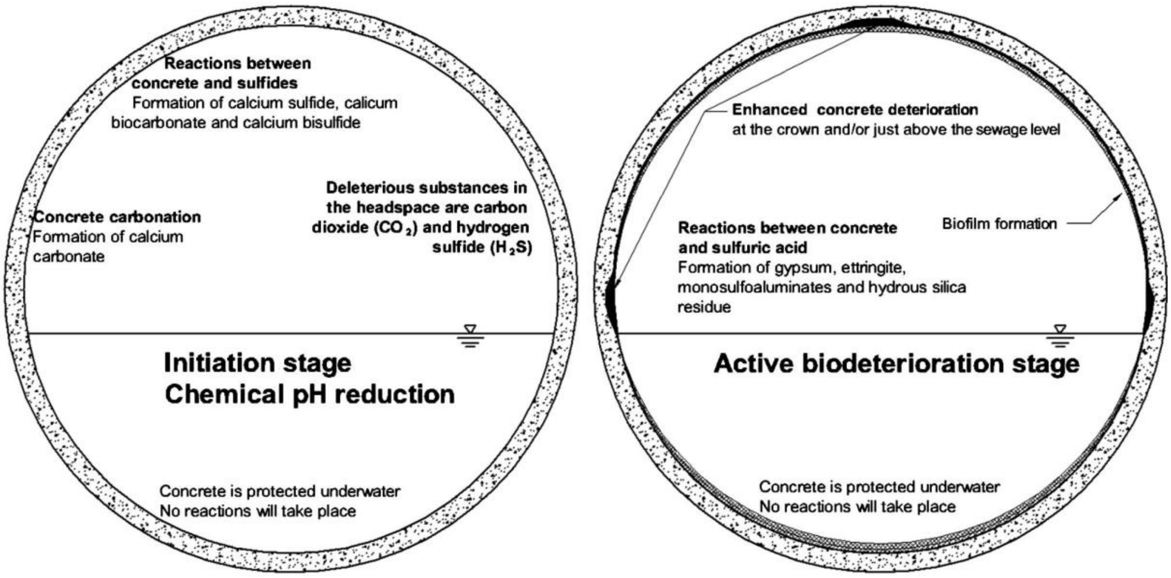

Figure 2.19 Chemical reactions in concrete sewer during deterioration (Hudon et al., 2011)

a) Carbonation

In this stage, carbon dioxide penetrates to the inside of concrete and reacts with the water present inside the concrete to form carbonic acid (shown in Eq. (2.11)). Portlandite being the least stable hydrate undergoes dissolution and reacts with carbonic acid forming calcium carbonate as per Eq. (2.12). Other hydrated phases such as CSH gel and calcium aluminate hydrates also react with carbonic acid to form calcium carbonate (as per Eq. 2.13 and 2.14) (Cerny and Rovnanikova, 2002). This carbonated layer occupies more space than the original hydrates, thus reducing the porosity of HCP and limits the further entry of carbon dioxide (Richardson, 2002). During this process, the pH of the concrete is reduced to about 8-9.

$$H_2O + CO_2 \rightarrow H_2CO_3 \tag{2.11}$$

$$Ca(OH)_2 + H_2CO_3 \rightarrow CaCO_3 + 2H_2O \tag{2.12}$$

$$CaO.SiO_2.zH_2O + H_2CO_3 \rightarrow CaCO_3 + SiO_2.(z+1)H_2O \tag{2.13}$$

$$kCaO.Al_2O_3.zH_2O + H_2CO_3 \rightarrow CaCO_3 + 2Al(OH)_3 + (z-2)H_2O \tag{2.14}$$

b) Hydrogen sulphide

Anaerobic bacteria such as Desulfovibrio break down the organic matter in the sewage producing H_2S gas in sewers. H_2S in solution acts as a weak acid and reacts with the hydrated cement paste of the concrete. As a result, the pH of the pore solution is dropped further. Calcium hydroxide reacts with hydrogen sulphide to form calcium sulphide as per Eq. (2.15). The calcium carbonate formed during the carbonation reactions also reacts with hydrogen sulphide forming calcium bicarbonate and calcium sulphide. Calcium sulphide further reacts with hydrogen sulphide forming calcium disulphide as per Eqs. (2.16) and (2.17) (Cerny and Rovnanikova, 2002). Roberts et al. (2002) performed experimental studies by exposing the concrete to varying concentrations of H_2S gas and measured the reduction in the pH of the pore solution. Okabe et al. (2006) also noticed similar reduction in pH for mortar coupons immersed in concrete sewers.

$$Ca(OH)_2 + H_2S \rightarrow CaS + 2H_2O \tag{2.15}$$

$$2CaCO_3 + H_2S \rightarrow Ca(HCO_3)_2 + CaS \tag{2.16}$$

$$CaS + H_2S \rightarrow Ca(HS)_2 \tag{2.17}$$

c) Organic acids

Gu et al. (1998) reported that a group of green fungi named Fusarium can grow at high pH levels and are capable of reducing pH of the pore solution to levels ideal for colonisation and growth of SOM. The authors report that these fungi produce wide range of organic acids such as acetic, oxalic acid etc which will initially react with the HCP of concrete cover. According to Zivica and Bajza (2001), there could be differences in the kinetics of attack based on the concentration of acid, the solubility of the salts that are formed etc. The flow of the sewage erodes these salts formed, exposing fresh surface to acid attack. Sometimes, if the salts formed are less soluble and having lower molar volume, they remain inside the matrix rendering a protective effect limiting the ingress of acid and further attack. Also, the ability of a concrete pipe to maintain the alkaline rich environment in the interface of steel reinforcement is essentially related to the aggressiveness of the acid and the neutralisation capacity of the system (which depends on the chemical composition of cementitious system and type of aggregates). Duchesne and Bertron (2013) state that the attack by organic acids results in the progressive decalcification of the hydrated and anhydrous phases present in the cementitious system. As pH falls below 2 due to progressive acid attack, the only reaction product left behind is amorphous silica gel. Very limited studies have focused on the effect of organic acids and hence it demands further investigation.

d) Sulphuric acid attack

According to Menendez et al. (2013), sulphuric acid attack on sewer pipes can be thought of as a combined sulphate and acid attack, in which the acid protons cause the dissolution of cement hydrates. Chatterjee and Goyns (2013) state that the oxidation of H_2S to sulphuric acid takes place in two ways: auto-oxidation process by the reaction of hydrogen sulphide combining with oxygen in an aqueous solution to form sulphuric acid (Eq. 2.18), or biologically due to aerobic SOMs, namely thiobacillus bacteria.

$$H_2S + 2O_2 \rightarrow H_2SO_4 \qquad (2.18)$$

The pH of the concrete reduces due to the microbial production of sulphuric acid. At this low pH, ettringite and monosulphate present in the cement matrix are destabilised and get converted to gypsum and aluminium hydroxide. However, ettringite may still crystallise in the inner layers where still higher pH persists. The basic reactions of HCP components with sulphuric acid are explained below (Eqs. 2.19 to 2.22). Calcium hydroxide is converted to gypsum while CSH is converted to gypsum and silica gel.

$$CH + H_2SO_4 \rightarrow C\underline{S}H_2 \text{ (gypsum)} \quad (2.19)$$

$$C_3A + 3\ C\underline{S}H_2 + 26H \rightarrow C_6A\underline{S}_3H_{32} \text{ (ettringite)} \quad (2.20)$$

$$2C_3A + C_6A\underline{S}_3H_{32} \rightarrow 3C_4A\underline{S}H_{12} \text{ (monosulphate)} \quad (2.21)$$

$$CSH \text{ gel} + H_2SO_4 \rightarrow C\underline{S}H_2 + SiO_2.aq \text{ (silica gel)} \quad (2.22)$$

The deteriorated layer comprising mainly of gypsum may allow further bacterial colonisation due to its higher porosity and its ability to retain moisture. According to Alexander and Fourie (2011), the gypsum layer formed binds together the insoluble silica residue in the gel layer, creating a physical barrier on the surface of the concrete, thus hindering the diffusion of ions involved in the reactions and slowing down the rate of attack. In the case of biogenic attack, wherein the production of acid by the bacteria is limited (unlike laboratory test with mineral acids), it is ideal to have a cementitious material with high neutralisation capacity (increased quantity of lime and alumina). This has implications while selecting aggregates which constitute significant volume of concrete. In bacteriogenic attack, it is preferable to use a limestone or dolomite aggregate which will act as sacrificial material protecting the dissolution of cement. Limestone or dolomitic aggregates get partly dissolved along with cementitious materials due to the action of acid. However, if siliceous aggregates are used, only the cementitious materials are attacked by acids. Cementing property is lost and aggregates pop out and fall, leading to increased degradation rate.

Interim Summary

Deterioration of concrete in sewer pipes due to biogenic sulphuric acid attack is a challenging problem which needs to be addressed by improving the material selection and mixture formulations. The deterioration mechanism of cementitious materials due to biogenic sewer corrosion is presented in detail in the above sections. It occurs in two stages resulting in the decalcification of hydrated cement paste products, the end products being gypsum and insoluble silica gel layer. The complete deterioration process is not yet fully understood and understanding the same demands further investigation, especially the deterioration due to various types of organic acids produced by microorganisms. According to Alexander and De Belie (2013), the gypsum layer plays a major role in the growth of bacteria and also helps in the bacterial colonisation by providing moisture. This aspect needs further investigation.

2.3.5 Development of test methods

Degradation of concrete due to acids is influenced by multitude of factors related to acid, cement as well as the test method. This creates a difficulty in finalising a single testing method which will address majority of the influencing factors altogether. Moreover, the assessment of cementitious materials is still hindered by the lack of standardised test or at least reference test methods. The response of given cementitious materials to acid attack clearly depends on architecture of tests as well as various other parameters (De Belie, 2008). The research studies focusing on the development of test methods are discussed in two sections; test methods to assess biogenic acid attack in sewer environment (commonly encountered inorganic acid) and the tests on organic acids.

2.3.5.1 Test methods to assess biogenic acid attack in sewers

In order to understand the mechanism of deterioration and to formulate the mixture for concrete sewer pipes, proper tests should be conducted. Hence, the objective of this section is to provide an overview of test methods developed and the test parameters used to assess the damage due to sulphuric acid attack in concrete sewer pipes. De Belie et al. (2002) preferred the use of laboratory based accelerated test methods in studying the acid attack phenomenon. Monteny et al. (2000) described different test methods for understanding degradation of concrete due to sulphuric acid. Most of the studies use concrete or mortar specimens of varying sizes and immerse them in aggressive solutions of varying concentration. In most of the cases, the acid solution is renewed at regular intervals, or the pH of the solution is maintained at a particular level by automatic titration arrangement. De Belie (2013) also critically reviewed various test methods to evaluate the performance of cement-based materials in aggressive acidic environments. According to the author, the choice of a particular test method will have a major effect on the usefulness of the test results. According to De Belie (2013), the kinetics results must be supported by micro-analytical characterisation techniques such as XRD, SEM to investigate the microstructural changes due to deterioration. De Graef et al. (2005) studied bacterial degradation of concrete using X-ray computed microtomography (CT). The following section describes various test methods developed by researchers.

2.3.5.2 Classification of test methods

The research performed on the development of test methods and subsequent assessment of resistance of concrete against corrosion of concrete in sewers can be grouped into three: chemical tests, microbiological tests and tests in situ, as illustrated in Figure 2.20.

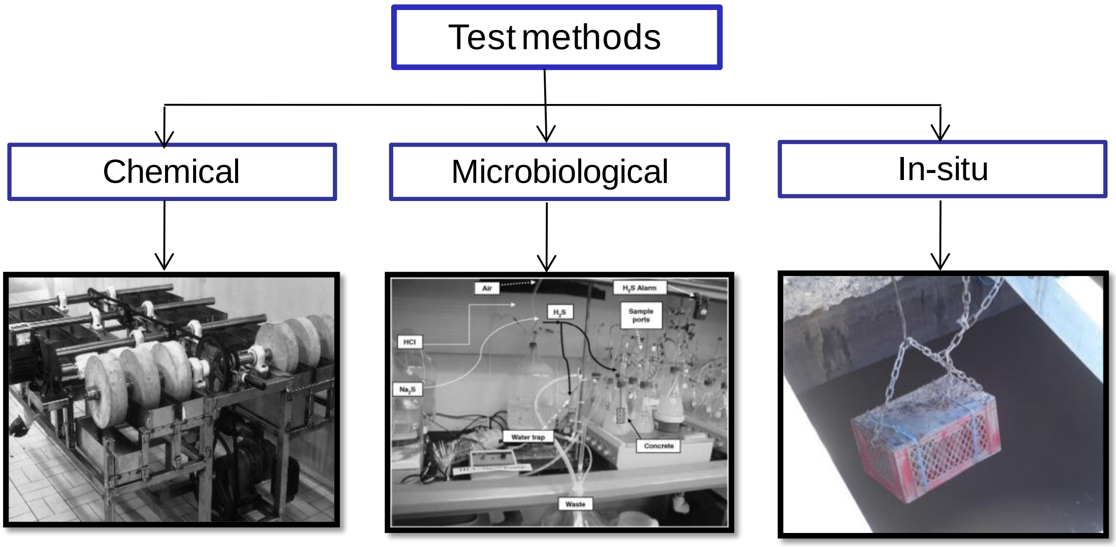

Figure 2.20 An overview of testing methods to assess acid attack
(adapted from De Belie et al., 2004; Padilla et al., 2010; Herisson et al., 2013)

a) Chemical tests

In chemical test, samples are immersed in mineral acid solutions for a period of time and the degradation is assessed using characterisation techniques and mechanical tests. Alexander and De Belie (2013) presented two dynamic test methods for assessing degradation of concrete specimens due to acid attack. Concrete mixtures are usually assessed for their suitability in sewers by an acid-insolubility test, which measures the total acid insoluble residue of a concrete mixture by digestion. According to Alexander and Fourie (2011), this test gives no information on possible interaction of various binders and aggregates, or on the kinetics of dissolution. The authors have developed a test method (shown in Figure 2.21) which uses hydrochloric acid to simulate the biogenic sulphuric acid attack inside the concrete sewers. Hydrochloric acid was used instead of sulphuric acid in order to simplify the test method and to simulate the worst case scenario inside the sewers. When sulphuric acid was used, the solution becomes saturated with gypsum just 2 hours after the immersion of specimen thereby slowing down the rate of attack. For this, it would be necessary to renew the sulphuric acid solution often. Hence, instead of sulphuric acid, hydrochloric acid was used. The test is carried out by immersing cylindrical concrete specimens in hydrochloric acid solution. In the immersed condition, the specimens are continuously rotated (using a mechanical arrangement) and brushed to remove the weak products that are formed. Acid resistance was evaluated by consistently measuring changes in mass and hydrogen ion consumption rates per unit surface area of the specimen.

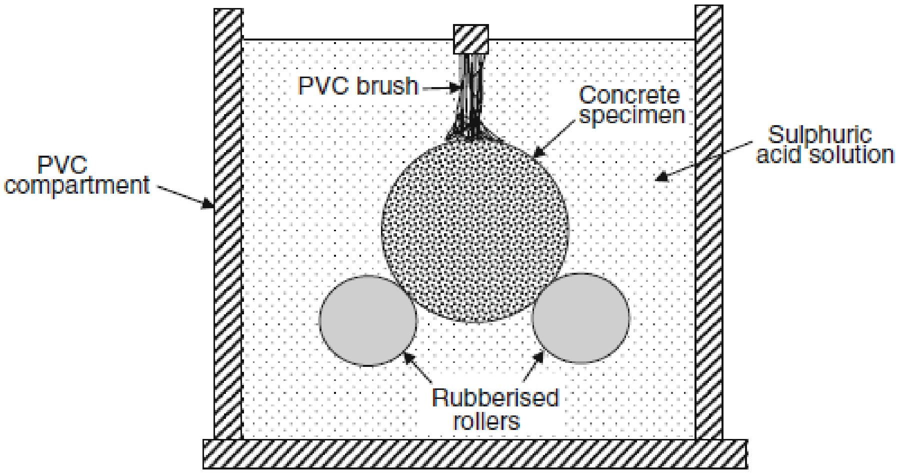

Figure 2.21 Cross-section of test rig for mineral acid test (Alexander and Fourie, 2011)

De Belie et al. (2002) developed an apparatus for accelerated degradation to simulate the deterioration of concrete in an automated and standardised way (Figure 2.22). Alternate wet-dry cycles along with abrasive action were used to accelerate the deterioration. The cylindrical concrete specimens are rotated in the acid solution followed by air drying. After every cycle of immersion, rotation and drying, the specimens are abraded with rotary brushes attached to the apparatus. The degradation was assessed in terms of changes in the diameter of specimens and surface roughness with the help of laser sensors. Harbulakova et al. (2014) carried out similar tests with sulphuric acid solutions using wet-dry cycles and abrasive action to accelerate the degradation. Similar chemical tests with sulphuric acid and hydrogen sulphide are reported by Herisson et al. (2013), Estokova et al. (2012).

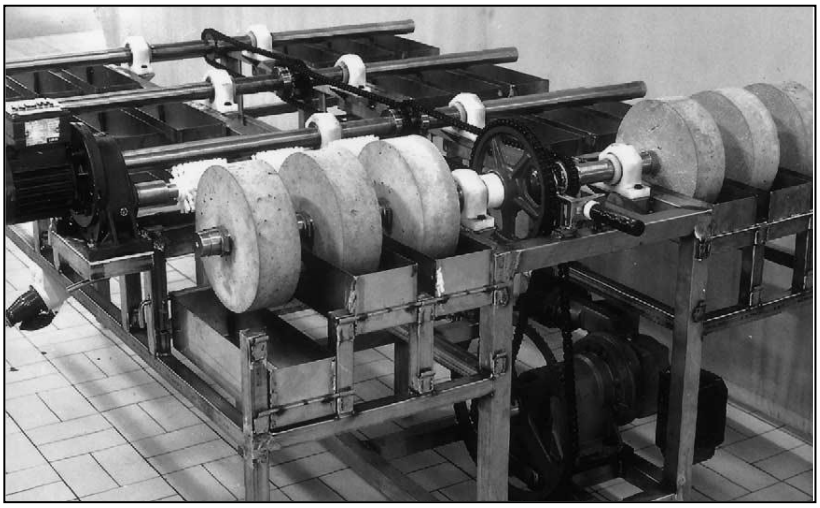

Figure 2.22 Test apparatus for measuring accelerated degradation (De Belie et al., 2004)

b) Microbiological tests

The basis of microbiological test is the immersion of specimen in a suspension containing bacteria and assessing the deterioration. Monteny et al. (2001) developed a microbiological test in which small concrete prisms (20 x 20 x 50 mm) were cut from concrete cylinders, attached on a glass plate and were exposed to a microbiological suspension. The suspension consists of bacteria, sulphur and other nutrients necessary to produce biogenic sulphuric acid. The parameters such as pH change, consumption of sulphate, and Ca^{2+} released were measured in addition to the changes in mass and height of the specimens. Similar procedure was followed by Harbulakova et al. (2014); the degradation was assessed in terms of changes in mass, visual changes in surface of the samples and leaching of cations. A lot of studies were done on biochemical accelerated test methods using microorganisms, however, with varied procedure and the method of assessment (Herisson et al., 2013; Hormann et al., 1997; Schmidt et al., 1997, De Belie et al., 2004; Sand et al., 1992; Lavigne et al., 2015). According to the authors, these accelerated tests using microorganisms simulate the mechanisms in concrete sewers better.

c) In-situ tests

Kiliswa (2016) conducted comprehensive investigations to study the deterioration in microstructure of Portland cement and calcium aluminate cement based concrete exposed to live sewer environment for 10 years in South Africa. The author also did monitoring of sewer parameters in-situ in two sewer sites in South Africa to bring improvements in the modelling of biogenic corrosion. The parameters investigated include the pH of sewage, sewer headspace temperature, relative humidity and H_2S concentration. Additionally, concrete specimens were exposed to live sewers and the surface pH was monitored on a regular basis for six months. Micro-analytical characterisation tests were conducted on the exposed samples in order to understand the deterioration mechanism.

Harbulakova et al. (2014) conducted similar in-situ experiments in the sewage networks in the city of Kosice. Leaching of ions such as Ca, Si, Fe were analysed along with the mass changes to study the degradation. Additionally, X-ray fluorescence was used in determining the chemical composition of the degraded concrete samples and the aggressive media. Similar in-situ test was carried out by Herisson et al. (2013) in which cylindrical mortar specimens were exposed in the headspace of sewer network. The parameters such as visual changes, changes in mass and surface pH were monitored on a regular basis to study the degradation.

Fernandes et al. (2012) did a case study investigation of acid attack on a long sewage system, 300 km long in Central Portugal. The sewers experienced premature deterioration just 2 years after the construction and a detailed study was conducted to understand the mechanism of deterioration. Concrete samples were collected from different locations having diverse exposure conditions. In some places, a white to yellowish putty-like product was excavated by hand (Figure 2.23). Strongest deterioration was observed in those structural elements in which aeration was deficient. Optical microscopy and SEM/EDS (Figure 2.24) confirmed that the soft putty-like product on the severely deteriorated surfaces was composed of gypsum with portions of silica and alumina gel, and residual siliceous particles of aggregate. The concrete mixture used in the construction consisted of cement CEM II/A-L 42.5R with limestone filler content of 16%, fly ash as mineral admixture, fluidifiers, crushed limestone for coarse aggregates and siliceous natural sand for fine aggregates. The water to binder ratio used was less than 0.45. However, it was noticed that the acid dissolved the cement paste and attacked the limestone aggregates directly. Siliceous aggregates were not attacked but showed a rim of gypsum surrounding the particles. Ettringite was locally detected in the concrete cores taken. The authors report that the sulphuric acid attack was predominant in the site despite the use of fly ash and low water to binder ratio in the concrete.

Figure 2.23 Deterioration of the concrete observed by site inspection (Fernandes et al., 2012)

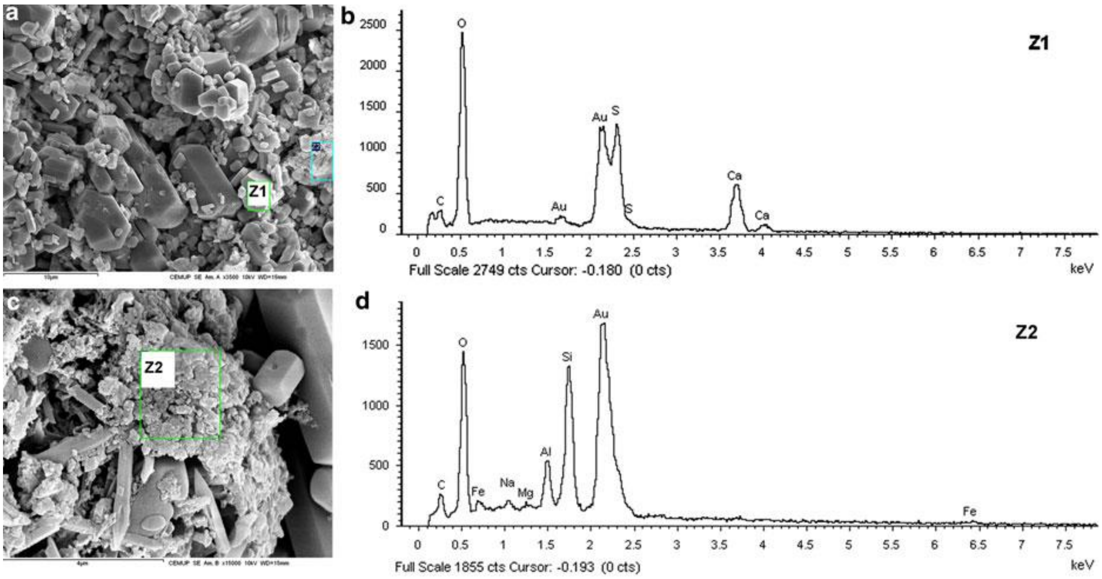

Figure 2.24 SEM/EDS analysis of putty like reaction product (Fernandes et al., 2012)

2.3.5.3 Differences between biogenic and chemical sulphuric acid attack

Although the reaction products formed (gypsum and ettringite) are same in chemical acid tests and biogenic tests, differences could exist between the two testing methods. In the case of biogenic test method, the nature of substratum influences the bacterial activity, which in turn, affects the quantity of sulphuric acid generated. In the case of chemical tests, a soft and pulpy layer of gypsum is formed on the outer surface, which acts as a protective barrier against further attack. However, in the case of bacteriologically produced sulphuric acid, this gypsum layer serves as an excellent stratum for the colonisation of bacteria. As the gypsum layer is porous, bacteria colonise inside producing more sulphuric acid near the unattacked matrix. Also, since the gypsum layer holds moisture, it safeguards the bacteria against dry conditions. The use of mechanical action in the form of abrasive action could have opposite effect on both chemical and biological attack. In the case of degradation by chemical acids, brushing removes the corroded layer, exposing relatively fresh surfaces for the attack. However, in the case of biological attack, brushing removes the bacterial colonies which in turn will retard the attack. But, if the gypsum layer is too thick that the availability of oxygen near the unattacked surface is limited for the growth of aerobic bacteria, brushing removes part of the gypsum layer and in this case, brushing could accelerate the kinetics. However, Grengg et al. (2017) opine that the microbial activity is not limited to the exterior deteriorated layer but present throughout the zone. Another bacteria known as Acidithiobacillus Ferrooxidans are detected even in deeper parts of the deteriorated zones which are deficient in oxygen, but able to secrete sulphuric acid. This portrays the severity of the attack in sewers.

It can be inferred that brushing the specimen while testing with mineral acids has a significant role to play in the deterioration process. Degradation kinetics of concrete exposed to acids and the effect of brushing the specimen is represented qualitatively in Figure 2.25. No brushing or rare brushing leads to low rate of degradation which is possibly due to the deposition of insoluble salts formed on the surface which acts as a surface protective barrier layer against further degradation. However, frequent brushing leads to removal of these corrosion products exposing inner concrete further to more deterioration resulting in higher rate of deterioration. This however, simulates the degradation in the zone between daily fluctuating sewage levels in which sewage flow causes regular dissolution and washing away of the gypsum products, thus continuously exposing fresh concrete to acid and resulting in accelerated loss of material owing to the combined effects of degradation and abrasive action.

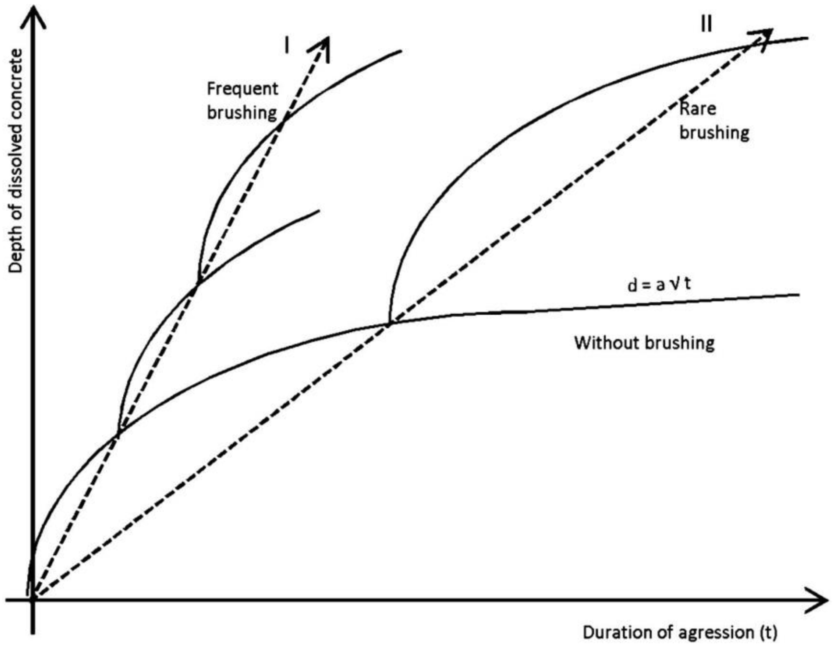

Figure 2.25 Alteration kinetics of concrete subjected to sulphuric acid attack illustrating the effect of brushing (Hudon et al., 2011)

2.3.5.4 Tests on organic acids

Bertron (2013) presented a detailed account of concrete structures exposed to various types of organic acids under various exposure conditions. The various types of tests for understanding the attack due to organic acids and effect of various test parameters were reviewed. According to the author, there is hardly any standard available for evaluating the performance of cementitious materials attacked by organic acids. The test procedure varied among the various researchers, depending on the objective. The corroded layers must be retained while understanding the mechanism of degradation by conducting a micro-analytical characterisation study. However, if the objective is to study the kinetics of degradation, the corroded layer may be removed on a regular basis either to accelerate the kinetics or to simulate the action of flowing effluents on concrete surface. As organic acids are weak in nature, test methods are highly influenced by the specificity of the acid. Special attention should be given on how the aggressiveness is maintained during the tests. Organic acids dissociate only partially. Moreover, they exhibit buffer zones which could significantly influence the quantity of acid consumed. These factors hence influence the degradation kinetics and must be kept in mind while developing a test method (Koenig and Dehn, 2016).

Larreur-Cayol et al. (2011a) analysed the degradation mechanism of cementitious materials caused by organic acids such as citric, tartaric and oxalic acid, the calcium salts of which are slightly soluble to insoluble, and their aggressiveness was compared to that of acetic acid that forms soluble salts. These acids differ in terms of poly-acidity and the characteristics of their calcium salt (pK_a and solubility). The degradation mechanisms were investigated using electron probe microanalysis, X-ray diffraction and scanning electron microscopy. Alteration kinetics was studied by mass loss and degraded layer depth measurements on cement paste specimens exposed to acidic solutions for one year. According to the authors, citric acid was the most aggressive of the organic acids studied followed by acetic, tartaric and oxalic acid. Acetic and tartaric acid have an intermediate aggressiveness and the degradation is caused by decalcification and progressive dissolution of cementitious phases (both hydrated and anhydrous).

Bertron et al. (2007) analysed the degradation mechanisms of cement-based materials immersed in a mixture of organic acids to simulate liquid manure at a pH of 4. The degradation mechanisms were studied using water intrusion porosimetry, electron microprobe analysis and X-ray diffraction. According to the author, the degradation of the cement matrix occurs by decalcification of hydrated phases and the formation of salts and silica gel containing aluminium and iron, which limits the kinetics of further degradation. The authors found that the differences in degradation mechanisms between the binders were negligible and mainly concerned with the stability of the anhydrous phases present in the binders. The authors opined that reduction in CaO/SiO_2 ratio and increased presence of elements such as iron and aluminium in the binder system would enhance the material resistance against acid attack.

2.3.5.5 Summary of test methods

The section critically reviewed literature on various test methods developed to assess deterioration of concrete due to biogenic sulphuric acid attack in concrete sewer environment. Some of them proposed accelerated chemical tests to simulate the phenomenon. In these chemical tests, cementitious samples are immersed in mineral sulphuric acid for a time period and the parameters related to the degradation are measured. This can only be considered as simulating the last step in the bio-deterioration process, and the initial pH reduction stages are not simulated by this method. Some tests also used periodic brushing in order to simulate the action of flowing sewage on the concrete surface. In general, there were differences in the findings when tested with chemical acids and biogenic acids (O'Connell et al., 2010; Herisson et al., 2013; Scrivener and De Belie, 2013). More investigation is needed in developing test methods which closely resemble the real-life scenarios. Contradictory results were reported between chemical and biological test methods (De Belie at al., 2004; Harbulakova et al., 2014). According to Scrivener and De Belie (2013), more research should be done to explore the relationship between the bacteria and the substratum on which it grows, as the latter significantly influences the bacterial activity, which further affects the production of sulphuric acid. Accelerated biochemical tests are better found to simulate the real conditions inside the sewer, but at the same time, difficult to be implemented in laboratories worldwide. However, accelerated tests done with mineral acids can be used in understanding the deterioration of concrete due to acid attack (O'Connell et al., 2010). Such tests can be used to study the interaction between cement and binders in the cementitious system.

According to De Belie (2013), the differences in the test method significantly affect the nature of degradation and consequently, the test results. The choice of degradation measure is important and it is necessary to state the test conditions along with the results. Often a combination of parameters should be used to assess the degradation. Bio-deterioration of concrete sewer pipes has not received much coverage in codes and standards and efforts are needed to address this issue. Various test methods and test parameters used to express the deterioration of concrete exposed to organic acids were also reviewed. It can be seen that relatively less number of studies are done on the effect of organic acids, some of which could be highly detrimental to the matrix. Based on the literature review, it can be concluded that new accelerated test methods have to be developed to study the degradation due to acid attack, which could be then used to evaluate the commonly available cement types and binders. Also, most of the studies were focused on only measuring mass loss and strength loss as the test parameters and conclusions are drawn based on one or two parameters, which may not hold true in all the cases. New test parameters need to be defined, which could better explain the level of degradation and a combination of test parameters should be used to assess the acid resistance.

2.3.5.6 Need for performance based approach

Generally, there is a notion to use a prescriptive approach while designing concrete mixes for various aggressive environments. The parameters such as minimum and maximum cement content, maximum water to binder ratio, minimum grade of concrete, and aggregate to cement ratio are used to design the mixes. Also, majority of the acid attack studies are restricted to the use of mass and strength changes as parameters to evaluate the performance of the concrete mixes. Acid attack is a phenomenon that is influenced by a variety of factors related to materials, acid and the test method by itself. A brief overview of the testing procedure found in the literature is presented in Figure 2.26. There is no consensus among the researchers in adopting a standard test procedure. Most of the testing was done without the replenishment of acid solution. If the solution is not replaced on a frequent basis, the aggressiveness of the solution will diminish quickly due to leaching of cations and consumption of acid ions which will affect the degradation kinetics. The duration of exposure can vary and it largely depends on the type of specimen, the size of specimen and the other testing conditions.

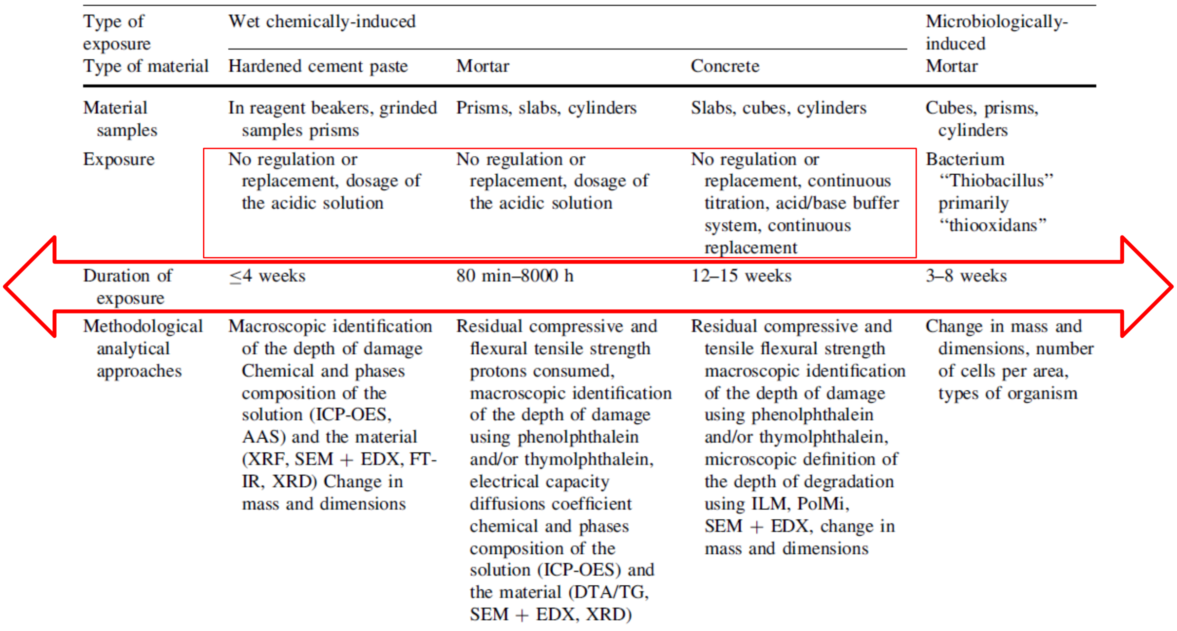

Type of exposure	Wet chemically-induced			Microbiologically-induced
Type of material	Hardened cement paste	Mortar	Concrete	Mortar
Material samples	In reagent beakers, grinded samples prisms	Prisms, slabs, cylinders	Slabs, cubes, cylinders	Cubes, prisms, cylinders
Exposure	No regulation or replacement, dosage of the acidic solution	No regulation or replacement, dosage of the acidic solution	No regulation or replacement, continuous titration, acid/base buffer system, continuous replacement	Bacterium "Thiobacillus" primarily "thiooxidans"
Duration of exposure	≤4 weeks	80 min–8000 h	12–15 weeks	3–8 weeks
Methodological analytical approaches	Macroscopic identification of the depth of damage Chemical and phases composition of the solution (ICP-OES, AAS) and the material (XRF, SEM + EDX, FT-IR, XRD) Change in mass and dimensions	Residual compressive and flexural tensile strength protons consumed, macroscopic identification of the depth of damage using phenolphthalein and/or thymolphthalein, electrical capacity diffusions coefficient chemical and phases composition of the solution (ICP-OES) and the material (DTA/TG, SEM + EDX, XRD)	Residual compressive and tensile flexural strength macroscopic identification of the depth of damage using phenolphthalein and/or thymolphthalein, microscopic definition of the depth of degradation using ILM, PolMi, SEM + EDX, change in mass and dimensions	Change in mass and dimensions, number of cells per area, types of organism

Figure 2.26 An overview of test procedures reported in literature
(adapted from Koenig and Dehn, 2016)

It is also important to decide upon the type of specimen (paste/mortar/concrete). The studies performed on concrete have got their own drawbacks due to large specimen size involved, which makes it a long term test to get salient results. Hence, accelerated tests need to be developed on smaller sized specimens. Moreover, it is the paste phase that is attacked by the acid and hence, it will be worth to study kinetics in cement paste instead of concrete itself. Paste study also allows uniform deterioration to be measured and the micro-analytical characterisation tests become less complicated to arrive at conclusions. However, the absence of ITZ in paste poses a serious limitation to the paste study. A mortar study may be conducted, to understand the influence of binders and ITZ. The quantification of parameters related to kinetics may then be more meaningful, especially while comparing the performance of various binders in resisting acid attack. It is also interesting to investigate if a model can be built to forecast the behaviour of mortar and concrete based on the observations of the paste study. There is an urgent need to shift from the prescriptive approach to performance based approach. For this, new accelerated methods should be developed and new performance indicators proposed based on the changes in the microstructure.

2.3.6 Achieving acid resistance

2.3.6.1 Review of test standards

Currently, there are hardly any codes or standards available for evaluating the material resistance to acid attack, especially the bio-deterioration of concrete sewers. American Concrete Institute (ACI, 2016) addresses this issue only by prescribing the durability requirements for concrete based on exposure conditions. Limits are specified on the parameters such as maximum w/c ratio, minimum cement content to be used, and the minimum grade of concrete etc. In addition, the code recommends the use of secondary coatings or linings to improve the durability. This prescription based approach needs to be changed to performance based approach.

In BS EN-206 (2013), acid attack is mentioned under the category of chemical attack when the concrete is exposed to natural soil and/or groundwater. The pH levels covered by the standard are 6.5 to 5.5, 5.5 to 4.5 and 4.5 to 4.0, which equate to the exposure classes XA1, XA2 and XA3, respectively. Here also, a prescriptive approach is followed by specifying maximum w/c ratio, minimum compressive strength of concrete and cement content to be used depending on the exposure class. However, the usefulness of EN-206, in its present state, is limited as the pH range specified is narrow in addition to its limited scope (soil and groundwater). Moreover, EN-206 recommends a special study for exposure to other aggressive chemicals outside its scope. The case of deterioration by organic acids is not covered by EN-206. The aggressiveness is only sorted based on the pH values, which is an inherent weakness of the existing standard. BS 8500-1 (2015) covers lower pH conditions up to 2.5, but limited to soil environments. Other aggressive environments and low pH levels are not well served by the concrete standards. The absence of standardised test method hinders the adequate evaluation of cementitious materials performance in acid environments. Moreover this absence is also a major obstacle to the evaluation of alternative binders in terms of performance and deterioration mechanisms and thus to their commercial development (Ramaswamy et al., 2017b).

Bio-deterioration of concrete is a severe durability issue especially in concrete sewer pipes and has hardly received wide coverage in the various national codes and standards. The Durable Concrete Structures Bulletin d'information No. 182 addresses the phenomenon by again following a prescriptive approach. Restrictions are imposed on the maximum w/c ratio and minimum cement content for concrete to be used in sewers. The design guide recommends reducing the turbulence in sewers, removal of growth of SOMs on the sewers, ensuring the adequate ventilation of the sewer pipes for removing the hydrogen sulphide gas from the sewer (Comité Euro-International du Béton, 1989).

A low water to cement (w/c) ratio is generally considered as the primary parameter for enhancing the concrete durability. However, according to Alexander and Fourie (2011), it is hard to explain the behaviour of concrete exposed to sulphuric acid based on the changes in w/c ratio or permeability of the matrix. Alternatively, the author proposes the attack to be classified based on the concentration of acid, as the severity of the attack in terms of the kinetics of degradation largely depends on the concentration of acid ions, especially in the cases of acids forming less soluble salts with higher molar volume. Various parameters affect the degradation process and literature seems to be inconclusive, demanding a shift to the performance based approach and further investigation in this regard.

2.3.6.2 Role of supplementary cementing materials

Use of supplementary cementing materials (SCM) makes concrete impermeable, and thus, expected to lead to more resistance to acid attack by reducing the rate of diffusion of acid ions. Monteny et al. (2003) investigated the influence of different concrete mixtures exposed to 0.5% sulphuric acid solution, using accelerated degradation test apparatus. The author found that the mix with silica fume showed poor resistance against sulphuric acid, despite its low permeability. The specimens were found to have expanded and undergone severe mass loss on brushing. O'Connell et al. (2012) and Monteny et al. (2003) noted the better performance of slag on exposure to sulphuric acid environment.

Furthermore, where previous studies have shown that the slag concrete had a higher resistance, De Belie et al. (2004) found High Sulphate Resistant Portland cement (HSR) more advantageous. In the microbiological tests, the concrete made with HSR performed marginally better than the slag cement concrete. According to the author, the inferior performance of slag in microbiological tests could be due to rapid colonisation of microbes on the surface of slag mixed concrete, resulting in increased production of acid.

Studies conducted by Roy et al. (2001) indicated that the use of binders such as silica fume, metakaolin and low calcium fly ash improved the acid resistance of mortar. Fly ash mix was found to be more resistant followed by metakaolin and silica fume. Another study by Chang et al. (2005) showed the beneficial effect of ternary blend of SCM, due to the synergistic effect. The concrete made with limestone aggregates and ternary blend with fly ash and silica fume showed improved resistance against sulphuric acid. Saricimen et al. (2003) found that high alumina based cementitious materials perform better compared to binary blends containing fly ash and silica fume on exposure to 2% sulphuric acid. In this case also, cement admixed with silica fume showed inferior resistance when compared to the other mixes. Fattuhi and Hughes (1988) investigated the sulphuric acid resistance of mortar and concrete. On exposure to 3% flowing sulphuric acid, the OPC + silica fume mix showed better performance followed by OPC + fly ash, OPC and Sulphate Resisting Cement (SRC) respectively. Another study by Attiogbe and Rizkalla (1988) showed that ASTM Type V cement had less resistance compared to Type I cement concrete on exposure to 1% sulphuric acid. Although it appears that the use of SCMs improves the acid resistance, the results published are not yet conclusive and this needs further study.

2.3.6.3 Role of special cement

Alexander and Fourie (2011) performed detailed investigations on various concrete mixtures made using common and special binders exposed to hydrochloric acid. The performance of concrete made with OPC, Calcium Aluminate Cement (CAC) and SCMs with acid soluble (calcareous) and acid insoluble aggregates were evaluated by exposing the specimens to both mineral acid (hydrochloric acid with pH = 1) and immersion in live sewer.

On exposure to mineral acid, the authors found that the concrete made with dolomite aggregate, OPC + silica fume showed superior performance when compared to the concrete with OPC and other SCMs such as slag, fly ash and metakaolin. The better performance was attributed to the slower dissolution of binder and improved ITZ in the case of OPC + silica fume concrete. The concrete made with CAC and dolomite aggregate was found only to be comparable to OPC, because of their higher porosity. However, the concrete made with CAC was found to outperform the OPC concrete when exposed to biogenic acid (immersion in live sewer). This improved performance was attributed to the ability of CAC in suppressing the metabolism of sulphur oxidising microorganisms, thereby limiting the production of acid. Herisson et al. (2013) also confirmed the superior performance of CAC in concrete exposed to biogenic acid environment. According to the authors, high aluminium content helps to stifle the bacterial activity, which resulted in the improved performance of CAC.

2.3.6.4 Influence of mix design

This section discusses the influence of various mix design factors like cement content, w/c ratio, coarse aggregate content, type of aggregate on the degradation kinetics on exposure to sulphuric acid.

Cement content

Cement being alkaline is vulnerable to acid attack. Results (Figure 2.27) showed that the mass loss of concrete specimens immersed in stronger sulphuric acid solutions (pH about 0.3) increased as the cement content of the mixture increased (Hewayde et al., 2007).

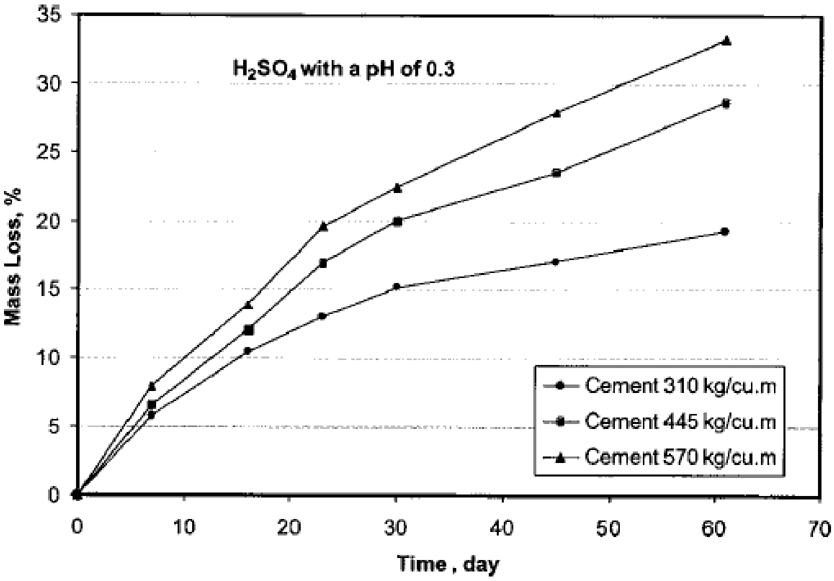

Figure 2.27 Effect of cement content on sulphuric acid attack (Hewayde et al., 2007)

Water to cement ratio

It is a proven fact that decreasing water to cement ratio in concrete results in significant improvement in durability and mechanical properties. However, Hewayde et al. (2007) observed that the mass loss of concrete specimens exposed to sulphuric acid solutions with pH < 1.5 decreased as the w/c ratio is increased (Figure 2.28). This shows that the acid resistance increases with an increase in the w/c ratio. This result was not justified by proper scientific explanations by the authors. Similar result was obtained in the study by Roy et al. (2001). As conventional approach to achieve durability is to lower the w/c of the mix, the effect of w/c in influencing the acid attack is worth investigating.

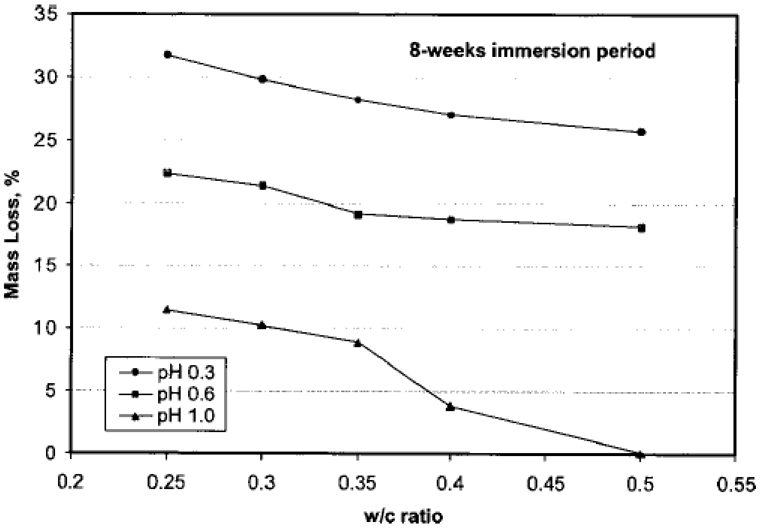

Figure 2.28 Effect of water to cement ratio on sulphuric acid attack (Hewayde et al., 2007)

Coarse aggregate content

The coarse aggregate content in concrete was also found to be an influencing factor affecting the kinetics at high concentration of sulphuric acid (pH < 1). According to Hewayde et al. (2007), the mass loss was found to increase with increase in the coarse aggregate content. At less pH of the solution, cement matrix could be easily attacked by acid, binding ability could be lost and if coarse aggregate content is high, it would result in fall out of aggregates from specimen, thus indicating higher mass loss. However, this effect was found to be minor on exposure to low concentrations of sulphuric acid.

Type of aggregate

Limestone (calcareous) and siliceous aggregates behave differently when they come into contact with acidic environment, owing to the changes in the mineralogy (Hughes and Guest, 1978). Chang et al. (2005) investigated sulphuric acid resistance of concrete made with limestone and siliceous aggregates using various binders. Based on the changes in mass and strength, the authors found that the concrete made with limestone aggregate and ternary cement with fly ash and silica fume showed better performance on exposure to 1% sulphuric acid. Four concretes (C2, C3, C4 and C6) were made with limestone coarse and fine aggregates whereas the two reference concretes (C1 and C5) were made with siliceous coarse and fine aggregates.

It is clear from Figure 2.29 and Figure 2.30 that the reference concrete C1, made with Portland cement and siliceous aggregates, had incurred severe mass loss with considerable loss of paste from the matrix and aggregates were exposed. For the concretes made with limestone aggregates, the attack occurred in both cement matrix and aggregates. It was found that the concrete (C6) made with limestone aggregates and a ternary blend containing cement, fly ash and silica fume showed the least degradation followed by the concrete (C5) made with siliceous aggregates and a ternary blend containing cement, slag and silica fume. This study highlighted that the use of limestone aggregates along with proper ternary blend of SCMs in concrete results in the enhanced resistance on exposure to sulphuric acid.

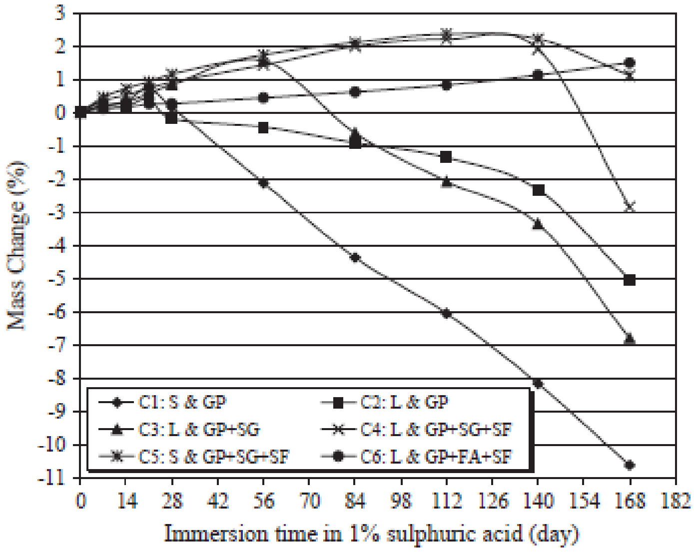

Figure 2.29 Mass loss of concrete made with various aggregates and SCMs after exposure to 1% sulphuric acid (Chang et al., 2005)

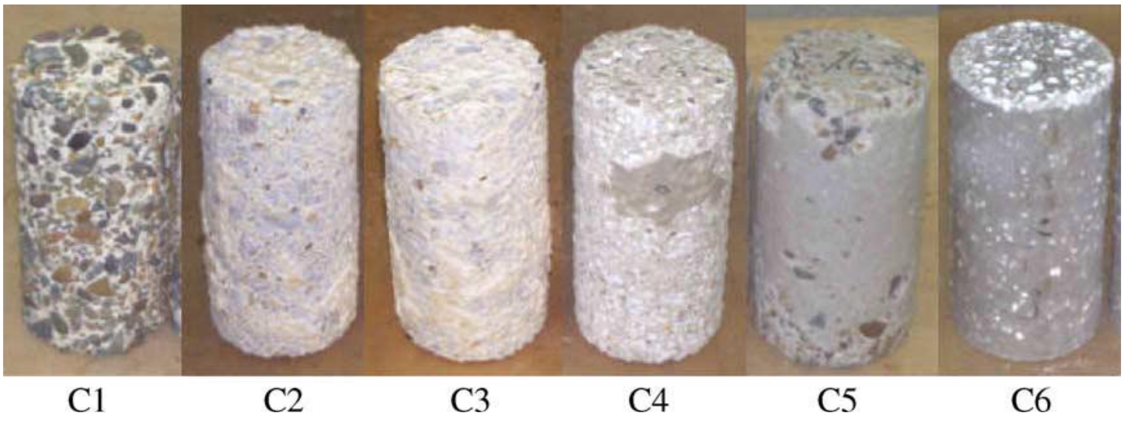

Figure 2.30 Concrete made with various aggregates and SCMs after exposure to 1% sulphuric acid (Chang et al., 2005)

Both chemical and microbiological tests conducted by De Belie et al. (2004) also showed that the aggregate type influences the kinetics of degradation. In the chemical test, the degradation depth for the concrete made with limestone aggregates was found to be smaller compared to concrete with siliceous aggregates. This improved performance of limestone aggregate concrete was attributed to its sacrificial protection of cement paste. As the acid attack is shared between aggregates and cement paste, the cement paste was found to be relatively more protected. Thus, it can be concluded that the relative rates of dissolution of binder and the aggregates govern the performance in acidic environment, as evident in the case of limestone aggregates.

2.3.6.5 Role of protective coatings

Monteny et al. (2001) investigated the influence of polymer type on concrete mixtures exposed to 0.5% sulphuric acid solution, using accelerated degradation test apparatus. Another study conducted by Monteny et al. (2003) showed that the use of polymers such as styrene-butadiene polymer and acrylic polymer resulted in more expansion and mass loss for the concrete specimens whereas vinyl copolymer and styrene acrylic ester polymer showed least expansion and better performance. De Muynck et al. (2009) investigated the effectiveness of various commercially available admixtures and surface treatments against sulphuric acid corrosion by means of chemical (accelerated degradation test) and microbiological tests. They found that the concrete coated with epoxy and polyurea performed better, with minimum changes in specimen surface roughness on acid exposure. Further studies conducted by Vipulanandan and Liu (2002, 2005) showed that the epoxy and polyurethane coated concrete could prolong the service life of sewer pipes as they perform better in sewer environment.

2.4 SUMMARY OF LITERATURE REVIEW AND NEEDS FOR THE RESEARCH

The available literature on the durability of cement-based materials in acidic environment was critically reviewed in this chapter. The concrete microstructure which consists of paste, aggregate and ITZ, was explained with its implications for the durability of concrete. In the process, the hydration of various common and advanced cementitious systems was detailed. Further, various factors affecting the durability of concrete were briefly reviewed. As acid attack is the topic of research, the general chemical reactions involved in chemical deterioration of concrete were summarised. The various sources of acidic media were reviewed, along with the general mechanism of acid attack. As acid attack is a phenomenon influenced by various factors, a detailed review was done on the influence of factors related to acid, materials and the test method. The alteration mechanisms by specific acids were critically studied and reviewed. An attempt was made to organise the mechanism into two; acids forming soluble salts and insoluble salts. Based on the review, a critical comparison was made between the mechanism of strong and weak acids. As the deterioration of concrete is a biogenic process, the mechanism was discussed in a separate section detailing the various processes and the various chemical reactions involved. The research studies focusing on the development of test methods were reviewed and organised in two sections; test methods to assess biogenic acid attack in sewer environment (commonly encountered inorganic acid) and the tests on organic acids. A section on acid resistance was provided in which a detailed discussion on the approach by various international standards was provided. Also, the influence of supplementary cementing materials, special cement, mix design factors and the protective coatings in resisting acid attack was reviewed and discussed.

Based on the extensive review, the following needs are identified for further research:

1. **Understanding the kinetics and mechanism of acid attack**

   Even though a number of studies have been carried out to study the effect of inorganic acids in concrete, there are limited studies on the effect of organic acids. This intricate mechanism of degradation is still not properly understood and further elaborate studies are required to investigate and explain the mechanisms of degradation and alteration kinetics in these aggressive conditions by developing new accelerated test methods and to formulate materials and mixtures that perform better in these environments. The various factors that influence the degradation kinetics should be investigated further to understand the phenomenon in a better way.

2. Development of accelerated test methods and proposal of better performance indicators

Currently, there are no codes or standards available for evaluating the resistance of materials to acid attack. The assessment of cementitious materials is still hindered by the lack of standardised test or at least reference test methods. The response of given cementitious materials to acid attack clearly depends on architecture of tests as well as various other parameters. Development of accelerated test methods is the pressing demand of today so as to design and evaluate the materials that perform well in these aggressive environments. There is a need to develop accelerated test methods which are simple, reliable and can be implemented in laboratories worldwide. The test method should be such that a variety of binders can be evaluated for their suitability in resisting acid solutions. Moreover, most studies focus just on measuring strength and mass loss on exposure to acid and do not focus on other possible degradation parameters. New test parameters are to be developed by considering a multitude of degradation parameters, which will help in the performance evaluation of various binder systems.

3. Assessment of the influence of type of binder and type of acidic environment

Sewer corrosion due to biogenic acid attack on concrete pipes is a grave durability issue faced worldwide. Premature failure of sewer pipes results in significant repair and maintenance costs. Concrete could also be attacked by various other acids present in industrial effluents such as organic acids, which are predominant in agricultural and agro-food effluents. Not much research has been done on the acid attack of cement-based materials by organic acids. The mechanism of attack and the kinetics could vary depending on the acid type. Hence, the study should be conducted by exposing the specimens to various acidic environments. More clarification is needed on the mechanism of degradation, the performance of various cement and binder types exposed to these aggressive environments.

As the use of mineral admixtures in concrete is increasing day by day, it is worth to study the role of these binders and their chemical composition in changing the alteration kinetics and the mechanism of degradation. The results depicting the influence of SCMs in acid attack, are in general, inconclusive. Contradictory results were obtained, especially for silica fume and slag incorporated mixes (Monteny et al., 2003; O'Connell et al., 2012; De Belie et al., 2004; Roy et al., 2001; Chang et al., 2005; Saricimen et al., 2003; Fattuhi and Hughes, 1988; Attiogbe and Rizkalla, 1988; Alexander and Fourie, 2011) and more detailed investigation must be conducted to validate the same. There are hardly any microstructural studies carried out to conclude the role of SCMs in resisting acid attack. Majority of the acid attack studies, especially on organic acids, were on paste specimens and the study needs to be extended to mortar so as to investigate effectively, the role of binders and ITZ in acid attack.

CHAPTER 3

MATERIALS AND METHODS

3.1 INTRODUCTION

This chapter discusses about the materials and experimental methods used in the study to investigate the alteration kinetics and the mechanism of degradation. The physical and chemical properties of the materials used in the study are described first. The details of mix proportions of paste and mortar are discussed in the subsequent section. This is followed by a section on experimental programme in which the various tests and test variables are described briefly. Two types of tests are carried out; immersion test with and without the abrasive action and dynamic test for accelerated degradation. The test parameters used to study the degradation kinetics and alterations in physico-mechanical properties are described in the next section. The parameters studied include mass changes, changes in pH of the acid solution, changes in the thickness of specimens, altered depth, changes in compressive strength, bulk density, ultrasonic pulse velocity and dynamic modulus of elasticity on acid exposure. The various micro-analytical characterisation techniques used to understand the mechanism of degradation are described in the last section. The characterisation techniques used in the study include X-ray tomography, X-ray diffraction, scanning electron microscopy, mercury intrusion porosimetry, thermogravimetric analysis and optical microscopy. A brief description of the various tests used to characterise the binders and aggregates are also given at the end of the chapter.

3.2 MATERIALS USED IN THE STUDY

This section describes the physical and chemical properties of the various materials used in the study, which include various types of binders, aggregates and superplasticizer.

3.2.1 Physical and chemical properties of binders

The binder materials used in the study include Ordinary Portland Cement (OPC 53 grade) conforming to IS 12269 (2013), Grade – I high alumina cement (HAC) conforming to IS 15895 (2011) and four supplementary cementing materials such as Class F fly ash (FA) (IS 3812 (Part 1), 2013), Ground granulated blast furnace slag (BFS), Silica fume (SF), limestone - calcined clay combination (LC2).

Ordinary Portland Cement with specific gravity and Blaine's fineness values of 3.15 and 318 m^2/kg respectively, and having a minimum 28th day compressive strength of 53 MPa, tested using mortar cubes of 70 mm size (IS 4031-Part 6, 2005) was used. Particle size distribution of cement was studied using laser diffraction technique and D_{50} (average particle size) of the cement was 19.41 µm. Loss on ignition of cement when tested as per IS 4032 (2005) was 3.43%. The particle size distributions of other binders were also studied using laser diffraction and are shown in Figure 3.1. The average particle sizes (D_{50}) of FA, BFS, LC2 and HAC were 23.74 µm, 12.61 µm, 13.10 µm and 11.22 µm respectively. The physical properties of the binders are summarised in Table 3.1.

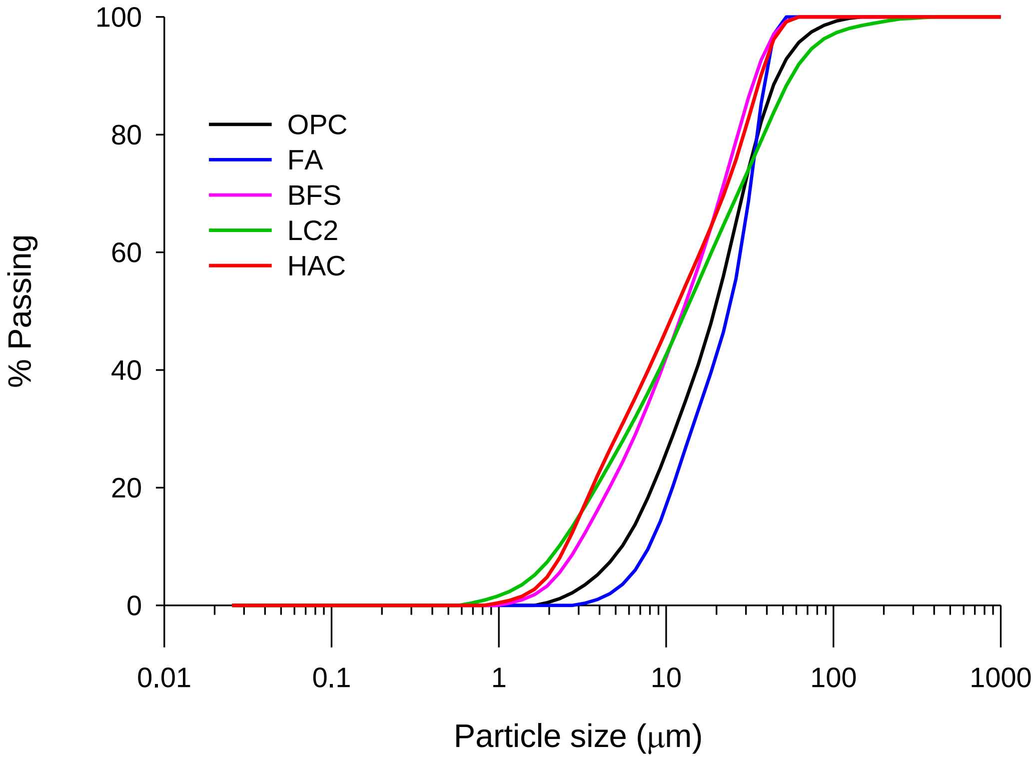

Figure 3.1 Particle size distribution of binders

Figure 3.2 shows the various binders used for the study. The oxide compositions of the binders were tested using X-ray fluorescence and the results are presented in Table 3.2. The mineralogical phases present in the binders were obtained from X-ray diffraction and the various mineralogical phases identified are shown in Figure 3.3.

OPC FA BFS

SF LC2 HAC

Figure 3.2 Binders used for the study

Table 3.1 Physical property of binders

Property	OPC	FA	BFS	SF	LC2	HAC
Specific gravity	3.15	2.21	2.88	2.05	2.60	2.97
Fineness (m^2/kg) by Blaine's air permeability	318	241	398	20000*	400	430
Loss on ignition (%)	3.43	0.08	-0.02	3.38	9.21	0.57

* surface area by BET

Table 3.2 Oxide composition of binders

Oxide composition	OPC	FA	BFS	SF	LC2	HAC
SiO_2	20.68	59.32	32.38	94.45	34.28	0.59
Al_2O_3	4.12	29.95	21.06	0.29	19.45	73.60
Fe_2O_3	5.44	4.32	1.87	0.10	3.43	0.12
CaO	60.36	1.29	31.46	0.20	28.29	24.31
MgO	0.83	0.61	8.57	0.59	1.38	0.28
K_2O	0.27	1.44	0.49	0.50	0.27	0.08
Na_2O	0.23	0.16	0.36	0.29	0.31	0.16
SO_3	2.46	0.17	-	0.20	1.58	0.38

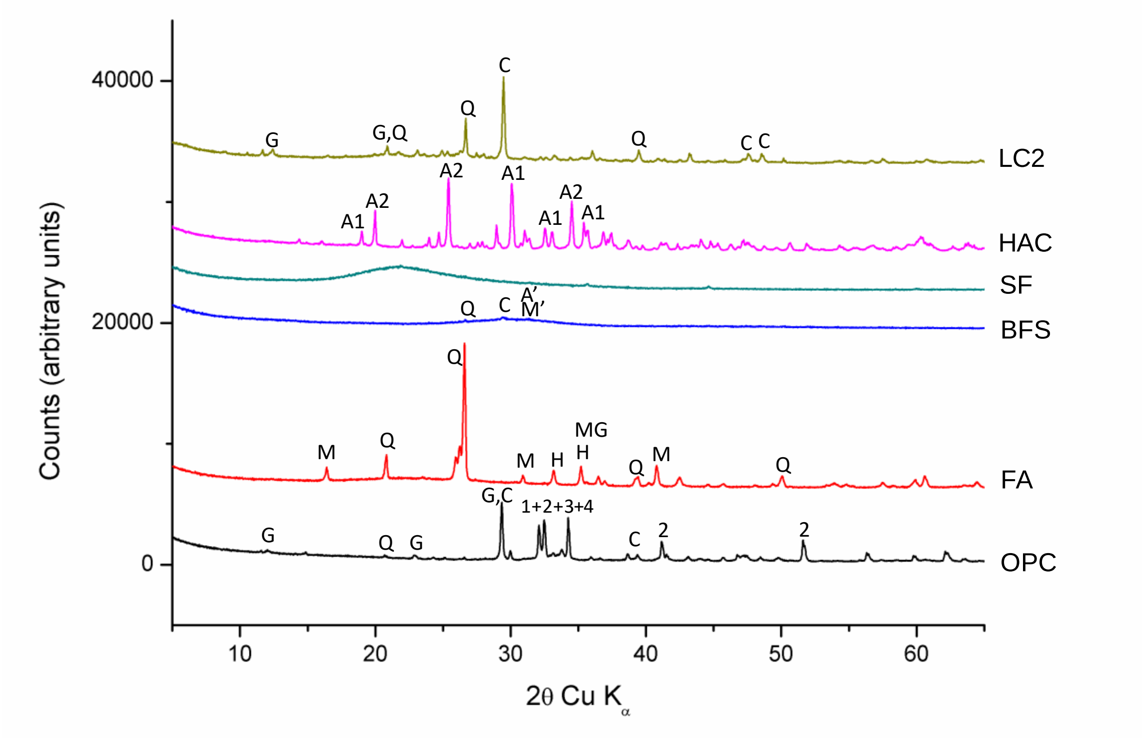

Figure 3.3 X-ray diffractogram of binders

The principal crystalline phases identified in OPC include gypsum (G), quartz (Q), calcite (C), alite (1), belite (2), tricalcium aluminate (C_3A, designated as 3), tetracalcium alumino-ferrite (C_4AF, designated as 4). The major crystalline phases in FA were identified as mullite (M), quartz (Q), hematite (H), and magnetite (MG). Slag was found to be amorphous and the crystalline phases present were marked as quartz (Q), calcite (C), akermanite ($Ca_2MgSi_2O_7$, designated as A'), and merwinite ($Ca_3MgSi_2O_8$, designated as M'). The diffractogram of silica fume was found to have amorphous silica, which is indicated by the halo around 22° 2θ. The main crystalline phases present in HAC were identified to be CA (calcium monoaluminate, designated as A1) and calcium dialuminate (CA_2, designated as A2). The principal crystalline phases present in the LC2 binder were gypsum (G), quartz (Q) and calcite (C).

3.2.2 Physical and chemical properties of aggregates

Two types of fine aggregates were used for making cement mortar. River sand (siliceous) and limestone (calcareous) aggregates were used as fine aggregates in mortar to study the influence of mineralogical nature of aggregate in resisting acid attack. The elemental composition and oxide composition of aggregates obtained by X-ray Fluorescence (XRF) are presented in Tables 3.3 and 3.4 respectively. The physical properties of aggregates are given in Table 3.5. Figure 3.4 shows the limestone aggregates, which are pulverised and used as graded fine aggregates in the study. The principal phases identified in river sand (designated as RS hereafter) and limestone aggregates (designated as LS hereafter) are quartz (Q) and calcite (C) respectively (using X-ray diffraction as shown in Figure 3.5).

Table 3.3 Elemental composition of aggregates from XRF

Element (%)	River sand	Limestone sand
O	47.90	29.10
Ca	1.92	68.45
Si	32.18	0.64
Al	8.26	0.24
Mg	0.36	1.06
Fe	2.27	0.25
Na	4.18	0.04
K	2.32	0.04
Ti	0.29	0.00

Table 3.4 Oxide composition of aggregates

Oxide (%)	River sand	Limestone sand
CaO	2.68	53.60
SiO_2	68.84	1.37
Al_2O_3	15.61	0.46
Fe_2O_3	3.24	0.36
MgO	0.59	1.75
Na_2O	3.12	0.05
K_2O	5.03	0.05
TiO_2	0.48	0.00

Table 3.5 Physical properties of aggregates

Aggregate type	Specific gravity	Water absorption (%)	Bulk density (kg/m^3)
River sand	2.62	1.60	1680
Limestone sand	2.70	0.35	1600

Figure 3.4 Limestone aggregates used in the mortar study

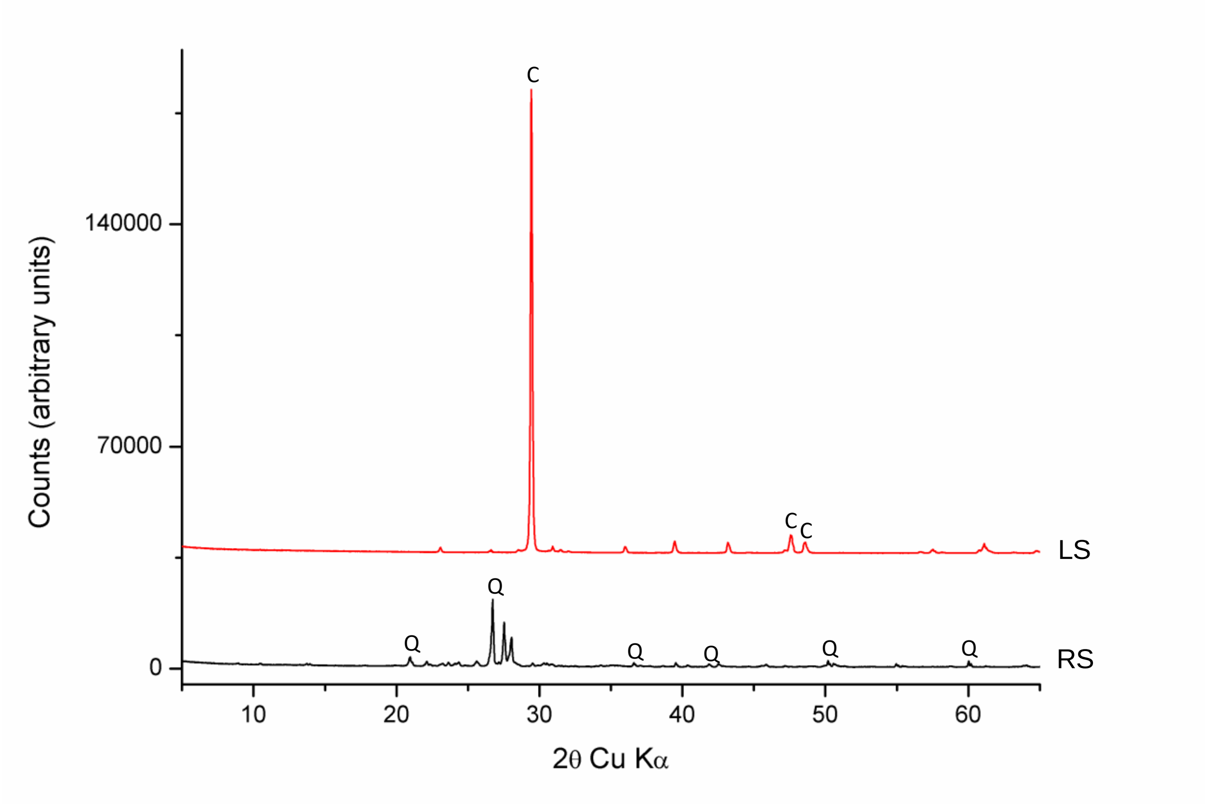

Figure 3.5 X-ray diffractogram of aggregates used in the study

Standard sand conforming to IS 650 (2008) was used as river sand for making mortar. The performance of the various binders in mortar exposed to acids was studied using this standard river sand as fine aggregate. In order to study the effect of mineralogical nature of aggregate, limestone aggregates were pulverised using a mechanical pulveriser and graded to the size of standard river sand. Aggregates passing 2 mm IS sieve and retained on 90 micron IS sieve were used for the study. The particle size distribution of the fine aggregate is given in Table 3.6.

Table 3.6 Grading of aggregates as per IS 650 (2008)

Particle size	Percent retained
Smaller than 2 mm and greater than 1 mm	33.33
Smaller than 1 mm and greater than 500 microns	33.33
Below 500 microns but greater than 90 microns	33.33

3.2.3 Properties of admixture

A new generation superplasticizer based on modified Polycarboxylic Ether (PCE) conforming to IS 9103 (2004) was used as chemical admixture. The properties of the superplasticizer used in the study are given in Table 3.7.

Table 3.7 Properties of superplasticizer

Property	Results
Appearance	Light brown liquid
Specific gravity	1.09
pH	6.70
% solids	40.40
Chloride ion content	< 0.2 %

3.3 MIX PROPORTIONS

Two types of specimens were tested for the acid resistance: paste and mortar. The details of the mix proportions used are presented below.

3.3.1 Cement paste

In order to study the role of binders in influencing the alteration kinetics due to acid attack, various paste mixes were prepared. The binders such as Class F fly ash (30% replacement), blast furnace slag (50% replacement), silica fume (10% replacement), and limestone calcined clay (45% replacement) were considered as mass replacements to OPC in addition to the control mix containing OPC only. These mixes were designated as FA30, BFS50, SF10 and LC2 respectively. Also a paste mix prepared only with high alumina cement (mix designated as HAC) was investigated for acid resistance.

All the paste mixes were prepared using distilled water with water to binder ratio of 0.40, which was chosen to ensure that most of the cement/binder grains were hydrated at the time of acid exposure (after 28 days of curing in saturated lime water) and the mix was workable without bleeding.

The mixing was done for about 3 minutes using a motorised hand blender (18000 rpm). In the case of binary mixes (i.e. OPC with one additional binder), dry mixing of OPC and binder was done initially before mixing with water. The details of the mix proportions and the notations for the mixes are presented in Table 3.8. Paste was poured into acrylic moulds (lubricated using thin oil) and specimens of size 10 × 10 × 60 mm (Figure 3.6) were demoulded after 24-36 hours. Polycarboxylic ether (PCE) based admixture at suitable dosage was used for the mix containing silica fume for improving the fluidity and dispersability. All specimens were initially cured in saturated lime water for a period of 28 days to avoid calcium leaching and to achieve sufficient strength before the acid exposure.

Table 3.8 Details of the mixes used in the paste study

Mix	Legend	Proportion used
OPC (control mix)	OPC	100% OPC only
OPC + fly ash	FA30	70% OPC + 30% FA
OPC + slag	BFS50	50% OPC + 50% BFS
OPC + silica fume	SF10	90% OPC + 10% SF
OPC + limestone calcined clay	LC2	55% OPC + 45% LC2
High alumina cement	HAC	100% HAC only

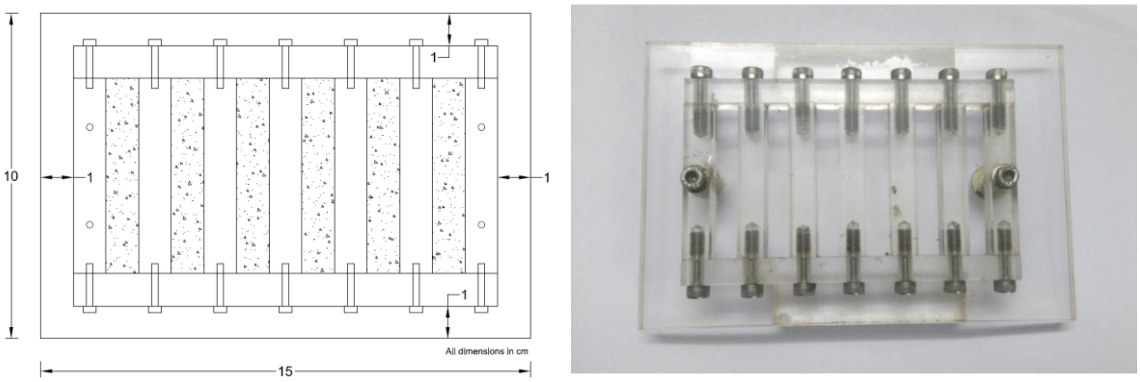

a) Top view of the mould for casting 10 × 10 × 60 mm specimens

b) Mould used for casting specimens for immersion test

Figure 3.6 Mould used for casting 10 × 10 × 60 mm paste and mortar specimens

3.3.2 Cement mortar

The study done on the paste was extended to mortar to investigate the role of binders and ITZ in acid attack. All mortars were made with a binder to aggregate ratio of 1:3 by mass. In order to study the role of various binders, a total of six mortar mixes were prepared: OPC, FA30, BFS50, SF10, LC2 (each mix with two w/b ratios of 0.40 and 0.55) and HAC (w/b ratio of 0.40). The replacement levels of the binders were the same as adopted in the paste study, explained in Table 3.8. All the above mortars were prepared using standard river sand as fine aggregate. Additionally, in order to study the effect of mineralogical nature of aggregate, LS mortar (with limestone fine aggregate) was prepared with OPC only as the binder (with a w/b of 0.40) and the performance in acids was compared with RS mortar (i.e. mortar prepared with standard river sand and OPC only as the binder).

A PCE based admixture at appropriate dosage was used for all the mortar mixes with a water to binder ratio of 0.40, as well as for the mix containing silica fume with water to binder ratio of 0.55. The mixing was done in a Hobart mixer (dry mixing for 1 minute followed by wet mixing for 3 minutes). Specimens of various sizes were prepared; prismatic specimens of 10 × 10 × 60 mm and 25 × 25 × 35 mm, cylindrical specimens of 25 mm diameter and 50 mm height, and cylindrical specimens of 25 mm diameter and 35 mm height. Specially fabricated acrylic moulds were used for casting prismatic specimens and plastic moulds were used for preparing cylindrical specimens. These moulds were lubricated with thin oil for the ease of demoulding. The mortar was placed in the moulds in layers, hand compacted and finished. The demoulding was done after 24-36 hours of casting. All mortar specimens were initially cured in saturated lime water for a period of 28 days, similar to the paste.

3.4 PREPARATION OF ACID SOLUTIONS

The different types of acids used in the paste study are sulphuric acid (1% and 3%), hydrochloric acid (1%), acetic acid (0.25M and 0.5M) and citric acid (0.5M). These acids are commonly encountered in practice; such acids differ in their solubility of calcium salts (refer Table 2.3) and the mechanism of attack and hence, are considered for the study. Among these acids, sulphuric and hydrochloric acids are strong inorganic acids, and acetic and citric acids are weak organic acids. Also, calcium salts of sulphuric and citric acids are less soluble while calcium salts of hydrochloric and acetic acids are highly soluble. Hence, these acids were selected so as to investigate the effect of type of acid, the solubility and kinetics of salt formation on acid attack. Commercially available acids were purchased and used in the study to prepare the acid solutions of various concentrations. Table 3.9 shows the quantity of acid used to prepare the acid solutions and Table 3.10 highlights the properties of acids. Citric acid was prepared by dissolving citric acid (anhydrous) in distilled water.

Table 3.9 Preparation of acid solutions

Acid	Concentration	Initial pH of the acid solution	Mass of acid per litre of distilled water (g/L)
Sulphuric	0.5%	1.31	5.10
Sulphuric	1%	0.99	10.20
Sulphuric (pH 2)	1%	2.00	10.20*
Sulphuric	3%	0.51	30.60
Hydrochloric	1%	0.56	28.57
Acetic	0.125M	2.84	7.53
Acetic	0.25M	2.68	15.06
Acetic (pH 4)	0.25M	4.00	15.06**
Acetic	0.5M	2.53	30.12
Citric	0.5M	1.72	96.06

* 7.8 g of NaOH is added per litre of distilled water to raise the pH to 2.00

** 2.75 g of NaOH is added per litre of distilled water to raise the pH to 4.00

Table 3.10 Properties of acids

Acid	Assay (%)	Specific gravity
Sulphuric	98	1.84
Hydrochloric	35	1.20
Acetic	> 99	1.049

3.5 EXPERIMENTAL PROGRAMME

As there is no specific standard existing for the testing of cementitious specimens in acids, research-based specially designed test set-ups and accelerated test methods are used in this study. The study has been subdivided into various phases. At first, field investigations were carried out to understand the broader picture of the problem. Deteriorated concrete samples from the site locations vulnerable to acid attack were collected for further characterisation studies. The micro-analytical characterisation studies were carried out on the samples, which include X-ray diffraction, X-ray micro-tomography, scanning electron microscopy and mercury intrusion porosimetry. X-ray micro-tomography and scanning electron microscopy (secondary imaging mode coupled with energy dispersive spectroscopy) were done to study the microstructural changes due to the deterioration by acids in real life conditions. The mineralogical changes were investigated using X-ray diffraction. The changes in the porosity and the pore structure of the matrix were investigated by using mercury intrusion porosimetry for the selected samples.

Next, laboratory tests were conducted to evaluate the performance of materials on exposure to acids. Studies were done on cement paste and mortar specimens. Two types of tests were done on paste; continuous immersion test (with and without abrasive action) and dynamic test for accelerated degradation. The alteration kinetics were studied by measuring parameters such as mass change, change in thickness, change in pH of the acid solution and altered depth (quantified based on X-ray tomography slice images) along with continuous visual observations on specimens. The characterisation techniques used to understand the mechanism of degradation in paste include X-ray micro-tomography, optical microscopy, X-ray diffraction, scanning electron microscopy, mercury intrusion porosimetry and thermogravimetric analysis. A test method known as dynamic test for accelerated degradation was developed, based on the existing slake durability test method.

Alteration kinetics in this test on paste specimens (25 mm cubes) was evaluated based on visual observations, mass changes and changes in pH of the acid solution.

The immersion test method and the study of alteration kinetics done on paste were further extended to mortar specimens in order to study the role of binders and ITZ in resisting the acid attack. The effect of parameters like size and shape of specimens, effect of pH of the acid solution were also studied. In addition to the measurement of parameters measured in the immersion test on paste, compressive strength and ultrasonic pulse velocity were measured on cylindrical mortar specimens at specific intervals of acid exposure to study the strength changes and changes in dynamic modulus of elasticity respectively. The characterisation tests were limited to X-ray diffraction, X-ray tomography, scanning electron microscopy and thermogravimetric analysis for the selected mortar samples.

As the aggregate type can affect the alteration kinetics significantly, the role of mineralogical nature of aggregates was studied by evaluating the alteration kinetics of mortar specimens made using calcareous aggregates (limestone aggregates). The microstructural alteration was captured using X-ray tomography imaging. The details of the test methods used to study the alteration kinetics and to understand the mechanism of degradation are discussed below.

3.6 TEST METHODS

3.6.1 Immersion test on paste

After the initial curing, the saturated mass and thickness of specimens (10 × 10 × 60 mm) were measured, after which they were exposed to various acids. In the paste study, the specimens (made with OPC and common binders) were exposed to 1% and 3% sulphuric acid, 1% hydrochloric acid, 0.25M and 0.5M acetic acid and 0.5M citric acid. The paste specimens made with special binders (HAC and LC2) were exposed only to sulphuric (1% and 3%) and acetic acid (0.25M and 0.5M). The volume ratio (i.e. volume of acid solution to volume of specimens) was kept fixed at 7 for the paste study.

Two specimens of the mix were kept fully immersed in a borosilicate glass beaker containing the acid solution and the beaker was then covered with an aluminium foil wrap in order to avoid carbonation and exposure to outside environment as much as possible (Figure 3.7). Figure 3.8 shows the acid exposure of paste specimens in progress. Acid solutions were renewed every week to maintain aggressiveness of the acid. This was done immediately after taking the measurements related to the kinetics. The immersion tests were done with and without periodic abrasive action. In the case of tests with abrasive action, brushing of specimens (with soft nylon brush) was done on a weekly basis just before the acid replenishment to remove the loosely held corroded particles, to expose relatively fresh matrix to the acid solution and thus to accelerate the testing. Also, periodic abrasive action is expected to simulate the action of flowing effluents on cementitious surfaces, as in the case of concrete sewers. Additionally, immersion tests were also done on paste specimens without brushing. In this case, the corroded layers will be preserved and this method could be useful to understand the mechanism of degradation. Also, the tests without abrasive action simulate a static acidic environment, where acids are present in a finite quantity. The degradation was arrested (by solvent exchange process using isopropanol) after six weeks of exposure for sulphuric, hydrochloric and acetic acids and after three weeks in the case of citric acid (due to rapid mass loss) and the specimens were stored in sealed zip lock covers inside a vacuum desiccator for further micro-analytical characterisation tests.

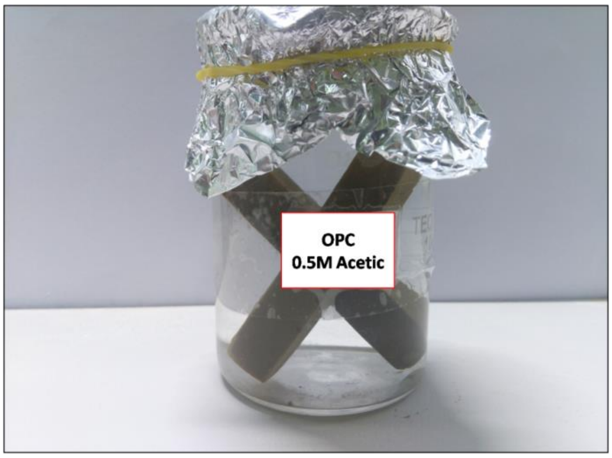

Figure 3.7 Immersion test set up for paste study

Figure 3.8 Acid exposure of paste specimens in progress

3.6.2 Dynamic test for accelerated degradation on paste

Another test method known as dynamic test for accelerated degradation was developed to simulate the effect of flowing effluents (sulphuric acid containing sewage water inside sewers). The test setup, based on the existing Slake Durability Test (IS 10050, 1996; ASTM D4644, 2008) is shown in Figure 3.9. In this method, ten cube specimens of size 25 mm (initially cured for 28 days in saturated lime water) were kept inside a wire-mesh cylinder (refer Figure 3.10), connected to a motor. The cylinder was immersed in acrylic tanks containing 1% sulphuric acid solutions (4.5 litres). The volume ratio (volume of acid to volume of specimens) was maintained at 29 so that the specimens are always immersed in the acid solution, even if the cylinders are not rotating. The motor runs at a specific speed (0-23 rpm), which can be controlled using a variable frequency drive attached to it. An automatic digital counter was also installed to count the total number of revolutions of cylinders.

Degradation of the specimen occurs in this test due to a combined action of acid attack and abrasive action among the specimens, when the cylinder is rotated at a specific constant speed. Acid solutions were renewed after every 5000 revolutions. An average of 12 hours interval was given in between every 1250 revolutions in order to allow the reactions to take place. The specimens inside the wired cylinder were kept immersed in the acid solution in static condition when the motor was not operating, allowing the degradation to continue. The test was continued until the total revolutions reached 20000 for the current study. However, the test could be extended for a longer exposure period. The test parameters such as mass change of the specimens and pH of the acid solution were monitored every 5000 revolutions just before the renewal of the acid solution.

The mass change of specimens after every 5000 revolutions was calculated based on the average initial mass of the specimens, measured before the start of the test (i.e. after 28 days of curing in saturated lime water). The test was repeated with another set of specimens immersed and subjected to 20000 revolutions in saturated lime water. The mass changes were measured after every 5000 revolutions. The net mass change was then estimated as the difference of the mass loss tested in acid solution and mass loss tested in saturated lime water.

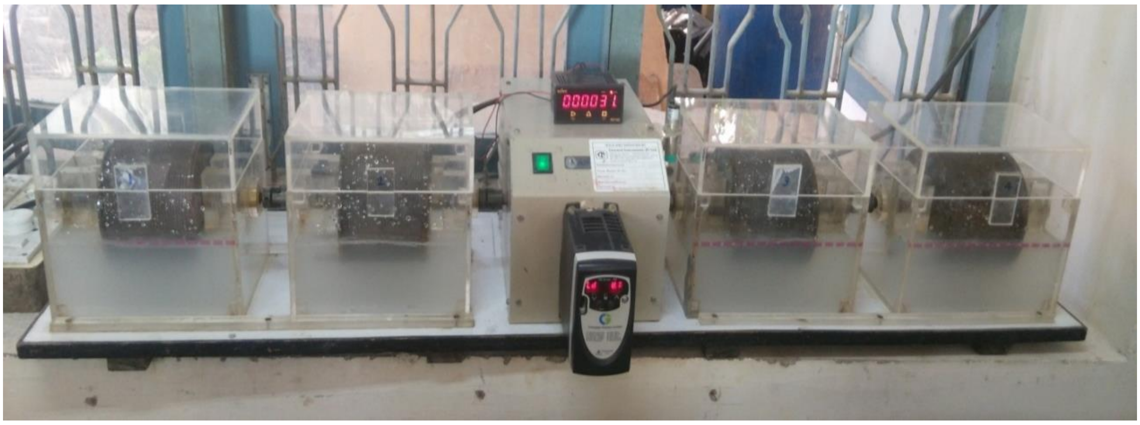

Figure 3.9 Test set up for dynamic test for accelerated degradation

Figure 3.10 Paste specimens placed inside the wired cylinder for the dynamic test for accelerated degradation

3.6.3 Immersion test on mortar

The immersion test carried out for paste was extended to mortar. Similar to the paste study, prismatic specimens of size 10 × 10 × 60 mm were used to study the degradation kinetics. After the initial curing, the saturated mass and thickness of specimens were measured after which they were exposed to various acids. The immersion tests on mortar were limited to exposure to sulphuric and acetic acid. Three concentrations of sulphuric acid (0.5%, 1% and 3%) and acetic acid (0.125M, 0.25M, 0.5M) were used. The volume ratio (i.e. volume of acid solution to volume of specimens) was kept fixed at 5 for the mortar study.

Three specimens of the same mix were kept fully immersed in a rectangular plastic container filled with the acid solution. The container was kept closed with a lid during the exposure to avoid carbonation reactions. Acid solutions were replenished on 2nd, 4th, 6th, 8th, and 12th weeks of acid exposure. The replenishment was done immediately after taking the measurements related to the evaluation of degradation kinetics. The immersion was carried out until a period of 16 weeks. Similar to the paste study, the tests were done with and without abrasive action. However, the tests with abrasion were limited to the specimens exposed to sulphuric acid wherein insoluble precipitates are formed. In the case of acetic acid, the immersion test was done without any abrasive action. Figure 3.11 and 3.12 show the immersion test on mortars in progress. After the exposure period, the degradation of specimens was arrested by slicing the specimens and immersing the pieces in isopropanol solution for 4 days (with frequent replenishment of isopropanol solution).

Additionally, the immersion tests were repeated for prismatic specimens of size 25 × 25 × 35 mm in order to study the influence of size of specimen on acid attack. For 25 × 25 × 35 mm specimens, the surface area to volume ratio (S/V = 0.217) was almost one half of the prismatic specimens of size 10 × 10 × 60 mm (S/V = 0.433). However, the study of size effect was limited to mortar with w/b of 0.55. Also, to study the effect of initial pH of the acid solution, the mortar specimens (10 × 10 × 60 mm) made with w/b of 0.40 were exposed to pH2 sulphuric acid (made by adding sodium hydroxide pellets to 1% sulphuric acid) and pH4 acetic acid (made by adding sodium hydroxide pellets to 0.25M acetic acid). The shape of the specimen could play a role in influencing the degradation kinetics, especially on exposure to sulphuric acid. Hence, to study this effect further, immersion test on mortar was also carried out using cylindrical specimens of size 25 mm diameter and height of 35 mm and the kinetics was compared with prismatic specimens of size 25 × 25 × 35 mm. The S/V ratios for both the specimen sizes were almost the same (S/V = 0.21), the only difference being in the shape of the specimen. This study, however, was restricted to mortar (w/b of 0.55) exposed to 3% sulphuric acid.

In all these immersion tests, the parameters such as mass changes, changes in pH of the acid solution and thickness changes of specimens were monitored regularly (just before the acid replenishment) to investigate the alteration kinetics and the detailed characterisation study was limited to selected mortar specimens exposed to sulphuric and acetic acids.

a) Immersion tests of mortar specimen of size 25 × 25 × 35 mm in progress (photograph taken just before taking measurements)

b) Immersion tests of mortar specimen of size 10 × 10 × 60 mm in progress

Figure 3.11 Immersion tests on mortar in progress

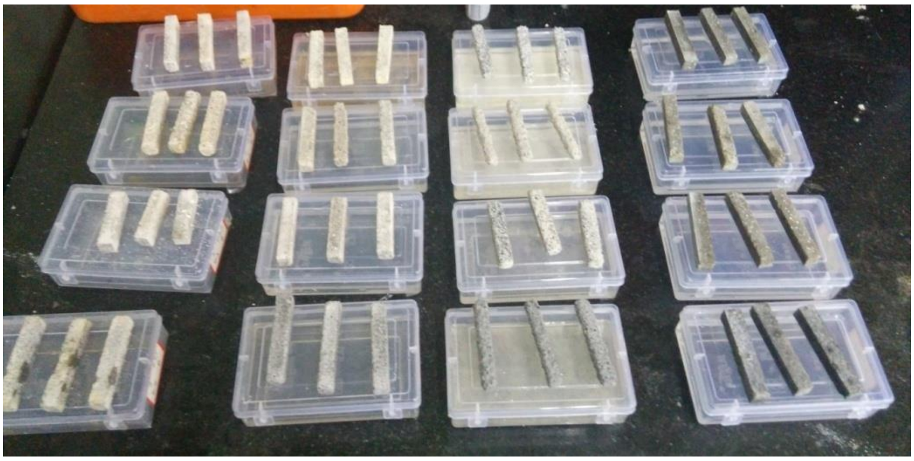

Figure 3.12 Mortar specimens wiped for taking mass measurements

3.7 DEGRADATION KINETICS

The term “degradation kinetics” and “alteration kinetics” are used synonymously in the study to describe the change of test parameters such as mass and thickness of specimens, altered depth, and changes in pH of the acid solution, on acid exposure. These parameters give an indication of the rate of degradation of the microstructure with acid exposure and hence the term “degradation kinetics” or “alteration kinetics”. This terminology is widely used in the acid attack studies (Bertron et al., 2005; Larreur-Cayol et al., 2011a). The following passages give the details of the various test measurements carried out to study the degradation kinetics.

3.7.1 Mass changes

The microstructural changes associated with the decalcification of hydrated products and subsequent salt formation in acid attack could manifest in the form of mass changes. Mass changes in the specimens were calculated with respect to the initial saturated mass (before the acid exposure) on a weekly basis, just before the renewal of acid solution. A positive value for the mass change in Eq. (3.1) indicates mass gain whereas a negative value indicates mass loss.

$$\text{Mass change (\%)} = \frac{M_t - M_0}{M_0} \times 100 \tag{3.1}$$

Where

M_0 = Average mass of the specimen before the acid exposure

M_t = Average mass of the specimen at age of exposure ‘t’

An electronic weighing balance having precision of 0.1 mg was used for measuring mass of the specimens (Figure 3.13). The balance was calibrated regularly with known weights for better accuracy in the measurements. In the case of no brushing, mass of the specimens was noted immediately after taking out the specimens (using a stainless steel tong) from the acid solution. The excess superficial water on the surface of the specimen was removed by wiping the specimen gently with a cotton cloth and the saturated mass was measured. In the case where brushing of specimens (with nylon brush) was done to remove the loosely held corroded particles (Figure 3.14) and to accelerate the testing, mass of the specimens before and after the brushing was noted. The parameters such as mass loss/gain, cumulative mass precipitated/leached and abraded were estimated based on the mass data collected, to demarcate the effect of abrasion and precipitation/leaching. In the case of no brushing, mass of the specimens was noted immediately after taking out the specimens from the acid solution, after wiping to remove the excess water.

Figure 3.13 Weighing balance used for taking mass measurements

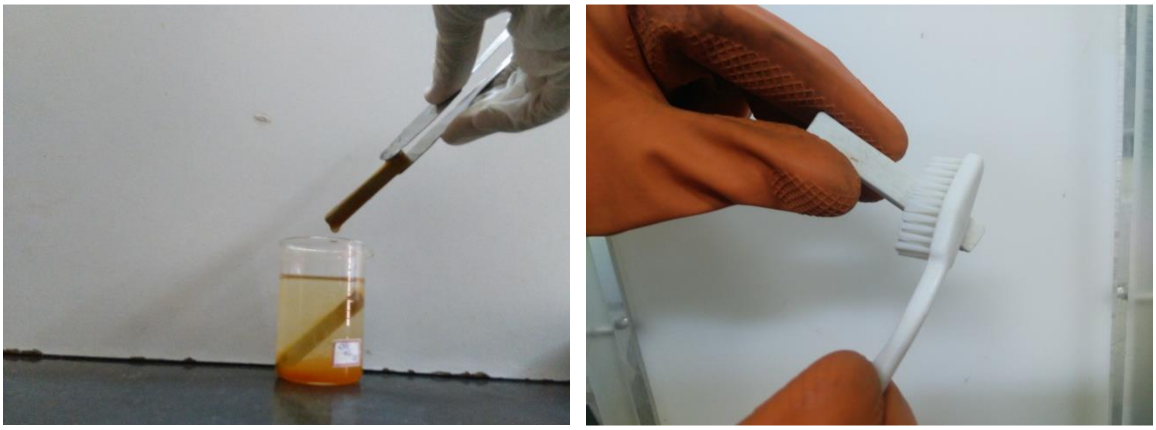

a) Taking out the specimens from the acid solution using a tong

b) Brushing of specimens using a soft nylon brush to remove the loosely held corroded particles

Figure 3.14 Steps involved in the paste study with brushing before taking the measurements

3.7.2 Changes in pH of the solution

The pH of an aqueous solution is a measure of its hydrogen ion concentration. During the acid attack, acid ions are neutralised by the various phases present in the cement hydrates. Subsequently, hydroxyl ions are released into the acid solution. The release of hydroxyl ions (or consumption of acid ions) during acid attack causes a rise in pH of the surrounding acid solution. These changes in pH of the acid solution (because of neutralisation) were monitored using a digital pH meter, on a regular basis just before the renewal of the acid. Figure 3.15 shows the digital pH meter (Eutech pH 5+) used in the study, which has an accuracy of ± 0.01 pH. The instrument has two components: an electronic meter and a pH probe. This pH probe consists of one reference electrode and a glass electrode. The immersion of this pH probe in an aqueous solution creates a potential difference between the two electrodes. The electronic meter connected with the pH probe interprets this potential difference and converts it to a scale of 0 to 14, thereby measuring the pH. Every time before the use, the pH meter was calibrated using standard calibration solutions of pH 4.01, 7.00 and 10.01. Also, after every use, the pH probe was dipped in deionised water and wiped dry with a cotton cloth to make it ready before the next use.

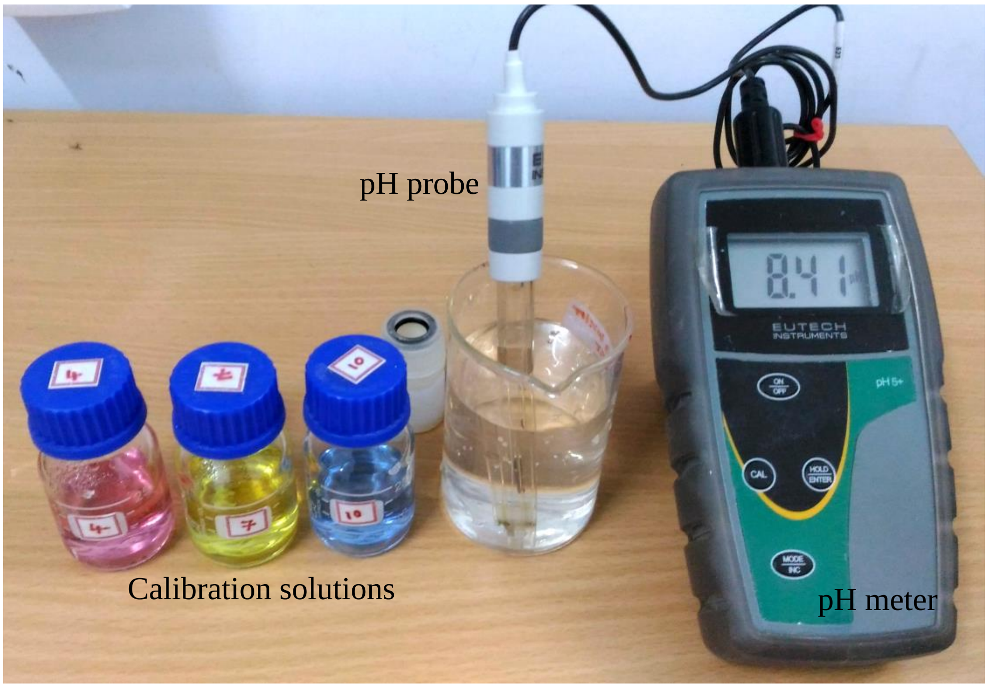

Figure 3.15 Eutech pH 5+ pH meter used in the study

3.7.3 Thickness changes

The specimens undergo either expansion or reduction in thickness depending on the solubility of the salt formed, the molar volume of the salt, its mesoscopic shape and the affinity towards the cementitious matrix. The change in thickness was calculated based on the initial thickness (at saturated surface dry state) before the acid exposure (Eq. 3.2). A positive value indicates expansion while a negative value refers to reduction (loss in thickness). The thickness of the specimens was measured using a digital caliper having sensitivity of 0.001 mm (Figure 3.16). When brushing was done, the thickness was measured only after the brushing of specimens. Each thickness used for the calculation is the average of six thickness readings taken along the length of the specimen.

$$\text{Thickness change (\%)} = \frac{T_t - T_0}{T_0} \times 100 \qquad (3.2)$$

Where,

T_0 = Average thickness of the specimen before the acid exposure

T_t = Average thickness of the specimen at age of exposure ‘t’

Figure 3.16 Digital caliper used for measuring the thickness

3.7.4 Altered depth

Mass losses and strength changes alone may not reveal a complete picture of deterioration as they depend on the type of acid and the solubility of salts formed. The technique adopted and the test parameters developed should be such that the results are indicative of the microstructural deterioration due to acid attack. Altered depth measurements are important as they give an idea about the time taken for the degradation front to reach the reinforcement to cause corrosion in reinforced concrete structures (Bertron, 2014). Hence, altered depth could be considered as a primary indicator of attack and any technique which can capture the altered depth needs to be used for investigating the degradation kinetics. Altered depth can be measured roughly using digital caliper or stereo zoom microscope based on visual changes (changes in colour of different zones of attack) by cutting the specimen perpendicular to its axis, but this is subject to errors and limitations in measurement accuracy. Alternatively, phenolphthalein solution can be sprayed to a fresh cut surface of the specimen and altered depth can be measured based on the colour changes. However, the complete altered depth due to decalcification and mineralogical zonation may not be picked correctly using this method and the measurement accuracy will be compromised on smaller sized specimens. As an alternative, X-ray tomography could be applied to investigate the same, and the methodology is discussed below.

At first, slice images of specimen were collected using X-ray tomography (explained in the section 3.9.1). Further, using the image analysis software ImageJ and by using the CT slice images, various parameters were determined to study the deterioration of paste and mortar specimens in acids. Figure 3.17(a) shows the specimen cross-section exposed to 0.5M acetic acid showing the mineralogical zonation. The schematic picture of this zonation, after the acid exposure is shown in Figure 3.17(b) indicating the various parameters related to depths/areas. The terms A_o, A_m, A_c in the Figure 3.17(b) denote the area of outer layer, middle layer and core layer respectively. A_f represents the final area of the specimen after the acid exposure whereas A_i represents the initial area of the specimen before the acid exposure. The term DD refers to the degraded depth (i.e. average thickness of the outer degraded layer) while DM refers to the average thickness (depth) of the middle layer (where decalcification is ongoing and partially complete). The depth of alteration/altered depth (DA) is defined as the sum of DD and DM. It is the depth for which the decalcification is effective in causing the deterioration. These depths are measured using the software ImageJ after calibrating the CT images (using the value of voxel resolution of specimen obtained in CT imaging). Each depth (DD and DM) used for the calculation is average of nine depth readings measured along the periphery of the cross-section of the specimen (avoiding the edges). The term DR refers to the average depth affected either due to the reactions and/or brushing. A positive value of DR indicates the thickness gain and a negative value indicates loss of thickness. If the final area of the cross-section after the exposure A_f is less than the initial area A_i, the corrected altered depth is estimated by adding DR to the DA. In the case of increase in area due to expansion (i.e. if A_f is larger than A_i), the DR value is not considered to find the corrected altered depth.

Similar to the depth measurements, area measurements are also done based on the image analysis of CT images. The areas defined in the Figure 3.17(b) (A_f, A_o, A_m and A_c) are estimated. As the area of the core layer varies with the extent of degradation, a parameter called area ratio is defined wherein the area of each layer is normalised with respect to the initial area before the attack. Normalizing with respect to the core area or final area of the specimen would result in area values bloated and this was hence avoided. The percentage of area decalcified is then arrived at by adding the area of outer and middle layers and expressing it as percentage of the initial area. The percentage of area shrunk or expanded was obtained by comparing the areas before and after the attack (Initial area was calculated based on the thickness readings obtained before the acid exposure using digital caliper).

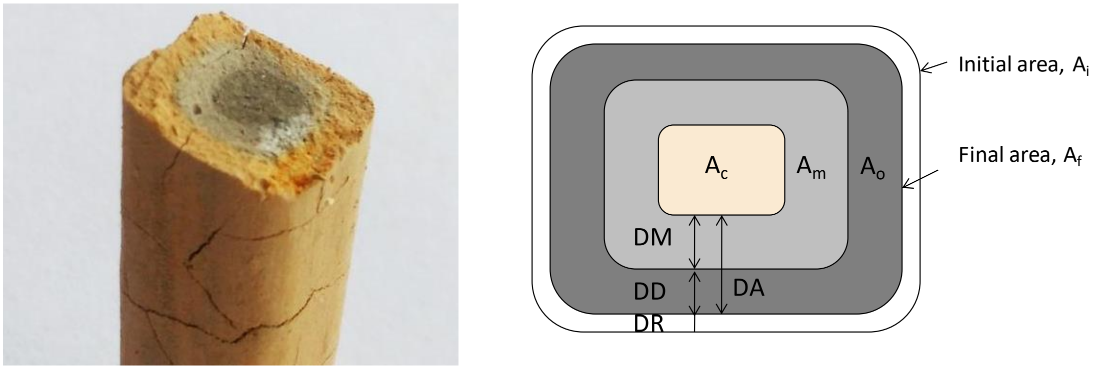

a) A close image of specimen cross-section exposed to 0.5M acetic acid

b) Schematic figure of slice image of specimen cross-section showing various areas/depths

Figure 3.17 Parameters used in the estimation of altered depth/area

3.8 ALTERATIONS IN PHYSICO-MECHANICAL PROPERTIES

Mortar cylinders of size 25 mm diameter and 50 mm height were fully immersed in plastic containers with a volume ratio of 5 for evaluating the changes in physico-mechanical properties (Figure 3.18). The specimens were taken out at specific intervals of acid exposure (at 6, 10 and 16 weeks) and tested for changes in compressive strength, changes in bulk density, changes in ultrasonic pulse velocity, and changes in dynamic modulus of elasticity. No abrasive action was used for the specimens.

Figure 3.18 Immersion test on mortar cylinders in progress to evaluate changes in physico-mechanical properties

3.8.1 Changes in strength

The compressive strength of the mortar specimens was tested using the CONTROLS Advantest9 testing machine as shown in Figure 3.19. The cylindrical mortar specimen of diameter 25 mm and height 50 mm was used for the testing. Three specimens were tested for each mix exposed to acid and the average value is reported as the mean compressive strength of the mix. Channel 3 in this instrument, having a maximum capacity of 250 kN, was used for testing. A loading rate of 70 N/s with peak sensitivity of 2 kN was used for performing the test. Figure 3.20 shows the typical failure pattern of specimens observed in the compression testing.

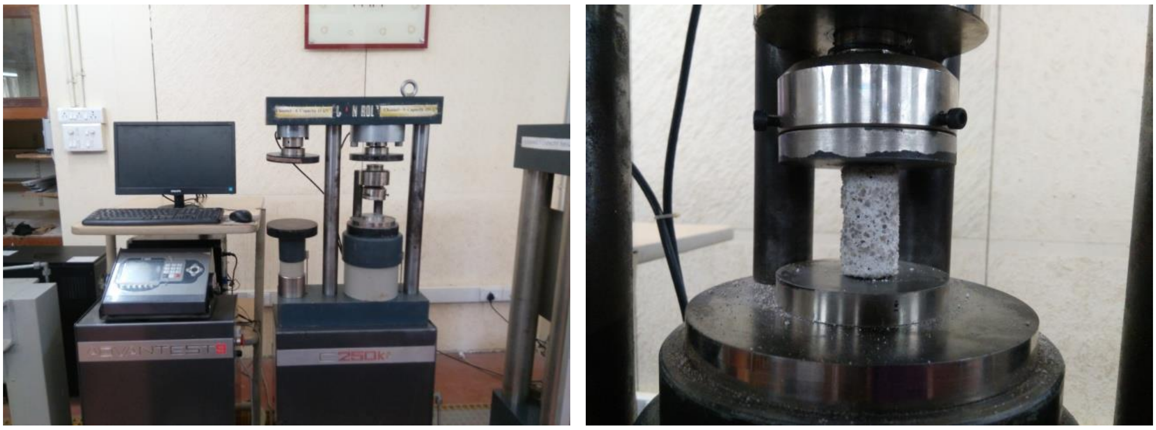

a) CONTROLS strength testing machine b) Compressive strength test in progress

Figure 3.19 CONTROLS Advantest9 testing machine used for testing compressive strength

Figure 3.20 Failure of cylindrical mortar specimen in compression

3.8.2 Changes in bulk density

The changes in mass and diameter of specimens result in changes in its bulk density which in turn will affect the dynamic modulus of elasticity. The bulk density of specimen in the saturated and surface dry condition was calculated based on the mass and volume of specimen at specific ages of acid exposure. At specific age of exposure, specimens were removed from the acid solution, and the excess wetness was wiped using cotton cloth. After measuring the mass, the volume of the specimen was estimated by measuring the average diameter (average of 3 readings) and average height of specimens (average of 3 readings) using the digital vernier caliper shown in Figure 3.16.

3.8.3 Changes in dynamic modulus of elasticity

The dynamic modulus of elasticity of the specimen is a measure of the quality of the interior of the specimen. It was calculated based on the values of Ultrasonic Pulse Velocity (UPV) and bulk density according to IS 13311 Part-I (2004), by assuming the Poisson's ratio of 0.17 for mortar (Eq. 3.3). The deterioration in the microstructure due to acid attack is expected to reflect in changes in the dynamic modulus of elasticity, and hence this test was carried out.

$$E = \rho \frac{(1+\mu)(1-2\mu)}{(1-\mu)} V^2 \tag{3.3}$$

Where,

E = dynamic modulus of elasticity (MPa)

ρ = average bulk density of the specimen (kg/m^3)

μ = Poisson’s ratio of the mortar

V = ultrasonic pulse velocity (m/s)

A term known as relative dynamic modulus of elasticity was then estimated as the ratio of dynamic modulus of elasticity of the mortar at specific age of acid exposure to the dynamic modulus of elasticity of the mortar before the exposure (i.e. after 28 days of initial curing) based on the Eq (3.4). UPV was obtained by testing mortar cylinders using transducers of 25 mm diameter before testing the compressive strength, using the Pundit lab UPV measuring instrument (Figure 3.21). The test was carried out on specimens in saturated and surface dry condition. High quality white grease was applied as a lubricant between the specimen surface and the transducer (Figure 3.22). A transducer frequency of 150 kHz and an excitation voltage of 500 V were used as the test settings.

$$\text{Relative E}= \frac{E_t}{E_0} \tag{3.4}$$

Where,

E = dynamic modulus of elasticity (GPa or MPa)

E_t = dynamic modulus of elasticity at age of acid exposure ‘t’ (GPa or MPa)

E_0 = dynamic modulus of elasticity before the acid exposure (i.e. t = 0) (GPa or MPa)

Figure 3.21 Pundit lab instrument for measuring ultrasonic pulse velocity

Figure 3.22 Ultrasonic pulse velocity testing of the attacked specimen in progress

3.9 MECHANISM OF DEGRADATION

The mechanism of degradation due to acid attack was studied using micro-analytical characterisation techniques such as X-ray micro-tomography, X-ray diffraction, scanning electron microscopy, optical microscopy, mercury intrusion porosimetry and thermogravimetric analysis. More details about these tests and the methodology used in the current study are discussed below.

3.9.1 X-ray micro-tomography

Tomography is a technique for digitally cutting a specimen open using X-rays to reveal its interior details and is derived from the Greek word “tomos” which means “cut” or “section”. X-ray Computed Tomography (CT) is a non-destructive technique for visualizing the interior features within solid objects, and for obtaining digital information on their three-dimensional (3D) geometries and properties. CT data have been applied to virtually every discipline of science and technology, and new applications are being continually discovered. Various researchers have used CT in studying the microstructure of building materials (Boel et al., 2008; Cesen et al., 2013; Stock, 2008; Diamond and Landis, 2007; Gallucci et al., 2007; Wong and Chau, 2005; Promentilla et al., 2009; Promentilla, 2011; Kim et al., 2012; Provis et al., 2012; Wei et al., 2013; Kim et al., 2013, Lu et al., 2006; Chotard et al., 2003; Chotard and Smith, 2003; Wang et al., 2014; Ponikiewski et al., 2014). X-ray CT has also been used in creating models to predict the permeability and elastic properties of cementitious materials (Zhang and Jivkov, 2016; Zhang, 2017). The tomography technique, being a non-invasive imaging technique, has the potential to be used as one of the prime techniques to characterise the microstructure and durability associated problems in cementitious systems such as sulphate attack (Naik et al., 2006; Stock et al., 2002), carbonation (Lydzba et al., 2014; Wan et al., 2014) and leaching (Burlion et al., 2006; Sugiyama et al., 2010). Optical and electron microscopy have been commonly used, for instance, as research tools to examine the microstructure of concrete, especially while investigating durability issues. However, the destructive or invasive way of specimen preparation prior to imaging of the cross-section may produce problematic artifacts and these techniques may not be suitable for quantifying altered depth. In addition, the limitations of observing a two-dimensional (2D) section of a three-dimensional structure from 2D microscopy must also be borne in mind. According to Diamond and Landis (2007), tomography being a 3D imaging technique, the microstructural features present in a 2D image such as air voids, sand grains, presence of cracks, hydrated and anhydrous phases etc. can be extended to trace such features in the third dimension, a capability unavailable to conventionally used microscopic techniques.

Deterioration of concrete in acidic environments results in premature degradation in terms of microstructural alteration of phases (mineralogical zonation) leading to mass changes, weakening of mechanical properties, increase in porosity due to calcium leaching etc. In past studies, tomography has been successfully used by researchers to characterise the microstructure evolution and deterioration associated with calcium leaching in cement-based materials (Wan et al., 2013; Rougelot et al., 2010; Koenig and Dehn, 2016; Dyer, 2016). However, most of the leaching studies were qualitative in nature, restricted to visualisation of degradation. Also, majority of the leaching studies were done using ammonium nitrate solution, which is a powerful leaching agent. The kinetics and the mechanism of attack due to ammonium nitrate differ from the other acids that attack the concrete. Limited studies are available on the application of tomography in studying the deterioration due to acid attack. It is evident from the literature that, tomographic imaging is an apt technique to investigate the attack due to various acids. Hence, in the current study, CT is used along with image analysis to understand the changes in microstructure and to extract useful parameters related to the deterioration in microstructure due to acid attack.

Computed tomography is a technique for obtaining volumetric measurements of the X-ray attenuation coefficient, creating images that map the variation of the X-ray attenuation coefficient within the objects. The schematic illustration of various processes involved in CT imaging is depicted in Figure 3.23.

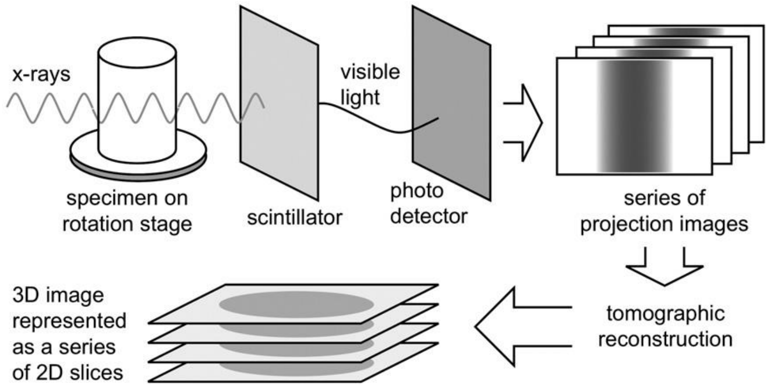

Figure 3.23 Schematic illustration of X-ray CT acquisition and reconstruction processes (adapted from Landis and Keane, 2010)

An X-ray beam is directed towards the specimen and the transmitted beam is recorded on a detector. According to Beer-Lambert law, the ratio of the number of transmitted to incident X-ray photons is related to the integral of the linear attenuation coefficient of the material along the path that the photons follow through the specimen. The resulting image (or radiograph) is a superimposed information or projection of a volume in a 2D plane. To get the 3D information, radiographic projections of the specimen are taken at many angles or projection views. In industrial CT scanners, the specimen is rotated and the X-ray source and detector are fixed in position, as shown in Figure 3.24. Once these projections are available, a reconstruction algorithm can be used to produce the contiguous two dimensional images which provide a discrete approximation of the distribution of X-ray attenuation coefficient within the volume of the imaged specimen. This two dimensional image is commonly referred to as slice because it corresponds to the cross-section of what would be seen if the specimen were sliced along the scan plane. Each slice is a matrix of voxels (volume element or 3D pixel) in which each voxel is associated with a grayscale value (GSV) that is related to the measured linear attenuation coefficient (Figure 3.25). For example, in an 8-bit CT image with voxels, with GSV that ranges from 0 to 255, the higher the X-ray attenuation coefficient of the material component, the higher the GSV of the corresponding voxel. Since the linear attenuation coefficient (LAC) is sensitive to the atomic composition and density (Bossa et al., 2015), CT technique could therefore provide nondestructive 3D visualisation and characterisation of internal structure without the time-consuming and difficult sectioning of specimen as is done in 2D microscopy techniques. As long as the spatial resolution is small with respect to the microstructural feature of interest, the volumetric image obtained from these measurements could provide valuable 3D structural information. Reconstruction is generally attenuation-conservative, allowing sub-voxel level details to be extracted. Quantitative measurements can be made from the resulting digital image data, including the spatial distribution and volume fraction of phases, as well as the changes in phases due to a range of mechanical or chemical phenomena.

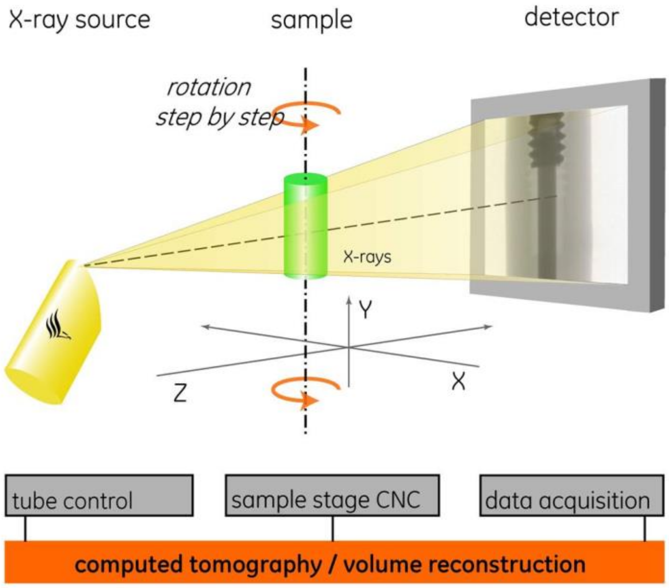

Figure 3.24 Cone beam configuration for CT data acquisition

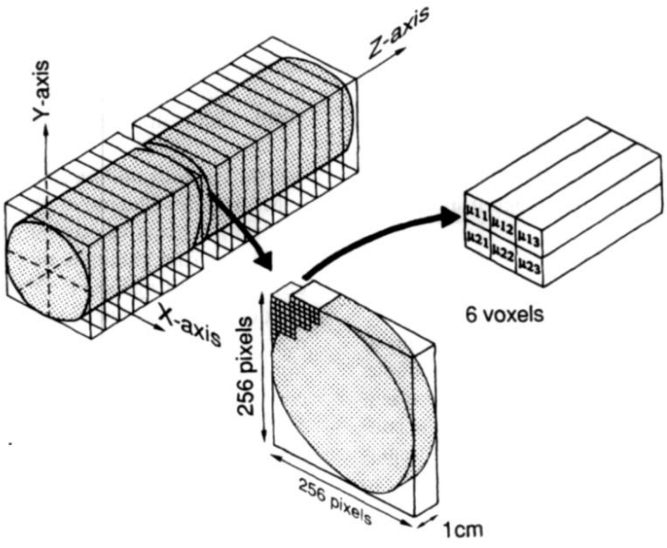

Figure 3.25 CT image illustrating the concept of pixel and voxel
(adapted from Jacobs et al., 1995)

The current study attempts to characterise the microstructure of the acid degraded specimens using X-ray computed micro-tomography. The tomography test setup at IIT Madras used for imaging (Figure 3.26), v|tome|x s is a versatile high resolution system consisting of both micro and nano focus tubes. To allow high flexibility, the v|tome|x s is equipped with both, a 180 kV / 15 W high-power nanofocus X-ray tube and a 240 kV / 320 W microfocus tube. Due to this unique combination, the system is an ideal tool for a wide range of applications from extreme high resolution scans of low absorbing materials as well as for 3D analysis of high absorbing objects up to 260 mm in diameter. The maximum voxel resolution for microfocus tube is less than 2 µm and for nanotube less than 1 µm. The maximum specimen mass that can be inspected is limited to 10 kg, while the maximum specimen size that can be imaged is of 420 mm height and 260 mm diameter. Cesium Iodide flat panel detector (pixels of 1024 × 1024) is used (for converting X-rays to light). In this study, only microfocus X-ray tubes were used and hence the term micro-tomography.

Figure 3.26 v|tome|x s – tomography setup used for imaging

Cubical samples of size approximately 10 mm were cut using diamond saw blade (Figure 3.27) from the end of the degraded specimens (as illustrated in Figure 3.28) and the control specimens immersed in lime water. The ends of the specimen are generally degraded more and hence, specimens are cut from the end for extracting maximum information about the deterioration. Solvent exchange process using isopropanol was used for specimen conditioning followed by drying. The dried specimens were then taken for the CT imaging.

Figure 3.27 Diamond tipped saw used in the study to cut thin slices of samples

A microfocus tube was used to generate X-rays (conical beam as shown in Figure 3.24) at a voltage of 65 kV and current of 120 µA. The specimen was rotated 360° and a total of 900 images were captured during the complete rotation of specimen in the stage, to reconstruct the 3D image. The data acquisition time was 333 milliseconds per image captured with an averaging of 4 frames per image. The total time for scanning a specimen was about 25 minutes. After the reconstruction process, the 3D image and 2D slice images were obtained. Figure 3.29 shows the schematic diagram of specimen showing the position of sections for obtaining 2D slice images from the 3D image. Sections 1-1 and 2-2 were cut to obtain the slice images (top view) through inside of the specimen and on the surface (degraded layer) respectively. Sections 3-3 and 4-4 were cut to obtain slice images (front view) through the surface (degraded layer) and from the inside of the specimen respectively.

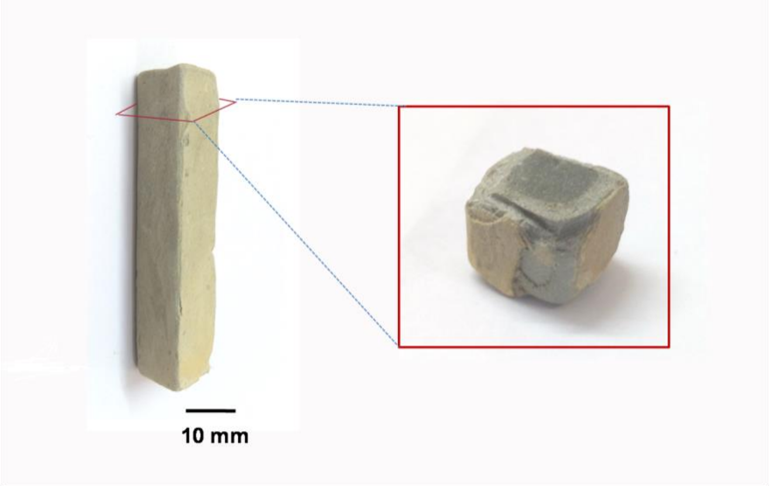

Figure 3.28 Specimen for X-ray CT imaging

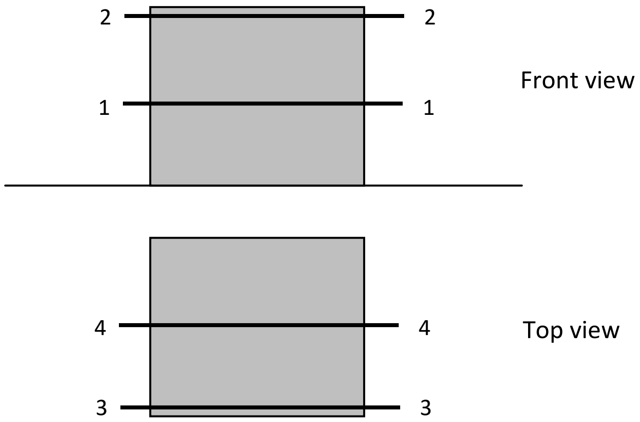

Figure 3.29 Schematic diagram of specimen showing sections for obtaining CT slice images

3.9.2 X-ray diffraction

X-ray diffraction (XRD) is one of the widely used analytical techniques in the characterisation of cement-based materials. Atoms present in the crystalline material interact with X-rays (of a single wavelength) producing an interference (XRD pattern), which consists of peaks of varying intensities at specific diffraction angles (Scrivener et al., 2016; Ramachandran and Beaudoin, 2001). The interference would be constructive, if the reflected X-rays from the successive atomic planes satisfy the Bragg's law for specific inclination of X-rays (as stated in Eq. 3.5). At other orientations, destructive interference takes place and no signal is generated.

$$n\,\lambda = 2d\ \sin\theta \tag{3.5}$$

Where,

d = lattice inter-planar spacing of the crystal

θ = X-ray incidence angle

λ = wavelength of characteristic X-rays

n = order of diffraction

Thus XRD produces patterns consisting of peak positions and the peak intensities that are characteristic of various crystal structures, which helps to identify their presence in the unknown tested samples. The output (X-ray diffractogram) is a plot between 2θ and the intensity of X-ray counts, where 2θ is the deviation angle between the incident and the scattered X-ray beam.

In this study, X-ray diffraction analysis was performed on the samples for the identification of reaction products (or new phases formed) on acid exposure. The study was restricted to the qualitative phase analysis. The decrease in the intensity of phase (in comparison to the peak intensity before the acid exposure) indicates the consumption of a phase during the reaction and vice versa. For field investigations, the thin slices of concrete samples collected from various locations were immersed in isopropanol for 4 days and subsequently dried. In order to prepare the sample for testing, mortar chunks were further separated from the concrete sample. The samples so collected were crushed gently using a mortar and pestle, and sand grains were separated as much as possible using sieves. The powdered sample passing through 75 μm was then taken for the testing.

For the laboratory study, both paste and mortar samples were tested. It is understood that the acid attack results in mineralogical zonation of materials. However, as it was difficult to separate the layers from the cross section (due to the small size of the specimens), the entire cross sections of the samples before and after the degradation were crushed to form the powder for testing. For this purpose, approximately 10 mm slices were cut from the prismatic paste and mortar specimens of size 10 × 10 × 60 mm. Further, the slices were immersed in isopropanol for 4 days (with regular replacement of isopropanol) and dried thereafter. The dried samples were kept in vacuum desiccator until testing. In the case of mortar samples, care was taken to remove the sand fractions as much as possible while grinding the samples. The samples were powdered using mortar and pestle and the powder passing 75 μm were taken for the testing. The main steps involved in the preparation of sample for XRD testing is shown in Figure 3.30.

The XRD testing was done using an X’Pert Pro PANalytical diffractometer (shown in Figure 3.31). The scanning range adopted was over the 2θ range from 5-65°. Cu-K_α radiation was used to generate X-rays with test settings of 45 kV voltage and a current of 30 mA. The identification of crystalline phases was carried out using the software, X’Pert HighScore Plus with Inorganic Crystal Structure Database (ICSD).

a) Samples cut using diamond tipped saw

b) Samples crushed using mortar and pestle and sieved through 75 µm sieve

c) Powdered sample placed inside a plastic vial inside zip lock covers

d) Samples kept inside desiccator until the time of testing

Figure 3.30 Steps involved in the preparation of samples for XRD testing

Figure 3.31 PANalytical X'Pert Pro instrument

3.9.3 Scanning electron microscopy

Scanning electron microscopy (SEM) is one of the most powerful and widely used techniques for studying the microstructure of cementitious materials (Scrivener et al., 2016; Ramachandran and Beaudoin, 2001; Stutzman, 2004; Stutzman and Clifton, 1999). A focused beam of electrons (by using electromagnetic condenser lenses) interact with the sample, undergoing a series of elastic and inelastic collisions with the atoms present in the sample. These collisions generate signals (such as secondary electrons (SEs), back scattered electrons (BSEs), characteristic X-rays) which are detected by various detectors in the microscope to form the image. These processes are schematically presented in Figure 3.32.

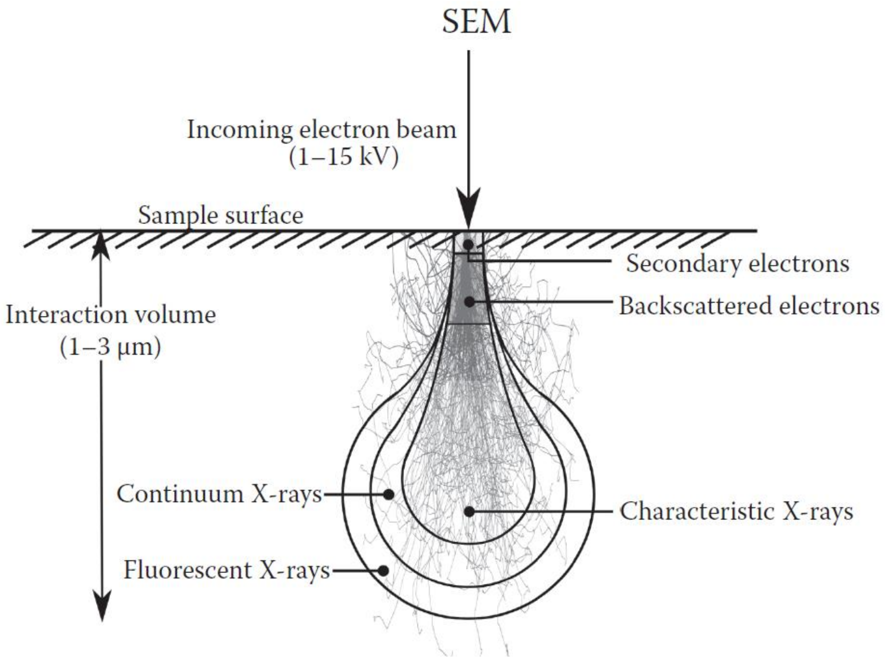

Figure 3.32 Schematic representation of the interaction of electrons with matter (Scrivener et al., 2016)

In this study, scanning electron microscopy in the secondary mode imaging was used to study the morphology of the products formed in various layers in the specimen exposed to acids. Secondary electrons (SEs) arise from the inelastic collisions between the electron beam and the loosely bound outer shell electrons in the sample. As a result of this inelastic collision, an electron is knocked out from the outer shell of an atom in the sample. These electrons have lower energy than the incident electrons. Hence, although they are generated throughout the interaction volume, they can escape only from the near surface of the specimen, and are caught by the SE detector. Due to this reason, the resolution of SE imaging is very good and it is widely used to study the topology and morphology of the particles making up the sample, and hence, used in this study.

Energy dispersive spectroscopy (EDS) equipped with the SEM facility is also used to study the elemental composition of either a spot or area in the sample. The working principle of EDS is similar to the X-ray fluorescence. The various elements present in the sample are identified based on the electronic transitions and the emission of X-rays (as a result of excitation by electrons) from the sample. The EDS plot is obtained in which the Y axis shows the X-ray counts (the number of X-ray signals received and processed by the detector) and the X-axis shows the energy level of those counts in electron volt (eV) which are characteristic of various elements present in the sample.

In the current research, SEM studies coupled with EDS were used for both the field and laboratory investigations to study the morphological changes of phases and to understand the mechanism of alteration. To study the morphology of the deteriorated concrete samples collected from the industries and to confirm the elemental composition of the reaction products, SEM studies were carried out with energy dispersive spectroscopy (EDS). The machine, Inspect F (shown in Figure 3.33), which has a field emission gun with high vacuum in the secondary electron mode, fitted with EDS detector was used. Flat samples cut using a diamond saw were immersed in isopropanol for 4 days followed by drying. The samples were fixed to the stainless steel stubs using a carbon tape and air blown to remove the loose particles, if any. The samples were then sputter coated with gold for 90 seconds to avoid charging during the imaging.

In the case of laboratory investigations, flat paste and mortar samples were cut from the prismatic specimen using a diamond tipped saw. These thin sliced samples were then immersed in isopropanol for 4 days followed by drying. The dried samples, loaded onto the stainless steel stubs, were sputter coated with gold for imaging as explained earlier. A scanning electron microscope named Quanta 200 FEG, (shown in Figure 3.34) which has a field emission gun with high vacuum, was used in secondary electron imaging mode. As the cut sample cross-section was relatively flat, EDS was used directly on the samples to determine the elemental composition of various phases observed. Figure 3.35 shows the photographs of different stages of sample preparation for SEM SE imaging.

Figure 3.33 Inspect F scanning electron microscope used in the study

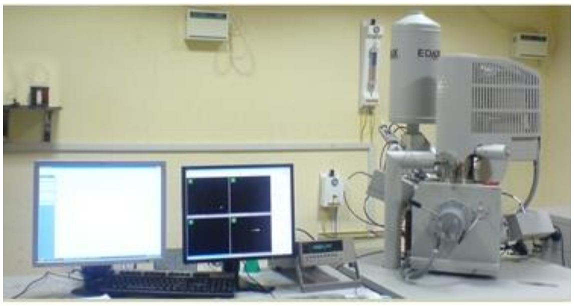

Figure 3.34 Quanta 200 FEG scanning electron microscope used for imaging

a) Thin samples cut using diamond tipped saw

b) Samples kept inside desiccator

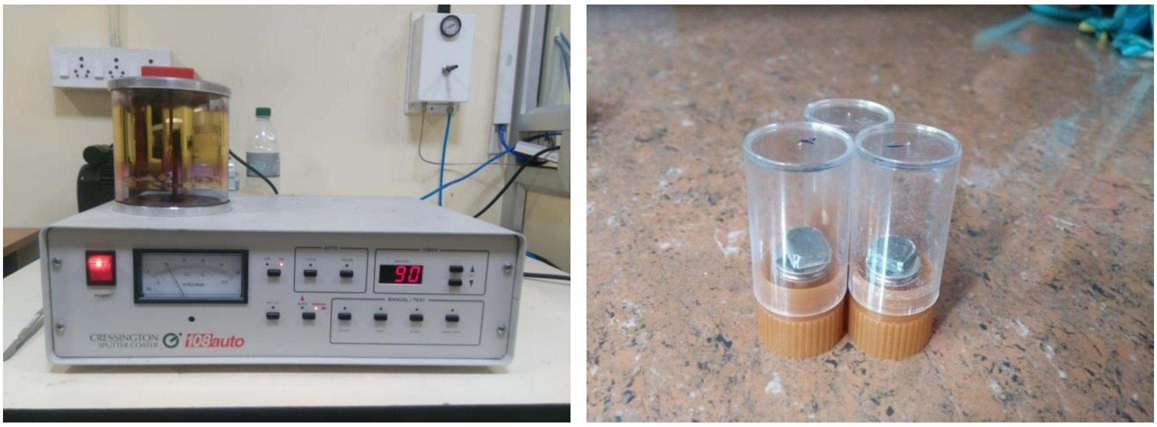

c) Samples sputter coated with gold

d) Coated samples placed in stubs for imaging

Figure 3.35 Steps involved in the preparation of samples for SEM imaging

3.9.4 Mercury intrusion porosimetry

Cementitious materials are porous in nature. The size of the pores in hydrated cement materials varies from microns to the nanoscale. The three main categories of voids/pores are compaction/air voids, capillary pores and gel pores. Only a few techniques are able to characterise the complex pore structure of hydrated cementitious materials. One of the commonly used techniques to investigate the pore structure in a quantitative way is mercury intrusion porosimetry (MIP). The technique gives reliable information about the pore size distribution and bulk density of porous solids. This technique is based on the intrusion of a non-wetting fluid (mercury) into porous structures under increasing pressure.

The principle of MIP is based on the relationship between the applied pressure and the corresponding volume of pores filled with mercury. Mercury is a non-wetting liquid having a contact angle with cementitious materials of 130–140°. The applied pressure and the resulting volume of mercury entering the pores of the tested material can be related to the entry pore diameter (pore size) and the amount of pores of the particular size as per the Washburn equation given below in Eq. (3.6).

$$\mathrm{P} = -\frac{2\gamma\cos\theta_c}{r} \tag{3.6}$$

Where,

γ is the surface tension of mercury

θ_c is the contact angle

P is the pressure

r is the radius of pore

In the current study, MIP was used to study the changes in pore structure of cementitious materials for both the field and laboratory investigations. MIP studies were conducted on the samples using a PASCAL 140/440 Series Porosimeter instrument from Thermo Scientific (shown in Figure 3.36). The instrument was capable of measuring the pore sizes from 100 µm to about 3.7 nm, by increasing the pressure from vacuum to 400 MPa.

The typical MIP plot is shown in Figure 3.37. The blue curve represents the cumulative intruded volume of mercury and the red curve gives the differential of the intruded curve. The pores present in the cementitious system are classified fundamentally into two; pores in the range 10 nm – 10 µm represent the capillary pores and pores in the range 1 – 10 nm classified as gel pores (Aligizaki, 2005). Additional parameters such as threshold diameter and the most likely diameter (sometimes called ‘critical diameter’) can also be estimated from the MIP curve. The threshold diameter is that pore size beyond which there is a rapid rise in the cumulative intruded volume. The most likely diameter is that pore size for which the incremental intruded volume is maximum. The other parameters such as bulk density of the porous samples can also be extracted based on the test data from the SOLID software interface connected with the MIP instrument.

Figure 3.36 PASCAL 140/440 Series Porosimeter instrument used for the study

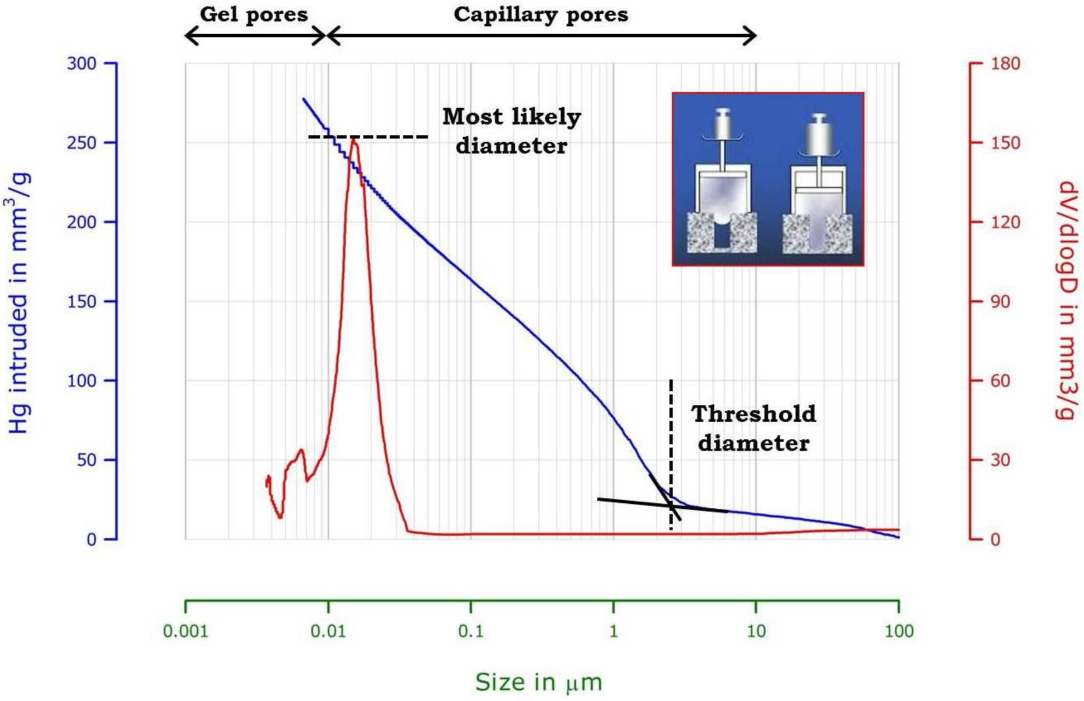

Figure 3.37 A typical MIP plot showing various porosity related parameters (Murugan, 2017)

The hydration/reactions of samples were arrested using a solvent exchange process using isopropanol, as explained earlier. In the case of field samples, mortar chunks were extracted from the concrete and dried samples of mass 0.5-1 g were used for testing. A pressure up to 400 MPa (which corresponds to a pore size of 3.7 nm diameter) was used during the test.

The use of MIP in the laboratory investigations was restricted to the testing of paste samples. In the paste study, approximately 10 mm thin slices were cut from the specimens (from the middle part of specimen) before and after the exposure using the diamond tipped saw as shown in Figure 3.27. As the entire cross section of the sample is cut, the porosimetry results are expected to reflect the overall changes in the pore structure of the material because of acid attack. Further, the cut slice was immersed in isopropanol for 4 days and the subsequently dried sample was further broken to 3-4 pieces so as to fit it inside the dilatometer and then tested.

3.9.5 Thermo-gravimetric analysis

Thermogravimetric analysis (TGA) is a widely used technique in the field of concrete technology. Measurements of bound water and Portlandite content by TGA are often used to explain the reaction of Portland cement or to evaluate the reactivity of SCMs. TGA is also used to identify amorphous hydrates present in the cementitious systems, such as CSH gel or AH_3, and can be used complementarily to other techniques such as X-ray diffraction (Scrivener et al., 2016).

Minerals and hydrates can undergo several thermodynamic alterations/reactions such as dehydration, dehydroxylation, decarbonation, oxidation, decomposition, phase transition or melting. These reactions are generally associated with mass changes or release of heat. The temperature at which these processes occur are typical for the mineral or hydrate. During TGA, the sample is heated at a constant rate and the mass of the sample is continuously recorded. TG curve plot is made with Y axis representing the mass of the sample and X axis representing the temperature. The differentiation of the thermogravimetric (TG) data gives the differential thermogravimetry (DTG) plot which allows a better resolution of the alteration (to identify the onset and end temperatures of the alteration) and in the identification of consecutive mass losses.

TGA was used in this study to determine the Portlandite and calcite contents of paste and mortar samples before and after the acid exposure. TGA is used as a complimentary technique to X-ray diffraction in order to understand the mechanism of degradation. The sample preparation and conditioning was explained earlier in the section on X-ray diffraction. The samples after immersion in isopropanol for 4 days were dried and ground to fine powder passing 75 μm sieve. The test was conducted from 30 °C to around 1000 °C, at a constant heat rate of 10 °C per minute in a nitrogen purged atmosphere. The paste study was done on the TGA instrument from Perkin Elmer (STA 6000) shown in Figure 3.38. Figure 3.39 shows the TGA instrument used for the mortar study (Model No. NETZSCH STA 449 F3 Jupiter).

Figure 3.38 Perkin Elmer STA 6000 used in the study (http://www.perkinelmer.com)

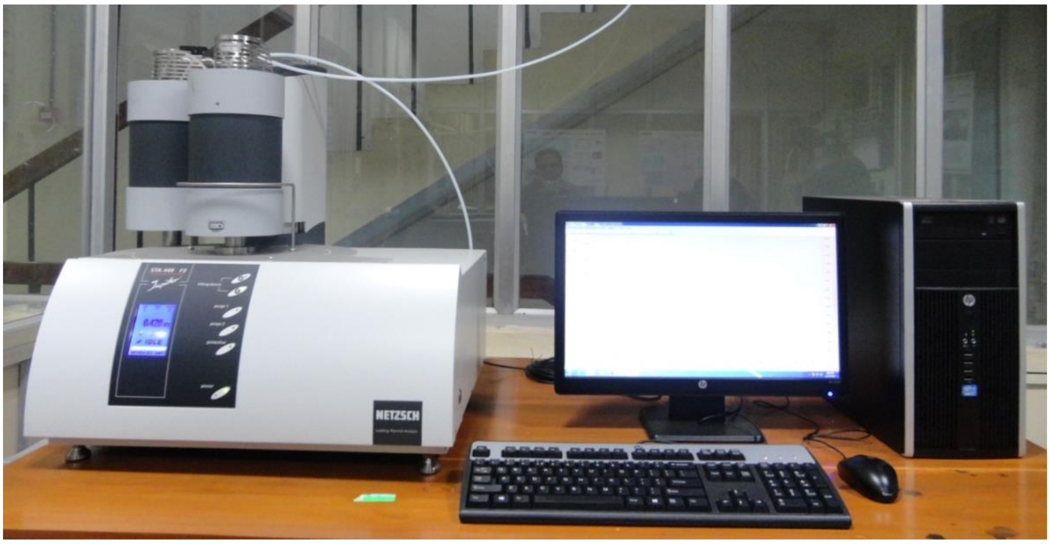

Figure 3.39 NETZSCH STA 449 F3 Jupiter – TGA instrument used for the study

3.9.6 Optical microscopy

Images collected from optical microscopes can provide useful information about the microstructure of the cementitious material especially when it undergoes microstructural alterations (Haneefa, 2014). These optical microscopes are generally equipped with reflected and transmitted modes. Polished opaque specimens can be viewed through reflected mode to study features such as different phases present in the system, their interfaces and relative proportions. A transmitted mode is used to study the mineralogy of thin sections in which semi-transparent specimens are viewed under the microscope. The mineralogy thus obtained depicts type, nature and volume proportions of minerals present, which can be correlated with material properties at macro (engineering) scales.

Figure 3.40 Olympus BX41 optical microscope used in the study

In the current study, the optical microscope in the reflected mode was used to visualise the microstructural alteration of OPC paste after the acid exposure. The mineralogical zonation could be captured in the images collected. The Olympus BX41 optical microscope, which was capable of 40X, 100X, 400X and 1000X magnifications owing to multiple objective lenses, was used in the study (Figure 3.40). The trinocular head enabled the capture of magnified images with a digital camera fitted in it. However, as it was found that X-ray tomography could be useful for getting more information, the study using optical microscope was limited to the OPC paste exposed to various acids to get a preliminary idea about the mineralogical zonation due to the acid attack.

3.10 CHARACTERISATION OF BINDERS AND AGGREGATES

The various binders and aggregates were characterised using techniques such as X-ray diffraction (explained in section 3.9.2), X-ray fluorescence, laser diffraction and loss on ignition test. The procedure and principle of these test methods are discussed below.

3.10.1 X-ray fluorescence

X-ray fluorescence (XRF) analysis is one of the useful analytical techniques in finding out the elemental composition in cementitious samples (Brouwer, 2003). The sample is bombarded with X-rays. This excites the sample to generate X-ray fluorescence radiation as shown in Figure 3.41 schematically. The incoming X-rays knock the individual electrons out of the atoms of the elements, primarily out of the inner atomic shells K and L. The resulting vacancies are filled up again by electrons from higher energy shells. The excess energy of these electrons is then emitted in the form of X-ray fluorescence radiation, which is characteristic for each element like a fingerprint and independent of the atom's chemical bond. The intensity of the radiation is proportional to the concentration of the element present in the sample. The elemental composition thus obtained can be further converted to the oxide composition.

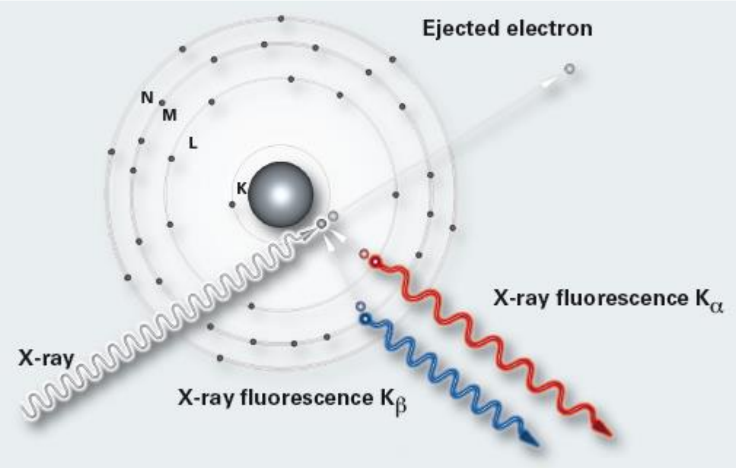

Figure 3.41 Working principle of XRF (https://www.bruker.com)

The oxide composition of various binders and aggregates used in the study was determined by XRF using Bruker S4-Pioneer aXS instrument (shown in Figure 3.42). The powder sample passing 75 µm was used for testing. A pressed pellet was prepared by mixing the sample and boric acid (binder) for the testing. SPECTRA^{plus} software package was used with the XRF instrument for the measurements.

Figure 3.42 Bruker S4-Pioneer aXS instrument

3.10.2 Laser diffraction

Laser diffraction is a widely used technique in the determination of particle size ranging from several microns to millimeters. The technique measures particle size distributions by measuring the angular variation in intensity of light scattered as a laser beam passes through a dispersion of particles in air or in a liquid. Large particles scatter light at small angles relative to the laser beam and small particles scatter light at large angles. The angular scattering intensity data is then analysed to calculate the size of the particles using the Mie theory of light scattering or Fraunhofer theory (Scrivener et al., 2016). The particle size is reported as a volume equivalent sphere diameter. A particular advantage is that the technique can generate a continuous measurement for analyzing process streams.

A volume distribution is calculated as the fundamental result, which is a plot between volume passing (%) and the particle size. The particle size distribution can then be plotted which is a plot between the % finer on the Y axis and particle size on the X axis (log scale). The terms D_{10}, D_{50} and D_{90} are also given as output where 10%, 50% and 90% of the particles are finer than these diameters in the particle size distribution curve (cumulative volume distribution).

In the current study, Microtrac S3500 particle size analyser (shown in Figure 3.43) was used to determine the particle size distribution of various binders used in the study. Isopropanol was used as a dispersant to disperse the binder materials with ultrasonic treatment during the testing. The D_{50} (in µm) estimated from the particle size distribution curve was reported as the average particle size of the binder sample tested.

Figure 3.43 Microtrac S3500 particle size analyser (https://www.microtrac.com/)

3.10.3 Loss on ignition

Loss on ignition (LOI) refers to the mass loss of a material when heated to high temperatures. It indicates the loss of volatile matter present in the material, which usually consists of combined water and carbon dioxide from carbonates. In this study, loss on ignition of various binders was determined as per IS 1727 (2004). About 1 gram of material (sample) in ceramic crucible of 25 mL capacity was placed in an oven at a temperature of 105 °C for 24 hours and weighed after cooling. This was further placed inside a muffle furnace and ignited to a temperature of 1050 °C for about 30 minutes. The temperature of the furnace was incrementally increased to 1050 °C. The crucible was cooled and the mass was measured. The difference between the oven dried sample and the mass after ignition represents the loss on ignition (Eq. 3.7), and is expressed as percentage of the oven dried mass before the ignition.

$$\mathrm{LOI} = \frac{\mathrm{M}_{105} - \mathrm{M}_{1050}}{\mathrm{M}_{105}} \tag{3.7}$$

Where,

M_{105} = Mass of the sample after heating to 105 °C

M_{1050} = Mass of the sample after ignition at a temperature of 1050 °C

3.11 SUMMARY

The physical and chemical properties of various materials used in the study such as binders, aggregates and superplasticizer are discussed in this chapter. The mix proportions used for making paste and mortar specimens and the details about the preparation of acid solutions are explained. Further, the experimental programme adopted in the study is explained followed by a detailed discussion on the testing methods used in the study. The various parameters used to study degradation kinetics are discussed. A detailed discussion is included on the various micro-analytical characterisation techniques used to understand the mechanism of degradation and to characterise the binders used in the study.

CHAPTER 4

FIELD INVESTIGATIONS

4.1 INTRODUCTION

This chapter discusses the micro-analytical characterisation of deteriorated concrete samples collected from two types of industries; a sewage treatment plant and a distillery plant in Tamil Nadu, India. These case study investigations were carried out in order to identify the possible areas where the acid attack could occur and also in understanding the nature and severity of the problem. The collected samples were tested using characterisation techniques such as X-ray diffraction, mercury intrusion porosimetry, scanning electron microscopy and X-ray micro-tomography and the results are presented in this chapter.

4.2 CASE STUDY 1: SEWAGE TREATMENT PLANT

4.2.1 Background and location details

Concrete is susceptible to attack by acids present in industrial effluents (Magniont et al., 2011). Of particular concern is the progressive dissolution of hydrated cementitious phases, resulting in the formation of a degraded layer on the surface (Pavlik, 1994a; Pavlik, 1994b; Pavlik, 1996). Sewage treatment plants (STPs), which treat domestic sewage and concrete sewer lines that transport the sewage, should also be taken into consideration (Sivakumar, 2017). The degradation that occurs in a STP is a result of the combined attack by sulphuric acid and organic acids such as acetic acid (Bertron et al., 2004). This sulphuric acid is produced biogenically because of the bacterial action of thiobacilli (Monteny et al., 2000; De Belie et al., 2004). Even though such degradation occurs at a very slow rate of 1 – 5 mm per year over a long period of time, the effects could be devastating as per Monteny et al. (2000). This also causes corrosion of steel if the acid permeates through the concrete cover depth. Since the degraded layer formed is soft and porous, it provides an excellent stratum for the growth of bacteria. This helps in causing further deterioration of concrete in these environments.

In this context, a site visit to Nesapakkam sewage treatment plant in Chennai, India was conducted to investigate the possible locations where acid attack can occur. The collection and treatment of wastewater for the city of Chennai has been divided into five zones. The STP visited is situated in Zone 4, which lies in the south-west of the city and is the smallest zone. There are 27 pumping stations to collect the wastewater in this zone. This collected wastewater is then conveyed to the treatment facility at Nesapakkam, which consists of three treatment plants. The first plant of 23 million litres per day (MLD) capacity, built in 1974, has been considered for this study. The wastewater collected in this plant is treated by Activated Sludge Process (ASP). The general layout of the plant is shown in Figure 4.1. Figure 4.2 shows the concrete deterioration from various locations of the plant, such as the screen and grit chamber, primary clarifier and aeration tank.

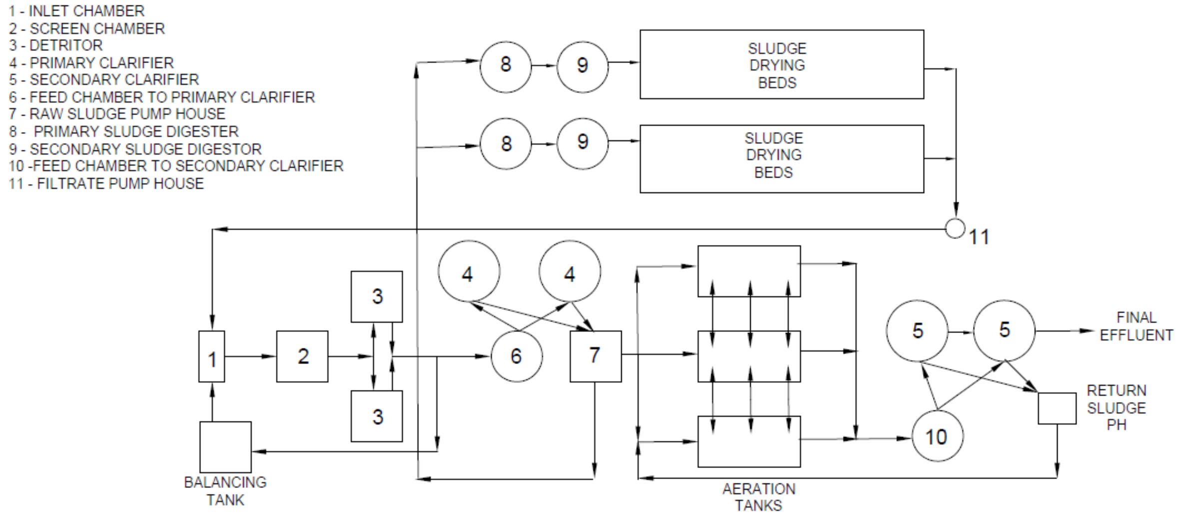

Figure 4.1 Layout of the Nesapakkam sewage treatment plant

4.2.2 Sample collection

The concrete samples were collected from various deteriorated locations of the plant, such as screen and grit chamber (which is always in contact with the raw flowing sewage), the primary clarifier (PC) and the secondary clarifier. Even though deterioration was observed in the aeration tank, samples could not be collected due to practical difficulties. All samples were collected by using a hammer and chisel from the zone that is subjected to alternate wetting and drying (just above the water level).

(a) Screening and grit chamber (b) Primary clarifier

(c) Concrete deterioration in primary clarifier (d) Aeration tank

Figure 4.2 Concrete deterioration in various locations of Nesapakkam sewage treatment plant in Chennai

4.2.3 Micro-analytical characterisation of samples

4.2.3.1 X-ray diffraction

Figure 4.3(a) shows the X-ray diffractogram of the sample taken from the screen and grit chamber (S/GC). From the diffractogram, it is clearly seen that there is gypsum (reaction product) formed along with calcite. Quartz is also observed in the diffractogram, which could be due to crushing of sand grains from the mortar while preparing the sample. Further, it is observed that Portlandite has been consumed completely in the attack due to decalcification by acids (both sulphuric and organic acids). Even though the screen and grit chamber hold only raw sewage, the effect of the attack is more pronounced here because of the continuous flow, which removes the deteriorated layers and exposes the fresh surface for attack. These findings are in agreement with a study conducted by Moradian et al. (2012), who also observed very high damage in the entrance channel, which is the first structure in any STP. Similar conclusions regarding the grit chamber have been drawn by O'Connell et al. (2010). Figure 4.3(b) shows the X-ray diffractogram of the white precipitate obtained from the primary clarifier sample (PC1). Gypsum was observed as the primary and dominant reaction product along with trace amounts of quartz. This gypsum might have formed primarily due to the reaction between sulphuric acid and Portlandite, suggesting that the primary clarifier is also susceptible to biogenic sulphuric acid attack. Portlandite is completely absent in the system. This could be due to the decalcification of Portlandite to form gypsum on reacting with sulphuric acid or dissolution of Portlandite due to the formation of soluble calcium salts on reaction with organic acids. The precipitate formed on the exposure of Ordinary Portland Cement (OPC) mortar immersed in 1% sulphuric acid (mineral acid) for a period of 1 month in laboratory condition was also analysed. It was confirmed that the reaction products were the same as found in the primary clarifier. Another interesting observation is that the precipitate samples collected from the outer layers were devoid of calcite, indicating that the calcite of acid attacked samples could only be present in the inner layers. This could be due to solubility of the calcite in acid solutions or the less availability of calcium hydrates (especially Portlandite) to form calcite in the outer layers.

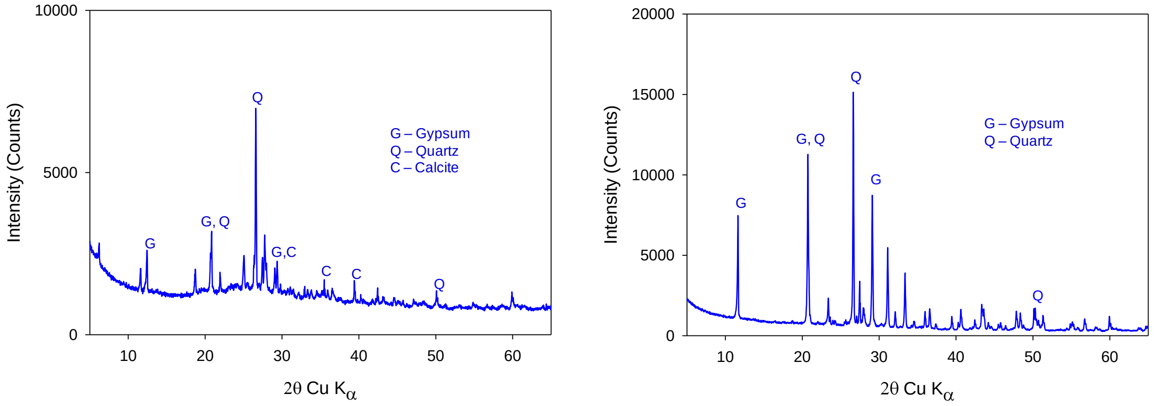

(a) S/GC (b) PC1

Figure 4.3 X-ray diffractograms of the samples collected from Nesapakkam sewage treatment plant

4.2.3.2 Mercury intrusion porosimetry

The variation in porosity of collected samples due to the deterioration was evaluated using mercury intrusion porosimetry (MIP). The cumulative pore volume curve and the derivative curve of the samples collected are shown in Figure 4.4. It can be noted that there is considerable increase in cumulative intruded volume due to the deterioration. A considerable shift (to right) in pore sizes for all the samples was also evident from Figure 4.4 when compared to the lab reference sample (M30 concrete sample named C1). This reinforces the fact that leaching leads to an increase in porosity due to decalcification of hydrated products and salt formation.

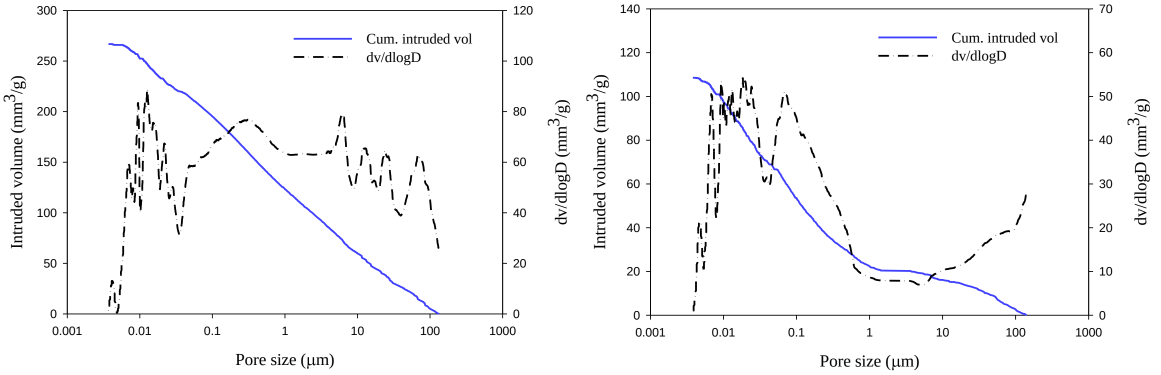

a) S/GC b) PC1

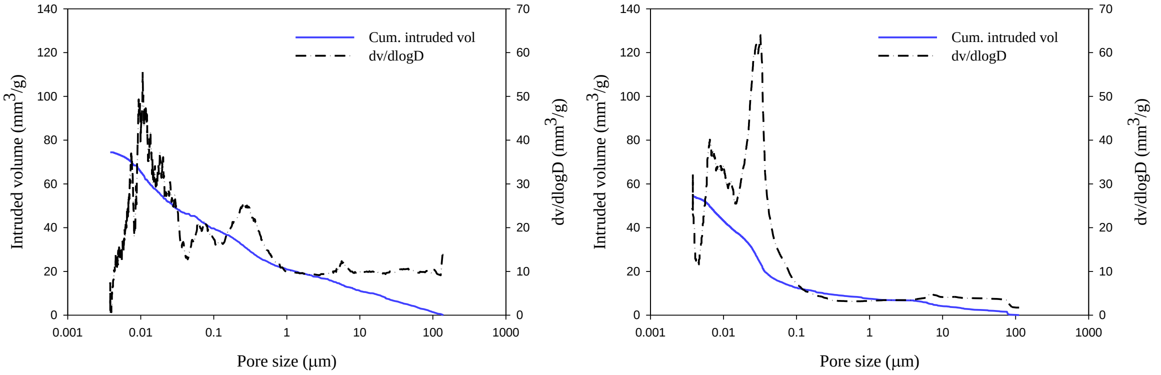

c) PC2 d) OPC M30 reference (C1)

Figure 4.4 MIP curve of samples collected from Nesapakkam sewage treatment plant

The various MIP related parameters are obtained from the test results and are presented in Table 4.1. The intruded volume and porosity were found to be higher for all the samples collected from the sewage treatment plant when compared to the reference concrete sample made in the lab (C1). This indicates the severity of attack experienced by these concrete structures. The intruded volume and the porosity were highest for the samples collected from the screen and grit chamber. This could be due to the high organic content of the samples resulting in the dissolution of hydrates by organic acids and due to the flowing action of sewage in the screen and grit chamber. The bulk density was found to be low due to increase in porosity. The samples collected from the primary clarifier also showed higher porosity, which was, however, lower than that of the screen and grit chamber samples. The porosity and intruded volume of the sample collected from secondary clarifier (sample named PC2) was found to be even lower and this could be due to the lower organic load present in the sewage at that location and relatively lower flow velocity of the sewage. As a result, bulk density was found to be higher.

Table 4.1 MIP test results of samples collected from Nesapakkam sewage treatment plant

Results	S/GC	PC1	PC2	C1
Total intruded volume (mm³/g)	266.7	108.5	74.4	54.9
Bulk density (g/cm³)	1.38	1.77	2.07	2.34
Porosity by Hg intrusion (%)	36.90	19.24	15.41	12.84
Threshold diameter (µm)	*	1.43	1.00	0.06

* Threshold diameter could not be determined as large sized pores were present

4.2.3.3 Scanning electron microscopy

Secondary electron microscopy imaging on the sample collected from the primary clarifier (PC1) shows the presence of gypsum, which is also confirmed by the X-ray diffractogram. Thick deposits of gypsum crystals (shown in Figure 4.5(a)) could be seen around the siliceous aggregates. Figure 4.6 shows a magnified image of gypsum deposits found in PC1 sample. The gypsum crystals were hexagonal-shaped with a columnar structure. The average size of the crystal was found to be 19 µm. These thick gypsum deposits were noted on the void areas and in interfacial transition zones (ITZ) around the aggregates. This reinforces the fact that Portlandite, which could be abundantly present in these areas, decalcified and converted to the final end product, gypsum. Energy dispersive spectroscopy (EDS) was done over the highlighted area shown in Figure 4.5(a) and the spectrum confirms the product as gypsum with prominent peaks of Ca, S and O.

Figure 4.5(b) shows another area of interest in which white gel-like deposits were observed along with gypsum. The EDS results show strong peaks of Si and O with traces of Al, S and Ca. This could be due to the amorphous gel formation after the decalcification of CSH gel and aluminate hydrates along with the gypsum formation. The gel thus formed is found to contain Al also. The imaging of the sample collected from the secondary clarifier is shown in Figure 4.5(c). It shows a magnified image of the interfacial transition zone (ITZ) around the aggregates. The ITZ was found to be porous due to formation of gypsum (as confirmed by EDS).

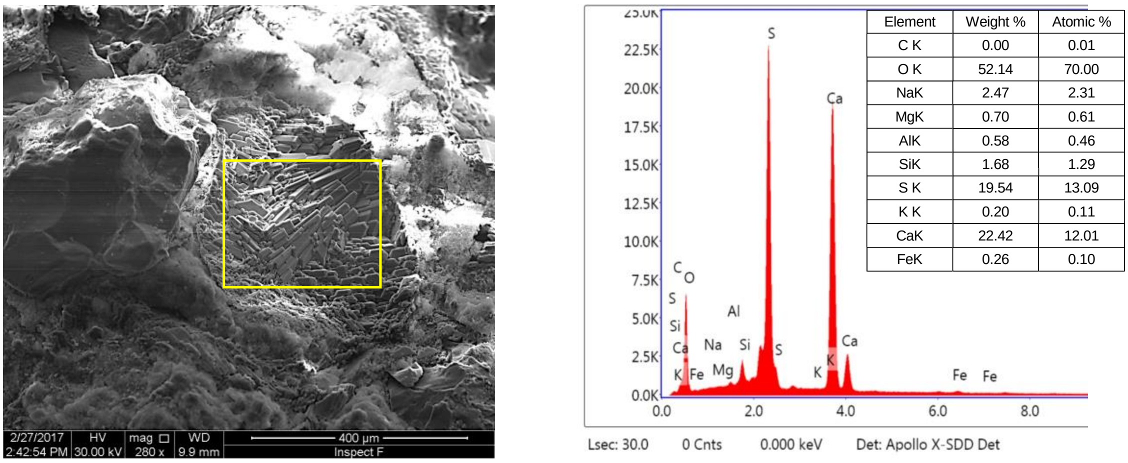

Element	Weight %	Atomic %
C K	0.00	0.01
O K	52.14	70.00
NaK	2.47	2.31
MgK	0.70	0.61
AlK	0.58	0.46
SiK	1.68	1.29
S K	19.54	13.09
K K	0.20	0.11
CaK	22.42	12.01
FeK	0.26	0.10

(a) Morphology of PC1 (left) and corresponding EDS (right) showing gypsum

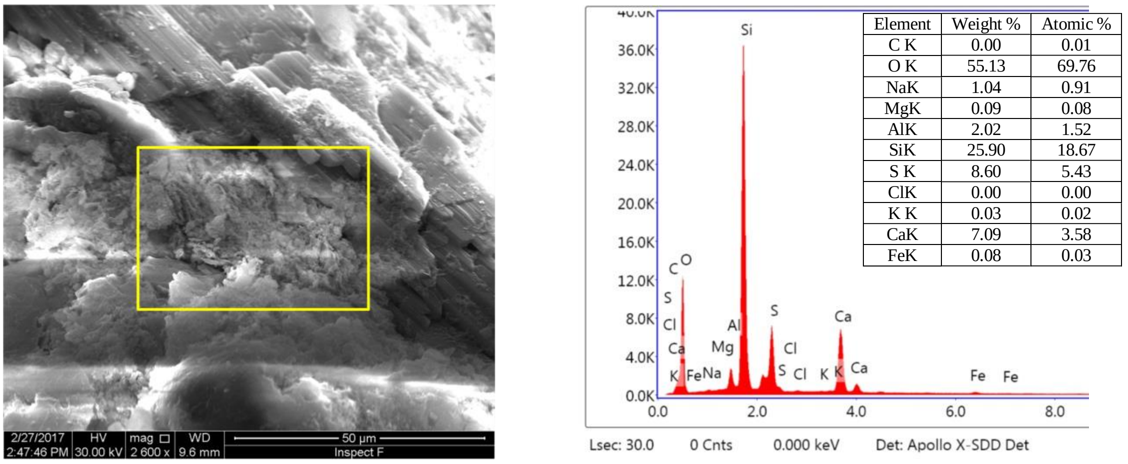

Element	Weight %	Atomic %
C K	0.00	0.01
O K	55.13	69.76
NaK	1.04	0.91
MgK	0.09	0.08
AlK	2.02	1.52
SiK	25.90	18.67
S K	8.60	5.43
ClK	0.00	0.00
K K	0.03	0.02
CaK	7.09	3.58
FeK	0.08	0.03

(b) Morphology of PC1 (left) and corresponding EDS (right) showing silica gel

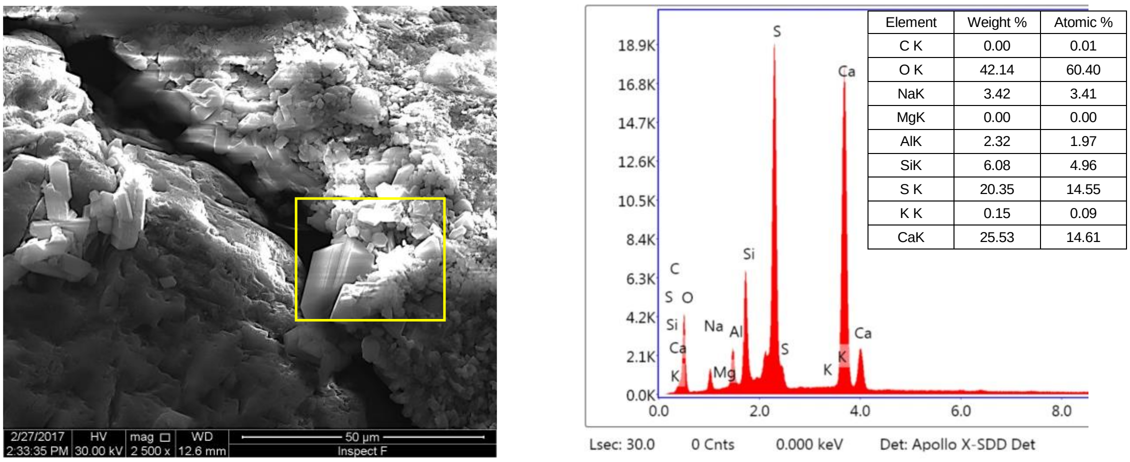

Element	Weight %	Atomic %
C K	0.00	0.01
O K	42.14	60.40
NaK	3.42	3.41
MgK	0.00	0.00
AlK	2.32	1.97
SiK	6.08	4.96
S K	20.35	14.55
K K	0.15	0.09
CaK	25.53	14.61

(c) Morphology of PC2 (left) and corresponding EDS (right) showing gypsum in the ITZ

Figure 4.5 SEM images of the samples from Nesapakkam sewage treatment plant

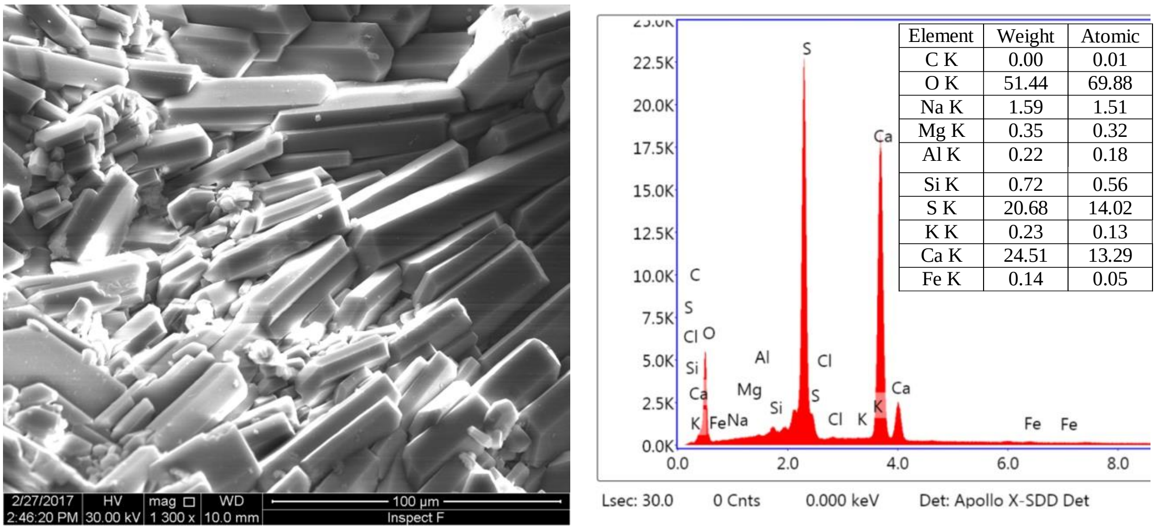

Element	Weight	Atomic
C K	0.00	0.01
O K	51.44	69.88
Na K	1.59	1.51
Mg K	0.35	0.32
Al K	0.22	0.18
Si K	0.72	0.56
S K	20.68	14.02
K K	0.23	0.13
Ca K	24.51	13.29
Fe K	0.14	0.05

a) Magnified image showing morphology of gypsum in PC1 sample

b) EDS of the area (left) showing gypsum

Figure 4.6 Morphology and EDS of gypsum present in sample collected from the primary clarifier of Nesapakkam sewage treatment plant

4.2.3.4 X-ray micro-tomography

X-ray CT imaging was done to understand the alteration in the microstructure and to view the macro porosity of the samples investigated. Figure 4.7(a) shows the top view, front view slice images and a 3D image of the samples collected from the screen and grit chamber (S/GC) of sewage treatment plant. The sample was found to be porous with macro voids identifiable from the images. More importantly, the paste was found to be very dark. The lower grayscale values of the pixels in the images suggest that the paste has been decalcified to a greater extent, comprising of silica gel. The 3D rendered image shows the outer surface that has degraded due to the combined action of abrasion due to the flowing sewage and the action of acids.

The sample collected from the primary clarifier (PC1) is shown in Figure 4.7(b). The slice images showed the microstructural zonation. An outer degraded layer and a relatively less deteriorated layer could be noted. The paste of outer layer appeared darker when compared to the inner layer. Macro voids were observed in these samples also. Traces of gypsum deposits (as a thin layer) could be noted from the front view slice image.

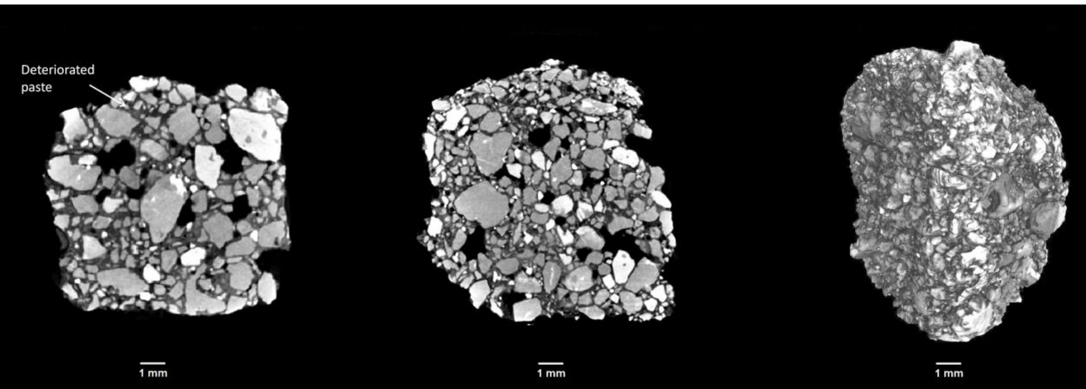

Top view Front view 3D image

(a) CT images of S/GC sample

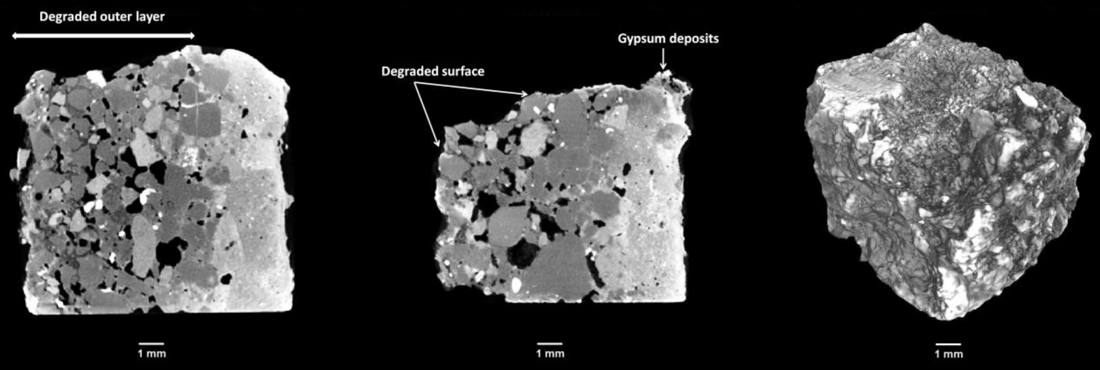

Top view Front view 3D image

(b) CT images of PC1 sample

Figure 4.7 X-ray CT images of samples collected from screen and grit chamber and primary clarifier

4.2.4 Summary – case study 1

The nature of deterioration of the concrete structures in a sewage treatment plant was investigated by using micro-analytical characterisation techniques. It can be ascertained that the primary cause of deterioration could be possibly due to the acids present in wastewater. The deterioration could also be due to the other aggressive chemicals present such as chlorides and sulphates. The X-ray diffraction study revealed the main reaction product to be gypsum and the microstructure was marked by the absence of Portlandite. The loss of Portlandite was attributable to the decalcification due to sulphuric acid to form gypsum. Also, the action of organic acids on Portlandite could cause its progressive dissolution to form soluble salts. The SEM images with EDS show gypsum bound with amorphous silica gel rich in aluminium. The porosimetry results showed higher intruded volume and porosity for all the samples, which indicate the deterioration in microstructure.

X-ray micro-tomography images also revealed the deteriorated microstructure of the samples collected, with severe deterioration in the samples collected from the screen and grit chamber. The observed porosity suggests that, in addition to the aggressiveness of the solutions, the continuous flow of sewage plays a major role in accelerating the attack.

4.3 CASE STUDY 2: DISTILLERY PLANT

4.3.1 Background and location details

Distillery spent wash is a highly polluting effluent from distillery industry and is generated from the fermentation of sugarcane based molasses to produce alcohol. Molasses based distilleries have a very high BOD and COD, rich in organic contents. The wastewater (effluent) generated from the distillation of fermented mash is known as spent wash. The spent wash has a temperature range of 70–80 °C, and is deep brown in color and acidic in nature (low pH about 4-5) with a high concentration of organic materials and solids (Mohana et al., 2009). On an average, 8–15 litres of spent wash effluent are generated for every litre of alcohol produced (Saha et al., 2005).

India has about 620 sugar mills and about 400 molasses based distilleries with an installed capacity of 400 billion litres of alcohol and a potential to generate, on an average, 40 billion litres of spent wash annually. If disposed untreated on land and in an uncontrolled manner, this toxic effluent may also be hazardous to vegetation and affect the ground water quality due to dissolved leachates and colour. The enormous quantity of effluents generated necessitates the storage for further treatment processes before its safe disposal as per the pollution control board regulations (Tewari et al., 2007; Pant and Adholeya, 2007). Often, these effluents are stored in large silos made with concrete. Concrete being highly alkaline due to the nature of its pore solution and chemical composition, is prone to damage by these chemically aggressive effluents. Anaerobic bacteria that thrive in these effluents consume the organic matter and produce a mixture of organic acids whose action on concrete can be highly detrimental (Larreur-Cayol et al., 2011a). The concrete deterioration due to acid attack in these aggressive environments is not well understood and needs further investigation.

A case study investigation was conducted in a molasses based distillery in Erode, Tamil Nadu, India wherein the concrete had shown deterioration due to the action of spent wash produced in the plant. The concrete tank which is used to store spent wash was seen to be experiencing premature deterioration; the resultant frequent repairs had huge cost implications for the plant. The objective of this study was to understand the nature of concrete deterioration caused by these effluents by employing a set of micro-analytical characterisation techniques. Concrete samples were collected from the deteriorated locations, just below the water level where the spent wash is stored and characterisation techniques were used to investigate the deterioration further.

4.3.2 Production of spent wash and its characteristics

Sugar is produced in the sugar mills from sugarcane. This process generates a viscous liquid by-product named molasses and leaves sugarcane based bagasse (residue after crushing of sugarcane) as an industrial waste. Molasses from sugar industry is taken to distillery industry for alcohol production. The production of alcohol involves the process of fermentation, which is followed by distillation, leaving the residual liquid waste as spent wash.

According to Mohana et al. (2009) and Saha et al. (2005), the production and the characteristics of the spent wash are highly variable. It depends upon the raw material properties and various aspects related to the production of ethanol. The spent wash is acidic, recalcitrant in nature, has an unpleasant obnoxious odour of burnt sugar, and has very high BOD and COD. It is also found to be rich in inorganic substances such as nitrogen, potassium, phosphates, calcium, and sulphates. The typical composition of distillery spent wash is shown in Table 4.2. The dark brown colour of spent wash is attributed to the thermal degradation of the reducing sugars and the presence of amino compounds. This is due to the formation of melanoidins and polyphenolic compounds/complexes. The formation of melanoidin is also largely responsible for the very high COD of the effluent.

Table 4.2 Typical composition of distillery spent wash (Mohana et al., 2009)

Parameters	Values	Parameters	Values
pH	3.0–4.5	Total dissolved solids (mg/L)	90,000–150,000
BOD (mg/L)	50,000–60,000	Chlorides (mg/L)	8000–8500
COD (mg/L)	110,000–190,000	Phenols (mg/L)	8000–10,000
Total solids (mg/L)	110,000–190,000	Sulphate (mg/L)	7500–9000
Total volatile solids (mg/L)	80,000–120,000	Phosphate (mg/L)	2500–2700
Total suspended solids (mg/L)	13,000–15,000	Total nitrogen (mg/L)	5000–7000

4.3.3 Sample collection

A large quantity of spent wash is generated by the molasses based distillery plant and stored in considerably large sized open tanks lined with concrete. Figure 4.8 shows the tank in which the spent wash in large quantity is stored for further treatment processes before its disposal to meet the environmental regulations. Concrete samples were collected using chisel and hammer from the severely deteriorated locations, just below the water level where the spent wash is stored. The aggressiveness of spent wash resulted in premature deterioration of concrete inside, demanding frequent maintenance and repair works. Samples for testing were collected before the repair work in the inside of the tanks was carried out. The photographs of the samples collected are shown in Figure 4.9.

Figure 4.8 Tank for storing spent wash in distillery plant

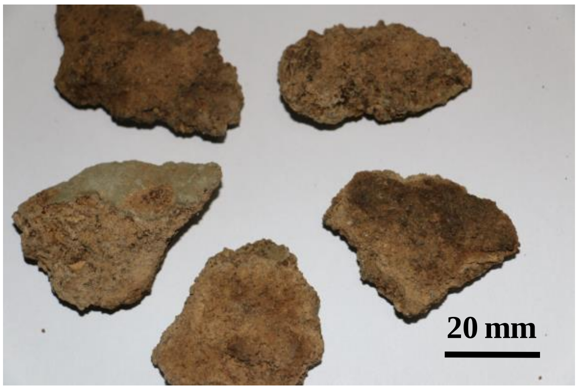

Figure 4.9 Deteriorated concrete samples collected from distillery plant

The samples appeared dark brown in colour due to the attack by spent wash and had pungent smell due to the ingress of spent wash into the concrete. The samples were found to be weak and relatively easy to chisel out. A set of micro-analytical characterisation techniques such as X-ray diffraction, scanning electron microscopy and

X-ray micro-tomography were then used to investigate the deterioration in detail and the results are discussed in the subsequent sections.

4.3.4 Micro-analytical characterisation of samples

4.3.4.1 X-ray diffraction

Two types of concrete samples were collected from the deteriorated locations of the tank wall. The sample collected from 0-5 mm from the surface was highly deteriorated, and is named as P_1 outer. Another sample was collected from approximately 5-10 mm from the surface and is named as P_1 inner. The X-ray diffractogram of the P_1 outer sample is shown in Figure 4.10(a). It can be seen from the diffractogram that the outer zone (0-5 mm) is mostly amorphous with a prominent amorphous silica band centered at 2θ of about 27°. The low pH of the spent wash resulted in severe decalcification of cementitious materials resulting in leaching and dissolution of crystalline hydrate phases in the outer zone. In the process, CSH gel and other hydrates containing Si and Al got converted to an amorphous gel rich in silica and alumina. Formation of silica gel and decalcification of Ca from hydrates increased the porosity of the matrix, thus having an impact also on the transport and mechanical properties.

As the spent wash is rich in sulphate and also contains sulphuric acid (added to the fermentation broth to adjust the pH), there could be additional phases formed due to its reaction with hydrates. The reaction of calcium bearing cement hydrates such as Portlandite, ettringite, CSH etc. with sulphuric acid led to formation of substantial quantity of gypsum. However, gypsum was found only at the depth of 0-5 mm from the surface due to the limited penetration of sulphuric acid and lower concentration of acid present in spent wash. Quartz peak was prominent in the diffractogram and this is mostly due to the unavoidable crushing of fine aggregates, which might be present during the preparation of sample for XRD analysis. Small quantity of calcite and hematite was also formed as secondary reaction products. Formation of calcite on the surface could be due to diffusion of carbon dioxide and subsequent reaction with Portlandite during the dry cycle when the tank was not in operation. It is interesting to note that hydrates such as ettringite, Portlandite and anhydrous phases such as alite and belite were totally absent in the outer zone. This confirms the aggressiveness of acids present in spent wash as the hydrates and anhydrous phases are finally converted to silica gel. The reaction of most of the organic acids (such as acetic acid) with the hydrates form calcium and aluminum salts which are soluble and leach to the outside solution, and are hence not detected in the diffractogram of the outer zone.

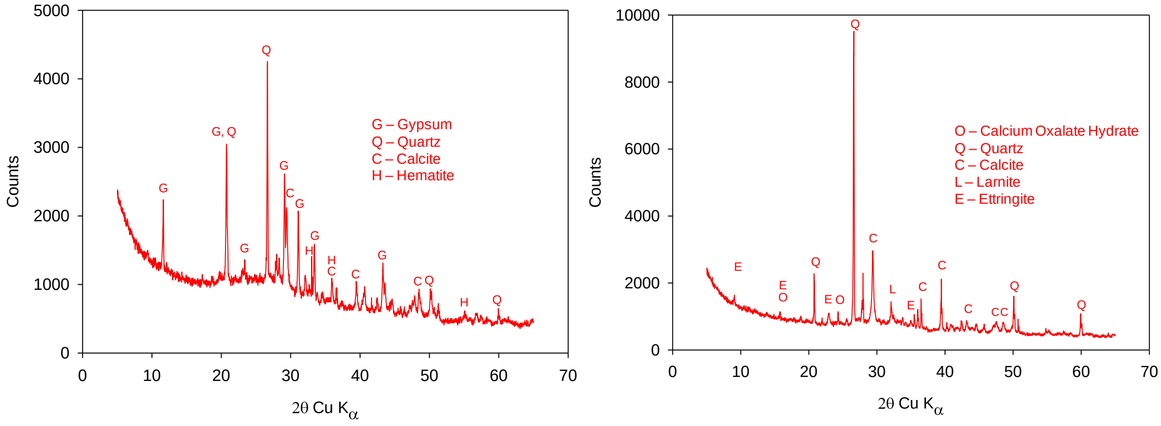

a) P_1 outer

b) P_1 inner

Figure 4.10 X-ray diffractogram of deteriorated concrete samples collected from distillery plant

The diffractogram of the sample P_1 inner is shown in Figure 4.10(b). Unlike the outer 5 mm, ettringite in small quantity is found to be stable in 5-10 mm zone. This could be due to the relatively higher pH at which ettringite is stable. Ettringite formation may be attributed to the combined sulphate and acid attack in which tricalcium aluminates are converted to ettringite. As the formation of gypsum was limited to the external surface, it was not observed in the 5-10 mm zone. The presence of quartz to some extent may be attributed to the crushing of fine aggregates at the time of sample preparation.

It was noted that the inner zone was less amorphous compared to the outer zone indicating less decalcification and degradation. Calcite was identified with its primary peak at 29.5°. A small quantity of anhydrous larnite (dicalcium silicate) was also observed in this zone. Oxalic acid present in spent wash could have reacted with various hydrates to form the salt, calcium oxalate hydrate, also known as Whewellite ($Ca(C_2O_4)H_2O$), which is less soluble and hence, traces of it were detected in the XRD pattern of P_1 inner sample. The precipitation of this salt could have a protective effect in limiting the progress of the reaction front as it could seal the porosity of the matrix to some extent, similar to gypsum in the case of lower concentrations of sulphuric acid. The other acids (primarily acetic acid) in the spent wash form soluble salts. Such salts leach into the solution and hence were not detected in the diffractogram. Overall, X-ray diffractograms suggest the fact that the deterioration is mainly due to combined action of a mixture of organic acids and sulphuric acid. The deterioration results in lixiviation of cementitious phases forming ettringite and gypsum in addition to a gel skeleton rich in silica and alumina, depending upon the depth from the surface.

4.3.4.2 Scanning electron microscopy

The degradation of concrete due to the action of various acids results in alteration in microstructure mainly due to the decalcification of calcium and aluminum bearing phases of hydrates. Electron micrographs were collected from the deteriorated regions in secondary electron mode. Figure 4.11(a) shows the morphology of the attacked surface (P_1 outer) at a magnification of 250x. The morphology presented in Figure 4.11(a) is typical of cementitious matrix that is decalcified by the action of acids. Loosely held particles along with aggregate phases (mainly quartz) were observed. In order to obtain more information about the reaction products formed, a magnified image (1000x) is taken in a void near to the aggregate phase and is shown in Figure 4.11(b). The major reaction products as confirmed by EDS results were observed to be gypsum and an amorphous gel rich in silica. These results were in line with the X-ray diffractograms obtained. Figure 4.12 shows the magnified image of the attacked surface showing the morphology of gypsum bound with silica gel.

The cement hydrates such as Portlandite, CSH, CASH, ettringite and calcium aluminates decalcify to form gypsum and a gel rich in alumina and silica on reaction with sulphuric acid present in spent wash. It is also observed that magnesium is also present in substantial quantities on attacked surface. The presence of magnesium points out the possibility that the concrete being tested may have had a binder admixed with slag at the time of construction because of its enhanced chemical resistance.

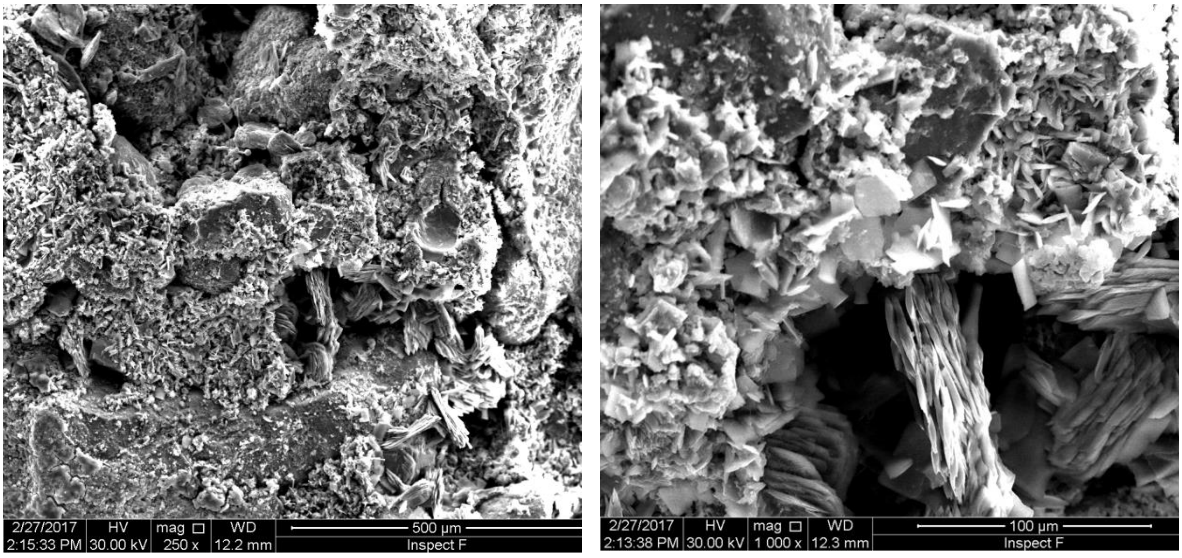

a) Morphology of acid interacted surface exhibits degradation

b) A close look at the acid interacted surface showing reaction products

Figure 4.11 Morphology of deteriorated samples collected from distillery plant

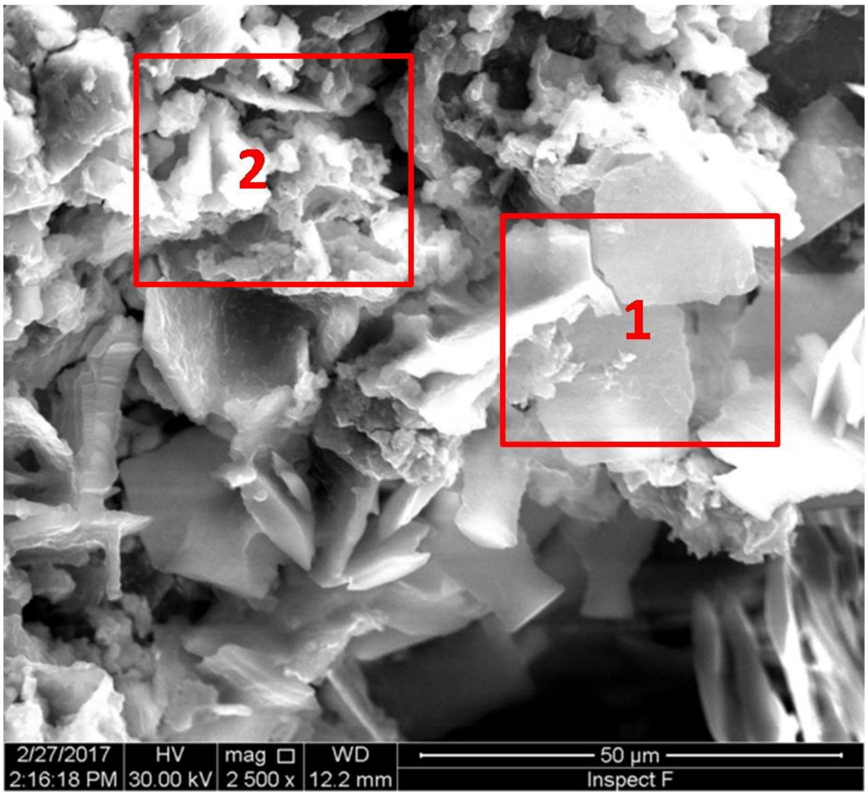

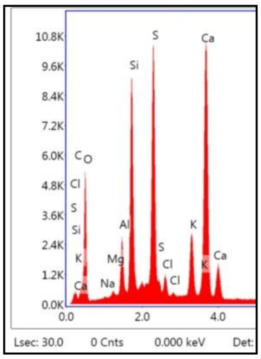

b) EDS of area 1

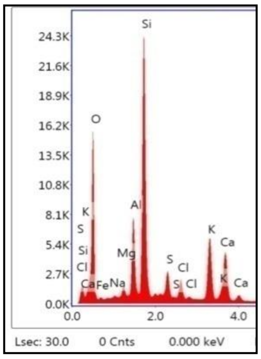

a) Secondary imaging showing the reaction products

c) EDS of area 2

Figure 4.12 A close look at the morphology of the attacked surface of the sample collected from distillery plant showing gypsum and silica gel

4.3.4.3 X-ray micro-tomography

Figure 4.13(a) shows the 3D rendered image of the sample collected from 0–5 mm from the surface (P_1 outer). The sample was found to be highly porous and weak. This was evident at the time of sample preparation for CT imaging. Mechanical and binding properties being lower, cubical shape was not obtained for the sample despite the use of high precision diamond saw cutting blade. The action of various organic acids on concrete resulted in dissolution of hydrates, especially Portlandite, on the surface and this led to the rough texture of the surfaces of specimens that is quite evident from the 3D rendered image. Figure 4.13(b) is obtained by performing suitable thresholding operation on the 3D reconstructed image using the software Volume Graphics (by moving the isobar line to the right) so that only highly dense particles in the matrix such as aggregates are visible in the 3D image. Siliceous aggregates are generally considered to be stable and inert to the attack by mild concentrations of various acids. From Figure 4.13(b), it can be inferred that the matrix is rich in aggregates. The 3D reconstructed image is processed further to get Figure 4.13(c), to highlight the various phases including the porosity. Coarse and fine aggregates appear light grey in colour due to higher density while porosity (voids) is seen as black in colour. The deteriorated paste phase appears as darker due to the decalcification of cement hydrates and associated reduction in density of the phases. It is seen only as a very thin layer around the aggregate phase. The high porosity of the samples is also clearly evident from Figure 4.13(c).

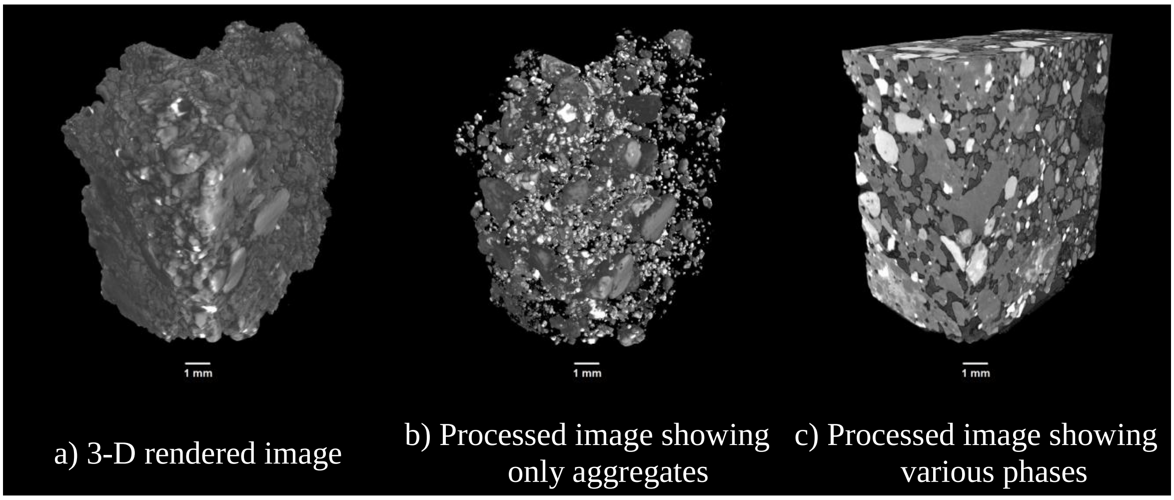

a) 3-D rendered image

b) Processed image showing only aggregates

c) Processed image showing various phases

Figure 4.13 X-ray CT images of P_1 outer sample

A stack of 2D slice images (top view and front view) were generated from the 3D reconstructed image. Figure 4.14(a) shows the top view slice image of the sample cut from 0-5 mm from the external surface (P_1 outer). It is evident that the deterioration is more pronounced at the exterior surface. The outer zone as depicted in Figure 4.14(a) appears very dark and this could be attributed to the severe decalcification of paste due to the attack of various acids forming silica gel, resulting in lower grayscale values of pixels in the 2D slice images. Sulphuric acid present in spent wash reacts with hydrates to form gypsum and is embedded in a gel skeleton rich in silica and alumina. Organic acids also react with hydrates to form calcium salts along with silica alumina gel. The formation of silica alumina gel results in dark appearance of paste in images. The specimen loses the binding ability due to the formation of this amorphous gel. Three mineralogical zones could be identified from the slice images; an outer zone which is severely degraded (zone 1), middle zone which has been decalcified (zone 2) and inner zone (zone 3) which is decalcified to a less extent (decalcification ongoing).

Conversion of hydrates to silica alumina gel results in reduction of volume and leads to formation of decalcification-related shrinkage cracks. These cracks around the aggregates are prominent in the slice images and this could have led to increased rate of deterioration due to further acid ingress towards inside. Some organic acids such as acetic acid present in spent wash form soluble salts on reaction with cement hydrates, which get leached away to the spent wash solution. This may be one of the reasons for the increased porosity of the specimen. The highly dense particles, which appear white in colour in slice images, could be ascribed to the possible use of aggregates containing limestone. The presence of limestone is ascertained from the calcite phase that is identified from the XRD analysis. The front view image of the specimen as shown in Figure 4.14(b) also confirms the very high porosity and cracking in the interfacial transition zones (ITZ) which could have led to the increased rate of degradation. It appears from the slice images that most of the pores are large in size and this could be possibly due to improper compaction done during the construction. Action of various acids along with the increased porosity has led to the rapid rate of degradation of the structure being investigated.

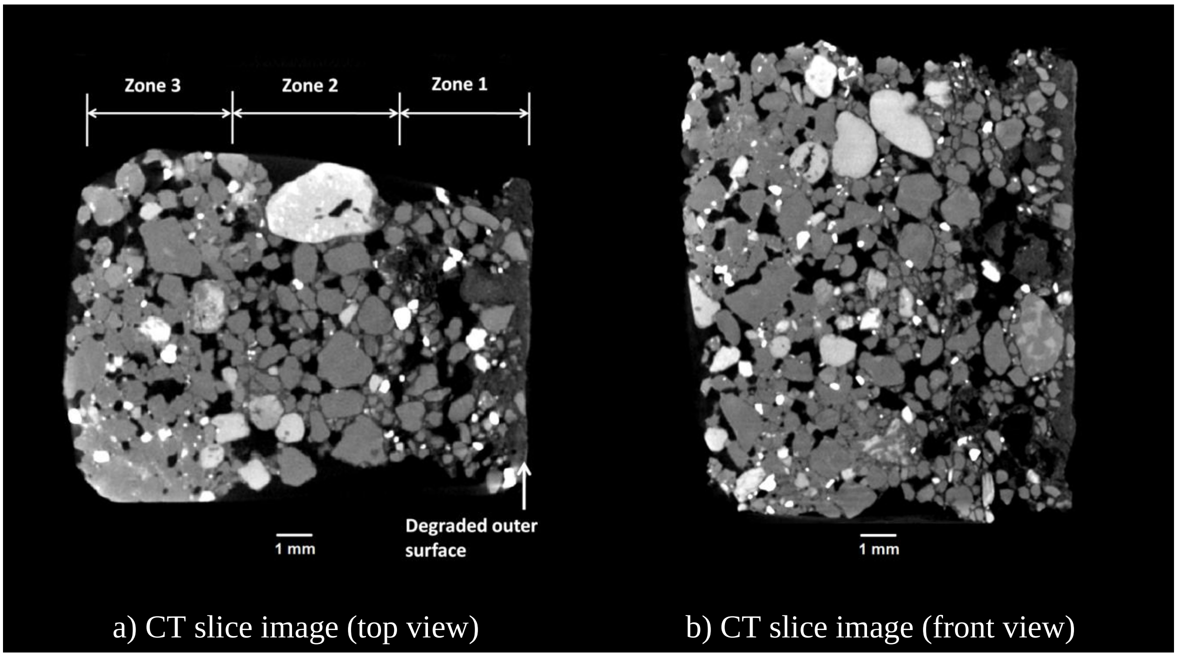

a) CT slice image (top view) b) CT slice image (front view)

Figure 4.14 X-ray CT images of P_1 outer sample showing deterioration

4.3.5 Summary – case study 2

The concrete deterioration due to the spent wash in molasses based distillery industry is investigated using micro-analytical characterisation techniques such as X-ray diffraction, scanning electron microscopy coupled with energy dispersive spectroscopy and X-ray computed micro-tomography. Distillery spent wash is a highly polluting effluent, rich in organic matter and the organic acids produced by anaerobic microorganisms thriving in these effluents along with sulphuric acid are highly detrimental to the cementitious matrix as they cause deterioration due to decalcification of hydrated products.

The alteration in microstructure due to decalcification results in mineralogical zonation. XRD results reveal that the outer zone (0-5 mm) has turned out to be mostly amorphous with a prominent amorphous silica band centered at 2θ of about 27°. The reaction of hydrates with sulphuric acid present in the spent wash led to gypsum formation in the 0-5 mm zone. A very small quantity of calcite and hematite was also formed as reaction products. It is observed that cement hydrates such as ettringite, Portlandite and anhydrous phases such as alite and belite are totally absent in the outer zone, which confirms the aggressiveness of the effluent. Unlike the outer 5 mm, ettringite in small quantity was found to be stable in 5-10 mm zone. This inner zone was found to be less amorphous compared to the outer zone, indicating less decalcification and degradation. Calcite was also identified with its primary peak at 29.5°. Traces of the less soluble salt, calcium oxalate hydrate ($Ca(C_2O_4)H_2O$) which is formed due to the reaction of oxalic acid with various hydrates were also detected in the diffractograms of the sample collected from 5-10 mm from the surface.

SEM and EDS results were found to be in line with the analysis results obtained based on XRD. The morphology of the acid interacted surface showed severe degradation. Loosely held particles comprising of silica gel along with aggregate phases (mainly quartz) are observed. The morphology of the attacked surface was typical of slag admixed concrete. Presence of magnesium in EDS results validates this conclusion that the concrete being tested might have been admixed with slag owing to its enhanced resistance to chemical attack. X-ray tomography images also revealed serious deterioration. The deteriorated paste appeared darker due to the decalcification of cement hydrates and associated reduction in density of the phases.

Sulphuric acid present in spent wash reacts with hydrates to form gypsum and is embedded in a gel skeleton rich in silica and alumina. Organic acids also react with hydrates to form calcium salts along with silica alumina gel. The formation of silica alumina gel results in dark appearance of paste in images. The specimen loses the binding ability due to the formation of this amorphous gel. Three mineralogical zones could be identified from the CT slice images; an outer zone which is severely degraded, middle zone which has been decalcified and inner zone which is decalcified to a less extent (decalcification ongoing). Some organic acids present in spent wash form soluble salts on reaction with cement hydrates that get leached away to the spent wash solution. This may be one of the reasons for the increased porosity of the specimens.

It is concluded that the severe and premature deterioration of concrete tanks in the sugar molasses based distillery industry is primarily due to the attack by various acids (sulphuric acid and organic acids) that are present in the spent wash. Calcium bearing hydrate phases are relatively not stable in these low pH aggressive acidic environments.

4.4 SUMMARY

Two case studies of concrete deterioration were presented; a case of sewage treatment plant and a molasses based distillery plant. The various micro-analytical characterisation tests such as X-ray diffraction, mercury intrusion porosimetry, scanning electron microscopy and X-ray micro-tomography were done in order to understand the deterioration in the samples collected. It can be inferred that the deteriorated concrete samples collected from both the industries has undergone severe decalcification, showing porous microstructure. Thus, it is imperative to develop and test new binders, which are resistant to these highly aggressive acidic environments. However, there are hardly any codes and standards available addressing the phenomenon. Accelerated laboratory test methods need to be developed which then can be used to test a variety of binders for their acid resistance. It is also important to study degradation kinetics and the mechanism of degradation of cement-based materials admixed with various binders. In this context, a detailed laboratory investigation was conducted on paste and mortar specimens made with common and special binder systems by developing accelerated immersion based test method. The kinetics and the mechanism of degradation of cementitious paste and mortar specimens exposed to various acidic solutions were studied and these results are discussed in the subsequent chapters.

CHAPTER 5

STUDY ON DEGRADATION KINETICS IN PASTE EXPOSED TO ACIDS

5.1 INTRODUCTION

This chapter deals with the laboratory investigations done on paste with various binders exposed to different acids. The first section presents the results of the continuous immersion test, which includes the parameters related to the kinetics of degradation. The results for common binder systems (OPC, FA30, BFS50, SF10) and special binder systems (HAC and LC2) are presented separately. The degradation kinetics is explained on the basis of mass changes, changes in pH of the acid solution, thickness changes and altered depth along with visual observations. An attempt was made to study acid attack using a dynamic test for accelerated degradation in paste and the kinetics was studied based on the visual observations, mass changes, and changes in pH of the acid solution.

5.2 VISUAL OBSERVATIONS – IMMERSION TEST

5.2.1 Common binder systems

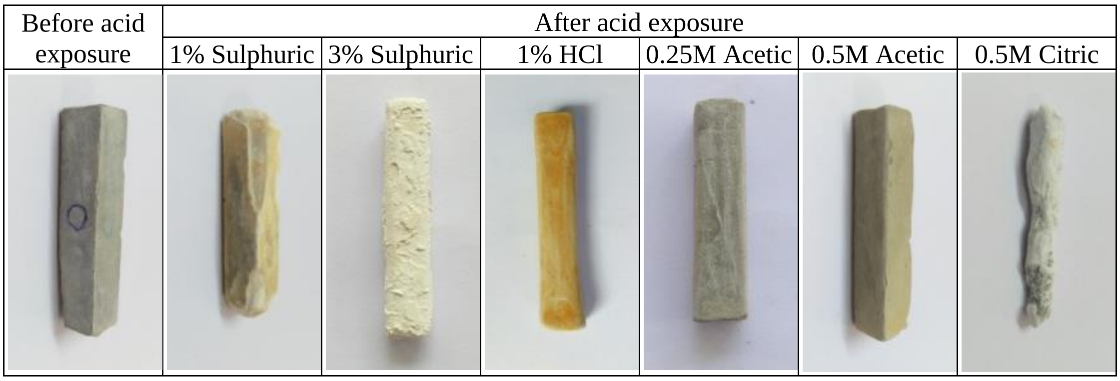

Figure 5.1 Aspect of OPC paste specimens before and after the acid exposure (B28)

The visual appearance of OPC specimens tested with periodic brushing (test method named B28) before and after the acid exposure (immersion test) is presented in Figure 5.1. The extent of degradation that could be visually examined can be linked essentially to the solubility of salts that are formed. The solubility of calcium and aluminium salts was presented earlier in Table 2.3. As indicated in Table 2.3, calcium sulphate salts formed due to sulphuric acid are sparingly soluble (2.4 g/L) and hence the salts precipitate on the specimen, once the solubility limit is reached in the solution. A white-yellow coloured precipitate (gypsum) was formed as a thin layer on the surface of the specimens on exposure to 1% sulphuric acid. It was soft in nature on prolonged exposure and could be removed due to brushing, especially at the edges (due to penetration from multiple directions). Hence, the degradation was more pronounced at the edges, similar to external sulphate attack. However, the gypsum formed on the lateral surfaces bound with silica and alumina gel was found to be adherent to the specimen and could not be easily removed despite brushing. Similar behaviour was noted for 3% sulphuric acid but the gypsum formed became soft on exposure and part of it was removed after the brushing.

Severe precipitation was observed in citric acid as the salts forming are almost insoluble (solubility of calcium salt is only 0.95 g/L). A white coloured salt was precipitated in substantial quantities on specimens immersed in 0.5M citric acid. X-ray diffraction study confirmed the salt as calcium citrate tetrahydrate ($Ca_3(C_6H_5O_7)_2.4H_2O$). Moreover, the salt formed was found to be loosely attached to the specimen and could be removed on prolonged exposure to the solution by itself and/or due to the periodic abrasive action.

As the calcium salts are soluble in the case of acetic and hydrochloric acid, the acid solution was found to be relatively clear with no precipitates of Ca salts. The specimens exposed to 1% HCl appeared to be shrunk and were orange-brown in colour. Even though a layer of degraded products was formed in the case of acetic acid, the degradation was not externally visible (for 0.25M and 0.5M concentrations of acid).

Similar observations were noted for the OPC specimen tested without the abrasive action (test method named WB28); the aspect of the OPC specimens is shown in Figure 5.2. The specimens made with other binders containing fly ash, slag and silica fume, exposed to the acids, were also similar in appearance to the OPC specimens, except to the fact that the degree of deterioration was different owing to the changes in the chemical composition of the hydrated matrix. The FA30, BFS50 and SF10 specimens after the acid exposure, tested with and without abrasive action are shown in Appendix A, Figures A-1 to A-6.

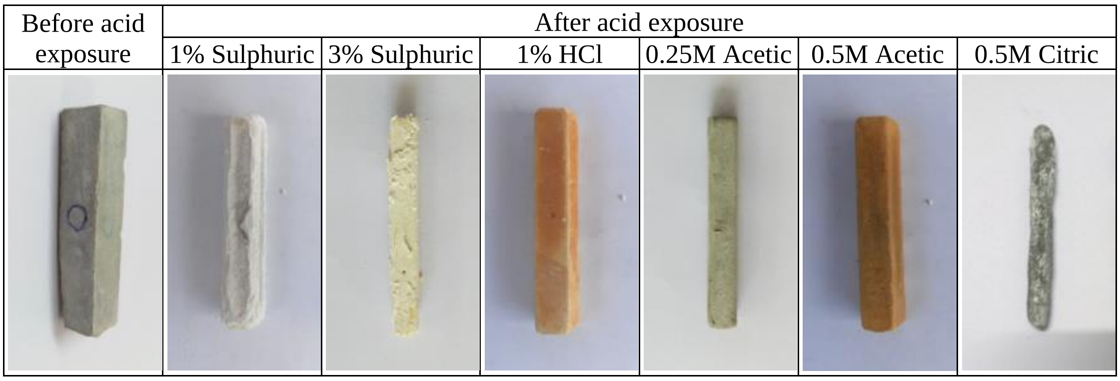

Figure 5.2 Aspect of OPC paste specimens before and after the acid exposure (WB28)

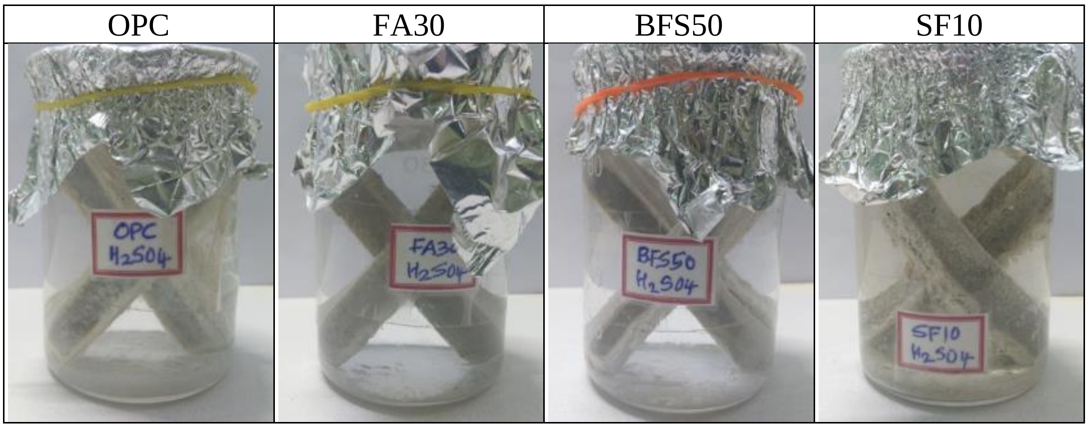

Figure 5.3 Acid solution and paste specimens exposed to 6 weeks of 1% sulphuric acid (WB28)

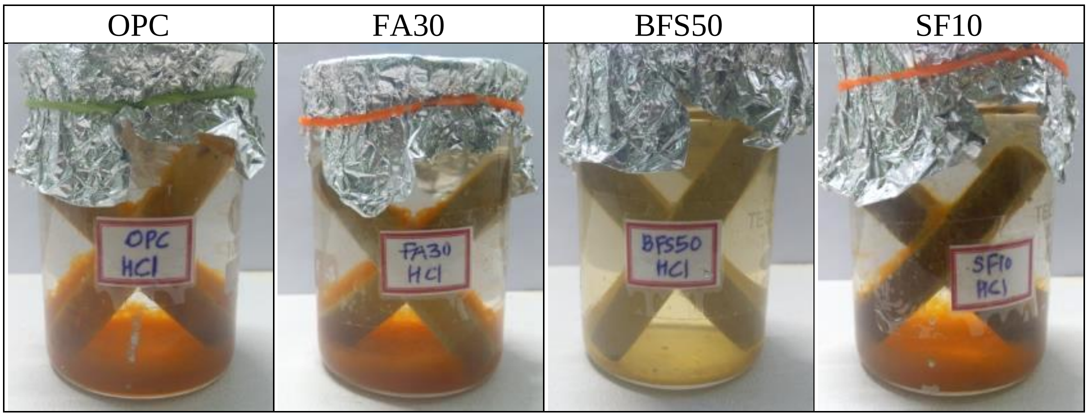

Figure 5.4 Acid solution and paste specimens exposed to 6 weeks of 1% hydrochloric acid (WB28)

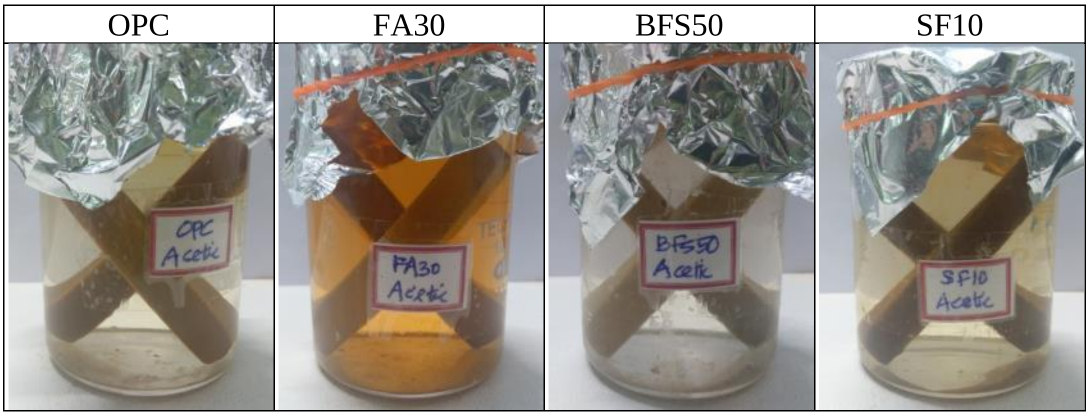

Figure 5.5 Acid solution and paste specimens exposed to 6 weeks of 0.5M acetic acid (WB28)

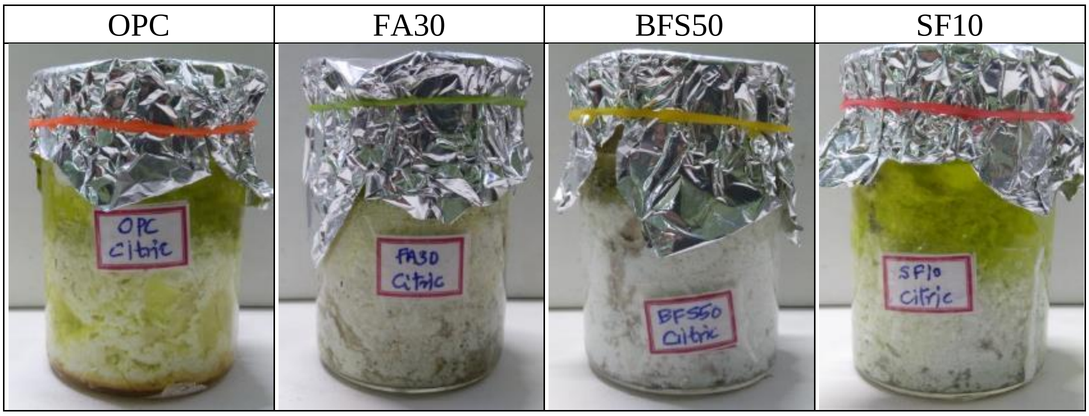

Figure 5.6 Acid solution and paste specimens exposed to 2 weeks of 0.5M citric acid (WB28)

Figures 5.3 to 5.6 show the acid exposure in progress. The sulphuric acid solution was found to be turbid due to the dissolution of gypsum in acid solution (Figure 5.3). A white coloured precipitate was formed on all the specimens exposed to sulphuric acid. The hydrochloric acid solution was found to be relatively clear. However, a brown coloured precipitate was observed on the bottom of the beakers, which could be possibly due to the dissolution of iron containing hydrates to form iron chloride/hydroxides (Figure 5.4). All the specimens appeared orange-brown in colour on acid exposure. The acetic acid solution was clear and no precipitates were observed on the specimens (Figure 5.5). Citric acid solution was found to be aggressive as the reactions with the cement matrix led to severe precipitation of salts (Figure 5.6). This behaviour was noted on all the mixes exposed to citric acid. As these salts are observed to be non-protective and loosely bound to the cement matrix, the precipitates got exfoliated from the specimen and were found to be deposited in the beakers.

5.2.2 Special binder systems

The paste specimens of LC2 and HAC before and after the acid exposure (immersion test without brushing) are shown in Figure 5.7 and Figure 5.8 respectively. The LC2 paste showed deterioration on exposure to sulphuric acid. The precipitation of gypsum was noted on the surface of the specimens. On exposure to 0.5M acetic acid, LC2 specimens showed extensive cracks on drying. Also, the specimens appeared darker in colour on exposure to acetic acid due to the decalcification. No salt precipitations were visually observed on HAC paste exposed to sulphuric acid. Instead, loss in thickness was noted. On exposure to acetic acid, HAC specimens showed no signs of deterioration on external appearance. However, the specimens broke on prolonged exposure to acetic acid by developing cracks. The visual observations of LC2 and HAC paste specimens before and after acid exposure, tested with brushing are given in Appendix A, Figures A-7 and A-8. The nature of degradation of specimens was found to be similar to the specimens tested without brushing.

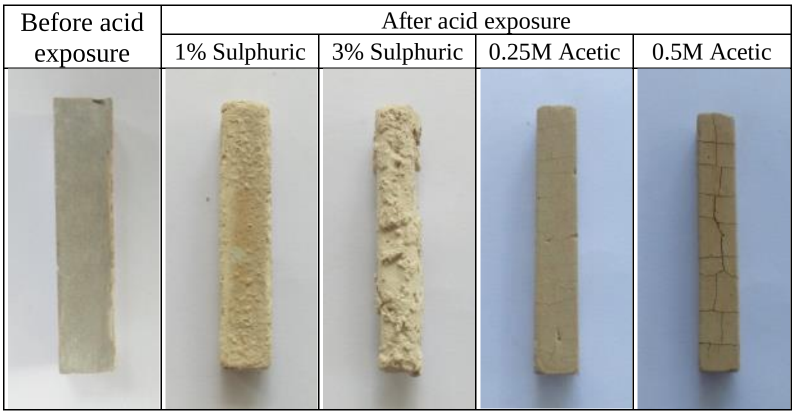

Figure 5.7 LC2 paste before and after acid exposure (without brushing)

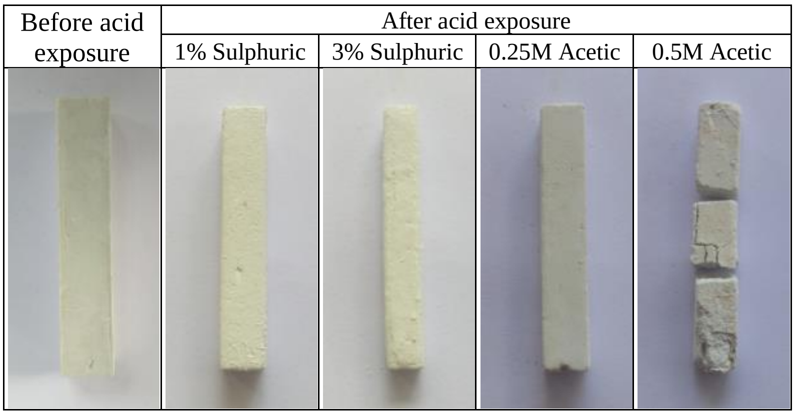

Figure 5.8 HAC paste before and after acid exposure (without brushing)

5.3 DEGRADATION KINETICS – IMMERSION TEST

The degradation kinetics of paste specimens were investigated by conducting immersion test. The kinetics of degradation was studied using parameters such as mass change of specimens, changes in pH of the acid solution, change in thickness of specimens, and altered depth. These results are discussed in the following sections.

5.3.1 Mass changes

5.3.1.1 Common binder systems

Mass change occurs due to alteration of certain phases to form new products. It is a direct measure of degradation. The mass changes were calculated with respect to the initial mass (before the acid exposure) on a weekly basis, just before the renewal of acid solution. A positive value for the mass change indicates mass gain whereas a negative value indicates mass loss. The mass changes of various common binder systems exposed to different acids are discussed below.

The mass changes of the various mixes on exposure to 1% sulphuric acid are shown in Figure 5.9. The specimens on exposure to 1% sulphuric acid had mass gain at early ages of exposure and started showing mass loss at prolonged exposure (at 4 weeks). The early mass gain is attributed to the formation of gypsum. Gypsum ($CaSO_4.2H_2O$) was precipitated as a white layer which binds together the insoluble residue in the gel layer (consisting of silica and alumina), creating a physical barrier on the surface of the paste, thus hindering the diffusion of ions involved in the reactions and slowing the attack rate (Gutberlet et al., 2015). The thickness of the gypsum layer increases until, at a certain thickness, the attack depends on the diffusion rate of the ions through this layer. In early days of exposure, it forms predominantly at the edges and then extends to cover the lateral surfaces of the specimen. This could have a protective effect on the degradation due to acid attack, thus resulting in lower mass loss when compared to the attack by other acids. In the case of no brushing, mixes OPC, FA30, BFS50 had considerable mass gain for an acid exposure of 6 weeks. However, SF10 specimens experienced mass loss on prolonged exposure. The gypsum formed in the specimen got delaminated, possibly due to destabilisation of gypsum and this led to loss of mass (0.69%) after 3 weeks.

Figure 5.9 (b) shows the mass changes of various mixes exposed to 1% sulphuric acid with periodic abrasive action in the form of brushing (B28). The abrasive action was found to accelerate the deterioration. The gypsum precipitated on the surface of the specimens could be removed due to the brushing action, thus exposing the relatively fresh surfaces to the acid. Hence, the mass loss for the specimens with brushing was found to be higher when compared to the testing without brushing. In the case of B28 specimens, OPC showed a higher mass loss of 7.13%. The performance of slag (BFS50) mix was found to be better when compared to FA30 and SF10. The gypsum formed on the slag specimens was found to be adherent to the matrix. Also, it was found to be covering the full lateral surface, thus creating a protective effect blocking the penetration of acid ingress further to the inside.

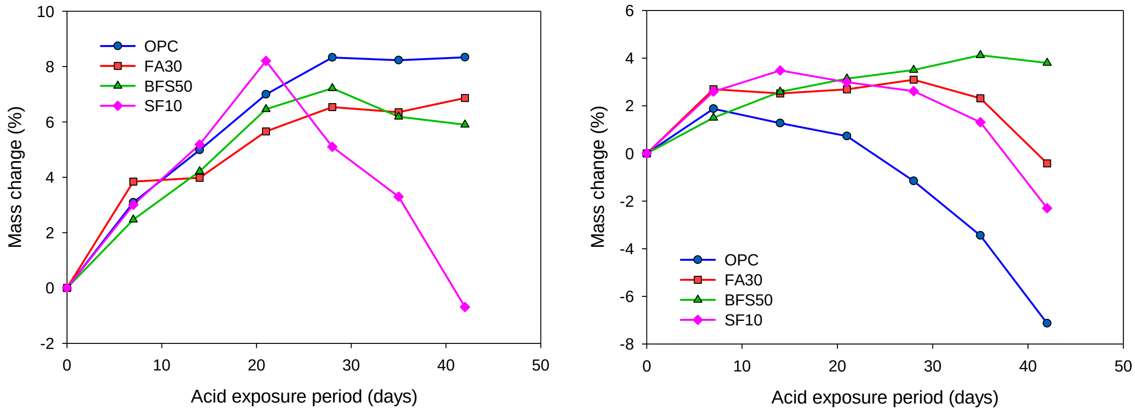

a) without brushing (WB28)

b) with brushing (B28)

Figure 5.9 Mass changes of paste on exposure to 1% sulphuric acid

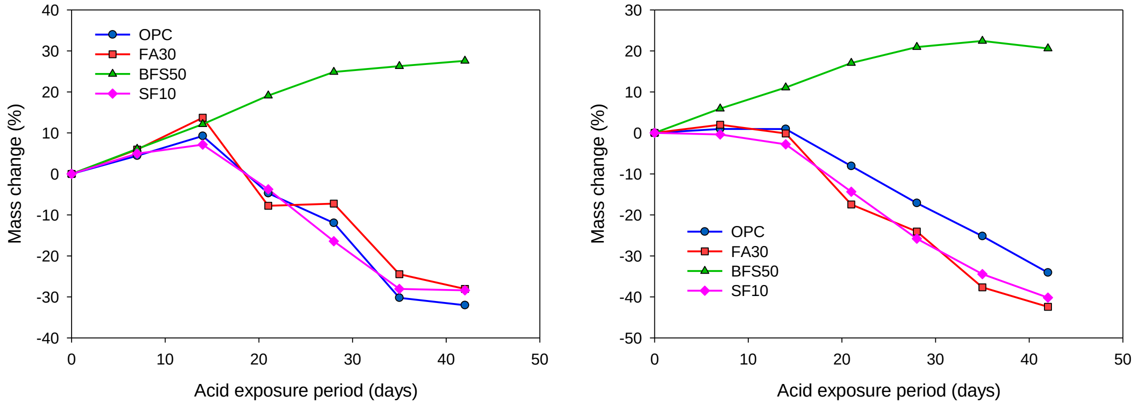

a) without brushing (WB28)

b) with brushing (B28)

Figure 5.10 Mass changes of paste on exposure to 3% sulphuric acid

Figure 5.10 shows the mass changes of various mixes exposed to 3% sulphuric acid. As the concentration is higher (pH = 0.51), the concentration gradient of acid ions between the solution and the external surface of the specimen is higher. This accelerates the kinetics of degradation. All mixes except slag showed mass loss. This is due the deterioration associated with the expansion of gypsum and subsequent exfoliation of the gypsum layer into the solution and/or due to the removal of the gypsum layer due to the brushing. The slag mix (BFS50) showed mass gain instead of mass loss even at 6 weeks of acid exposure. However, this considerable mass gain (27.6% for WB28 and 20.6% for B28) is associated with formation of thick layer of gypsum bound with silica gel rich in alumina. The enhanced adhesion of gypsum with the silica gel layer led to mass gain instead of mass loss for both cases, with and without brushing. The performance of mixes such as FA30 and SF10 was found to be comparable to the OPC mix at higher concentration of sulphuric acid (3%).

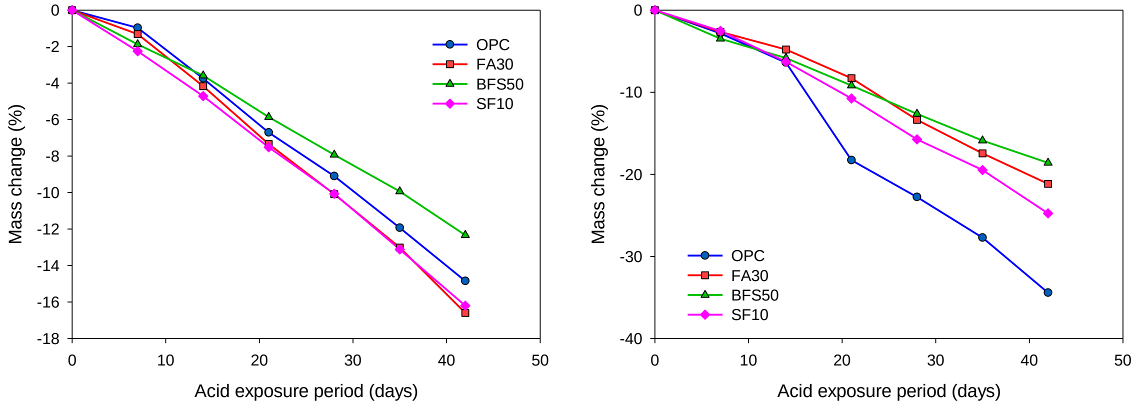

a) without brushing (WB28)

b) with brushing (B28)

Figure 5.11 Mass changes of paste on exposure to 1% hydrochloric acid

Figure 5.11 shows the mass changes of various mixes exposed to 1% hydrochloric acid. As the calcium and aluminium salts are highly soluble, no precipitates were observed on the specimens. Leaching was the driving process leading to the deterioration of the microstructure. The salts being soluble leach out into the solution leaving the inner matrix porous. Hence, all the specimens exposed to HCl showed mass loss at all ages. The mass loss was found to increase at a constant rate with the exposure period. In this case also, brushing accelerated the deterioration but the extent of acceleration was less when compared to sulphuric acid. The abrasive action was found to remove the weak corroded particles in the outer degraded layer, which comprises of a Si-Al gel. In both the cases, with and without brushing, the performance of slag was found to be better as the mass loss was less when compared to the other mixes. The lower mass loss in the slag system may be ascribed to the less availability of Portlandite in the system and increased alumina content adding to the stability of the corroded layer.

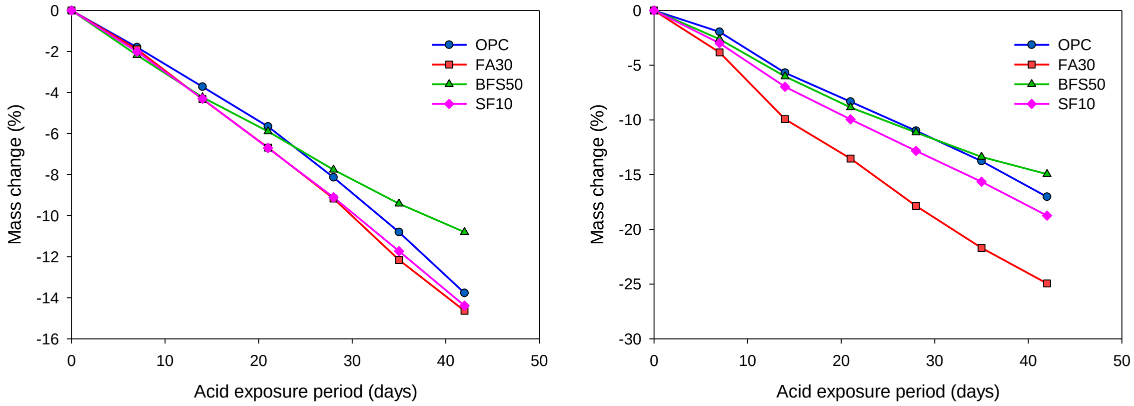

a) without brushing (WB28) b) with brushing (B28)

Figure 5.12 Mass changes of paste on exposure to 0.25M acetic acid

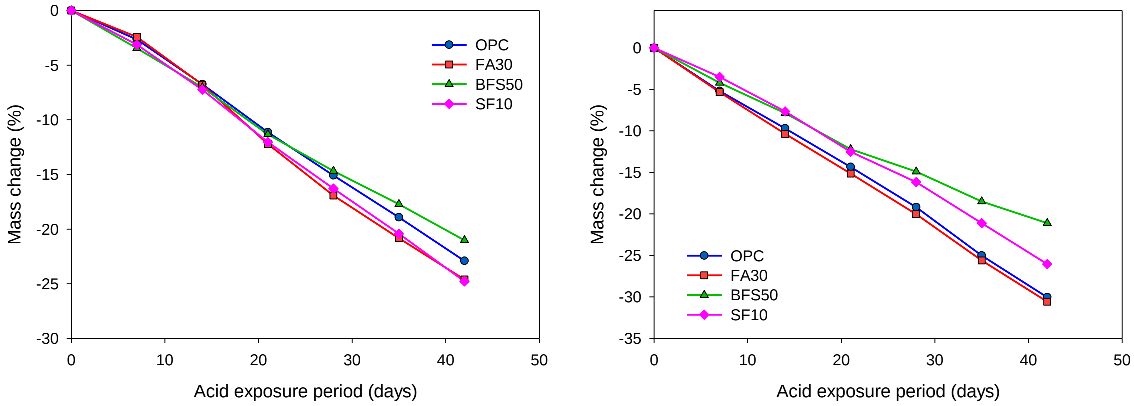

a) without brushing (WB28) b) with brushing (B28)

Figure 5.13 Mass changes of paste on exposure to 0.5M acetic acid

Acetic acid, although considered as a weak organic acid, was found to be aggressive to the cementitious medium leading to strong calcium leaching. The enhanced aggressiveness of acetic acid may be attributed to solubility of salt and the buffer action property exhibited by the acid (Koenig and Dehn, 2016). Mass loss was observed at all ages and was found to vary linearly with time of exposure. The variation of mass changes on exposure to 0.25M and 0.5M acetic acid are shown in Figures 5.12 and 5.13. The degradation kinetics was almost similar to 1% HCl for the concentration studied (0.5M). Similar to HCl, the kinetics got accelerated due to brushing but to a less extent compared to sulphuric acid. This could be due to the fact that the salts formed are soluble and hence they do not precipitate in the matrix, thus limiting the role of abrasion in accelerating the rate of degradation. The performance of slag was found to be better irrespective of the concentration of acid and the test method (WB28 or B28). Similar results depicting the improved performance of slag in acetic acid were reported by Bertron et al. (2004 and 2007). This points out to the hypothesis that the reduction in Portlandite content and the presence of more alumina in the hydrated products of BFS50 system led to the enhanced acid resistance. It is also noted that the kinetics of mixes such as OPC, FA30 and SF10 were similar and hardly distinguishable at lower concentration of acetic acid (0.25M). This justifies the need to investigate the acid attack by developing tests using higher concentrations of acid and/or the use of abrasive action. Despite the lower initial Ca content in FA30 mix, the performance of the mix was found to be the worst on exposure to 0.25M and 0.5M acetic acid. The depth of decalcification was found to be higher in the case of FA30 mix compared to the other mixes and this aspect is explained in the section 5.3.3 pertaining to the altered depth measurements based on X-ray tomography.

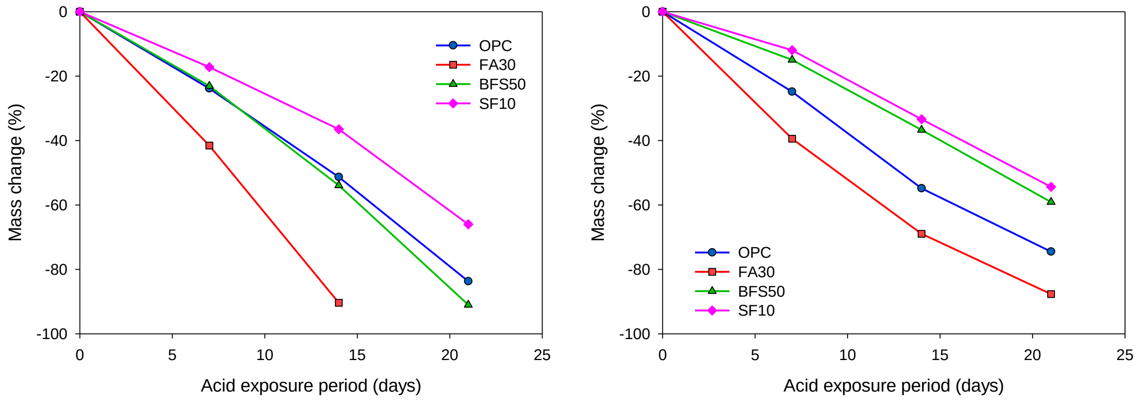

a) without brushing (WB28) b) with brushing (B28)

Figure 5.14 Mass changes of paste on exposure to 0.5M citric acid

Citric acid was the most aggressive among the acids, as it led to rapid mass loss (Figure 5.14). Hence, the degradation was stopped after three weeks of exposure. The aggressiveness may be ascribed to a combination of factors such as non-protective nature and high molar volume of the salt, poly acidic nature and buffer action exhibited by the acid and the high concentration (0.5M) being used (Bertron, 2013; Koenig and Dehn, 2016; Ramaswamy and Santhanam, 2016). Citric acid is polyacidic as it dissociates to give multiple protons at their respective pK_a values of 3.14, 4.76 and 6.40 and this could lead to a sustained attack, if the pH of the solution is in the range of pK_a values. The reaction of citric acid with the matrix led to severe precipitation of salts having very high molar volume (Larreur-Cayol et al., 2011a) and low affinity with the cement matrix. This makes the salt non-protective, defragmenting by itself from the matrix and getting deposited in the beakers.

Among the mixes studied, the performance of silica fume (SF10) was found to be better. Also, it is noted that the performance of mixes such as FA30 and BFS50 was not satisfactory as the mass loss was considerably higher. This behaviour may be attributed to the presence of more alumina in the cementitious system. Citric acid on dissociation could react with alumina forming complexes (Al and Ca cations form complexes with the conjugated bases (i.e. anions of acids)) that could increase the degradation kinetics (Bertron and Duchesne, 2013). According to De Windt et al. (2015), the strong chelating effect of citric acid may be the one of the main reasons to the very high aggressiveness of the acid. This is because; the formation of complexes can act as a pump for the Ca from the cement phases. Moreover, aluminium competes to form complexes with citrate ion, resulting in increased degradation (Dyer, 2016; De Windt et al., 2015). Hence, a system containing amorphous silica such as SF10 was found to improve the citric acid resistance. The role of abrasion was found to be minimal as the salt precipitated was exfoliated by itself and only a thin layer remained on the surface of the specimen.

To summarise the effect of type of acid, the variation of mass of OPC mix with age of exposure is presented in Figure 5.15. The immersion test with periodic abrasive action in the form of brushing accelerated the kinetics of degradation for all acids. The kinetics and aggressiveness of acids differ and the aggressiveness essentially depends on the solubility of salts formed. Also, factors such as concentration of acid, molar volume of salt, poly-acidity nature and buffer action of acid also influence the kinetics. At low concentration of sulphuric acid (1%), the gypsum formed acts as a protective coating, which limits the kinetics, at early ages. At higher concentration of sulphuric acid, gypsum is formed in enormous quantity and the expansive pressures exerted lead to cracking and mass loss. Acids such as acetic acid and hydrochloric acid form soluble salts that leach out to the solution, thus resulting in mass loss at all ages. The aggressiveness of citric acid could be attributed to the very low solubility of the calcium salt, polyacidic nature and complexolysis coupled with its non-protective nature due to the high molar volume and low affinity with the cementitious matrix. This leads to higher mass when compared to other acids for the concentrations studied.

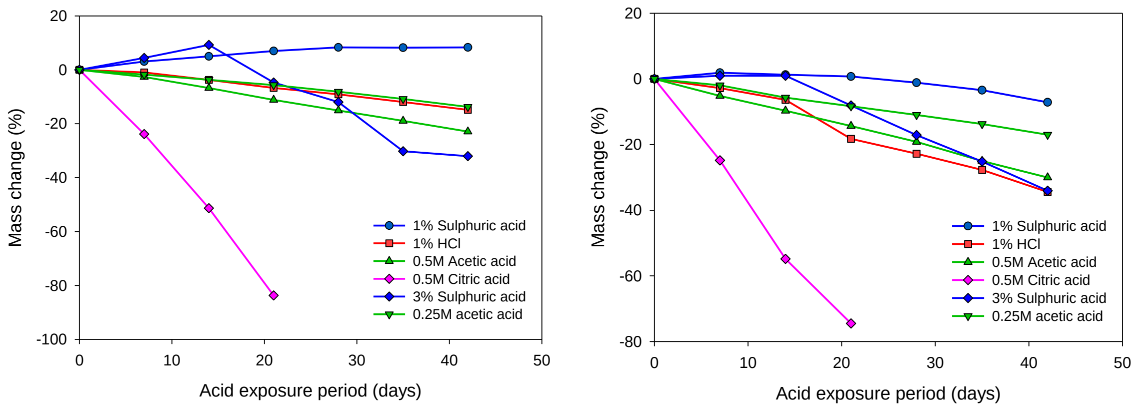

a) without brushing (WB28) b) with brushing (B28)

Figure 5.15 Variation of mass changes of OPC paste on exposure to various acids

Effect of concentration of acid on degradation kinetics

The concentration of acid is an important factor influencing the kinetics of degradation. As concentration of acid increases, more acid ions are available for the reaction. Also, the increased concentration gradient leads to more diffusion of acid ions to the inside of the specimen. Figures 5.16 and 5.17 show the effect of concentration of sulphuric and acetic acid on the mass changes of OPC specimens. It is evident that the kinetics of degradation increased to a significant extent on increasing the concentration of sulphuric acid from 1% to 3%. The variation of mass loss on exposure to acetic acid was found to be linear with age of exposure. Also, the mass loss was found to be directly proportional to the concentration of acetic acid. The mass loss observed for 0.5M acetic acid was almost double the mass loss observed for 0.25M acetic acid.

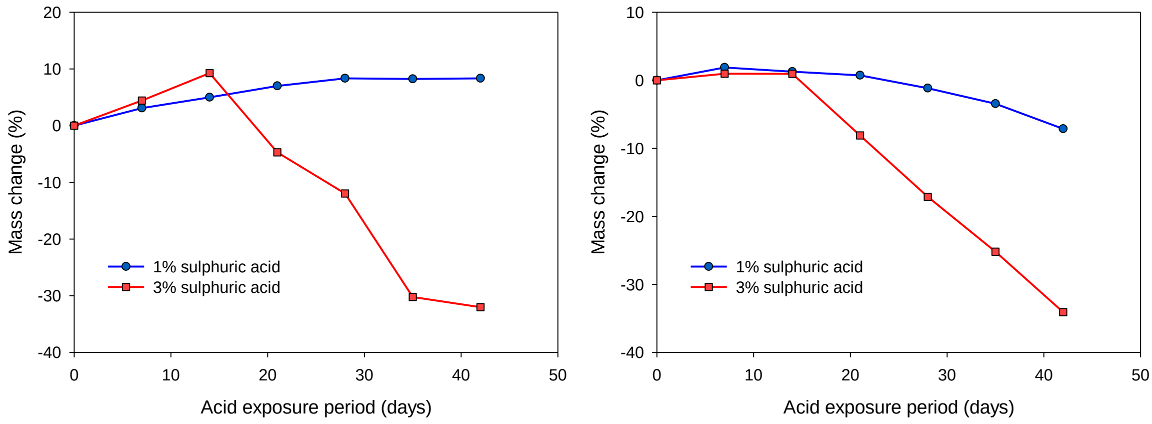

a) without brushing (WB28) b) with brushing (B28)

Figure 5.16 Effect of concentration of sulphuric acid on mass changes of OPC paste

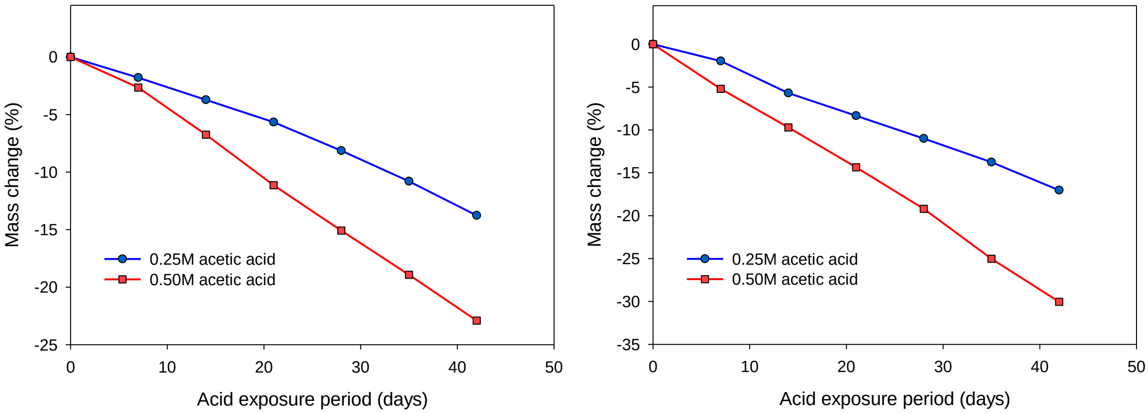

a) without brushing (WB28) b) with brushing (B28)

Figure 5.17 Effect of concentration of acetic acid on mass changes of OPC paste

Effect of abrasion and precipitation/leaching on degradation kinetics

Abrasive action in the form of periodic brushing is done for removing the weak corroded particles formed due to the reaction, thus accelerating the rate of degradation. Based on the mass data obtained in the B28 method (test with brushing), cumulative amount of mass precipitated/leached and abraded was calculated in terms of % of the initial mass of specimens before the exposure; the data for the exposure to various acids are presented in Figure 5.19 to 5.22. In the case of 1% sulphuric acid, the increase in mass of specimens (before brushing) of the current week compared to the mass (after brushing) of the previous observation was considered to be the amount of precipitate formation (gypsum). For all other acids, as leaching/acidolysis was prominent, mass of specimens reduces with exposure period and the decrement in mass (i.e. difference in mass of the specimen for the current week before brushing and the mass of the specimen after brushing of the previous week) was attributed as leached mass. This parameter involves any mass loss due to leaching of ions into the solution and any mass getting collected in the beakers due to detachment from the specimen. The abraded mass is indicative of the mass of the weak products that gets removed due to abrasive action and is calculated by taking the difference between the mass before and after brushing for the current week. The abraded mass is also an indicator of the stability of the corroded layer.

For better understanding, the variation of cumulative mass precipitated or leached and mass abraded is plotted as % of the initial mass of the specimen with the age of exposure for the OPC mix and is shown in Appendix A, Figures A-15 to A-17. If the cumulative abraded mass curve overtakes the cumulative mass precipitated, it indicates the onset of mass loss. In the case of leaching-dominant processes where a decrement of mass is observed with the age of exposure, cumulative mass abraded and cumulative mass leached are plotted to understand the contribution of leaching and abrasion on the degradation kinetics and this is shown in Figure 5.18. It is observed that leaching was the predominant contributor to mass loss for all the mixes. In the case of citric acid, the contribution of leaching was significantly higher when compared to abrasion for FA30 mix. This in turn led to more mass loss when compared to other mixes. However, leaching was found to be relatively less dominant in the case of SF10 mix on exposure to citric acid. A layer of white precipitate attached to the specimen could be removed by abrasion and the effect of abrasion was higher in the case of SF10 mix on exposure to citric acid. Another interesting observation is that, the contribution of abrasion was found to be lower for BFS50 for most of the acids. This suggests that the corroded layer in BFS50 is comparatively more stable due to the presence of alumina in the degraded layer.

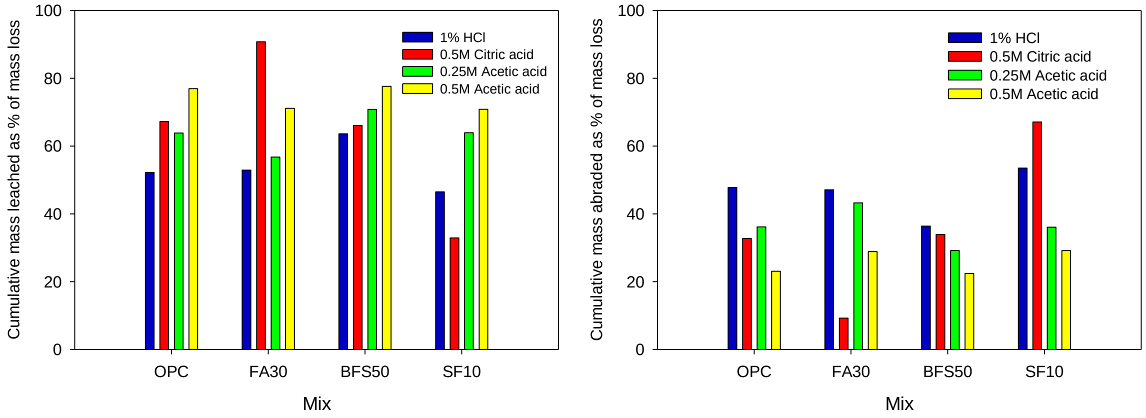

a) Cumulative mass leached

b) Cumulative mass abraded

Figure 5.18 Effect of leaching and abrasion on the mass loss of paste

The variation of cumulative mass precipitated and abraded of various paste mixes on exposure to 1% and 3% sulphuric acid is shown in Figures 5.19 and 5.20. On exposure to 1% sulphuric acid, more precipitates were formed in the case of SF10 and OPC mix. This could be due to the availability of more lime in the systems. The performance of silica fume in paste was not found to be effective. This could be possibly due to the silica fume particles (originally used in the densified form) not getting de-densified in the paste, causing the pozzolanic property of silica fume to be not utilised. Less precipitates were formed in the case of FA30 and BFS50 and this could be due to the surface-protective effect limiting the diffusion of acid ingress and hence the formation of more reaction products. Also, the abrasion resistance of the corroded layer was found to be more in the case of FA30 and BFS50 compared to OPC and SF10 mixes, as the cumulative mass abraded was found to be less compared to the OPC and SF10 (Figure 5.19(b)). This explains the reason partly for the enhanced resistance of FA30 and BFS50 against 1% sulphuric acid. However, the protective effect found in 1% sulphuric acid was not observed in 3% sulphuric acid for FA30 and BFS50 mixes. The amount of precipitates formed was found to be higher for BFS50 on exposure to 3% sulphuric acid. However, the gypsum formed was tightly bound to the matrix in BFS50 mix and this led to enhanced resistance against the abrasion of the corroded layer. The cumulative mass abraded in the case of other mixes was greater than the cumulative mass precipitated and hence resulted in mass loss even at the early ages of exposure to 3% sulphuric acid.

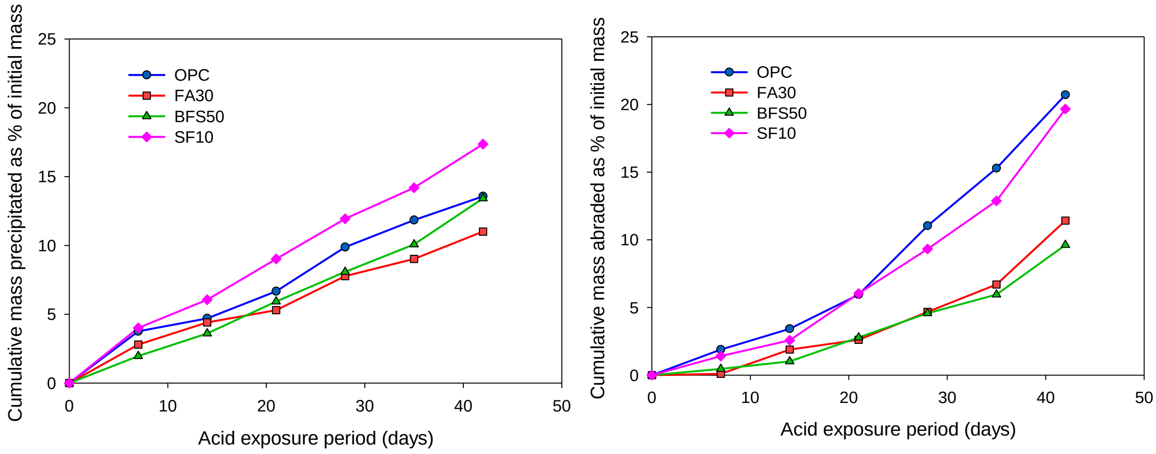

a) Cumulative mass precipitated

b) Cumulative mass abraded

Figure 5.19 Variation of cumulative mass precipitated and abraded of paste mixes on exposure to 1% sulphuric acid

The variations of cumulative mass leached and abraded of various paste mixes on exposure to 0.25M and 0.5M acetic acid are shown in Figures 5.21 and 5.22. The variation of mass leached was found to be linear for all the mixes studied. It is noted that the FA30 mix showed more leaching of mass when exposed to 0.25M and 0.5M acetic acid as compared to BFS50. Also, FA30 mix showed poor abrasion resistance as the mass abraded was found to be higher when compared to all the other mixes. The BFS50 mix showed good resistance against abrasion of the corroded layer for both 0.25M and 0.5M acetic acid (cumulative mass abraded being the least among the paste mixes, evident from Figure 5.21(b) and 5.22(b)). The variation of cumulative mass leached and abraded of paste mixes for 1% hydrochloric acid and 0.5M citric acid are shown in Appendix A (Figures A-18 and A-19).

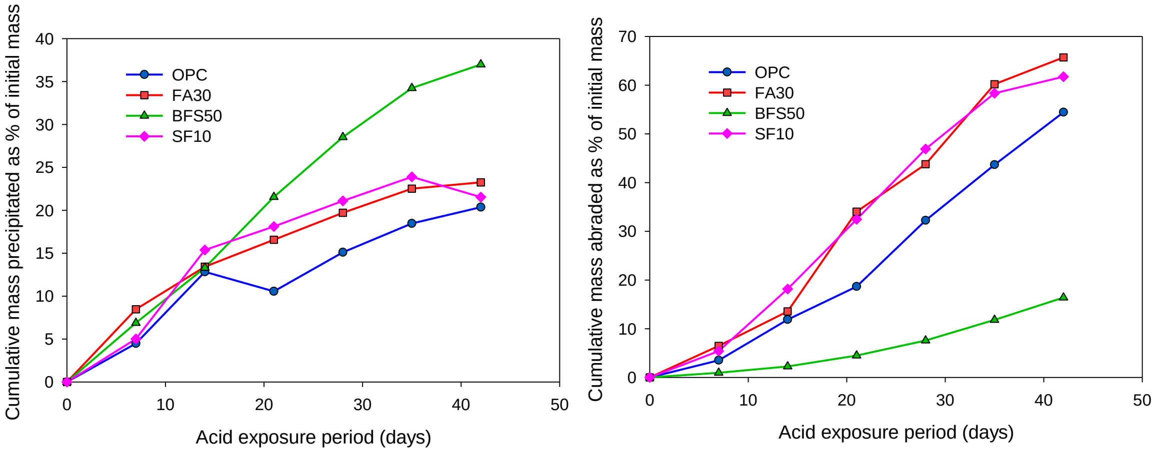

a) Cumulative mass precipitated b) Cumulative mass abraded

Figure 5.20 Variation of cumulative mass precipitated and abraded of paste mixes on exposure to 3% sulphuric acid

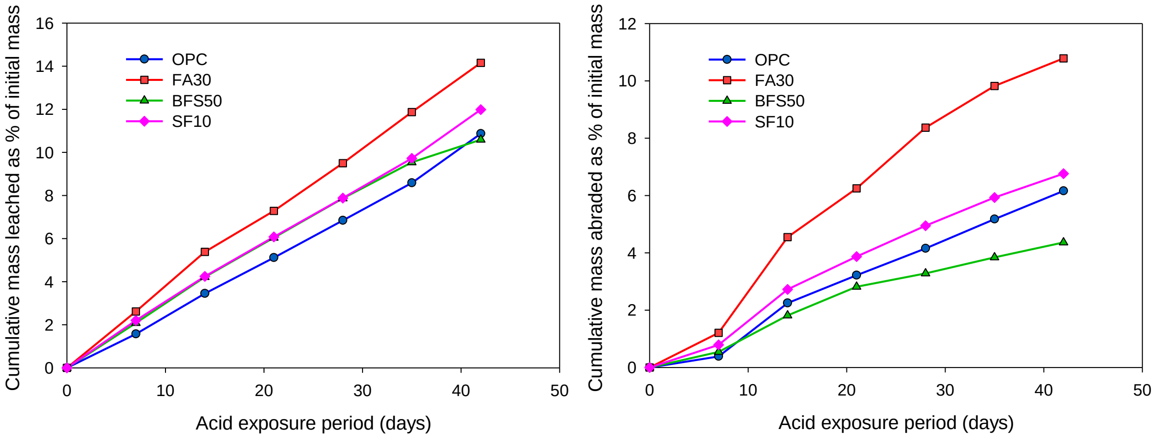

a) Cumulative mass leached b) Cumulative mass abraded

Figure 5.21 Variation of cumulative mass leached and abraded of paste mixes on exposure to 0.25M acetic acid

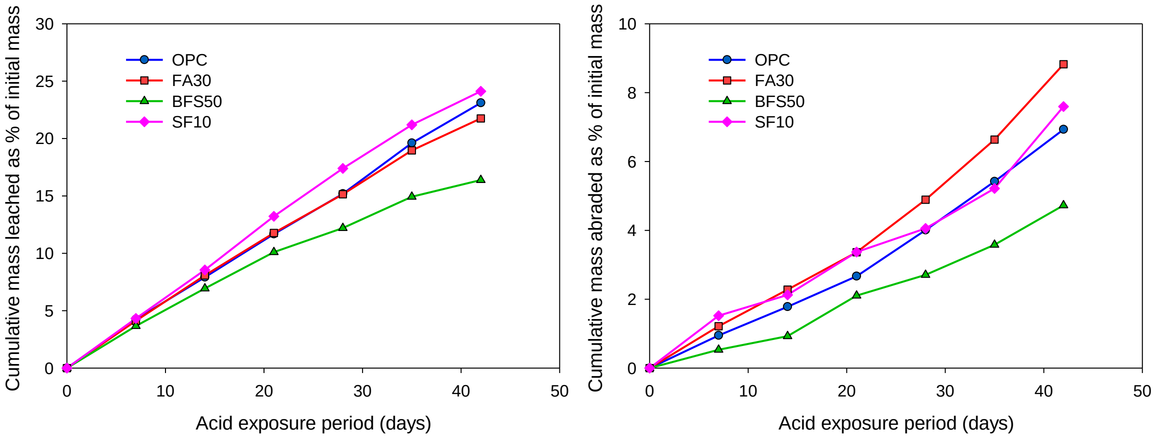

a) Cumulative mass leached b) Cumulative mass abraded

Figure 5.22 Variation of cumulative mass leached and abraded of paste mixes on exposure to 0.5M acetic acid

5.3.1.2 Special binder systems

The mass changes of LC2 and HAC paste were compared with the control mix containing OPC only. The LC2 paste showed mass gain for both tests with and without brushing, on exposure to 1% sulphuric acid (Figure 5.23). This could be due to the conversion of calcium bearing hydrates in LC2 system to gypsum. But the mass gain of LC2 paste was found to be lower than OPC. This could be due to reduced amount of precipitates formed and reduced availability of Portlandite in the LC2 binder system. The test results with brushing show that the performance of LC2 paste is better than OPC and HAC. Contrary to the behaviour of OPC and LC2 paste, no mass gain was observed for HAC paste (for the tests with and without brushing). Instead, mass loss was observed for HAC paste on exposure to sulphuric acid. This could be due to changes in the hydration products in the HAC system (marked by the absence of Portlandite and formation of calcium aluminate phases).

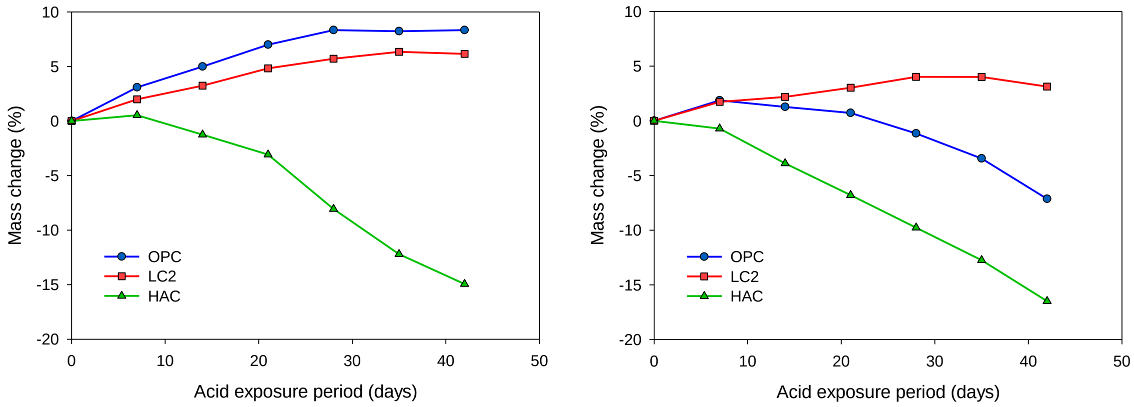

a) without brushing b) with brushing

Figure 5.23 Mass changes of LC2 and HAC paste on exposure to 1% sulphuric acid

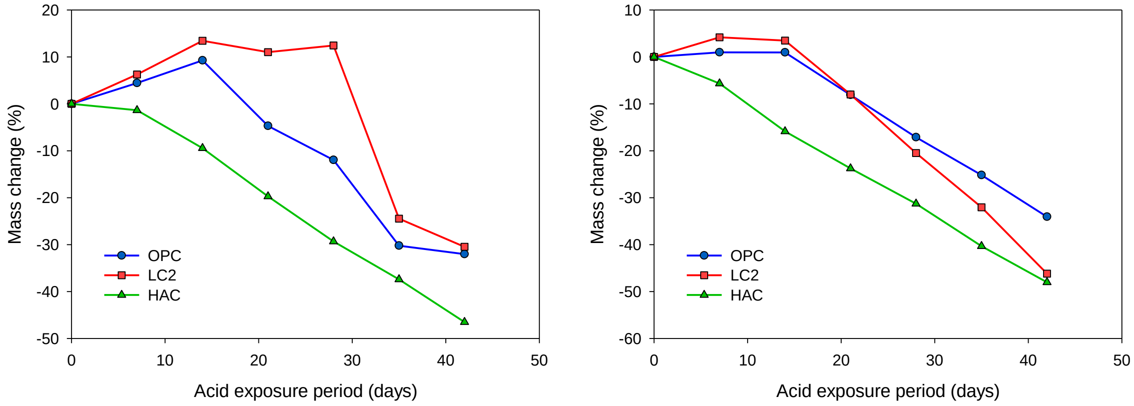

a) without brushing b) with brushing

Figure 5.24 Mass changes of LC2 and HAC paste on exposure to 3% sulphuric acid

On exposure to 3% sulphuric acid, all the mixes had severe mass loss on prolonged exposure. The HAC paste performed poorly as the mass loss was found to be higher compared to the OPC and LC2 paste (Figure 5.24). Unlike the OPC and LC2 paste wherein mass loss was due to the expansion related damage due to formation of gypsum, HAC paste suffered mass loss without the formation of insoluble salts in large quantities. It is also noted that the improved performance of LC2 paste evident in 1% sulphuric acid was not observed at higher concentration of 3%.

The performance of LC2 paste was comparable to fly ash paste for 3% sulphuric acid. In the case of tests with brushing, the LC2 mix had higher mass loss compared to OPC. This higher mass loss could be associated with the lower permeability, early age pore refinement and lower Ca/Si of the CSH gel in the case of LC2 paste. Also, the pozzolanic reaction of LC2 might have consumed the free lime thus exposing the CSH gel to be directly attacked by the acid solution. The lower the permeability, higher could be the expansive pressure exerted by the gypsum that crystallises inside the pores leading to cracking and mass loss.

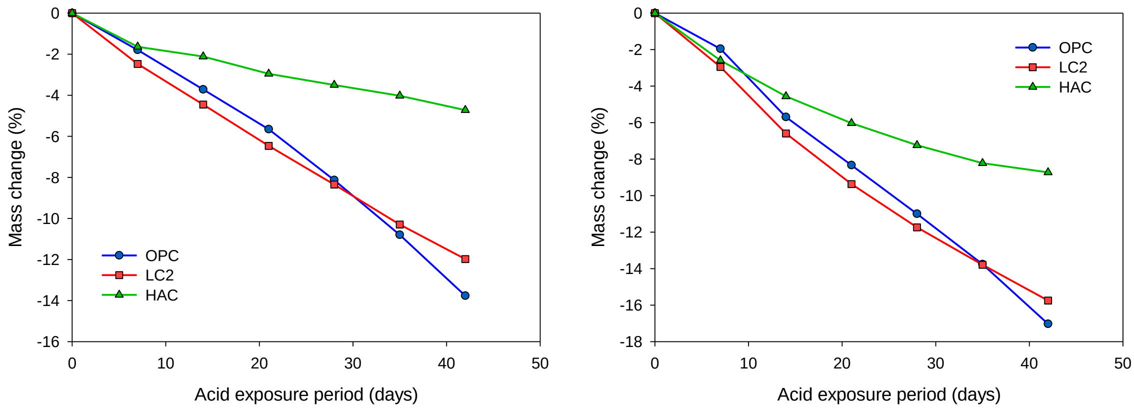

a) without brushing b) with brushing

Figure 5.25 Mass changes of LC2 and HAC paste on exposure to 0.25M acetic acid

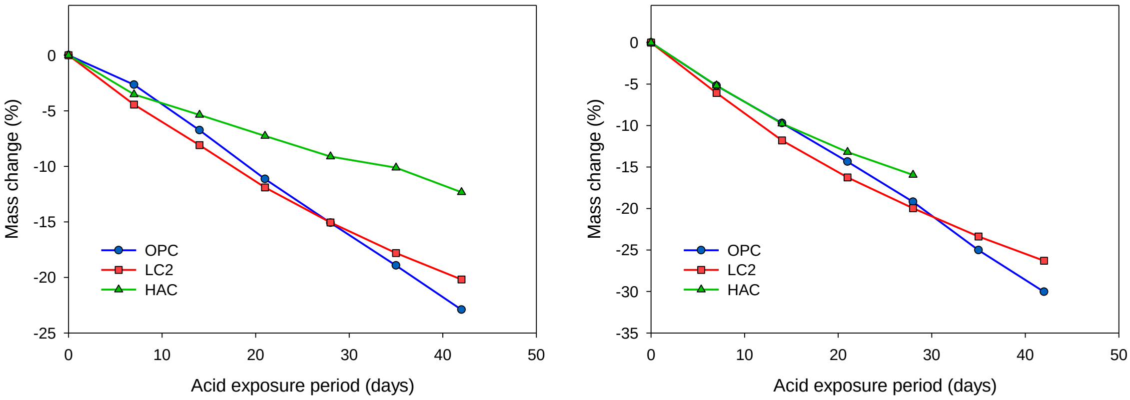

a) without brushing b) with brushing

Figure 5.26 Mass changes of LC2 and HAC paste on exposure to 0.5M acetic acid

On exposure to acetic acid, the HAC mix showed better performance as mass loss was found to be less when compared to the OPC and LC2 pastes. The mass loss of LC2 was only comparable to OPC on exposure to 0.25M acetic acid (for test with and without brushing) as shown in Figure 5.25. The mass loss trends for OPC and LC2 in 0.5M acetic acid were similar to 0.25M acetic acid except the fact that the kinetics are almost doubled compared to 0.25M acetic acid. Even though it can be seen that the HAC paste had less mass loss at 0.5M acetic acid, the specimens became weak and brittle on prolonged exposure to acetic acid. According to Dyer (2017), the acid resistance (in terms of mass loss) of HAC paste could be attributed to the enhanced neutralisation capacity of HAC on exposure to acetic acid. The mechanical properties reduced considerably (for smaller sized specimens of 10 × 10 × 60 mm) and led to fracture of specimens (at 28 days of exposure) in multiple locations for the tests with brushing (Figure 5.26).

Figures 5.27 and 5.28 show the effect of concentration of acid on the mass changes of LC2 paste and HAC paste respectively. A significant increase in the degradation kinetics was observed in the case of sulphuric acid when the concentration was varied from 1% to 3% for both the pastes. In the case of acetic acid, the variation of mass loss was found to be linear and the behaviour was similar to the other SCM pastes such as FA30 and BFS50. The abrasive action was found to increase the kinetics of LC2 paste in the case of sulphuric acid and its effect was found to be minimal in the case of acetic acid. These observations were consistent with the observations of the paste made with common binders. The effect of abrasion was also less pronounced in the case of HAC paste as there was no formation of insoluble precipitates in the matrix (Figure 5.28).

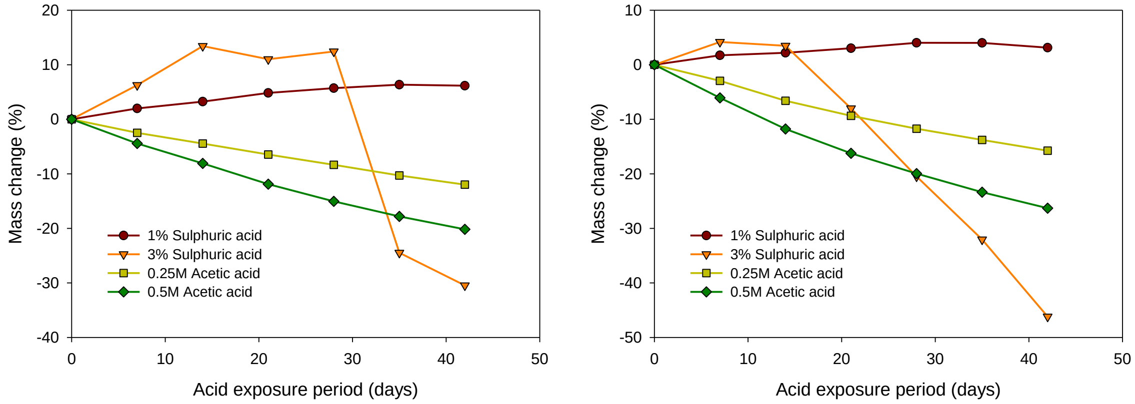

a) without brushing b) with brushing

Figure 5.27 Effect of concentration of acid on mass changes of LC2 paste on exposure to sulphuric and acetic acid

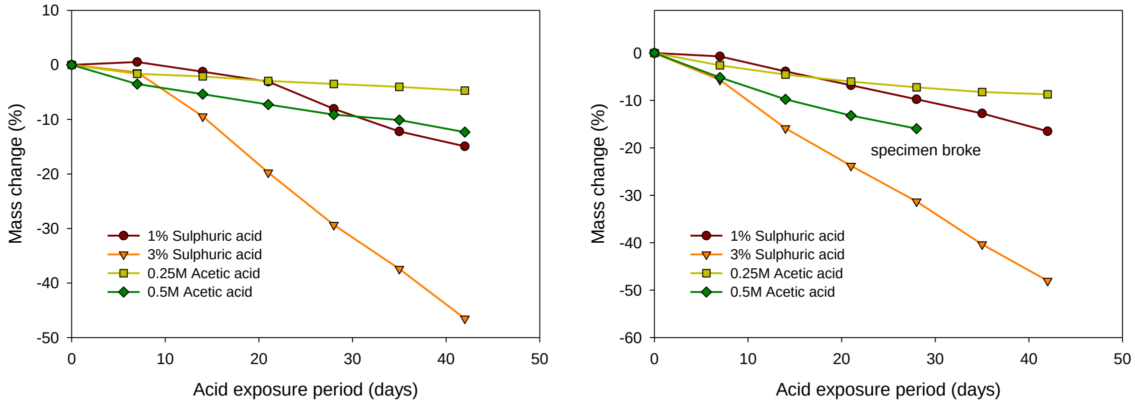

a) without brushing b) with brushing

Figure 5.28 Effect of concentration of acid on mass changes of HAC paste on exposure to sulphuric and acetic acid

Additional analysis was done based on the mass data collected for the tests with brushing in order to get a better understanding of the kinetics. It can be seen that the effect of leaching was much higher when compared to the effect of abrasion for both LC2 and HAC pastes on exposure to acetic acid (Figure 5.29). Among the mixes, the effect of leaching for HAC paste was found to be comparatively less when compared to the OPC and LC2 pastes and the effect of abrasion was found to be more for HAC paste when compared to the OPC and LC2 pastes. Also, it is seen that, as the concentration of acetic acid was increased from 0.25M to 0.5M, the effect of leaching increased and the effect of abrasion was found to decrease for all the paste mixes. In the case of 1% sulphuric acid, OPC had more precipitate formation when compared to LC2 (Figure 5.30). Hence, the effect of abrasion was also found to be higher for OPC as the layer of soft gypsum could be removed on abrasive action. It can also be noted that the cumulative mass precipitated in HAC paste is negative. This indicates that there is no formation of insoluble precipitates on the specimen unlike the case of OPC and other SCM pastes. In the case of 3% sulphuric acid, the LC2 paste experienced considerable mass gain due to the formation of gypsum and hence, the effect of abrasion was also found to be higher when compared to OPC paste (Figure 5.31). This explains the higher mass loss for LC2 paste in 3% sulphuric acid. In the case of 0.25M acetic acid, the cumulative mass leached in terms of % of the initial mass was found to be less for HAC paste and the trends were comparable for OPC and LC2 (Figure 5.32). On exposure to 0.5M acetic acid, the cumulative mass abraded (as % of the initial mass) was found to be higher for HAC paste when compared to the OPC and LC2 (Figure 5.33). The specimen thickness of HAC paste reduced and the specimens broke on prolonged exposure to 0.5M acetic acid.

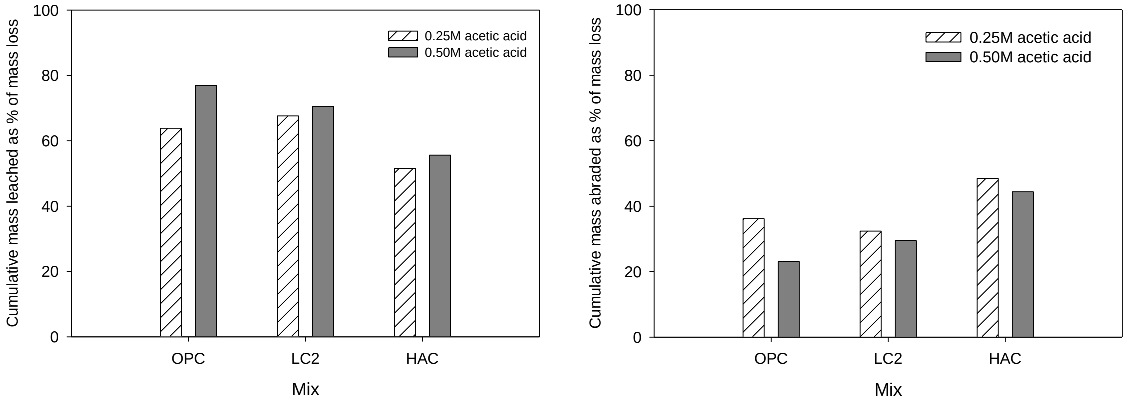

a) Cumulative mass leached b) Cumulative mass abraded

Figure 5.29 Effect of leaching and abrasion on degradation kinetics of LC2 and HAC paste mixes on exposure to acetic acid

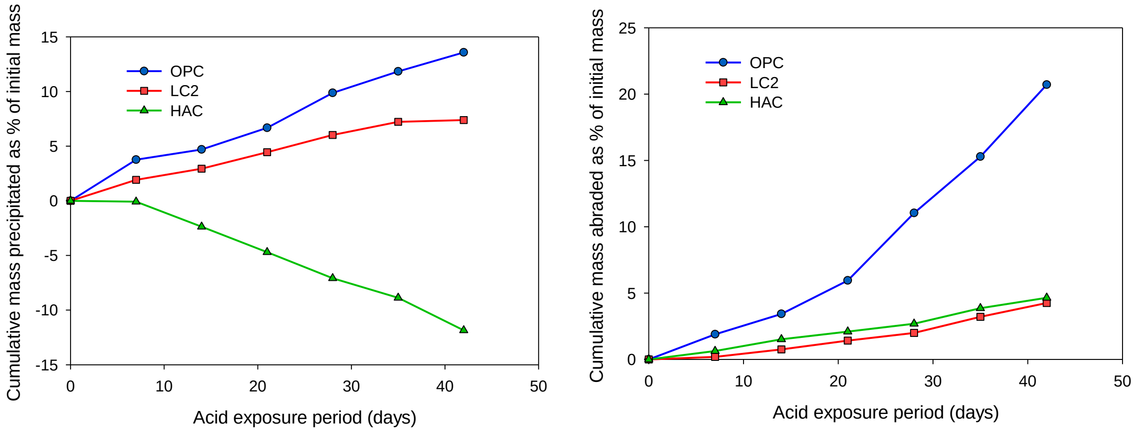

a) Cumulative mass precipitated b) Cumulative mass abraded

Figure 5.30 Variation of cumulative mass precipitated and abraded of LC2 and HAC paste mixes on exposure to 1% sulphuric acid

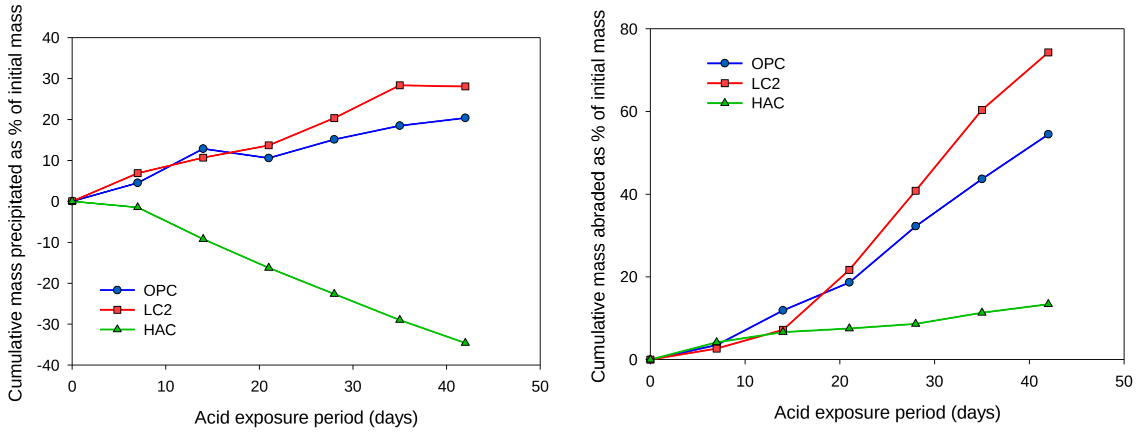

a) Cumulative mass precipitated b) Cumulative mass abraded

Figure 5.31 Variation of cumulative mass precipitated and abraded of LC2 and HAC paste mixes on exposure to 3% sulphuric acid

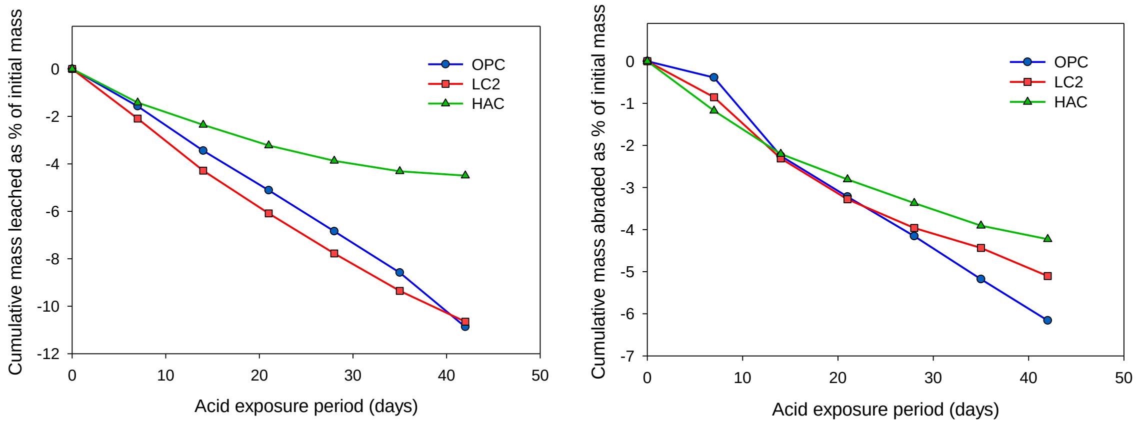

a) Cumulative mass leached b) Cumulative mass abraded

Figure 5.32 Variation of cumulative mass leached and abraded of LC2 and HAC paste mixes on exposure to 0.25M acetic acid

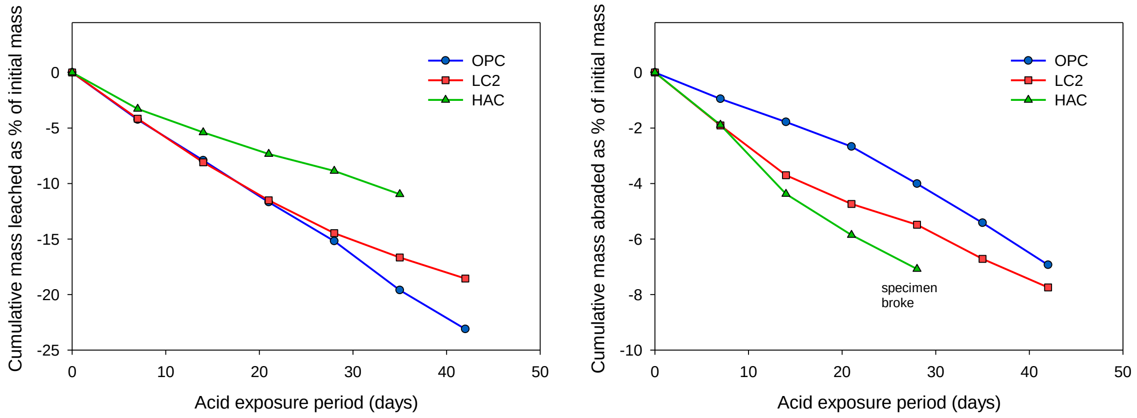

a) Cumulative mass leached b) Cumulative mass abraded

Figure 5.33 Variation of cumulative mass leached and abraded of LC2 and HAC paste mixes on exposure to 0.5M acetic acid

5.3.2 Changes in pH of the solution

5.3.2.1 Common binder systems

Acid attack is a classic example of acid - base reaction to form salt and water. In this process, ions such as calcium, aluminium etc. from the cementitious system react with the acid solution. Acid protons are consumed and to maintain the equilibrium, hydroxyl ions are released into the solution. This neutralisation process causes a rise in pH of the acid solution. Hence, measuring pH on regular basis could be another possible measure of the degradation kinetics as it gives an idea about the hydrogen ion consumption rate or in other words, the neutralisation capacity of the system. Most of the studies are conducted in static curing conditions without the frequent renewal of acid. This practice is incorrect, especially on exposure to lower concentrations of acids. The solution needs to be replenished frequently so that the aggressiveness of acid is maintained for the attack to be sustained. An automated titration system is ideal, but not practical to be implemented in all laboratories. Hence, monitoring pH of the acid solution on a regular basis with periodic renewal of acid is highly essential when testing for acid attack.

The typical plot showing variation of pH of the acid solution with each solution renewal is shown in Figure 5.34. It is a cyclic plot showing increase in pH of the acid solution after every 7 days of exposure each time back to the pH of the values of the fresh acid solution. However, this cyclic plot becomes difficult to understand if the dataset is large, consisting of various binder systems. Hence, in order to simplify the representation, only the pH of the solution measured just before each renewal is shown in subsequent Figures 5.35 to 5.41. The initial pH of the solution is shown in each figure and it has to be understood that the solution is replenished with the fresh acid solution with the initial pH until the end of the exposure.

Figures 5.35 to 5.41 show the variation of pH of the acid solution for various acids and their concentrations. It can be seen that there is a rapid increase in pH for the 7th day compared to the initial pH for all the acids. This must be due to the rapid neutralisation process when the cementitious material comes into contact with acid solution. Even though the specimens are wiped to remove the excess lime on the surface after the initial lime water curing, reaction of any remnant lime could also contribute to a sudden rise in pH.

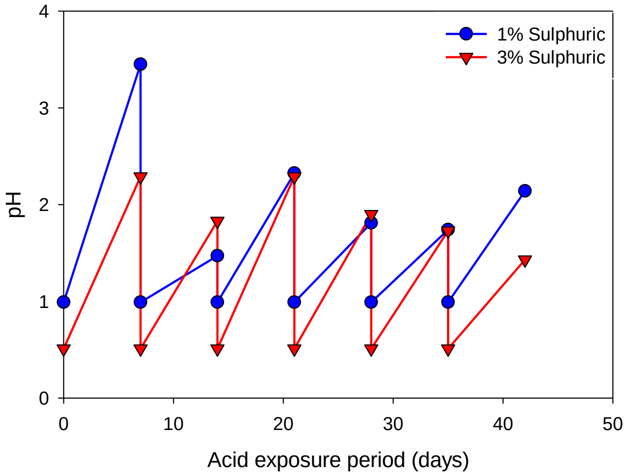

Figure 5.34 Typical graph showing changes in pH of the acid solution

In the case of 1% sulphuric acid, the increase in pH for the 14th day was less. This could be due to the protective effect offered by the gypsum, which coats the surface of the specimen. However, on prolonged exposure, there is a marginal increase in pH of the solution and this indicates that the reaction proceeds inward and neutralisation reactions subsequently take place. In the case of 3% sulphuric acid, the pH of the solution decreases with the age of exposure. This could be due to the reduced availability of Portlandite and/or due to the growth in the thickness of the gypsum layer. The pH of the OPC system is more when compared to the other binder systems. This is possibly due to the increased quantity of Portlandite present in OPC system when compared to other cementitious systems which are pozzolanic and consume the lime.

Similar trend was observed in the case of 1% HCl, 0.25M and 0.5M acetic acid solutions. Despite the presence of more alumina, which can enhance the neutralisation capacity of the system, the pH of the solution in the case of FA30 and BFS50 was found to be less when compared to OPC and SF10. This could be due to less amount of Portlandite available for the reaction and the enhanced stability of aluminate hydrates (as the pH is greater than 3). Also, this leads to an assumption that Al^{3+} is relatively stable when compared to Ca^{2+}. On exposure to 0.5M citric acid, it is noted that the pH increase is greater for the slag system. The pH evolution for the other binder systems was comparable. The increased pH in the case of slag system reconfirms the fact that aluminate hydrates react with dissociated citric acid to form complexes. The higher mass loss of BFS50 compared to OPC and SF10 is in alignment with these observations leading to enhanced degradation kinetics.

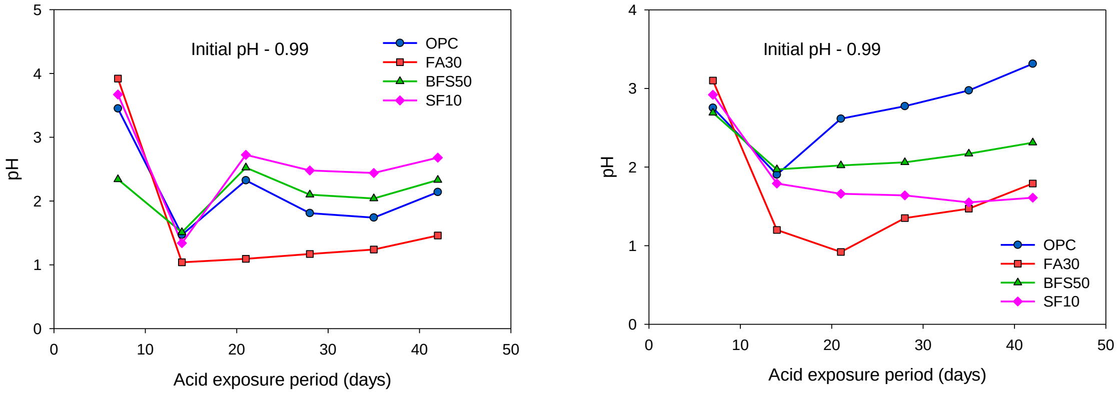

a) without brushing (WB28)   b) with brushing (B28)

Figure 5.35 Changes in pH of the acid solution on exposure to 1% sulphuric acid

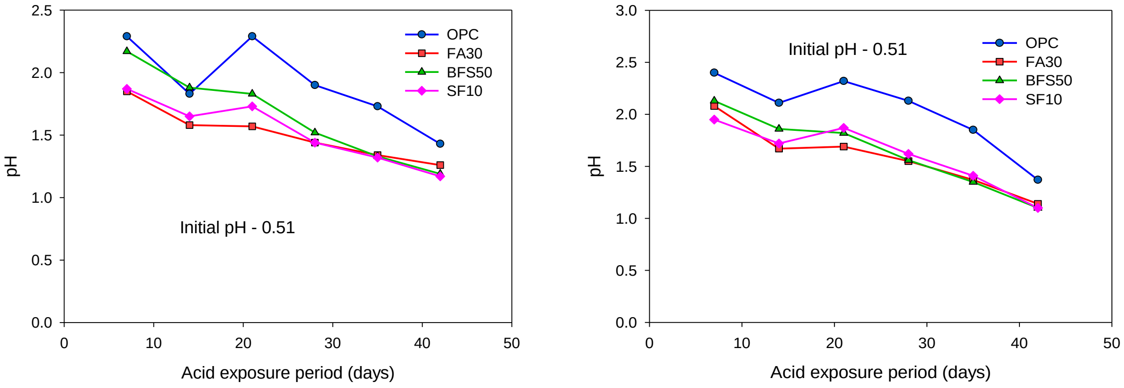

a) without brushing (WB28)   b) with brushing (B28)

Figure 5.36 Changes in pH of the acid solution on exposure to 3% sulphuric acid

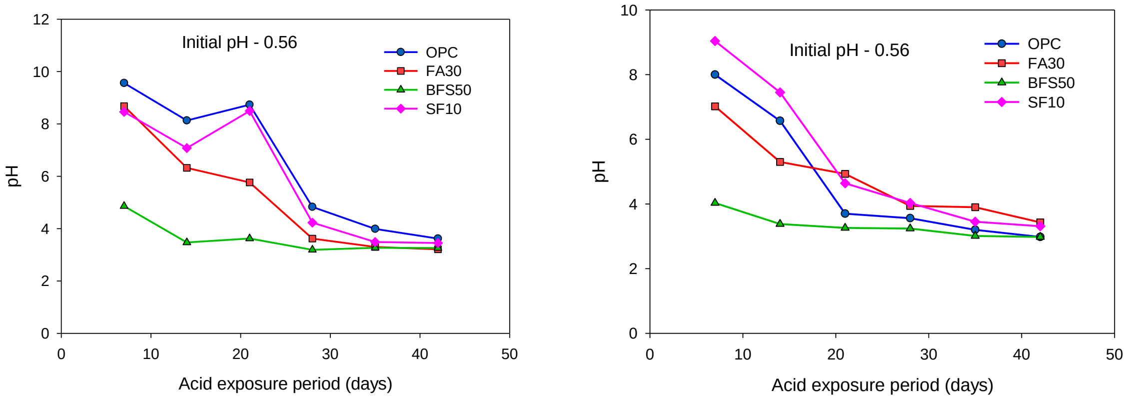

a) without brushing (WB28)   b) with brushing (B28)

Figure 5.37 Changes in pH of the acid solution on exposure to 1% hydrochloric acid

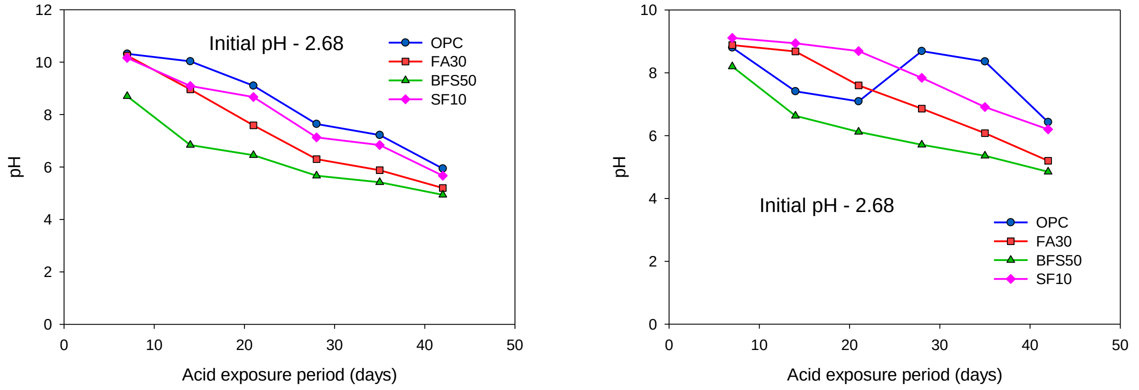

a) without brushing (WB28) b) with brushing (B28)

Figure 5.38 Changes in pH of the acid solution on exposure to 0.25M acetic acid

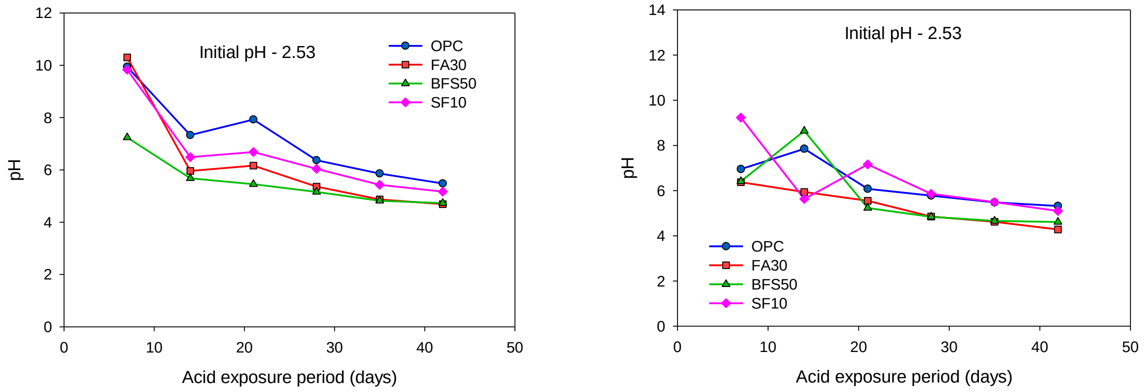

a) without brushing (WB28) b) with brushing (B28)

Figure 5.39 Changes in pH of the acid solution on exposure to 0.5M acetic acid

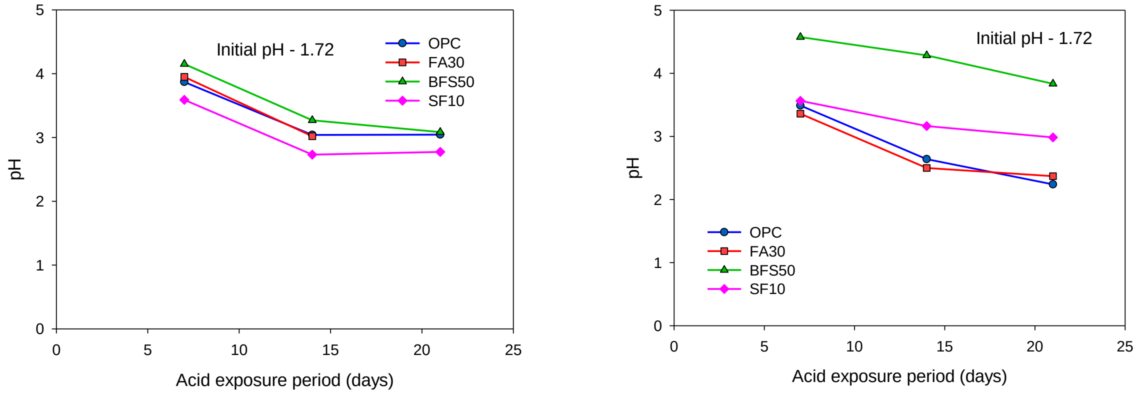

a) without brushing (WB28) b) with brushing (B28)

Figure 5.40 Changes in pH of the acid solution on exposure to 0.5M citric acid

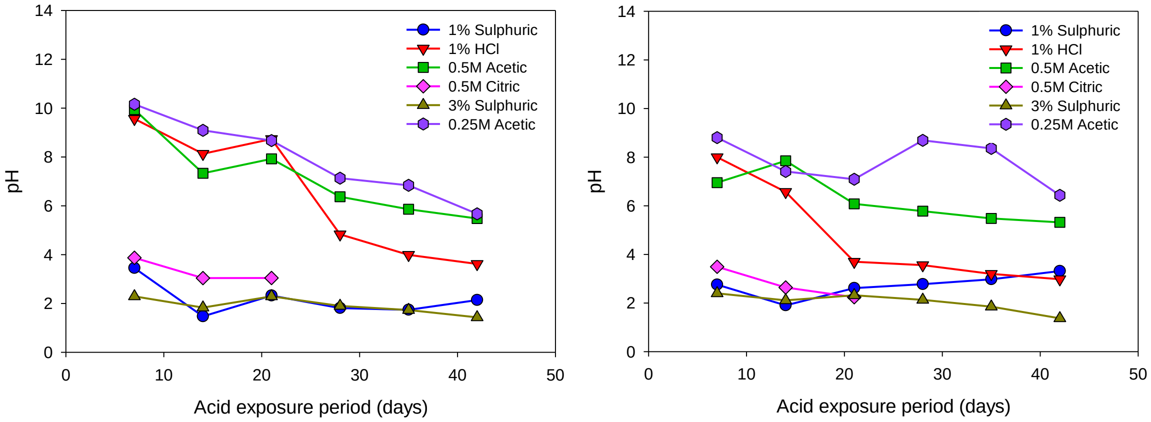

a) without brushing (WB28) b) with brushing (B28)

Figure 5.41 Changes in pH of the acid solution of OPC paste on exposure to various acids

To summarise the observations on changes in pH of the acid solution, the variation of pH of the solution for OPC mix on exposure to various concentrations/acids is shown in Figure 5.41. The trends were similar for the tests with and without brushing. In general, the pH of the solutions for all acids was found to decrease with acid exposure period, the pH drop being more prevalent in the case of HCl and acetic acid. The reduction in pH suggests the fact that calcium leaching reduces over time. The increase in thickness of corroded outer layer and its influence in limiting the kinetics further along with diminishing Portlandite availability may be the factors responsible for this behaviour. Despite the buffer action, the pH observed is highest in the case of acetic acid. In the case of citric acid, the decrease in pH with exposure period is marginal. However, considering the considerable reduction in mass and surface area of specimens with exposure (i.e. reduction in the availability of hydrates in the matrix), it can be concluded that the degradation kinetics in citric acid is unaffected with the time of exposure and continues to attack the specimen inward. It is observed that the increase in pH is greater for those acids which form soluble salts. The pH of the solution starts to increase rapidly after the renewal of the acid solution. The higher pH evolution demands the necessity for periodic renewal of acid/automatic titration system for maintaining the aggressiveness of the solution. The increase in the pH for the acids which form sparingly soluble salts, was found to be marginal.

5.3.2.2 Special binder systems

Figure 5.42 shows the changes in the pH of acid solution for LC2 and HAC paste on exposure to 1% sulphuric acid. A considerable difference was observed between the HAC paste and the other mixes (OPC and LC2). Similar trend was observed in the case of 3% sulphuric acid also (Figure 5.43). The lower pH of the acid might have triggered the dissolution of CA phases present in the HAC system. The presence of more Al^{3+} ions could be the reason for the increased neutralisation and hence higher pH of the acid solution.

However, the reverse trend was observed in the case of acetic acid (Figures 5.44 and 5.45). The OPC paste showed higher pH of the solution followed by LC2 and HAC. It can be inferred that, the pH rise in acetic acid could be proportional to the initial calcium content of the binder system. In the case of acetic acid, the pH rise was rapid when compared to the sulphuric acid. This means that the pH of the pore solution is higher for most of the exposure period (pH of the acid solution > 4). In these conditions, aluminate hydrates could possibly be more stable leading to less dissociation and hence less pH rise of the acid solution (Lavigne et al., 2016). This explains the less pH of the acid solution observed in the case of binder systems containing more alumina (HAC and LC2 compared to OPC).

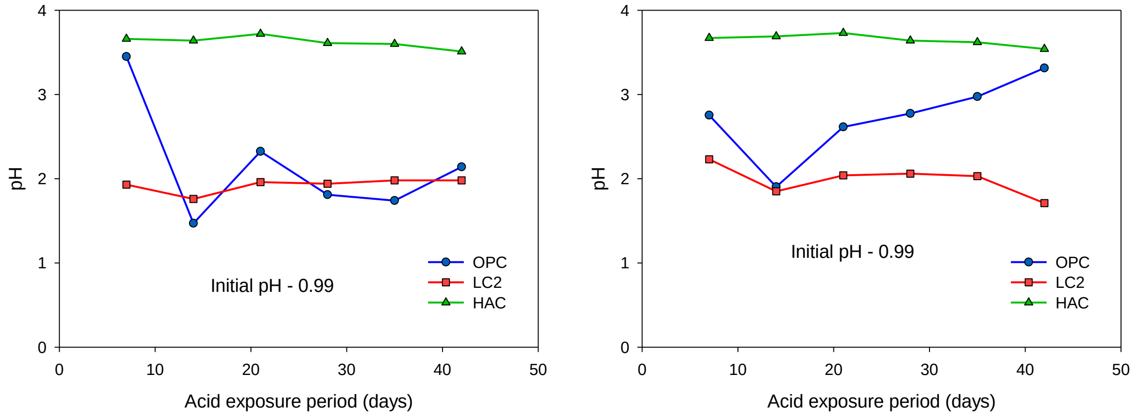

a) without brushing b) with brushing

Figure 5.42 Changes in pH of acid solution for LC2 and HAC paste on exposure to 1% sulphuric acid

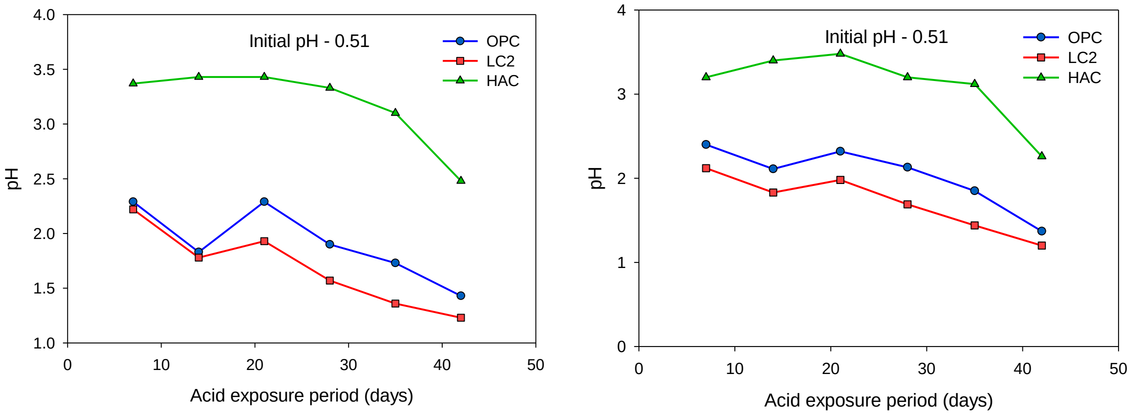

a) without brushing b) with brushing

Figure 5.43 Changes in pH of acid solution for LC2 and HAC paste on exposure to 3% sulphuric acid

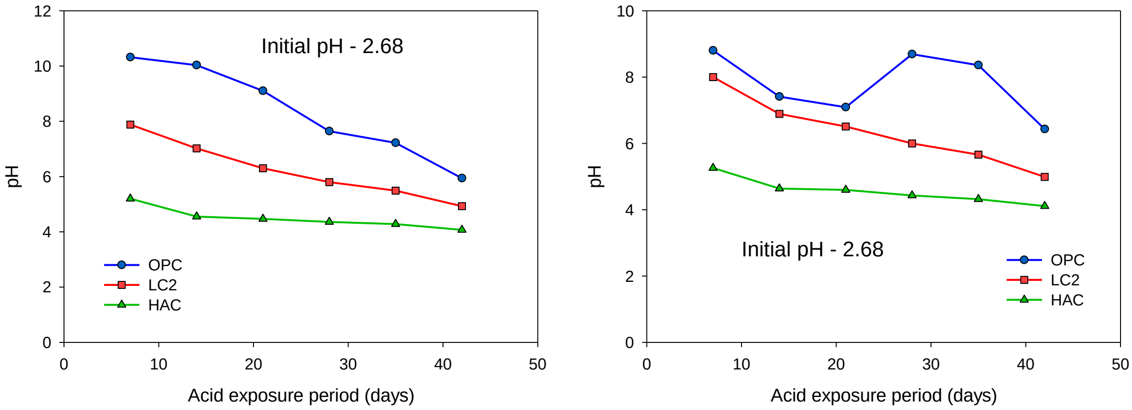

a) without brushing b) with brushing

Figure 5.44 Changes in pH of acid solution for LC2 and HAC paste on exposure to 0.25M acetic acid

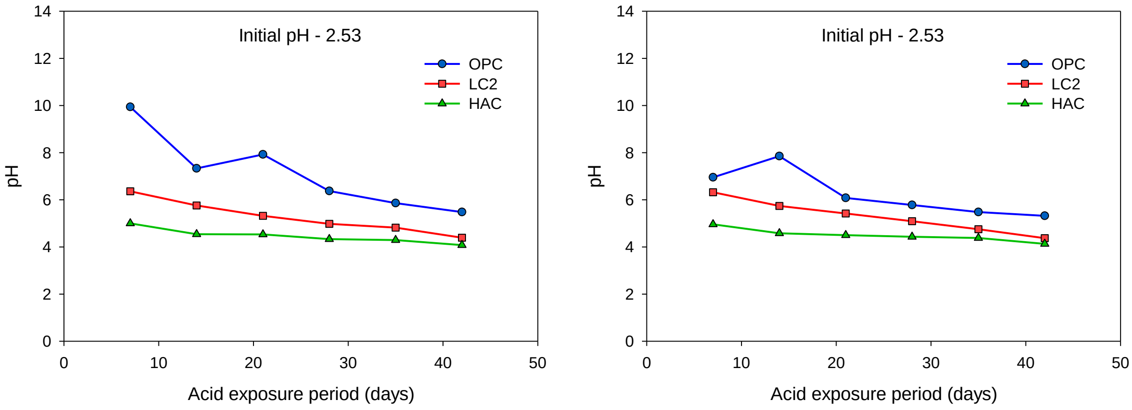

a) without brushing b) with brushing

Figure 5.45 Changes in pH of acid solution for LC2 and HAC paste on exposure to 0.5M acetic acid

5.3.3 Altered depth

5.3.3.1 Common binder systems

Using the image analysis software ImageJ and by using the CT slice images, various parameters were determined (the methodology is explained in the section 3.7.4) to study the deterioration of paste mixes in acids (tested without brushing) and these are presented in Tables 5.1 and 5.2. The area of various layers was quantified and the data presented in Table 5.1 are average of 10 slice images.

On exposure to 1% and 3% sulphuric acid, the percentage area decalcified was higher for mixes made with SCMs. This increased area of decalcification may be attributed to the reduced availability of Portlandite, which results in the direct attack of CSH gel, as suggested by Amin and Bassuoni (2018). SF10 mix showed significant expansion when compared to the other mixes on exposure to 1% sulphuric acid. The BFS50 mix showed an increase in the area (1.6%) while the other mixes experienced significant area loss on exposure to 3% sulphuric acid. On exposure to 1% HCl, the BFS50 mix had the least area that was decalcified. These observations are in alignment with the mass change results. The area that shrunk was also less for BFS50 on exposure to 1% HCl. On exposure to acetic acid, the decalcified area was higher for FA30 mix and least for BFS50 mix for concentrations of 0.25M and 0.5M. The superior performance of slag in acetic acid environment was evident also based on the thickness changes, as the area that shrunk was found to be the least for BFS50 when compared to the other mixes. On exposure to 0.5M citric acid, the binder systems which contain alumina (FA30 and BFS50) experienced greater loss in area and had greater area that was decalcified when compared to the OPC and SF10 mixes.

It is further noted that the area of outer degraded layer is less for specimens exposed to 1% sulphuric acid. This reinforces the fact that the gypsum layer formed is protective and restricts the further penetration of acid into the specimen.

Calcium leaching associated with the high solubility of calcium chloride salts resulted in higher areas for the outer degraded layer for the specimens exposed to HCl. Acetic acid attack resulted in strong calcium leaching leading to serious deterioration of microstructure, which is evident from the fact that the area of core was the least (only 3-15% of the initial area).

Table 5.1 Altered area measurements based on CT image analysis (WB28)

Mix	Acid	Concentration	Area as % of the initial area of the specimen				
			Area of outer layer	Area of middle layer	Area of specimen decalcified	Area of core layer	Area expanded/lost
OPC	Sulphuric	1%	11.13	15.02	26.15	75.18	1.34
FA30	Sulphuric	1%	8.01	24.39	32.41	69.82	2.22
BFS50	Sulphuric	1%	5.58	28.94	34.53	65.96	0.49
SF10	Sulphuric	1%	9.06	19.60	28.66	84.06	12.72
OPC	Sulphuric	3%	10.39	0.00	10.39	39.19	-50.42
FA30	Sulphuric	3%	32.26	6.41	38.67	24.11	-37.22
BFS50	Sulphuric	3%	59.63	0.00	59.63	41.95	1.59
SF10	Sulphuric	3%	22.82	0.00	22.82	40.19	-36.99
OPC	HCl	1%	18.39	35.02	53.42	31.80	-14.78
FA30	HCl	1%	38.00	0.00	38.00	46.11	-15.89
BFS50	HCl	1%	18.69	0.00	18.69	76.75	-4.56
SF10	HCl	1%	22.05	0.00	22.05	69.33	-8.62
OPC	Acetic	0.25M	14.80	21.27	36.08	47.99	-15.93
FA30	Acetic	0.25M	32.61	14.72	47.33	37.07	-15.60
BFS50	Acetic	0.25M	41.56	3.28	44.84	64.31	9.15
SF10	Acetic	0.25M	24.72	17.52	42.25	47.34	-10.41
OPC	Acetic	0.5M	53.62	22.02	75.64	15.40	-8.95
FA30	Acetic	0.5M	79.98	2.94	82.93	3.01	-14.06
BFS50	Acetic	0.5M	65.14	12.67	77.80	18.45	-3.74
SF10	Acetic	0.5M	56.60	18.18	74.78	14.48	-10.75
OPC	Citric	0.5M	4.83	0.00	4.83	17.21	-77.95
FA30	Citric	0.5M	5.21	0.00	5.21	10.80	-83.98
BFS50	Citric	0.5M	8.11	1.70	9.81	3.83	-86.36
SF10	Citric	0.5M	5.91	0.00	5.91	23.52	-70.57

Table 5.2 Altered depth measurements based on CT image analysis (WB28)

Mix	Acid	Concentration	DD (µm)	DM (µm)	DA (µm)	DR (µm)	Total altered depth (µm)
OPC	Sulphuric	1%	276	1373	1649	34	1649
FA30	Sulphuric	1%	227	1887	2114	57	2114
BFS50	Sulphuric	1%	82	1647	1729	13	1729
SF10	Sulphuric	1%	183	1037	1220	323	1220
OPC	Sulphuric	3%	437	0	437	-1525	1962
FA30	Sulphuric	3%	1177	390	1567	-1095	2662
BFS50	Sulphuric	3%	2023	0	2023	44	2023
SF10	Sulphuric	3%	1196	0	1196	-1035	2231
OPC	HCl	1%	545	1278	1824	-396	2220
FA30	HCl	1%	1244	0	1244	-427	1671
BFS50	HCl	1%	489	0	489	-118	607
SF10	HCl	1%	620	0	620	-220	840
OPC	Acetic	0.25M	466	717	1184	-424	1608
FA30	Acetic	0.25M	1155	540	1695	-421	2116
BFS50	Acetic	0.25M	1189	70	1259	238	1259
SF10	Acetic	0.25M	752	610	1362	-274	1636
OPC	Acetic	0.5M	1699	1105	2804	-236	3040
FA30	Acetic	0.5M	3422	375	3797	-376	4173
BFS50	Acetic	0.5M	2091	599	2690	-95	2785
SF10	Acetic	0.5M	1765	959	2724	-277	3001
OPC	Citric	0.5M	374	0	374	-2742	3116
FA30	Citric	0.5M	472	0	472	-3054	3526
BFS50	Citric	0.5M	746	220	966	-3161	4127
SF10	Citric	0.5M	388	0	388	-2467	2855

As the salt formed in the case of citric acid is non-protective and loosely bound to the matrix, the outer degraded layer was thin, and this is evident from lower area of the outer degraded layer. However, considerable area of the specimen (on formation of precipitate) had already exfoliated and deposited in the beakers. This area lost from the specimen also should be added to the % area of the specimen decalcified to get the correct idea about the deterioration. The parameters defined such as % area decalcified, % area of the core, and alteration depths are quantitative data extracted from the CT images. These parameters serve as more direct indicators of degradation and hence, should be used as complimentary data along with the mass changes for the performance evaluation of materials while investigating degradation kinetics. Thus, CT images can be used to quantify parameters which are linked with alteration in microstructure, to explain the behaviour of cement-based materials when exposed to various acids.

In order to extract more useful data from the CT images, depths were measured based on the methodology explained in section 3.7.4. The altered depth (DA) measurements thus estimated for the various binder systems exposed to various acids without brushing are presented in the Figures 5.46 to 5.48.

On exposure to 1% sulphuric acid, the depth of outer gypsum layer was found to be very less when compared to other acids (less values of DD). The middle decalcified layer (comprising of silica gel and iron/aluminium hydroxides) was found to be adjacent to the gypsum layer. The depth of alteration (DA) was found to be high when compared to 3% sulphuric acid. However, in the case of 3%, the exfoliation of gypsum layer resulted in lower value of DD but higher value of DR (due to loss of mass).

The altered depth of BFS50 was found to be lower when compared to the other mixes on exposure to HCl and acetic acids. In the case of citric acid, the altered depths of FA30 and BFS50 were found to be higher when compared to OPC and SF10. These observations were found to be in good alignment with the mass measurements and area measurements previously explained. The altered depth of SF10 was found to be the least considering also the depth of the specimen removed (DR). It is concluded that the altered depth measurements (DA) should be reported along with the DR values, especially in the cases of acids that form less soluble salts having higher molar volume. If the depth removed (DR) values are negative, those measurements should be added with the altered depth (DA) to get the total depth which is affected in the specimen due to acid attack. The area and depth measurements were repeated for the specimens tested with brushing (B28) and the results are presented in Appendix A (Tables A-2 and A-3, Figures A-20 to A-22). These observations were also in alignment with the conclusions drawn for the case without brushing.

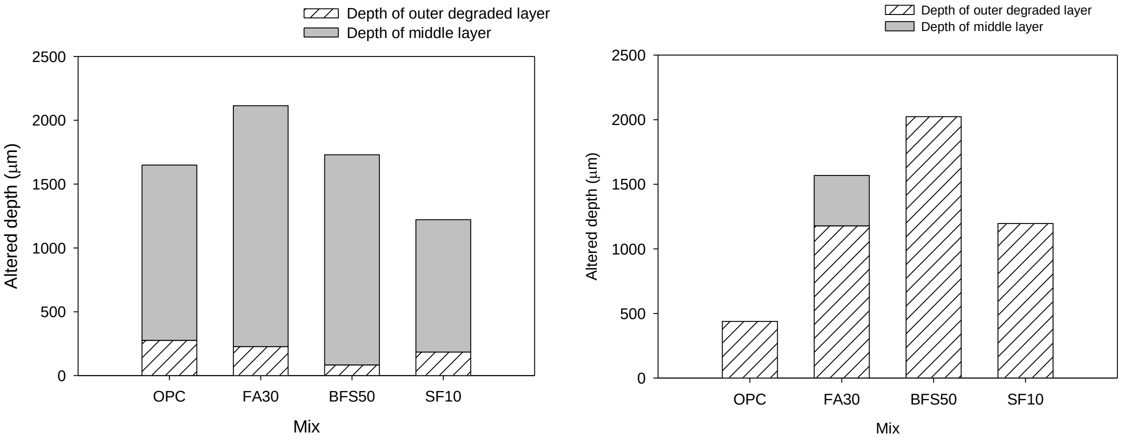

a) 1% sulphuric acid b) 3% sulphuric acid

Figure 5.46 Altered depth of paste exposed to sulphuric acid (without brushing)

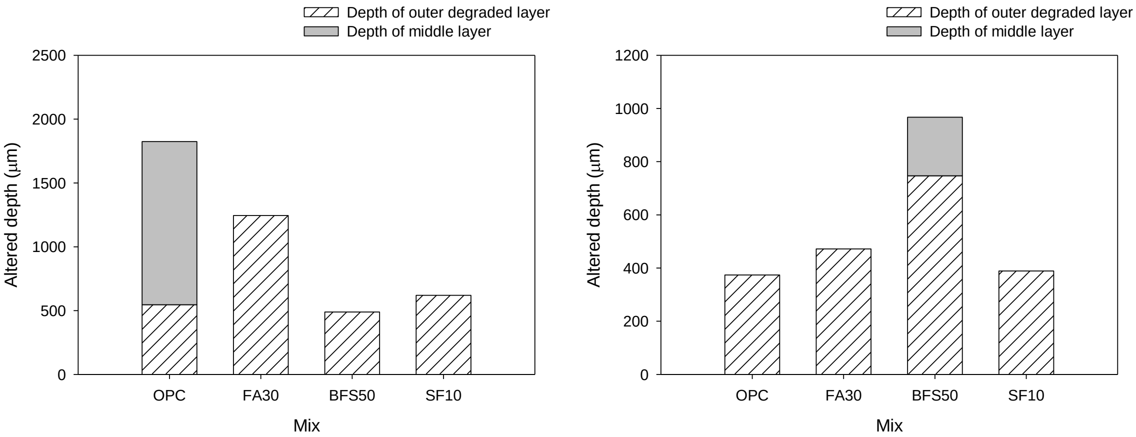

a) 1% hydrochloric acid b) 0.5M citric acid

Figure 5.47 Altered depth of paste exposed to hydrochloric and citric acid (without brushing)

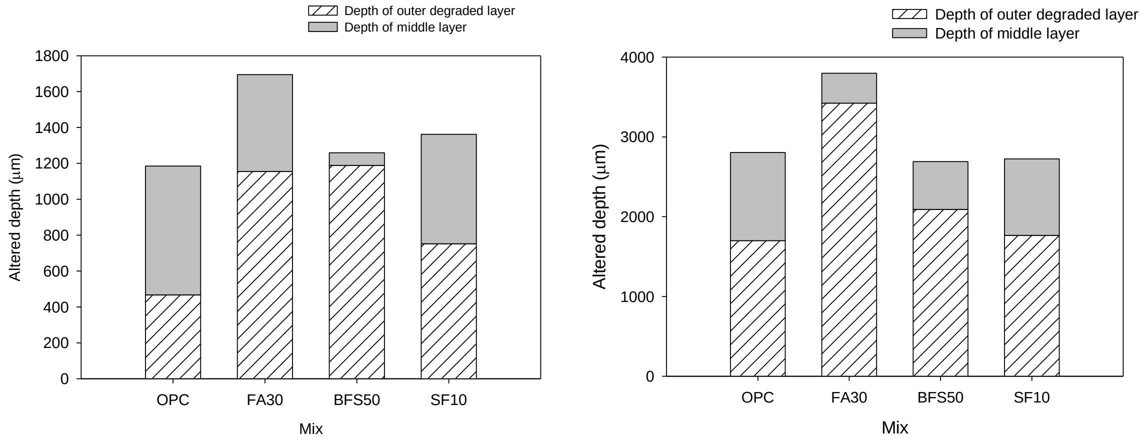

a) 0.25M acetic acid b) 0.5M acetic acid

Figure 5.48 Altered depth of paste exposed to acetic acid (without brushing)

5.3.3.2 Special binder systems

Table 5.3 summarises the various parameters associated with the estimation of altered area and depths of paste made with special binders such as HAC and LC2. The decalcified area (as % of initial area) for HAC paste was found to be significantly less when compared to LC2 paste for all concentrations of sulphuric and acetic acid. Apparently, the altered depth of the HAC paste (after accounting for the depth expanded/shrunk) was found to be less when compared to LC2 paste. This difference may be attributed to the changes in the chemical composition of these two binder systems. Thus, based on the altered depth/area measurements, the performance of HAC seems to be better on exposure to both sulphuric and acetic acid.

Figure 5.49 shows the altered depth of the paste mixes on exposure to 1% sulphuric acid tested with and without brushing. In both the cases, it can be seen that the depth of the outer degraded layer of OPC is less than LC2. Similar trend was observed for 3% sulphuric acid and 0.25M acetic acid also (Figure 5.50). The higher degraded layer depths for LC2 indicate the direct attack on CSH gel, similar to the observations in the case of common binder systems.

Table 5.3 Altered area/depths of LC2 and HAC paste exposed to sulphuric and acetic acid

Method	Mix and acid	as % of the initial area			DD (µm)	DM (µm)	DA (µm)	DR (µm)	Total alteration depth (µm)
		Area decalcified	Area unattacked	Area expanded /shrunk					
B28	LC2 S 1%	19.06	64.15	-16.79	1110.5	0	1110.5	-479.6	1590
B28	HAC S 1%	2.62	71.33	-26.05	130.0	0	130.0	-742.2	872
WB28	LC2 S 1%	27.15	72.04	-0.81	834.5	0	834.5	-21.2	856
WB28	HAC S 1%	5.13	97.38	2.51	135.0	0	135.0	+65.5	135
WB28	LC2 S 3%	26.66	22.96	-50.38	1422.5	0	1422.5	-1580.8	3003
WB28	HAC S 3%	4.90	45.04	-50.06	209.5	0	209.5	-1495.9	1705
WB28	LC2 A 0.25M	37.47	51.42	-11.12	1191.2	0	1191.3	-300.0	1491
WB28	HAC A 0.25M	18.79	72.16	-9.06	520.0	0	520.0	-242.8	763

S- sulphuric, A – acetic

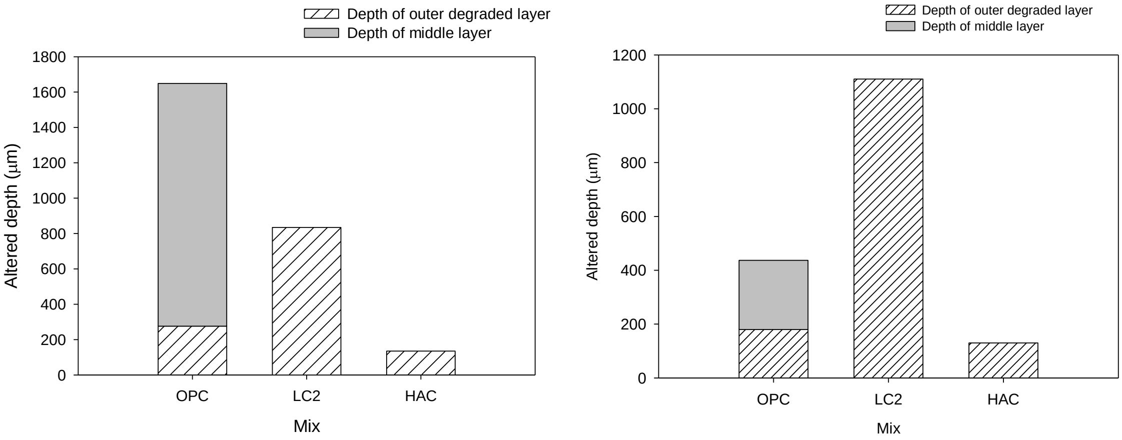

a) without brushing b) with brushing

Figure 5.49 Altered depth of LC2 and HAC paste exposed to 1% sulphuric acid

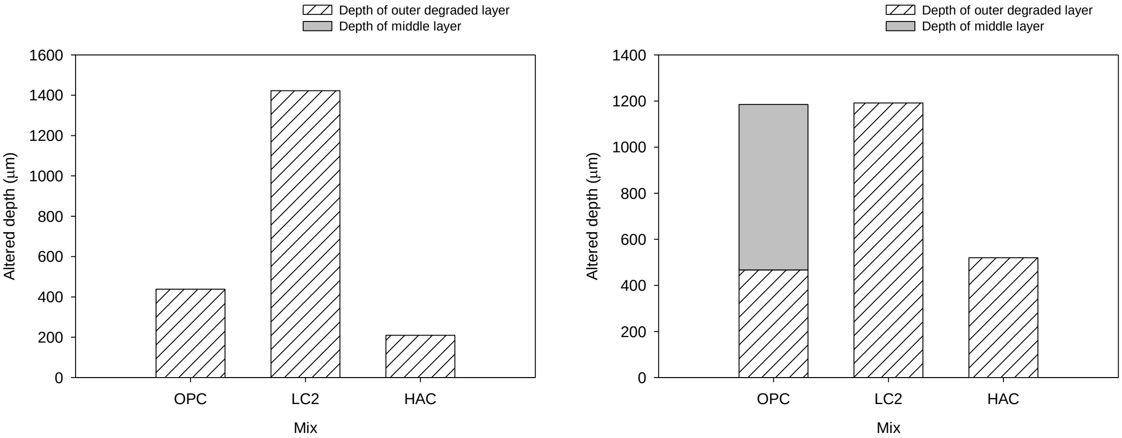

a) 3% sulphuric acid (without brushing) b) 0.25M acetic acid (without brushing)

Figure 5.50 Altered depth of LC2 and HAC paste exposed to 3% sulphuric acid and 0.25M acetic acid (without brushing)

5.3.4 Thickness changes

5.3.4.1 Common binder systems

Specimens undergo either expansion or reduction in thickness depending on the solubility of the salt formed. The change in thickness was calculated based on the initial thickness before the acid exposure. A set of 12 readings were taken along the length specimen, and reported as the average thickness at a particular age of exposure. Tables 5.4 and 5.5 show the thickness changes after the exposure period for the tests done without brushing (WB28) and with brushing (B28) respectively. A positive value indicates expansion while a negative value refers to reduction (loss in thickness). All specimens on exposure to 1% sulphuric acid without abrasion experienced increase in thickness. The increase in thickness is due to the precipitation of gypsum layer on the surface of the specimen. However, all mixes except BFS50 showed a reduction in thickness on exposure to 3% sulphuric acid. This is due to the destabilisation and subsequent delamination of gypsum in the acid solution. But, in the case of BFS50, there was a substantial increase in thickness. This is due to the considerable expansion because of the gypsum layer adhering to the cement matrix. Even though there was an increase in thickness of 22.7%, the specimen surface became soft in nature due to the thick gypsum layer in the acid solution.

As leaching was a dominant process and salts formed were soluble, specimens exposed to HCl and acetic acid underwent reduction in thickness. This reduction in thickness could be attributed to a combination of decalcification associated shrinkage and/or thickness of the corroded layer lost due to brushing. All mixes on exposure to HCl and acetic acid underwent reduction in thickness, the reduction being the least in the case of BFS50 mix. The loss in thickness was greater for the specimens in citric acid, as the mass loss was severe. The precipitate formed in citric acid has low solubility (0.95 g/L at 25 °C), and was loosely adhered to the specimen. The salt does not have a protective effect on the matrix due to the high molar volume of the salt (Larreur-Cayol et al., 2011a), 518.4 cm^3/mol when compared to CSH (108-125 cm^3/mol) and Portlandite (33 cm^3/mol). This led to rapid loss of thickness at just three weeks of exposure and hence degradation was stopped after 3 weeks itself for further characterisation tests. In the case of citric acid, the mixes containing alumina such as FA30 and BFS50 incurred higher loss of thickness as the degradation kinetics were found to be enhanced in such mixes. The losses of thickness calculated were, in general, in good alignment with the mass changes observed.

Table 5.4 Changes in thickness of paste on exposure to various acids (WB28)

Mix	Without brushing (WB28)					
	1% Sulphuric	3% Sulphuric	1% HCl	0.25M Acetic	0.5M Acetic	0.5M Citric
OPC	+13.40	-7.70	-3.29	-2.15	-2.56	-49.59
FA30	+3.76	-2.83	-4.04	-2.94	-3.31	-57.76*
BFS50	+11.55	+22.77	-1.99	-1.16	-1.29	-58.85
SF10	+8.10	-4.02	-3.22	-3.09	-2.00	-35.80

* after 2 weeks of exposure

Table 5.5 Changes in thickness of paste on exposure to various acids (B28)

Mix	With brushing (B28)					
	1% Sulphuric	3% Sulphuric	1% HCl	0.25M Acetic	0.5M Acetic	0.5M Citric
OPC	+0.03	-10.73	-8.58	-4.09	-4.21	-34.37
FA30	+4.21	-12.57	-10.72	-9.27	-5.67	-50.41
BFS50	+8.14	+21.31	-5.64	-2.71	-3.59	-31.48
SF10	+3.12	-14.59	-9.63	-5.82	-4.22	-19.68

In the case of tests with brushing, all mixes on exposure to 1% sulphuric acid showed expansion. The mixes such as OPC, FA30 and SF10 showed an increase in thickness although there was a mass loss at the end of the exposure period. This can be explained due to the formation of gypsum in large quantities and the difference in densities of cement matrix and the gypsum layer. Additionally, this may also be due to mass loss from edges of specimens, which is reflected in mass loss but not in the reduction of thickness measured using digital caliper.

In the case of 3% sulphuric acid, all mixes except BFS50 experienced substantial reduction in thickness due to expansion and delamination associated with gypsum formation. The BFS50 mix showed thickness increase similar to the observation in the test without brushing (WB28). This has already been observed to be due to the enhanced adherence of gypsum layer with the cementitious matrix and increased resistance against abrasion. All specimens had a reduction in thickness on exposure to HCl and citric acids, the thickness reduction being the minimum for BFS50. The better performance of SF10 mix on exposure to citric acid was evident in B28 also, as the thickness loss was found to be the minimum when compared to the other mixes.

5.3.4.2 Special binder systems

The thickness changes of specimens made with special binders exposed to sulphuric and acetic acids were compared with OPC and the results are presented in Table 5.6. On exposure to 1% sulphuric acid, LC2 specimens had thickness gain owing to the formation of gypsum adherent to the matrix. However, the inferior performance of HAC was evident as the exposure to 1% sulphuric acid led to thickness loss in both the test methods (with and without brushing). On exposure to higher concentration of sulphuric acid, the special binders had higher thickness losses compared to OPC for the tests with and without brushing. On exposure to 0.25M and 0.5M acetic acid, LC2 and HAC pastes had reduction in thickness and the thickness changes were comparable to OPC.

Table 5.6 Changes in thickness of paste (with special binders) on exposure to various acids

Method	With brushing (B28)				Without brushing (WB28)			
Acid / Mix	1% Sulphuric	3% Sulphuric	0.25M Acetic	0.5M Acetic	1% Sulphuric	3% Sulphuric	0.25M Acetic	0.5M Acetic
OPC	+0.03	-10.73	-4.09	-4.21	+13.40	-7.70	-2.15	-2.56
LC2	+4.52	-17.69	-2.41	-6.16	+8.26	-7.97	-2.15	-2.87
HAC	-8.26	-23.76	-4.36	-4.62	-7.50	-22.29	-2.14	-2.02

5.4 DYNAMIC TEST FOR ACCELERATED DEGRADATION

An attempt was made to investigate the phenomenon of acid attack by conducting a dynamic test for accelerated degradation using paste specimens (restricted to evaluation of common binder systems) by modifying the test setup of the slake durability apparatus. The methodology of the test was detailed in the section 3.6.2 and the test results are discussed below.

5.4.1 Visual observations

Figure 5.51 shows the paste specimens after 20000 revolutions in 1% sulphuric acid solution. A thin layer of gypsum could be seen in all the mixes. More deterioration associated with the loss of mass due to the abrasion between the specimens inside the cylinder is also evident from the images. The specimens were also exposed to saturated lime water solution for 20000 revolutions in the apparatus and the visual observation of specimens is shown in Figure 5.52.

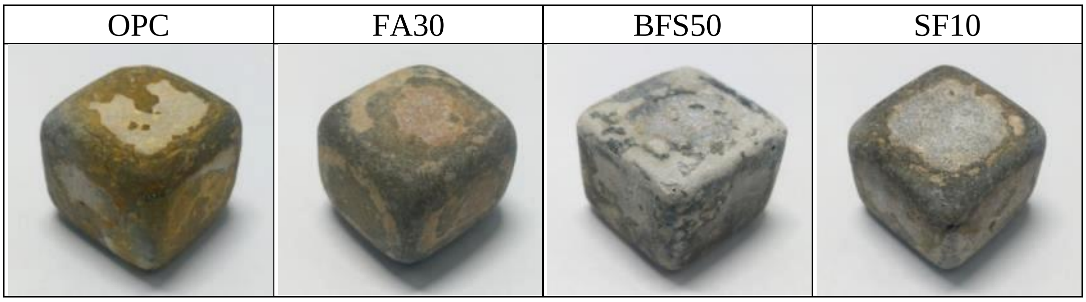

Figure 5.51 Specimens after 20000 revolutions exposed to 1% sulphuric acid in dynamic test apparatus for accelerated degradation

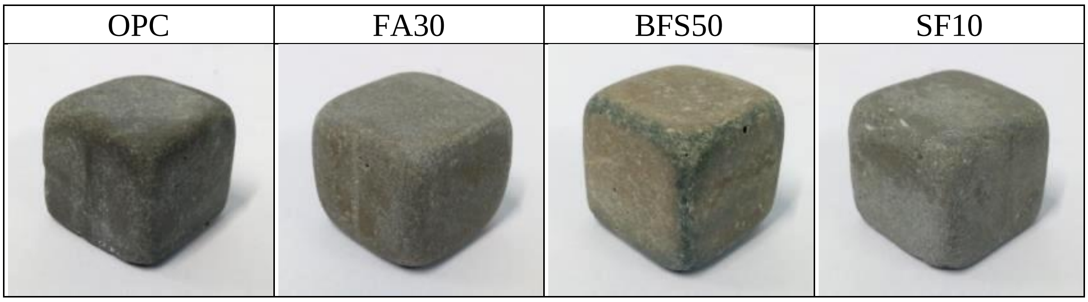

Figure 5.52 Specimens after 20000 revolutions exposed to saturated lime water in dynamic test apparatus for accelerated degradation

5.4.2 Mass changes

The mass changes of specimens were calculated based on the initial mass before the start of the test (i.e. after 28 days of curing in saturated lime water). The mass of the specimens was measured after every 5000 revolutions in the apparatus. An average of 12 hours interval was given in between successive 1250 revolutions in order to allow the reactions to take place. The mass changes were estimated after 20000 revolutions in 1% sulphuric acid and saturated lime water solution and the difference in mass loss was calculated and reported as the effective mass change. The details of measurements carried out during the test are provided in the Appendix A (Table A-1).

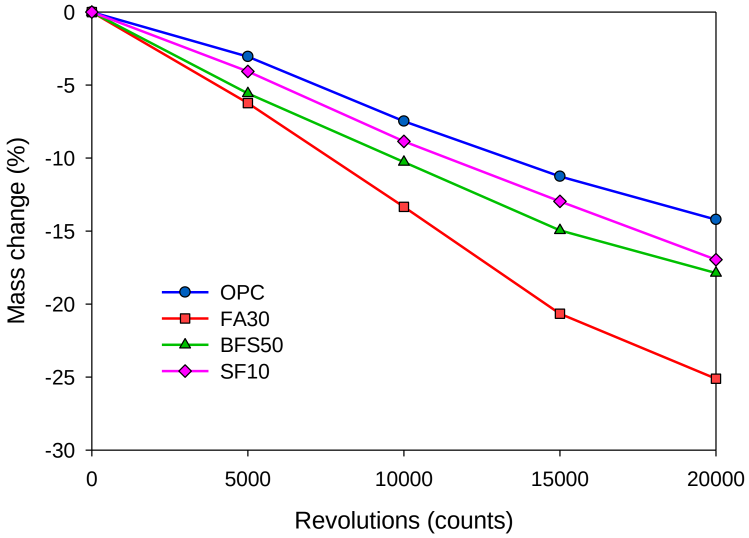

Figure 5.53 Mass changes of paste after 20000 revolutions in 1% sulphuric acid in dynamic test for accelerated degradation

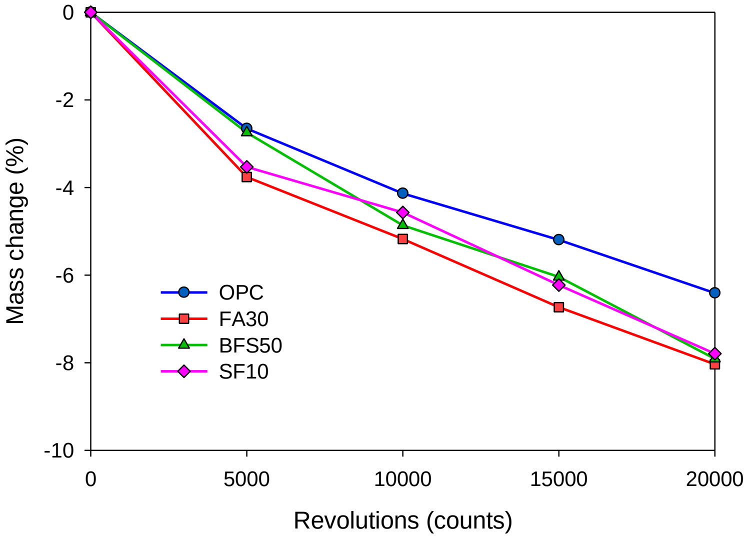

Figure 5.54 Mass changes of paste after 20000 revolutions in saturated lime water in dynamic test for accelerated degradation

Figures 5.53 and 5.54 show the variations in mass change during 20000 revolutions on exposure to 1% sulphuric acid and saturated lime water respectively. It can be seen that the mass loss is less for OPC and SF10 when compared to FA30 and BFS50. The mass loss was also found to vary linearly with respect to the revolution counts. The trend in mass loss was similar to the mass change in saturated lime water. This indicates that the effect of abrasion is more predominantly reflected in the test result. The net mass loss after calculating the difference of mass loss on exposure to acid and saturated lime water is shown in Figure 5.55. Based on the net mass change, the performance of FA30 and BFS50 was seen to be inferior compared to OPC and FA30. However, these results were contrary to the mass changes noted during the continuous immersion test with and without periodic abrasion. The evolution of pH of the acid solution for the various mixes is shown in Figure 5.56. As the revolution counts increased, there was an increase in the pH of the acid solution. However, there was hardly any salient difference in the pH of the acid solution between the mixes.

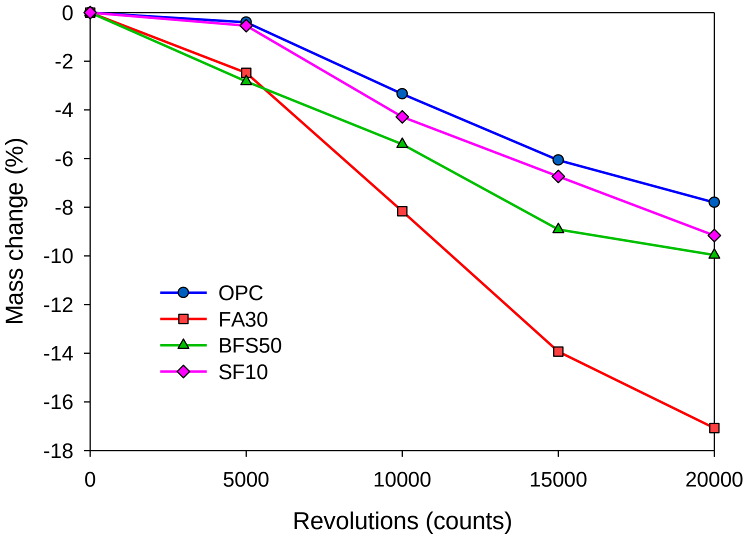

Figure 5.55 Net mass change of paste after 20000 revolutions on exposure to 1% sulphuric acid in dynamic test for accelerated degradation

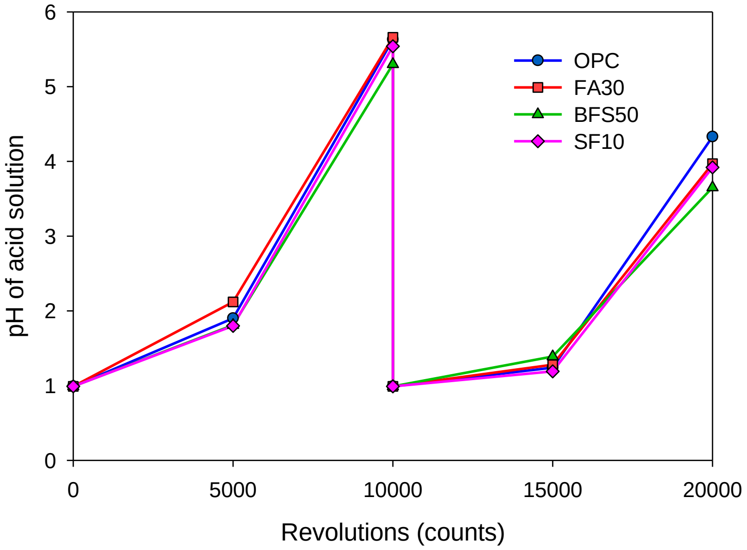

Figure 5.56 Measured pH of the acid solution on exposure of paste to 1% sulphuric acid in dynamic test for accelerated degradation

The test had limitations as it was not reflecting the actual mechanism of attack. It seems that the test favours the mixes that have better strength and therefore better abrasion resistance. However, this could be further developed to quickly assess the acid resistance of various binder systems. The experience with the testing indicates that the specimens need to be exposed to the acid solutions for a considerable time period so that the reaction products can be formed and the real potential of the material can be assessed. Also, the test has to be continued for increased number of revolutions by giving sufficient time period between revolutions. Based on the test results, it seems that this test method may be more suitable for the mortar specimens rather than paste specimens. In the case of mortar specimens, the role of ITZ is also important and accelerated results could be possibly obtained using this test.

5.5 SUMMARY

The degradation kinetics of paste was investigated by conducting accelerated immersion test. The test was conducted with and without the abrasive action to simulate the action of flowing and static effluents respectively. The paste specimens made with common binders were exposed to sulphuric, hydrochloric, acetic and citric acids. The special binders were exposed to sulphuric and acetic acid. The test results show that the acid attack is primarily influenced by the solubility of calcium salt and its properties such as molar volume, and its affinity with the inner cement matrix.

Among the acids tested, citric acid was the most aggressive which resulted in severe mass and thickness loss in the specimens. The OPC and SF10 paste mixes showed less mass losses and thickness changes on exposure to 0.5M citric acid compared to FA30 and BFS50 pastes. On exposure to other acids such as sulphuric, hydrochloric and acetic acids, the performance of slag paste was better compared to the other common binders based on the mass changes. In the case of special binders, the LC2 paste showed better performance compared to OPC and HAC on exposure to 1% sulphuric acid, while the HAC paste showed less mass loss on exposure to acetic acid followed by LC2 and OPC. Overall, the alternative binders showed good resistance only in the case of lower concentrations of acids. It is also noted that the altered depths of pastes made with common and special binders were in general higher than OPC. It is inferred that the choice of the binders in acidic environment should be made based on the use of multitude of parameters related to kinetics. The degraded paste was then analysed using micro-analytical characterisation techniques to understand the mechanism of degradation and these results are presented in the next chapter.

CHAPTER 6

MICRO-ANALYTICAL INVESTIGATION OF PASTE EXPOSED TO ACIDS

6.1 INTRODUCTION

This chapter deals with the micro-analytical characterisation studies done on paste with different binders exposed to acids. The various characterisation techniques used to study the mechanism of degradation include optical microscopy, X-ray tomography, X-ray diffraction, scanning electron microscopy, mercury intrusion porosimetry, and thermo-gravimetric analysis.

6.2 MICRO-ANALYTICAL CHARACTERISATION

6.2.1 Optical microscopy

The images of cut paste specimens of OPC after the degradation (tested with brushing, method named B28) were collected using an optical microscope fitted with a digital camera and these images are shown in Figures 6.1 to 6.3. Prior to the imaging, the reactions were stopped by immersing the cut specimens in isopropanol for 4 days with constant replenishment of isopropanol. A magnification of 40X was used for collecting the images. A white coloured gypsum layer with a small transition layer of iron hydroxides (brown in colour) can be seen on exposure to sulphuric acid. A thin layer of light grey coloured region is also observed just to the inside of the brown ring. This indicates the middle layer, which is partially decalcified. Similarly, an outer amorphous silica gel layer with brown iron hydroxide rings was observed in the case of HCl. The specimens exposed to acetic acid also showed distinct mineralogical zonation consisting of outer degraded layer, an inner middle layer that was partly decalcified and the central core layer which was not attacked. However, only a thin outer degraded layer was observed in the case of citric acid. From the micrographs, it is evident that the altered depth was greater in the case of acetic acid.

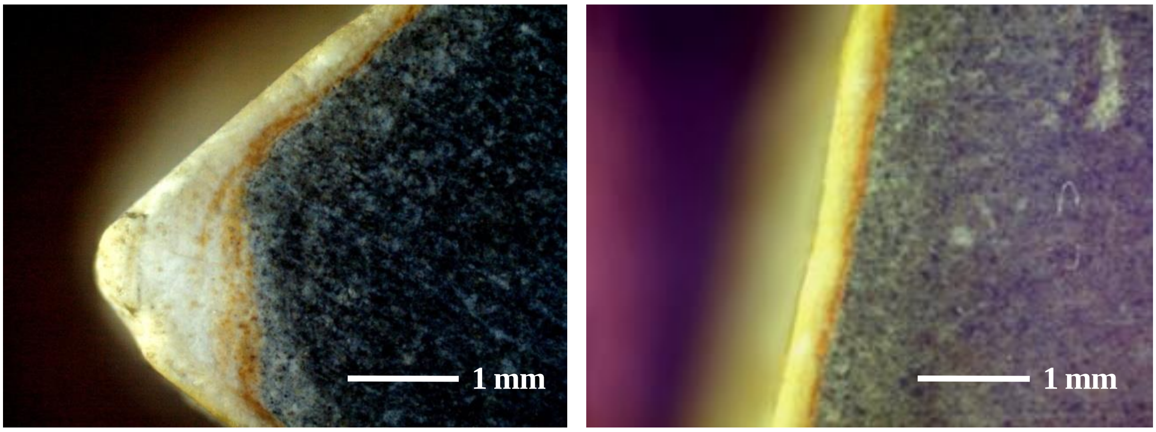

Gypsum layer at the edges | Thin layer of gypsum on the lateral surface

Figure 6.1 Optical micrographs of OPC paste exposed to 1% sulphuric acid (B28)

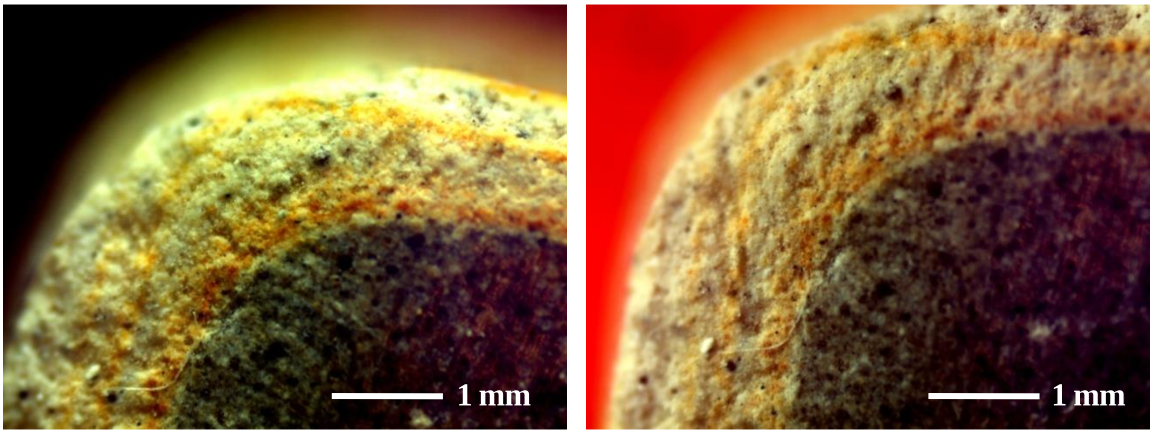

White corroded layer with brown rings of iron hydroxide

Figure 6.2 Optical micrographs of OPC paste exposed to 1% hydrochloric acid (B28)

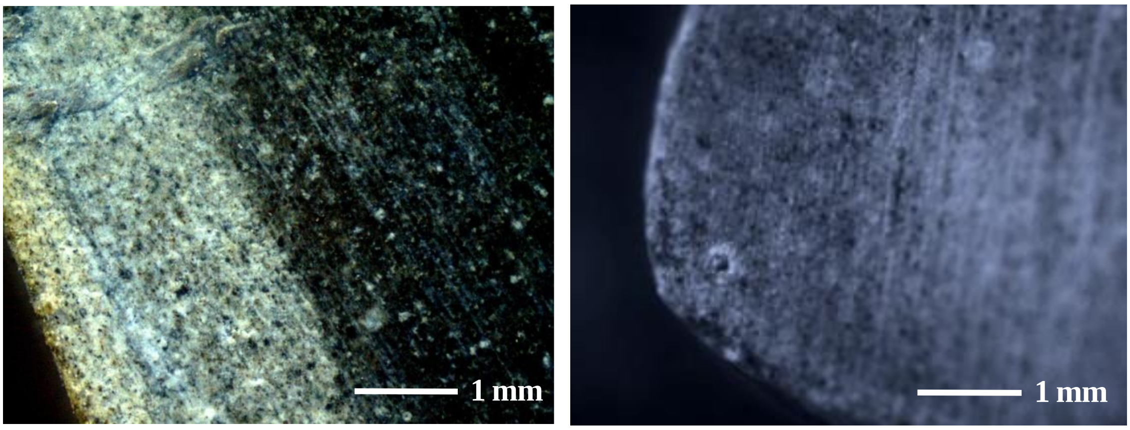

Degraded layer on exposure to 0.5M acetic acid

A thin layer of white coloured precipitate on exposure to 0.5M citric acid

Figure 6.3 Optical micrographs of OPC paste exposed to 0.5M acetic acid and 0.5M citric acid (B28)

6.2.2 X-ray micro-tomography

6.2.2.1 Common binder systems

The CT slice images, 3D rendered image and illustrative image showing void porosity of the control mix cured in saturated lime water are shown in Figure 6.4. The slice images obtained from both the inside (section 1-1 in Figure 3.29) and the surface of the sample (section 2-2 in Figure 3.29) show uniform microstructure. The 16 bit images obtained from CT were converted to 8 bit images before performing the image analysis. The 8 bit CT images thus obtained, had a grayscale values (GSV) ranging from 0 to 255. Pure black regions in the slice images refer to the voids (pixels with GSV less than 50), white regions refer to the very dense/anhydrous particles (pixels with GSV greater than 250) and gray coloured regions indicate the various hydrated phases formed, depending on the GSV. The void porosity as shown in Figure 6.4 is obtained by performing image segmentation. The voxels with GSV less than 50 were considered to be voids and visualised in Figure 6.4. The CT images of other mixes before the acid exposure (i.e. mixes FA30, BFS50 and SF10 cured in saturated lime water) are shown in Appendix B, Figures B-1 to B-3.

The specimens after the degradation (Figure 6.5) clearly show the mineralogical zonation due to alteration in phases (demarcated by white/black lines in Figure 6.5), which is a characteristic feature of acid attack. Darker portions in the CT slice images are mostly deteriorated, and have less density (mainly due to decalcification) and GSVs when compared to the sound unattacked zones. An attempt was also made to evaluate the porosity changes due to leaching. However, as the voxel resolution obtained is in the range of 9.77 - 15.51 μm for a specimen size of approximately 10 mm, only macro voids were visible, the effect of which is minimal in the deterioration due to acid attack and hence, not considered for the detailed analysis further. Three distinct zones could be identified in all acids: inner zone named as core, middle layer and the outer layer. The outer layer is degraded and decalcification is almost complete. The middle layer could be called as progression/reaction front for the attack to proceed inward wherein the decalcification is ongoing and is partly completed. The inner core zone is unattacked and the microstructure is very similar to the one before the attack.

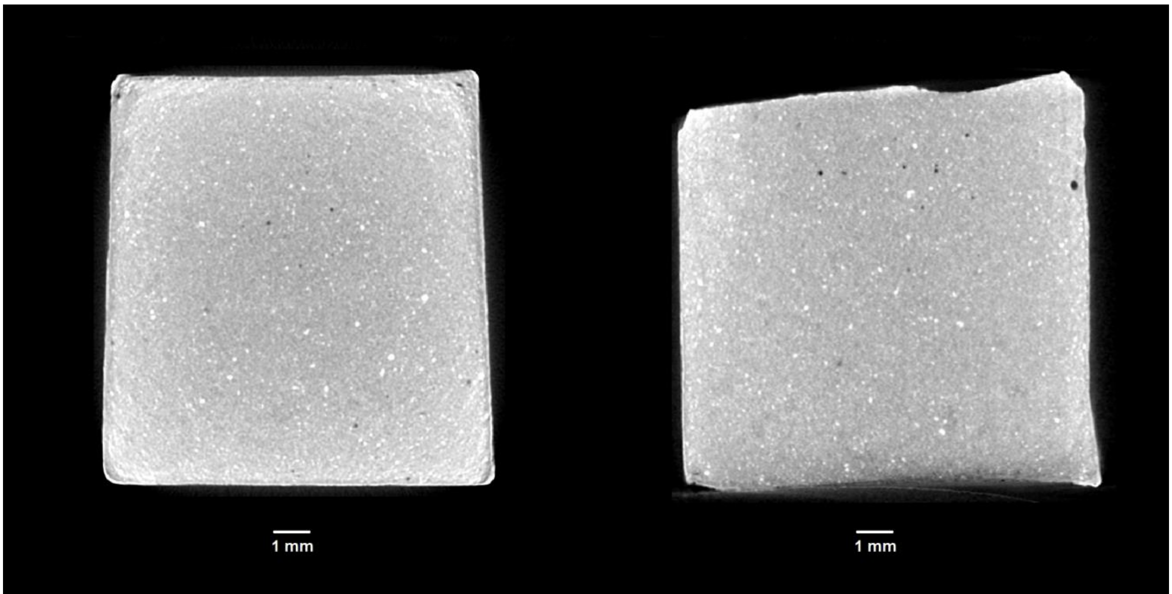

a) Top view (slice image) - inside b) Front view (slice image) – surface

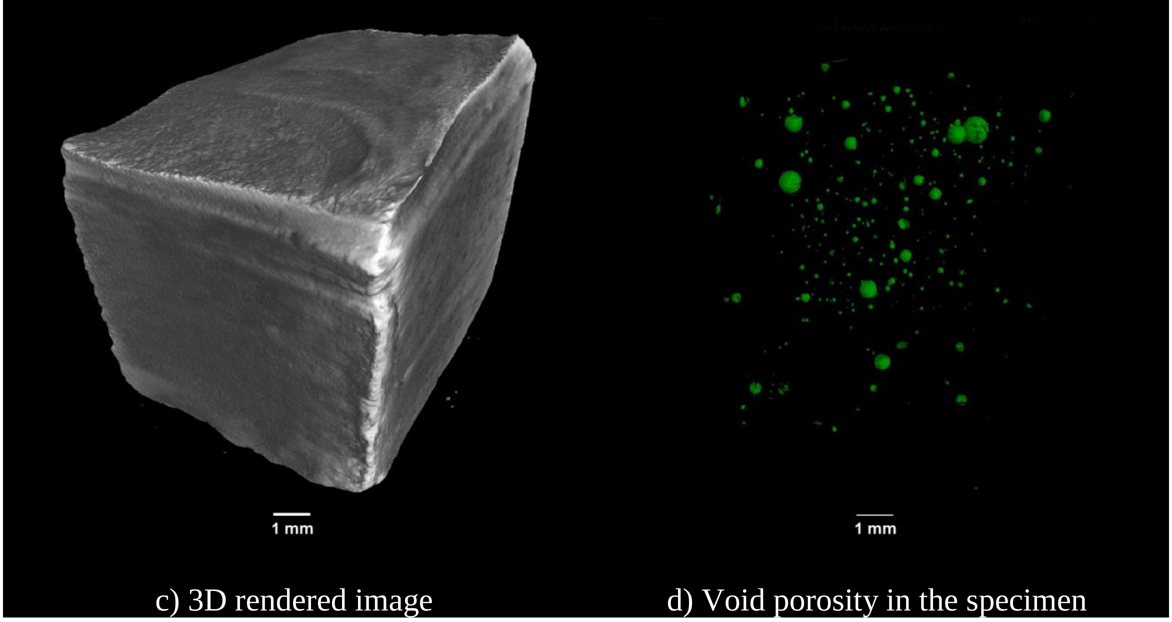

c) 3D rendered image d) Void porosity in the specimen

Figure 6.4 CT images of OPC paste specimen before acid exposure

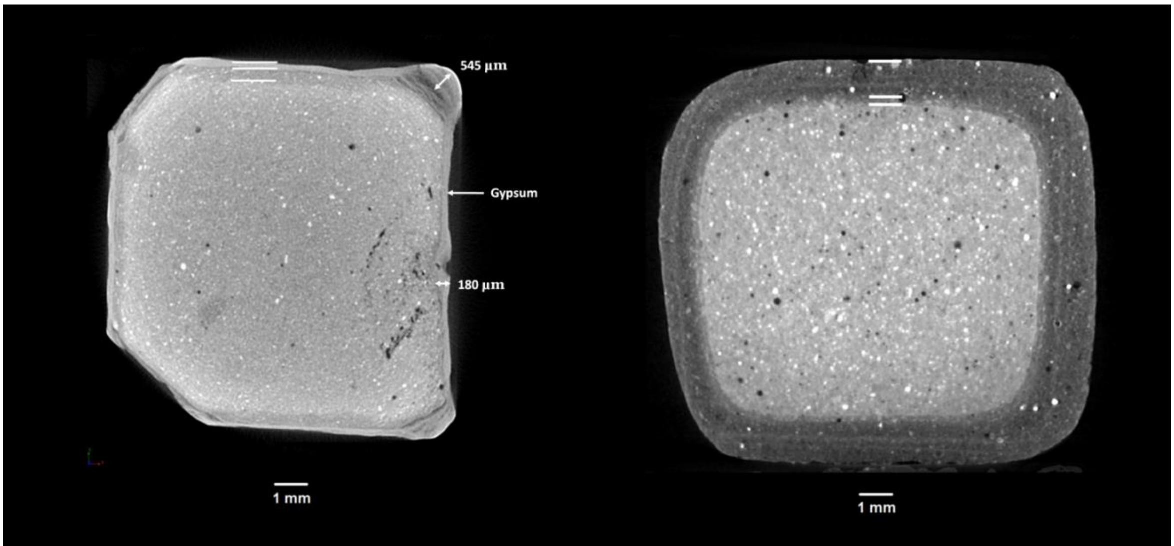

a) 1% sulphuric acid b) 1% hydrochloric acid

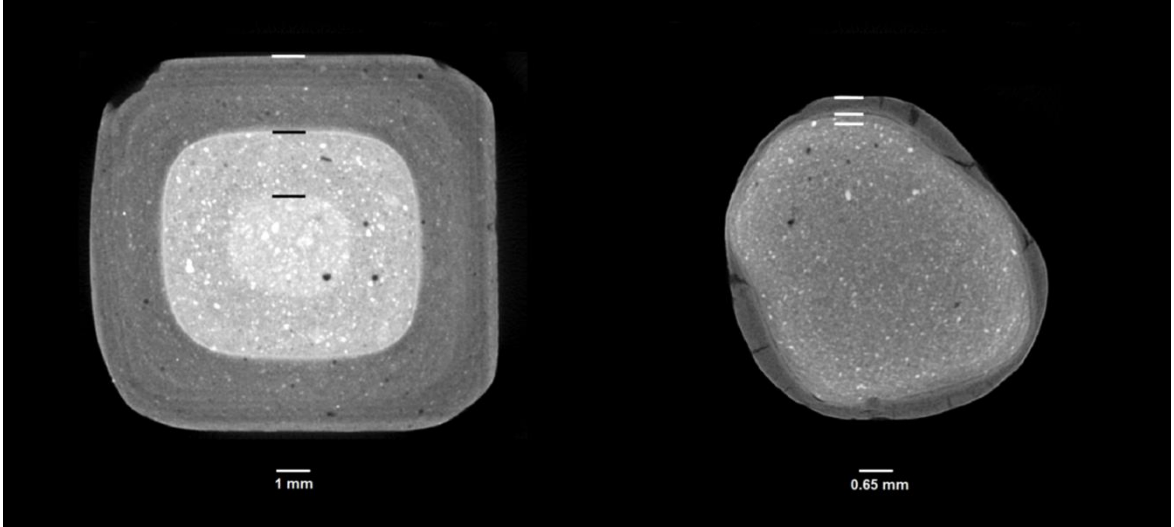

c) 0.5M acetic acid d) 0.5M citric acid

Figure 6.5 CT slice images (top view) of OPC paste exposed after acid exposure (test with brushing)

A thin layer of gypsum (white-yellow coloured precipitate on visual observation) bound with silica-alumina gel skeleton can be seen as an outer layer covering the specimen in the 2D slice images of OPC specimens exposed to sulphuric acid (Figure 6.5(a)). Calcium from the hydrates such as Portlandite and CSH gel leaches out to the exterior and combines with sulphate ions from the acid solution to form gypsum. As the solubility of the gypsum in the acid solution is less, it precipitates and adheres to the surface of the specimen. Decalcification of hydrates leads to formation of amorphous gel rich in silica and alumina which can be seen along with gypsum. The thickness of gypsum layer was more at the edges (due to penetration of acid from more than one direction) and less on the lateral surfaces. The average thickness of the layer at the edges was 545 µm, compared to 180 µm on the surfaces. The layer was soft in nature and could be removed due to brushing, especially at the edges. Edges that were more deteriorated due to decalcification appeared dark. However, no cracks were observed on the gypsum which was adhered on the lateral surface, thus confirming the protective nature of gypsum (Gutberlet et al., 2015), which played a role in limiting the degradation kinetics against further attack for the concentration of the acid studied (1%). Gypsum can be considered to be an expansive precipitate (solubility of 2.4 g/L at 20 °C) which might have blocked the pore spaces left behind by the decalcification of hydrated products, predominantly Portlandite, thus restricting the ingress of the acid further. The thickness of the middle layer which was undergoing the process of decalcification (partly decalcified) was found to be about 257 µm.

In the case of HCl, a thick layer of degraded products comprising mainly of amorphous silica gel (about 869 µm) was formed uniformly over the edges and on the surfaces (Figure 6.5(b)). The outer layer (orange brown) was darker and porous (lower GSV of pixels in the outer layer), which could be attributed to the severe decalcification of hydrates and consequently weak properties of the silica gel layer thus formed. Decalcification associated shrinkage cracks (map cracking due to changes in volume on conversion of hydrated products to silica gel) were seen on the external surface of the altered zone. Precipitate formation as in the case of sulphuric acid was not observed, as leaching and acidolysis were the driving processes of deterioration. Also, as the silica gel was adherent to the matrix and was not soft when compared to gypsum, deterioration at edges that was observed in sulphuric acid was absent in this case. Hence, the mass loss was predominantly due to combined effect of leaching and abrasive action. Calcium and aluminium salts being highly soluble (solubility of 745 g/L and 458 g/L respectively at 20 °C) leach out into the acid solution, leaving the silica gel porous, which results in further acid ingress, thus leading to greater degraded depth of the outer layer. As a result, the observed mass loss was higher (34.43%). However, despite the thick outer layer, the thickness of middle layer was found to be less (about 107 µm).

Even though acetic acid is generally considered as a weak acid, it was found to be highly detrimental to the cement matrix in this study. Both the outer and the middle layer were observed to be thicker as evident from Figure 6.5(c) (1825 µm and 1550 µm respectively), leaving only a small area of core that was left behind unattacked. The outer layer was severely decalcified as evident from the low GSV of pixels from CT images. Even anhydrous grains (white dots in images) were absent in the outer layer and this points out the instability of anhydrous grains and that the outer layer had completely turned amorphous. In addition to these three zones observed in all cases, a thin dense intermittent layer between the outer and the middle layer was observed in the specimens exposed to acetic acid and this may be ascribed to the formation of aluminium and/or iron bearing products which get deposited as a thin layer of hydroxides. Aluminium and iron also leach from the hydrates at a very low pH and get finally converted to corresponding hydroxides, which are seen as a thin brown ring encircling the middle layer. More importantly, the altered depth was found to be the highest among the acids studied (about 3375 µm), thus confirming the aggressiveness of acetic acid. The outer zone and the middle layer were found to be very weak with respect to the mechanical properties such as strength and hardness (Bertron et al., 2004). The mechanism of attack being leaching/acidolysis was similar to HCl. The calcium acetate salt that forms is soluble (solubility of 347 g/L at 20 °C) and leaches out making the outer layer porous (undissolved), with primarily silica gel (Bertron et al., 2007). Hence, the mass loss observed after six weeks was also higher (30.04%). The higher aggressiveness and alteration depth could also be due to properties such as specificity, buffer action and complexation properties exhibited by acetic acid (Koenig and Dehn, 2016; De Windt et al., 2015).

Citric acid was found to be the most aggressive among the acids studied for the concentration investigated. On exposure to citric acid, a white coloured salt due to calcium citrate tetrahydrate ($Ca_3(C_6H_5O_7)_2.4H_2O$) of very low solubility (0.95 g/L at 25 °C) was precipitated in substantial quantities on the specimens (Ramaswamy and Santhanam, 2016). The salt being totally non-protective as it was loosely attached to the matrix, led to almost complete dissolution of the outer degraded layer. Hence, it was seen only as a thin layer about 303 µm (dark layer with lower grayscale values for pixels) in CT images, as a majority of this zone underwent dissolution and got eroded away due to leaching and/or brushing. The shape of the specimen was highly distorted due to the formation of loosely adhered precipitates which were further removed by brushing/leaching. As the salt possesses a higher molar volume compared to hydrated products such as Portlandite and CSH (Larreur-Cayol et al., 2011a), it resulted in the formation of cracks in the outer layer as shown in Figure 6.5(d). As a result, the precipitate gets exfoliated from the specimen, goes into the acid solution and deposited in the beakers. Hence, the outer layer was restricted close to the surfaces only. This process of deterioration resulted in severe loss of mass (74.51%) and thickness, which is evident from the CT images. The higher aggressiveness could also be due to polyacidity and complexation properties of citric acid (Dyer, 2016; Ramaswamy and Santhanam, 2016). However, the thickness of the middle layer was observed to be less (196 μm) as in the case of sulphuric acid and HCl. As the outer degraded layer undergoes dissolution, the altered depth alone cannot be used as an indicator of degradation. In this case, loss of thickness is also important and must be taken into consideration.

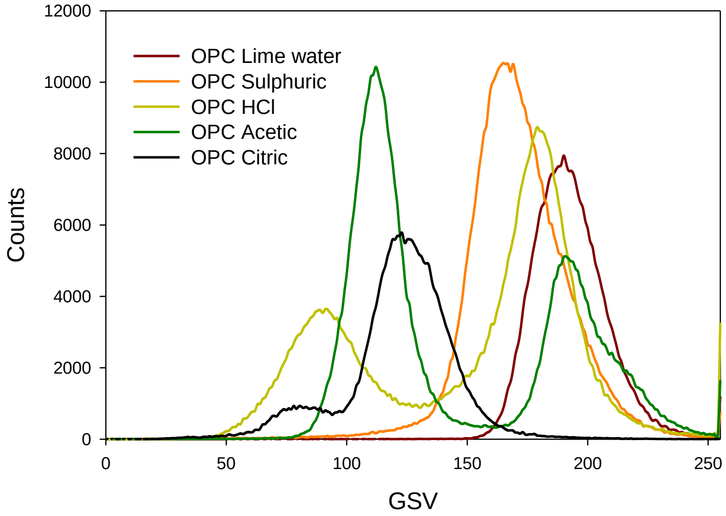

Figure 6.6 Histogram of CT images of OPC paste (with brushing)

The image analysis software called ImageJ was used for the detailed analysis of the tomography images to extract quantitative data. Histograms were plotted from the 8-bit images obtained from 2D slice images (based on Figure 6.5) and are shown in Figure 6.6. It can be seen that the histograms of acid attacked specimens shift to left when compared to the reference (OPC in lime water for 28 days), indicating the reduction of grayscale values. Histograms of all specimens are standardised with respect to the grayscale value of anhydrous grains, i.e. histograms are adjusted so that GSV of anhydrous grains in all the cases is equal to 255. As grayscale values are proportional to the attenuation coefficient and hence the density of the phases, it validates the fact that there is density reduction of cementitious phases associated with decalcification and weakening of microstructure associated with the degradation process. However, as the grayscale values may vary slightly on adjusting the brightness and contrast of the images after the reconstruction process, histograms are better used only qualitatively to assess the degree of deterioration.

Similarly, the variation of grayscale values of pixels of CT slice images can be plotted with the distance from the external surface of specimen by selecting and analyzing the image using rectangular selections of the area of image using 'plot profile' feature in ImageJ. In the case of citric acid, as the shape is not well defined, the average of six plot profile data obtained by drawing lines on images is taken to draw the GSV plot profile. The GSV profile data thus obtained is shown in Figure 6.7 a-e. On exposure to acids such as HCl, acetic and citric acids, there was a considerable reduction in GSV near the external surface, which indicates a remarkable reduction in density and constitutes the outer degraded layer. A gradual increase of GSV was observed towards the inner part of the image after the degraded layer and this could be attributed to the gradual decalcification of Portlandite and other hydrated products, and this forms the progression front for the attack to proceed inward. The GSV of the core zone is higher compared to the middle and outer layers. In the case of sulphuric acid, an increase of GSV can be observed near the external surface and this could be due to the formation of calcium sulphate salts.

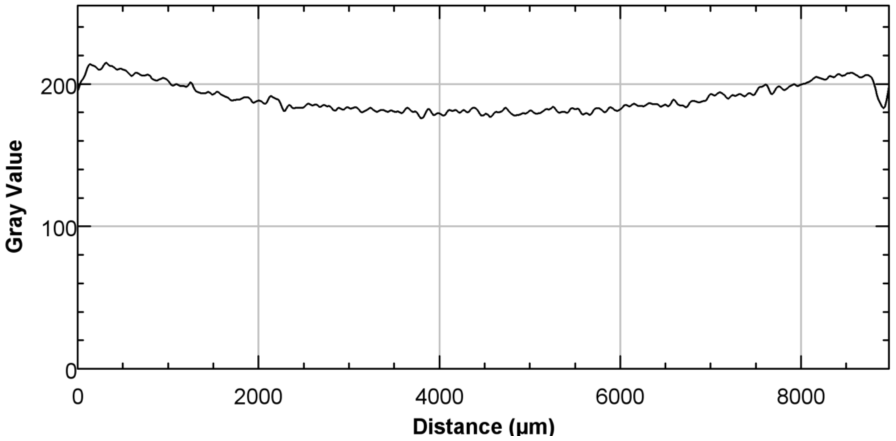

(a) OPC in saturated lime water

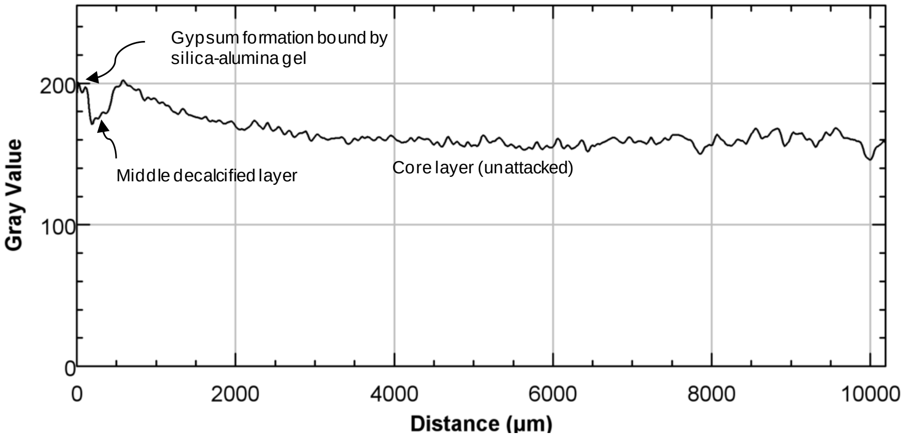

(b) OPC in 1% sulphuric acid

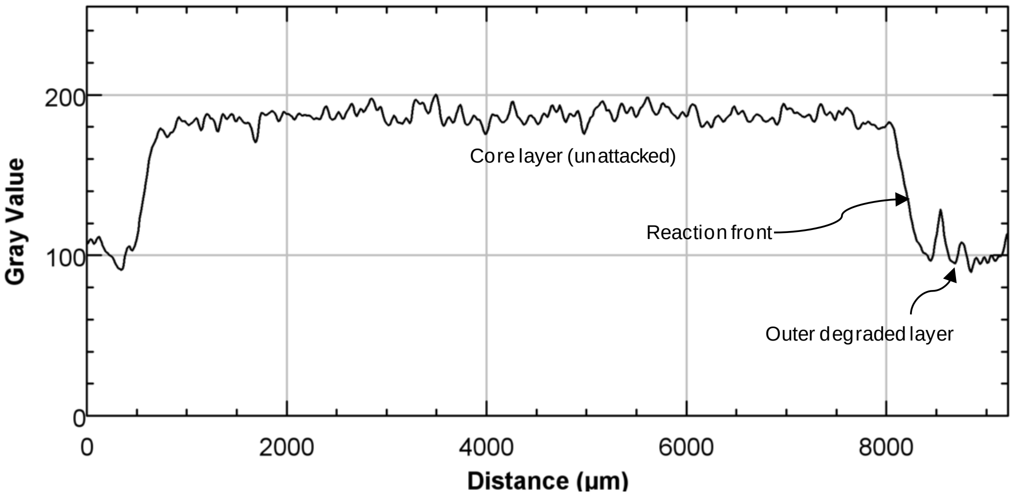

(c) OPC in 1% hydrochloric acid

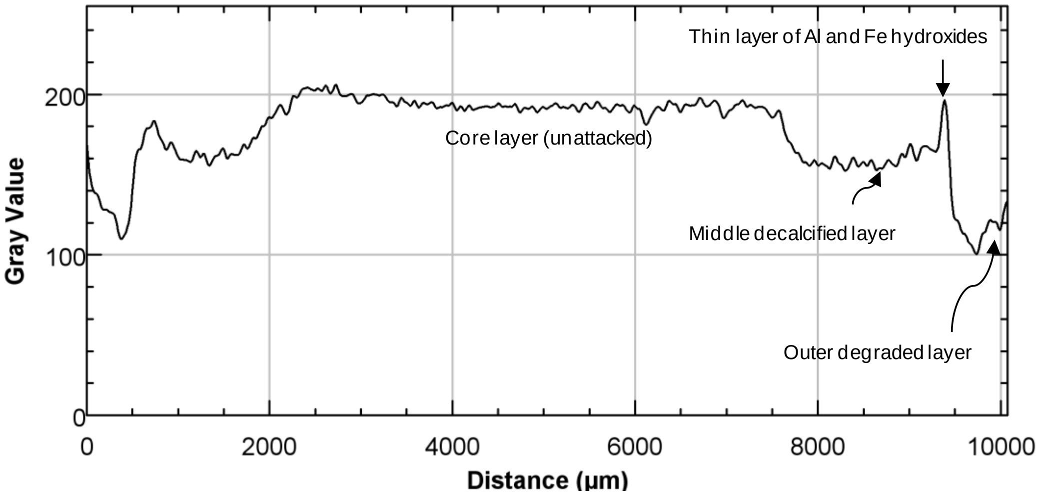

(d) OPC in 0.5M acetic acid

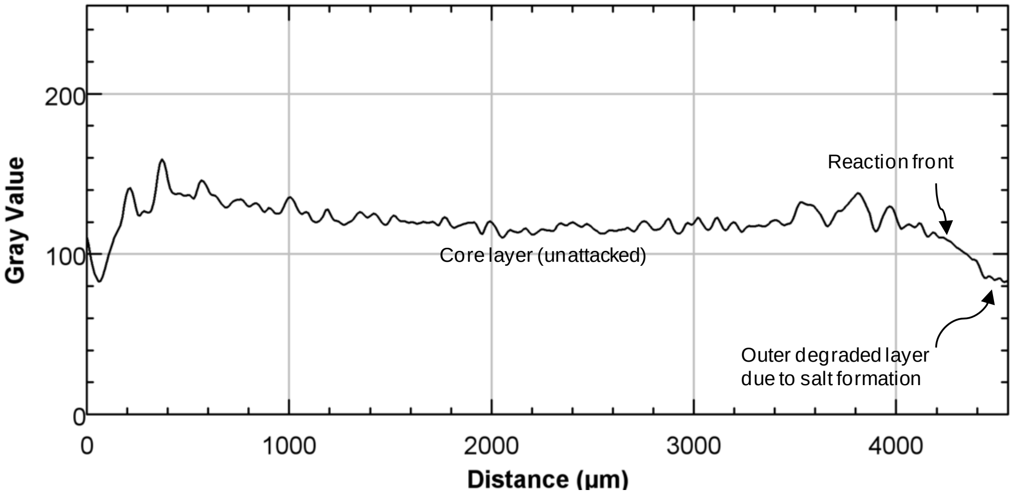

(e) OPC in 0.5M citric acid

Figure 6.7 GSV profile of CT images of OPC paste specimens exposed to acids (with brushing)

Figures 6.8 to 6.11 show the CT images of OPC, FA30, BFS50 and SF10 mixes on exposure to 1% sulphuric acid without the application of abrasive action. In the case of OPC (Figure 6.8), a thin layer of gypsum was found to form along with a decalcified layer comprising of amorphous silica gel. The deterioration was more evident on the edges due to penetration from multiple directions. The top view slice image cut through the degraded layer appears dark due to the formation of silica gel. The 3D rendered image shows the deterioration at the edges due to expansion created by the formation of gypsum on prolonged exposure to acid. Thin bands of gypsum and silica gel are found in FA30 specimen also (Figure 6.9). Similar bands of reaction products filled with gypsum and brucite were observed and reported by Santhanam et al. (2003) in the case of external sulphate attack. The slice cut through the degraded layer shows the delamination of gypsum from the lateral surface. The top view slice image cut through the degraded layer also shows the cracking in the degraded layer, which leads eventually to the loss of mass.

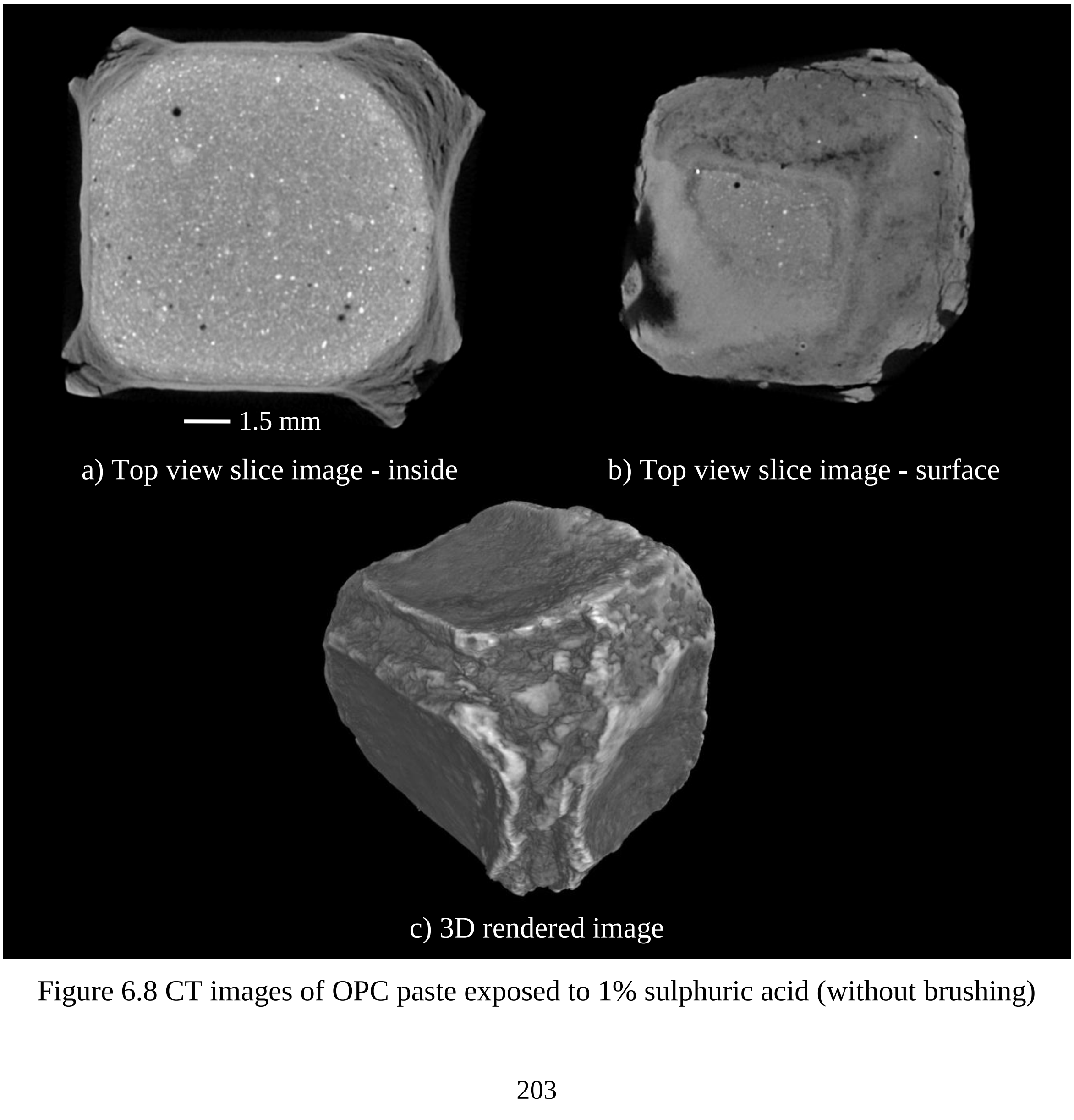

a) Top view slice image - inside

b) Top view slice image - surface

c) 3D rendered image

Figure 6.8 CT images of OPC paste exposed to 1% sulphuric acid (without brushing)

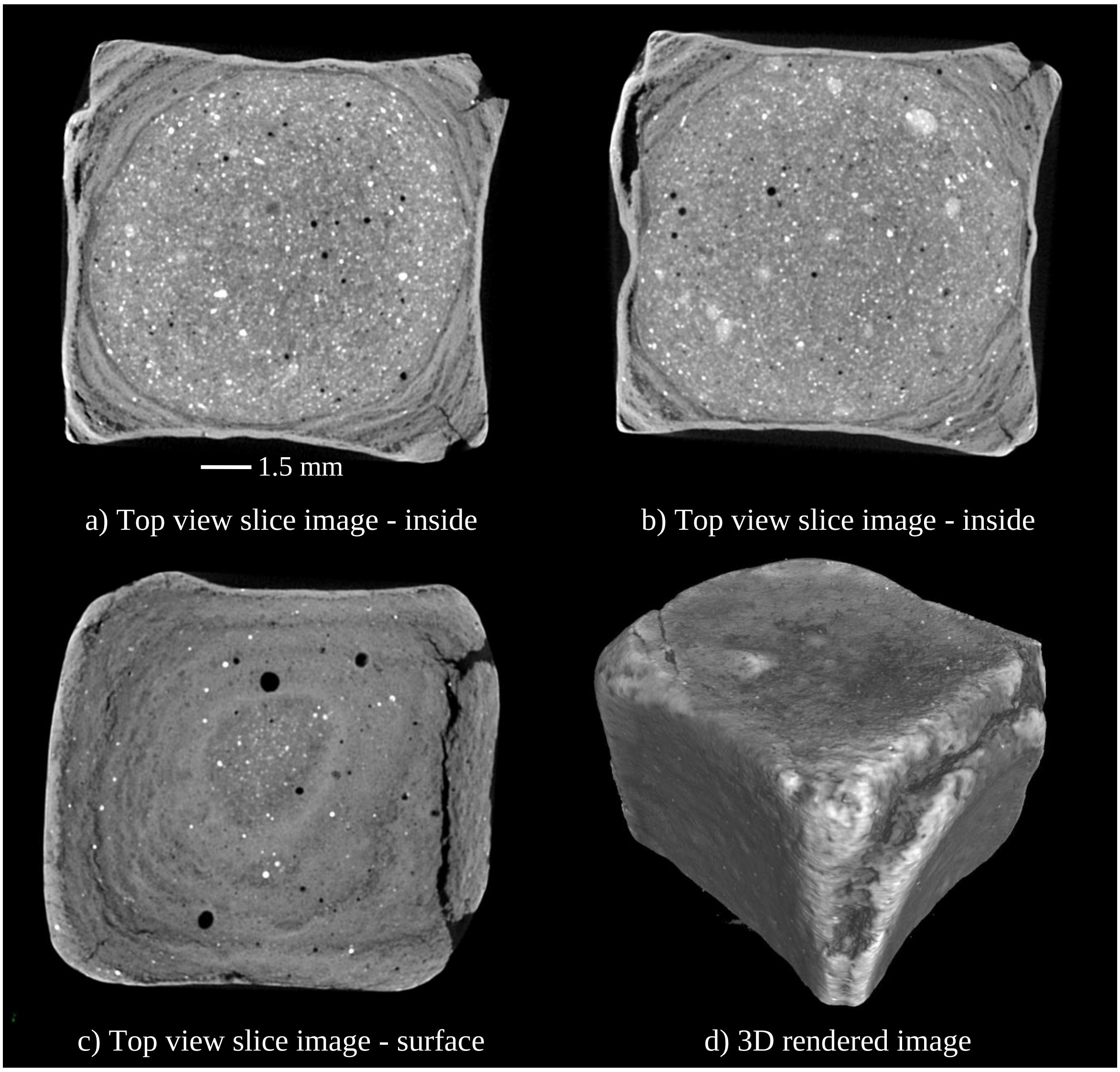

a) Top view slice image - inside

b) Top view slice image - inside

c) Top view slice image - surface

d) 3D rendered image

Figure 6.9 CT images of FA30 paste exposed to 1% sulphuric acid (without brushing)

The CT slice images of BFS50 mix reveal the gypsum (outer layer) and the presence of multiple layers of silica gel along with aluminium/iron hydroxides (Figure 6.10). Similar bands of degraded layers of cementitious pastes were reported by Murugan and Santhanam (2018), on exposure to 0.5M nitric acid. It is evident from the image that the gypsum layer is adherent to the lateral surface of the specimen. The front view slice images through the degraded layer show delamination of gypsum layer. This thick deposit of reaction products led to mass gain and increase in thickness when compared to the other mixes. In the case of SF10 mix, extensive delamination was observed from the CT images (Figure 6.11).

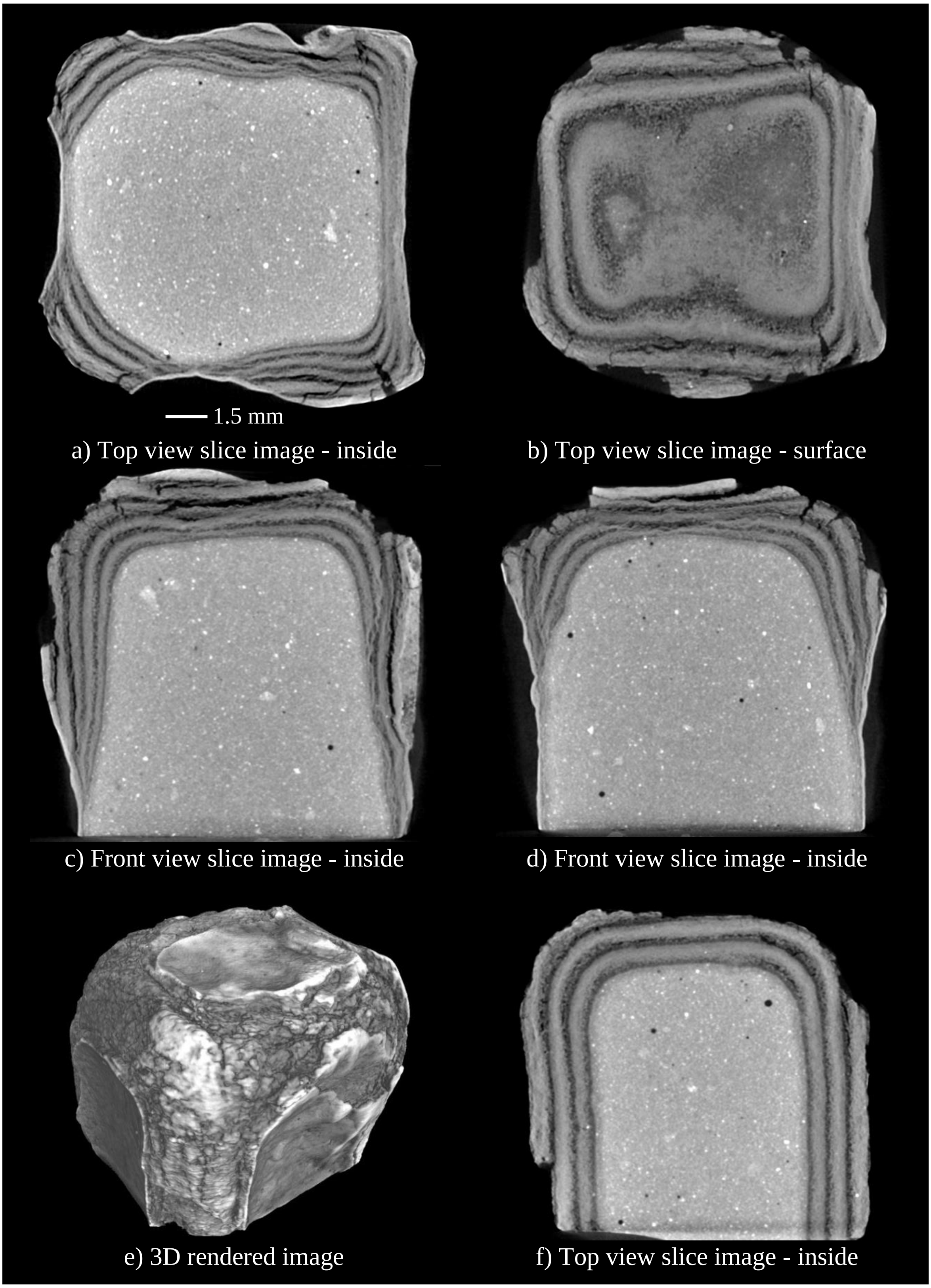

a) Top view slice image - inside

b) Top view slice image - surface

c) Front view slice image - inside

d) Front view slice image - inside

e) 3D rendered image

f) Top view slice image - inside

Figure 6.10 CT images of BFS50 paste exposed to 1% sulphuric acid (without brushing)

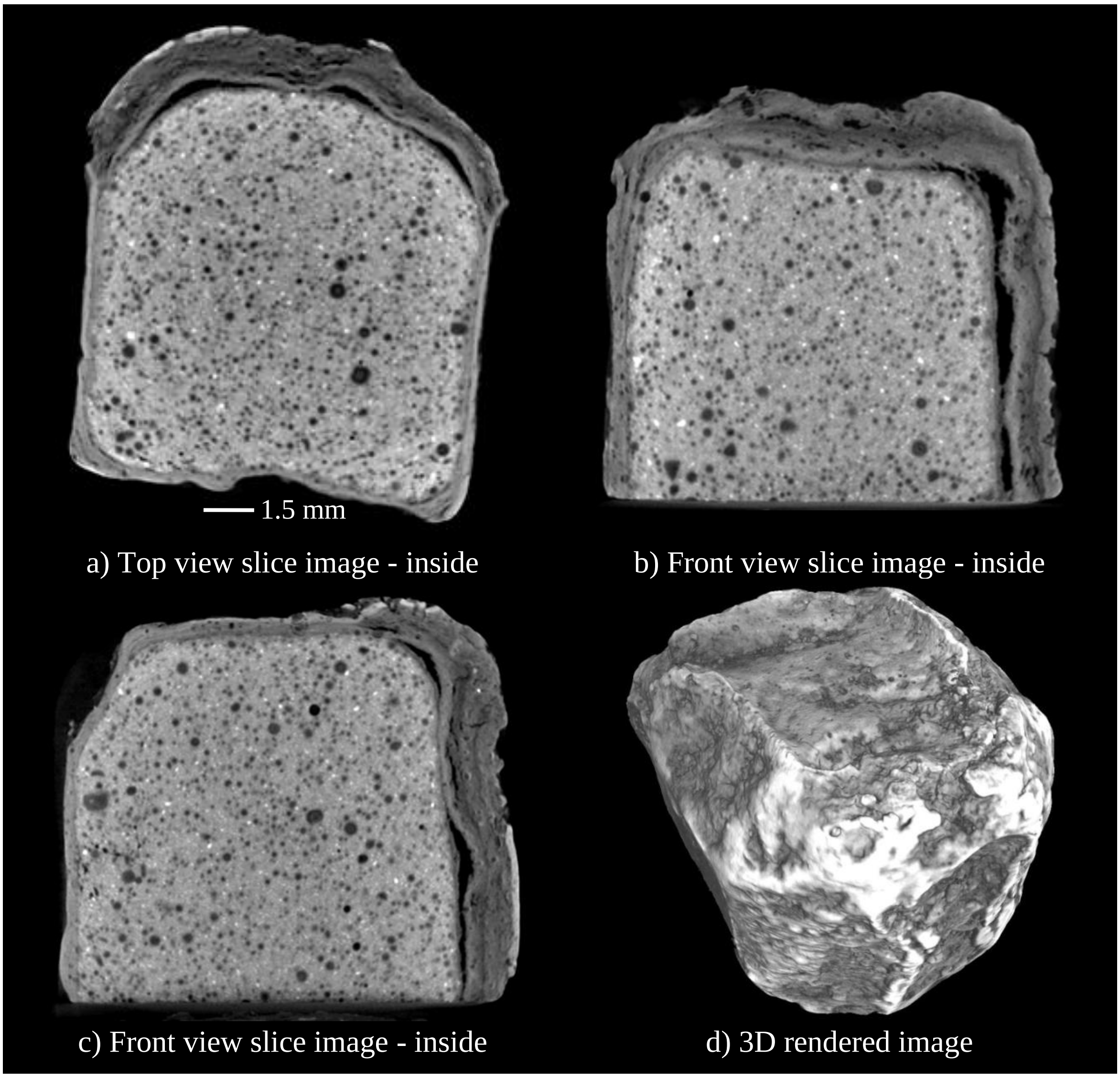

Figure 6.11 CT images of SF10 paste exposed to 1% sulphuric acid (without brushing)

Figures 6.12 to 6.15 show the CT images of OPC, FA30, BFS50 and SF10 mixes on exposure to 3% sulphuric acid without the application of abrasive action. In the case of OPC, only a thin layer of gypsum was seen around the specimen (Figure 6.12). The degraded layers which are formed earlier got delaminated at the end of 6 weeks of exposure leaving only a thin layer of gypsum. The 3D rendered image hence appeared smooth because most of the degraded layer has already been lost at the end of exposure period. Similar to the observations for 1% concentration, thick degraded layer was observed in the CT slice images of FA30 and BFS50. The delamination of the degraded layer and the associated damage due to the expansion was also evident from the CT images (Figure 6.13 and 6.14). In the case of SF10 mix, the observation was similar to OPC as most of the degraded layer had already been exfoliated and got collected in the beaker. The CT images show the delamination of previously formed degraded layers, thus trying to expose the freshly formed degraded layer (Figure 6.15).

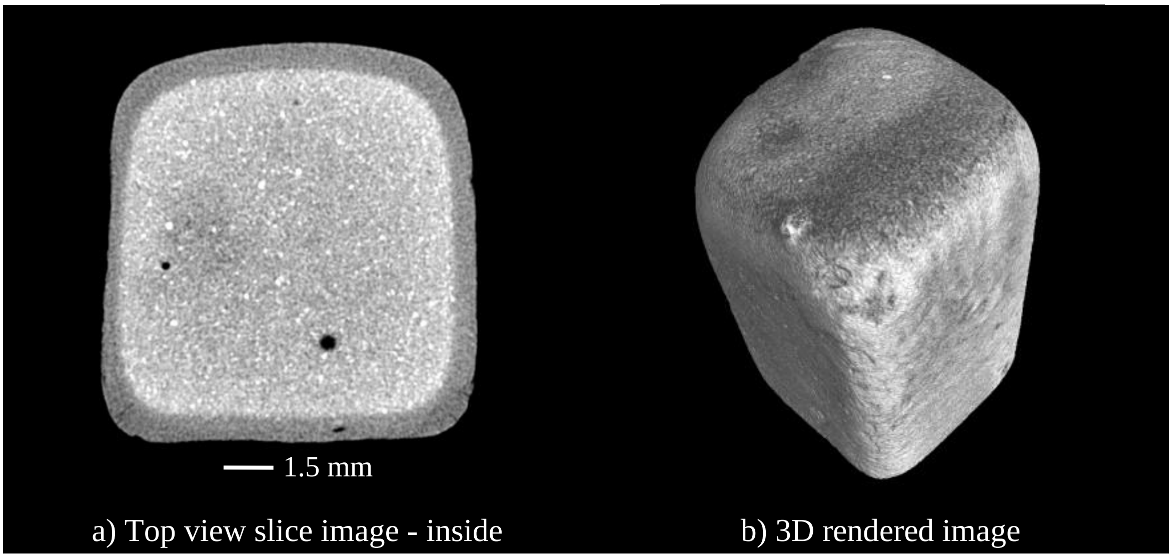

a) Top view slice image - inside b) 3D rendered image

Figure 6.12 CT images of OPC paste exposed to 3% sulphuric acid (without brushing)

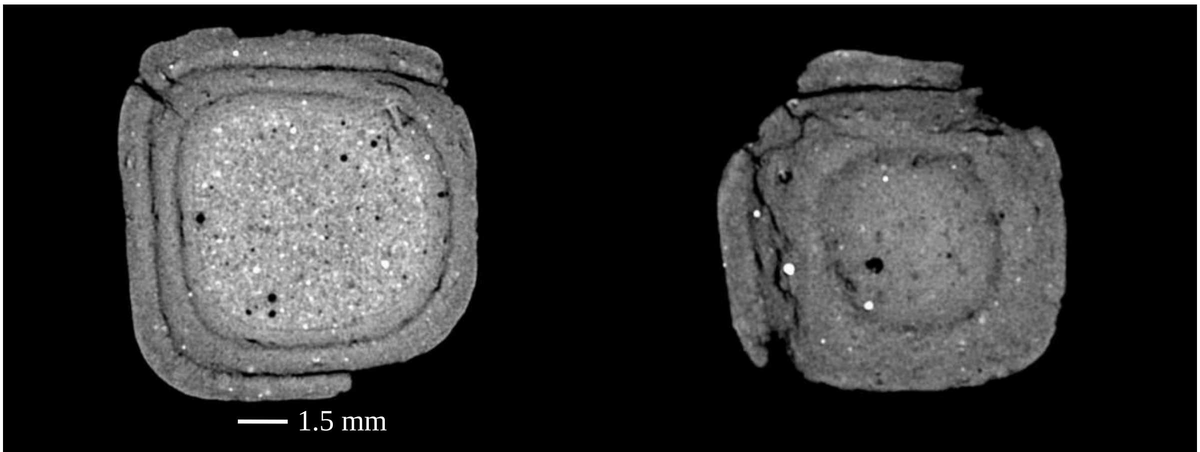

a) Top view slice image - inside b) Top view slice image - surface

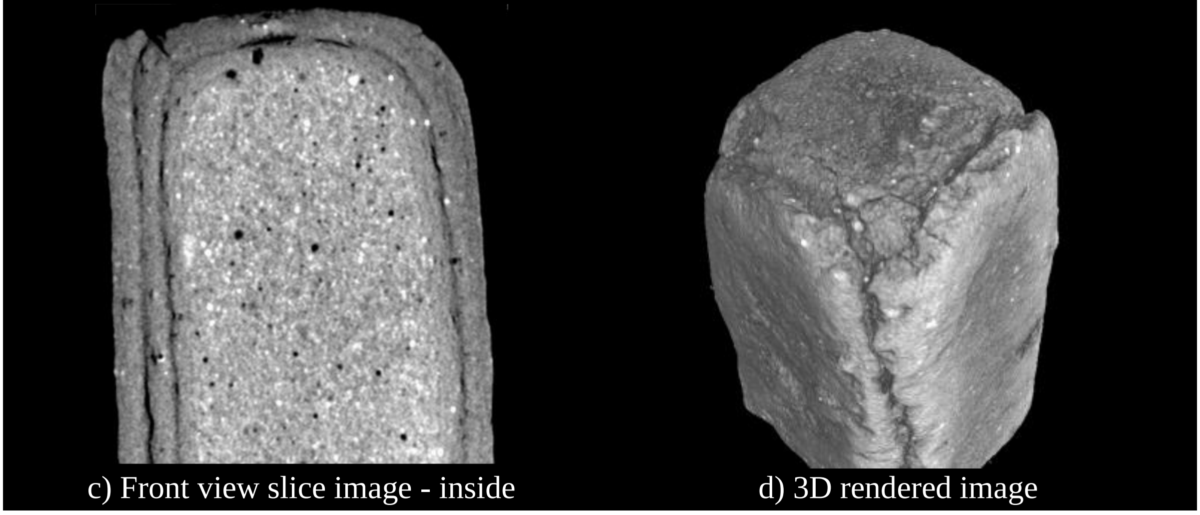

c) Front view slice image - inside d) 3D rendered image

Figure 6.13 CT images of FA30 paste exposed to 3% sulphuric acid (without brushing)

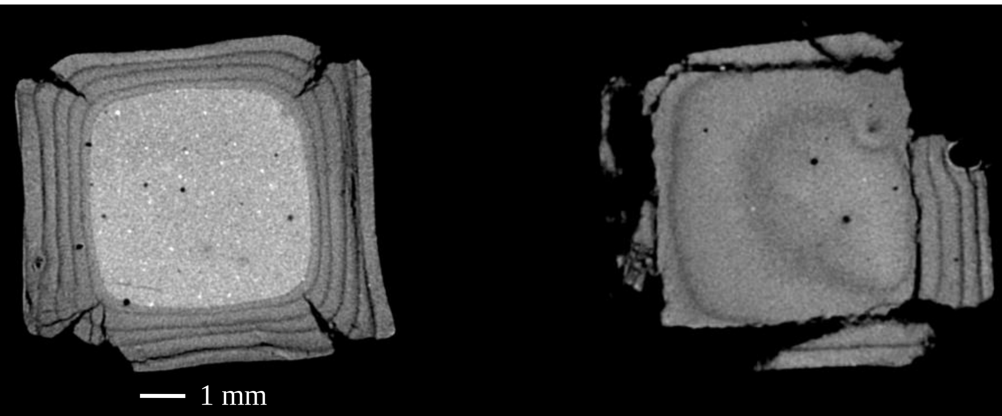

a) Top view slice image - inside b) Top view slice image - surface

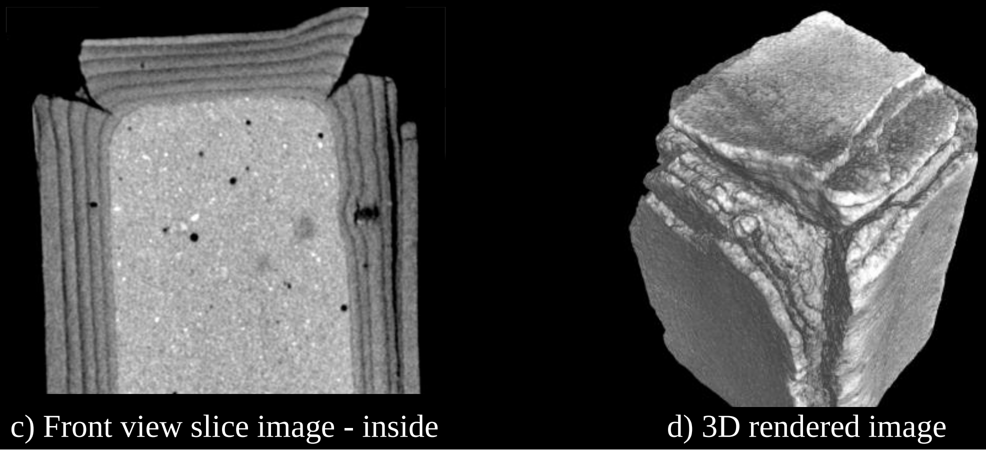

c) Front view slice image - inside d) 3D rendered image

Figure 6.14 CT images of BFS50 paste exposed to 3% sulphuric acid (without brushing)

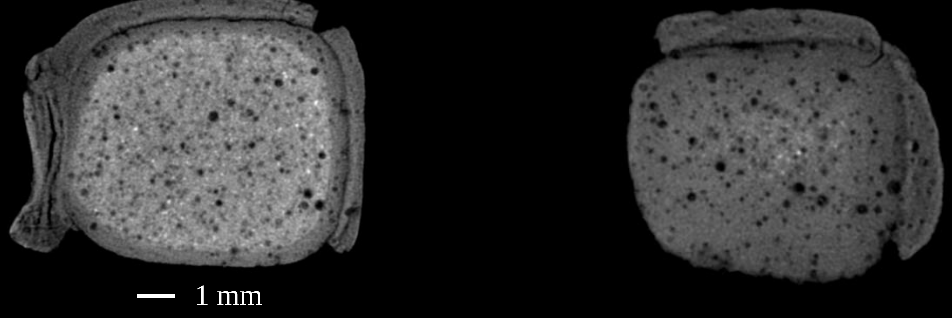

a) Top view slice image - inside b) Top view slice image - surface

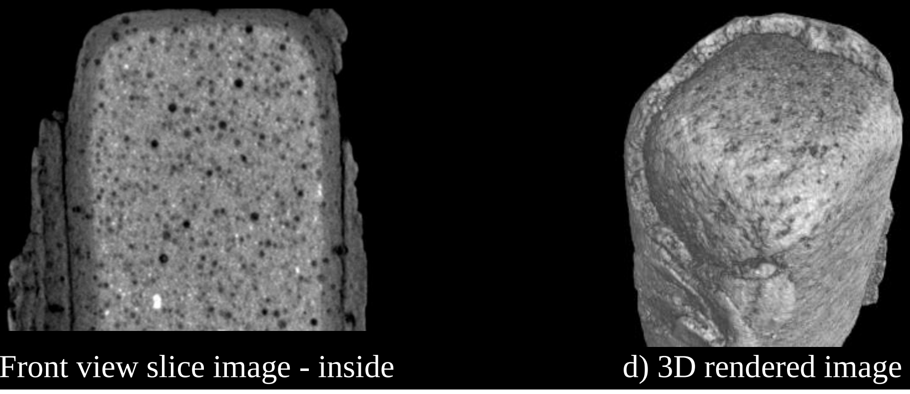

c) Front view slice image - inside d) 3D rendered image

Figure 6.15 CT images of SF10 paste exposed to 3% sulphuric acid (without brushing)

Figures 6.16 to 6.19 show the CT images of OPC, FA30, BFS50 and SF10 mixes on exposure to 1% hydrochloric acid without the application of abrasive action. The top view slice images of all specimens show distinct mineralogical zonation. A thick degraded layer comprising of silica alumina gel could be seen in all the mixes, the thickness of the degraded layer being greater for FA30. In the case of OPC and SF10, a middle layer which is partially decalcified is also visible from the CT images. The external degraded layer shows extensive shrinkage cracks on drying. This could be associated with the shrinkage due to the decalcification of hydrated products (Chen et al., 2006; Murugan and Santhanam, 2018). The 3D rendered images show less deterioration compared to sulphuric acid as there was no precipitation induced damage.

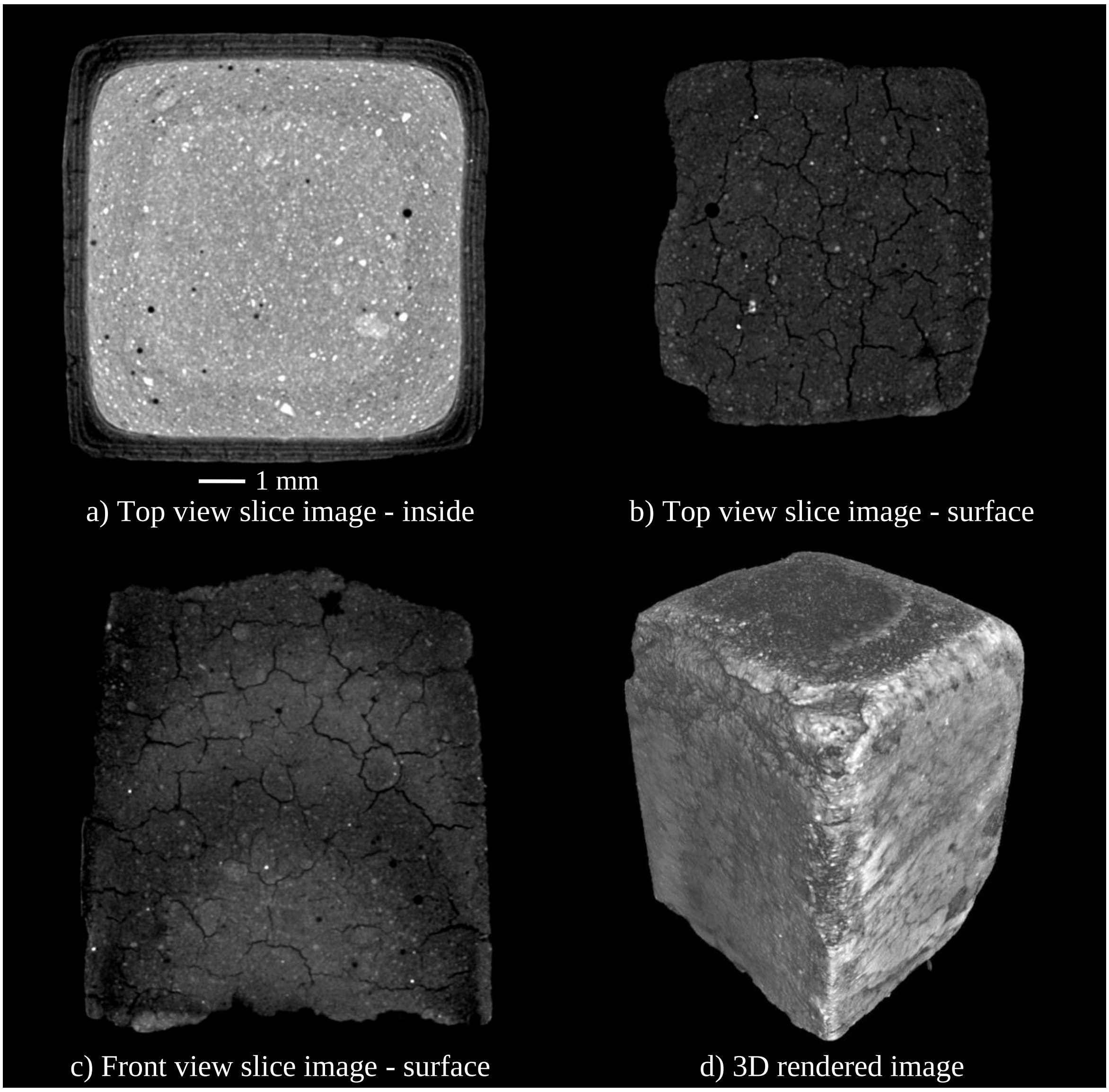

a) Top view slice image - inside

b) Top view slice image - surface

c) Front view slice image - surface

d) 3D rendered image

Figure 6.16 CT images of OPC paste exposed to 1% hydrochloric acid (without brushing)

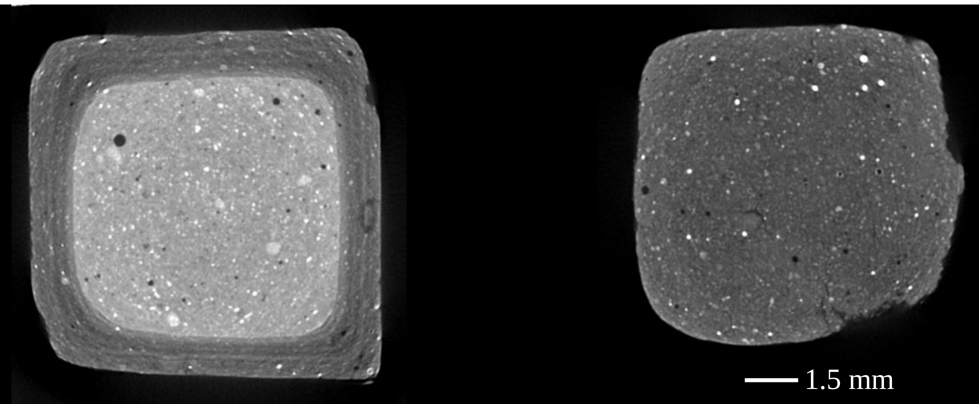

a) Top view slice image - inside

b) Top view slice image - surface

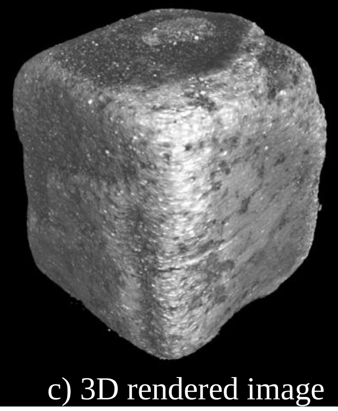

c) 3D rendered image

Figure 6.17 CT images of FA30 paste exposed to 1% hydrochloric acid (without brushing)

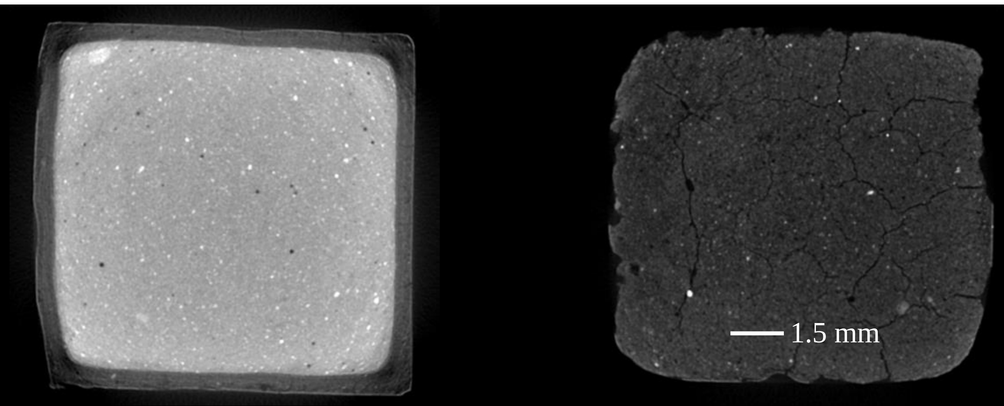

a) Top view slice image - inside

b) Top view slice image - surface

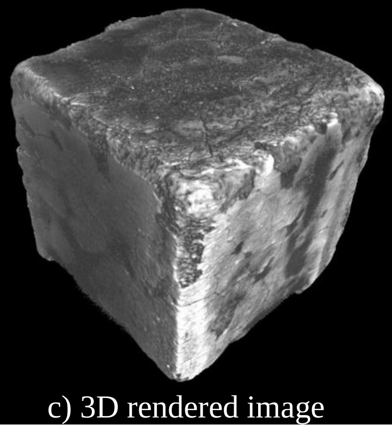

c) 3D rendered image

Figure 6.18 CT images of BFS50 paste exposed to 1% hydrochloric acid (without brushing)

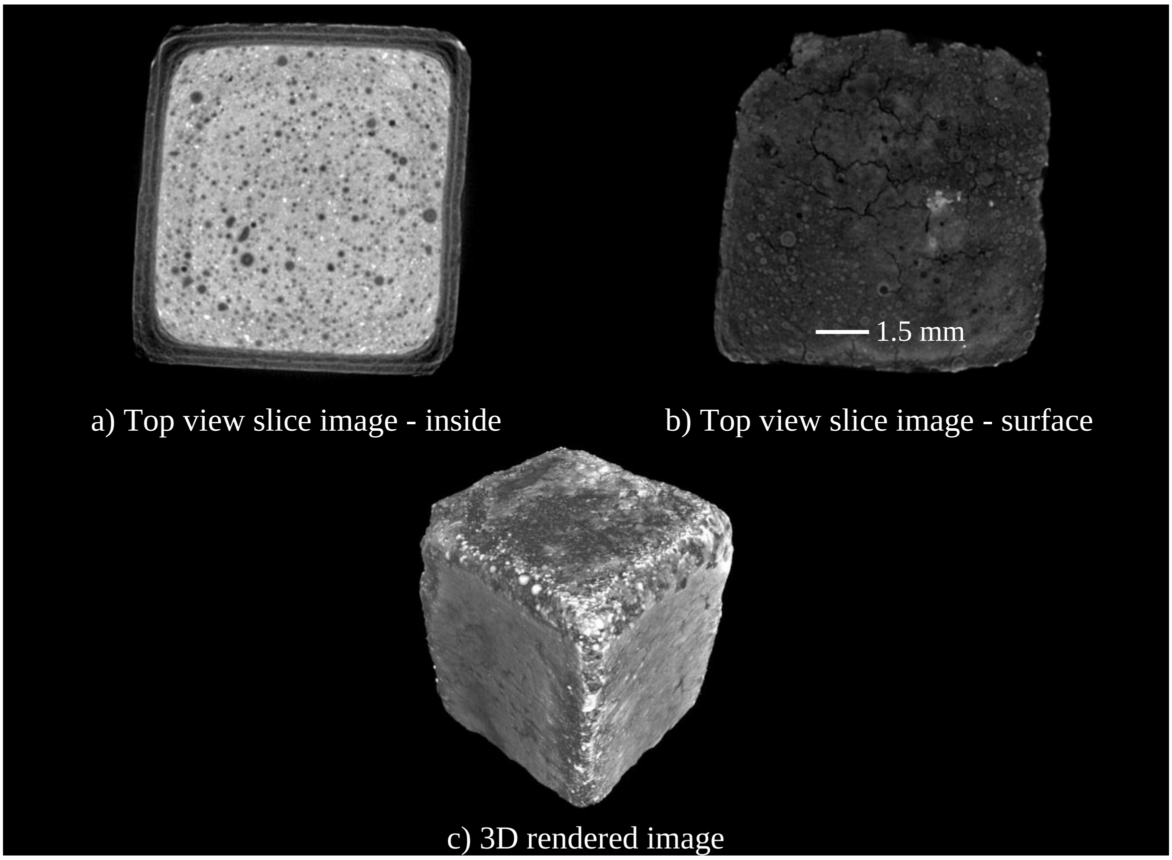

a) Top view slice image - inside

b) Top view slice image - surface

c) 3D rendered image

Figure 6.19 CT images of SF10 paste exposed to 1% hydrochloric acid (without brushing)

Figures 6.20 to 6.23 show the CT images of OPC, FA30, BFS50 and SF10 mixes on exposure to 0.5M acetic acid without the application of abrasive action. The mineralogical zonation was similar to the hydrochloric acid as the mechanism of degradation was identical (i.e. due to the formation of soluble salts leaching out into the solution). However, the thickness of the degraded layer was found to be higher for 0.5M acetic acid. The slice images through the degraded layer appeared dark indicating severe decalcification. Large cracks were evident in the slice images cut through the degraded layers. These indicate the weak mechanical property of the silica gel layer that is formed. Similar to HCl, in addition to the outer degraded layer, a thick middle layer could be observed on OPC and SF10 mixes. This middle layer might have undergone partial decalcification. The depth of degraded layer was found to be higher for FA30 when compared to other mixes. The depths of degraded layers of other mixes were comparable. As the salts are soluble, external visual deterioration, as evident from the 3D rendered image for all the mixes, was less in the case of acetic acid. In the case of 0.25M acetic acid, the microstructural change was similar except that the thickness of the degraded layers was less as the concentration was one half of 0.5M acetic acid. The CT images for specimens exposed to 0.25M acetic acid are shown in Appendix B, Figures B-4 to B-7.

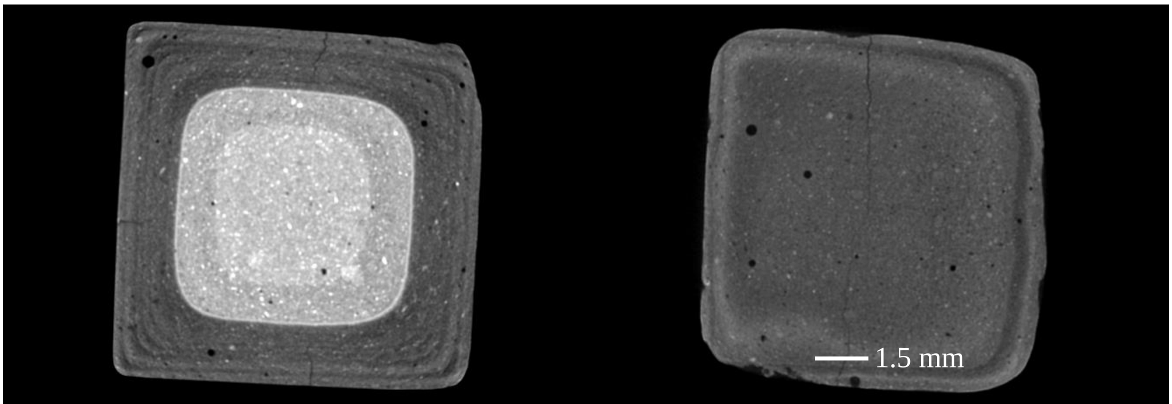

a) Top view slice image - inside

b) Top view slice image - surface

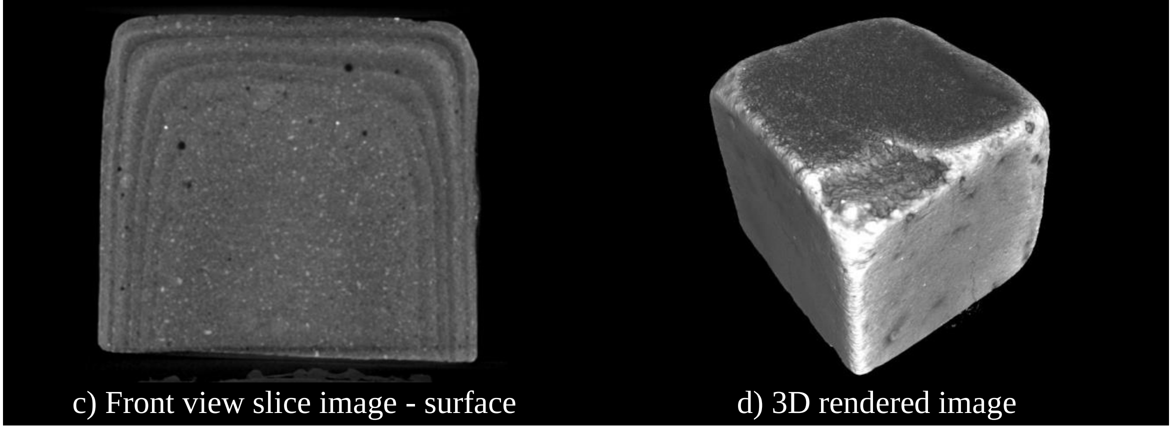

c) Front view slice image - surface

d) 3D rendered image

Figure 6.20 CT images of OPC paste exposed to 0.5M acetic acid (without brushing)

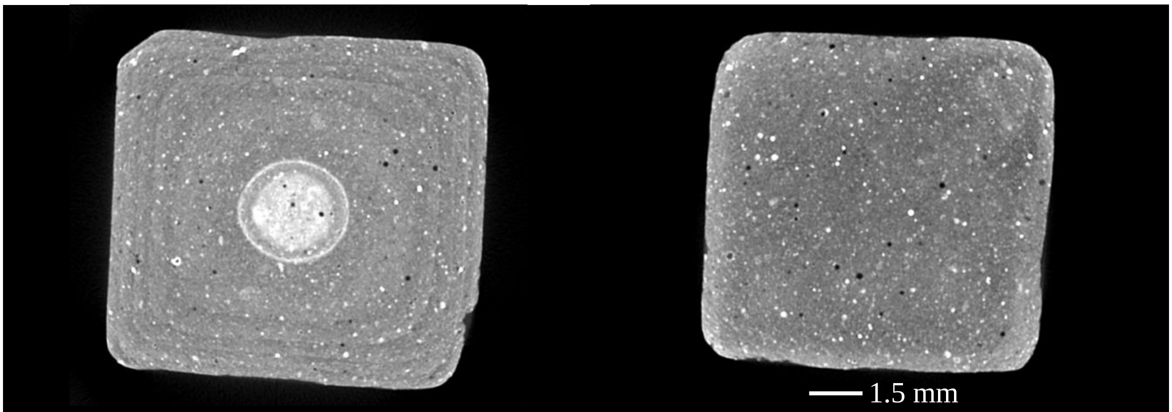

a) Top view slice image - inside

b) Top view slice image - surface

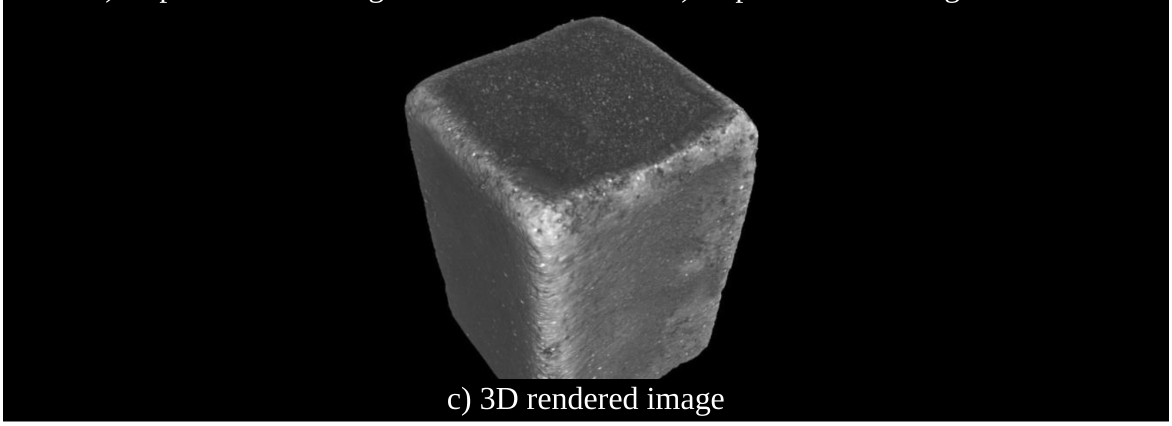

c) 3D rendered image

Figure 6.21 CT images of FA30 paste exposed to 0.5M acetic acid (without brushing)

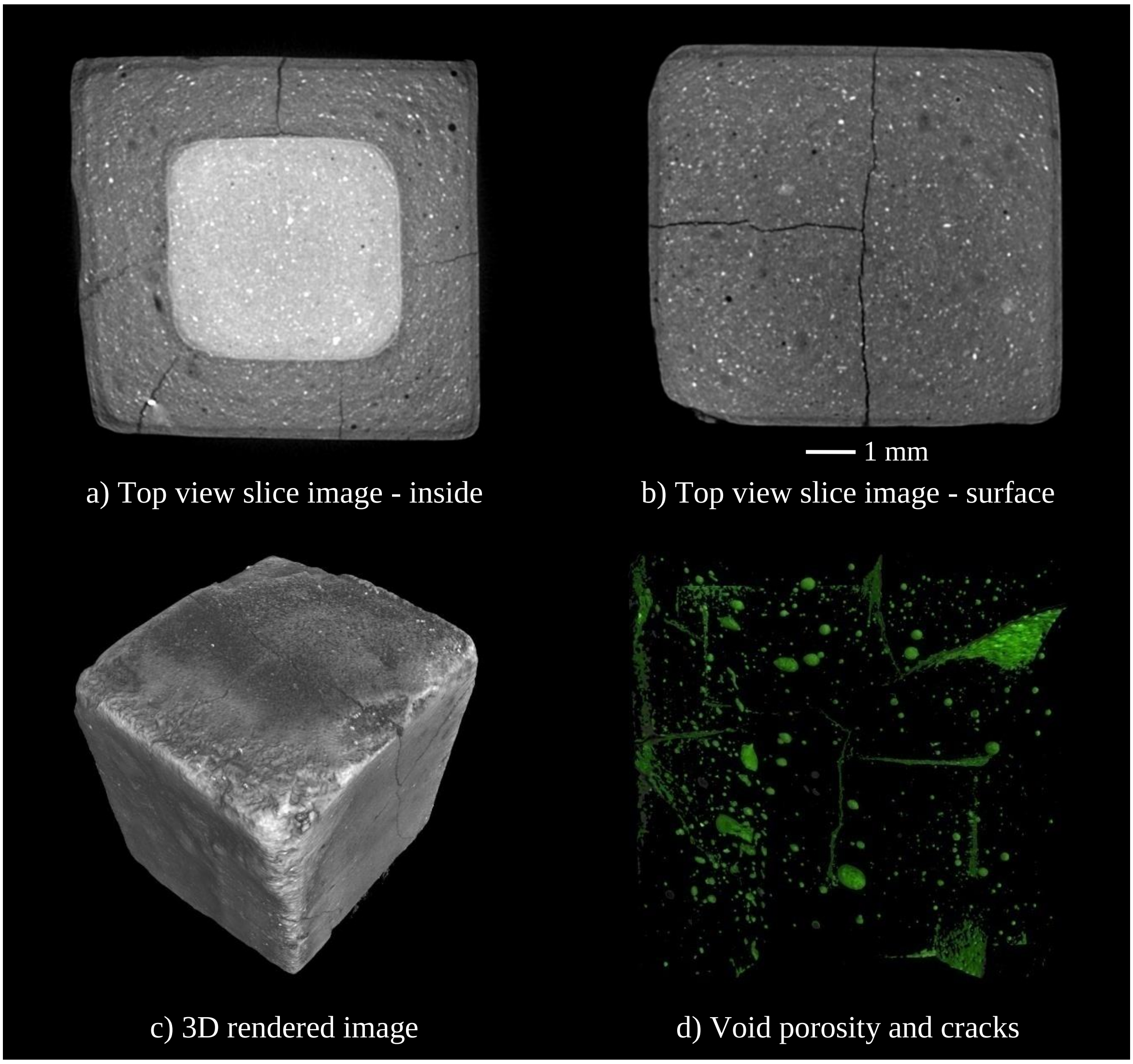

a) Top view slice image - inside

b) Top view slice image - surface

c) 3D rendered image

d) Void porosity and cracks

Figure 6.22 CT images of BFS50 paste exposed to 0.5M acetic acid (without brushing)

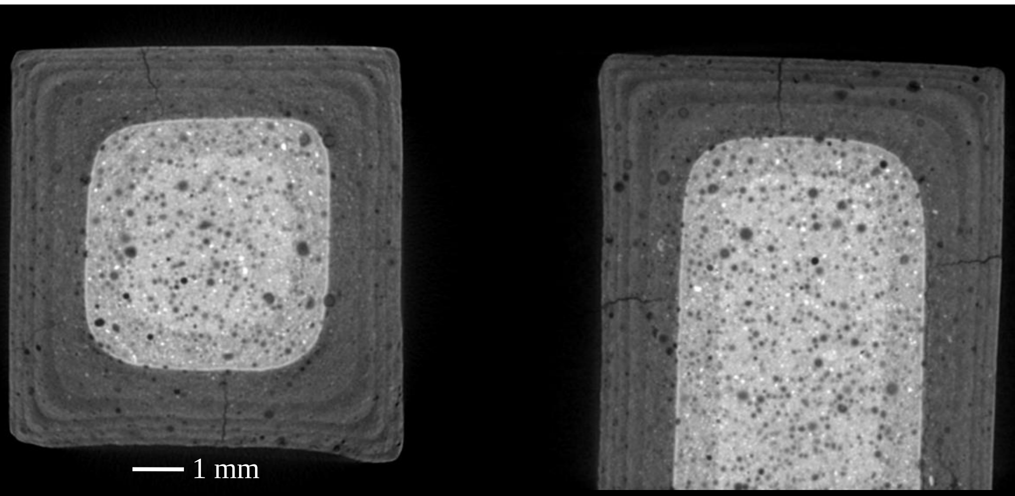

a) Top view slice image - inside

b) Front view slice image - inside

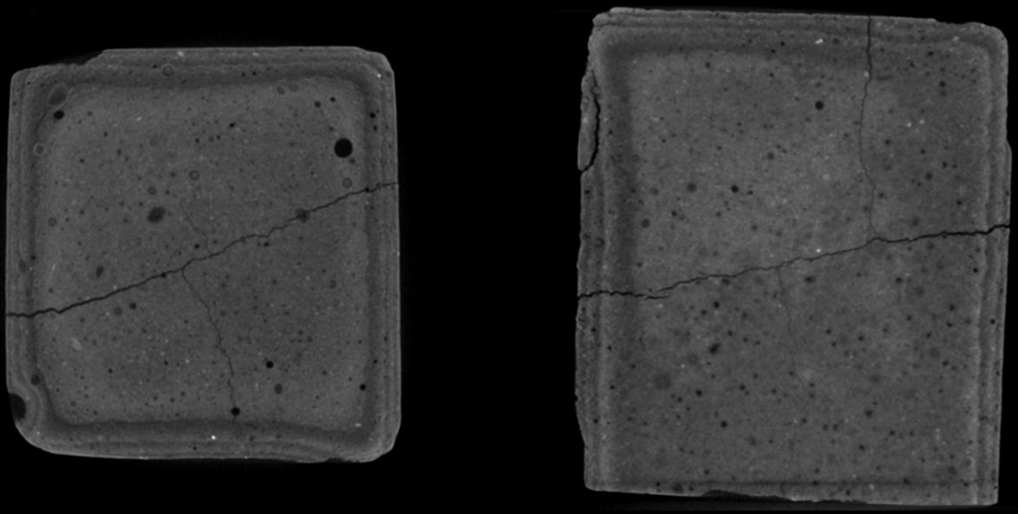

c) Top view slice image - surface

d) Front view slice image - surface

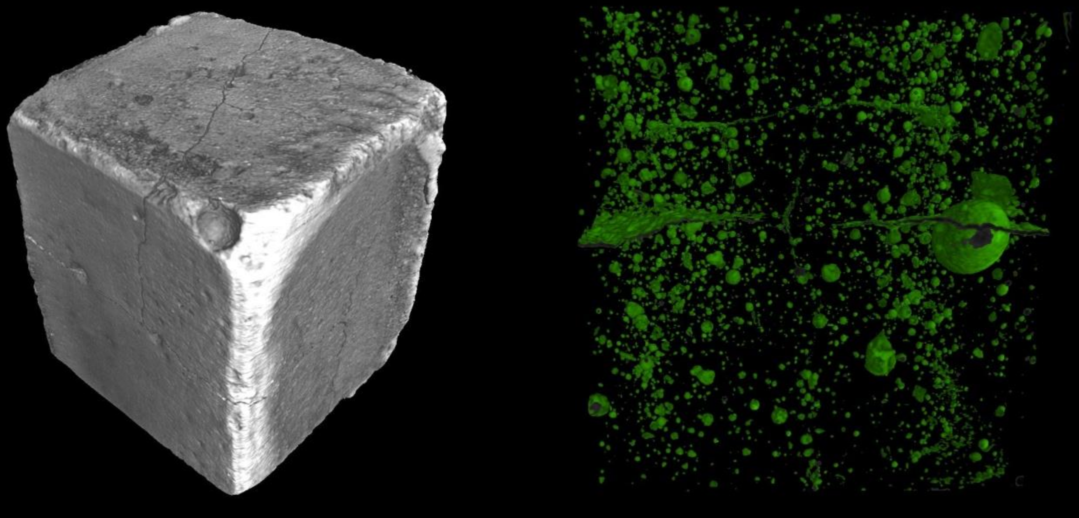

e) 3D rendered image

f) Void porosity and cracks

Figure 6.23 CT images of SF10 paste exposed to 0.5M acetic acid (without brushing)

Figures 6.24 to 6.27 show the CT images of OPC, FA30, BFS50 and SF10 mixes on exposure to 0.5M citric acid without the application of abrasive action. Higher aggressiveness and rapid loss of mass and thickness are evident from images of the specimens exposed to citric acid. The top view and front view slice images for all the mixes showed extensive cracking of the outer degraded layer. This could be due to the expansion induced by the higher molar volume of the calcium salt that is formed. Also, the thickness of the outer layer was found to be less when compared to other acids. This indicates the non-protective nature of the salt. The salt having low affinity with the matrix gets exfoliated and the layer subsequently defragments away into the solution. Among all the mixes, the thickness of the outer degraded layer for BFS50 mix was found to be the highest. As explained in the earlier sections on mass changes, the presence of alumina could enhance the degradation kinetics when exposed to citric acid. The severe damage and the loss of mass/thickness were evident from the 3D rendered images of all the mixes. The CT images of the specimens tested with abrasion were also found to be similar to the specimens without abrasion, except for the fact that the thickness of the degraded layer could be different owing to the removal of corroded layer due to the periodic brushing. These CT images are shown in Appendix B, Figures B-8 to B-27.

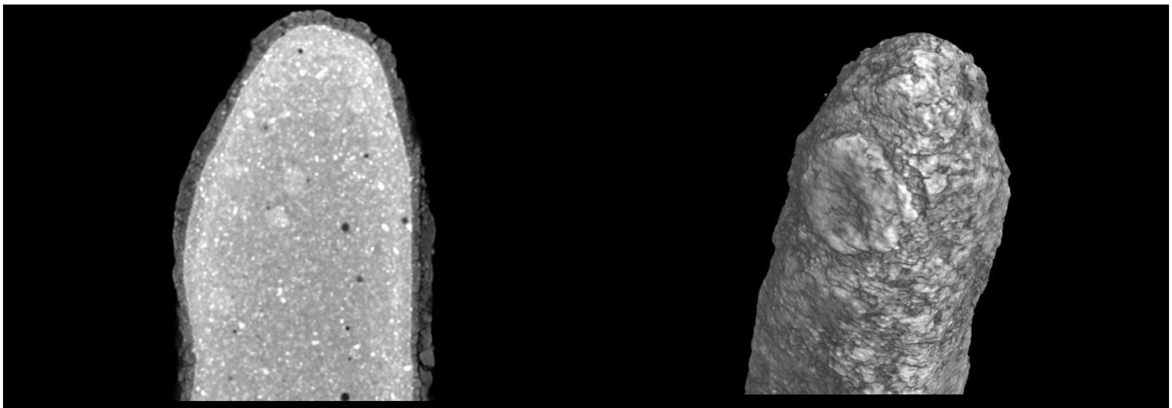

a) Front view slice image - surface

b) 3D rendered image

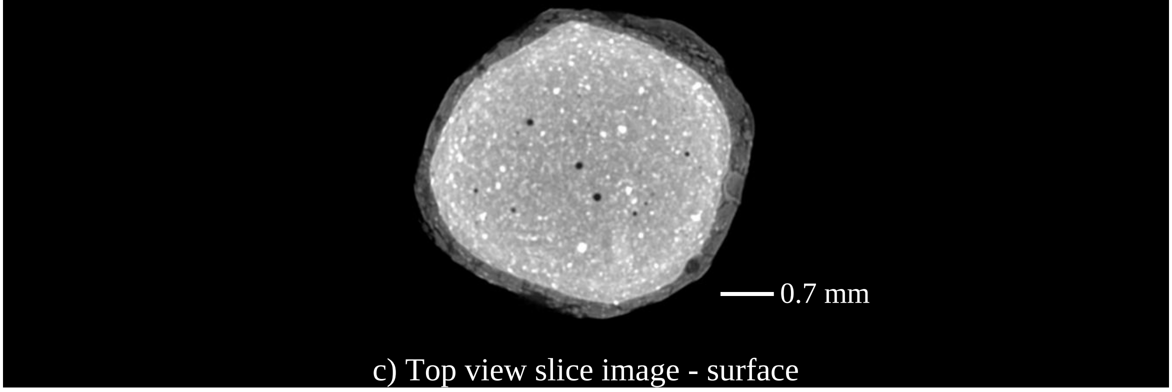

c) Top view slice image - surface

Figure 6.24 CT images of OPC paste exposed to 0.5M citric acid (without brushing)

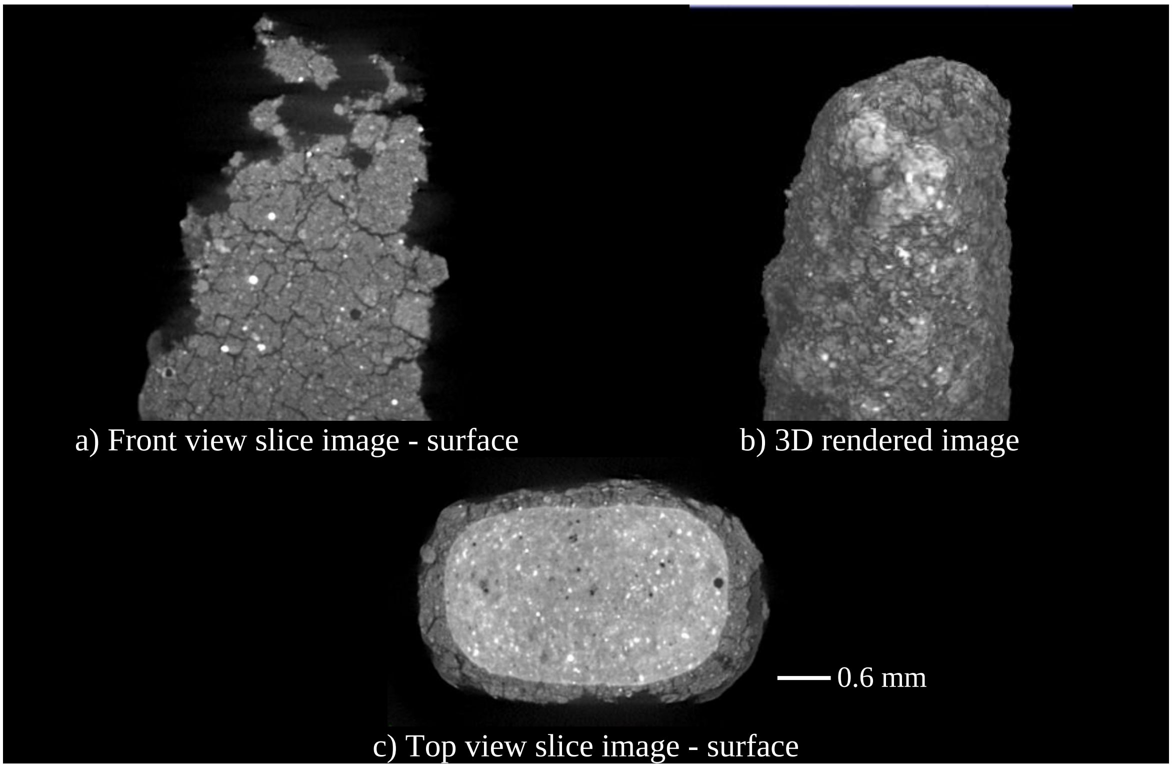

a) Front view slice image - surface

b) 3D rendered image

c) Top view slice image - surface

Figure 6.25 CT images of FA30 paste exposed to 0.5M citric acid (without brushing)

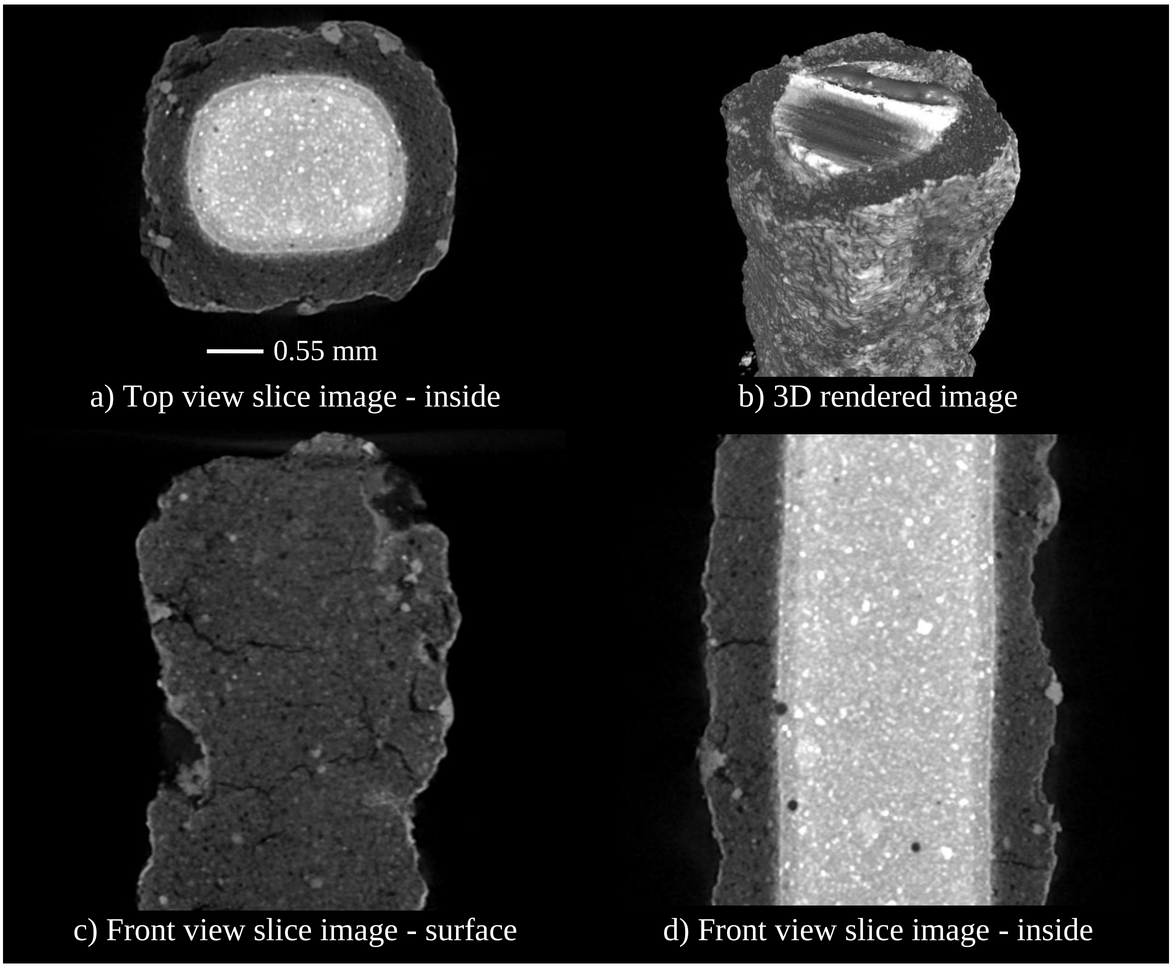

a) Top view slice image - inside

b) 3D rendered image

c) Front view slice image - surface

d) Front view slice image - inside

Figure 6.26 CT images of BFS50 paste exposed to 0.5M citric acid (without brushing)

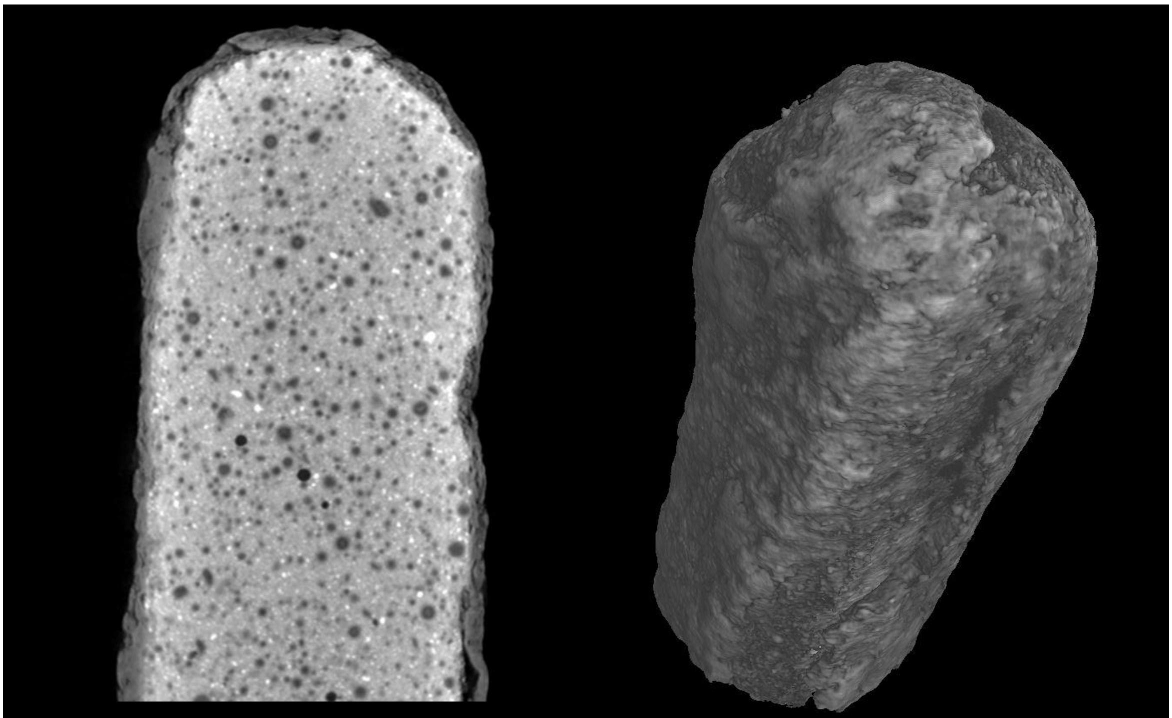

a) Front view slice image - inside

b) 3D rendered image

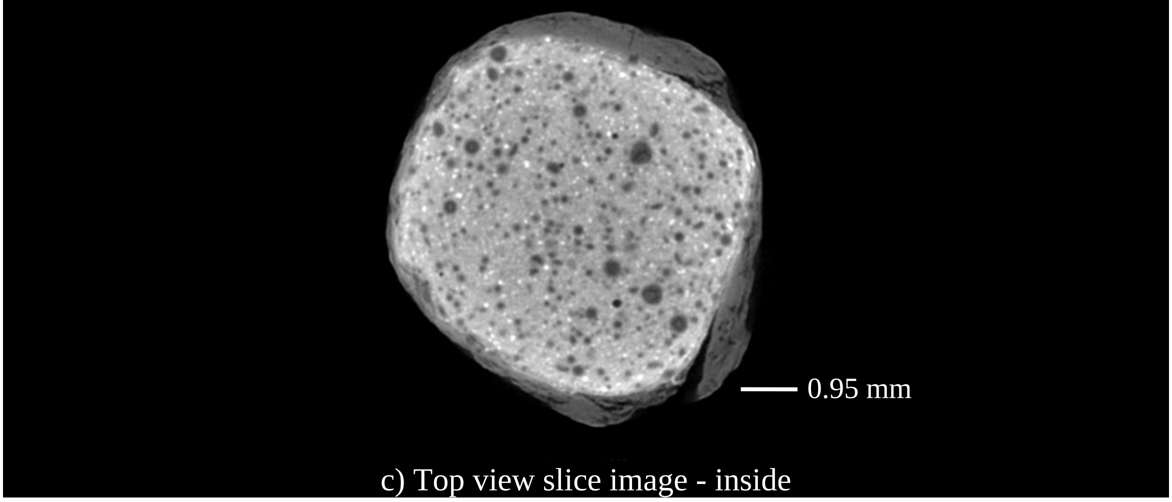

c) Top view slice image - inside

Figure 6.27 CT images of SF10 paste exposed to 0.5M citric acid (without brushing)

6.2.2.2 Special binder systems

Tomography imaging was done on the paste specimens made with special binders, LC2 and HAC, before and after the acid exposure to understand the microstructural changes. The CT images of the LC2 and HAC paste samples before the acid exposure are shown in Figures 6.28 and 6.29 respectively. The LC2 paste after exposure to 1% sulphuric acid (without brushing) showed considerable deterioration, which is visualised in Figure 6.30. The CT slice image, shown in Figure 6.30(a) indicated layers of degradation products on the surface of the specimen. Similar to the other SCM systems, various thin layers of gypsum and silica gel could be seen. On prolonged exposure, these layers exert expansive pressure and undergo delamination. This delamination of the gypsum layer is also evident in Figures 6.30(a) and 6.30(b). Figure 6.30(c) shows a CT slice image cut through the degraded layer showing gypsum bound with silica gel (dark coloured area). The deterioration was more predominant at the edges when compared to the lateral surfaces as shown in Figure 6.30(d). However, less deterioration was visible for HAC paste exposed to 1% sulphuric acid without brushing (Figure 6.31). The CT images cut through the inside of the specimen and the surface only showed less microstructural changes. Only a thin layer of degraded products was evident from the CT slice image. The 3D rendered image appeared smooth which confirms that there is no precipitation of insoluble salts. Nevertheless, the exposure resulted in considerable reduction in thickness of HAC paste on exposure to 1% sulphuric acid. Similar observations were made in the case of tests with brushing also and these CT images are presented in Appendix B (Figures B-28 and B-29).

The LC2 paste on exposure to 3% sulphuric acid, however, had considerable deterioration. The alteration depth was found to be higher and several bands of gypsum and silica gel could be seen from the slice image shown in Figure 6.32. The CT slice image cut through the degraded layer indicated a dark layer comprising of silica gel. The gypsum formed was found to be non-protective as expansion cracks were seen in the front view slice image shown in Figure 6.32(c). The 3D rendered image shown in Figure 6.32(d) indicates the severity of deterioration, exposing the relatively inner areas to fresh acid solution. However, even on exposure to 3% sulphuric acid, HAC paste showed less deterioration based on the CT images (Figure 6.33). The outer degraded layer was found to be thin and considerable loss of thickness was also observed. Also, the inner layers of the HAC paste appeared to be more porous. This could be due to the possible conversion of metastable hydrated products such as CAH_{10} and C_2AH_8 to C_3AH_6 and AH_3. The conversion process results in the increase of porosity and strength loss. This may possibly be the reason for the brittle behaviour shown by the specimens on prolonged exposure in acidic media.

On exposure to 0.25M acetic acid, the LC2 paste showed a thick degradation layer comprising of silica gel (Figure 6.34). The CT slice images of LC2 were similar to the FA30 and BFS50 paste explained in earlier sections. The outer layer was found to be weak in the mechanical properties as cracks were evident from the CT images (Figure 6.34(a) and 6.34(b)). The 3D rendered image showed less deterioration from outside as the salts formed were soluble, though there was deterioration inside. The HAC paste on exposure to 0.25M acetic acid also showed two layers, a relatively thinner outer degraded layer and an inner core layer (Figure 6.35). Unlike the case of LC2 paste, no cracks were found on the surface of the HAC paste sample.

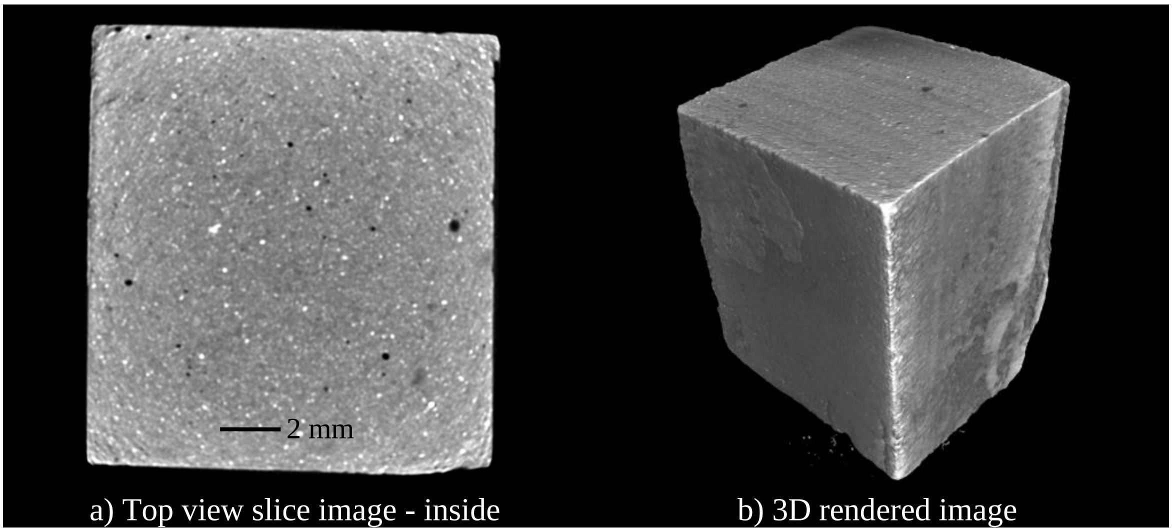

a) Top view slice image - inside

b) 3D rendered image

Figure 6.28 CT image of LC2 paste before the acid exposure

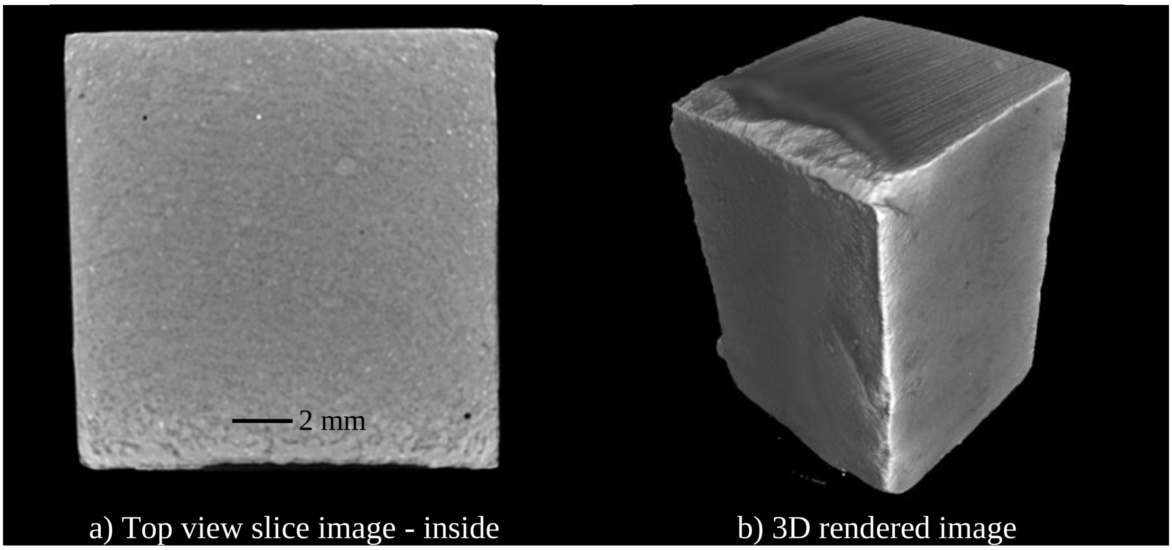

a) Top view slice image - inside

b) 3D rendered image

Figure 6.29 CT image of HAC paste before the acid exposure

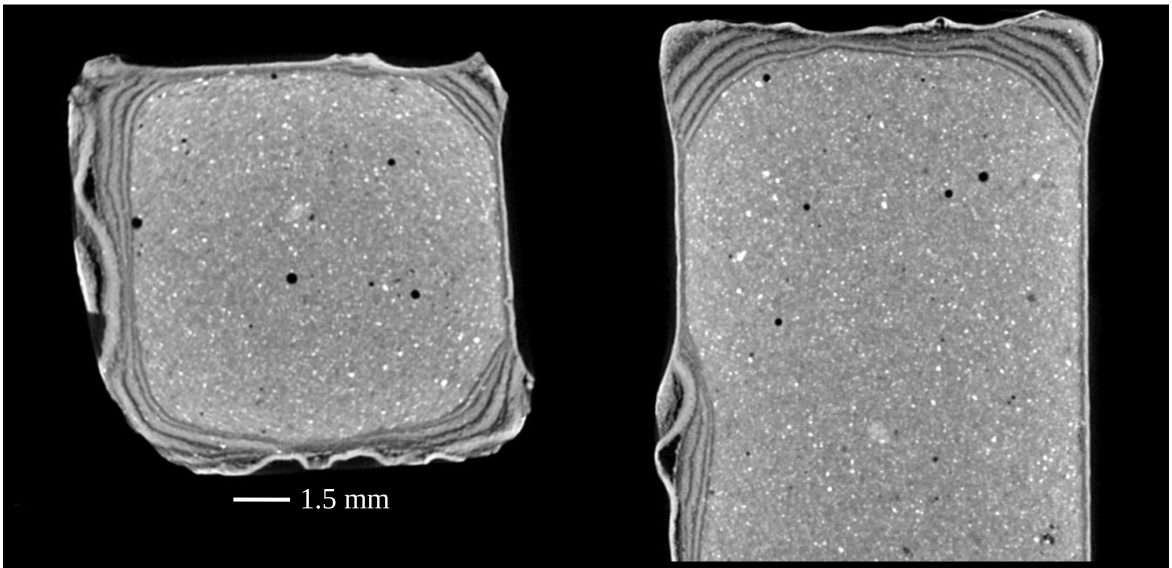

a) Top view slice image - inside b) Front view slice image - inside

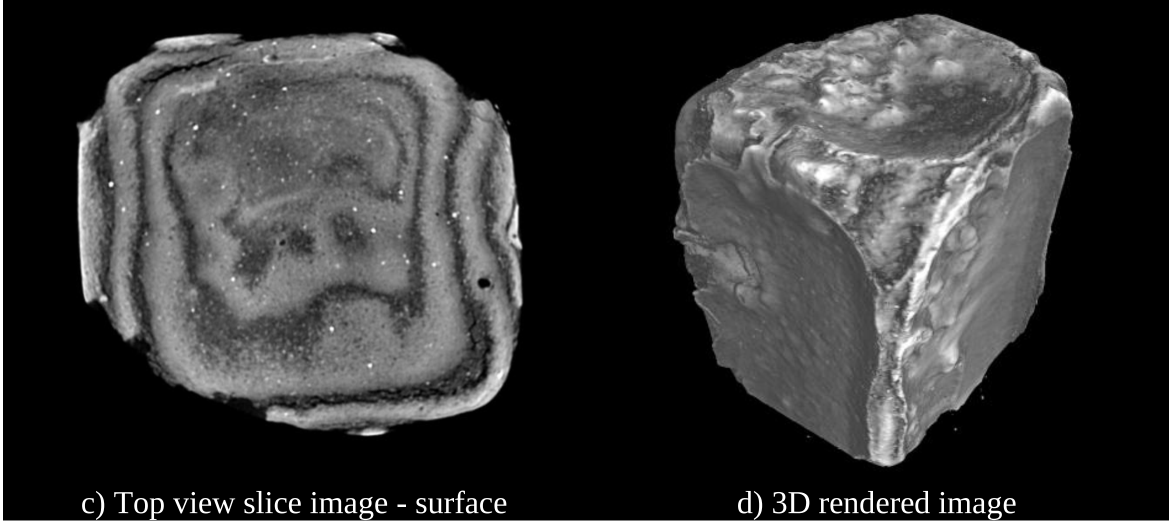

c) Top view slice image - surface d) 3D rendered image

Figure 6.30 CT images of LC2 paste exposed to 1% sulphuric acid (without brushing)

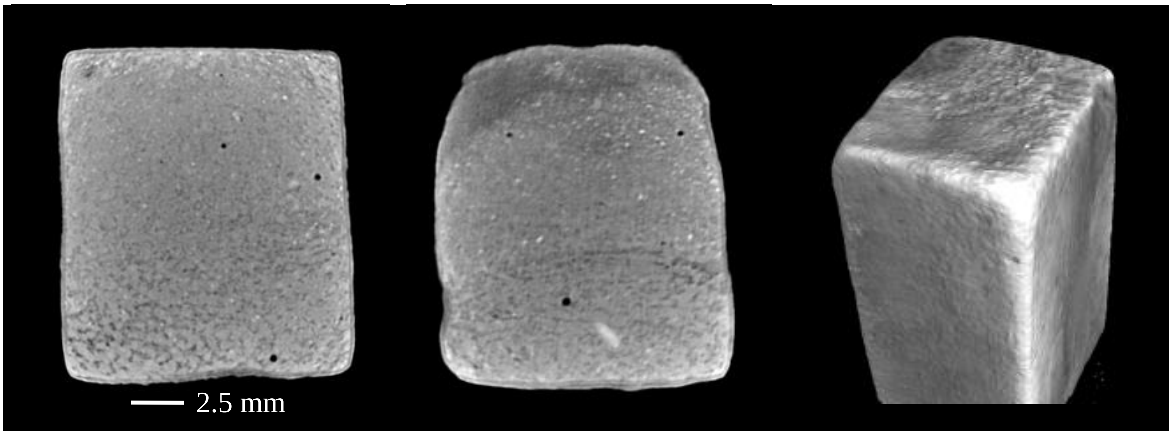

a) Top view slice image - inside b) Top view slice image - surface c) 3D rendered image

Figure 6.31 CT images of HAC paste exposed to 1% sulphuric acid (without brushing)

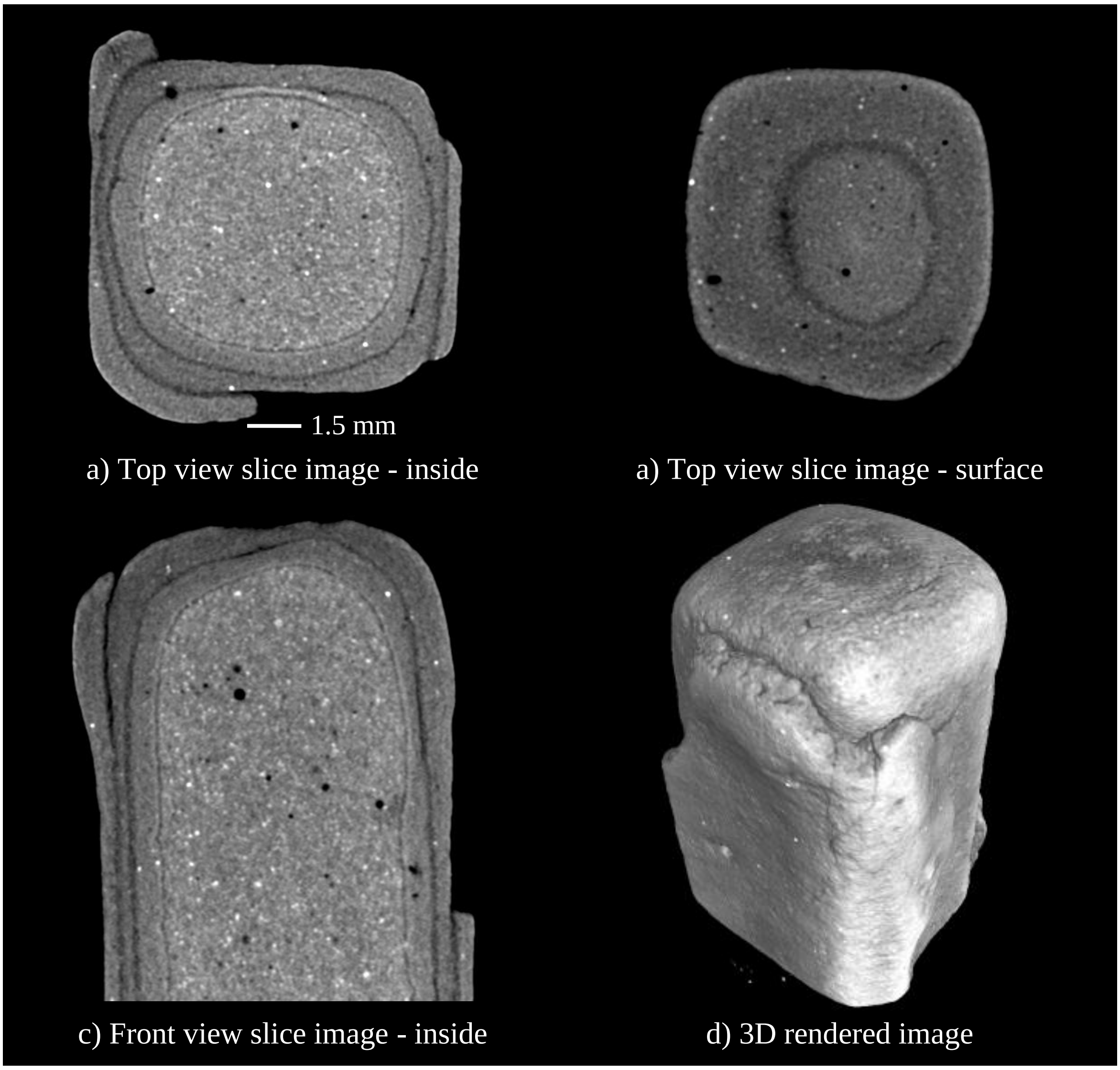

a) Top view slice image - inside

a) Top view slice image - surface

c) Front view slice image - inside

d) 3D rendered image

Figure 6.32 CT images of LC2 paste exposed to 3% sulphuric acid (without brushing)

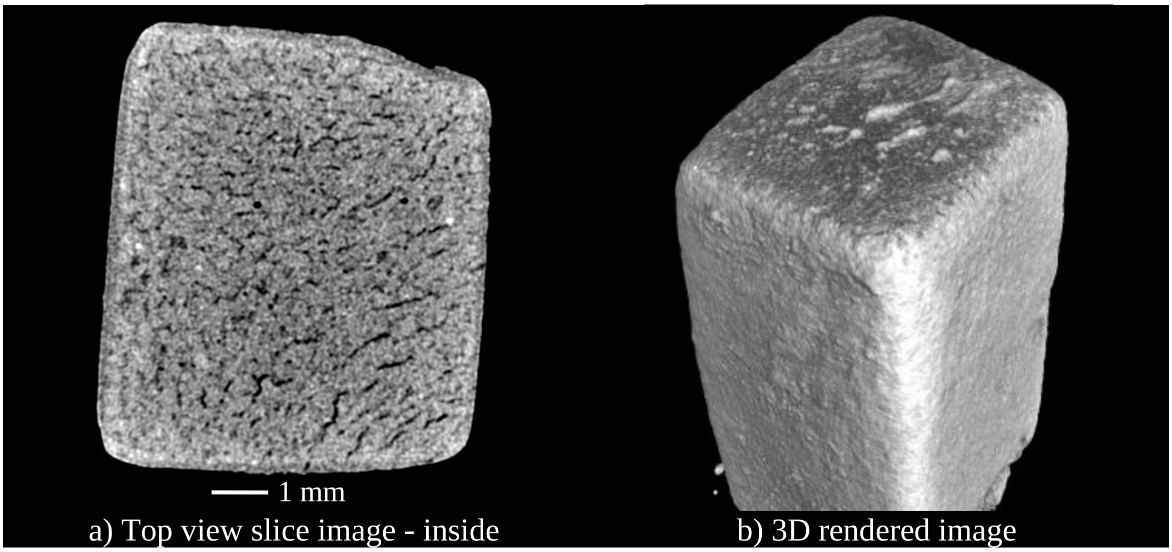

a) Top view slice image - inside

b) 3D rendered image

Figure 6.33 CT images of HAC paste exposed to 3% sulphuric acid (without brushing)

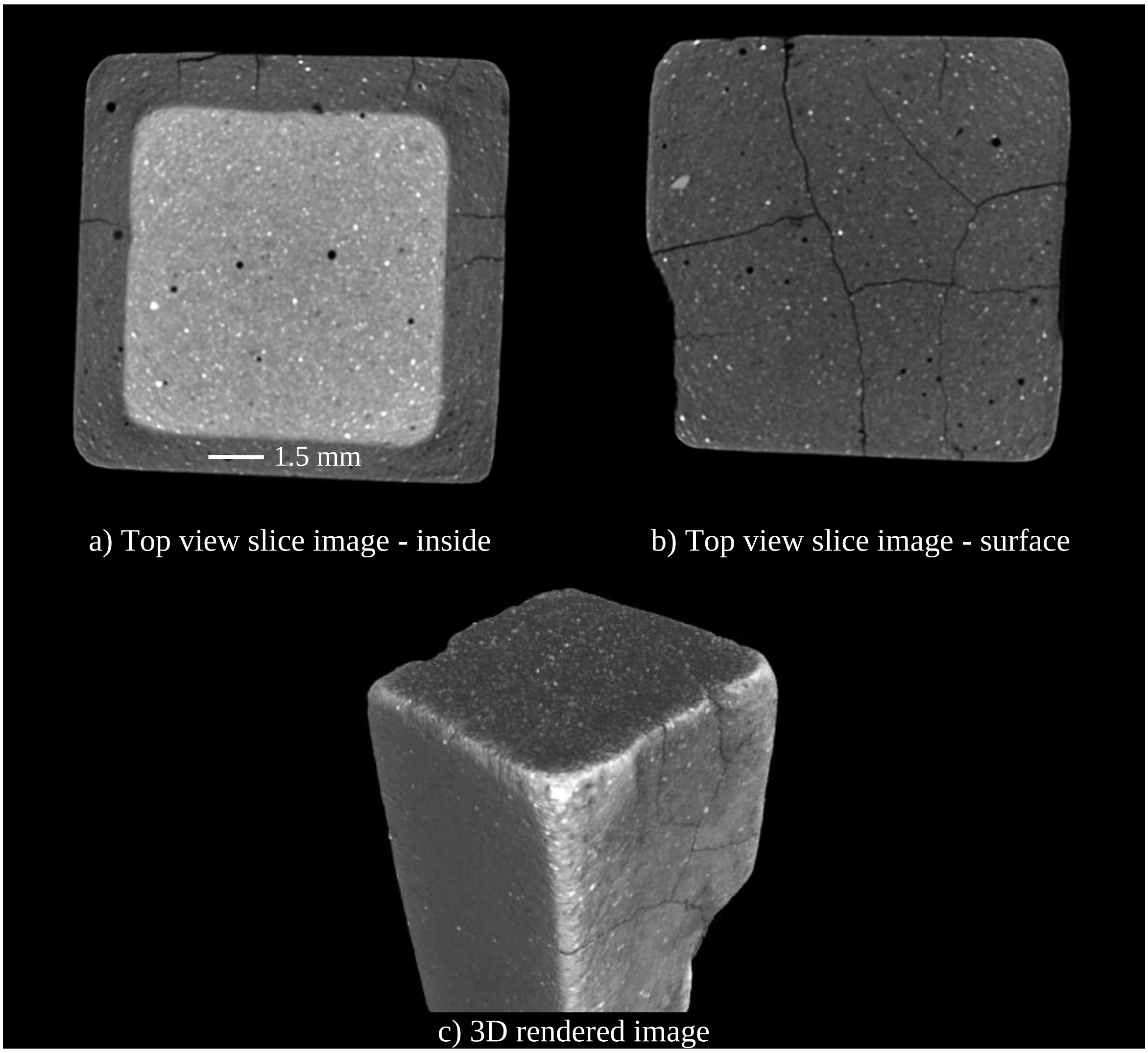

a) Top view slice image - inside

b) Top view slice image - surface

c) 3D rendered image

Figure 6.34 CT images of LC2 paste exposed to 0.25M acetic acid (without brushing)

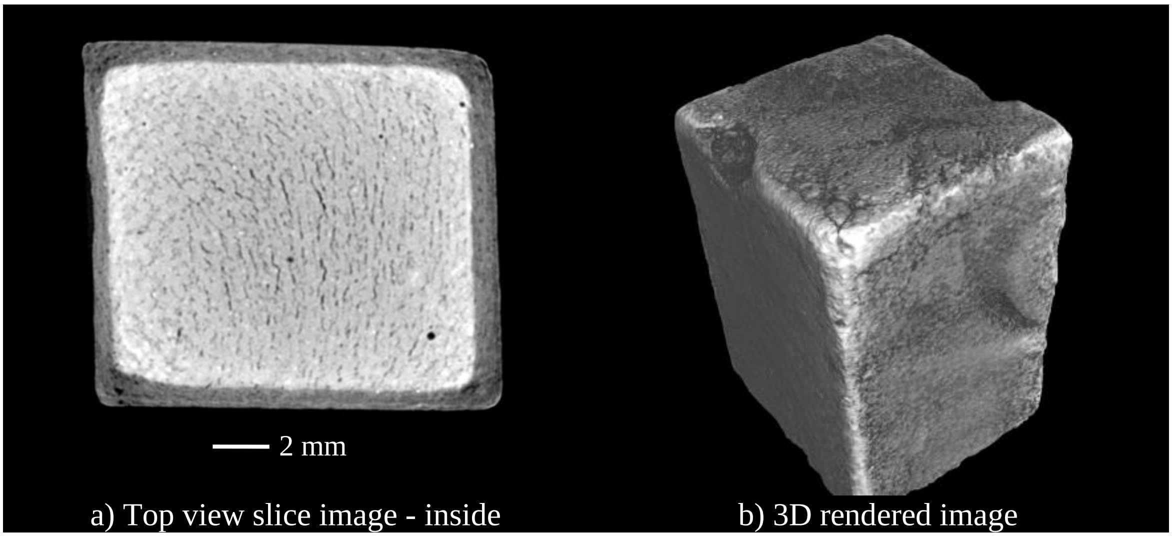

a) Top view slice image - inside

b) 3D rendered image

Figure 6.35 CT images of HAC paste exposed to 0.25M acetic acid (without brushing)

6.2.3 Mercury intrusion porosimetry

The variation in porosity due to acid attack was evaluated using mercury intrusion porosimetry (MIP). The cumulative pore volume curve of OPC specimens before and after the attack is shown in Figure 6.36. The legends, L, S, H, A and C refer to OPC specimens exposed to lime water (reference), 1% sulphuric, 1% HCl, 0.5M acetic and 0.5M citric acid solutions respectively. It can be noted that there is considerable increase in cumulative intruded volume due to acid attack. This reinforces the fact that leaching leads to increase in porosity due to decalcification of hydrated products and salt formation. The porosity increase could then affect the transportation properties, leading to further ingress of acids and deterioration. The differential of cumulative intruded volume curve is plotted in Figure 6.37.

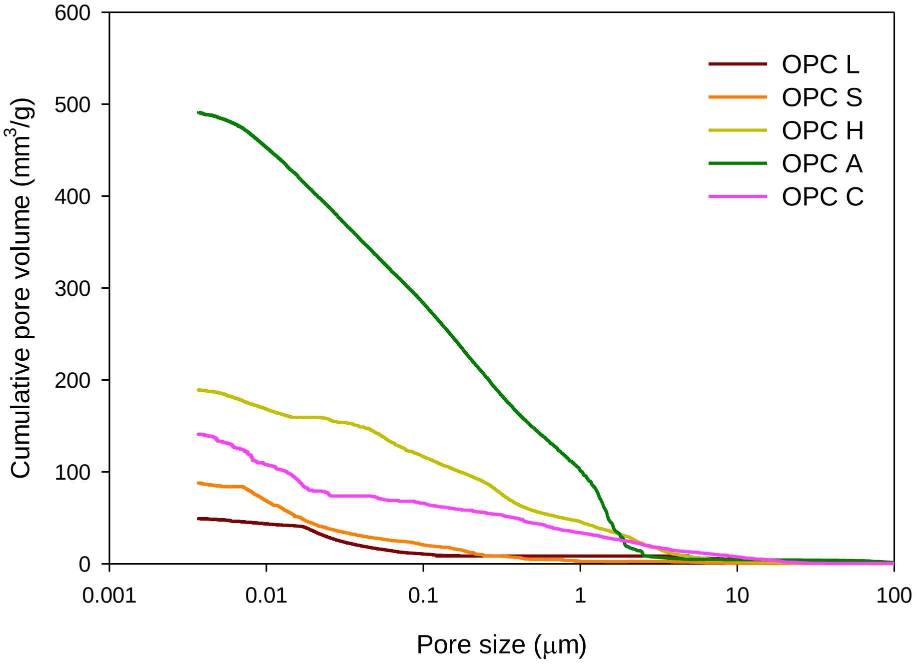

Figure 6.36 Cumulative pore volume curve of OPC paste exposed to acids

It can be seen from Figure 6.37 that there is a considerable shift (to right) in pore sizes for all the mixes on exposure to acid solution. MIP related parameters are deduced from the test results and are presented in Table 6.1. Threshold diameter and total intruded volume is obtained from Figure 6.36 whereas modal pore diameter is obtained from Figure 6.37. Intruded volume is highest for mixes on exposure to acetic acid due to strong leaching. Total intruded volume is also considerably high for specimens exposed to HCl and citric acid. Porosity is higher and bulk density is lowest for OPC mixes on exposure to acetic acid. Protective effect of gypsum layer in limiting the degradation is evident as the intruded volume is less for OPC specimens exposed to sulphuric acid. Threshold diameter is highest for OPC exposed to citric acid and this may be attributed to the extent of micro cracks present in the outer degraded layer (due to the high molar volume of calcium citrate tetra hydrate salt compared to Portlandite and CSH). The increase in threshold diameter and intruded volume due to acid attack points out the fact that acid attack results in microstructural deterioration, thus having an impact on durability properties. The cumulative intruded pore volume and the differential curves for the other paste mixes exposed to various acids are shown in Appendix B, Figures B-30 to B-36.

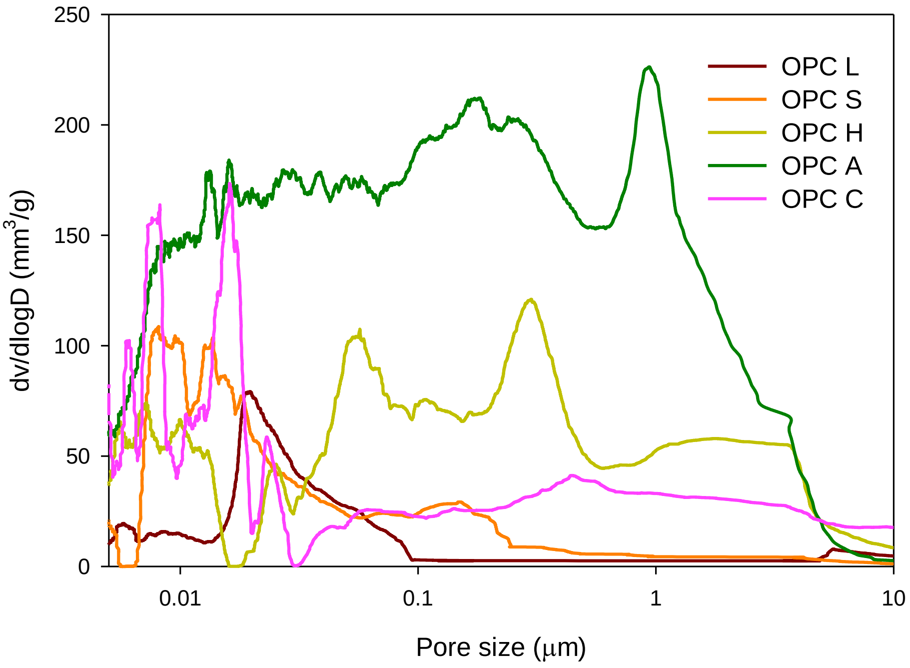

Figure 6.37 Differential intruded volume curve of OPC paste exposed to acids

Table 6.1 Summary of parameters of OPC paste based on MIP results

Results	OPC L	OPC S	OPC H	OPC A	OPC C
Total intruded volume (mm³/g)	49.15	88.28	189.42	491.72	141.1
Bulk density (g/cm³)	2.06	1.77	1.69	1.16	1.78
Porosity by Hg intrusion (%)	10.14	15.66	32.09	57.08	25.18
Modal pore diameter (μm)	0.0197	0.0037	0.0037	1.0215	0.0082
Threshold diameter (μm)	0.1	1	4	2	20

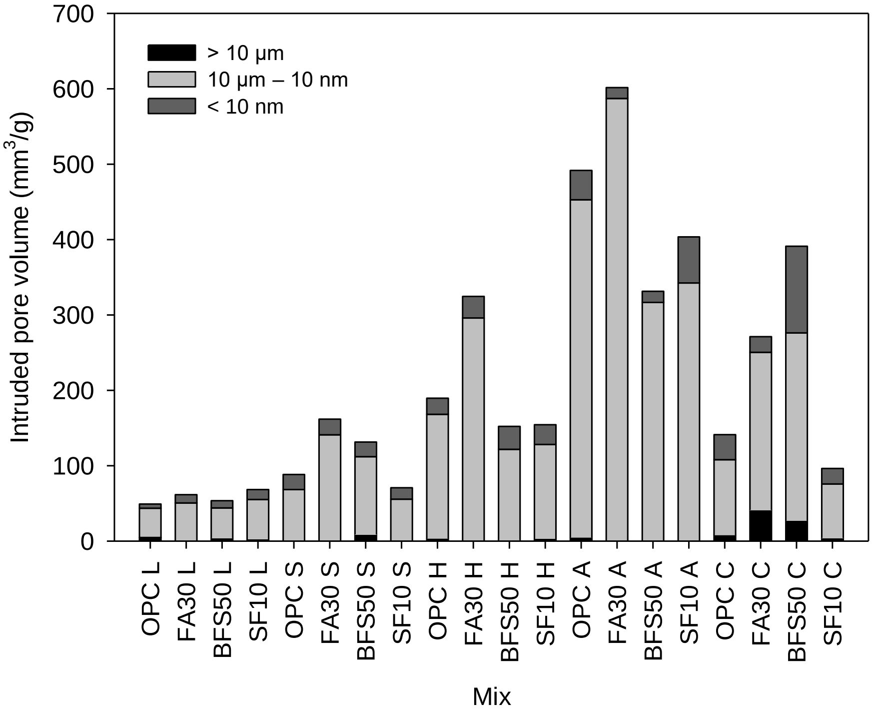

Figure 6.38 Classification of intruded pore volume of paste exposed to acids

The pore volume data obtained from MIP is further classified into three; pores greater than 10 µm are classified as macro pores, pores of size 10 µm – 10 nm are classified as capillary pores and pores finer than 10 nm are treated as gel pores (Aligizaki, 2005). The pore volume data thus classified are shown in Figure 6.38. It can be observed that there is a substantial increase in the capillary porosity due to the acid attack.

The increase in the capillary porosity was found to be lower for paste exposed to 1% sulphuric acid. This could be due to the limited penetration of sulphuric acid into the specimens. The increase in capillary porosity was found to be higher for the paste exposed to 0.5M acetic acid. The altered depth comprising of silica gel is greater for acetic acid and this resulted in considerable increase in capillary porosity. The increase in the capillary porosity of the paste means that the acid solution can diffuse to the inside of the cementitious matrix faster on acid exposure. Table 6.2 shows the MIP related parameters of the paste mixes before the acid exposure (i.e. after 28 days of curing in saturated lime water). The porosity values of the control mixes are comparable. The MIP parameters of paste exposed to various acids are shown in Tables 6.3 to 6.6. There was a reduction in the bulk density and increase in the porosity values for all mixes except SF10. In the case of SF10, the degraded gypsum layer has already been delaminated by the time of testing, which possibly might have resulted in the minimal changes in the porosity. However, as the degraded layers (gypsum bound with silica gel) were adherent to the surface and as the degraded depths were higher, the FA30 and BFS50 mixes showed greater reduction in the bulk density and greater increase in the intrusion porosity.

In the case of 1% hydrochloric acid, the reduction in the bulk density and the increase in the porosity were substantial. The FA30 mix showed the greatest reduction in bulk density and hence, greater increase in the intrusion porosity, while the porosity was the least for the BFS50 mix. These are in alignment with the mass changes as FA30 had the highest mass loss while BFS50 had the minimum. Similar results were obtained in the case of 0.5M acetic acid. The decrement in the bulk density and the increase in intrusion porosity were higher for 0.5M acetic acid. It is observed that the bulk density reduction and porosity increase in the mixes are higher where acids form soluble salts. The FA30 mix had the lowest bulk density and the highest porosity among all the mixes investigated on exposure to 0.5M acetic acid. The BFS50 mix showed better performance as the bulk density was higher and intrusion porosity also was lower when compared to the other mixes. These observations are found to be in tune with the mass changes noted where BFS50 had the lowest mass loss and FA30 registered the highest mass loss.

In the case of citric acid, the improved performance of OPC and SF10 was evident from the MIP results also as there was less reduction in the bulk density and less increase in the intrusion porosity. The lower reduction in the bulk density in the case of OPC and SF10 may be due to the fact that the precipitated layer of salt being non-protective has already worn out into the solution leaving only a very thin layer of salt attached to the specimen (evident from the CT images). However, the FA30 and BFS50 mix had substantial reduction in the bulk density, which resulted in the greater increase in the intrusion porosity when compared to OPC and SF10. These observations can be correlated to the mass changes and thickness of the corroded layer remaining on the specimen. In the case of FA30 and BFS50, the thickness of the outer degraded layer (salt) attached to the specimen was found to be greater. Also, cracks were evident in the outer degraded layer of the specimens. This might have resulted in the lowering of bulk density of the sample and subsequently in the increase of mercury intrusion porosity. Thus, mercury intrusion porosimetry helped to reconfirm the observations made through mass changes and CT imaging.

Table 6.2 Summary of MIP parameters of paste before acid exposure

Mix	Intruded volume (mm^3/g)	Bulk density (g/cm^3)	Porosity by Hg intrusion (%)
OPC L	49.15	2.06	10.14
FA30 L	61.44	1.84	11.30
BFS50 L	53.57	1.95	10.43
SF10 L	68.29	1.97	13.45

Table 6.3 Summary of MIP parameters of paste exposed to 1% sulphuric acid

Mix	Intruded volume (mm^3/g)	Bulk density (g/cm^3)	Porosity by Hg intrusion (%)
OPC S	88.28	1.77	15.66
FA30 S	161.70	1.70	27.54
BFS50 S	131.27	1.75	22.97
SF10 S	70.66	2.03	14.34

Table 6.4 Summary of MIP parameters of paste exposed to 1% hydrochloric acid

Mix	Intruded volume (mm^3/g)	Bulk density (g/cm^3)	Porosity by Hg intrusion (%)
OPC H	189.42	1.69	32.09
FA30 H	324.47	1.27	41.30
BFS50 H	152.10	1.65	25.14
SF10 H	154.35	1.67	25.85

Table 6.5 Summary of MIP parameters of paste exposed to 0.5M acetic acid

Mix	Intruded volume (mm^3/g)	Bulk density (g/cm^3)	Porosity by Hg intrusion (%)
OPC A	491.72	1.16	57.08
FA30 A	601.52	0.97	58.63
BFS50 A	331.21	1.24	41.02
SF10 A	403.48	1.35	54.58

Table 6.6 Summary of MIP parameters of paste exposed to 0.5M citric acid

Mix	Intruded volume (mm^3/g)	Bulk density (g/cm^3)	Porosity by Hg intrusion (%)
OPC C	141.10	1.78	25.18
FA30 C	271.08	1.41	38.12
BFS50 C	391.05	1.27	49.61
SF10 C	96.32	1.97	19.01

6.2.4 Thermo-gravimetric analysis

TGA was done on paste samples to understand the chemical transformations in materials before and after the acid exposure. The primary objective of conducting TGA is to estimate the Portlandite and calcite content. Figure 6.39 shows the TGA/DTG curve of OPC paste before the acid exposure (i.e. after 28 days curing in saturated lime water). The first peak of DTG is due to the dehydroxylation of hydrated products such as CSH gel, AF_t and AF_m. The second major peak with the peak transformation temperature of 434.7˚C indicates the dehydroxylation of Portlandite. The third peak having peak transformation temperature of 684.9˚C refers to the decarbonation reaction of the calcium carbonate phases (calcite, valerite, aragonite etc.). Table 6.7(a) shows the quantity of Portlandite and calcite estimated for the OPC paste exposed to various acids.

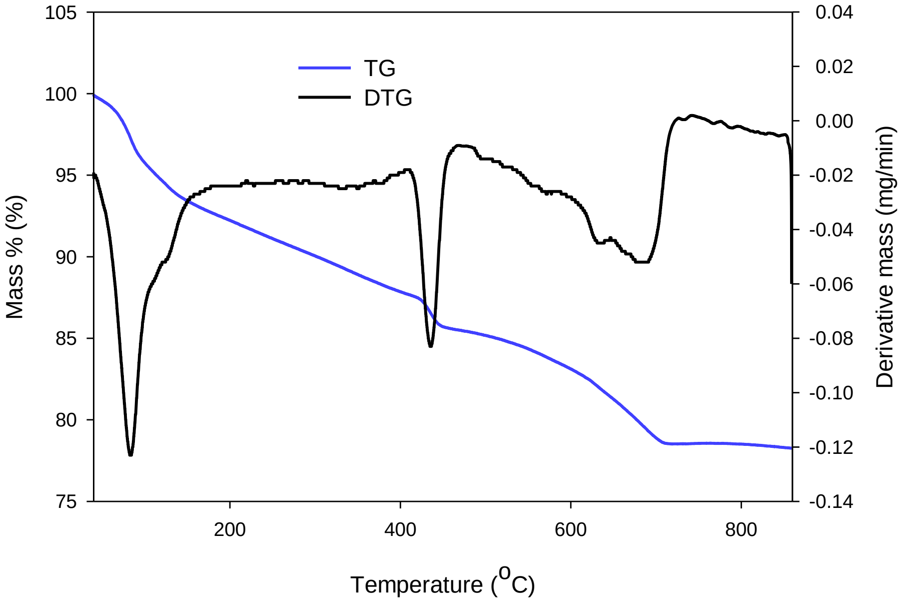

Figure 6.39 TGA/DTG curve of OPC paste before the acid exposure

The TGA/DTG curve of OPC paste exposed to 1% sulphuric acid for 6 weeks is shown in Figure 6.40. In addition to the transformation of CSH gel, an additional peak is visible which is due to the loss of water from the gypsum that is formed as a reaction product. Gypsum formation is due to the reaction between Portlandite or CSH gel with the sulphuric acid solution. The Portlandite content in the system reduces (26.9% reduction) owing to the formation of gypsum, as indicated in the results in Table 6.7(a).

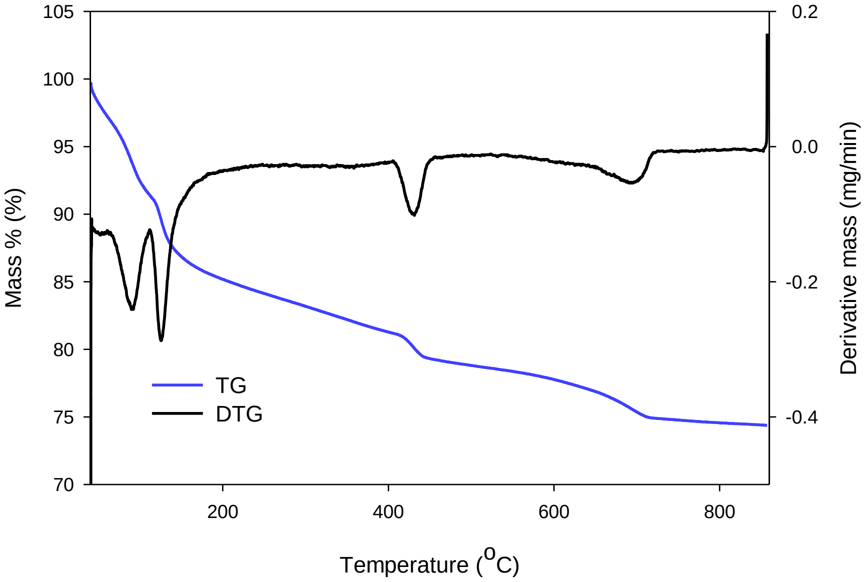

Figure 6.40 TGA/DTG curve of OPC paste after exposure to 1% sulphuric acid

Figure 6.41 shows the TGA/DTG curve of OPC paste on exposure to 1% hydrochloric acid. In addition to the regular three peaks due to CSH, $Ca(OH)_2$ and $CaCO_3$, a wide transformation could also be seen just before the dehydroxylation of $Ca(OH)_2$. This could possibly due to the loss of water from amorphous silica gel which is formed as a reaction between the CSH gel and the acid. There was a reduction in Portlandite by 49.4% which indicates the extent of decalcification when exposed to acids like HCl, which form soluble salts.

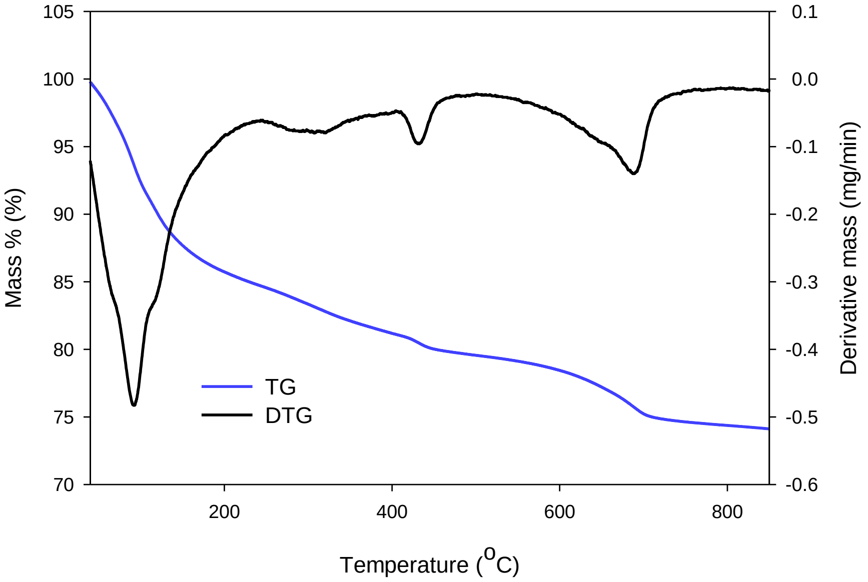

Figure 6.41 TGA/DTG curve of OPC paste after exposure to 1% hydrochloric acid

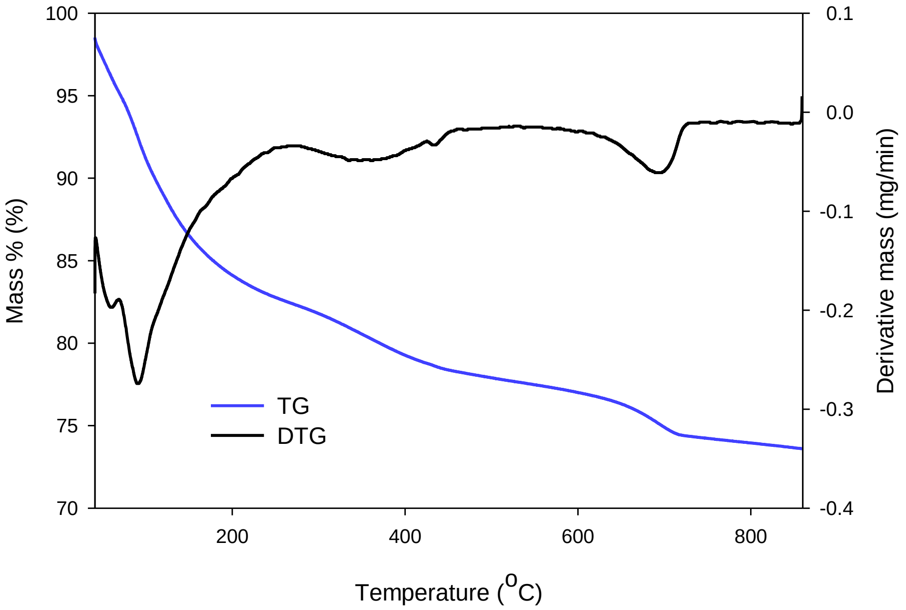

Figure 6.42 TGA/DTG curve of OPC paste after exposure to 0.5M acetic acid

Figure 6.42 shows the TGA/DTG curve of OPC paste after exposure to 0.5M acetic acid for a period of 6 weeks. The TGA/DTG curve was similar to the one for 1% HCl. Portlandite has been almost completely consumed by the acid (reduction of 80.6%) and only 2.13% Portlandite is estimated to be left in the specimen after the acid exposure. There is also a reduction in the calcite content, which could be due to dissolution of calcite in acidic conditions.

The TGA /DTG curve of OPC paste after 3 weeks exposure to citric acid is shown in Figure 6.43. The peak due to silica gel was not evident. Moreover, there is a less reduction in Portlandite content of the system (by 18.3%) when compared to 1% HCl and 0.5M acetic acid. This could be due to two reasons; the degraded layer attached to the specimen is very thin and already the precipitates which were formed due to decalcification of hydration products have exfoliated from the specimen. Hence, the specimen tested has shown increased Portlandite content. Except to the fact that there is a thin layer of precipitate adhering to the specimen, the microstructure of specimen exposed to citric acid was similar to the one before the attack as evident from the CT images.

The TGA/DTG curves for the other paste mixes exposed to various acids are detailed in Appendix B, Figures B-37 to B-39. Table 6.7 (b-d) shows the Portlandite and calcite contents of the paste specimens of FA30, BFS50 and SF10 before and after the exposure to various acids. In the case of FA30, there is a reduction in Portlandite content by 52.7% and 68.9% on exposure to 1% sulphuric and 0.5M citric acid respectively. This reduction is attributed to the thick corroded layer present on the specimen even after the exposure. The entire Portlandite in the system was found to be consumed in the case of exposure to acids that formed soluble salts (HCl and acetic acid). This explains partly the poor performance of FA30 in such acid environments.

In the case of BFS50, the free lime was consumed during the hydration process of slag system and less Portlandite content was present in BFS50 when compared to the OPC system. A reduction of Portlandite by 3.08%, 38.8%, 100% and 24.6% was calculated for BFS50 paste exposed to 1% sulphuric, 1% hydrochloric, 0.5M acetic and 0.5M citric acid respectively. All the Portlandite present in the system had been completely consumed on reaction with acetic acid. This could lead to direct attack of CSH gel further, due to the non-availability of Portlandite in the matrix. In the case of SF10, a reduction in Portlandite of 2.6% and 22.1% is estimated on exposure to 1% sulphuric and 0.5M citric acid. Similar to the other mixes, the Portlandite consumption was found to be greater on exposure to 1% hydrochloric and 0.5M acetic acids (reduction of 54.2% and 100%). Further details about the TGA results are shown in Appendix B, Table B-1.

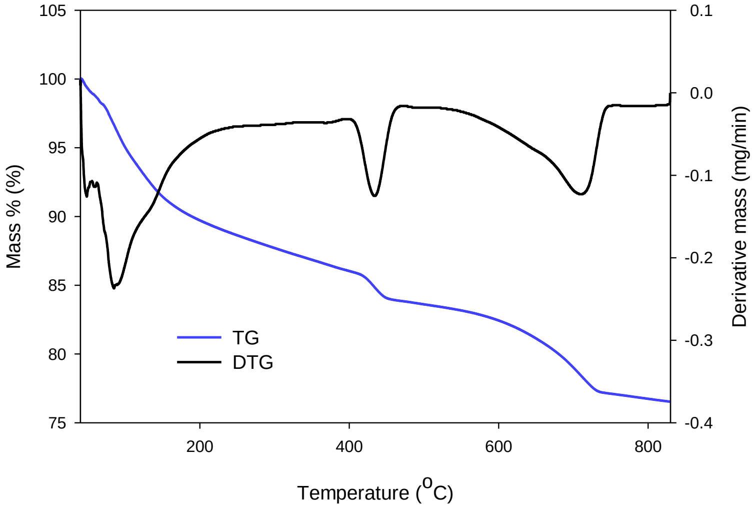

Figure 6.43 TGA/DTG curve of OPC paste after exposure to 0.5M citric acid

Table 6.7 Estimation of Portlandite and calcite contents of paste before and after acid exposure

Mix	Solution	$Ca(OH)_2$ (%)	$CaCO_3$ (%)
OPC	Saturated lime water	10.98	13.85
OPC	1% sulphuric acid	8.02	8.06
OPC	1% hydrochloric acid	5.56	11.77
OPC	0.5M acetic acid	2.13	8.90
OPC	0.5M citric acid	8.97	15.48

a) OPC paste

Mix	Solution	$Ca(OH)_2$ (%)	$CaCO_3$ (%)
FA30	Saturated lime water	8.46	18.45
FA30	1% sulphuric acid	4.00	8.63
FA30	1% hydrochloric acid	0.00	7.76
FA30	0.5M acetic acid	0.00	2.02
FA30	0.5M citric acid	2.63	12.19

b) FA30 paste

Mix	Solution	$Ca(OH)_2$ (%)	$CaCO_3$ (%)
BFS50	Saturated lime water	5.20	6.58
BFS50	1% sulphuric acid	5.04	6.40
BFS50	1% hydrochloric acid	3.18	8.50
BFS50	0.5M acetic acid	0.00	2.67
BFS50	0.5M citric acid	3.92	11.11

c) BFS50 paste

Mix	Solution	$Ca(OH)_2$ (%)	$CaCO_3$ (%)
SF10	Saturated lime water	9.35	11.38
SF10	1% sulphuric acid	9.11	9.94
SF10	1% hydrochloric acid	4.28	12.34
SF10	0.5M acetic acid	0.00	4.50
SF10	0.5M citric acid	7.28	19.00

d) SF10 paste

6.2.5 Scanning electron microscopy

Scanning electron microscopy in the secondary electron imaging mode coupled with energy dispersive spectroscopy was used to investigate the microstructural changes due to the acid attack. The primary objective of using SEM was to study the morphology and nature of the reaction products across the zones that are formed due to the attack. After the acid exposure, paste specimens (tested without abrasion) were cut and reactions were arrested using solvent exchange process using isopropanol. The dried samples were coated with gold and taken for imaging in secondary mode (sample preparation was discussed in the section 3.9.3).

Figures 6.44 and 6.45 show the morphology of the outer degraded layer of OPC specimen exposed to 6 weeks in 1% sulphuric acid. Prismatic deposits of gypsum along with loosely held silica gel are evident from the image. The gypsum formed due to the decalcification of Portlandite and CSH gel could block the pores created due to decalcification, thus creating a protective effect at lower concentrations of sulphuric acid. CSH gel reacts with acid ions and undergoes decalcification to form gypsum and silica gel, which is amorphous in nature. The image of the middle decalcified layer (Figure 6.46) showed cracks which could be due to decalcification and associated shrinkage. The EDS indicated that the Ca/Si ratio was low. The decalcified area had the presence of alumina which is stable and binds with the silica gel. The inner core that is not attacked by the acid showed the presence of normal hydrates rich in calcium (Figure 6.47).

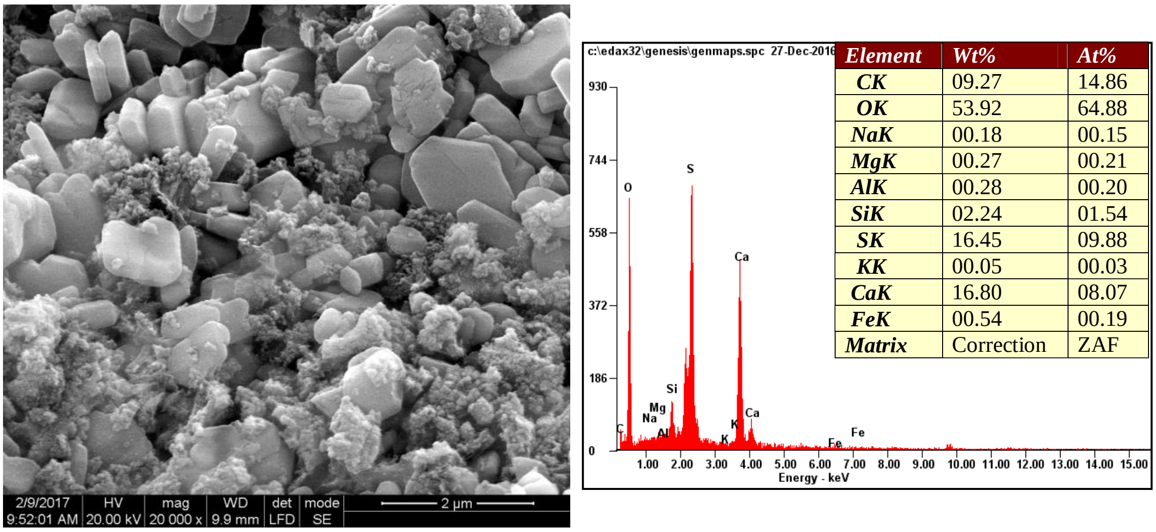

Element	***Wt%***	***At%***
CK	09.27	14.86
OK	53.92	64.88
NaK	00.18	00.15
MgK	00.27	00.21
AlK	00.28	00.20
SiK	02.24	01.54
SK	16.45	09.88
KK	00.05	00.03
CaK	16.80	08.07
FeK	00.54	00.19
Matrix	Correction	ZAF

Figure 6.44 Morphology and EDS spectrum of outer degraded layer of OPC paste exposed to 1% sulphuric acid

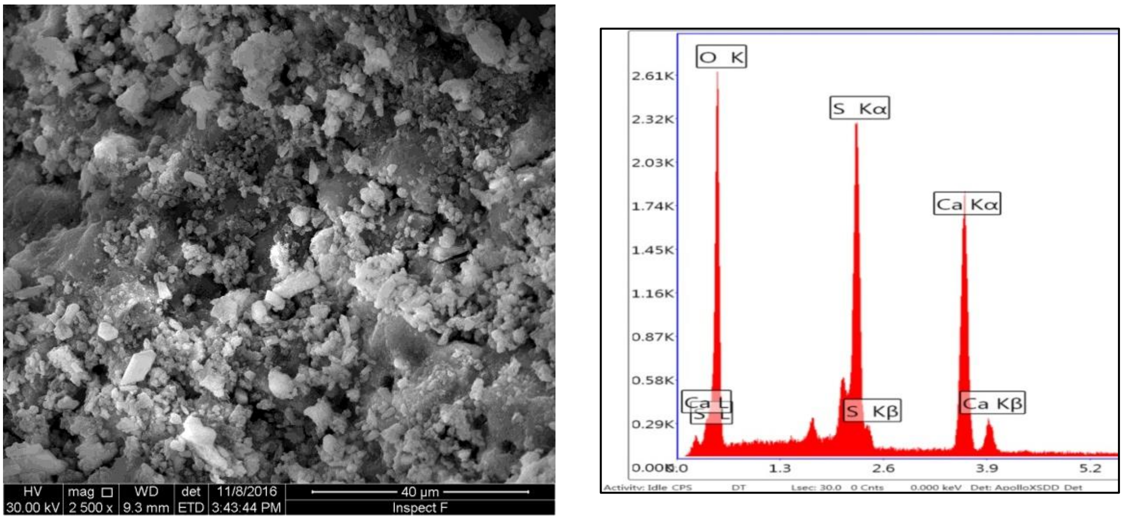

Figure 6.45 Morphology and EDS spectrum of outer degraded layer of OPC paste exposed to 1% sulphuric acid showing gypsum and silica gel

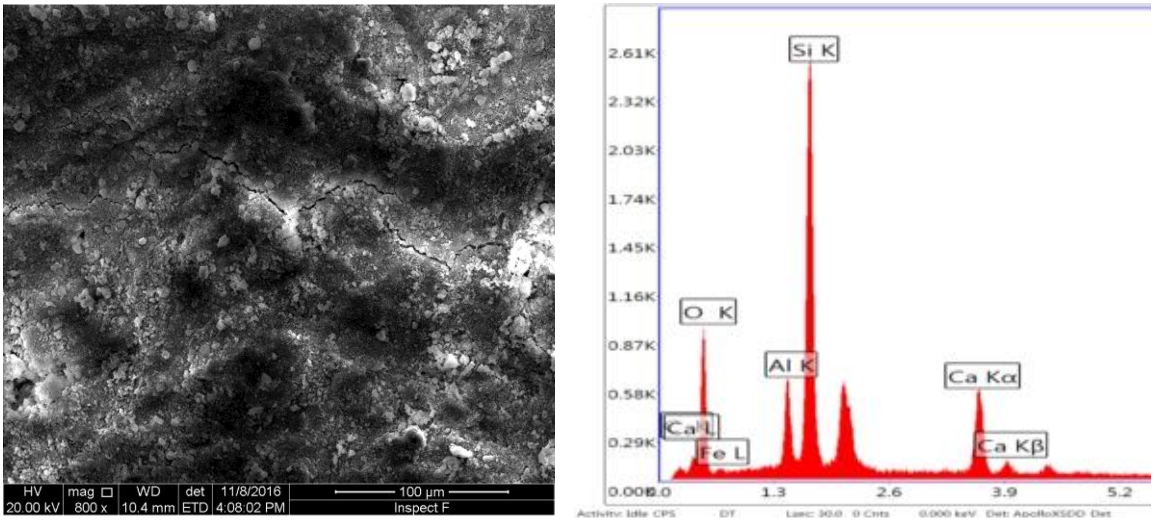

Figure 6.46 Morphology and EDS spectrum of middle decalcified layer of OPC paste exposed to 1% sulphuric acid showing cracks and loss of calcium

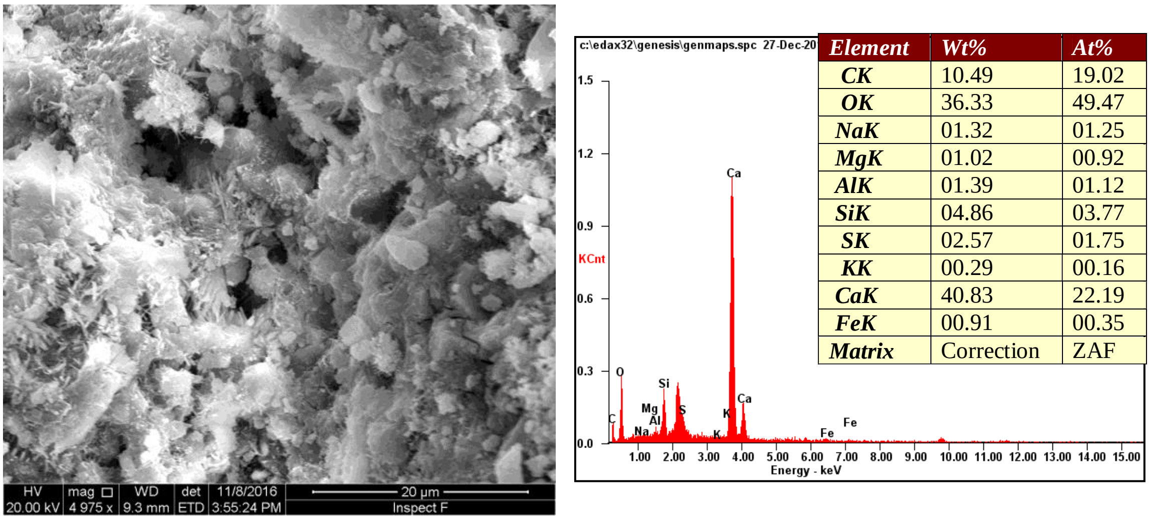

Element	*Wt%*	*At%*
CK	10.49	19.02
OK	36.33	49.47
NaK	01.32	01.25
MgK	01.02	00.92
AlK	01.39	01.12
SiK	04.86	03.77
SK	02.57	01.75
KK	00.29	00.16
CaK	40.83	22.19
FeK	00.91	00.35
Matrix	Correction	ZAF

Figure 6.47 Morphology and EDS spectrum of core layer of OPC paste exposed to 1% sulphuric acid showing hydrates rich in calcium

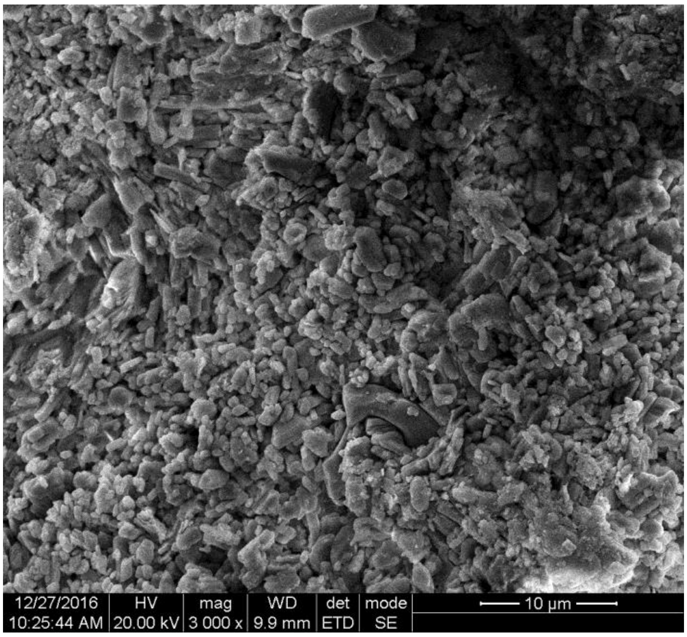

Figure 6.48 Morphology of outer degraded layer of FA30 paste exposed to 1% sulphuric acid showing thick deposits of gypsum

Figure 6.48 shows the electron micrograph of the outer degraded layer of FA30 paste exposed to 1% sulphuric acid showing large deposits of gypsum. The gypsum was observed to be fine-sized, which could possibly block the capillary pore spaces created by the decalcification of Portlandite and CSH gel. Figure 6.49 shows a magnified image of the degraded layer and its corresponding EDS spectrum of the area indicating the presence of gypsum. The presence of silica in the EDS spectrum denotes the fact that the gypsum is bound with silica gel. Figure 6.50 shows another magnified image of the degraded layer showing gypsum and loosely bound silica gel.

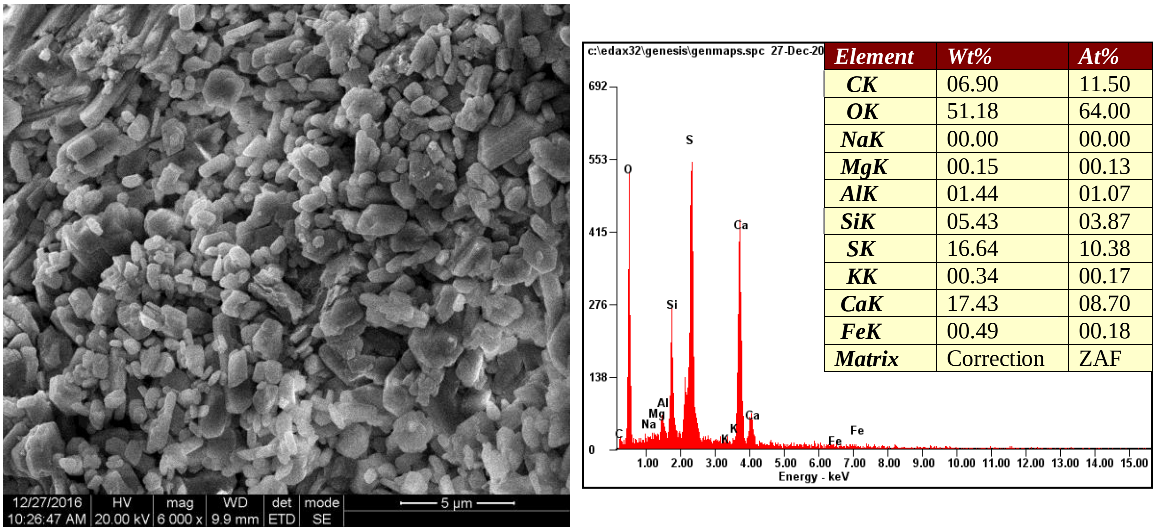

Element	*Wt%*	*At%*
CK	06.90	11.50
OK	51.18	64.00
NaK	00.00	00.00
MgK	00.15	00.13
AlK	01.44	01.07
SiK	05.43	03.87
SK	16.64	10.38
KK	00.34	00.17
CaK	17.43	08.70
FeK	00.49	00.18
Matrix	Correction	ZAF

Figure 6.49 Morphology and EDS spectrum of outer degraded layer of FA30 paste exposed to 1% sulphuric acid showing gypsum

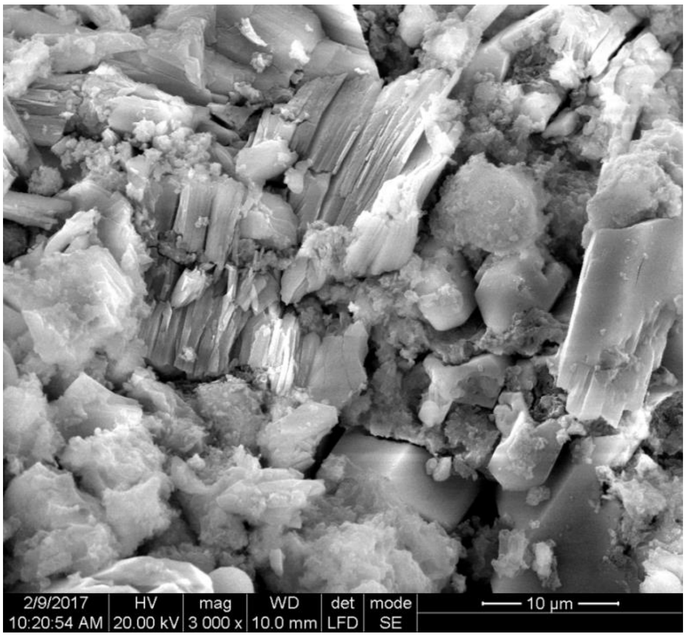

Figure 6.50 A magnified image showing morphology of outer degraded layer of FA30 paste exposed to 1% sulphuric acid

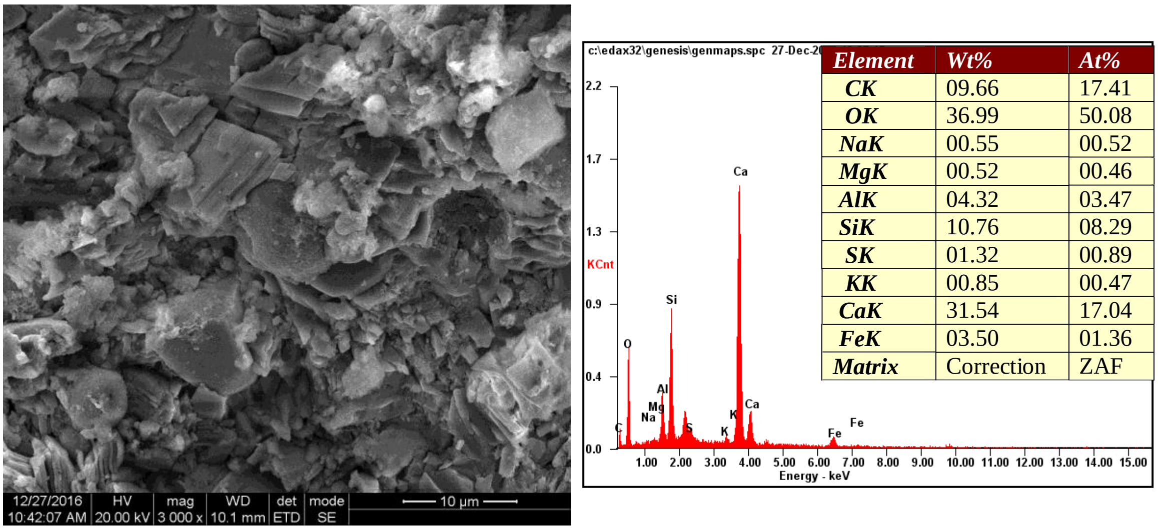

Element	*Wt%*	*At%*
CK	09.66	17.41
OK	36.99	50.08
NaK	00.55	00.52
MgK	00.52	00.46
AlK	04.32	03.47
SiK	10.76	08.29
SK	01.32	00.89
KK	00.85	00.47
CaK	31.54	17.04
FeK	03.50	01.36
Matrix	Correction	ZAF

Figure 6.51 Morphology and EDS spectrum of core layer of FA30 paste exposed to 1% sulphuric acid showing calcium rich hydrated products

The core unattacked layer showed large crystals of Portlandite with other hydrated products and the area was found to be rich in elements such as calcium and aluminium (Figure 6.51).

Figures 6.52 to 6.54 show the morphology of outer degraded layer of BFS50 paste exposed to 1% sulphuric acid. The morphology of the reaction products was similar to the other mixes. Figure 6.53 shows the EDS spectrum of the products formed in the outer degraded layer. However, it appears that the outer layer is less porous in the case of

BFS50 mix. Figure 6.55 shows the magnified image of the gypsum which can be seen as prismatic deposits closely packed in the outer layer. Figure 6.56 shows the micrograph of the outer degraded layer of SF10 paste exposed to 1% sulphuric acid. Long prismatic crystals of gypsum could also be seen in the outer layer. The growth of such crystals could have resulted in the expansion causing the delamination of gypsum layer leading to mass loss on prolonged exposure to sulphuric acid. The decalcified area without gypsum appeared dark and was identified as silica gel as shown in the EDS spectrum in Figure 6.57.

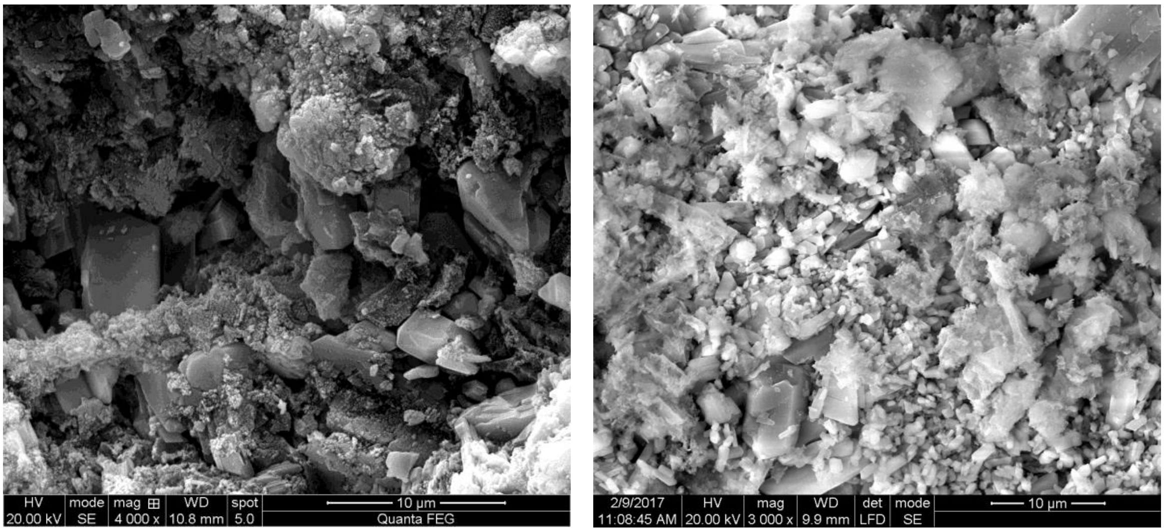

a) magnified view of outer degraded layer

b) outer degraded layer

Figure 6.52 Morphology of outer degraded layer of BFS50 paste exposed to 1% sulphuric acid showing gypsum and silica gel

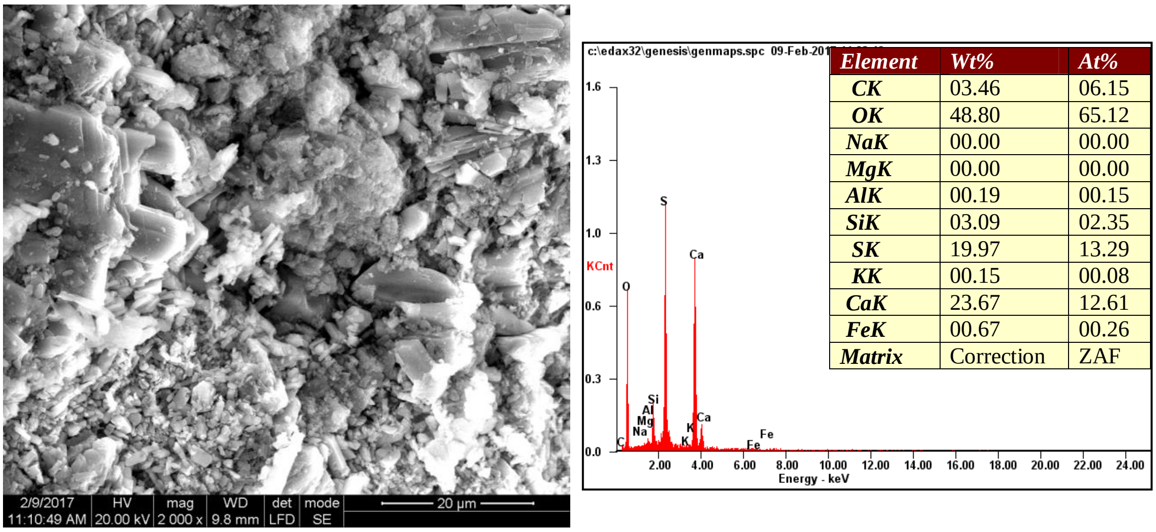

Element	*Wt%*	*At%*
CK	03.46	06.15
OK	48.80	65.12
NaK	00.00	00.00
MgK	00.00	00.00
AlK	00.19	00.15
SiK	03.09	02.35
SK	19.97	13.29
KK	00.15	00.08
CaK	23.67	12.61
FeK	00.67	00.26
Matrix	Correction	ZAF

Figure 6.53 Morphology and EDS spectrum of outer degraded layer of BFS50 paste exposed to 1% sulphuric acid showing gypsum

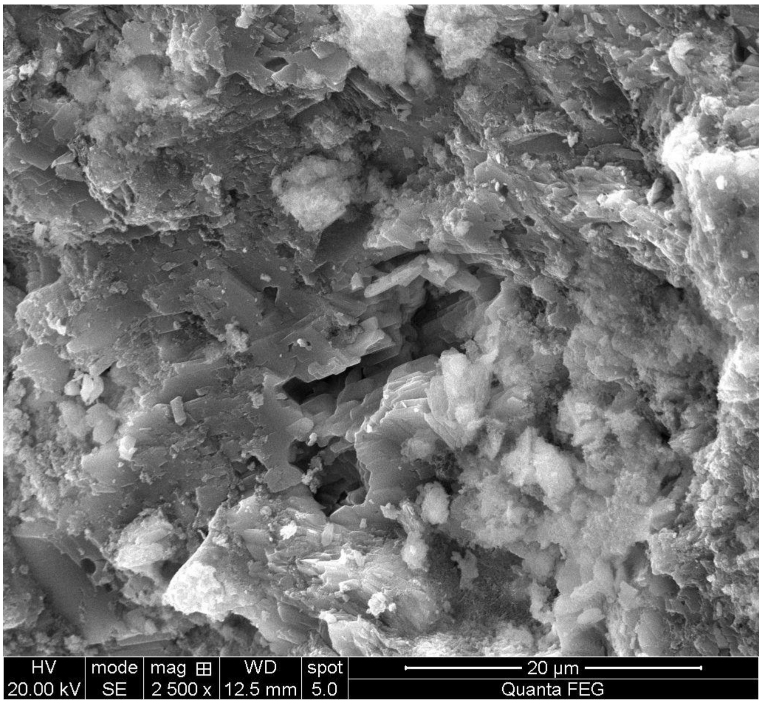

Figure 6.54 Outer degraded layer of BFS50 paste exposed to 1% sulphuric acid showing gypsum bound with silica gel

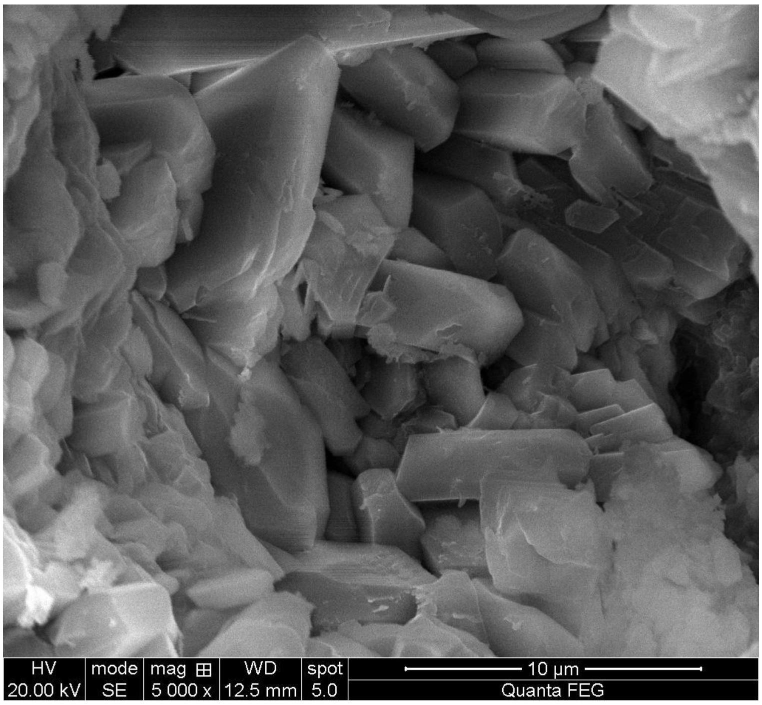

Figure 6.55 A close view of the morphology of gypsum formed in the BFS50 paste exposed to 1% sulphuric acid

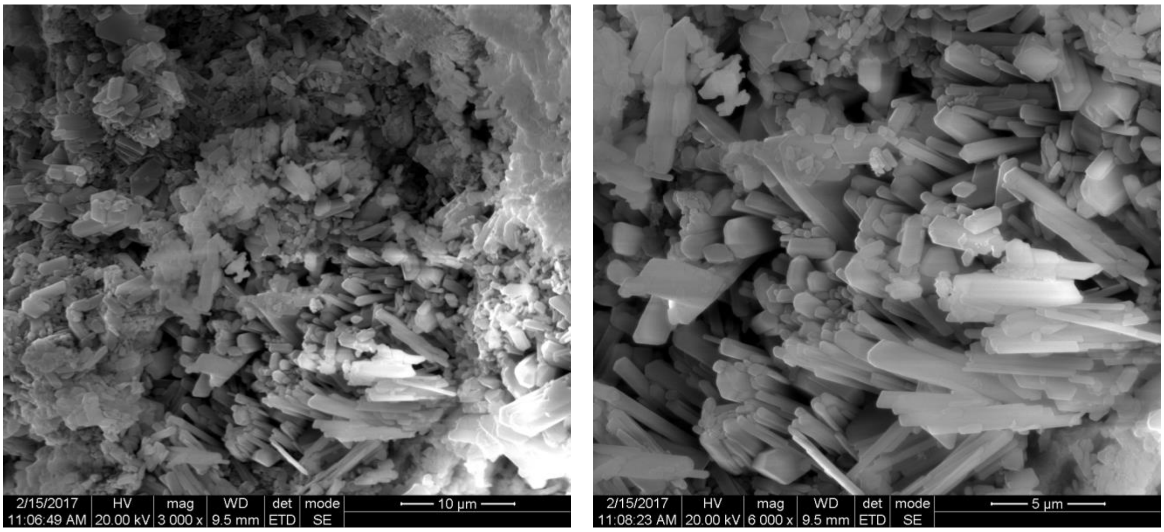

a) Needle like gypsum deposits b) A close view of gypsum deposits

Figure 6.56 Outer degraded layer of SF10 paste exposed to 1% sulphuric acid showing thick deposits of gypsum

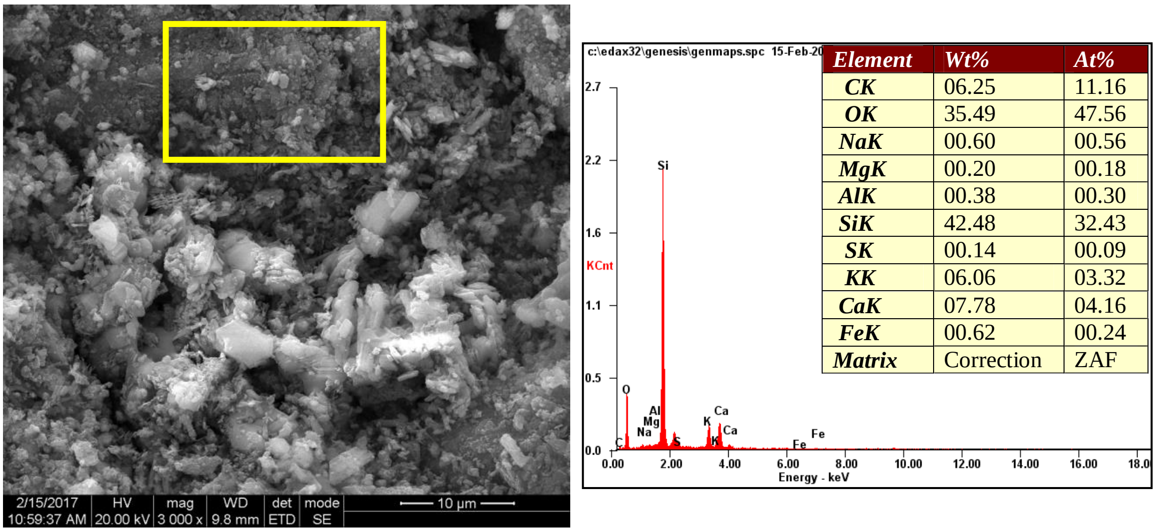

Element	*Wt%*	*At%*
CK	06.25	11.16
OK	35.49	47.56
NaK	00.60	00.56
MgK	00.20	00.18
AlK	00.38	00.30
SiK	42.48	32.43
SK	00.14	00.09
KK	06.06	03.32
CaK	07.78	04.16
FeK	00.62	00.24
Matrix	Correction	ZAF

Figure 6.57 Morphology and EDS spectrum of outer degraded layer of SF10 paste exposed to 1% sulphuric acid showing silica gel and gypsum

Figures 6.58 to 6.64 show the micrographs of various paste mixes exposed to 6 weeks of 1% hydrochloric acid. The outer degraded layer of OPC paste in Figure 6.58 shows the deterioration in the microstructure. The extensive decalcification of hydration products has transformed all calcium bearing phases to silica gel. The salts being soluble have leached to the solution leaving the matrix comprising only of silica gel. The pores created by the decalcification are left empty as the salts were soluble and hence the matrix appeared highly porous. The EDS spectrum (Figure 6.59) showed that the outer degraded layer is rich with silica gel containing alumina and devoid of calcium bearing phases. As evident from the EDS spectrum shown in Figure 6.60, the inner core layer was found to be rich with normal hydrates rich in calcium.

The morphology of the degraded layers of the other mixes was found to be similar. In the case of FA30 (Figure 6.61), the silica gel was also found to be rich in alumina and iron. This could be possibly due to the decalcification of aluminium and iron bearing hydrates forming aluminium hydroxide and iron hydroxide in the outer layers which are relatively more stable at low pH. The inner core layer was found to be rich in calcium (Figure 6.62). Some calcite like crystals also could be seen in the inner core layer. Figures 6.63 and 6.64 show the micrographs of the degraded layer of BFS50 and SF10 paste exposed to 1% hydrochloric acid comprising of porous silica gel. The high porosity of the silica gel layer as evident from the micrographs of all the mixes might have resulted in the further ingress of acid into the inside.

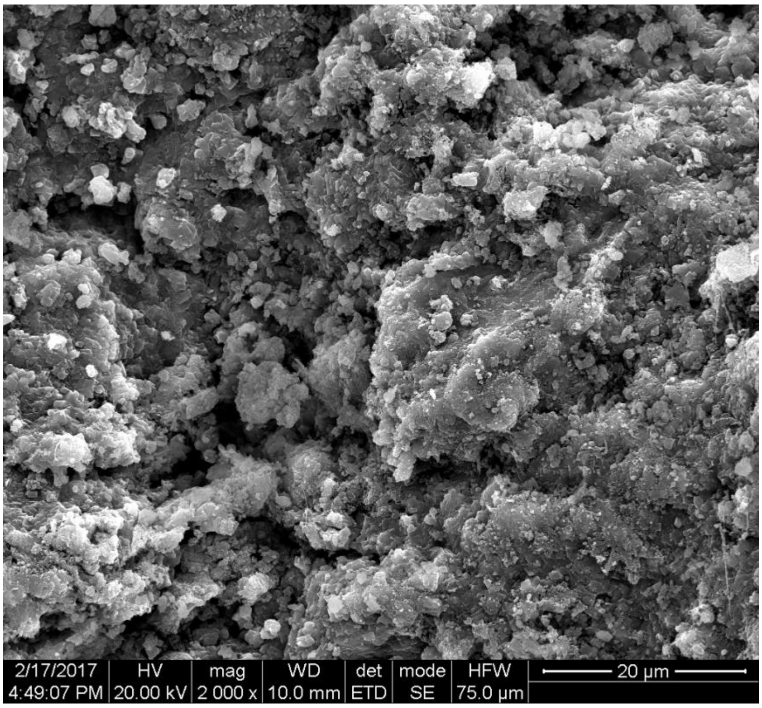

Figure 6.58 Outer degraded layer of OPC paste exposed to 1% hydrochloric acid showing deterioration

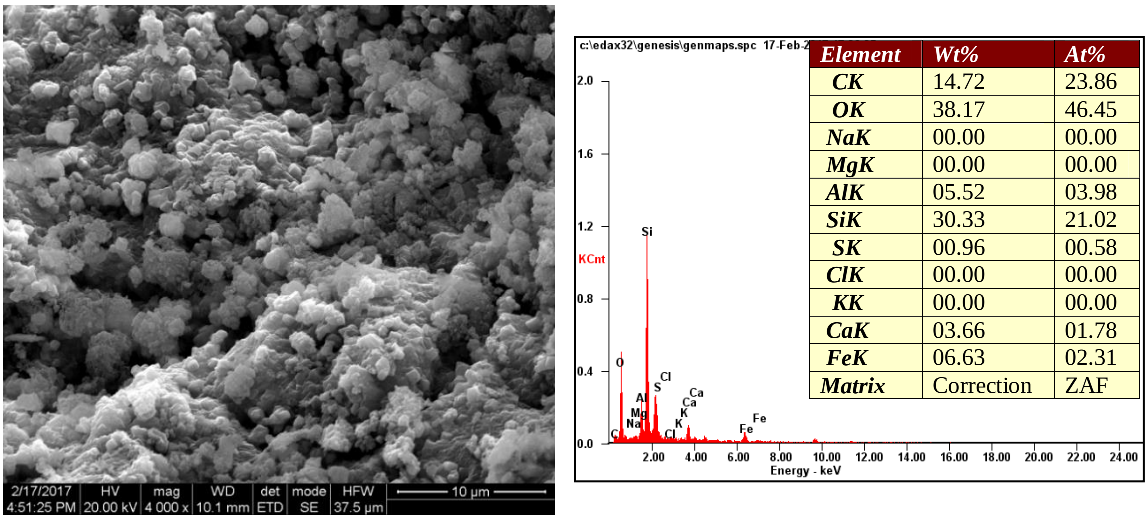

Element	Wt%	At%
CK	14.72	23.86
OK	38.17	46.45
NaK	00.00	00.00
MgK	00.00	00.00
AlK	05.52	03.98
SiK	30.33	21.02
SK	00.96	00.58
ClK	00.00	00.00
KK	00.00	00.00
CaK	03.66	01.78
FeK	06.63	02.31
Matrix	Correction	ZAF

Figure 6.59 Morphology and EDS spectrum of outer degraded layer of OPC paste exposed to 1% hydrochloric acid showing silica gel

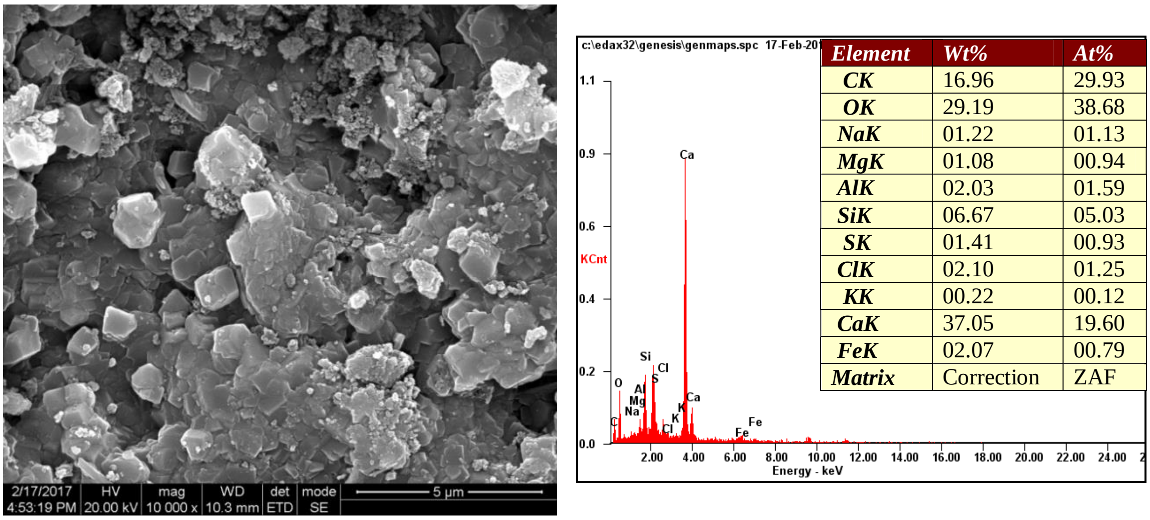

Element	Wt%	At%
CK	16.96	29.93
OK	29.19	38.68
NaK	01.22	01.13
MgK	01.08	00.94
AlK	02.03	01.59
SiK	06.67	05.03
SK	01.41	00.93
ClK	02.10	01.25
KK	00.22	00.12
CaK	37.05	19.60
FeK	02.07	00.79
Matrix	Correction	ZAF

Figure 6.60 Morphology and EDS spectrum of inner core layer of OPC paste exposed to 1% hydrochloric acid showing microstructure rich in calcium

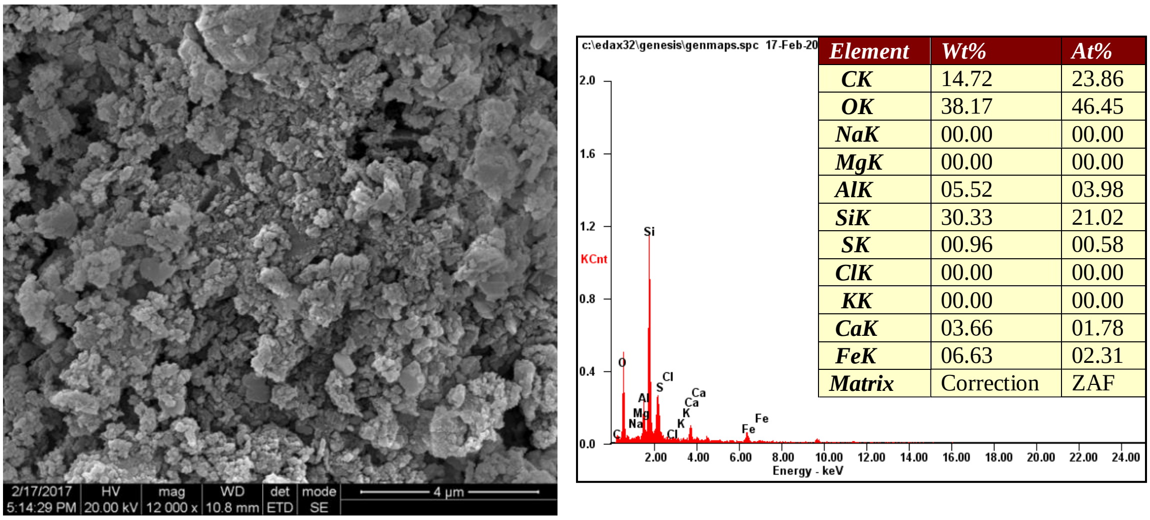

Element	Wt%	At%
CK	14.72	23.86
OK	38.17	46.45
NaK	00.00	00.00
MgK	00.00	00.00
AlK	05.52	03.98
SiK	30.33	21.02
SK	00.96	00.58
ClK	00.00	00.00
KK	00.00	00.00
CaK	03.66	01.78
FeK	06.63	02.31
Matrix	Correction	ZAF

Figure 6.61 Morphology and EDS spectrum of outer degraded layer of FA30 paste exposed to 1% hydrochloric acid showing porous microstructure and silica gel

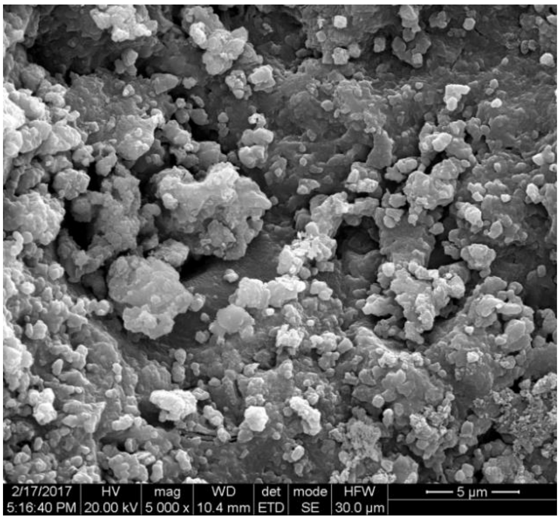

Element	Wt%	At%
CK	16.48	28.42
OK	29.48	38.17
NaK	01.25	01.12
MgK	01.20	01.02
AlK	01.79	01.38
SiK	17.48	12.90
SK	02.31	01.49
ClK	01.84	01.08
KK	00.46	00.25
CaK	26.67	13.78
FeK	01.04	00.39
Matrix	Correction	ZAF

Figure 6.62 Morphology and EDS spectrum of inner core area of FA30 paste exposed to 1% hydrochloric acid

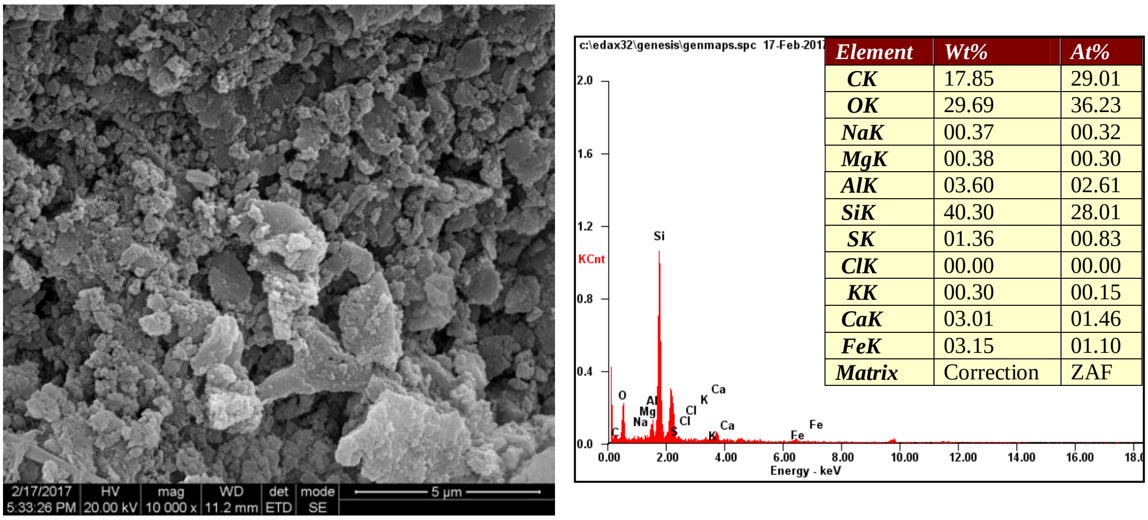

Element	Wt%	At%
CK	17.85	29.01
OK	29.69	36.23
NaK	00.37	00.32
MgK	00.38	00.30
AlK	03.60	02.61
SiK	40.30	28.01
SK	01.36	00.83
ClK	00.00	00.00
KK	00.30	00.15
CaK	03.01	01.46
FeK	03.15	01.10
Matrix	Correction	ZAF

Figure 6.63 Morphology and EDS spectrum of outer degraded layer of BFS50 paste exposed to 1% hydrochloric acid showing deterioration and silica gel

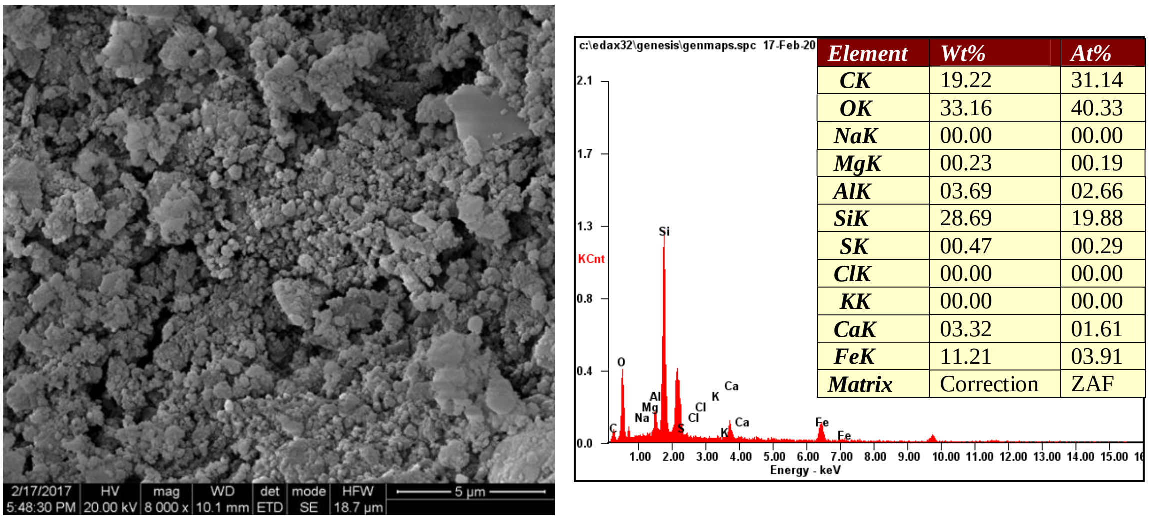

Element	Wt%	At%
CK	19.22	31.14
OK	33.16	40.33
NaK	00.00	00.00
MgK	00.23	00.19
AlK	03.69	02.66
SiK	28.69	19.88
SK	00.47	00.29
ClK	00.00	00.00
KK	00.00	00.00
CaK	03.32	01.61
FeK	11.21	03.91
Matrix	Correction	ZAF

Figure 6.64 Morphology and EDS spectrum of outer degraded layer of SF10 paste exposed to 1% hydrochloric acid showing deterioration and silica gel

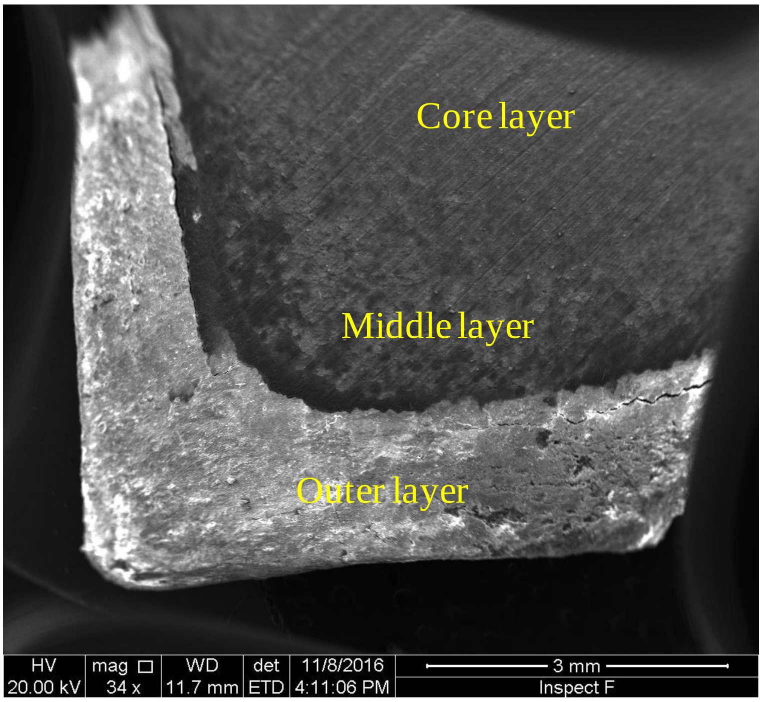

Figure 6.65 Micrograph of OPC paste exposed to 0.5M acetic acid showing mineralogical zonation

The micrograph of OPC paste exposed to 0.5M acetic acid is shown in Figure 6.65. The three zones identified in the CT images could be seen in the micrograph also; the outer layer which is severely deteriorated, an inner middle layer which is partially decalcified and the inner core which is not yet attacked by the acid solution. Extensive cracks along the junction between the outer and the middle layer are also evident, which reconfirms the weak mechanical properties of the silica gel that is formed as the end product after the reactions. The morphology and the EDS spectrum of the outermost degraded layer is shown in Figure 6.66. The layer showed severe degradation of microstructure and the matrix appeared porous which explains the large shift in the pore sizes, a reduction in the bulk density, an increase of mercury intruded volume, increase of capillary porosity etc. observed in the analysis of MIP results. The high porosity of the outer layer implies that the acid ions and salts can diffuse faster in either direction, thus resulting in the larger alteration depths when compared to those acids which form less soluble salts. Besides the considerable loss of calcium from the matrix, the degraded layer was found to be enriched in aluminium and iron when compared to the inner layers. However, the inner layer as shown in Figure 6.67 was found to be with normal hydrates without any decalcification.

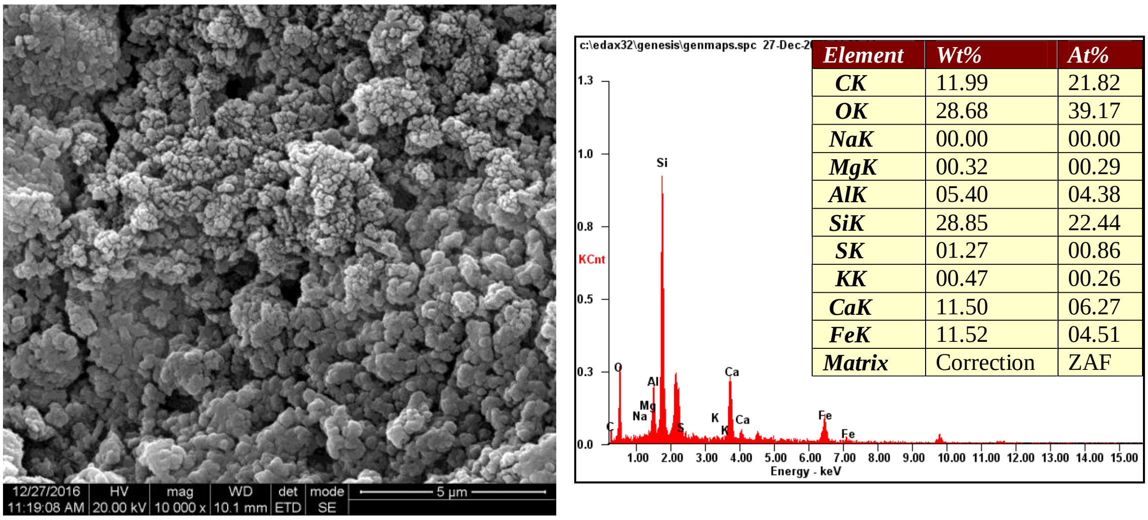

Element	Wt%	At%
CK	11.99	21.82
OK	28.68	39.17
NaK	00.00	00.00
MgK	00.32	00.29
AlK	05.40	04.38
SiK	28.85	22.44
SK	01.27	00.86
KK	00.47	00.26
CaK	11.50	06.27
FeK	11.52	04.51
Matrix	Correction	ZAF

Figure 6.66 Morphology and EDS spectrum of outer degraded layer of OPC paste exposed to 0.5M acetic acid showing deterioration and silica gel

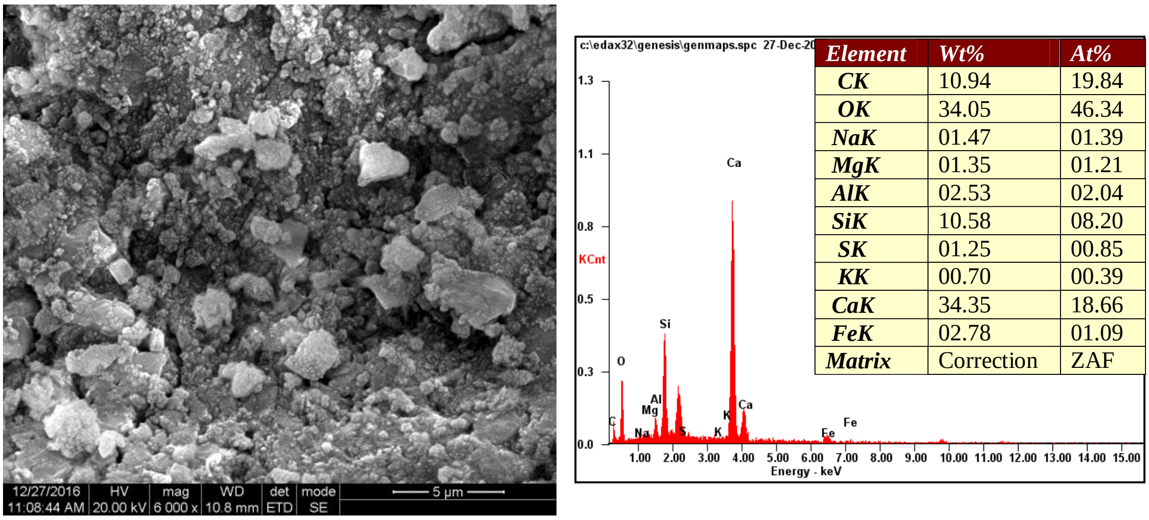

Element	Wt%	At%
CK	10.94	19.84
OK	34.05	46.34
NaK	01.47	01.39
MgK	01.35	01.21
AlK	02.53	02.04
SiK	10.58	08.20
SK	01.25	00.85
KK	00.70	00.39
CaK	34.35	18.66
FeK	02.78	01.09
Matrix	Correction	ZAF

Figure 6.67 Morphology and EDS spectrum of inner core layer of OPC paste exposed to 0.5M acetic acid showing hydration products rich in calcium

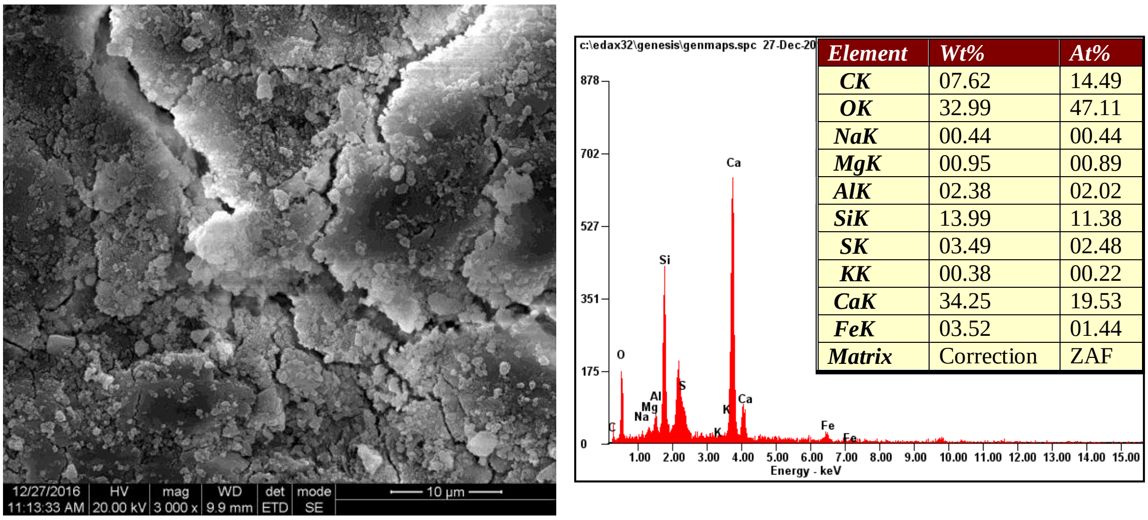

Element	Wt%	At%
CK	07.62	14.49
OK	32.99	47.11
NaK	00.44	00.44
MgK	00.95	00.89
AlK	02.38	02.02
SiK	13.99	11.38
SK	03.49	02.48
KK	00.38	00.22
CaK	34.25	19.53
FeK	03.52	01.44
Matrix	Correction	ZAF

Figure 6.68 Morphology and EDS spectrum of the middle layer of OPC paste exposed to 0.5M acetic acid showing cracks

Figure 6.68 shows the morphology and the EDS spectrum of middle layer of OPC paste exposed to 0.5M acetic acid. The decalcification shrinkage cracks were evident from the micrograph. It was found that the middle layer was not completely decalcified as some calcium is still present in it. It was also found that the area is enriched with sulphur, which could have moved out from the inner layer. The attacked FA30 paste showed similar morphology (Figures 6.69 and 6.70). The micrograph as shown in Figure 6.69 appeared to be porous, and filled with silica-alumina gel skeleton. Unlike the OPC paste, it was found that the inner layer was also affected by the decalcification to a large extent. The EDS spectrum shown in Figure 6.71 revealed that the inner area is devoid of calcium. These observations are in alignment with the larger alteration depths measured and high mass loss observed while investigating the alteration kinetics.

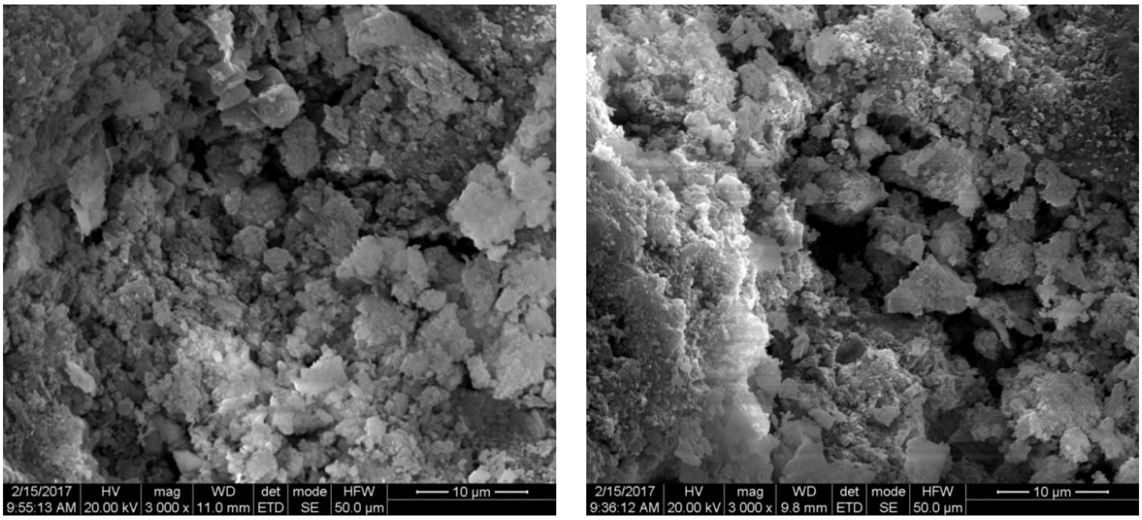

Figure 6.69 Morphology of the outer degraded layer of FA30 paste exposed to 0.5M acetic acid showing porous and deteriorated microstructure

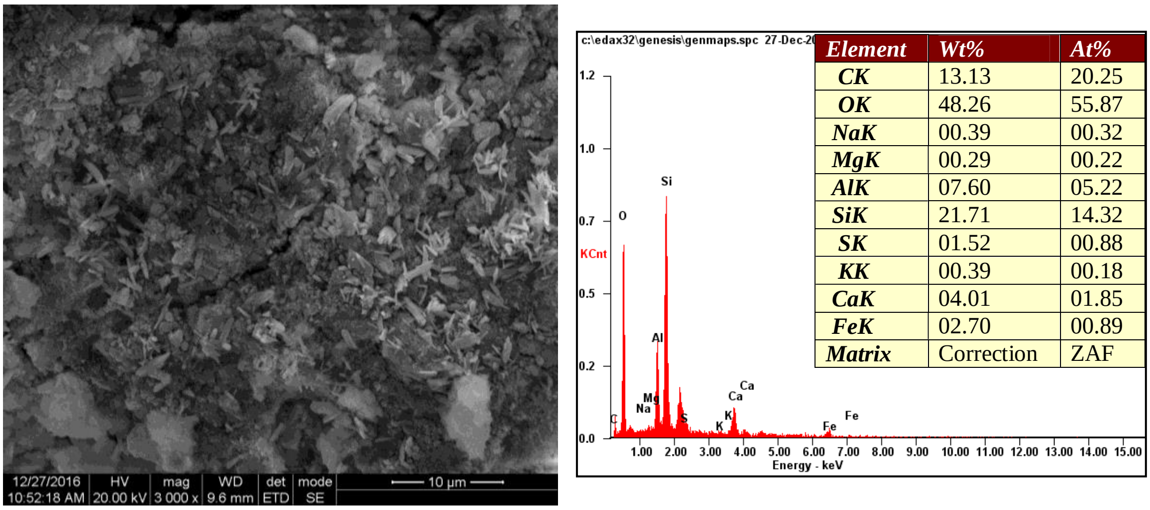

Element	***Wt%***	***At%***
CK	13.13	20.25
OK	48.26	55.87
NaK	00.39	00.32
MgK	00.29	00.22
AlK	07.60	05.22
SiK	21.71	14.32
SK	01.52	00.88
KK	00.39	00.18
CaK	04.01	01.85
FeK	02.70	00.89
Matrix	Correction	ZAF

Figure 6.70 Morphology and EDS spectrum of the outer degraded layer of FA30 paste exposed to 0.5M acetic acid showing alumina enriched silica gel

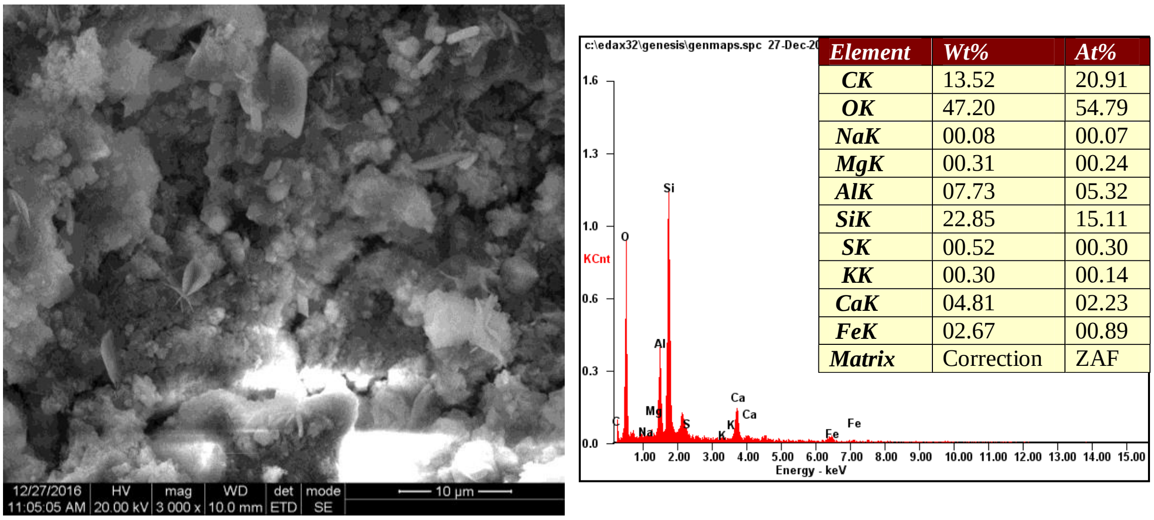

Element	Wt%	At%
CK	13.52	20.91
OK	47.20	54.79
NaK	00.08	00.07
MgK	00.31	00.24
AlK	07.73	05.32
SiK	22.85	15.11
SK	00.52	00.30
KK	00.30	00.14
CaK	04.81	02.23
FeK	02.67	00.89
Matrix	Correction	ZAF

Figure 6.71 Morphology and EDS spectrum of the inner core layer of FA30 paste exposed to 0.5M acetic acid showing severe decalcification

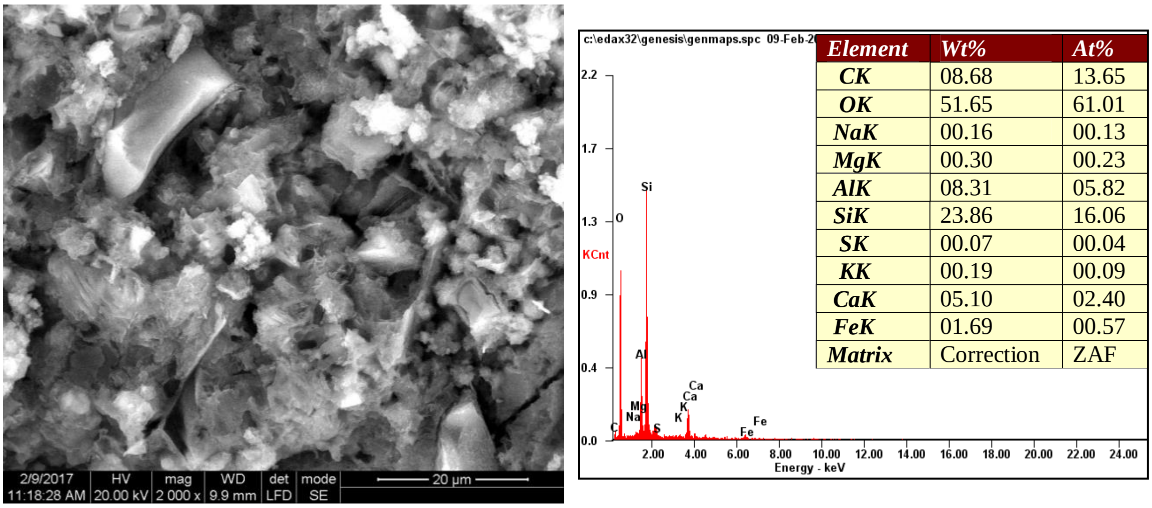

Element	Wt%	At%
CK	08.68	13.65
OK	51.65	61.01
NaK	00.16	00.13
MgK	00.30	00.23
AlK	08.31	05.82
SiK	23.86	16.06
SK	00.07	00.04
KK	00.19	00.09
CaK	05.10	02.40
FeK	01.69	00.57
Matrix	Correction	ZAF

Figure 6.72 Morphology and EDS spectrum of the outer degraded layer of BFS50 paste exposed to 0.5M acetic acid

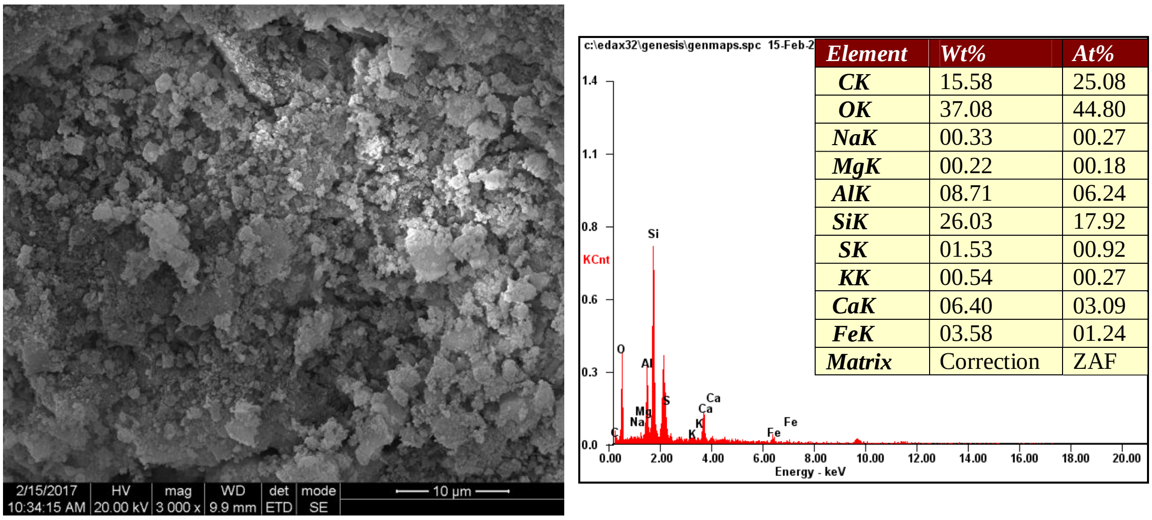

Element	Wt%	At%
CK	15.58	25.08
OK	37.08	44.80
NaK	00.33	00.27
MgK	00.22	00.18
AlK	08.71	06.24
SiK	26.03	17.92
SK	01.53	00.92
KK	00.54	00.27
CaK	06.40	03.09
FeK	03.58	01.24
Matrix	Correction	ZAF

Figure 6.73 Morphology and EDS spectrum of the outer degraded layer of BFS50 paste exposed to 0.5M acetic acid showing silica gel

The acetic acid attacked BFS50 paste also showed similar morphology (Figure 6.72 and 6.73) of the outer degraded layer which comprises of silica alumina gel. A magnified micrograph image shown in Figure 6.74 revealed the severity of decalcification. The microstructure was granular and highly porous (Figure 6.75). However, the morphology of the middle layer as shown in Figures 6.76 to 6.78 was found to be dissimilar. The middle layer deficient in calcium was found to be enriched with flower-like structures rich in sulphur. The sulphur from the inner core layer may have migrated towards these locations and got transformed to these flower-like structures. Figure 6.78 shows the magnified image of the middle layer and the EDS spectrum reveals the decalcification (due to low Ca/Si ratio) and the increased concentration of sulphur. Similar morphology for the middle layer was reported by Murugan and Santhanam (2018) in the case of paste exposed to 0.5M nitric acid, in which the authors classified these crystals as ‘thaumasite-like’.

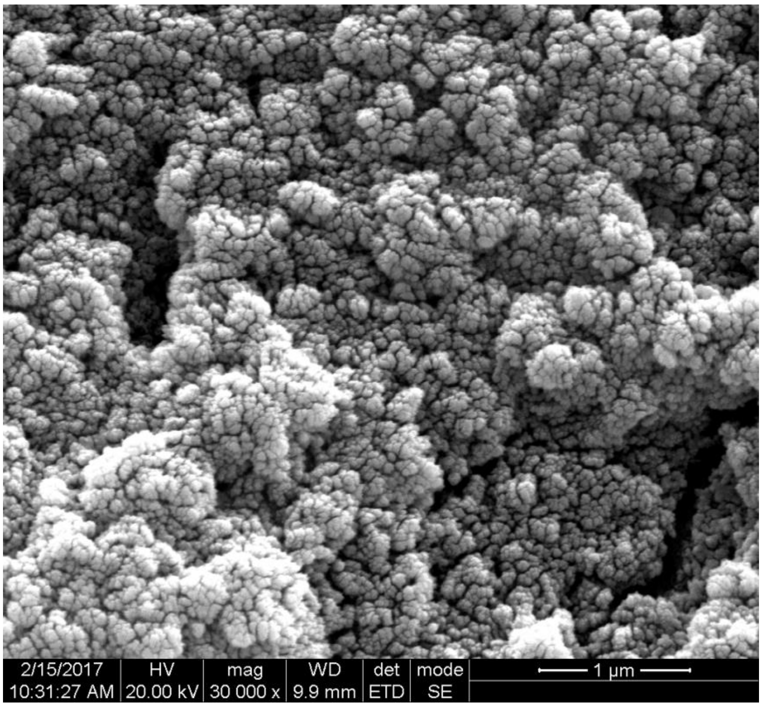

Figure 6.74 A magnified micrograph showing the degraded layer of BFS50 paste exposed to 0.5M acetic acid

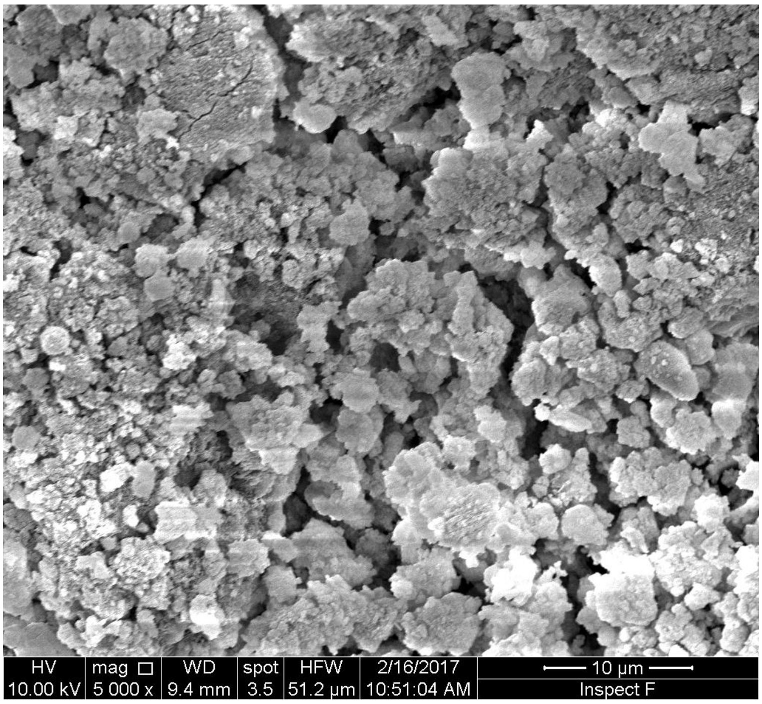

Figure 6.75 Micrograph showing the degraded layer of BFS50 paste exposed to 0.5M acetic acid showing the porous and disintegrated microstructure

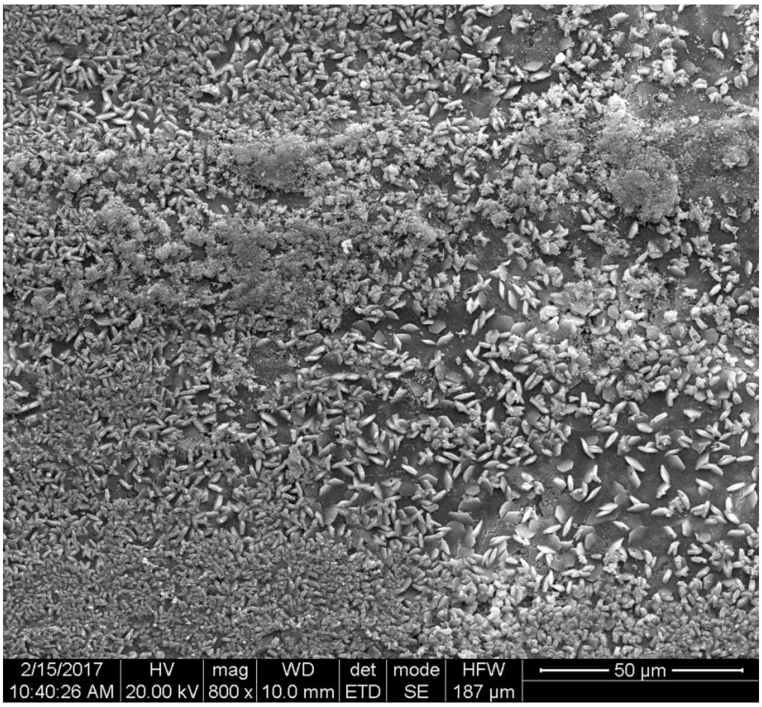

Figure 6.76 Micrograph of the middle layer of BFS50 paste exposed to 0.5M acetic acid showing decalcified microstructure rich in sulphur

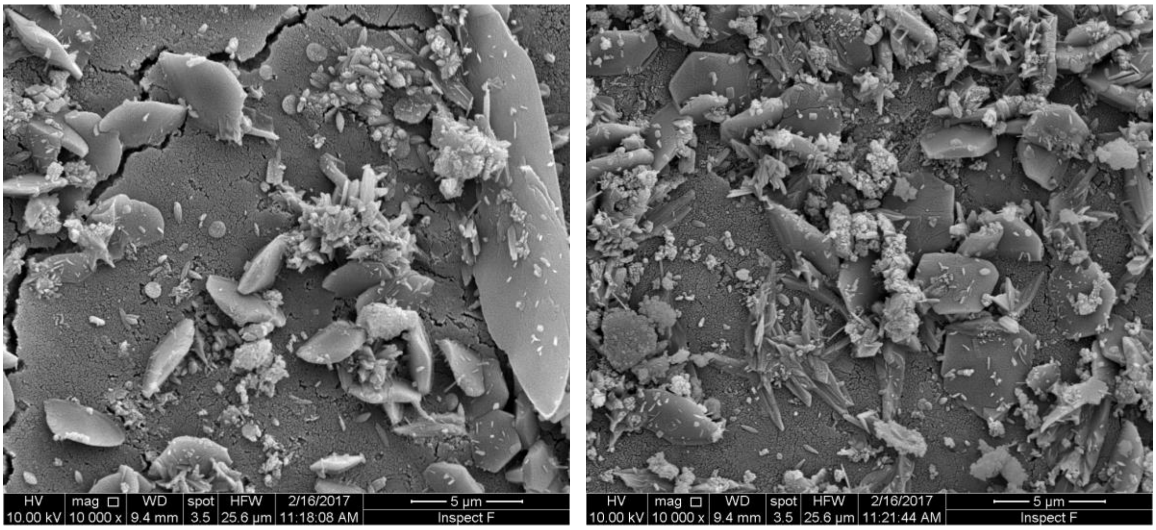

a) middle decalcified layer showing cracks due to decalcification

b) microstructure of middle layer showing ongoing decalcification of hydrates

Figure 6.77 Micrographs showing the decalcification in the middle layer of BFS50 paste exposed to 0.5M acetic acid

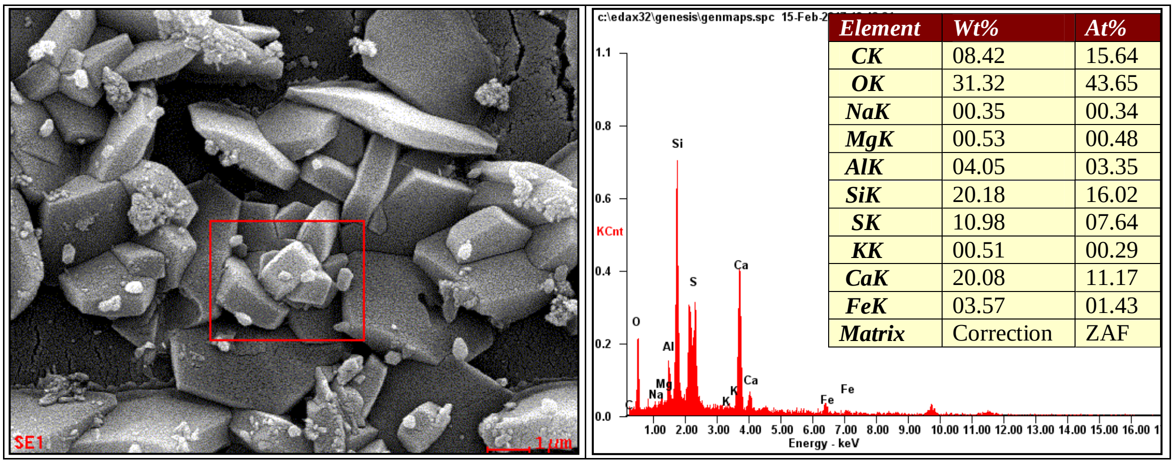

Element	Wt%	At%
CK	08.42	15.64
OK	31.32	43.65
NaK	00.35	00.34
MgK	00.53	00.48
AlK	04.05	03.35
SiK	20.18	16.02
SK	10.98	07.64
KK	00.51	00.29
CaK	20.08	11.17
FeK	03.57	01.43
Matrix	Correction	ZAF

Figure 6.78 Morphology and EDS spectrum of the middle layer of BFS50 paste exposed to 0.5M acetic acid showing enrichment of sulphur

A micrograph (Figure 6.79) captured at the junction between the outer layer and the middle layer of BFS50 paste showed the difference in the microstructure and porosity of these layers. The outer layer was found to be disintegrated and porous with loose deposits of silica gel residue while the middle layer, even though partially decalcified, was found to be less porous with precipitates of flower like structures containing sulphur in it. Figures 6.80 and 6.81 show the morphology and EDS spectrum of the inner core layer which is not attacked by the acetic acid. As evident from the EDS spectrum (Figure 6.80), the area was found to be filled with normal hydrates rich in calcium. The SF10 paste affected by acetic acid also showed granular disintegrated porous microstructure of the outer degraded layer (Figure 6.82).

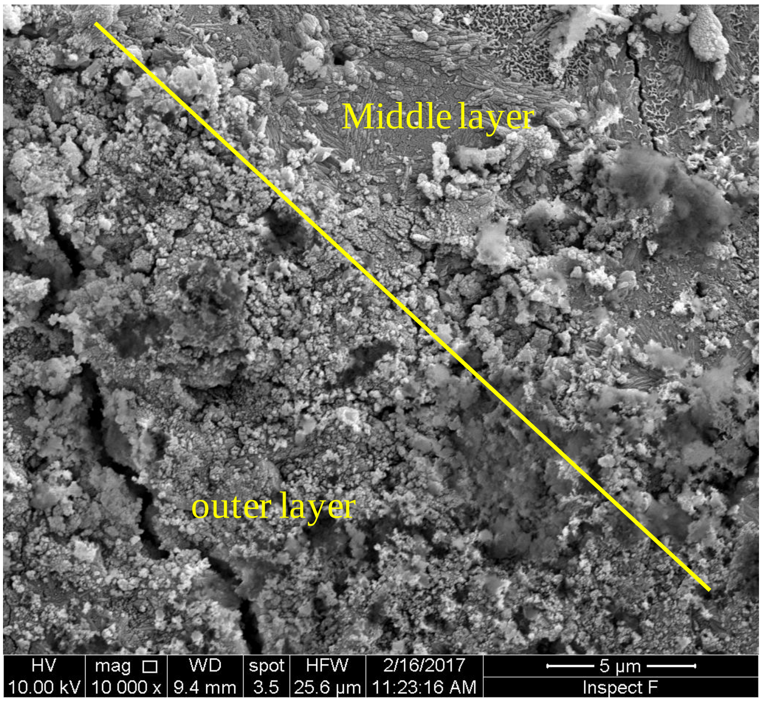

Figure 6.79 Micrograph showing the junction of outer and middle layers of BFS50 paste exposed to 0.5M acetic acid

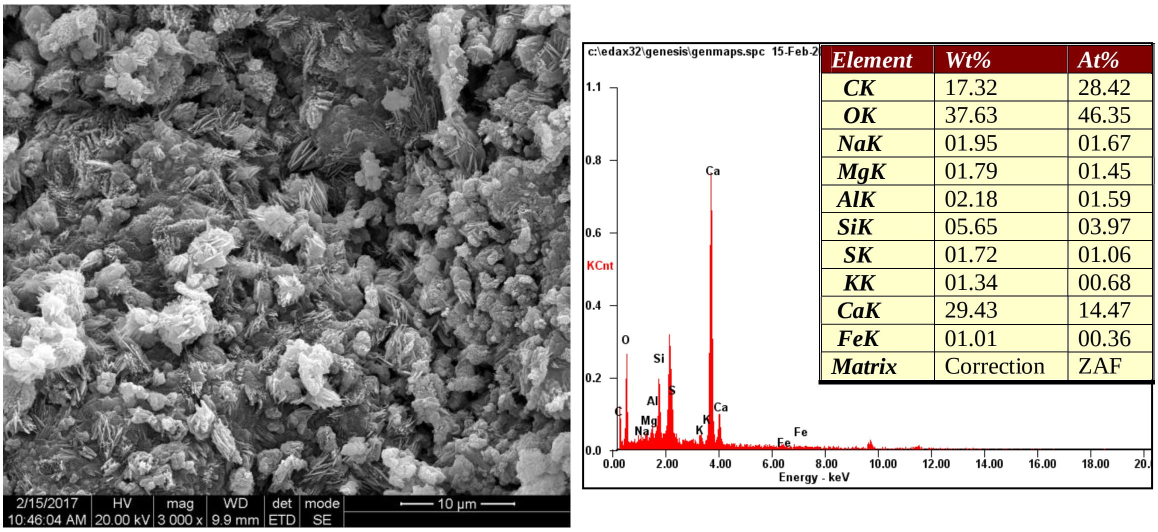

Element	*Wt%*	*At%*
CK	17.32	28.42
OK	37.63	46.35
NaK	01.95	01.67
MgK	01.79	01.45
AlK	02.18	01.59
SiK	05.65	03.97
SK	01.72	01.06
KK	01.34	00.68
CaK	29.43	14.47
FeK	01.01	00.36
Matrix	Correction	ZAF

Figure 6.80 Morphology and EDS spectrum of the inner core layer of BFS50 paste exposed to 0.5M acetic acid showing calcium rich hydrates

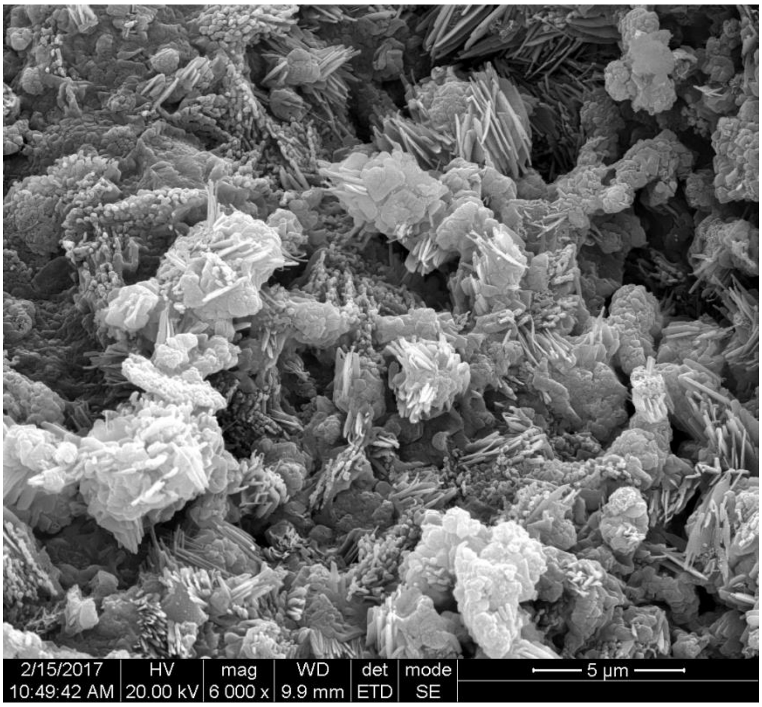

Figure 6.81 A magnified micrograph showing the microstructure of the inner core layer of BFS50 paste exposed to 0.5M acetic acid

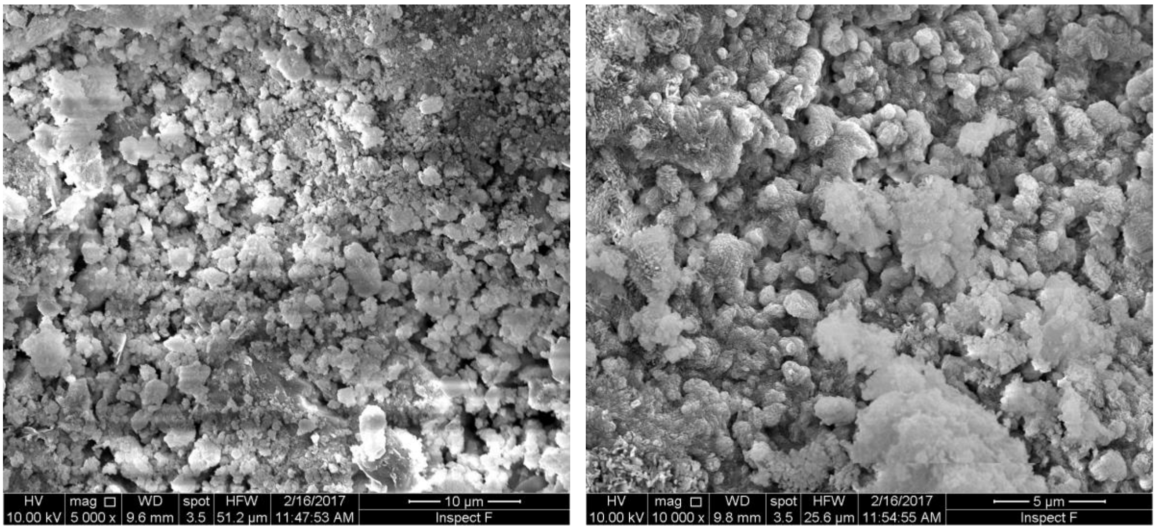

Figure 6.82 Morphology of the outer degraded layer of SF10 paste exposed to 0.5M acetic acid

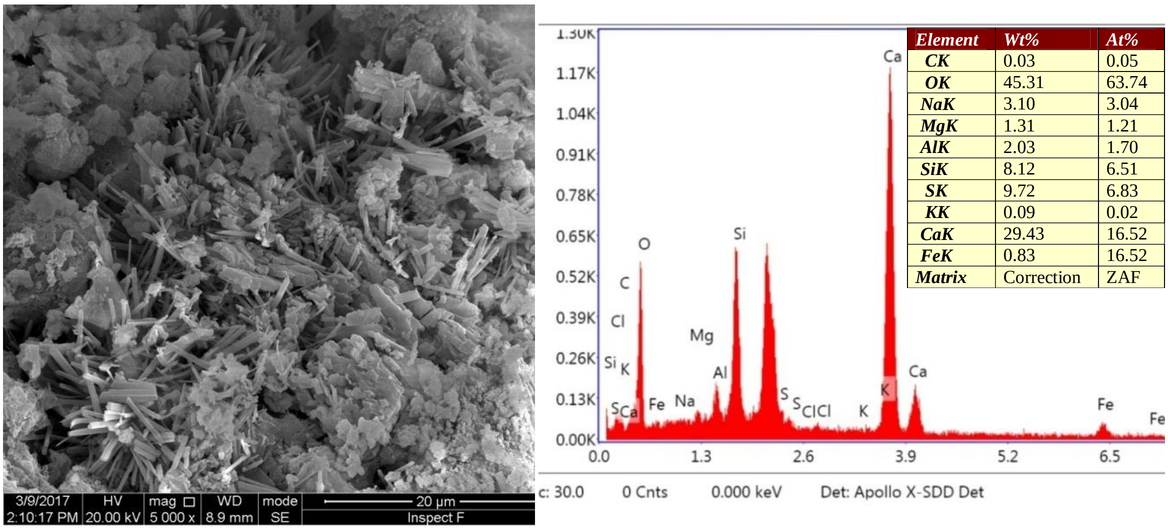

Element	**Wt%**	**At%**
CK	0.03	0.05
OK	45.31	63.74
NaK	3.10	3.04
MgK	1.31	1.21
AlK	2.03	1.70
SiK	8.12	6.51
SK	9.72	6.83
KK	0.09	0.02
CaK	29.43	16.52
FeK	0.83	16.52
Matrix	Correction	ZAF

Figure 6.83 Morphology and EDS spectrum of the outer degraded layer of OPC paste exposed to 0.5M citric acid showing precipitation of salts

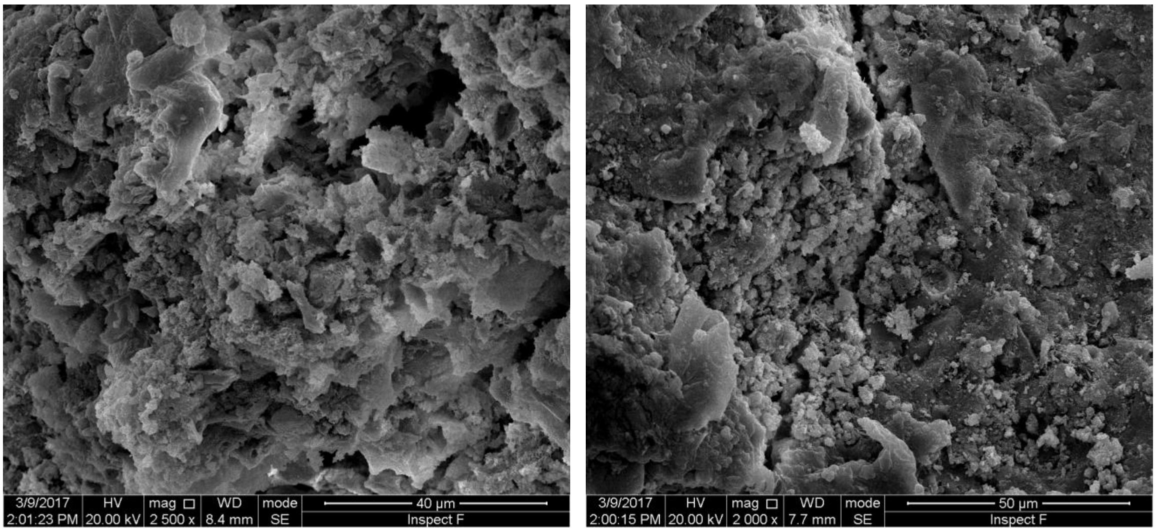

a) salt deposits

b) degraded layer showing cracks

Figure 6.84 Micrograph of the outer degraded layer of OPC paste exposed to 0.5M citric acid showing precipitation of salts and cracks

The microstructural features of citric acid attack were different from the other acids. Figures 6.83 and 6.84 show the morphology of the outer degraded layer of OPC paste exposed to 6 weeks of 0.5M citric acid. The SEM images showed severe precipitation of calcium citrate tetra hydrate salts in the outer degraded layer. The salt was found to be loosely attached to the matrix which apparently consists of the silica gel after the decalcification of hydrates. The needle like structure of salt is known to possess high molar volume when compared to the original hydrates. This resulted in expansive pressure and in the associated deterioration. Figures 6.85, 6.86 and 6.88 show the morphology and EDS spectrum of the outer degraded layers of FA30, BFS50 and SF10 paste exposed to

0.5M citric acid respectively. In all these SEM images, the severity and aggressiveness of the citric acid was evident as the salt was less soluble which precipitated within the decalcified matrix (as in Figure 6.87) possessing high molar volume and low affinity to the matrix. This explains the higher mass loss and loss of thickness noted while evaluating the degradation kinetics.

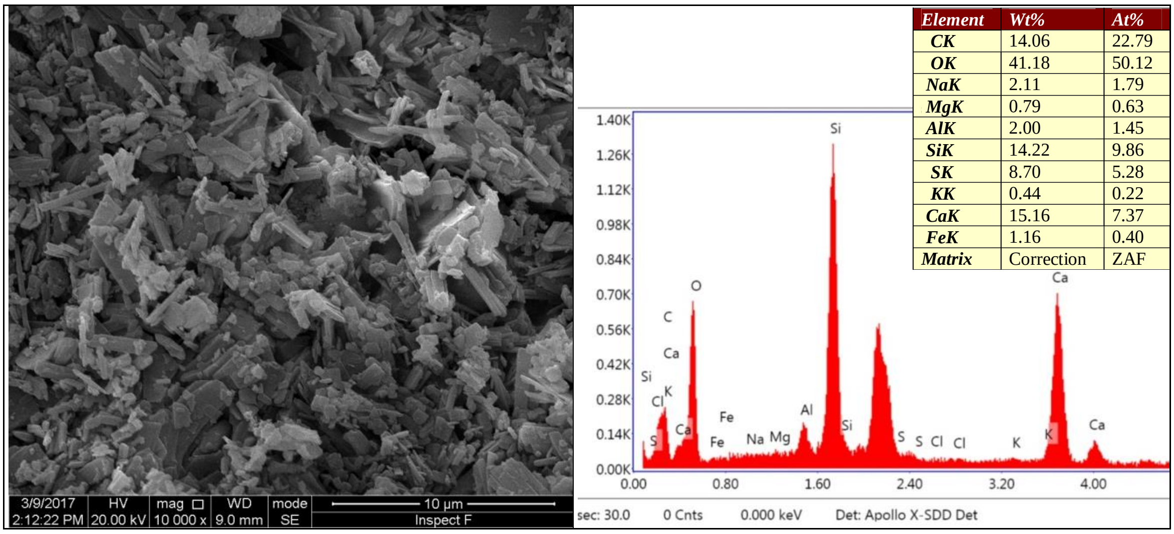

Element	Wt%	At%
CK	14.06	22.79
OK	41.18	50.12
NaK	2.11	1.79
MgK	0.79	0.63
AlK	2.00	1.45
SiK	14.22	9.86
SK	8.70	5.28
KK	0.44	0.22
CaK	15.16	7.37
FeK	1.16	0.40
Matrix	Correction	ZAF

Figure 6.85 Morphology and EDS spectrum of outer degraded layer of FA30 paste exposed to 0.5M citric acid

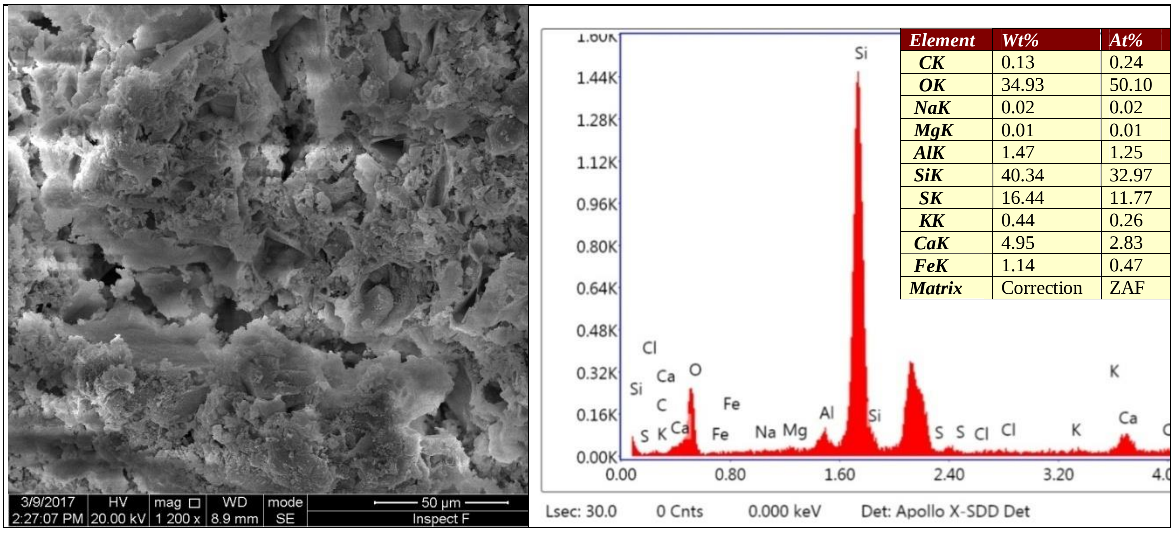

Element	Wt%	At%
CK	0.13	0.24
OK	34.93	50.10
NaK	0.02	0.02
MgK	0.01	0.01
AlK	1.47	1.25
SiK	40.34	32.97
SK	16.44	11.77
KK	0.44	0.26
CaK	4.95	2.83
FeK	1.14	0.47
Matrix	Correction	ZAF

Figure 6.86 Morphology and EDS spectrum of outer degraded layer of BFS50 paste exposed to 0.5M citric acid

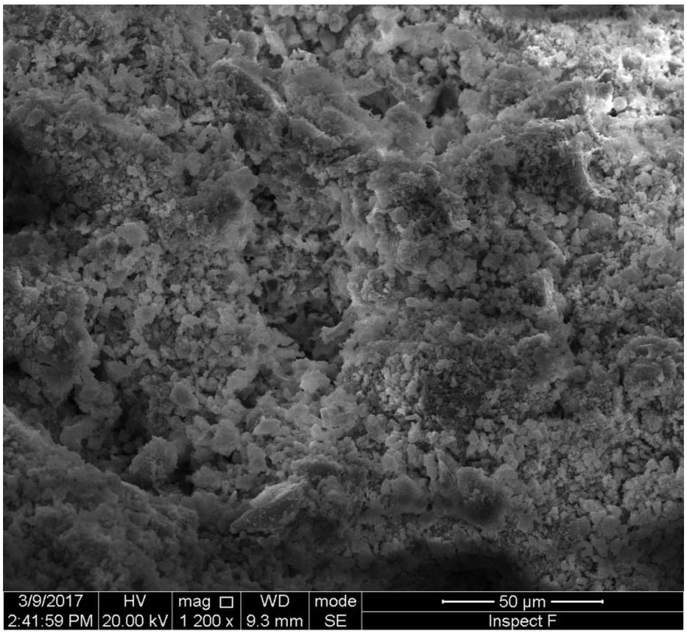

Figure 6.87 Micrograph of outer degraded layer of SF10 paste exposed to 0.5M citric acid showing precipitation of calcium citrate salts

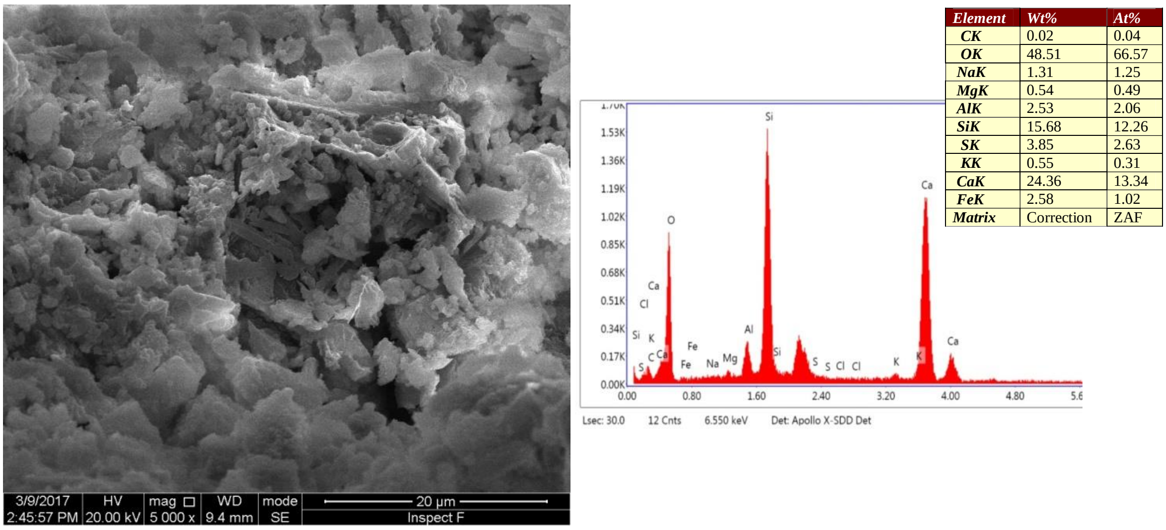

Element	Wt%	At%
CK	0.02	0.04
OK	48.51	66.57
NaK	1.31	1.25
MgK	0.54	0.49
AlK	2.53	2.06
SiK	15.68	12.26
SK	3.85	2.63
KK	0.55	0.31
CaK	24.36	13.34
FeK	2.58	1.02
Matrix	Correction	ZAF

Figure 6.88 Morphology and EDS spectrum of outer degraded layer of SF10 paste exposed to 0.5M citric acid

Line scan mapping of elements was done along the attacked layers of the paste. Averages of 16 frames were taken for the imaging operations. Figure 6.89 shows the line scan elemental profile of OPC paste exposed to 0.5M acetic acid. It can be seen that there is a substantial removal of calcium from the outer degraded layer as it gets leached away to the solution as calcium acetate. There is a reduction in the concentration of calcium also in the middle layer which is the progression front. This reduction could be due to the dissolution of Portlandite. There is an increased concentration of silicon in the outer layer due to the formation of silica gel. Also, it is evident that there is an increased concentration of aluminium and iron in the outer layer as they leach to the outside. Figure 6.90 shows the line scan elemental profile of FA30 paste exposed to 0.5M acetic acid. The profile shows that the entire specimen has undergone decalcification as there is deficiency of calcium throughout the depth of the specimen. These observations match with the altered depth measurements, CT imaging and the SEM secondary electron micrographs. An increased concentration of iron very near to the external surface could also be seen. In the case of BFS50 paste exposed to acetic acid, the line profile was similar to OPC paste (Figure 6.91). There is progressive loss of calcium from the inner layer moving towards the outer degraded layer. Similar to OPC paste, the outer layer was found to have increased concentration of elements such as aluminium, iron and silicon.

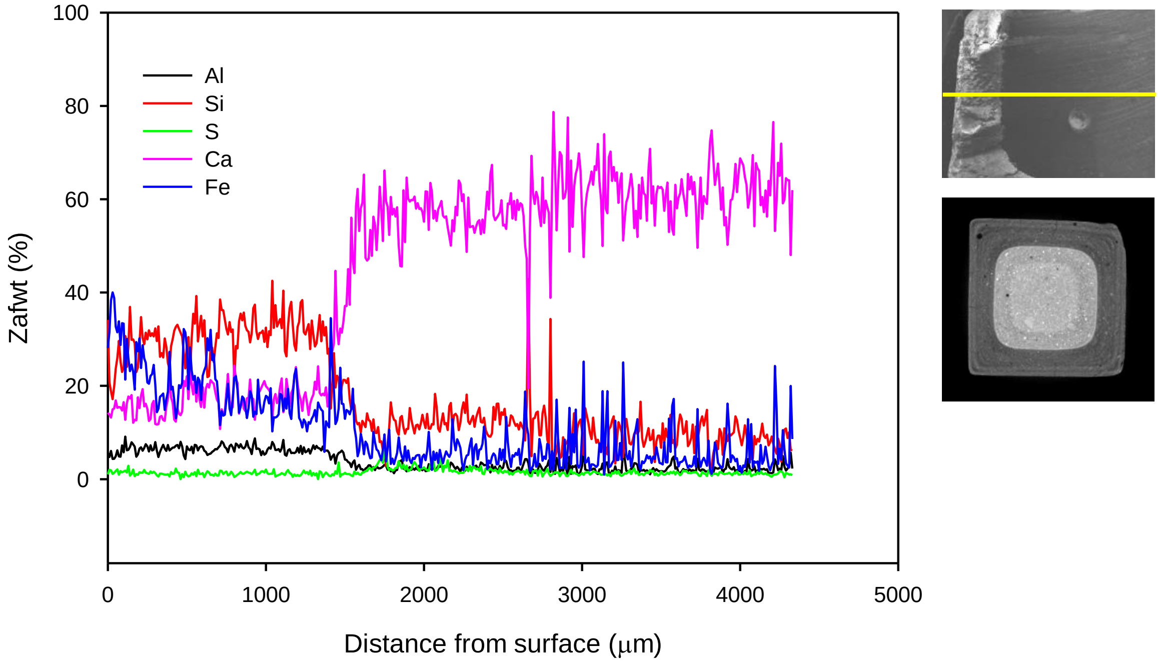

Figure 6.89 Line scan profile of OPC paste exposed to 0.5M acetic acid

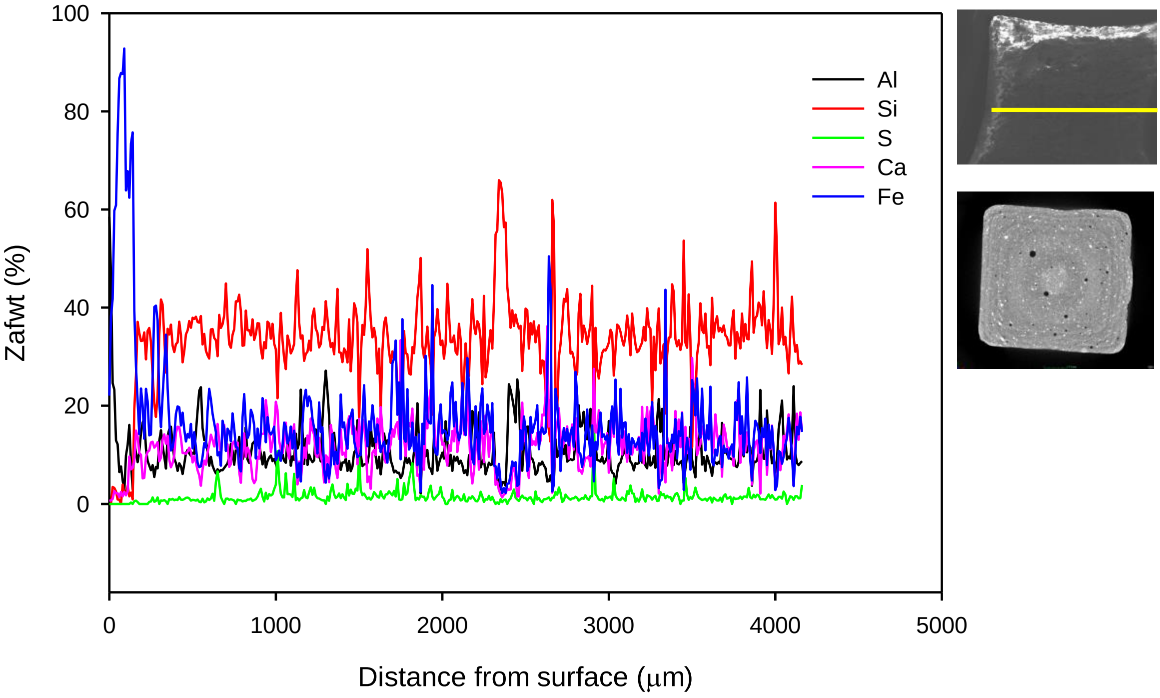

Figure 6.90 Line scan profile of FA30 paste exposed to 0.5M acetic acid

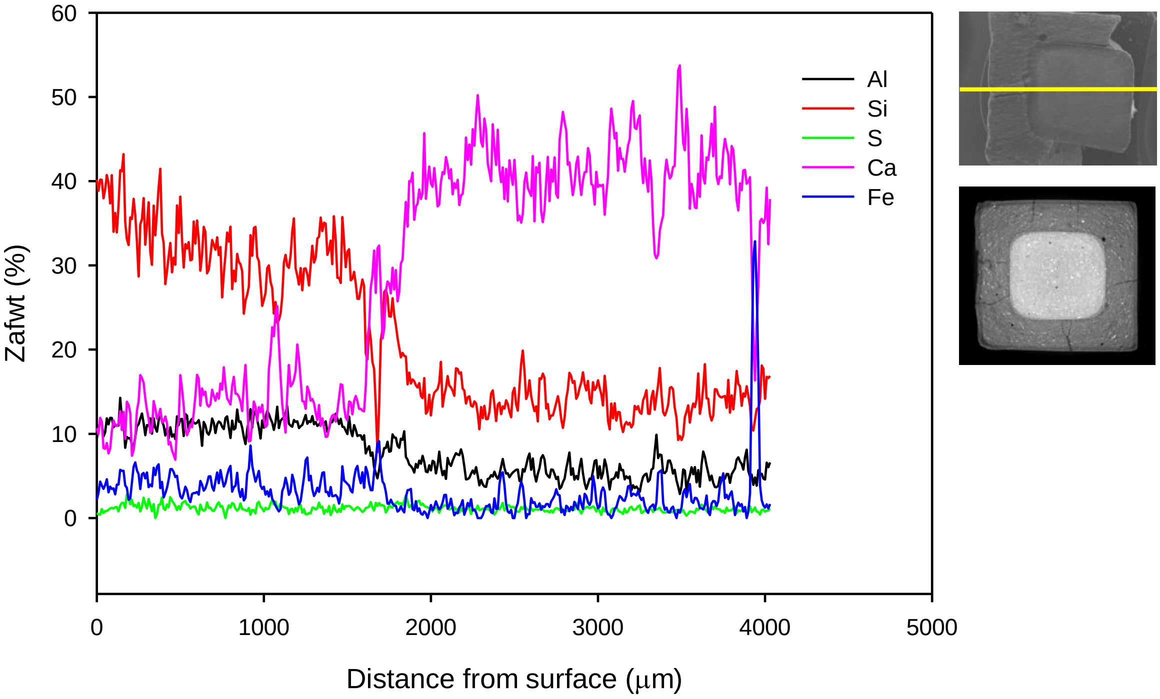

Figure 6.91 Line scan profile of BFS50 paste exposed to 0.5M acetic acid

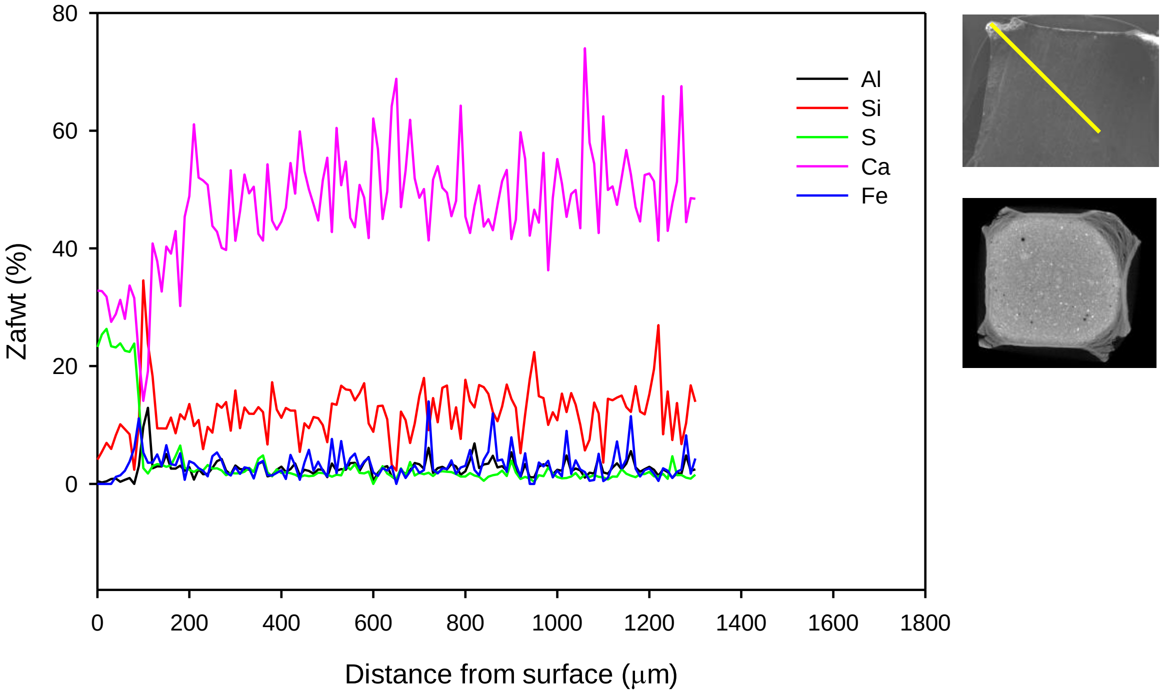

Figure 6.92 Line scan profile of OPC paste exposed to 1% sulphuric acid

Figure 6.92 shows the line scan elemental profile of OPC paste exposed to 1% sulphuric acid. As evident from the Figure 6.92, the depth of decalcification was found to be less. There is a marginal drop of calcium in the middle decalcified layer and considerable loss of calcium in the outer layer. The increased concentration of sulphur (from the migration of sulphate ions of the acid) in the outer layer is due to the formation of gypsum. An increased concentration of silicon, aluminium and iron is noticed at the depth (around 100 μm from the surface) where there is a substantial increase of sulphur. This suggests the fact that there is a layer of silica gel bound with alumina and iron just beneath the gypsum layer. The line scan profile of FA30 paste exposed to 1% sulphuric acid (Figure 6.93) was also similar to that of the OPC paste with a hike in concentration of aluminium, silicon and iron just adjacent to the gypsum layer (evident from the zoomed portion of the line profiles as shown in Figure 6.94).

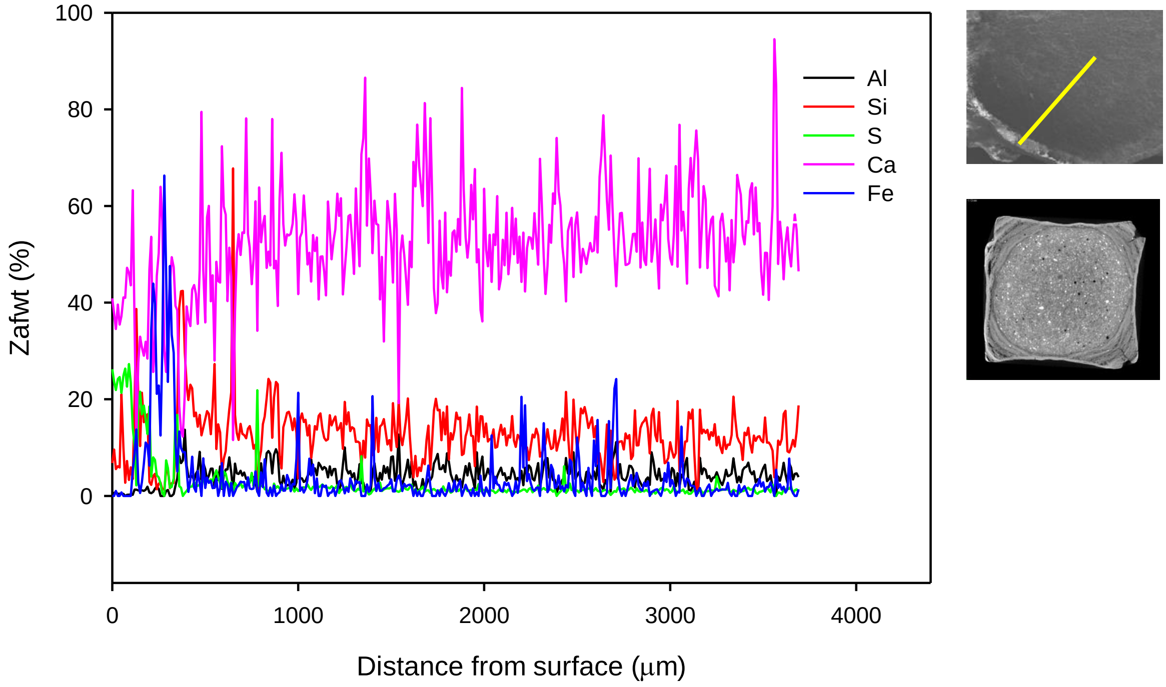

Figure 6.93 Line scan profile of FA30 paste exposed to 1% sulphuric acid

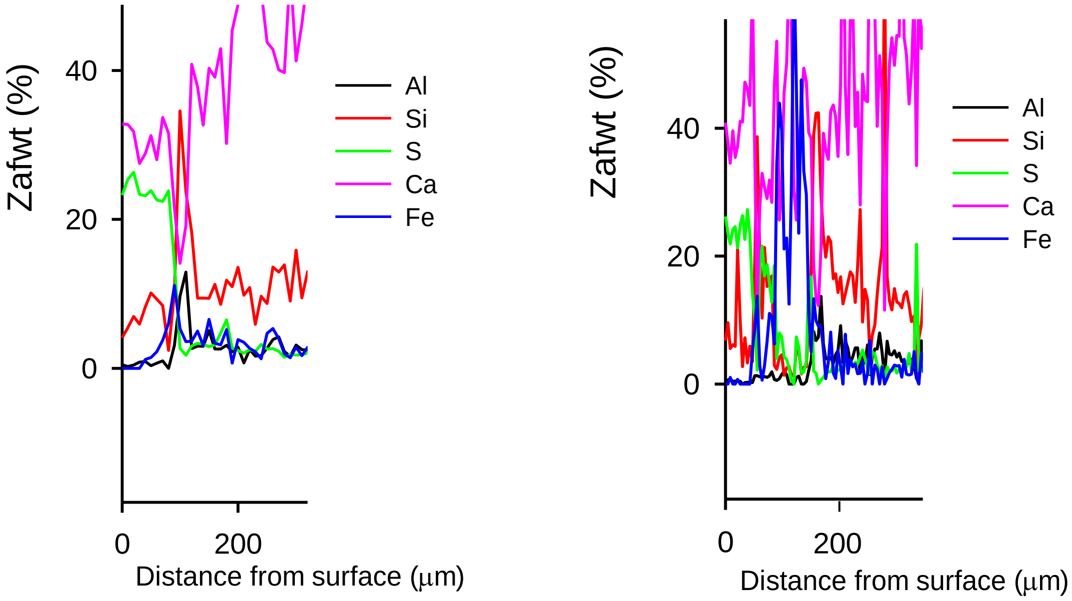

a) OPC paste

b) FA30 paste

Figure 6.94 A zoomed image showing the line scan profile of OPC and FA30 paste near to the external surface on exposure to 1% sulphuric acid

6.2.6 X-ray diffraction

6.2.6.1 Common binder systems

X-ray diffraction study is carried out on powdered samples in order to understand the mineralogical transformations due to the acid attack. The X-ray diffractograms for the control paste before the acid exposure are shown in Figure 6.95. Crystalline hydrated phases such as ettringite (E), Portlandite (P) were identified in the OPC mix along with other crystalline phases such as gypsum, quartz, calcite, anhydrous phases such as brownmillerite (B), larnite (C_2S) and hatrurite (C_3S). Similar phases were present in the other mixes.

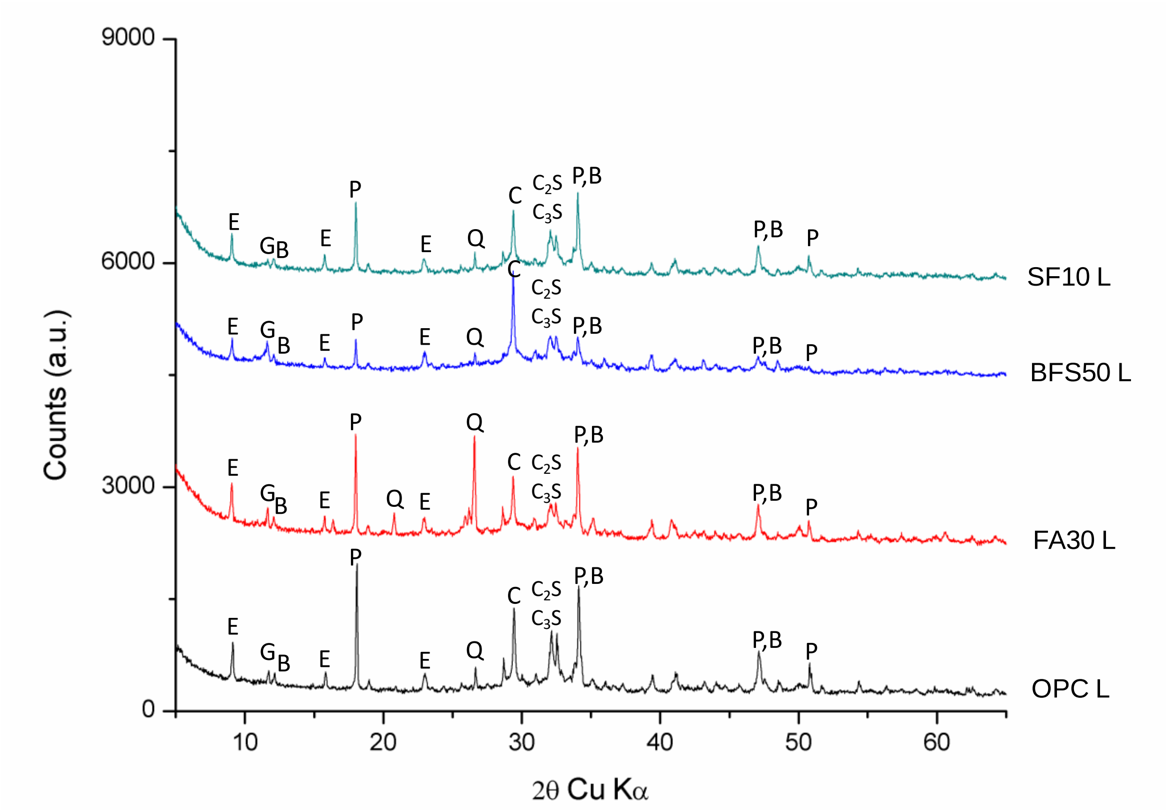

Figure 6.95 X-ray diffractograms of paste mixes before the acid exposure

Figure 6.96 shows the X-ray diffractograms of OPC paste exposed to various acids (S – 1% sulphuric, H – 1% hydrochloric, A – 0.5M acetic and C – 0.5M citric acid). On exposure to 1% sulphuric acid, it is seen that there is an increase in the peak intensity for ettringite. Gypsum was formed as the main reactive product which is due to the reaction between calcium-bearing hydrates and sulphuric acid. The formation of ettringite could be due to the reaction of calcium aluminates with the gypsum. A minor reduction in the

Portlandite phase was noted which indicates that Portlandite near the external surface is consumed for the reaction to form gypsum in the outer degraded layer. As the penetration of acid is limited to few microns from the external surface, Portlandite was present intact in the inner layers as evident from the Portlandite peaks exposed to sulphuric acid. There was also a reduction in the peak intensity for anhydrous phases such as C_2S and C_3S on exposure to sulphuric acid. The damage to the specimens on exposure to sulphuric acid can thus be attributed to the formation of gypsum and ettringite. Ettringite, being less stable in acidic environments, converts back to gypsum on the external surfaces. But ettringite may be present in the middle layer where decalcification is partially completed or yet to start.

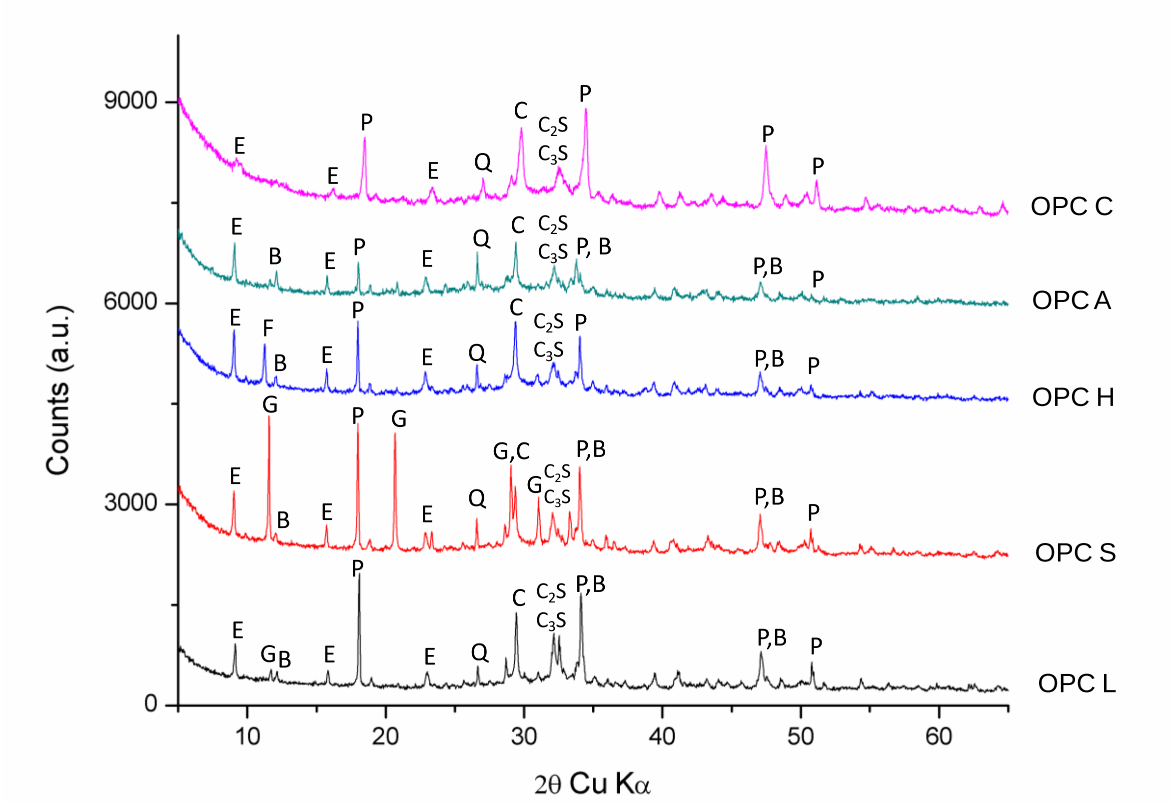

Figure 6.96 X-ray diffractograms of OPC paste before and after acid exposure

On exposure to 1% hydrochloric acid, as the salts were soluble, they do not form precipitates within the matrix and hence are not detected in the X-ray diffractogram. The strong peak at 11.19° 2θ indicates the formation of Friedel’s salt which could be due to the reaction between calcium aluminate hydrates and hydrochloric acid. There was a clear reduction in the intensity of peaks for Portlandite and anhydrous phases. A small increase in the ettringite peak suggests that it may be formed in the middle layers where more concentration of sulphur is made available because of the concentration gradient induced by the attack. This increased concentration of sulphur in the middle layer was earlier confirmed in the SEM imaging. Additionally, an increase in the amorphous area centered around 27˚ 2θ suggests the decalcification of CSH gel to form an amorphous silica gel. A minor reduction in the peak of calcite was noted as calcite in the outer degraded layer is soluble in acid solution.

The alteration in the OPC paste attacked by acetic acid was also found to be similar to hydrochloric acid as the mechanism of the degradation is similar. All crystalline peaks of hydrated phases have undergone reduction and there was a formation of an amorphous hump centered around 27˚ 2θ indicating the formation of silica gel due to the reaction between CSH gel and hydrochloric acid. An increase in the peak intensity of quartz is also noted which could be due to the decalcification of anhydrous calcium silicates. The substantial reduction of the Portlandite may be ascribed to the greater alteration depth of acetic acid.

On exposure to citric acid, calcium citrate tetrahydrate is formed in substantial quantities. However, as the salt possesses high molar volume and low affinity with the matrix, it defragments from the matrix and gets collected in the test beakers. Hence, only a thin layer of precipitate was present in the specimens that were crushed for testing XRD. As a result, only less quantities of salt were noted. There was a reduction in the peak intensities for phases such as Portlandite, C_2S, C_3S and ettringite on reaction with citric acid.

In order to understand the mechanism further, an attempt was made to separate the various layers formed in OPC paste exposed to sulphuric, hydrochloric and acetic acid and the XRD patterns for these samples are shown in Figure 6.97. The XRD of the outer layer of OPC paste exposed to sulphuric acid showed that only gypsum is present in the outer layer and no other crystalline phases were noted. An amorphous hump in the 20 – 30˚ 2θ range confirms the formation of silica gel which is bound with the gypsum in the outer layer as supported by the CT images and SEM imaging. The outer layer of OPC paste exposed to hydrochloric acid was amorphous as no major crystalline hydrated peaks were found which indicate the severity of decalcification. Only trace quantities of quartz, calcite and brownmillerite were noted in the outer layer along with amorphous silica gel. The presence of minor amount of brownmillerite suggests that iron and aluminium are stable in the degraded layers, the presence of which is responsible for the increased concentration of aluminium and iron in the EDS spectrum of the SEM images. Acetic acid was even aggressive as the outer layer of OPC paste was turned completely amorphous owing to the formation of silica gel. Only quartz and brownmillerite were found to be stable in the outer degraded layer. Even calcite was not noted in the outer layer as it might have been dissolved by the acid solution. Samples were also collected from the relatively thick middle layer of OPC paste exposed to acetic acid. It was found that the layer is less amorphous when compared to the outer degraded layer. The presence of higher intensities of quartz, calcite and brownmillerite were noted. However, there were no traces of hydrated crystalline phases present even in the middle layer which reconfirms the hypothesis that the middle layer has undergone partial or full decalcification and constitutes the progression front for the further attack to progress inward.

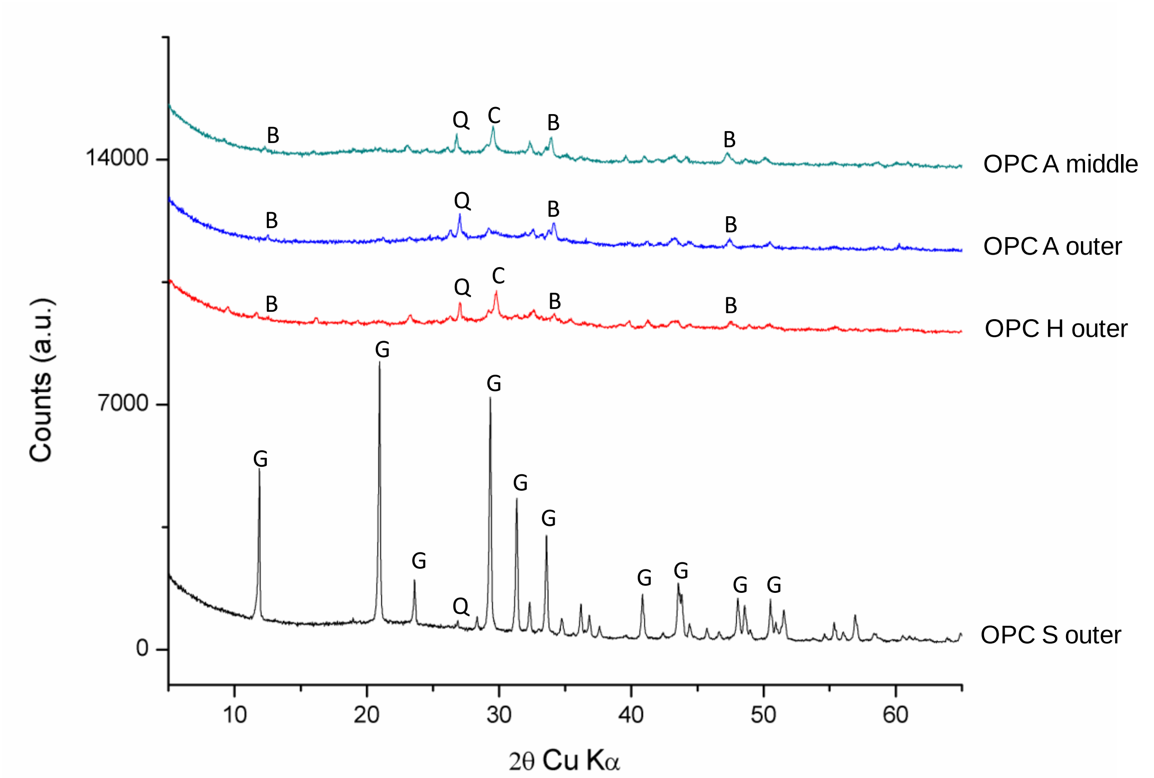

Figure 6.97 X-ray diffractograms of various layers formed on OPC paste exposed to acids

Figure 6.98 shows the X-ray diffractogram patterns of paste made with various binders when exposed to 1% sulphuric acid. The XRD patterns for all the mixes appear to be similar, the variation being in the amount of reactive products formed. It is seen that higher quantity of ettringite and gypsum is formed in FA30 when compared to OPC. This increased precipitation is noticed on microscopy images and in the corresponding mass gain while investigating the alteration kinetics. An increase in the peak intensity of gypsum in BFS50 is also supported by the visual observations and mass changes as the amount of precipitate formed was found to be higher. In the case of BFS50 mix, this led to a protective effect limiting the kinetics when compared to the other mixes. In the case of SF10 mix, the amount of gypsum formed based on the XRD pattern was found to be less when compared to other mixes. This may be due to the delamination of gypsum already formed by the end of exposure period and hence only less degraded layer was present in the SF10 sample prepared for the analysis. On exposure to 3% sulphuric acid, the major reaction product was gypsum (Figure 6.99). As it was formed in greater quantities, other minor peaks were masked by the gypsum peaks. The mixes FA30 and BFS50 showed higher peak intensities of gypsum. The increased amount of gypsum despite the pozzolanic reactions in FA30 and BFS50 indicates that there is decalcification of CSH gel to form additional gypsum.

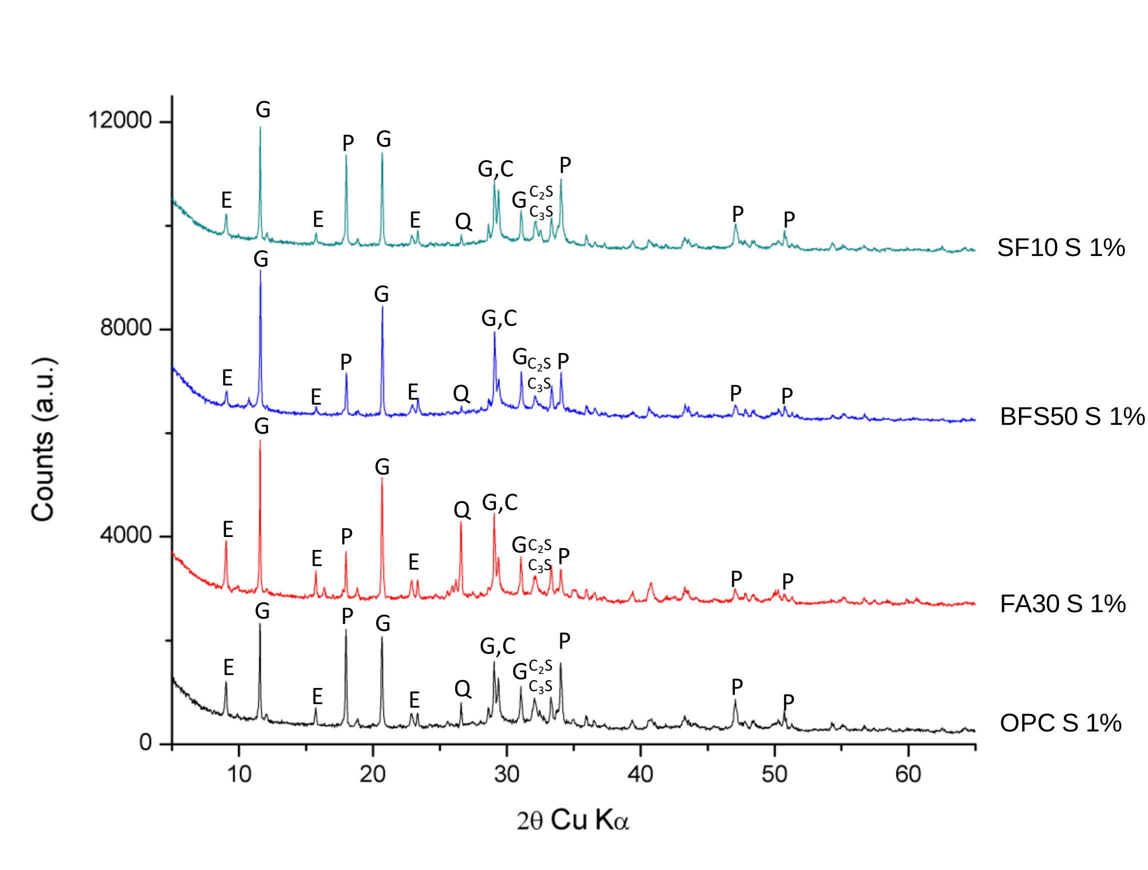

Figure 6.98 X-ray diffractograms of paste on exposure to 1% sulphuric acid

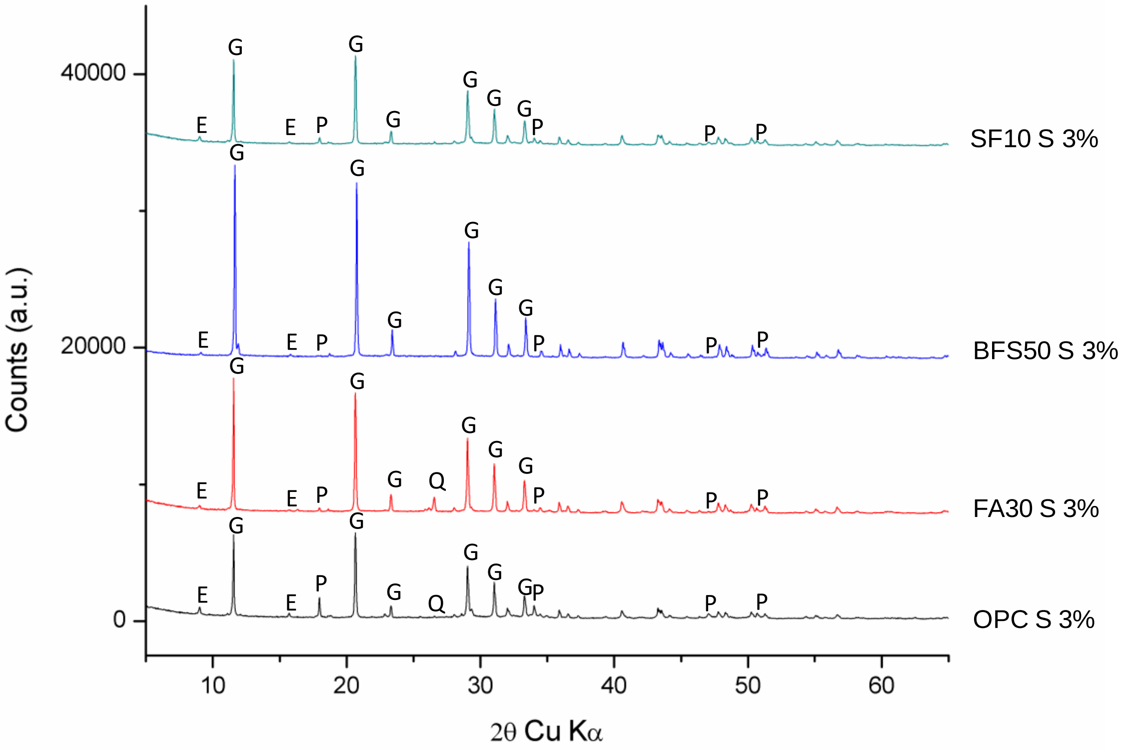

Figure 6.99 X-ray diffractograms of paste on exposure to 3% sulphuric acid

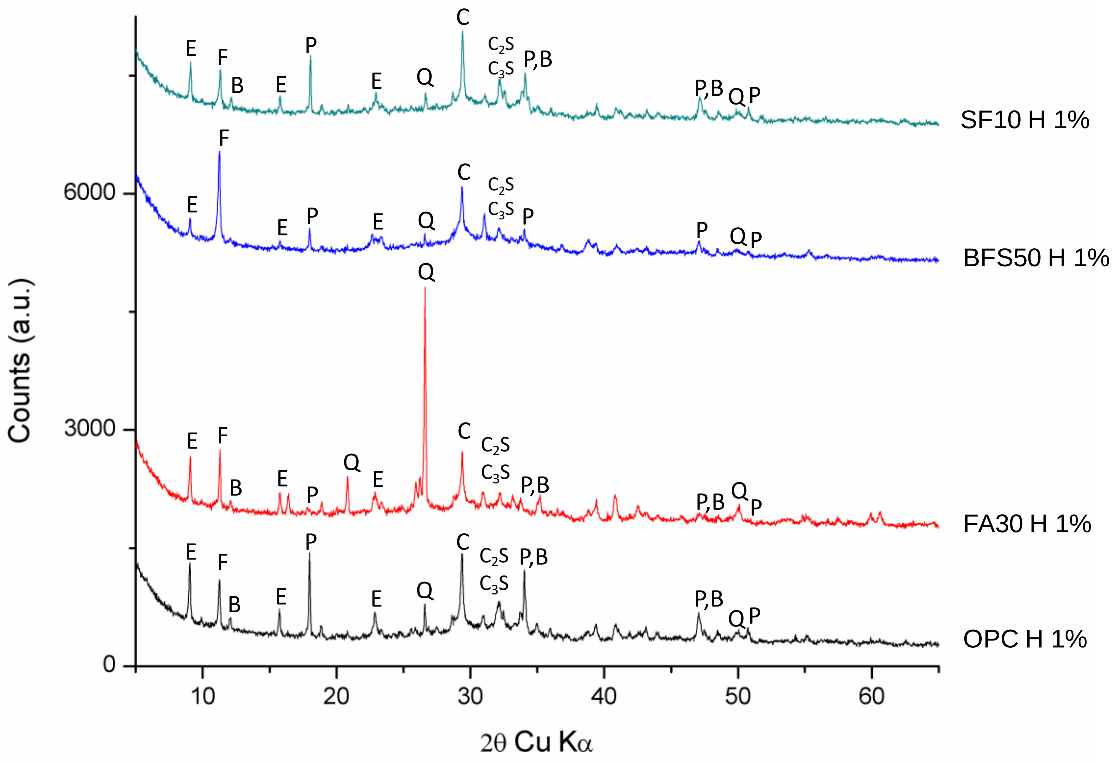

Figure 6.100 X-ray diffractograms of paste on exposure to 1% hydrochloric acid

On exposure to 1% hydrochloric acid (Figure 6.100), the major reaction products formed in all the mixes were amorphous silica gel and Friedel's salt. Figure 6.101 shows the X-ray diffractogram of paste exposed to 0.25M acetic acid. The consumption of Portlandite is evident from the Figure 6.101. All mixes showed reduction in the peak intensity of the crystalline hydrated phases. In the case of FA30, presence of mullite was observed in the sample even after the acid exposure (peaks at 2θ of 16.32°, 25.8° and 32.99°). In the case of higher concentrations of acetic acid (0.5M) as shown in Figure 6.102, only trace quantities of Portlandite were present in OPC and SF10 samples. The ettringite formation was also less in 0.5M acetic acid as it may be less stable at higher concentrations of acid solution.

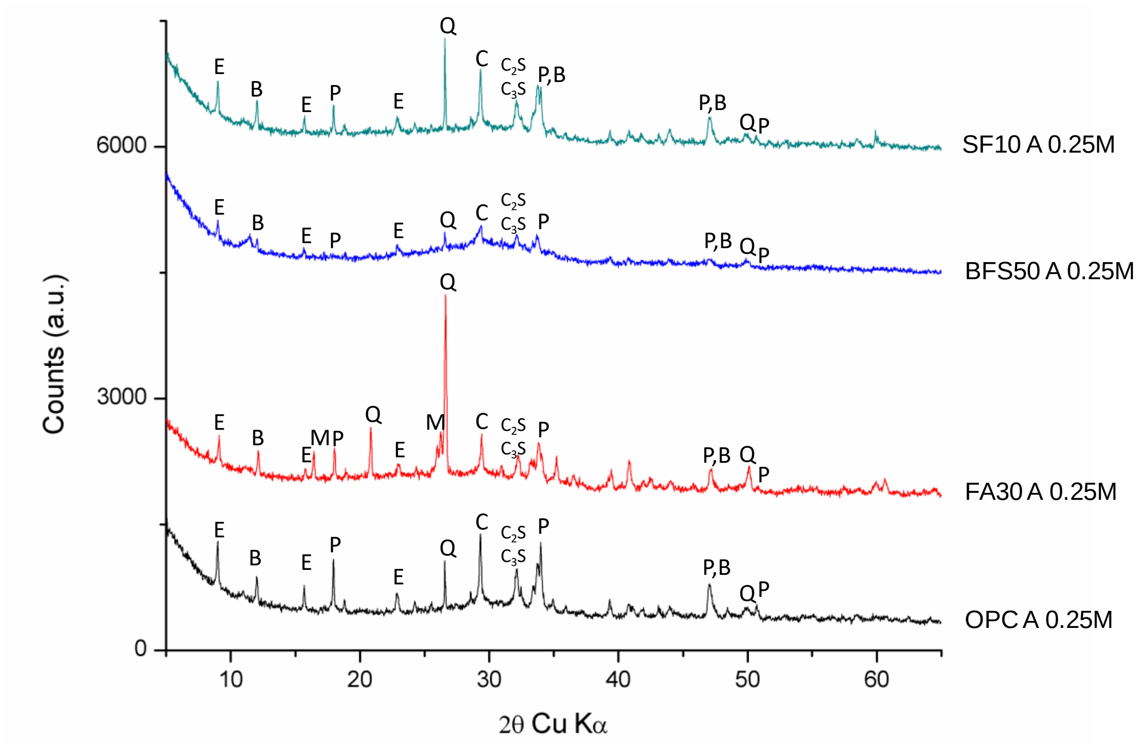

Figure 6.101 X-ray diffractograms of paste exposed to 0.25M acetic acid

In the case of 0.5M citric acid, FA30 and BFS50 showed severe damage as all the hydrated phases were consumed during the attack (Figure 6.103). Only quartz and calcite were present along with the calcium salt in the fly ash paste whereas minor quantities of hydrates were still present in the inner core in the case of slag paste. The conclusions based on the XRD patterns for the fly ash and slag were supported by the mass changes explained earlier. The improved resistance of OPC and SF10 paste against citric acid was evident from the diffractograms as peaks of ettringite, Portlandite, and anhydrous phases were still present in the sample after the acid exposure.

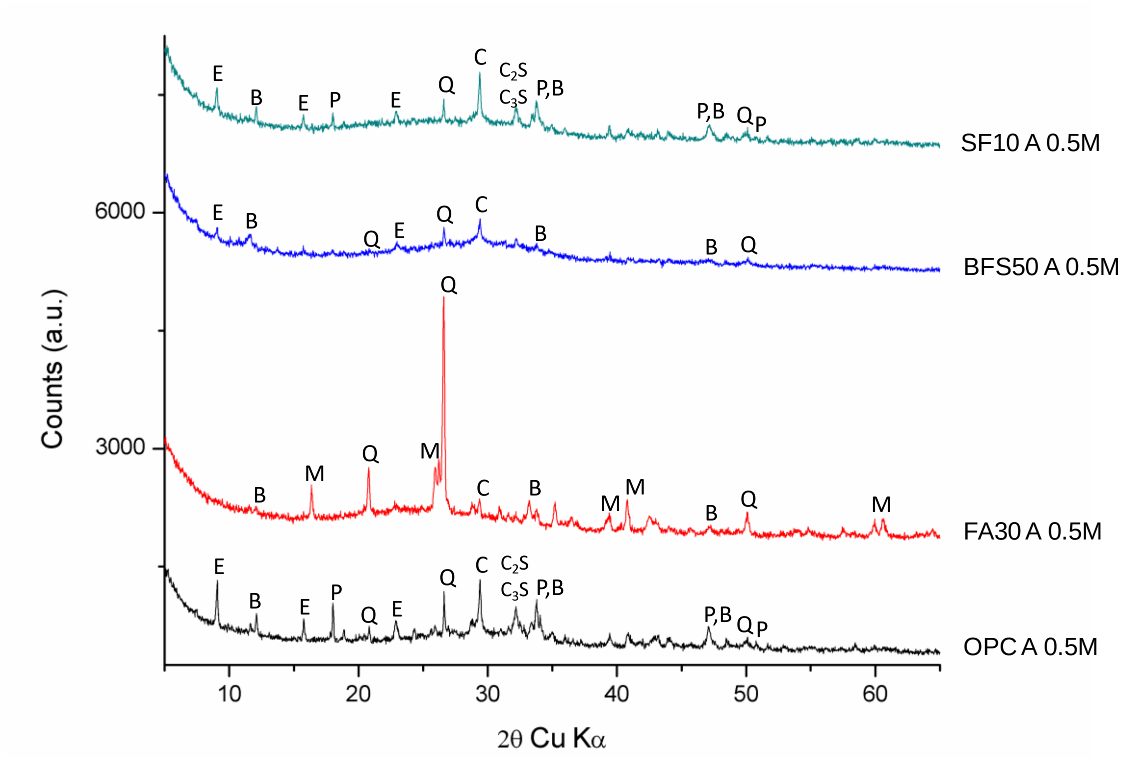

Figure 6.102 X-ray diffractograms of paste exposed to 0.5M acetic acid

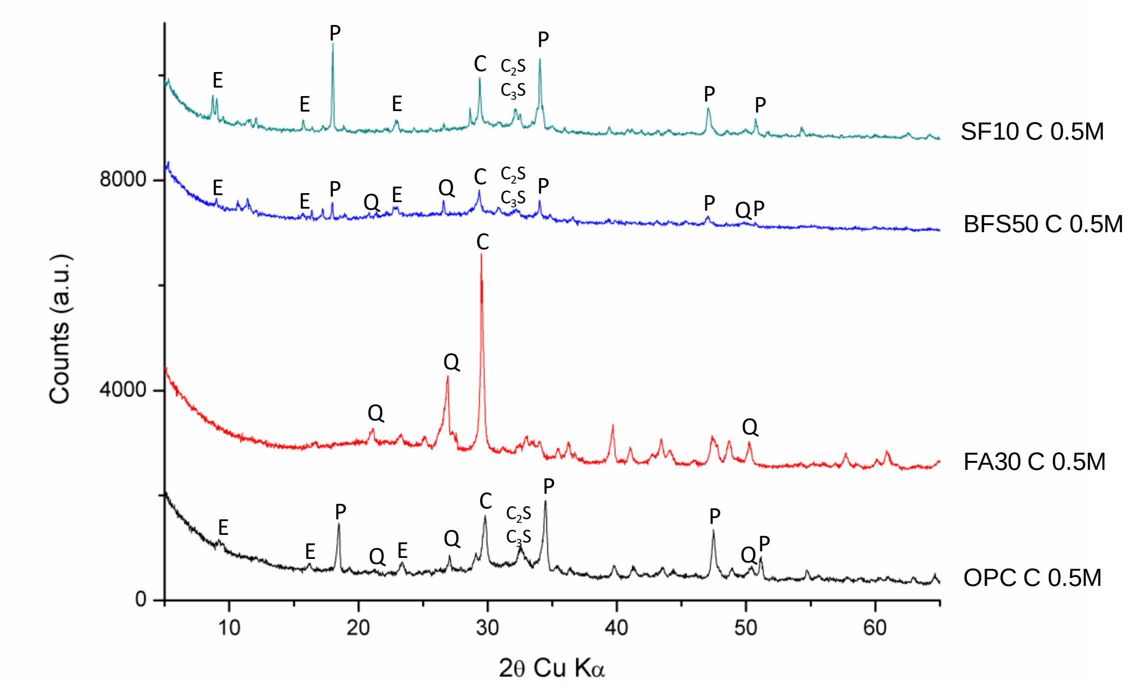

Figure 6.103 X-ray diffractograms of paste exposed to 0.5M citric acid

6.2.6.2 Special binder systems

The mineralogical changes in the LC2 and HAC paste due to acid attack were analysed using X-ray diffractograms. Figure 6.104 shows the X-ray diffractogram of LC2 paste before and after exposure to sulphuric acid. The LC2 paste before the exposure showed hydrated products such as ettringite, monocarboaluminate, Portlandite, calcite and amorphous CSH gel. Other crystalline phases present were quartz, gypsum, C_3S and C_2S. Almost the entire Portlandite was consumed by the LC2 binder for its pozzolanic reaction producing CSH and CASH gel.

On exposure to 1% sulphuric acid, an increase in the peak intensities for ettringite was observed. This indicates that the ettringite formed may be stable in the middle or inner layers which are less affected by the decalcification. Gypsum was formed as the main reaction product owing to the reaction between sulphates of the acid and the calcium bearing hydrates and constituted the outer degraded layer along with silica gel rich in alumina. On exposure to 3% sulphuric acid, a reduction in ettringite peak indicates that it is less stable in very low pH environment. In these conditions, ettringite might have converted to gypsum and aluminium hydroxide on reacting with carbon dioxide. An increase in the peak intensity of gypsum was observed, which could be due to formation of large deposits of gypsum, as the concentration gradient is higher.

Figure 6.105 shows the X-ray diffractogram of LC2 paste before and after exposure to acetic acid. On exposure to 0.25M acetic acid, the LC2 paste showed dissolution of crystalline phases. A reduction in the peak intensities for ettringite and calcite were observed. The amorphous area at 20-30˚ 2θ indicates that the CSH gel is being decalcified to form soluble calcium acetate salt and silica gel. The calcite present in the system is also attacked as it is soluble in acid solution. The quartz peak also was found to increase. On exposure to 0.5M acetic acid, the specimen loses its crystallinity (reduction in peaks of crystalline hydrated phases) due to increased formation of silica gel.

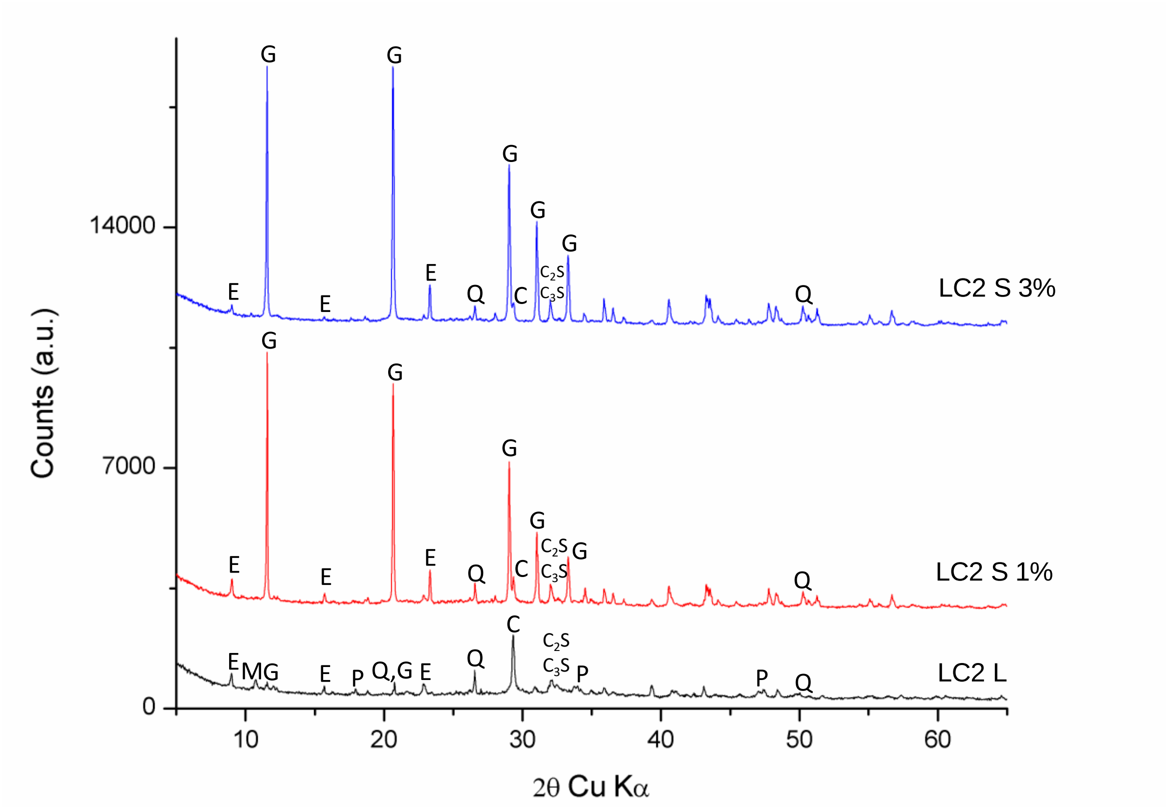

Figure 6.104 X-ray diffractogram of LC2 paste before and after exposure to sulphuric acid

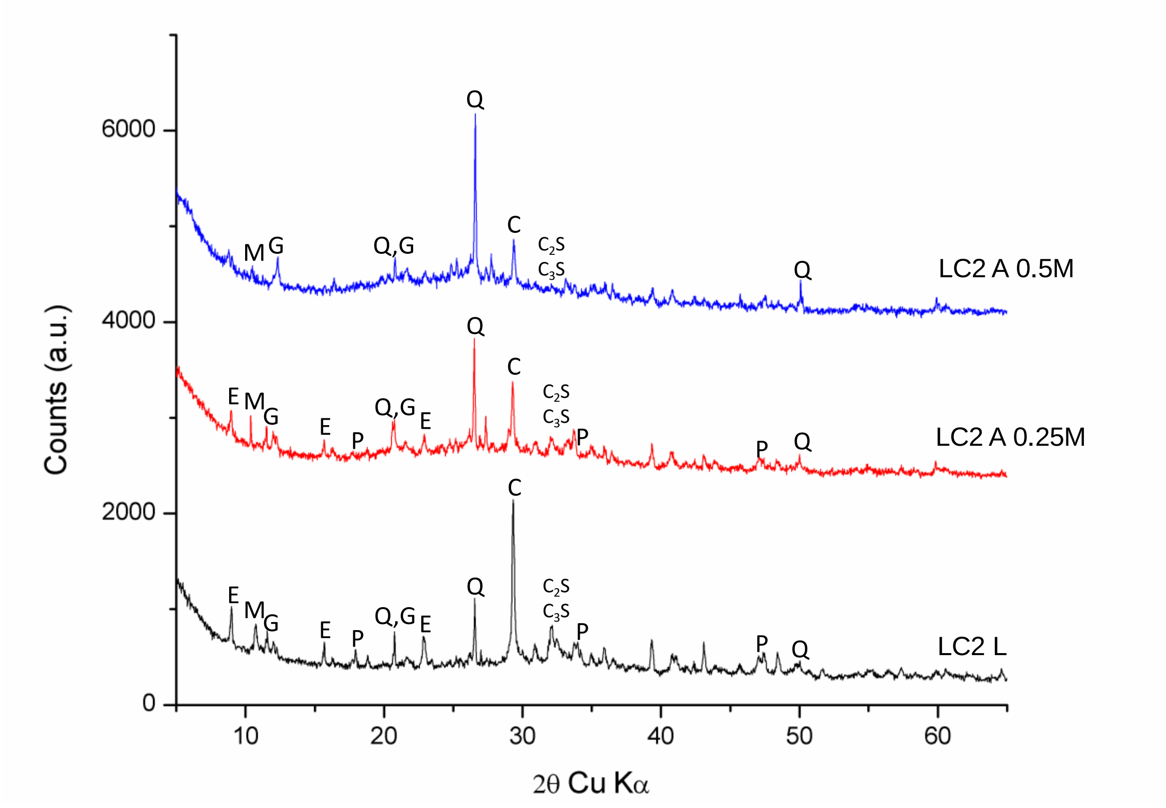

Figure 6.105 X-ray diffractogram of LC2 paste before and after exposure to acetic acid

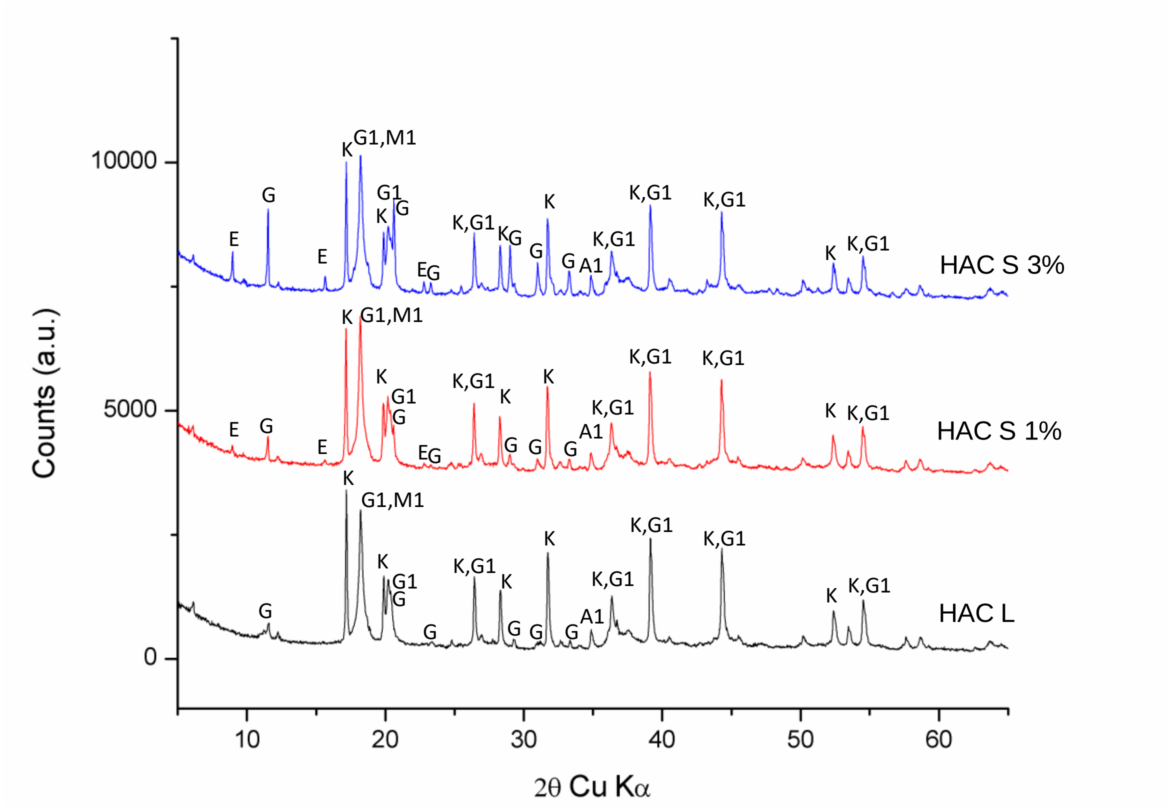

Figure 6.106 X-ray diffractogram of HAC paste before and after exposure to sulphuric acid

The X-ray diffractogram of HAC paste before and after exposure to sulphuric acid is shown in Figure 6.106. The hydrated phases identified in HAC paste (before exposure) include katoite (C_3AH_6, designated as K), gibbsite (AH_3, designated as G1), mayenite ($C_{12}A_7$, designated as M1), calcium mono-aluminate (CA, designated as A1) along with other crystalline phases such as gypsum (G). On exposure to 1% sulphuric acid, the reaction products formed were identified as gypsum, ettringite and amorphous AH_3. Calcium aluminate hydrates (C_3AH_6) react with sulphuric acid to form gypsum/ettringite and AH_3 on the surface of the specimen (Lavigne et al., 2016). Unlike the case of LC2 and other binder systems, silica gel was not formed in attacked HAC paste. Instead, the end product may be amorphous AH_3 on the surface. As the amount of calcium present in the HAC system is limited, gypsum is formed only in less amount compared to calcium dominant binder systems. It is inferred that katoite phase is mainly consumed during the reactions as evident from the reduction in the peak intensity of K (C_3AH_6) observed in the XRD pattern. The dissolution of C_3AH_6 along with the formation of ettringite and gypsum resulted in the deterioration of HAC paste on exposure to 1% sulphuric acid. The diffractogram for 3% sulphuric acid was similar to 1% sulphuric acid except that the peak intensities of gypsum were higher, indicating more formation of gypsum. It can also be noted that there is only a marginal reduction in the peak intensity for C_3AH_6 which suggests that the deterioration is limited to the external surface of the specimen.

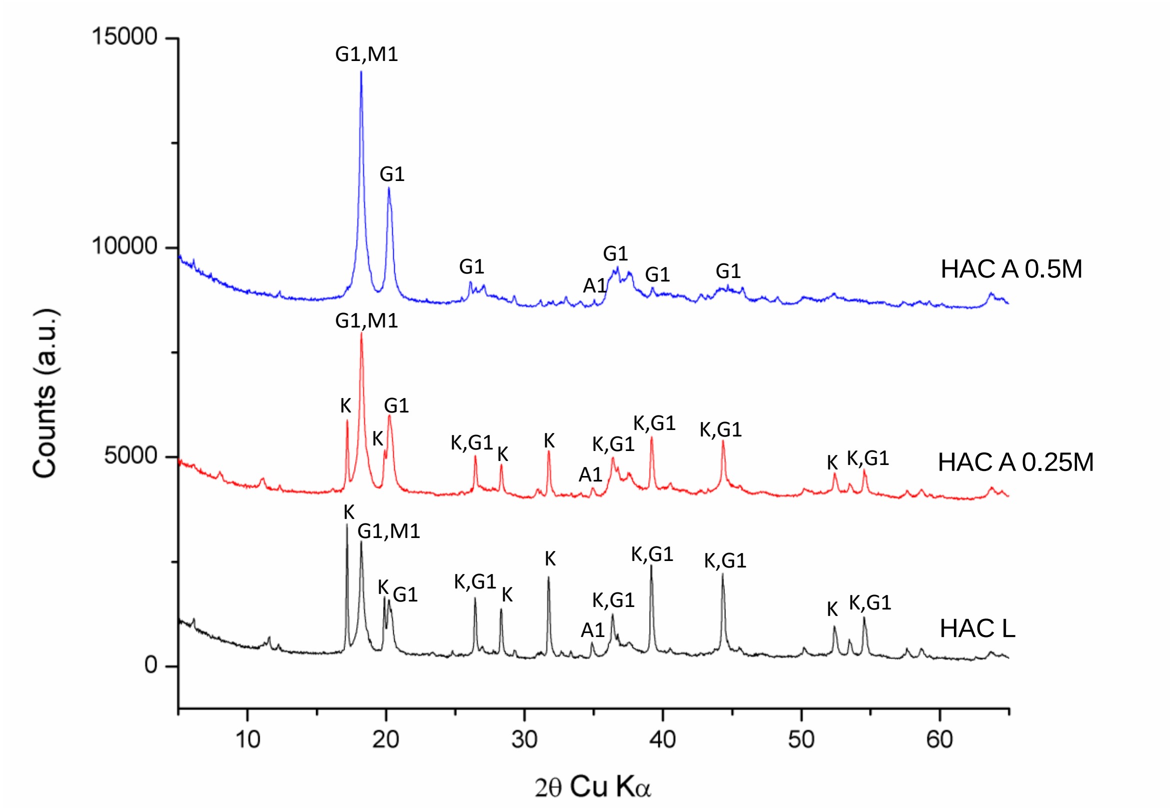

Figure 6.107 X-ray diffractogram of HAC paste before and after exposure to acetic acid

The X-ray diffractogram of HAC paste before and after the exposure to acetic acid is shown in Figure 6.107. A considerable reduction in the peak intensity of C_3AH_6 was observed in the diffractogram of paste exposed to 0.25M acetic acid, which suggests that the dissolution of C_3AH_6 in acid solution has resulted in the formation of silica gel and amorphous AH_3. The salts being soluble leach out into the solution. The diffractogram pattern was similar in the case of 0.5M acetic acid. However, the material loses its crystalline behaviour, which is evident from the Figure 6.107. Thus, the conversion of C_3AH_6 to amorphous AH_3 might have resulted in the increase of porosity and reduction of strength on exposure to acetic acid.

6.3 SUMMARY

The paste attacked by acids was subjected to micro-analytical characterisation tests in order to understand the microstructural changes and to know the basic mechanism of degradation. The deterioration in the microstructure was evident from the CT images and SEM images. The mineralogical changes were studied using XRD. TGA was used to quantify the Portlandite content to estimate its consumption during the attack. MIP was done on paste samples (made with common binders) to evaluate the changes in porosity and pore structure due to the attack. In the case of special binders such as LC2 and HAC, the characterisation of paste was limited to XRD and tomography.

Tomography imaging indicated the mineralogical zonation and further enabled the quantification of altered depth. MIP results revealed increase in capillary porosity due to acid attack, the increase being more in the case of acids that form soluble salts. The reaction products formed were identified using SEM and XRD analysis. TGA results showed reduction in the Portlandite content on acid exposure, especially on exposure to acetic acid.

Laboratory investigations on paste are useful in studying the degradation kinetics and the mechanism of degradation. However, it is important to extend the investigations to mortar in order to study the role of binders and ITZ in acid attack, which are discussed in the next chapter.

CHAPTER 7

INVESTIGATIONS ON MORTAR EXPOSED TO ACIDS

7.1 INTRODUCTION

This chapter deals with the laboratory investigations done on mortar with various binders exposed to two acids that are predominantly encountered by the concrete structures: sulphuric and acetic acid. The first section provides the discussion on the investigation of degradation kinetics by continuous immersion test. The kinetics are explained by means of visual observations, changes in mass and thickness of specimens, changes in pH of the acid solution and altered depth. A brief discussion on the effect of concentration of acid, effect of water to binder ratio of the mix, effect of size and shape of specimens and abrasion on the kinetics is also provided. This is followed by a discussion on changes in the physico-mechanical properties of mortar exposed to acids. The last section details the characterisation techniques employed to understand the alteration mechanism in mortar and the influence of interfacial transition zone. The characterisation techniques used include X-ray tomography, X-ray diffraction, scanning electron microscopy and thermo-gravimetric analysis.

7.2 VISUAL OBSERVATIONS

7.2.1 Common binder systems

The aspect of OPC mortar specimens before and after the acid exposure (for 4 months) without the abrasive action is presented in Figure 7.1. The visual observations were similar to the paste specimens. Mortar specimens exposed to sulphuric acid showed gypsum formation. The aggregates were seen to protrude out in the case of higher concentrations of sulphuric acid. As observed in the paste, less damage was externally visible on the mortar specimens exposed to acetic acid. As the salt formed in sulphuric acid (gypsum) is less soluble and known to have protective effect in limiting degradation kinetics, additional immersion tests were carried out on mortar specimens with periodic abrasive action in the form of brushing to accelerate the kinetics and also in simulating the action of flowing effluents on cement-based materials. The mortars made with SCMs after the acid exposure also appeared similar to OPC mortar, and the visual observations are presented in Appendix C (Figures C-1 to C-3).

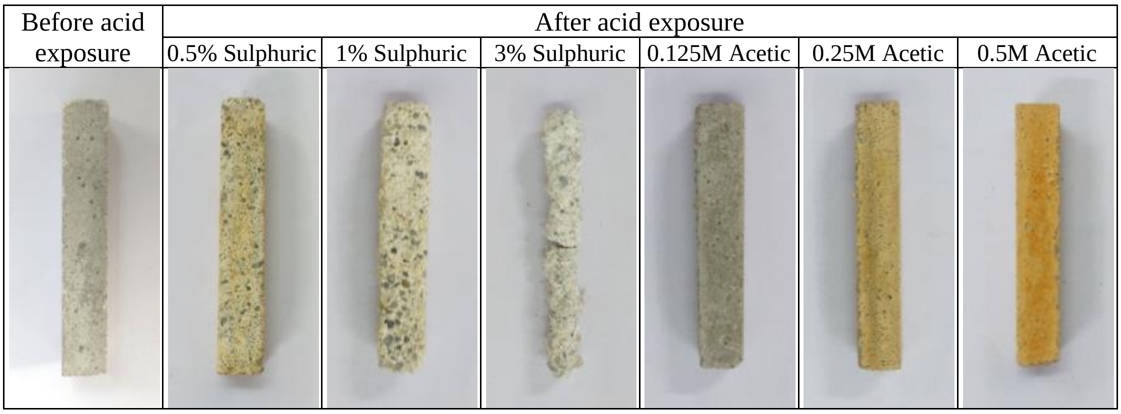

Figure 7.1 OPC mortar (w/b 0.40) specimens before and after acid exposure

7.2.2 Special binder systems

The aspect of LC2 and HAC mortar specimens before and after the acid exposure are shown in Figures 7.2 to 7.4. A white coloured precipitation due to gypsum along with exposed aggregates was observed in the case of LC2 mortar exposed to 1% sulphuric acid. In the case of 3% sulphuric acid, the complete matrix of LC2 mortar got disintegrated within the test period of 4 months and reported as 100% mass loss. On exposure to acetic acid, the LC2 mortar specimens appeared darker in colour owing to the formation of silica gel. The HAC mortar specimens on exposure to 1% and 3% sulphuric acid showed severe deterioration and this manifested in terms of mass loss and reduction in thickness of specimens. The deterioration of HAC mortar was evident also in the case of exposure to acetic acid. The specimen was found to be having loose deposits on its surface and appeared to be porous on exposure.

Before exposure	After acid exposure					
	Without brushing				With brushing	
	1% Sulphuric	3% Sulphuric	0.25M Acetic	0.5M Acetic	1% Sulphuric	3% Sulphuric
		*				*

* 100% mass loss, specimen got disintegrated completely

Figure 7.2 LC2 mortar specimens before and after acid exposure (w/b 0.40)

Before exposure	After acid exposure					
	Without brushing				With brushing	
	1% Sulphuric	3% Sulphuric	0.25M Acetic	0.5M Acetic	1% Sulphuric	3% Sulphuric
						

Figure 7.3 HAC mortar specimens before and after acid exposure (w/b 0.40)

Before exposure	After acid exposure					
	Without brushing				With brushing	
	1% Sulphuric	3% Sulphuric	0.25M Acetic	0.5M Acetic	1% Sulphuric	3% Sulphuric
		*				*

* 100% mass loss, specimen got disintegrated completely

Figure 7.4 LC2 mortar specimens before and after acid exposure (w/b 0.55)

7.3 DEGRADATION KINETICS

7.3.1 Mass changes

7.3.1.1 Common binder systems

The mass changes were calculated based on the initial mass before the acid exposure. Figures 7.5 to 7.7 show the mass changes of mortar mixes after exposure to 0.5%, 1%, 3% sulphuric acid respectively. In order to study the effect of pH of the acid solution, additional immersion test was carried out on mortar specimens exposed to 1% sulphuric acid by raising its pH to 2.0 by adding caustic soda into the acid solution. Figure 7.8 shows the mass changes on exposure to pH2 sulphuric acid. Unlike the paste, the degradation kinetics in mortar was found to be different. All the mixes on exposure to mild and moderate concentrations of sulphuric acid showed early mass gain due to formation of gypsum on the surface of the specimen and showed mass loss at later ages due to the destabilisation of gypsum caused by prolonged exposure in acid solution.

At higher concentrations of sulphuric acid (3%), all the mixes showed mass loss due to severe expansive pressure exerted by the gypsum, which is formed in substantial quantities at early ages itself (Figure 7.7). It was found that abrasion accelerated the kinetics for specimens exposed to 0.5% and 1% sulphuric acid while the effect was minimal on exposure to 3% sulphuric acid. It was found that the SCM mixes performed better on exposure to lower concentrations of sulphuric acid, with SF10 mix outperforming the other mixes. This was totally different from the paste study. In the paste study, severe delamination of gypsum layer was noted in SF10 paste leading to more mass loss but in mortar, the lower mass loss may be attributed to the improved pozzolanic reaction between de-densified silica fume particles and the free lime present in the cementitious system and the subsequent densification of the ITZ. In the case of higher concentrations of sulphuric acid, the performance of SCM mixes was found to be ordinary and the difference between the mixes was minimal, the performance of FA30 being the worst, showing complete disintegration of specimen on acid exposure. Torii and Kawamura (1994) also found that the SCM mortar incorporating fly ash and silica fume performed poorly on exposure to high concentration of sulphuric acid. In the case of pH2, the deterioration observed was very limited and all the mixes except OPC incurred minor mass loss (within 1.5%) and the difference was too small to be comparable across the mixes (Figure 7.8). The effect of concentration of sulphuric acid on the degradation kinetics of OPC mortar (w/b 0.40) is shown in Figure 7.9. It can be noted that the kinetics to a large extent depends on the concentration of sulphuric acid.

The water to binder ratio (w/b) of the mix is one of the parameters that could alter the kinetics, and hence tests were done at a w/b of 0.55 also. The mass changes are presented in Figures 7.10 to 7.13. The trends in the mass changes were similar to the results obtained for a w/b of 0.40. However, the mass changes of mortar for a higher w/b of 0.55 were found to be less when compared to 0.40 on exposure to sulphuric acid. This aspect will be explained later in the section discussing the effect of w/b. Similar to mortar of w/b 0.40, the SCM mixes showed better resistance with respect to mass changes on exposure to 1% sulphuric acid and their performance was found to be ordinary at higher concentration (3%) of sulphuric acid. The effect of concentration of sulphuric acid on the degradation kinetics of OPC mortar (w/b 0.55) is shown in Figure 7.13.

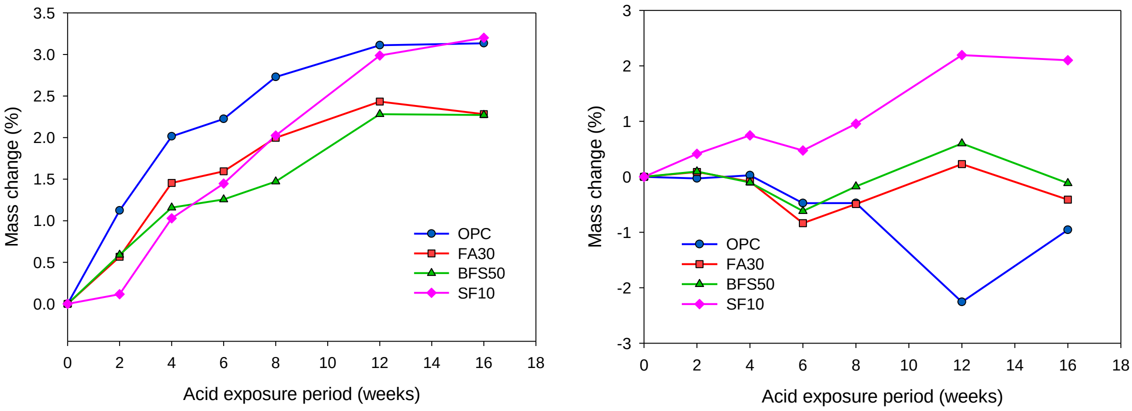

a) without brushing b) with brushing

Figure 7.5 Mass changes of mortars exposed to 0.5% sulphuric acid (w/b 0.40)

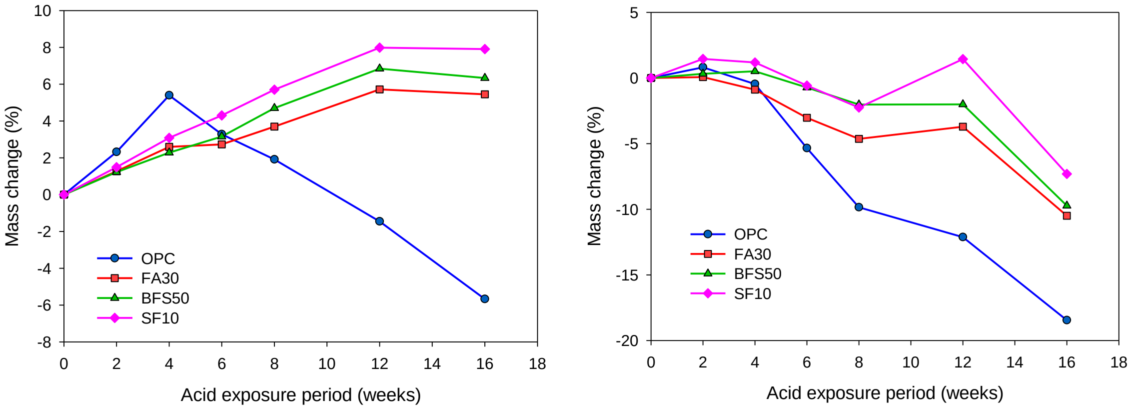

a) without brushing b) with brushing

Figure 7.6 Mass changes of mortars exposed to 1% sulphuric acid (w/b 0.40)

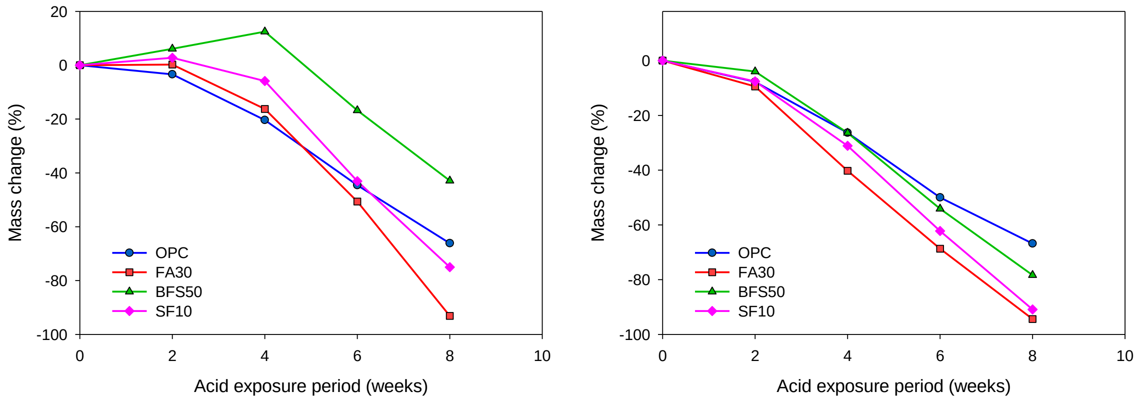

a) without brushing b) with brushing

Figure 7.7 Mass changes of mortars exposed to 3% sulphuric acid (w/b 0.40)

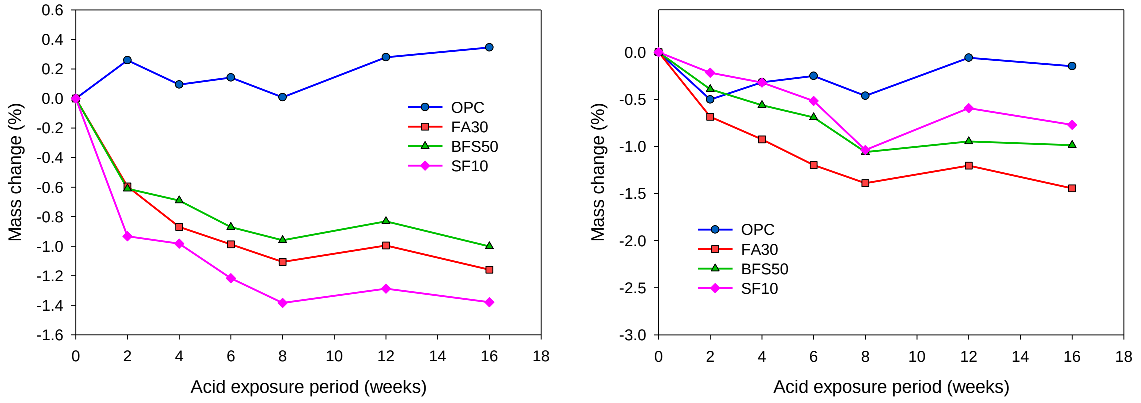

a) without brushing b) with brushing

Figure 7.8 Mass changes of mortars exposed to pH2 sulphuric acid (w/b 0.40)

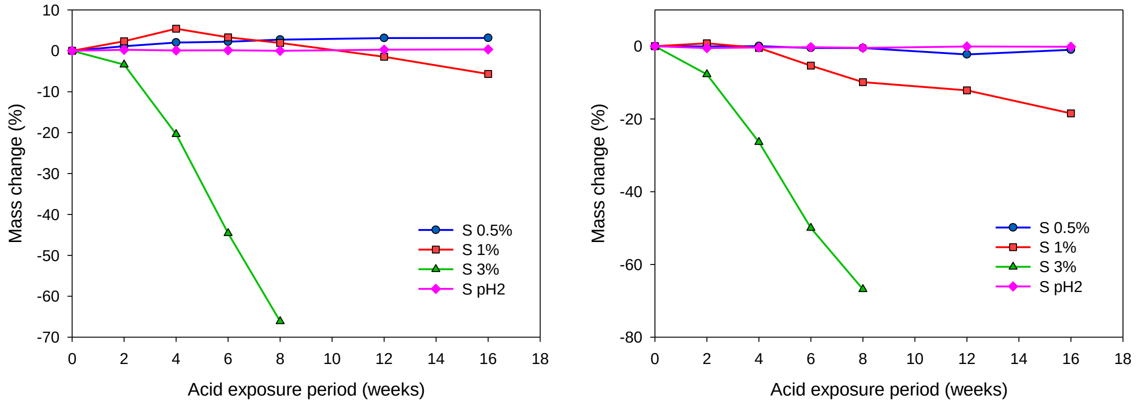

a) without brushing b) with brushing

Figure 7.9 Mass changes of OPC mortar exposed to sulphuric acid (w/b 0.40)

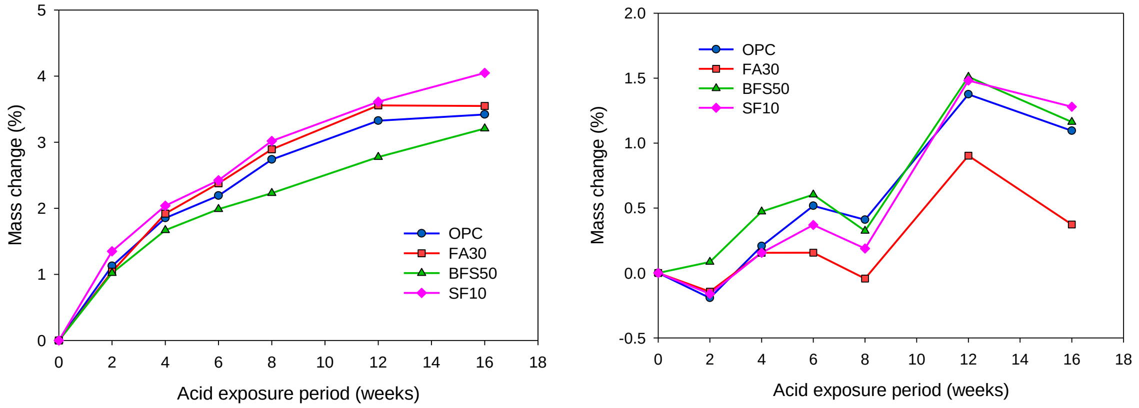

a) without brushing b) with brushing

Figure 7.10 Mass changes of mortars exposed to 0.5% sulphuric acid (w/b 0.55)

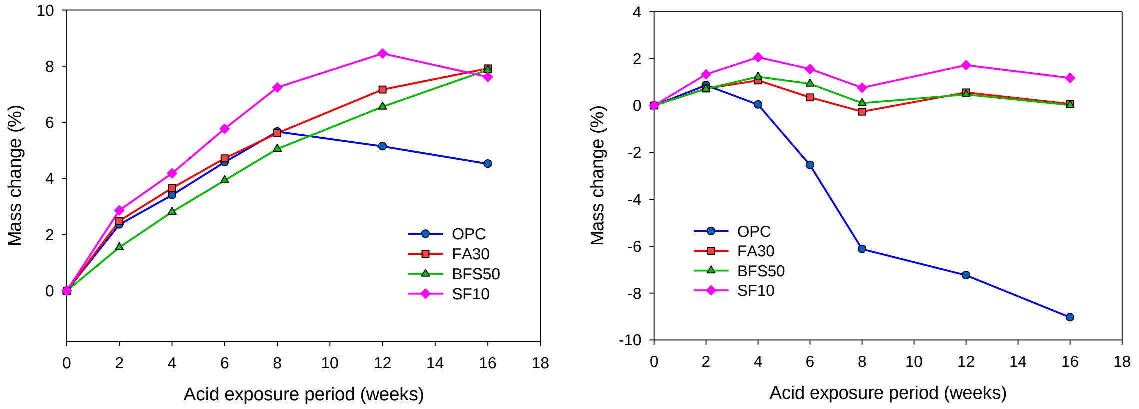

a) without brushing b) with brushing

Figure 7.11 Mass changes of mortars exposed to 1% sulphuric acid (w/b 0.55)

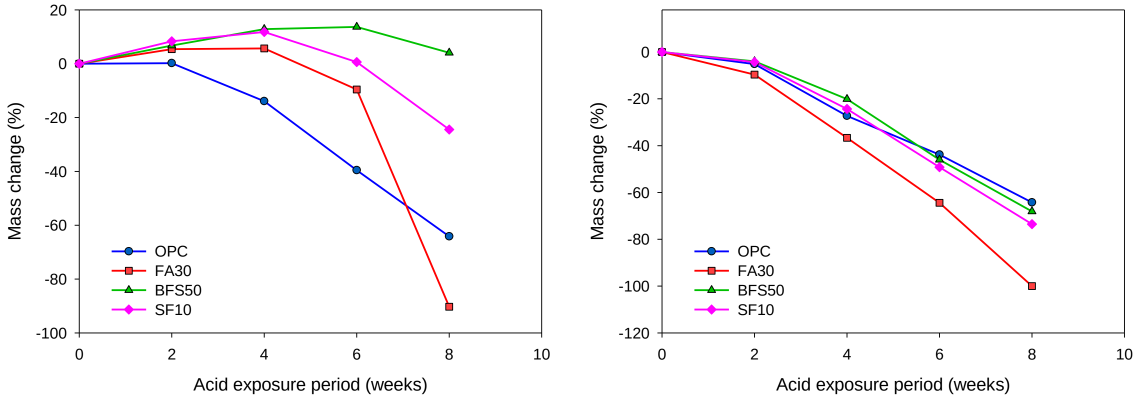

a) without brushing b) with brushing

Figure 7.12 Mass changes of mortars exposed to 3% sulphuric acid (w/b 0.55)

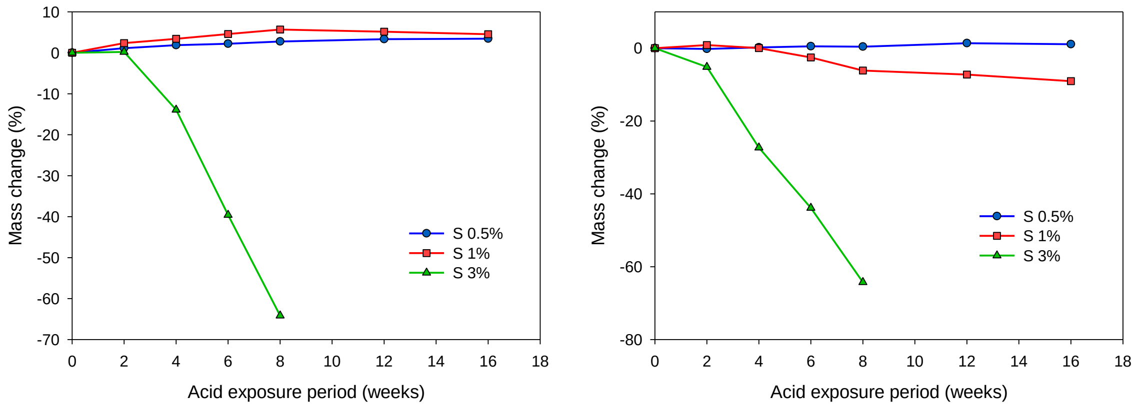

a) without brushing b) with brushing

Figure 7.13 Mass changes of OPC mortar exposed to sulphuric acid (w/b 0.55)

The mortar specimens (w/b 0.40) exposed to acetic acid showed mass loss due to leaching of soluble salts and these mass changes are shown in Figures 7.14 to 7.18. It is seen earlier in the paste studies that that the effect of abrasion in accelerating the kinetics is minimal, as the salts do not precipitate on the surface, to be removed by abrasion. Hence, the exposure to acetic acid is done only without the abrasion. On exposure to lower concentration of acetic acid (0.125M), the BFS50 mix performed better followed by SF10 and OPC for a water to binder ratio of 0.40. However in the case of mortar at a water to binder ratio of 0.55, the mass change curves for the mixes were close, and could not be compared. Similar results were observed for 0.25M acetic acid. In the case of 0.5M acetic acid, the trends were similar for both water to binder ratios of 0.40 and 0.55. The mass losses for FA30 and BFS50 were less when compared to OPC and SF10. Also, the variation in the mass loss was found to be almost linear when the acid was replenished at regular equal intervals. Moreover, the mass changes were found to be directly proportional to the concentration of acetic acid.

In order to investigate the effect of pH of the solution, additional mortar specimens were exposed to 0.25M acetic acid, the pH of which was elevated to 4.00 by adding caustic soda to the acid solution, and the corresponding mass changes are shown in Figure 7.17. However, no specific conclusions could be made as the mass losses of the mixes were very close to each other. This has implications on the development of test methods for acid attack studies. If the tests are done at lower concentrations of acids, the results may not be distinguishable and it is better to conduct accelerated testing by exposing the specimen to higher concentrations of acids so as to explore the potential of various binder systems.

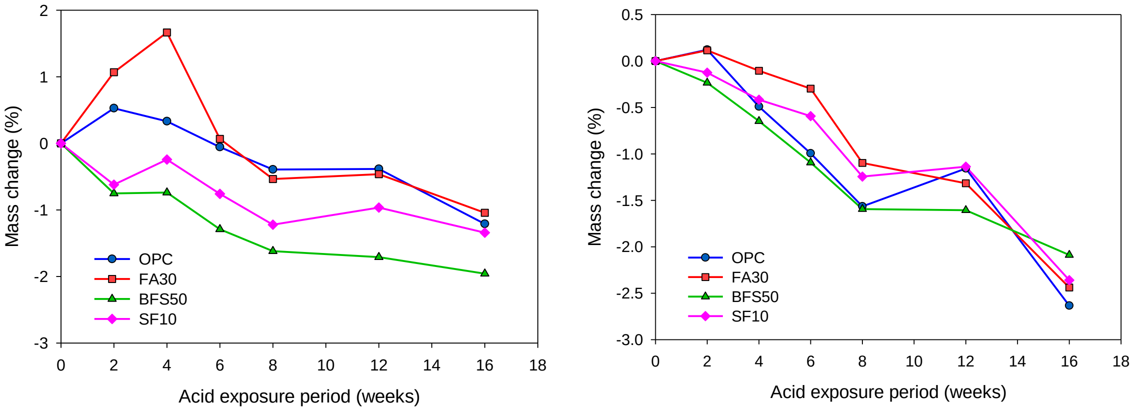

a) w/b 0.40 b) w/b 0.55

Figure 7.14 Mass changes of mortars exposed to 0.125M acetic acid

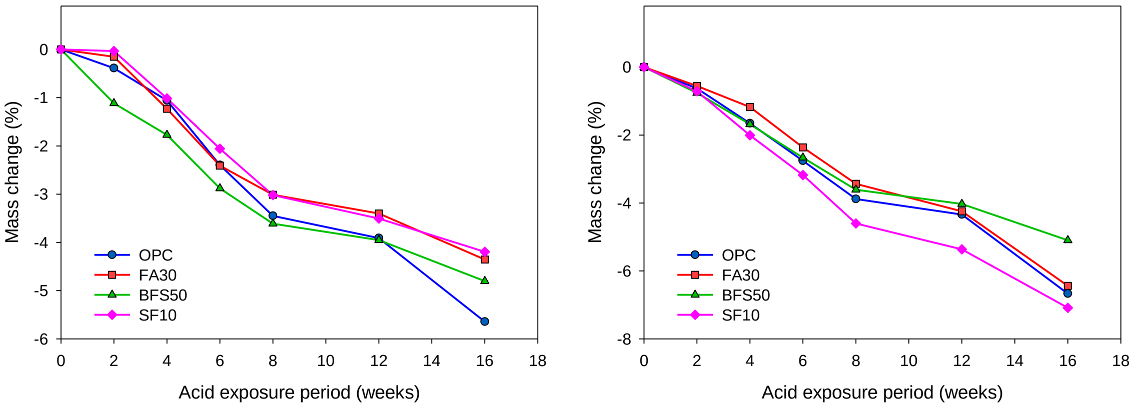

a) w/b 0.40 b) w/b 0.55

Figure 7.15 Mass changes of mortars exposed to 0.25M acetic acid

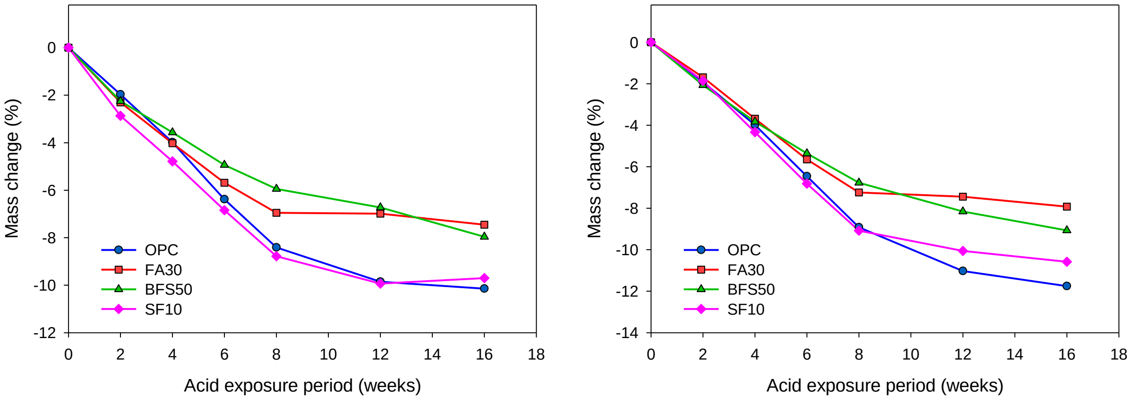

a) w/b 0.40 b) w/b 0.55

Figure 7.16 Mass changes of mortars exposed to 0.50M acetic acid

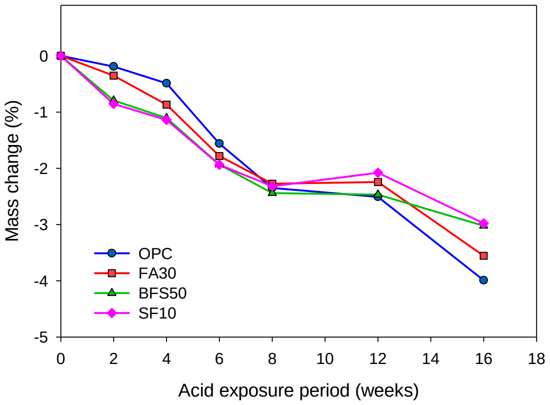

Figure 7.17 Mass changes of mortars (w/b 0.40) exposed to pH4 acetic acid

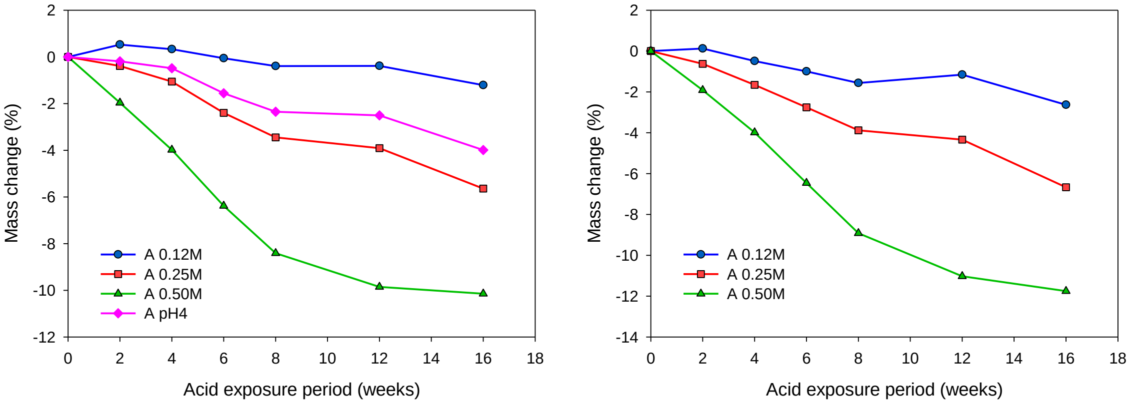

a) w/b 0.40

b) w/b 0.55

Figure 7.18 Mass changes of OPC mortar exposed to acetic acid

7.3.1.2 Effect of influencing factors on degradation kinetics

The degradation kinetics due to acid attack could be affected by a variety of factors such as concentration of acid, water to binder ratio of the mix, use of abrasion in the test method, the size of the specimens, pH of the acid solution etc. It can be seen that there is a tremendous increase in the mass changes on increasing the concentration of sulphuric acid from 1% to 3% (Figure 7.13). Also, contrary to the expectations, the mix with higher water to binder ratio was found to have less mass loss when exposed to 1% sulphuric acid (for both the tests with and without brushing) and the effect of w/b ratio is shown in Figure 7.19. This behaviour can be explained based on the porosity of the paste phase. In the case of lower w/b of 0.40, the paste might be less porous and the matrix experiences greater expansive pressure due to the formation of expansive gypsum. As the space available is limited, gypsum offers higher pressure creating cracks and this result in higher mass loss. But mortar made with higher water to binder ratio may be porous so as to accommodate the expansion offered owing to the formation of gypsum. The better performance of mortar with higher water to binder ratio was even evident marginally at higher concentration of 3% sulphuric acid. These observations were found to be consistent with the results reported by Amin and Bassuoni (2018) and Hewayde et al. (2017). The abrasive action also accelerated the kinetics at lower concentrations of sulphuric acid (for both water to binder ratios of 0.40 and 0.55) (Figure 7.20). This could be due to the removal of gypsum layer attached to the matrix. However, the effect was found to be minimal at 3% sulphuric acid as the gypsum layer, being unstable at very low pH, delaminates itself from the matrix.

Unlike sulphuric acid, the use of lower water to binder ratio resulted in the improved performance (lower mass loss) on exposure to acetic acid for both 0.25M and 0.50M acetic acid (Figure 7.21). This may be attributed to the reduced permeability of the paste at low w/b, which further reduces the ingress of acid by diffusion. Also, as the salts are soluble in the case of acetic acid, they do not exert crystallization pressure when the porosity is less. These observations have important implications on the design of concrete mixes, as similar behaviour is expected in the concrete although the kinetics could be different owing to the size effects. Thus, in order to understand the effect of size of specimen (i.e. effect of surface area to volume ratio of specimen), additional tests were carried out on mortar specimens of size 25 × 25 × 35 mm. The size was selected so as to have one half the surface area to volume ratio when compared to the specimens earlier tested (of size 10 × 10 × 60 mm).

The mass changes and pH of these 25 × 25 × 35 mm prisms made with various binders on exposure to various concentrations of sulphuric and acetic acid are provided in Appendix C (Figures C-9 to C-12, C-14 to C-20, C-22 to C-24). In general, the trends were similar to the smaller size specimens. The improved performance of SF10 mix at lower concentrations, and of BFS50 and FA30 specimens at higher concentrations of sulphuric acid were observed in 25 × 25 × 35 mm specimens also. The superior performance of BFS50 on exposure to higher concentrations of acetic acid was also evident. Figure 7.22 depicts the effect of surface area to volume ratio on leaching kinetics. The effect of size was found to be minimum in the case of sulphuric acid. However, the size effect was significant on exposure to acetic acid; smaller sized specimens with higher surface area to volume ratio had higher mass loss when compared to specimens with less surface area to volume ratio (Figure 7.23). The effect of shape of specimen was also explored in the case of exposure to 3% sulphuric acid (Figure 7.24). The alteration kinetics was studied on mortar cylinders of size 25 mm diameter and 35 mm height. The size was selected so as to have almost same surface area to volume ratio to that of 25 × 25 × 35 mm prisms. Specimens with edges (25 × 25 × 35 mm) showed more mass change and deterioration when compared to cylindrical mortar specimens. This increased deterioration on prismatic specimens could be due to penetration of acids from two directions near to the edges resulting in more deterioration near to the edges. The effect of initial pH of the acid solution also influenced the alteration kinetics. The deterioration was significantly higher on exposure to 1% sulphuric acid (with initial pH 0.99) when compared to exposure to pH2 sulphuric acid (Figure 7.25). In the case of pH2 sulphuric acid, deposits of sodium sulphate salt were noted on the specimen surface (due to the reaction between sulphuric acid and sodium hydroxide). Increased mass loss was also observed on exposure to 0.25M acetic acid (with initial pH 2.68) when compared to pH4 acetic acid (Figure 7.26).

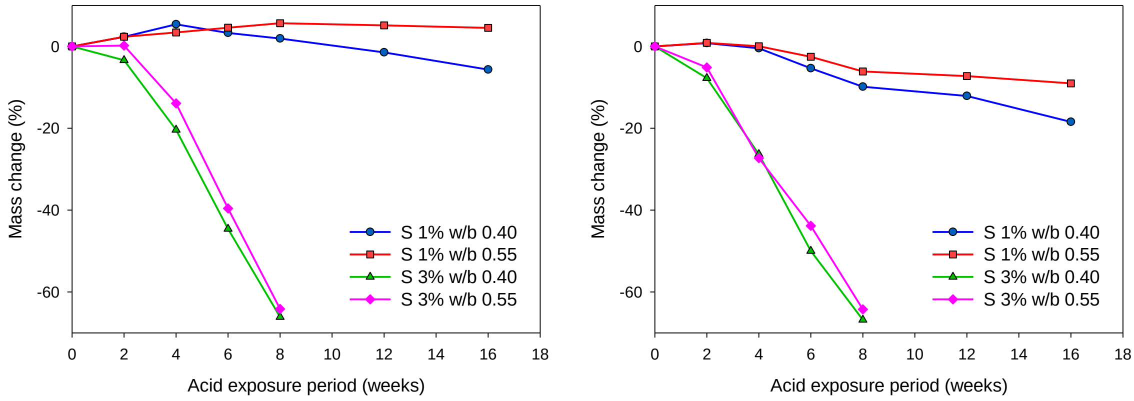

a) without brushing b) with brushing

Figure 7.19 Effect of water to binder ratio on mass changes of OPC mortar exposed to sulphuric acid

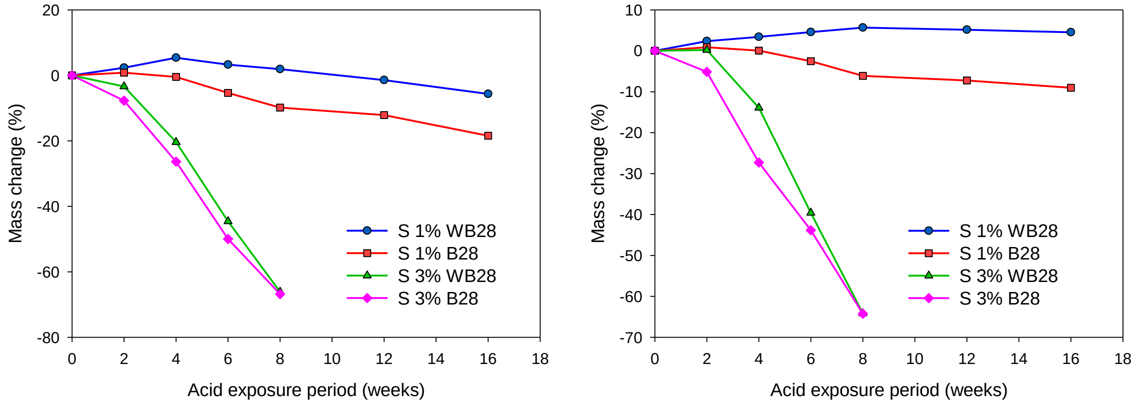

a) w/b 0.40 b) w/b 0.55

Figure 7.20 Effect of abrasion on mass changes of OPC mortar exposed to sulphuric acid

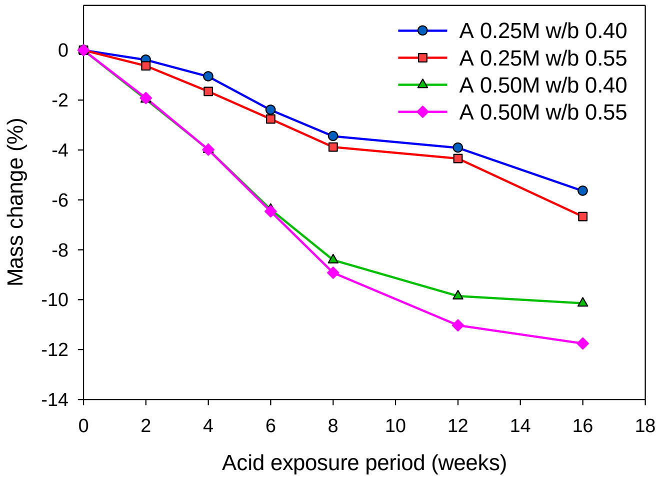

Figure 7.21 Effect of water to binder ratio on mass changes of OPC mortar exposed to acetic acid

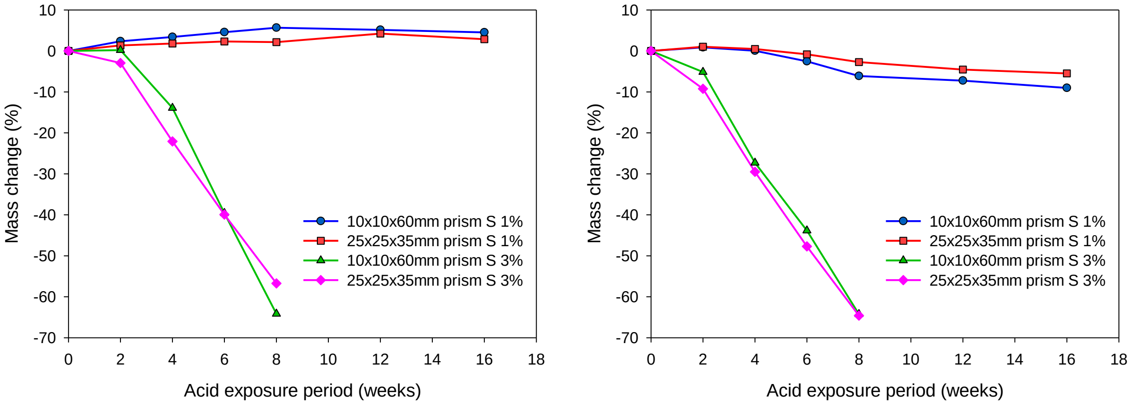

a) without brushing

b) with brushing

Figure 7.22 Effect of size of the specimen on mass changes of OPC mortar exposed to sulphuric acid (w/b 0.55)

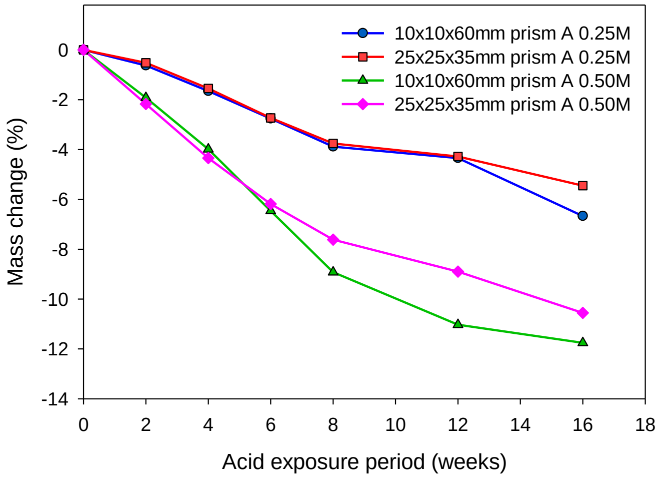

Figure 7.23 Effect of size of the specimen on mass changes of OPC mortar exposed to acetic acid (w/b 0.55)

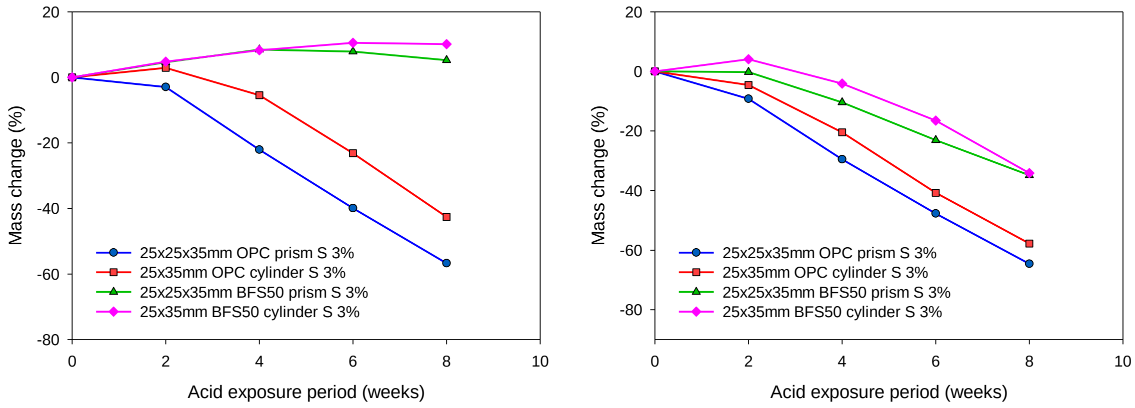

a) without brushing b) with brushing

Figure 7.24 Effect of shape of the specimen on mass changes of mortar exposed to sulphuric acid (w/b 0.55)

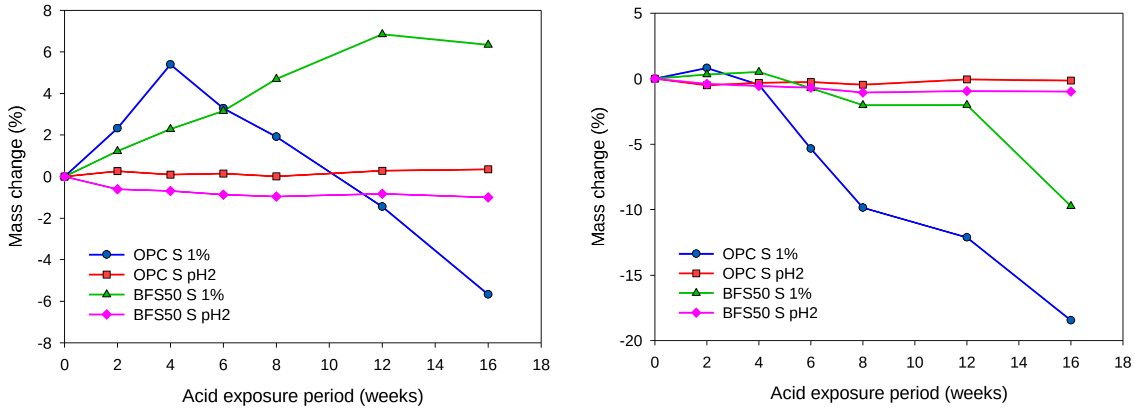

a) without brushing b) with brushing

Figure 7.25 Effect of pH on the mass changes of mortar exposed to sulphuric acid (w/b 0.40)

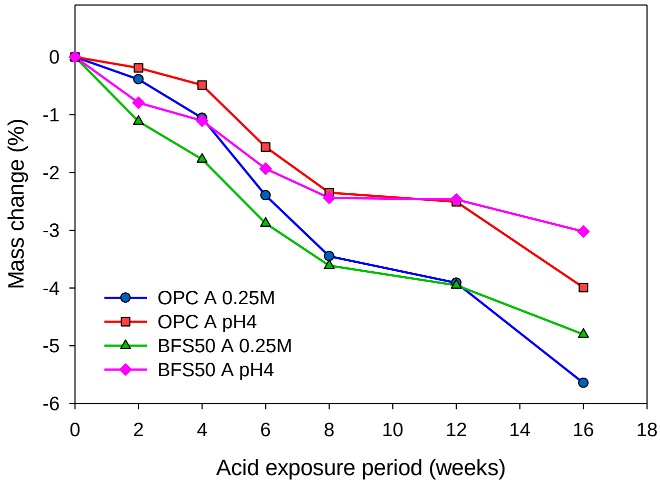

Figure 7.26 Effect of pH on the mass changes of mortar exposed to acetic acid (w/b 0.40)

7.3.1.3 Special binder systems

The mass changes of LC2 and HAC mortar on exposure to 1% sulphuric acid were compared to the OPC mortar and the results are shown in Figure 7.27. It is found that the mortar testing gave accelerated results compared to the paste. The potential of LC2 binder was evident in mortar as the mass losses for both w/b ratios (0.40 and 0.55) were less when compared to OPC and HAC mortar. The HAC mortar suffered severe degradation as the mass loss was found to be the higher. This indicates that the ITZ of HAC mortar is highly affected due to the attack. The higher mass loss could also be attributed to the possible conversion reaction of its metastable hydrated products to C_3AH_6 and AH_3 thereby increasing the porosity and reducing the strength.

Similar to the observations made in the case of common binders, the use of higher w/b ratio for LC2 mortar resulted in lower mass loss when compared to a lower w/b ratio of 0.40. This reconfirms the fact that strong mixture formulations made with very low w/b ratios may not be always durable in sulphuric acid environments. Instead, it is better to adopt a mix with a marginally higher w/b ratio so as to minimise the damage due to expansive stresses exerted by gypsum. However, the performance of LC2 mortar was found to be the worst on exposure to 3% sulphuric acid (Figure 7.28). As explained earlier in the section on paste study, this higher damage could be due to the excessive pressure exerted by the gypsum resulting in severe cracking and damage. Also, the limited availability of Portlandite in the system leads to a direct attack on CSH gel, thus affecting the integrity of the specimen. In such situations, the performance of HAC and OPC mortar was found to better when compared to LC2 mortar. The trends in the mass loss for 3% were found to be similar for tests with and without brushing.

The beneficial action of LC2 binder was noted on exposure to acetic acid (similar to slag mortar). On exposure to 0.25M and 0.5M acetic acid, the LC2 mortar with a w/b 0.40 had the least mass loss when compared to the other mixes including LC2 mortar with w/b 0.55 (Figure 7.29). The improved performance of LC2 mortar with respect to mass changes on exposure to acetic acid may be attributed to early age pore refinement, lower Portlandite content, and less permeability seen in limestone calcined clay systems (Dhandapani et al., 2018). At high concentration of acetic acid (0.5M), the HAC mortar performed the worst. The mass loss was higher and the specimen broke into many pieces along the length of the specimens indicating the extent of deterioration. The effect of concentration of sulphuric and acetic acid on the mass changes of LC2 and HAC mortar for a w/b of 0.40 is summarised in Figure 7.30. It can be inferred that the special mortars like LC2 mortar and HAC mortar are effective only at moderate concentrations of acids such as 1% sulphuric and 0.25M acetic acid. The performance of LC2 mortar was found to be ordinary on exposure to high concentrations of acid. Similarly, HAC mortar showed better performance only at lower concentrations of sulphuric and acetic acid only and has to be used with a note of caution as there is a possibility that conversion reaction of its metastable hydrates could result in poor microstructure and less durability.

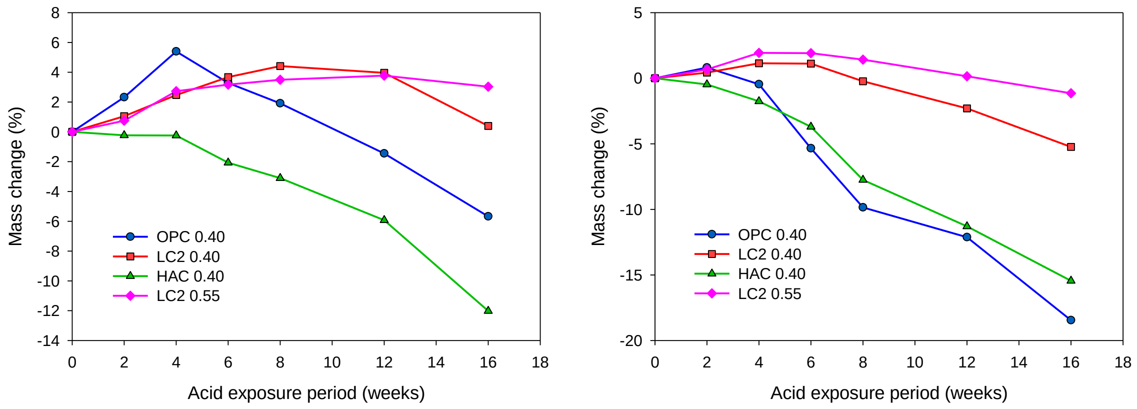

a) without brushing b) with brushing

Figure 7.27 Mass changes of LC2 and HAC mortar on exposure to 1% sulphuric acid

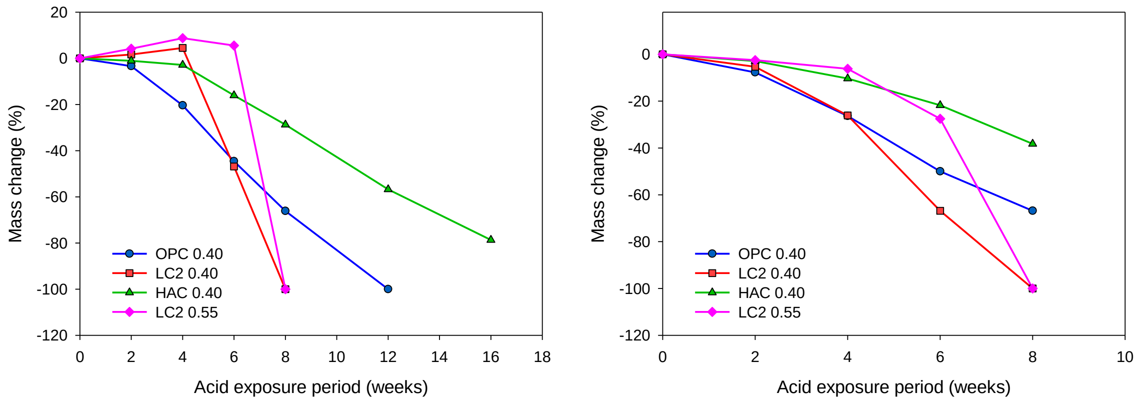

a) without brushing b) with brushing

Figure 7.28 Mass changes of LC2 and HAC mortar on exposure to 3% sulphuric acid

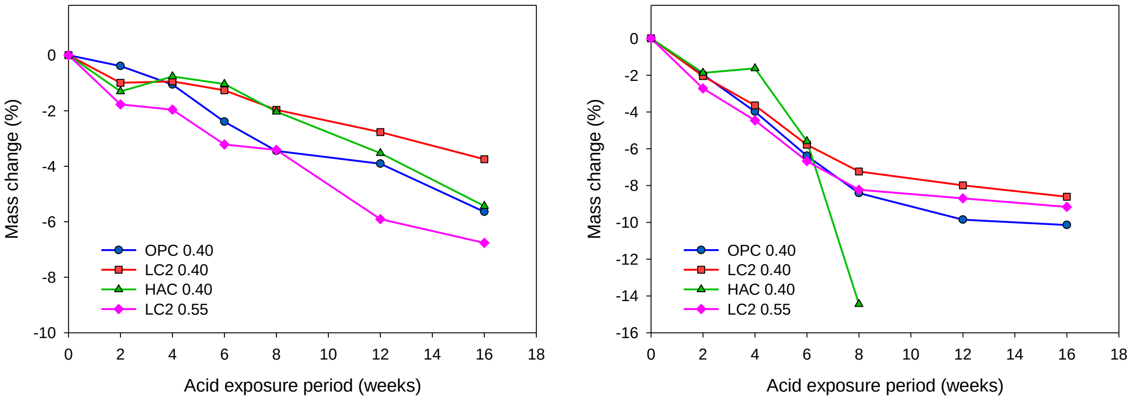

a) 0.25M acetic acid b) 0.5M acetic acid

Figure 7.29 Mass changes of LC2 and HAC mortar on exposure to 0.25M and 0.5M acetic acid

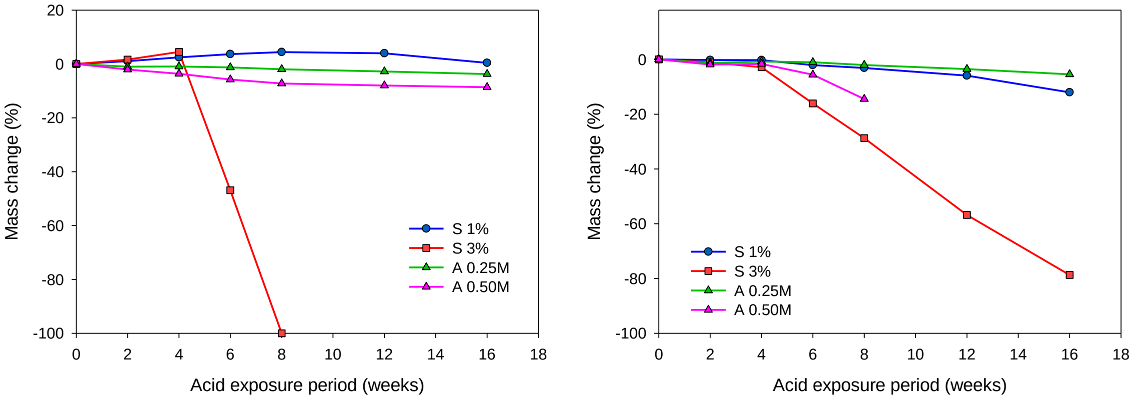

a) LC2 b) HAC

Figure 7.30 Effect of concentration of acid on mass changes of LC2 and HAC mortar on exposure to sulphuric and acetic acid (w/b 0.40)

7.3.2 Changes in pH of the acid solution

7.3.2.1 Common binder systems

The change in pH of the acid solution is indicative of the chemical alterations of the cementitious matrix. Figures 7.31 to 7.34 show the pH rise of the acid solution measured on exposure to sulphuric acid (mortar with w/b 0.40). In general, on exposure to sulphuric acid, there is a decline in the pH of acid solution with age of exposure, which indicates that the reaction rate decreases with age of exposure. A marginal increase in pH observed after 8th week on exposure to 1% sulphuric acid could be due to increase in the time period between successive acid replenishments.

In the case of 0.5% sulphuric acid, it is observed that the pH rise in SCMs containing alumina is the least (FA30 and BFS50). The average pH of the acid solution is above 3 and this could imply that aluminate hydrates remain stable and do not dissociate into the solution and hence, they does not contribute to the neutralisation process and thus result in less pH rise compared to OPC and SF10. This conclusion was proved correct as the observation was found to be different on exposure to higher concentrations of sulphuric acid (above 1%). As the average pH was less than 3 for most of the exposure period, aluminate and iron hydrates become unstable and convert to their respective hydroxides, and in the process, they enhance the neutralisation process elevating the pH of the acid solution. This was evident in the case of BFS50 as the pH was found to be higher when compared to the other mixes on exposure to higher concentrations of sulphuric acid. In the case of pH2, a marginal rise in pH was initially noted (above 7) which could probably be due to very less concentration of acid ions in the system. Even a smaller release of hydroxyl ions could significantly elevate the pH of the acid solution and the differences between the mixes were very minimal. The changes in pH for the mortar with w/b of 0.55 followed a similar trend to mortar with w/b of 0.40 and these observations are shown in Appendix C (Figures C-6 to C-8).

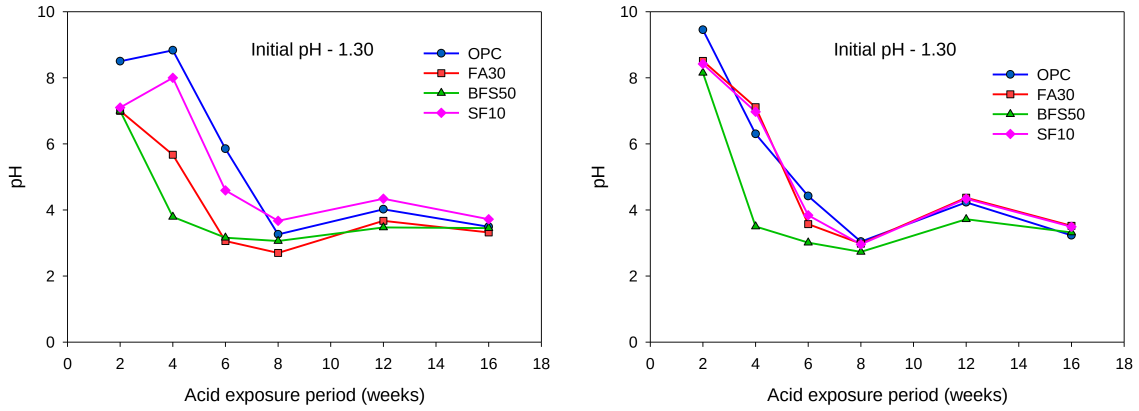

a) without brushing

b) with brushing

Figure 7.31 Changes in pH of acid solution exposed to 0.5% sulphuric acid (mortar w/b 0.40)

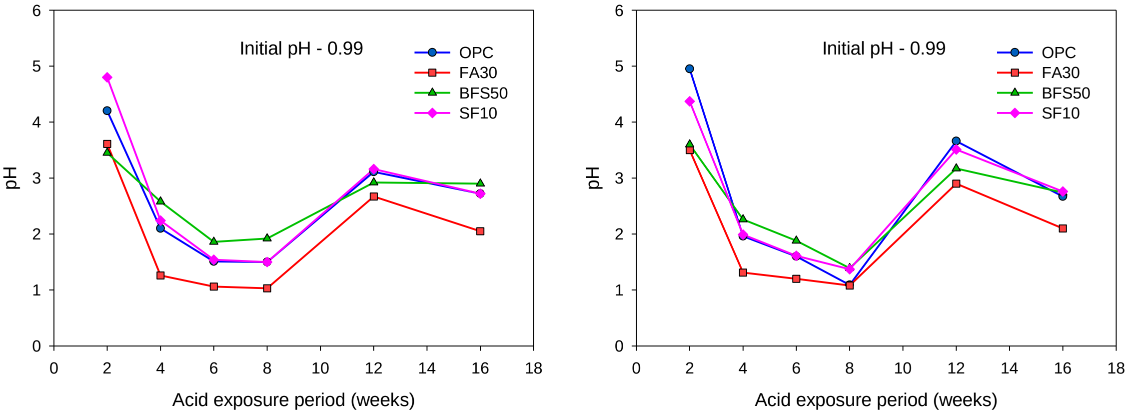

a) without brushing

b) with brushing

Figure 7.32 Changes in pH of acid solution exposed to 1% sulphuric acid (mortar w/b 0.40)

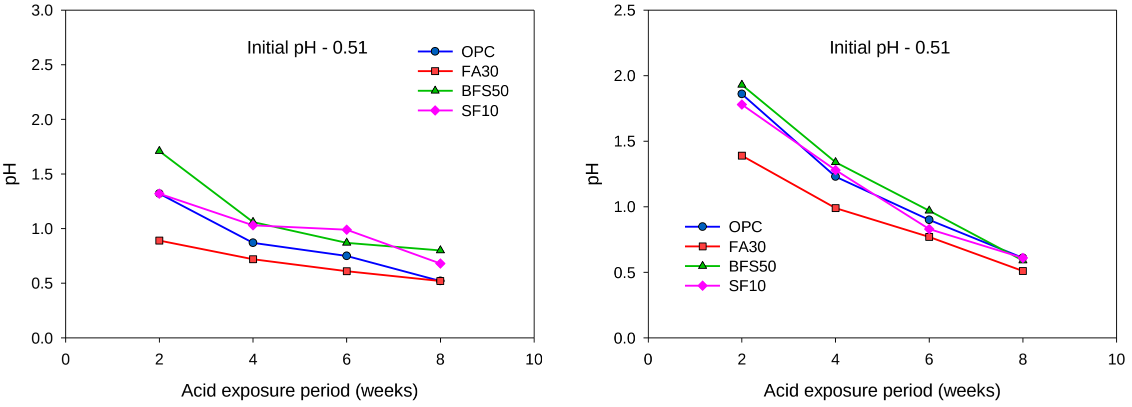

a) without brushing

b) with brushing

Figure 7.33 Changes in pH of acid solution exposed to 3% sulphuric acid (mortar w/b 0.40)

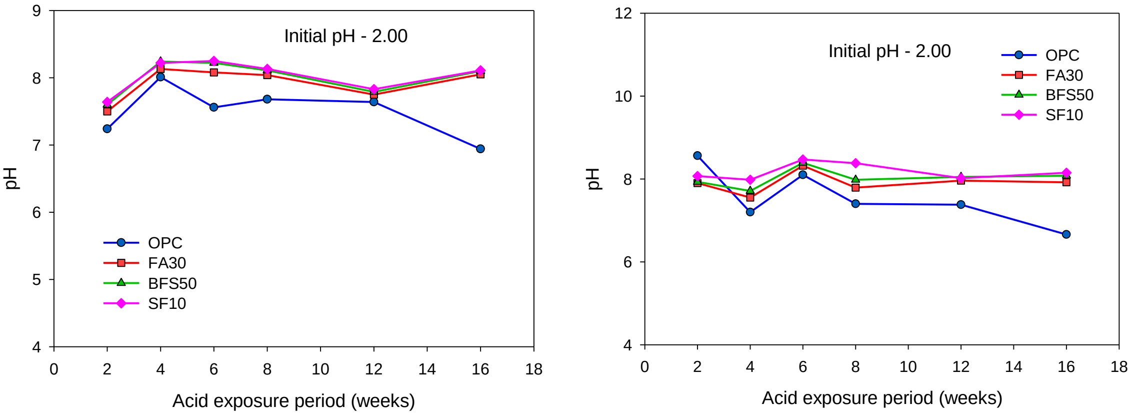

a) without brushing

b) with brushing

Figure 7.34 Changes in pH of acid solution exposed to pH2 sulphuric acid (mortar w/b 0.40)

Figures 7.35 to 7.38 show the changes in pH of the acid solution on exposure to various concentrations of acetic acid. The trends in the pH changes were very similar to the observations made during the paste study. The pH rise was found to decline over the age of exposure. This could be due to the buildup of the outer degraded layer and the limited availability of hydrates such as Portlandite near to the external surface of the specimen. It is also noted that the pH rise is very high compared to sulphuric acid. Despite the buffer action of acetic acid close to its pK_a value, the pH values of the acid solution are still found to be high for 0.125 and 0.25M concentrations. This implies that there is strong calcium leaching leading to an increase in the pH values. It is also observed that the pH rise for mortar with w/b of 0.55 is in general higher than the mortar made with w/b of 0.40. The higher porosity of the paste at a higher w/b of 0.55 might have contributed to increase in leaching and subsequently resulted in higher pH of the acid solution and marginally higher mass loss compared to lower w/b ratio of 0.40.

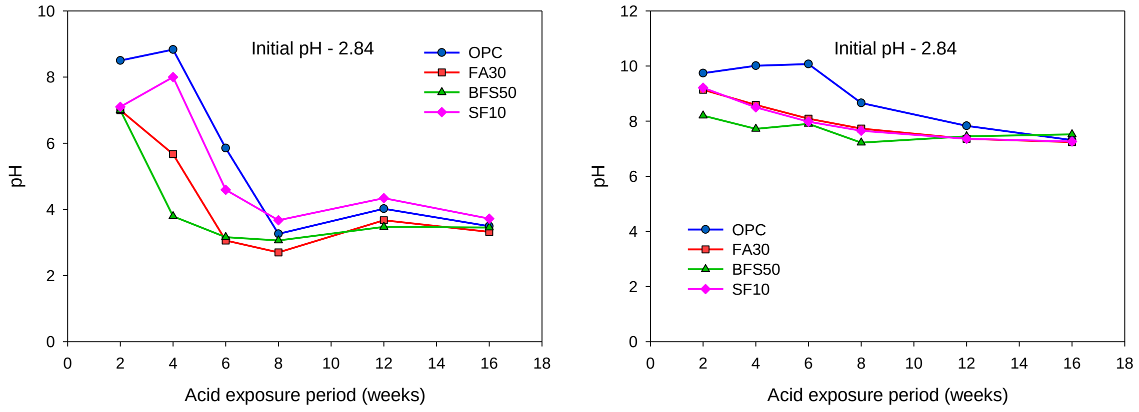

a) w/b 0.40

b) w/b 0.55

Figure 7.35 Changes in pH of acid solution exposed to 0.125M acetic acid (mortar)

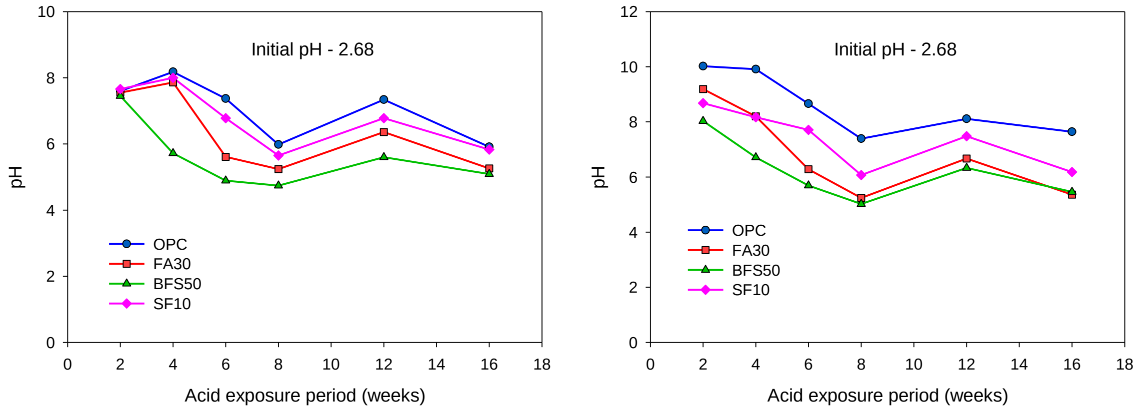

a) w/b 0.40

b) w/b 0.55

Figure 7.36 Changes in pH of acid solution exposed to 0.25M acetic acid (mortar)

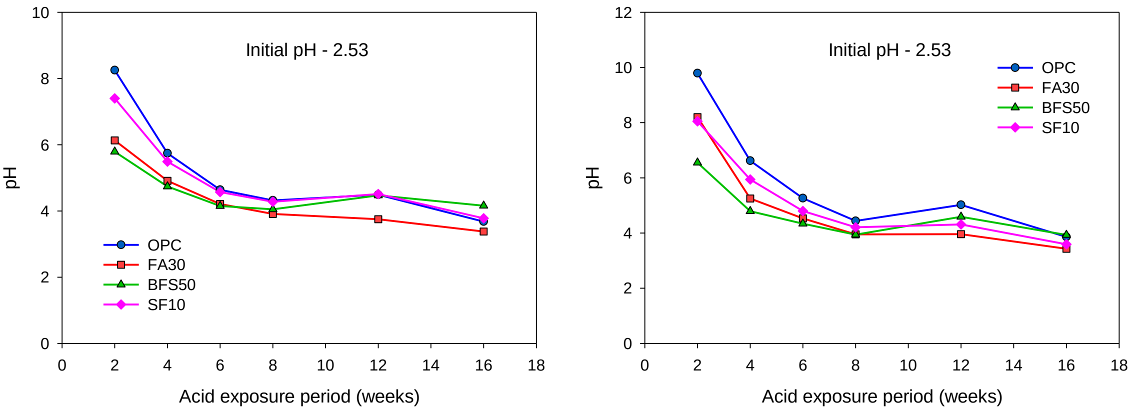

a) w/b 0.40 b) w/b 0.55

Figure 7.37 Changes in pH of acid solution exposed to 0.50M acetic acid (mortar)

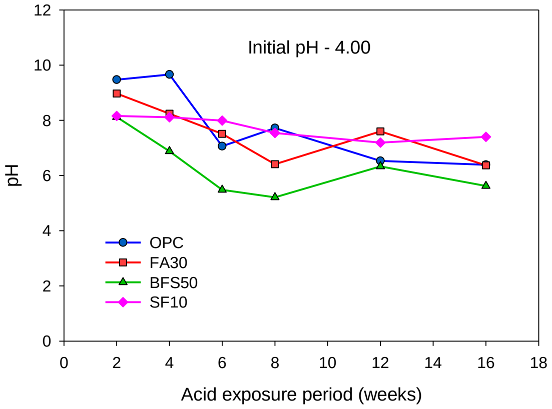

Figure 7.38 Changes in pH of acid solution exposed to pH4 acetic acid (mortar w/b 0.40)

7.3.2.2 Special binder systems

The changes in pH of the acid solution for mortar with LC2 and HAC followed a similar trend to the paste. On exposure to 1% and 3% sulphuric acid, the HAC mortar showed highest rise in the pH of the acid solution (Figures 7.39 and 7.40). As explained earlier, this could be attributed to the dissociation of aluminium hydrates enhancing the neutralisation. The LC2 binder system which has alumina in it also showed higher pH when compared to OPC mortar. However, in the case of acetic acid, the OPC mortar showed higher pH followed by LC2 and HAC for 0.25M acetic acid and the pH values were comparable for 0.5M acetic acid (Figure 7.41).

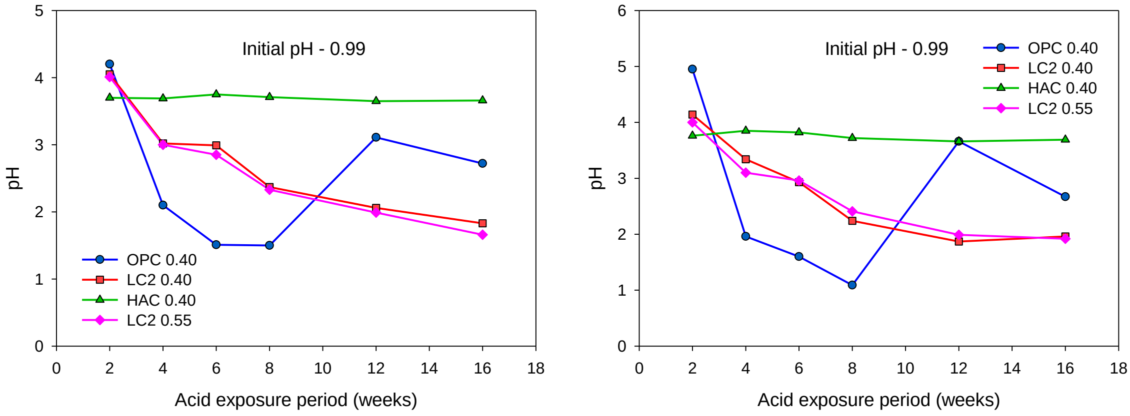

a) without brushing b) with brushing

Figure 7.39 Changes in pH of the acid solution for LC2 and HAC mortar exposed to 1% sulphuric acid

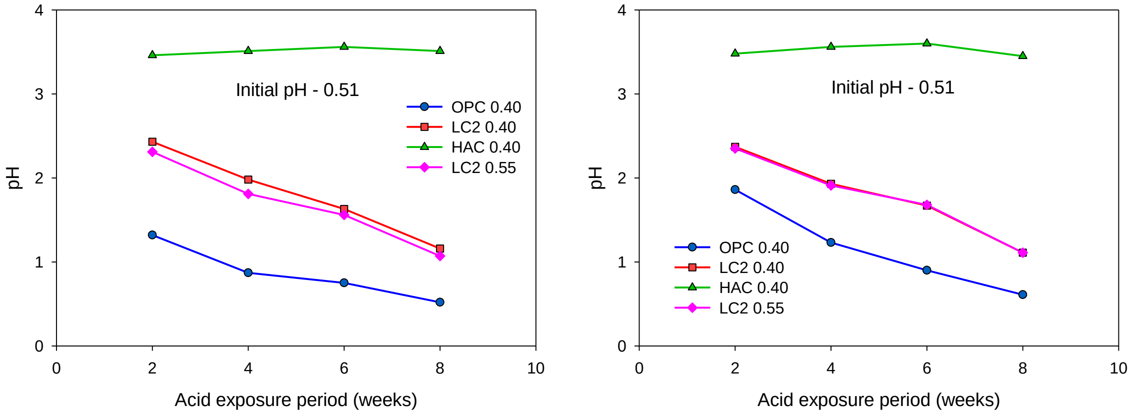

a) without brushing b) with brushing

Figure 7.40 Changes in pH of the acid solution for LC2 and HAC mortar exposed to 3% sulphuric acid

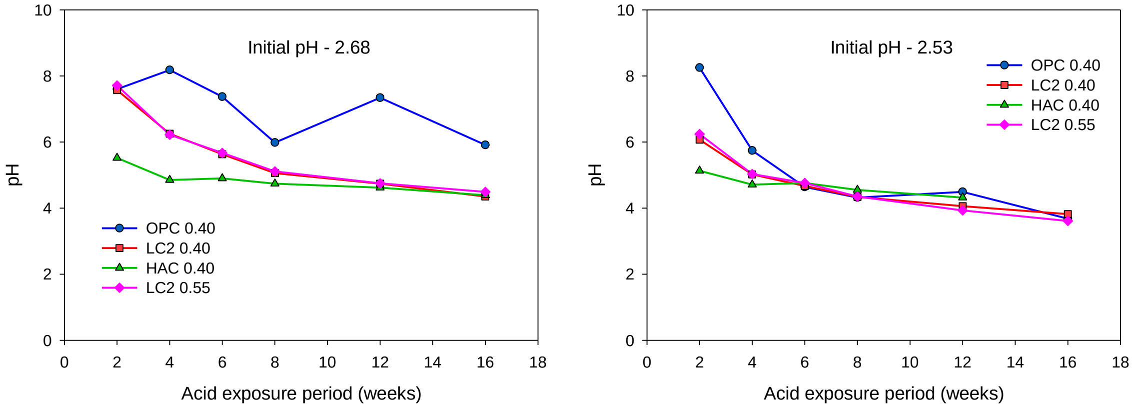

a) 0.25M acetic acid b) 0.5M acetic acid

Figure 7.41 Changes in pH of the acid solution for LC2 and HAC mortar exposed to acetic acid (without brushing)

7.3.3 Altered depth

7.3.3.1 Common binder systems

As done in the paste study, altered depth of specimens was determined from image analysis of the CT images. However, the middle decalcified layer, which was prominent in the paste, was not evident in the CT images of the mortar, probably due to the limitations in the voxel resolution in the imaging. Hence, in the case of mortar, altered area presented in the Table 7.1 is the area of the degraded layer and the altered depth presented is the sum of degraded depth and any depth removed due to the reactions. It can be seen that the alteration depths of SCM mixes are in general higher than OPC on exposure to acetic acid (Figure 7.42). This could be due to direct attack on CSH gel due to the limited availability of Portlandite in such systems (Amin and Bassuoni, 2018).

Among all the mixes, the alteration depth of FA30 was the highest and this observation was consistent with the measurement on paste. Even though mass loss may be less for FA30, the altered depth/area was found to be higher; the % area unattacked being only 22.3% and 18.3% of the initial area (for w/b ratios of 0.40 and 0.55 respectively) before the exposure to 0.25M acetic acid. The altered depths for SCM mixes were found to be greater at higher water to binder ratios, which could be due to the increased permeability of the paste and ITZ. The increased altered depth and reduced unattacked area for SCM mixes were also observed on exposure to 1% sulphuric acid. However, altered depths and areas were comparable for both mortars with w/b ratios of 0.40 and 0.55 on exposure to 1% sulphuric acid.

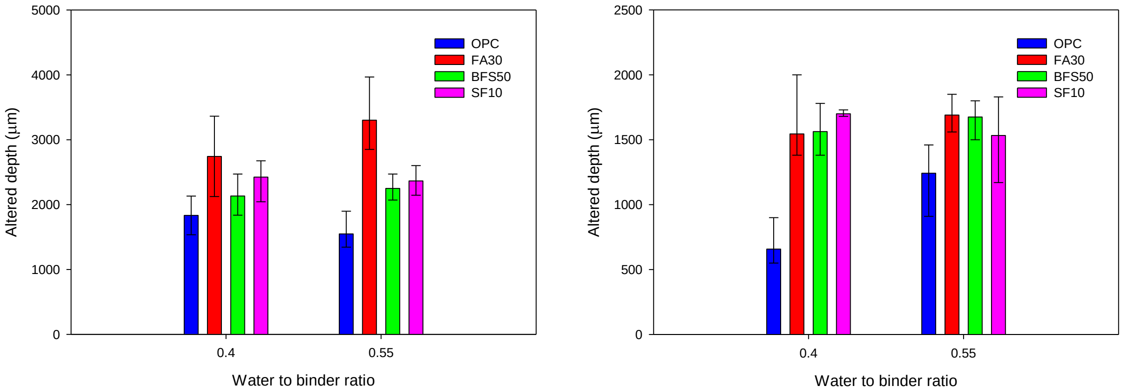

a) 1% sulphuric acid b) 0.25M acetic acid

Figure 7.42 Altered depth of mortar exposed to sulphuric and acetic acid based on image analysis of CT images

Table 7.1 Altered area and depth of mortar exposed to sulphuric and acetic acids based on CT image analysis

Mix	w/b	Acid	Conc.	(As % of the initial area)			Average degraded depth (μm)	Depth due to expansion/ shrinkage (μm)	Total alteration depth (μm)
				% area degraded	% area unattacked	% area expanded/ shrunk			
OPC	0.4	Acetic	0.25M	58.1	41.9	-1.81	1834	-46	1880
FA30	0.4	Acetic	0.25M	77.7	22.3	-4.09	2743	-108	2850
BFS50	0.4	Acetic	0.25M	67.9	32.1	-5.56	2133	-144	2276
SF10	0.4	Acetic	0.25M	67.5	32.5	-4.97	2423	-128	2552
OPC	0.55	Acetic	0.25M	45.1	54.9	-8.25	1549	-225	1774
FA30	0.55	Acetic	0.25M	81.7	18.3	-5.55	3301	-146	3447
BFS50	0.55	Acetic	0.25M	64.3	35.7	-7.14	2249	-189	2438
SF10	0.55	Acetic	0.25M	60.5	39.5	-17.21	2365	-464	2829
OPC	0.4	Sulphuric	1%	25.3	74.7	-10.74	658	-282	940
FA30	0.4	Sulphuric	1%	46.4	53.6	-0.96	1545	-25	1570
BFS50	0.4	Sulphuric	1%	52.0	48.0	+10.13	1563	+253	1563
SF10	0.4	Sulphuric	1%	51.1	48.9	+3.81	1700	+103	1700
OPC	0.55	Sulphuric	1%	36.2	63.8	+5.51	1242	+137	1242
FA30	0.55	Sulphuric	1%	44.0	56.0	-12.92	1690	-341	2031
BFS50	0.55	Sulphuric	1%	50.2	49.8	+4.61	1675	+115	1675
SF10	0.55	Sulphuric	1%	49.5	50.5	+3.99	1533	+100	1533

Note: Positive value indicates expansion and negative value indicates section loss in the specimens

7.3.3.2 Special binder systems

Table 7.2 summarises the parameters used for estimating the degraded area and alteration depth of LC2 and HAC mortar exposed to sulphuric and acetic acid. It can be seen that the degraded areas and alteration depths (after accounting for the depth expanded/shrunk) for LC2 mortar (w/b 0.40) and HAC mortar are comparable on exposure to 0.25M acetic acid. Also, it can be inferred that the degradation based on the % area degraded and alteration depth for LC2 mortar (w/b 0.40) is less than the same mortar made with w/b of 0.55. This reaffirms that lower w/b ratio mixes may be more durable against acetic acid environments.

On exposure to 1% sulphuric acid, the effect of w/b ratio was found to be minimal in the case of LC2 mortar. In other words, the influence of transport properties is minimal in influencing the kinetics in the case of sulphuric acid. Among all the mortar mixes, the performance of HAC mortar was found to be better compared to LC2 mortars as the % degraded area and alteration depths were found to be less in the case of HAC mortar.

Figure 7.43 shows the comparison of altered depths (as measured from the CT images without accounting for any depth expanded or removed) for LC2 and HAC mortars with OPC mortar. It can be seen that the altered depth is greater for LC2 mortar when compared to OPC mortar in the case of 1% sulphuric acid and 0.25M acetic acid. This increased depth of alteration was observed to be similar to carbonation process wherein the SCM systems with less Portlandite seem to have increased carbonation depths due to direct attack on CSH/ pozzolanic CSH gel (Papadakis, 2000; Antoni, 2013).

Table 7.2 Altered area/depths of LC2 and HAC mortar exposed to sulphuric and acetic acid

Mix	w/b	Acid and concentration	as % of the initial area		% area expanded/ shrunk	Average degraded depth (μm)	Depth due to expansion /shrinkage (μm)	Total alteration depth (μm)
			Area degraded	Area unattacked				
OPC	0.40	Acetic 0.25M	58.10	41.90	-1.81	1834.0	-46.0	1880
LC2	0.40	Acetic 0.25M	56.75	43.25	-11.39	2176.2	-301.3	2478
HAC	0.40	Acetic 0.25M	56.86	43.14	-21.97	2255.0	-591.9	2847
LC2	0.55	Acetic 0.25M	67.87	32.13	-9.01	2905.5	-239.4	3145
OPC	0.40	Sulphuric 1%	25.30	74.70	-10.74	658.0	-282.0	940
LC2	0.40	Sulphuric 1%	47.00	53.00	-7.64	1595.0	-212.4	1807
HAC	0.40	Sulphuric 1%	18.37	81.63	-27.38	550.0	-759.1	1309
LC2	0.55	Sulphuric 1%	47.54	52.46	-10.25	1925.0	-271.7	2197

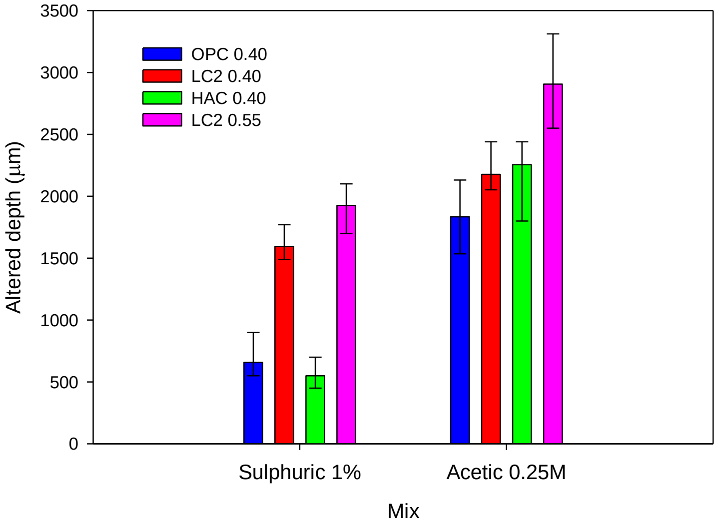

Figure 7.43 Altered depth of LC2 and HAC mortar after 16 weeks exposure to sulphuric and acetic acid (without brushing)

7.3.4 Thickness changes

7.3.4.1 Common binder systems

In order to know whether there is expansion/reduction in thickness on acid exposure, the thickness was measured before and after the acid exposure. Table 7.3 shows the average thickness changes of mortar after acid exposure tested without brushing where the corroded layers are not disturbed. It can be inferred that all mortar specimens on exposure to mid and moderate concentrations of sulphuric acid (< 1%) had expansion due to the formation of gypsum. Excessive reduction in thickness was observed on exposure to 3% sulphuric acid due to the delamination and destabilisation of gypsum at this aggressive low pH environment. In the case of pH2 sulphuric acid, hardly any precipitation was observed and the measurements indicated a minor reduction in thickness, which was reflected in the mass changes also (small mass loss).

In the case of acetic acid, as the salts are soluble, most of the specimens showed a small reduction in thickness and there was no expansion. However, the thickness changes observed in mortar were much less than that observed in paste specimens. This could be due to the presence of fine aggregates hindering the thickness measurements in mortar. In the case of tests with brushing also, all mortar specimens showed expansion for mild and moderate concentrations of sulphuric acid and severe loss of thickness in the case of 3% sulphuric acid (Table 7.4). Similar analyses were carried out for other mortar specimens tested with w/b of 0.55 (of size 10 × 10 × 60 mm and 25 × 25 × 35 mm) and these results are shown in Appendix C (Tables C-1 and C-2).

Table 7.3 Thickness changes of mortar after acid exposure without brushing (w/b 0.40)

	Without brushing (WB28)							
Mix	0.5% Sulphuric	1% Sulphuric	3% Sulphuric	1% sulphuric pH2	0.125M Acetic	0.25M Acetic	0.5M Acetic	0.25M acetic pH4
OPC	+1.39	+2.77	-24.29	-0.83	+1.40	-0.40	-1.06	-0.14
FA30	+3.55	+6.94	-58.28	-0.32	-4.79	+0.20	-0.02	-1.34
BFS50	+3.62	+7.21	-22.06	-0.21	-0.56	-0.09	+0.47	-0.14
SF10	+2.32	+7.18	-54.75	-0.51	-1.17	-1.49	-1.21	-1.23

Table 7.4 Thickness changes of mortar after acid exposure with brushing (w/b 0.40)

Mix	With brushing (B28)			
	0.5% Sulphuric	1% Sulphuric	3% Sulphuric	1% sulphuric pH2
OPC	+0.35	+0.23	-31.97	+1.05
FA30	+0.84	+5.72	-81.94	+0.68
BFS50	+2.11	+5.16	-20.15	+1.05
SF10	+1.63	+4.30	-69.91	+1.27

7.3.4.2 Special binder systems

The thickness changes of mortar specimens made with special binders after the acid exposure were compared with OPC mortar and the results are presented in Table 7.5. The LC2 mortar specimens had thickness gain on exposure to 1% sulphuric acid whereas HAC mortar had loss in thickness. The better performance of LC2 in 1% sulphuric acid was not observed in the case of 3% sulphuric acid as the entire specimen disintegrated on acid exposure. The HAC mortar also showed double the thickness loss when compared to the OPC mortar on exposure to 3% sulphuric acid. The thickness changes of all the mortar mixtures on exposure to acetic acid was very less, as there was no precipitation of secondary products. Also, siliceous aggregates remained in the matrix with silica gel, which caused less change in thickness.

Table 7.5 Thickness changes of mortar made with special binders after acid exposure

Mix	w/b	Without brushing (WB28)				With brushing (B28)	
		1% Sulphuric	3% Sulphuric	0.25M Acetic	0.5M Acetic	1% Sulphuric	3% Sulphuric
OPC	0.40	+2.77	-24.29	-0.40	-1.06	+0.23	-31.97
LC2	0.40	+3.14	-100	+1.25	-2.51	+2.72	-100
LC2	0.55	+3.26	-100	-2.33	-1.53	+3.11	-100
HAC	0.40	-2.26	-45.81	+1.48	+0.60	-2.35	-37.83

7.4 ALTERATIONS IN PHYSICO-MECHANICAL PROPERTIES

7.4.1 Strength changes

7.4.1.1 Common binder systems

The cylindrical mortar specimens of 25 mm diameter and 50 mm height were tested for the compressive strength before and after acid exposure at regular intervals. The photographs of specimens after the acid exposure are shown in Appendix C (Figures C-25 to C-28). The decalcification of hydrated products and changes in porosity could result in changes in compressive strength of mortar. On exposure to 0.5% sulphuric acid, a marginal drop in compressive strength was noted (Figure 7.44). The reduction in compressive strength was considerable on exposure to 16 weeks in 1% sulphuric acid (Figure 7.45). It is noted that the mortar with higher w/b of 0.55 had less reduction in the compressive strength when compared to mortar made with w/b of 0.40. There was a substantial reduction in the compressive strength of mortar on exposure to 3% sulphuric acid (Figure 7.46). The OPC and BFS50 mortars had greater residual compressive strength after 10 weeks of exposure in 3% sulphuric acid. In the case of pH2 sulphuric acid, the changes in the compressive strength were not noticeable even after 16 weeks of exposure as the deterioration was very minimal (Figure 7.47).

The reduction in the compressive strength was more pronounced in the case of exposure to acetic acid (Figures 7.48 to 7.51). A progressive loss of strength was evident for all mixes exposed to various concentrations of acetic acid. It is inferred that the mixes with lower w/b ratio of 0.40 had less reduction in the compressive strength when compared to mortar with w/b of 0.55. This could be due to the reduced permeability and porosity of paste leading to less deterioration and increased strength due to lower w/b ratio. On exposure to 0.25M and 0.5M and pH4 acetic acid, the BFS50 mix had greater compressive strength when compared to the other mixes, at the end of the exposure period. The improved performance of slag could be attributed to the consumption of lime, reduced permeability and presence of more alumina, which adds stability to the corroded layer. An attempt was made to measure the altered depths of strength-tested specimens using digital vernier caliper of sensitivity 1 µm. These results are presented and summarised in Appendix C (Figures C-32 to C-37 and Table C-11).

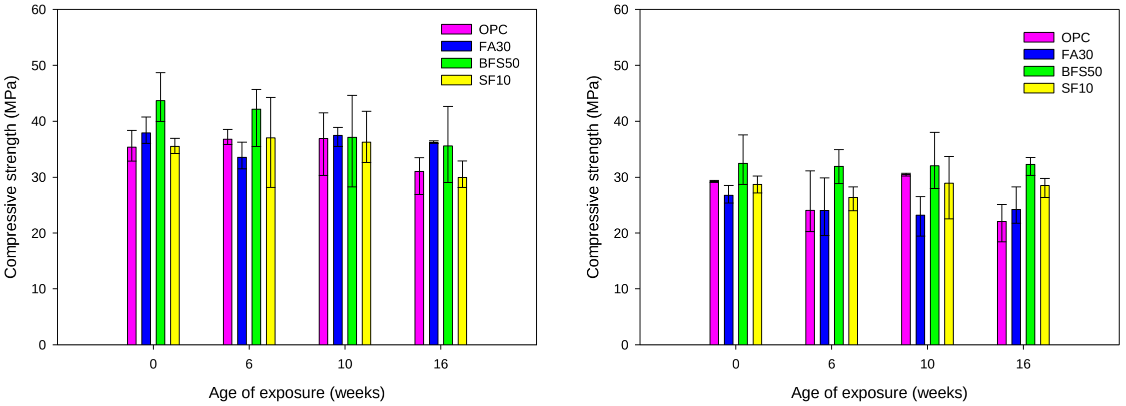

a) w/b 0.40 b) w/b 0.55

Figure 7.44 Changes in compressive strength of mortar exposed to 0.5% sulphuric acid

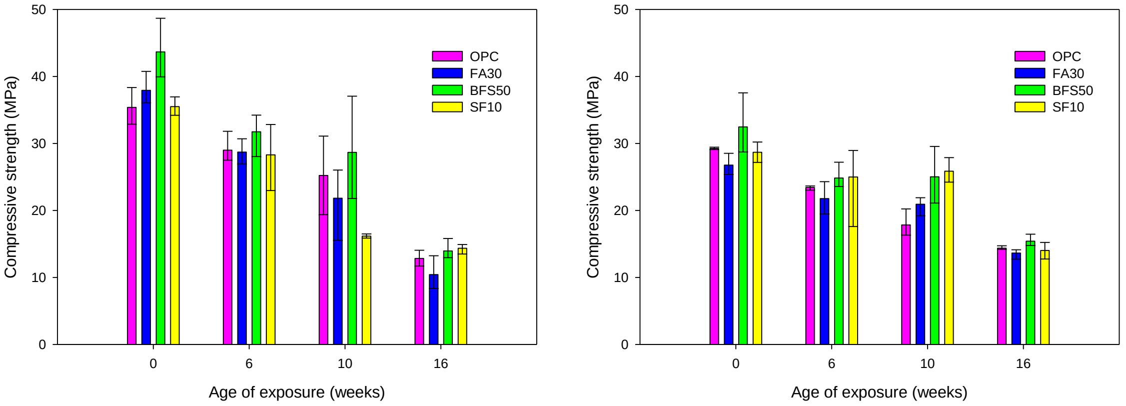

a) w/b 0.40 b) w/b 0.55

Figure 7.45 Changes in compressive strength of mortar exposed to 1% sulphuric acid

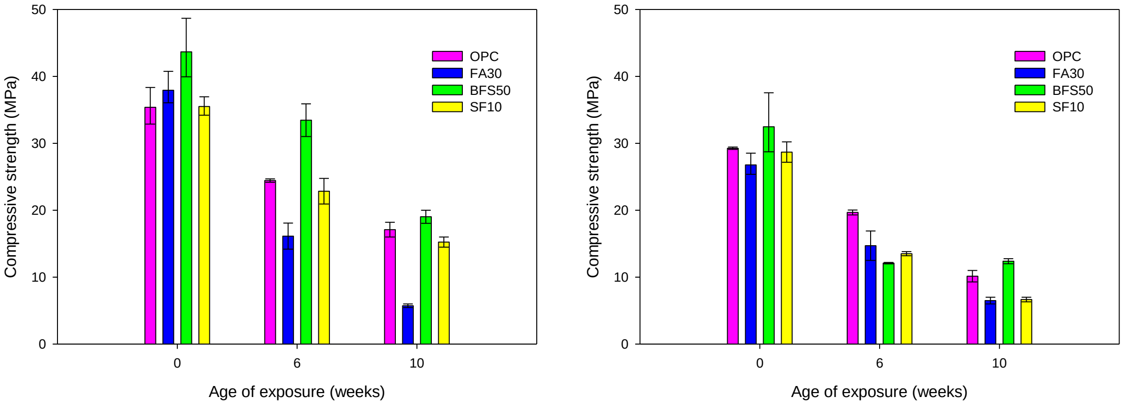

a) w/b 0.40 b) w/b 0.55

Figure 7.46 Changes in compressive strength of mortar exposed to 3% sulphuric acid

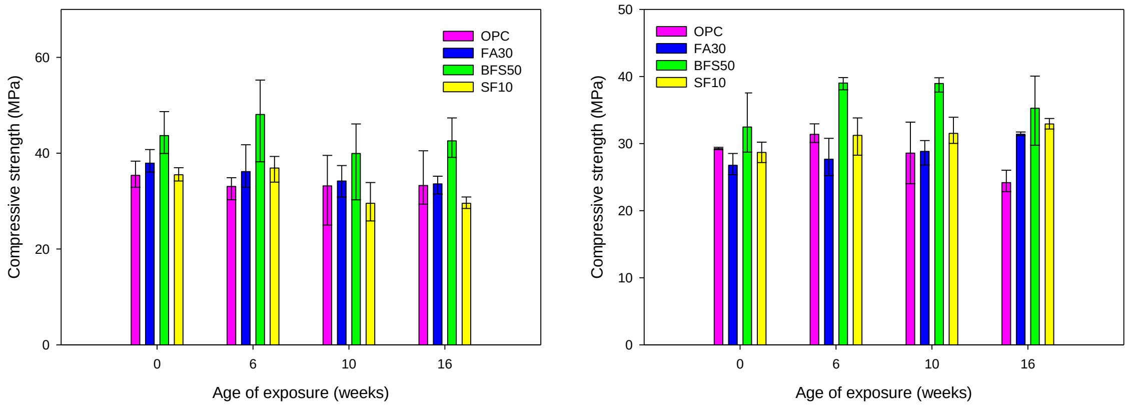

a) w/b 0.40 b) w/b 0.55

Figure 7.47 Changes in compressive strength of mortar exposed to pH2 sulphuric acid

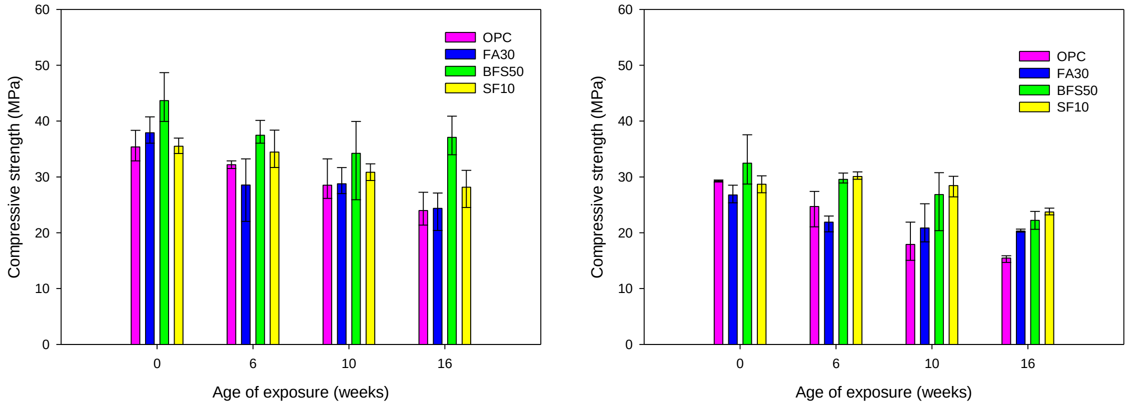

a) w/b 0.40 b) w/b 0.55

Figure 7.48 Changes in compressive strength of mortar exposed to 0.125M acetic acid

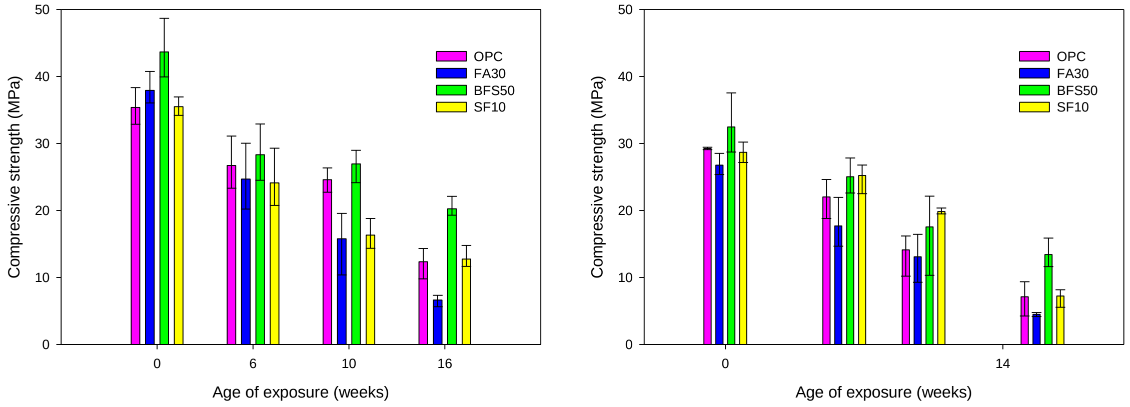

a) w/b 0.40 b) w/b 0.55

Figure 7.49 Changes in compressive strength of mortar exposed to 0.25M acetic acid

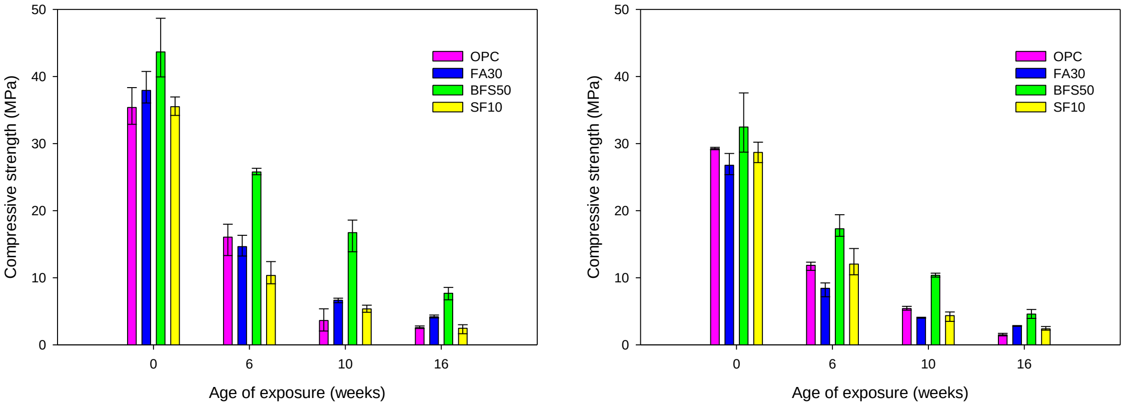

a) w/b 0.40 b) w/b 0.55

Figure 7.50 Changes in compressive strength of mortar exposed to 0.50M acetic acid

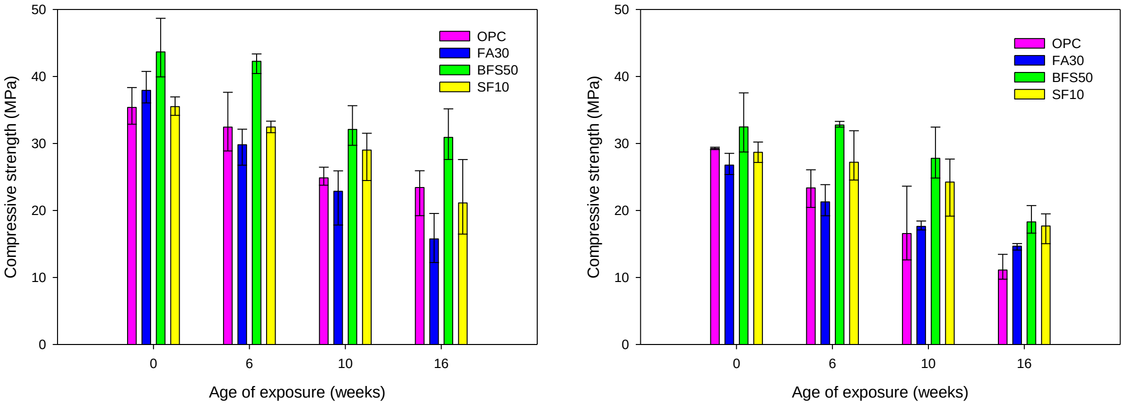

a) w/b 0.40 b) w/b 0.55

Figure 7.51 Changes in compressive strength of mortar exposed to pH4 acetic acid

7.4.1.2 Special binder systems

The photographs of mortar specimens after exposure to acids are shown in Appendix C (Figures C-29 to C-31). The strength tests on mortar showed that the LC2 mortar (w/b 0.40) and HAC mortar (w/b 0.40) had better residual compressive strength after 16 weeks of exposure in 1% sulphuric acid (Figure 7.52). A progressive drop in compressive strength was observed in all mixes. However, on exposure to 3% sulphuric acid, the performance of OPC and HAC mortar were found to be much better when compared to LC2 mortars of w/b 0.40 and 0.55. These are consistent with the mass change observations wherein the LC2 mortar showed the highest mass loss for 3% sulphuric acid. On exposure to 0.25M acetic acid, the residual strengths of OPC, LC2 (w/b 0.40) and HAC mortars were comparable as shown in Figure 7.53. For a higher concentration of 0.5M acetic acid, the LC2 mortar (w/b 0.40) and OPC mortar showed higher residual strength compared to

HAC mortar and LC2 mortar (w/b 0.55). Altered depths were also measured using digital caliper and these results are shown in Appendix C (Figures C-38 and C-39).

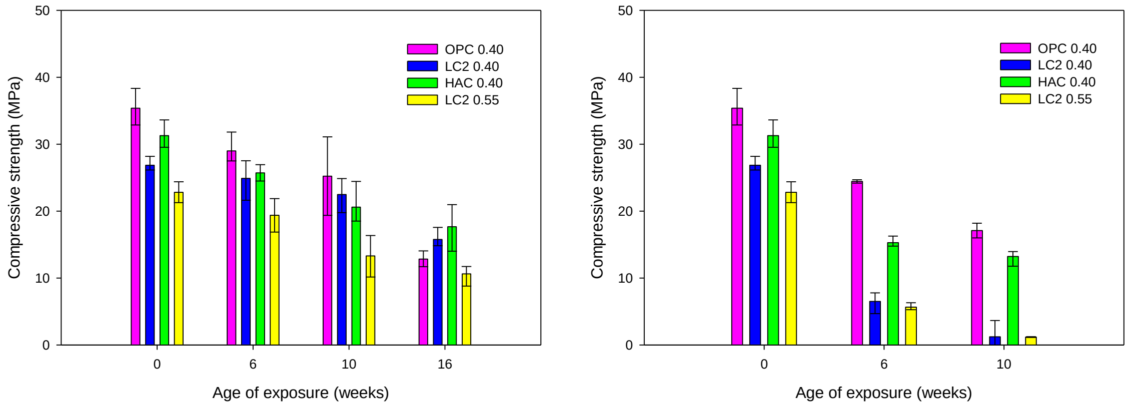

a) 1% sulphuric acid b) 3% sulphuric acid

Figure 7.52 Strength changes of LC2 and HAC mortar on exposure to sulphuric acid

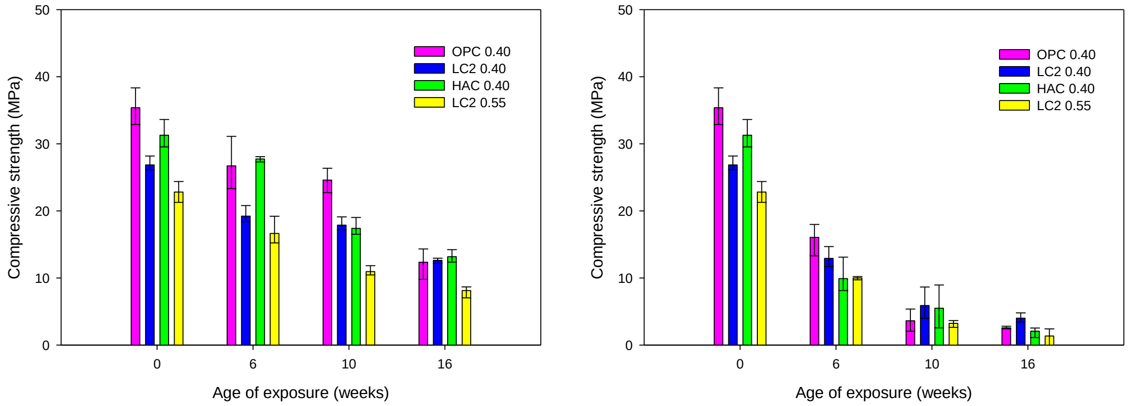

a) 0.25M acetic acid b) 0.5M acetic acid

Figure 7.53 Strength changes of LC2 and HAC mortar on exposure to acetic acid

7.4.2 Dynamic modulus of elasticity

7.4.2.1 Common binder systems

Ultrasonic pulse velocity test was carried out on the mortar cylinders in saturated surface dry condition just before performing the compressive strength test. Bulk density was calculated based on the mass of the specimen, the average diameter and height of the specimen. The dynamic modulus of elasticity of mortar was then calculated based on the bulk density and ultrasonic pulse velocity. Relative dynamic modulus of elasticity was then estimated as the ratio of the dynamic modulus of elasticity of mortar at specific age of acid exposure to the dynamic modulus of elasticity of mortar tested before the acid exposure. The variations in the dynamic modulus of elasticity of various mortar mixes on exposure to various concentrations of sulphuric and acetic acid are provided in Appendix C (Figures C-40 to C-46). It is seen that the variability in the test results for dynamic modulus of elasticity is less than the variability observed in the strength tests. A drop in the dynamic modulus of elasticity is observed for all the mortar mixes on exposure to various concentrations of sulphuric and acetic acids, the reduction being more predominant in the case of acetic acid. In general, it is evident that the BFS50 had greater residual dynamic modulus of elasticity in all the concentrations of sulphuric and acetic acid studied.

Tables C-3 to C-10 in Appendix C give the details of the changes in physico-mechanical properties such as strength, bulk density and dynamic modulus of elasticity for mortar mixes with two w/b ratios of 0.40 and 0.55 exposed to sulphuric and acetic acid. It can be inferred that there is a considerable drop in the bulk density of mortar on exposure to acetic acid. This could be attributed to the mass loss due to leaching and the subsequent increase in the porosity of the specimens. The UPV values were found to reduce considerably in the case of prolonged exposure to acetic acid, especially at higher concentrations of acid, implying that the matrix had already undergone severe deterioration. Table 7.6 summarises the observations pertaining to the variations in the relative dynamic modulus of elasticity upon acid exposure. In general, it is seen that as the concentration of acid is increased, there is a drop in the relative E value. Also, in the case of sulphuric acid attack, the relative E value after 16 weeks of exposure for mortar with higher w/b ratio of 0.55 was found to be higher than for mortar with a w/b of 0.40 (due to less damage). Hence, it is suggested that the use of marginally higher w/b ratios may be desirable in order to have less deterioration in the case of sulphuric acid attack.

Based on the relative E values after 16 weeks of exposure to 1% sulphuric acid, the performance of FA30 and SF10 mortar was found to better when compared to OPC and BFS50 mixes. In the case of acetic acid, it is found that the relative E values of lower w/b ratio of 0.40 are higher than mortar with higher w/b ratio of 0.55. Hence, the use of lower w/b ratio may be appropriate when designing the concrete mixes exposed to acetic acid environments. The BFS50 mix had greater relative E value after 16 weeks of acetic acid exposure when compared to the other mixes for all concentrations of acetic acid.

Table 7.6 Changes in relative dynamic modulus of elasticity of mortar with acid exposure

Mix	Acid	Concentration	w/b 0.40			w/b 0.55		
			Age (weeks)			Age (weeks)		
			6	10	16	6	10	16
OPC	Sulphuric	0.50%	1.04	0.87	0.76	0.94	0.93	0.83
OPC	Sulphuric	1.00%	0.95	0.66	0.51	0.95	0.69	0.59
OPC	Sulphuric	3.00%	0.52	-	-	0.51	0.00	0.00
OPC	Sulphuric	pH2	1.05	0.88	0.89	0.96	0.88	0.90
OPC	Acetic	0.12M	0.90	0.89	0.76	0.98	0.93	0.70
OPC	Acetic	0.25M	0.88	0.85	0.57	0.82	0.78	0.50
OPC	Acetic	0.50M	0.71	0.65	0.22	0.79	0.58	0.07
OPC	Acetic	pH4	0.98	0.87	0.74	0.88	0.89	0.68
FA30	Sulphuric	0.50%	0.99	0.86	0.71	1.02	0.90	0.85
FA30	Sulphuric	1.00%	0.85	0.67	0.49	0.98	0.77	0.64
FA30	Sulphuric	3.00%	0.52	-	-	0.60	-	-
FA30	Sulphuric	pH2	1.02	0.81	0.84	0.97	0.93	0.86
FA30	Acetic	0.12M	0.82	0.86	0.71	0.96	0.88	0.72
FA30	Acetic	0.25M	0.79	0.76	0.52	0.91	0.80	0.49
FA30	Acetic	0.50M	0.71	0.59	0.17	0.76	0.50	0.15
FA30	Acetic	pH4	0.81	0.83	0.61	0.91	0.82	0.56
BFS50	Sulphuric	0.50%	0.99	0.82	0.76	0.90	0.84	0.79
BFS50	Sulphuric	1.00%	0.89	0.67	0.47	0.85	0.69	0.49
BFS50	Sulphuric	3.00%	0.48	-	-	0.45	-	-
BFS50	Sulphuric	pH2	1.00	0.77	0.85	0.98	0.83	0.78
BFS50	Acetic	0.12M	0.99	0.95	0.81	0.81	0.86	0.68
BFS50	Acetic	0.25M	0.92	0.86	0.67	0.76	0.78	0.55
BFS50	Acetic	0.50M	0.83	0.78	0.47	0.75	0.60	0.27
BFS50	Acetic	pH4	0.94	0.96	0.74	0.79	0.79	0.59
SF10	Sulphuric	0.50%	0.95	0.80	0.72	0.90	0.90	0.77
SF10	Sulphuric	1.00%	0.84	0.67	0.48	0.91	0.73	0.60
SF10	Sulphuric	3.00%	0.46	-	-	0.46	-	-
SF10	Sulphuric	pH2	0.92	0.84	0.78	0.92	0.83	0.77
SF10	Acetic	0.12M	0.95	0.88	0.72	0.88	0.90	0.73
SF10	Acetic	0.25M	0.82	0.75	0.52	0.76	0.75	0.44
SF10	Acetic	0.50M	0.72	0.60	0.09	0.72	0.53	0.09
SF10	Acetic	pH4	0.87	0.85	0.64	0.85	0.84	0.60

Note: The degradation for 3% sulphuric acid was stopped at 10 weeks. As the surface of the specimen was rough due to degradation, UPV measurements could not be carried out for 3% exposure at 10 weeks of exposure.

7.4.2.2 Special binder systems

A continuous drop in the values for dynamic modulus of elasticity was observed for all mortar specimens exposed to sulphuric and acetic acid. In general, it can be seen that the HAC mortar showed higher dynamic modulus of elasticity especially at early ages of acid exposure. Similar performance was also observed in the case of limestone mortar. The increased values for dynamic modulus of elasticity may be due to the changes in the chemical composition of the system. The relative dynamic modulus of elasticity of LC2 and HAC mortar exposed to sulphuric and acetic acid are presented in Table 7.7. Compatible with the other results, the LC2 and HAC mortar showed higher values for the residual dynamic modulus of elasticity (i.e. after 16 weeks of acid exposure) in the case of 1% sulphuric acid (Figure 7.54). It appears that the HAC mortar showed greater residual dynamic modulus of elasticity on acid exposure. Apparently, the relative dynamic modulus of elasticity for HAC mortar at the end of exposure period was higher on exposure to 1% sulphuric acid (0.92), 0.25M acetic acid (0.98) and 0.5M acetic acid (0.54). However, this was not reflected in the mass changes and visual observations. Considering the behaviour with respect to mass changes also, LC2 mortar with w/b 0.55 may be more suitable for exposure to low concentrations of sulphuric acid. At high concentrations (3%), it is clear that the performance of LC2 is ordinary and hence the use of HAC may be preferred when compared to the LC2 system. On exposure to acetic acid, LC2 mortar (w/b 0.40) and HAC mortar (w/b 0.40) are recommended based on the values of relative dynamic modulus of elasticity and mass changes. Additional information about changes in bulk density along with other physico-mechanical parameters are presented in Appendix C (Tables C-12 to C-14).

Table 7.7 Relative dynamic modulus of elasticity of LC2 and HAC mortar exposed to sulphuric and acetic acid

Mix	w/b	Solution	Concentration	Age (weeks)		
				6	10	16
LC2	0.40	Sulphuric	1%	0.84	0.74	0.76
HAC	0.40	Sulphuric	1%	1.18	1.11	0.92
LC2	0.55	Sulphuric	1%	0.89	0.73	0.73
LC2	0.40	Acetic	0.25M	0.84	0.72	0.67
HAC	0.40	Acetic	0.25M	1.08	0.97	0.98
LC2	0.55	Acetic	0.25M	0.81	0.69	0.64
LC2	0.40	Acetic	0.5M	0.70	0.56	0.55
HAC	0.40	Acetic	0.5M	0.87	0.62	0.54
LC2	0.55	Acetic	0.5M	0.65	0.50	0.42

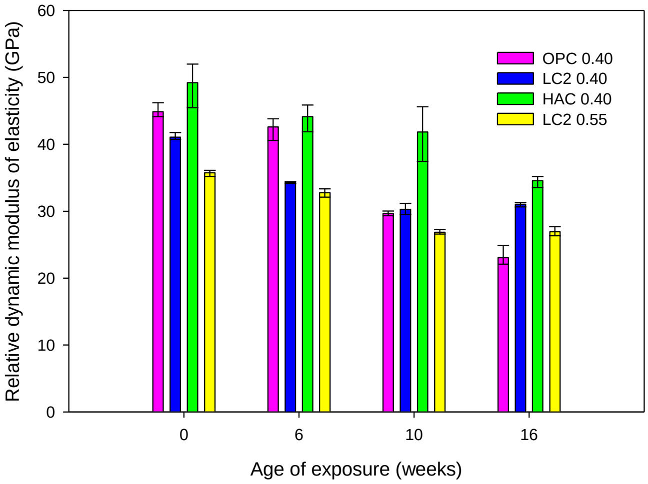

Figure 7.54 Changes in dynamic modulus of elasticity of LC2 and HAC mortar on exposure to 1% sulphuric acid

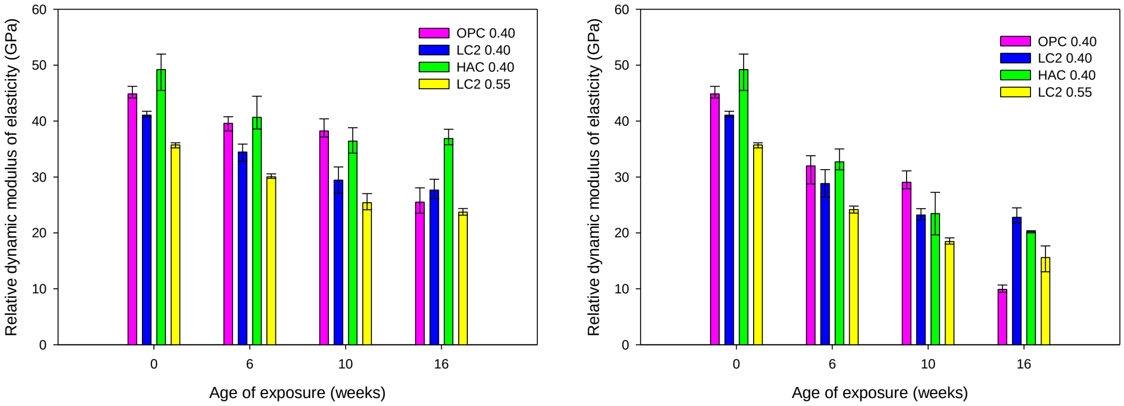

a) 0.25M acetic acid b) 0.5M acetic acid

Figure 7.55 Changes in dynamic modulus of elasticity of LC2 and HAC mortar on exposure to acetic acid

7.5 MECHANISM OF DEGRADATION

7.5.1 X-ray micro-tomography

7.5.1.1 Common binder systems

X-ray tomography imaging was done on mortar samples after the acid exposure. Figure 7.56 shows the CT slice images of mortar samples (w/b 0.40) exposed to 16 weeks immersion in 1% sulphuric acid without the application of abrasive action. The OPC mortar showed degradation on the surface as the gypsum layer was found to destabilise on prolonged exposure, exposing the aggregates. The decalcification of the outer layer is clearly evident as the GSV of the outer layer was less when compared to the inner layer which is not attacked. Also, cracking around the ITZ was visible in the CT image. The SCM binder systems showed similar degradation. However, the extent of delamination was less as the degraded layer was found to be more adherent to the matrix. The CT images of mortar (w/b 0.55) exposed to 1% sulphuric acid also showed similar degradation and these images are provided in the Appendix C, Figure C-55.

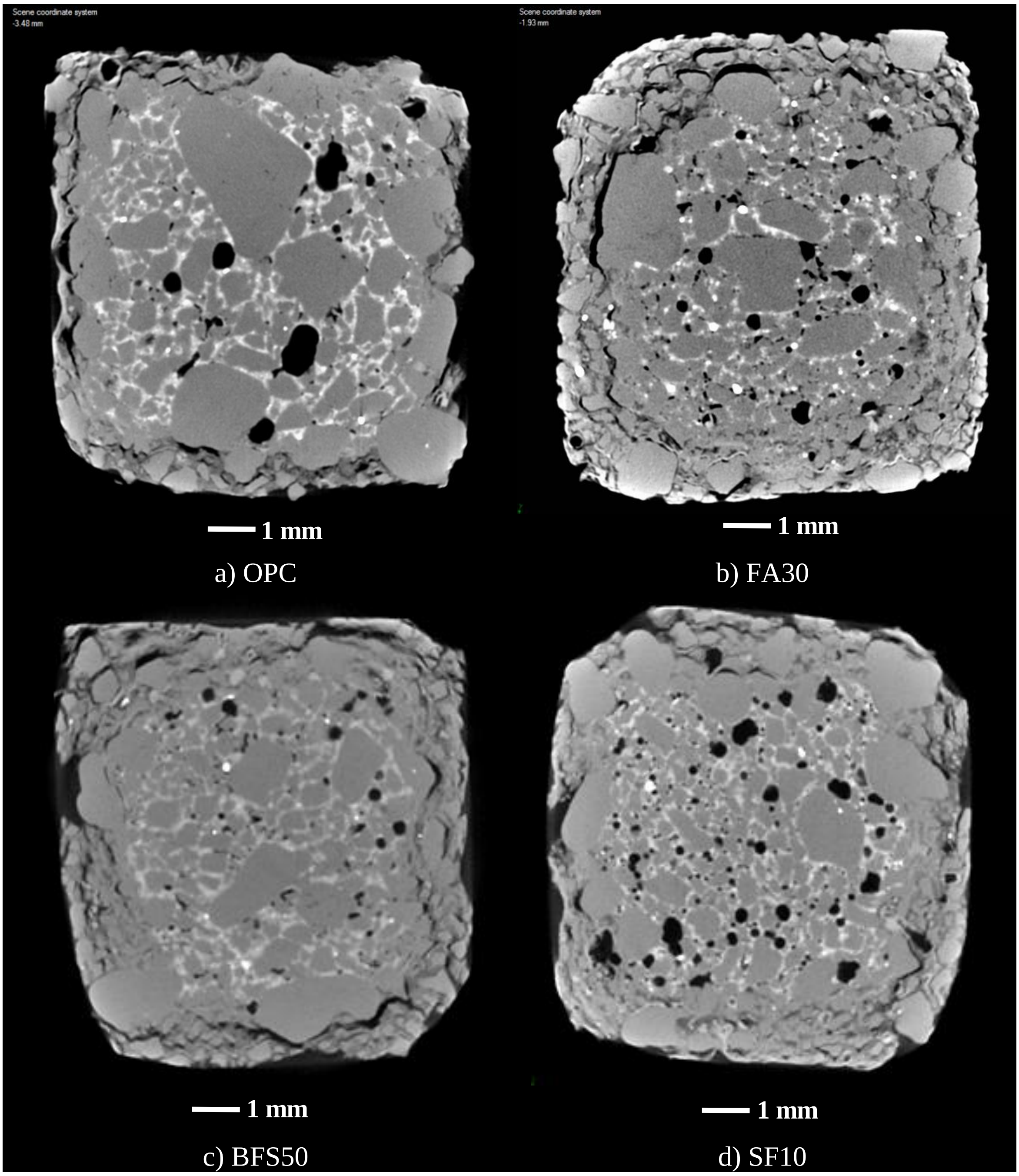

a) OPC b) FA30 c) BFS50 d) SF10

Figure 7.56 Top view CT slice images of mortar (w/b 0.40) after exposure to 1% sulphuric acid

It can also be noted that the depth of degraded layer in SCM mixes was higher compared to the OPC. This could be due to the consumption of lime either for hydration reactions or due to the acid attack. In effect, the limited availability of Portlandite in SCM systems led to direct attack on CSH gel and this might have led to higher degradation depths of the outer layer. The cracking around the aggregates in the outer degraded layer was also visible in the SCM mortar samples. In the case of exposure to pH2 sulphuric acid, hardly any deterioration was noted from the CT images when compared to 1% sulphuric acid (Figure 7.57). This again emphasises the need for the accelerated testing to ascertain the performance of various binder systems.

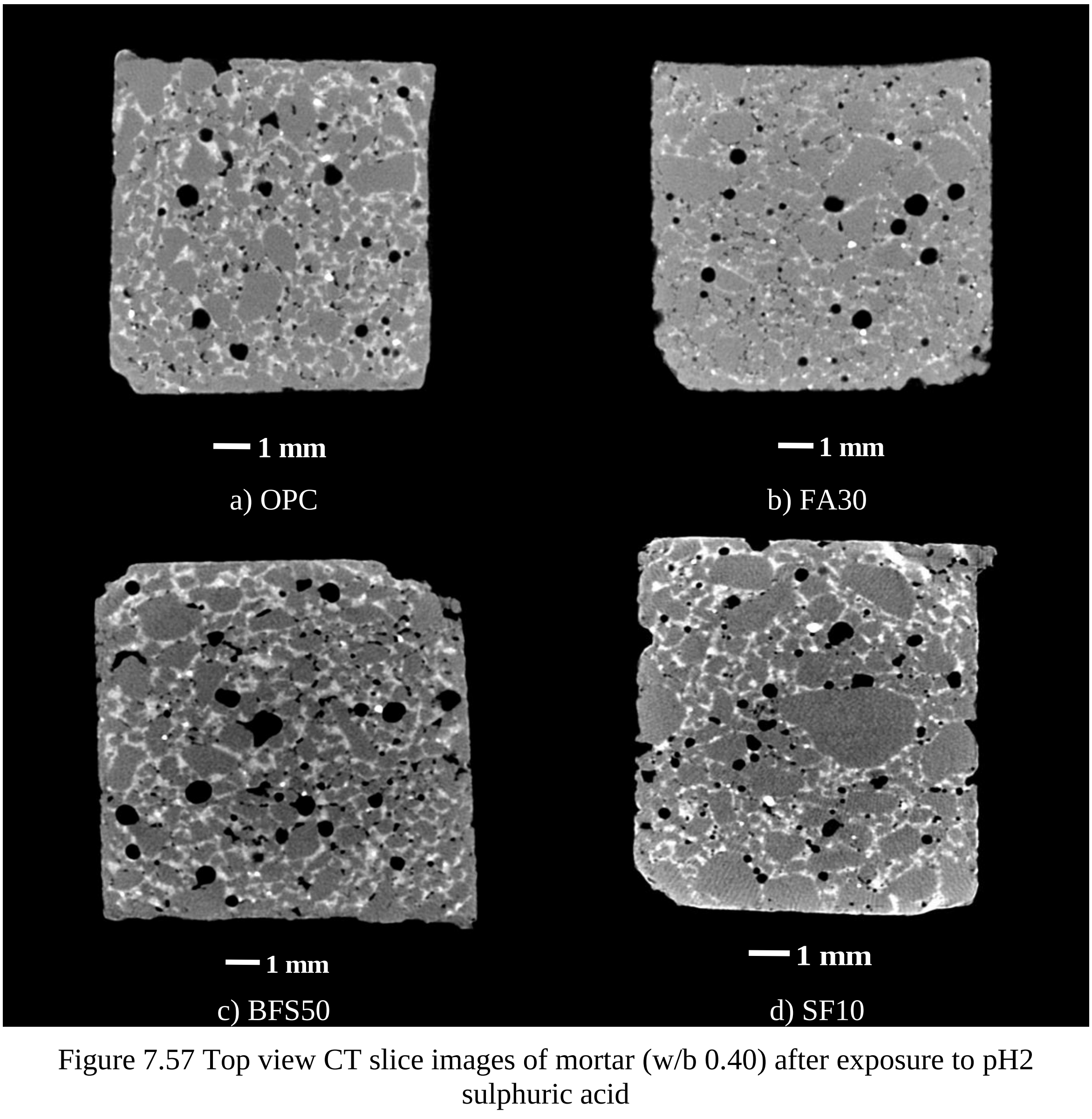

Figure 7.57 Top view CT slice images of mortar (w/b 0.40) after exposure to pH2 sulphuric acid

The mortar samples exposed to acetic acid showed less deterioration outside but had severe degradation inside the specimen as evident from the Figures 7.58 to 7.61. The acid had penetrated to the full cross-section of the specimen for all the mixes on exposure to 0.5M acetic acid (mortar with w/b 0.40), as evident from Figure 7.58. The paste phase in the mortar appeared dark due to this decalcification. The kinetics in terms of altered depth was found to be higher in mortar when compared to the paste. Hence, it can be inferred that the ITZ in mortar accelerated the degradation kinetics. The paste near the ITZ being more permeable than the bulk paste could be the reason behind this faster progression of decalcification to the inside. Similar to mortar with w/b 0.40, the mortar having w/b 0.55 was also found to have deteriorated completely as evident from the CT images shown in Appendix C (Figure C-56).

The CT images of mortar (w/b 0.40) exposed to 0.25M acetic acid are shown in Figure 7.59. The depth of degradation was found to be less when compared to 0.5M acetic acid. The paste phase in the inner layer appeared brighter compared to the outer degraded layer. This indicates that the inner layer is not much affected by the attack. It is also observed that the depths of degradation of SCM mixes were higher compared to the OPC, the depth being highest for FA30. Similar degradation was evident in the mortar with a w/b of 0.55 and these images are shown in Appendix C (Figure C-57). In the case of 0.125M acetic acid, the degradation depth was found to be limited when compared to 0.25M acetic acid (Figure 7.60) for mortar with w/b of 0.40. The inner layers were not yet attacked by the acid. The mortar with w/b 0.55 showed similar results and these are presented in Appendix C (Figure C-58). In the case of pH4 acetic acid, the degradation depths were higher than 0.125M and were marginally less than 0.25M (Figure 7.61). This could be attributed to the buffer action property of acetic acid. Even though the initial pH is 4, which is less than the pKa value of the acetic acid, it dissociates to supply more acid ions at pKa value. Also, large amount of hydroxyl ions has to be released to increase the pH of the acid solution if the pH is in the range of pKa ± 1. These factors might have contributed to the increased aggressiveness of pH4 acetic acid.

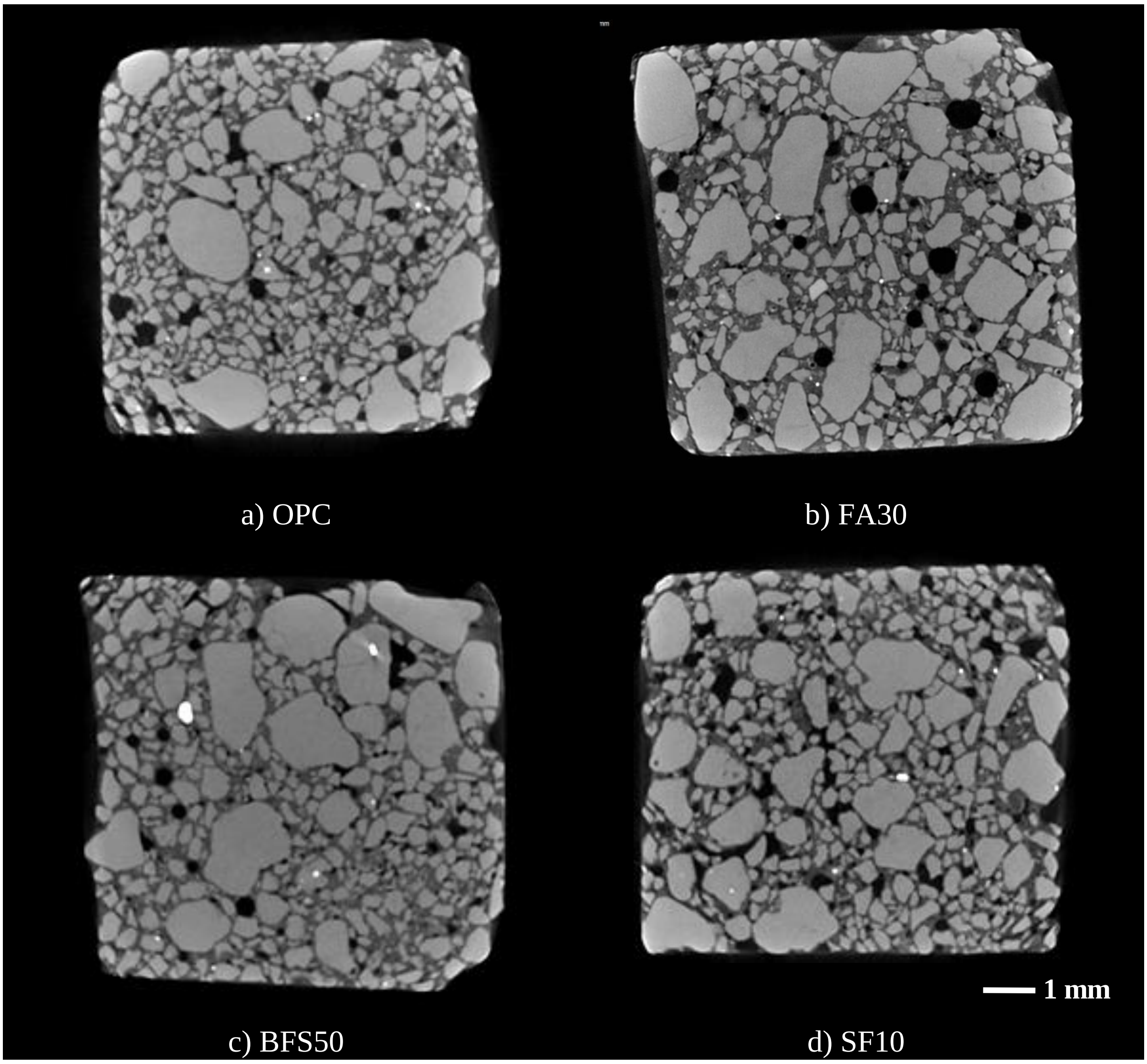

Figure 7.58 Top view CT slice images of mortar (w/b 0.40) after exposure to 0.5M acetic acid

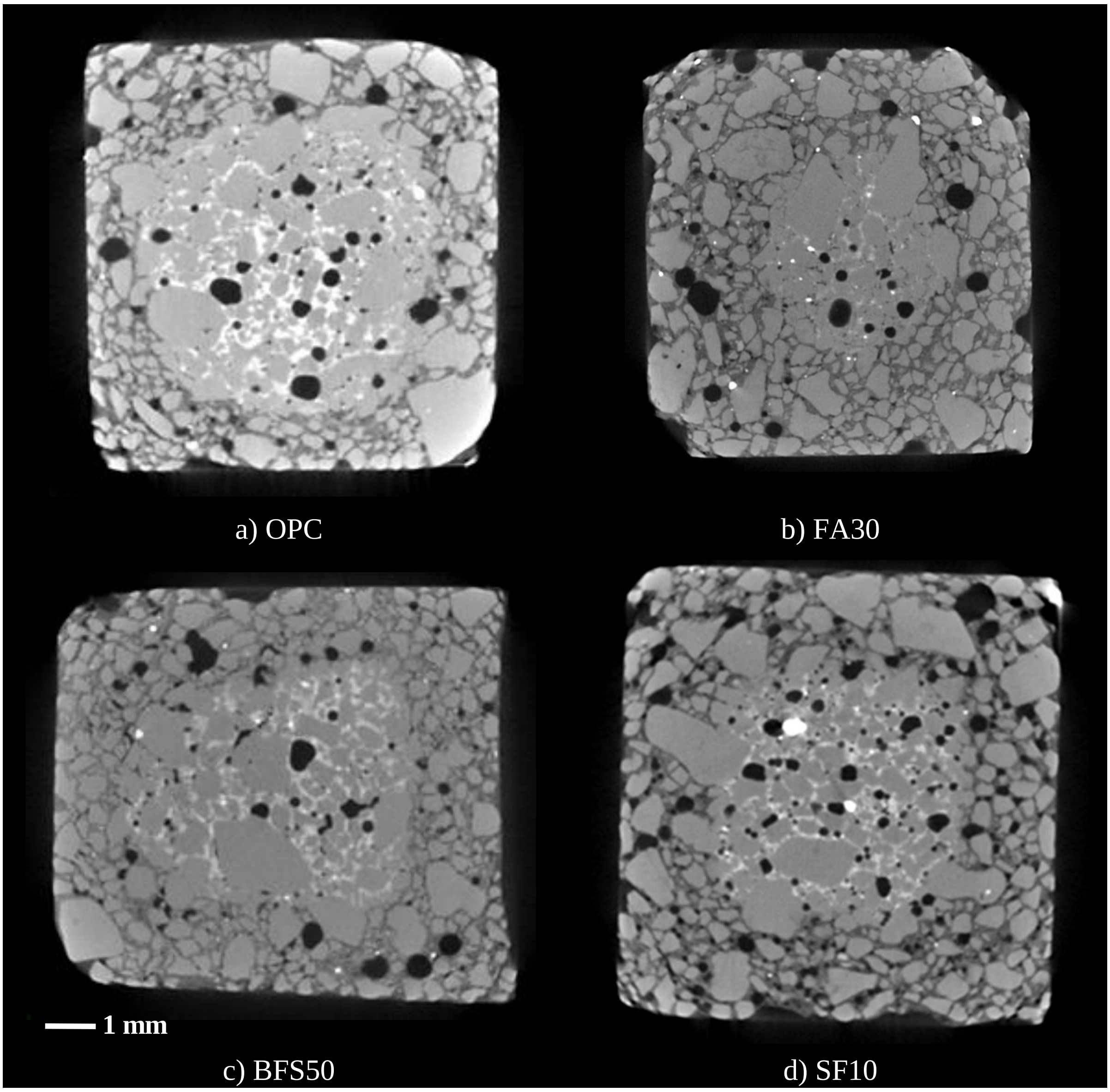

a) OPC

b) FA30

c) BFS50

d) SF10

Figure 7.59 Top view CT slice images of mortar (w/b 0.40) after exposure to 0.25M acetic acid

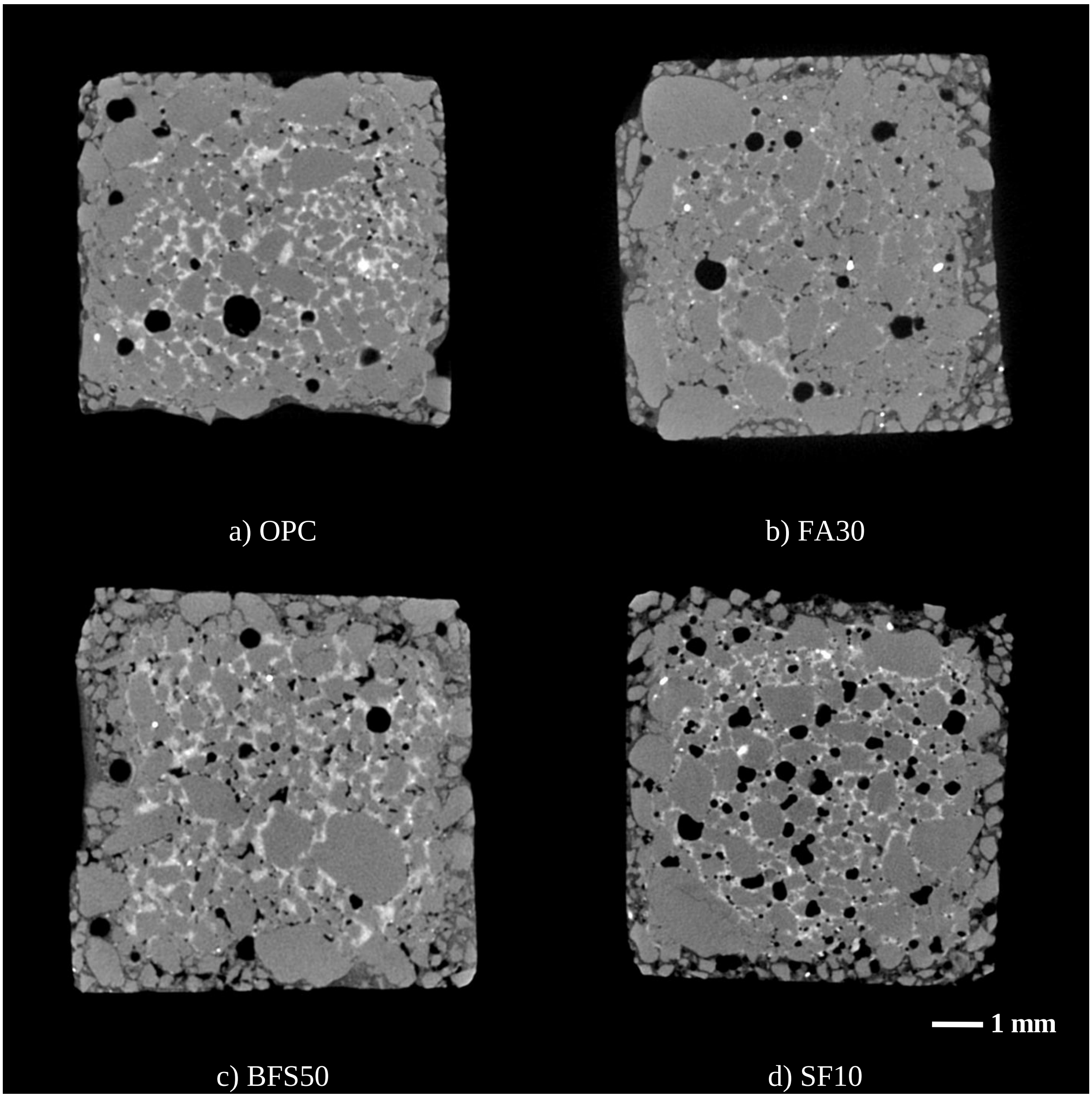

a) OPC

b) FA30

c) BFS50

d) SF10

Figure 7.60 Top view CT slice images of mortar (w/b 0.40) after exposure to 0.125M acetic acid

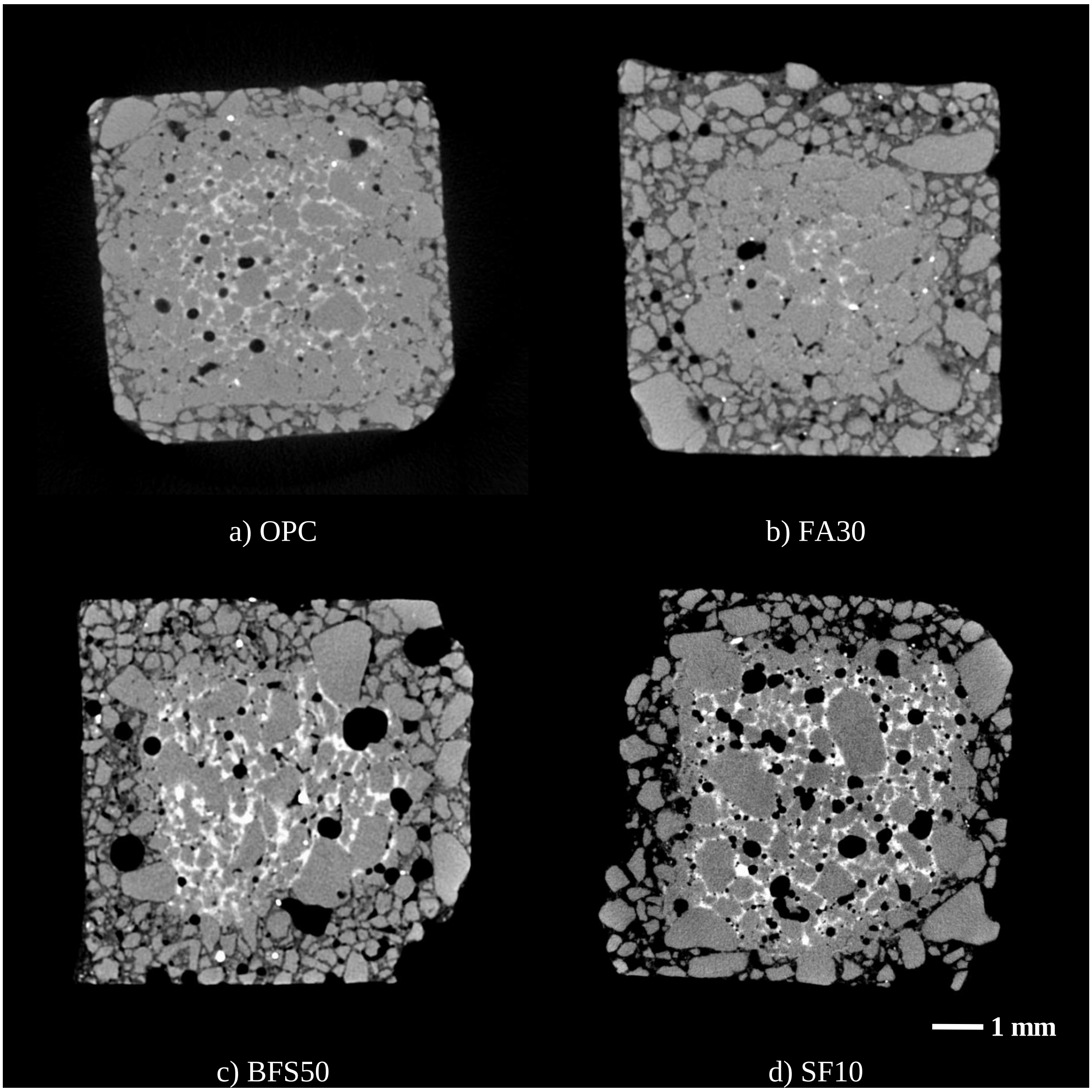

Figure 7.61 Top view CT slice images of mortar (w/b 0.40) after exposure to pH4 acetic acid

The CT images of cylindrical mortar specimens (w/b 0.40) of size 25 × 25 × 35 mm after the exposure to 10 weeks of 3% sulphuric acid are shown in Figures 7.62 to 7.66. The CT slice image of OPC mortar showed severe degradation at the periphery of the specimen (Figure 7.62). It is clearly evident that a portion of the degraded layer has already been exfoliated from the specimen at the time of testing. This reconfirms the instability of the corroded layers in OPC mortar. The front view slice image showed severe and continuous cracking, which could lead to delamination of the outer layer further. The 3D rendered image showed the rough surface texture of the specimen wherein the aggregates are exposed. The CT slice image cut through the external degraded layer shows the microstructure of gypsum formed. The gypsum layer was found to be highly porous with wide cracks around the aggregates, which could have formed due to the expansive pressure exerted by the gypsum formation.

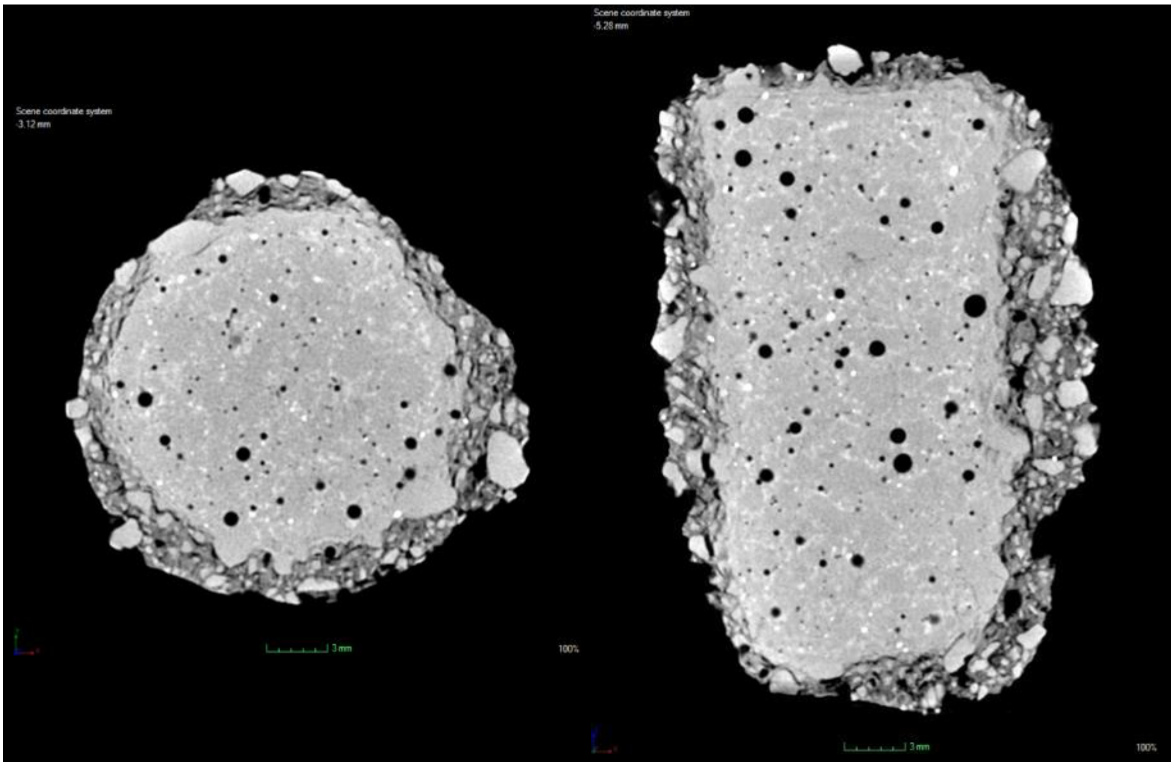

a) Top view slice image - inside

b) Front view slice image - inside

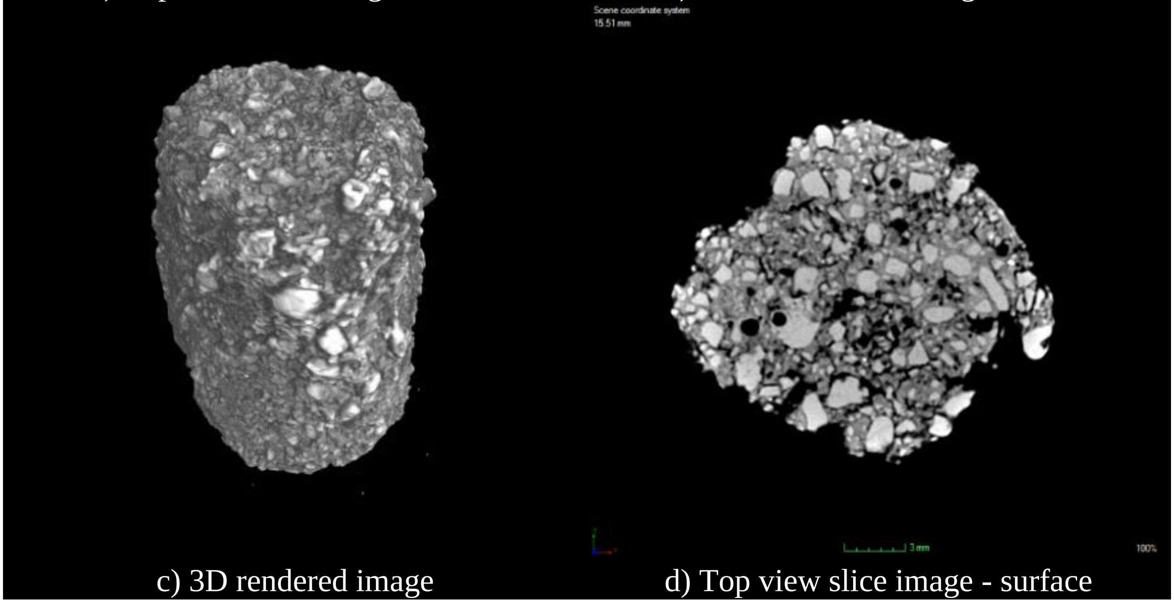

c) 3D rendered image

d) Top view slice image - surface

Figure 7.62 CT images of OPC mortar cylinder (w/b 0.40) after exposure to 3% sulphuric acid

The CT images of FA30, BFS50 and SF10 mortar exposed to 3% sulphuric acid are shown in Figures 7.63 to 7.65 respectively. The deterioration was found to be different from the OPC mortar. Thick degraded layer comprising of gypsum and silica gel was observed in all the SCM mixes. This could be due to the increased amount of CSH gel available in SCM system and limited availability of Portlandite. In the case of FA30 and BFS50, the degraded layer was found to adhere strongly with the matrix. The crack formation around the ITZ was also visible. In the case of SF10, the degradation was found to be severe when compared to FA30 and BFS50, and extensive crack formation was seen in the degraded layer. The CT images cut through the degraded layer for the SCM mortar samples were identical to the OPC mortar showing cracks associated with gypsum formation and expansion. Additionally, front view CT slice images were collected wherein the image represents the section plane passing through the degraded layer (Figure 7.66). All the mortar samples showed severe cracking around the aggregates, which could have led to the increased degradation kinetics. The extent of cracking in BFS50 was less though when compared to the other mixes.

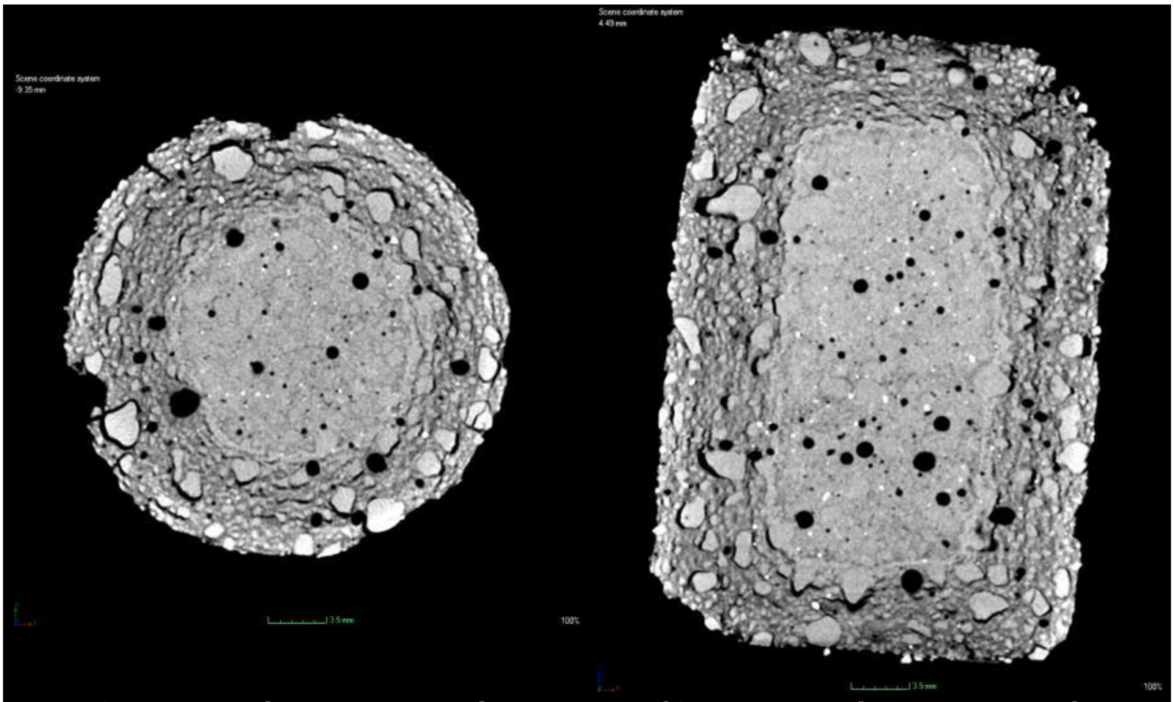

a) Top view slice image - inside b) Front view slice image - inside

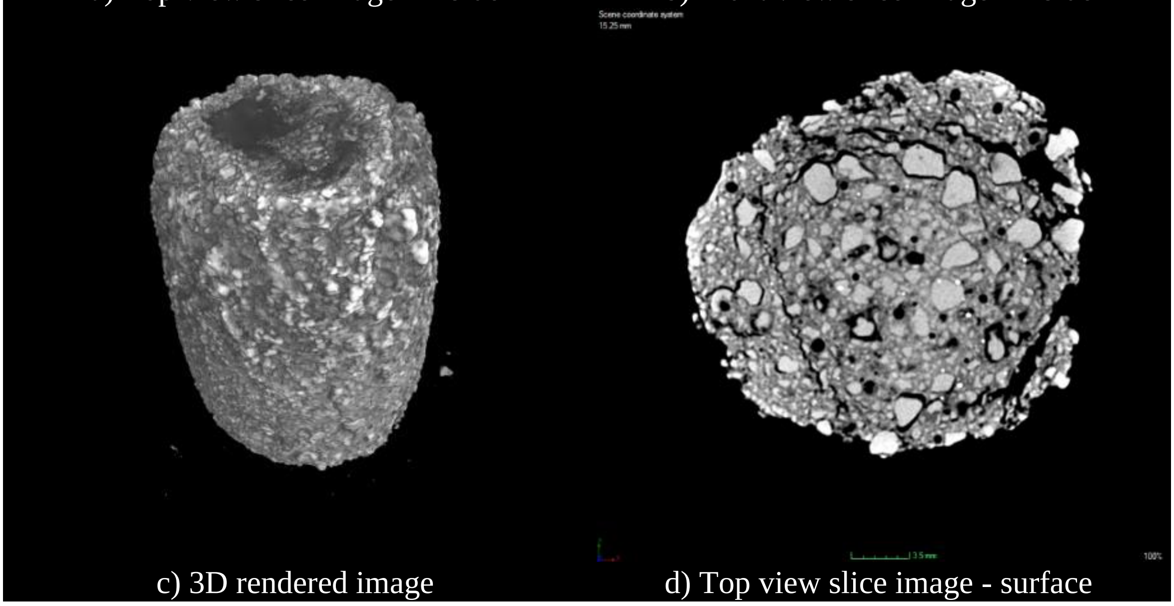

c) 3D rendered image d) Top view slice image - surface

Figure 7.63 CT images of FA30 mortar cylinder (w/b 0.40) after exposure to 3% sulphuric acid

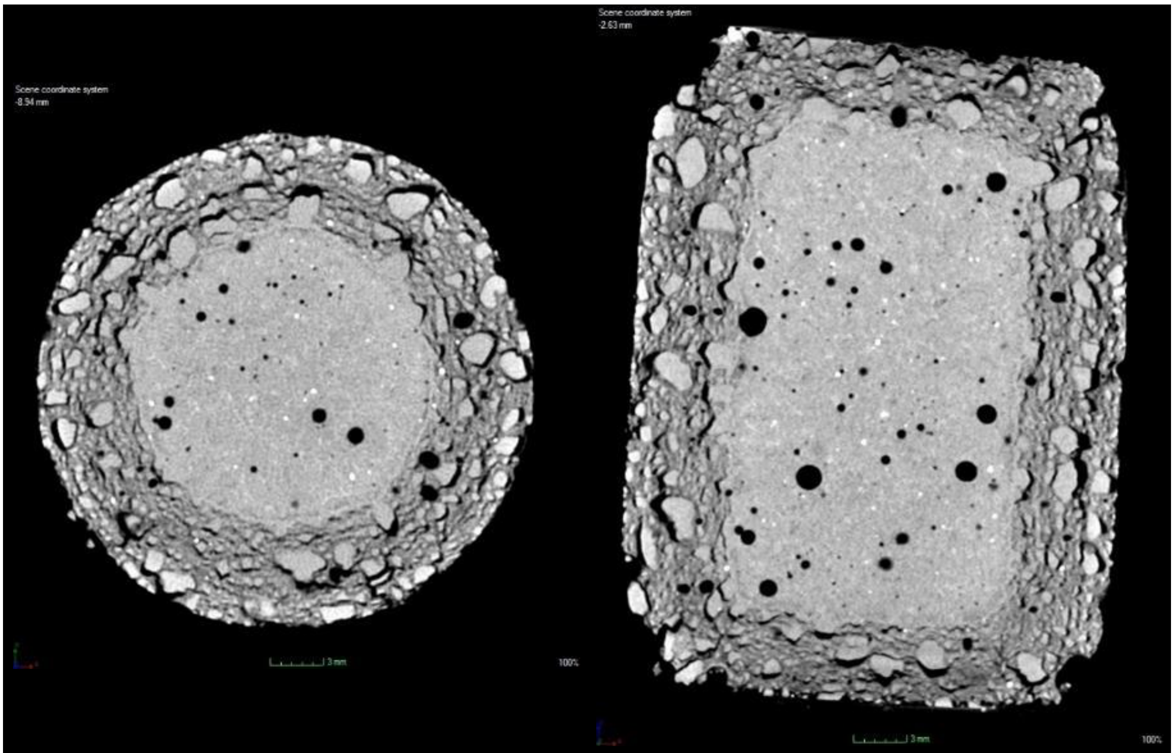

a) Top view slice image - inside

b) Front view slice image - inside

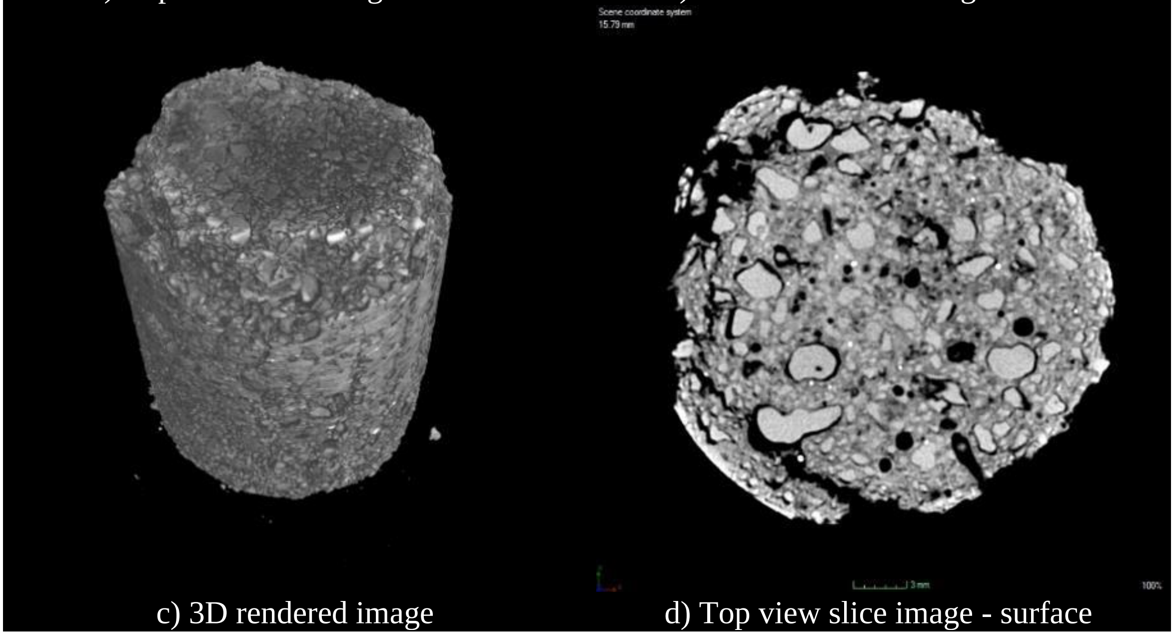

c) 3D rendered image

d) Top view slice image - surface

Figure 7.64 CT images of BFS50 mortar cylinder (w/b 0.40) after exposure to 3% sulphuric acid

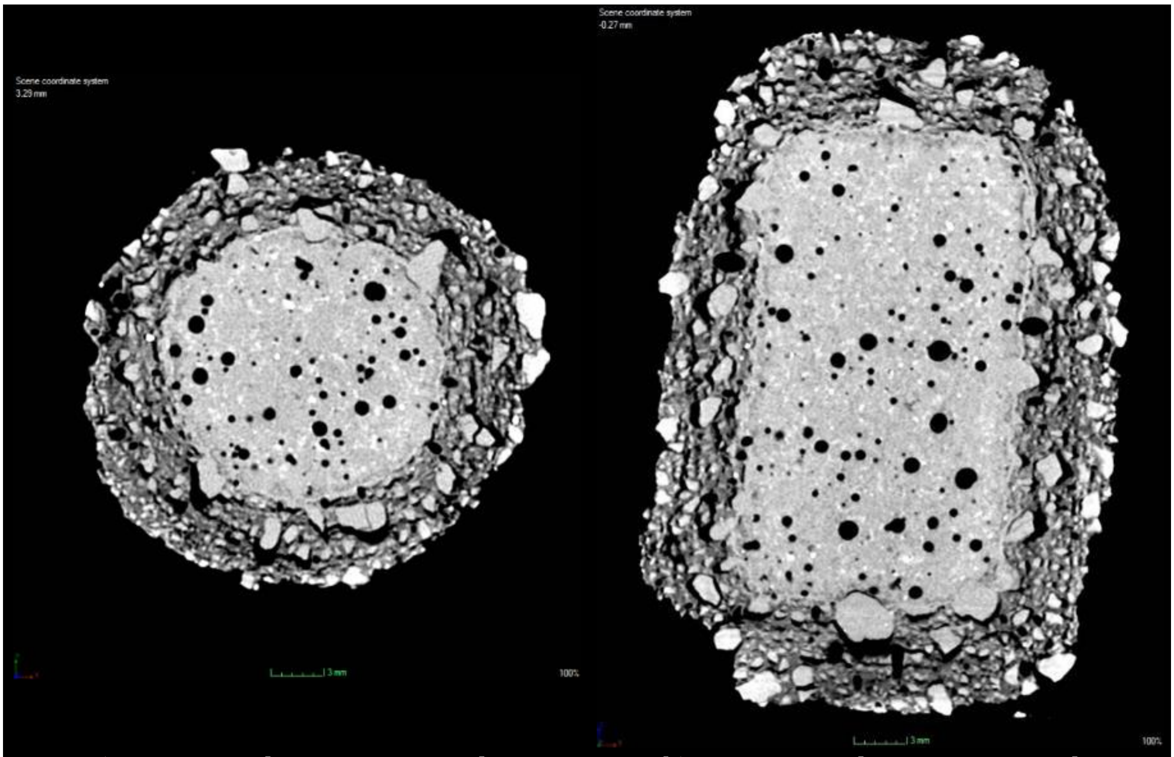

a) Top view slice image - inside b) Front view slice image - inside

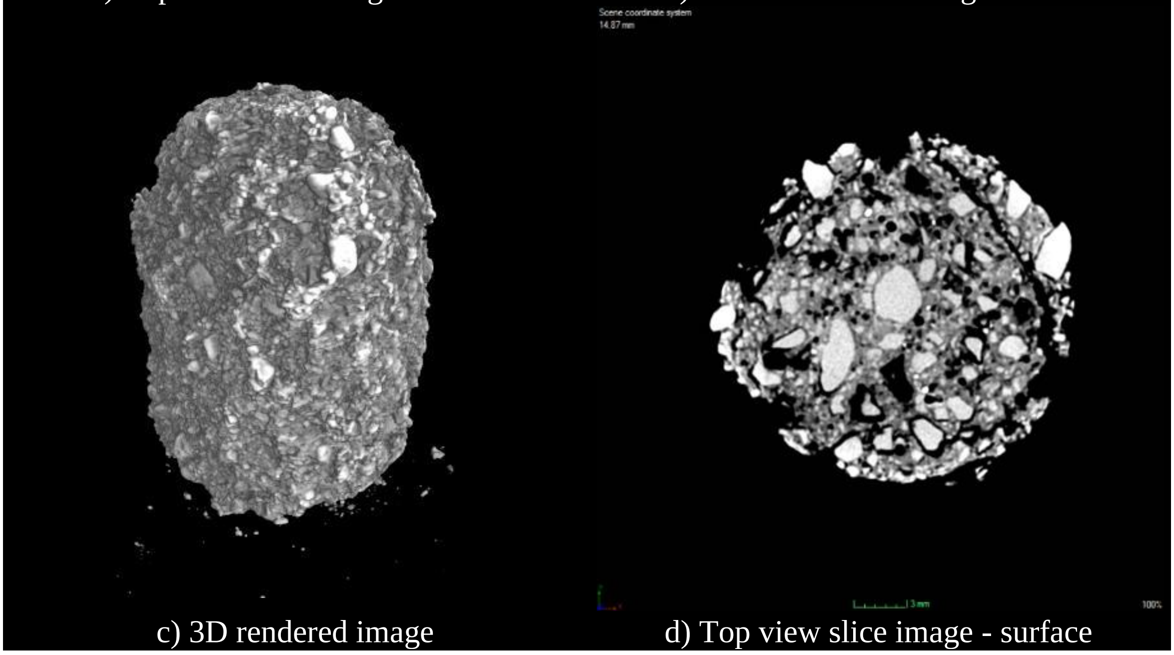

c) 3D rendered image d) Top view slice image - surface

Figure 7.65 CT images of SF10 mortar cylinder (w/b 0.40) after exposure to 3% sulphuric acid

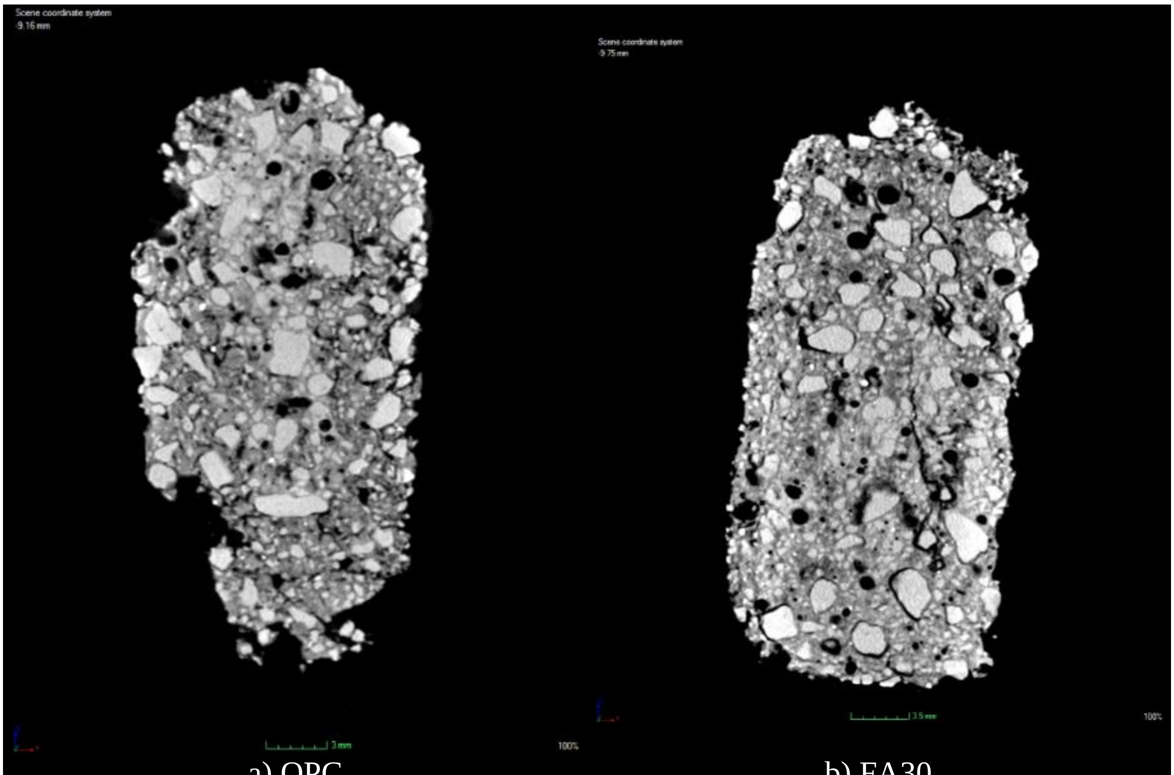

a) OPC b) FA30

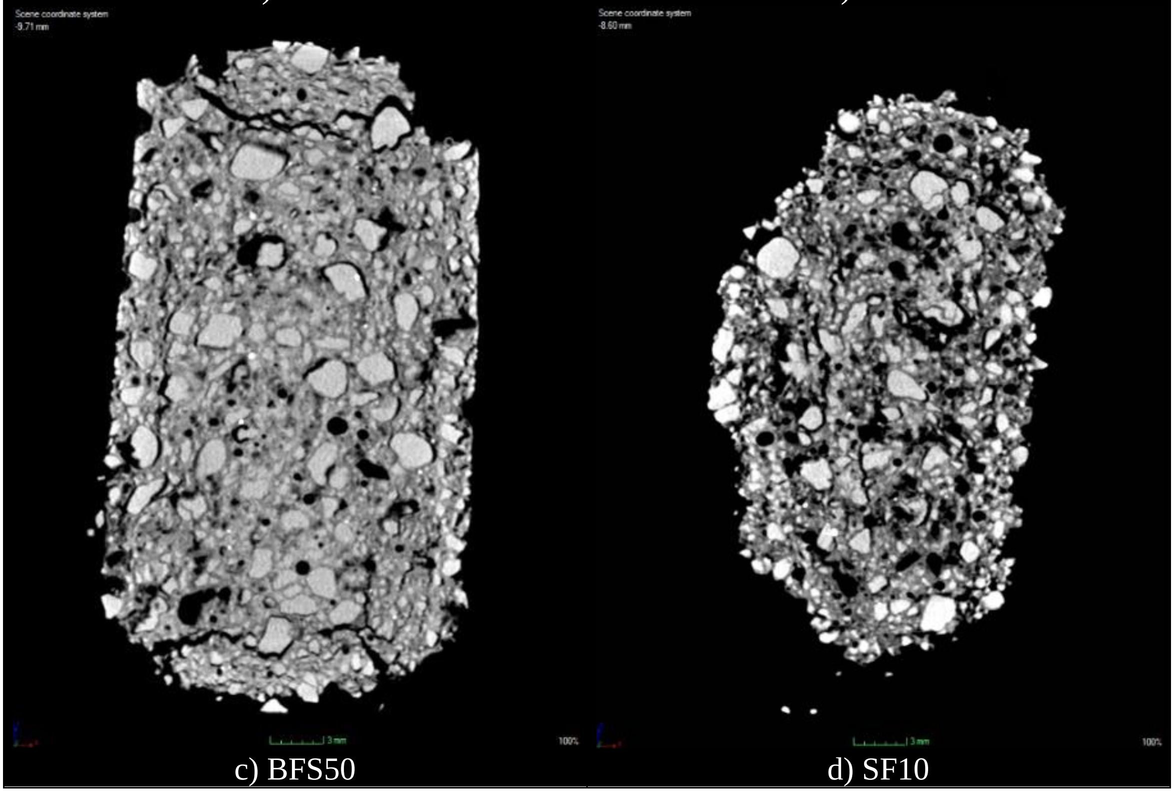

c) BFS50 d) SF10

Figure 7.66 Front view CT slice images cut through the degraded layer of mortar after exposure to 3% sulphuric acid showing extensive cracking around ITZ

7.5.1.2 Special binder systems

The CT slice images of all the mortar samples exposed to 1% sulphuric acid showed degradation in the outer layer (Figure 7.67). The cracks due to gypsum formation were evident in the images. These cracks were seen to be formed around the ITZ which indicates that the attack in mortar progresses through the ITZ. It can also be noted that the depth of degradation of outer layer for HAC mortar was comparatively less than the LC2 mortar. Also, the microstructure of the inner layer of HAC mortar appears to be porous with micro-cracks developed in it. As explained earlier, this could be due to the strength reduction associated with the conversion of hydrated products. The 3D rendered image shown in Figure 7.68 indicates that LC2 mortar had degradation due to precipitates which are expansive in nature. The HAC mortar, however, shows reduction in volume without any damage typically seen due to expansive precipitates.

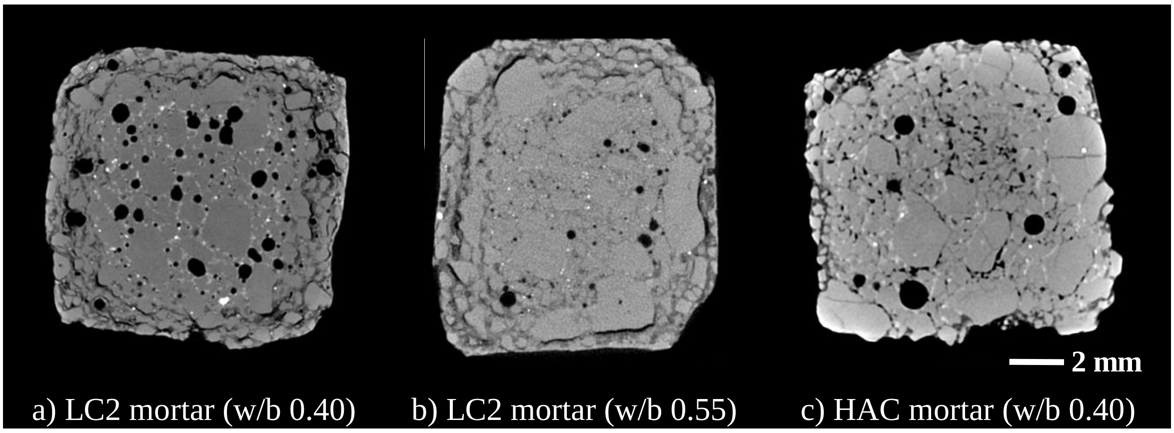

a) LC2 mortar (w/b 0.40) b) LC2 mortar (w/b 0.55) c) HAC mortar (w/b 0.40)

Figure 7.67 CT images of LC2 and HAC mortar on exposure to 1% sulphuric acid

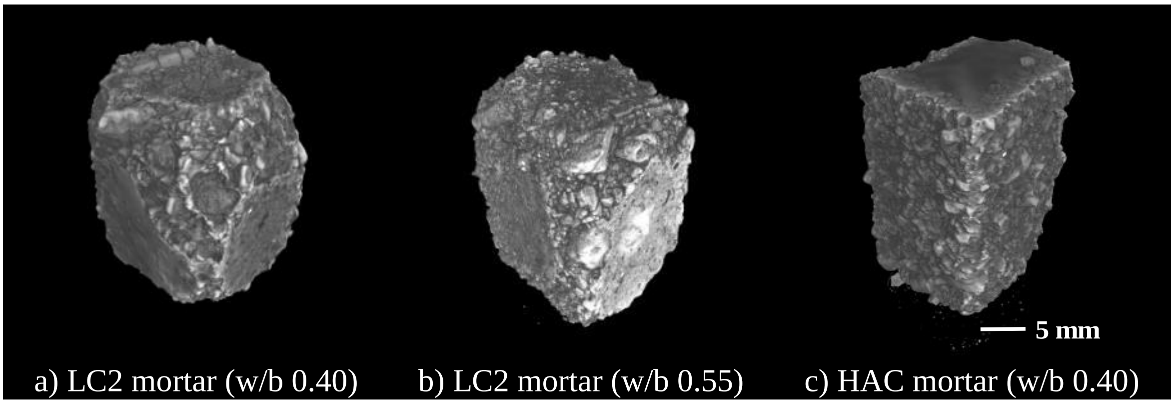

a) LC2 mortar (w/b 0.40) b) LC2 mortar (w/b 0.55) c) HAC mortar (w/b 0.40)

Figure 7.68 3D rendered CT images of LC2 and HAC mortar on exposure to 1% sulphuric acid

The LC2 and HAC mortar on exposure to 0.25M acetic acid showed extensive decalcification of the outer layer (Figure 7.69). The paste in the degraded layer appeared dark which indicates full decalcification to silica gel. The CT image of HAC mortar showed aggregate loss from the specimen, which indicates the severity of attack due to acetic acid. Based on the 3D rendered image shown in Figure 7.70, the HAC mortar seems to have more deterioration compared to LC2 mortar. Similar observations could be noted on specimens exposed to 0.5M acetic acid as shown in Figure 7.71, wherein the entire cross-section of the specimen has been decalcified for LC2 and HAC mortar. More deterioration could be noted for HAC mortar in the 3D rendered images as shown in Figure 7.72.

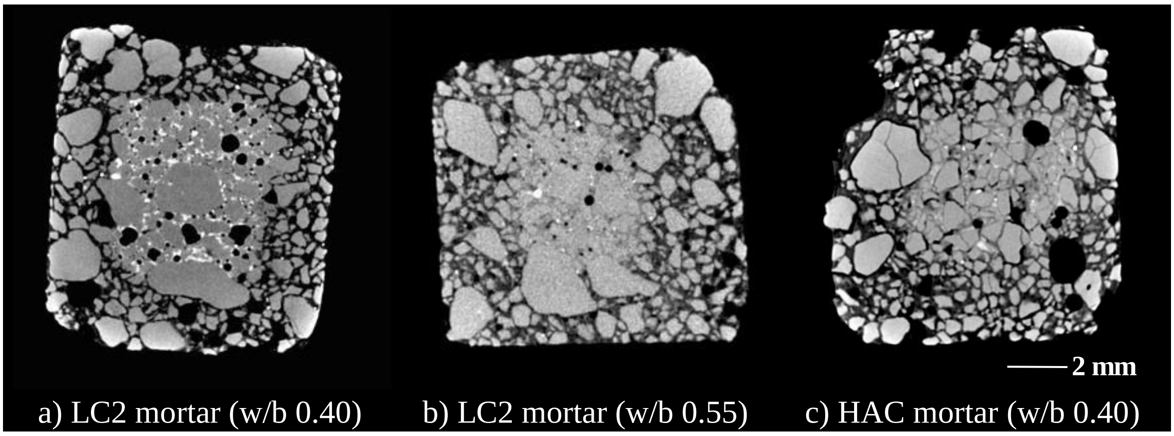

a) LC2 mortar (w/b 0.40) b) LC2 mortar (w/b 0.55) c) HAC mortar (w/b 0.40)

Figure 7.69 CT images of LC2 and HAC mortar on exposure to 0.25M acetic acid

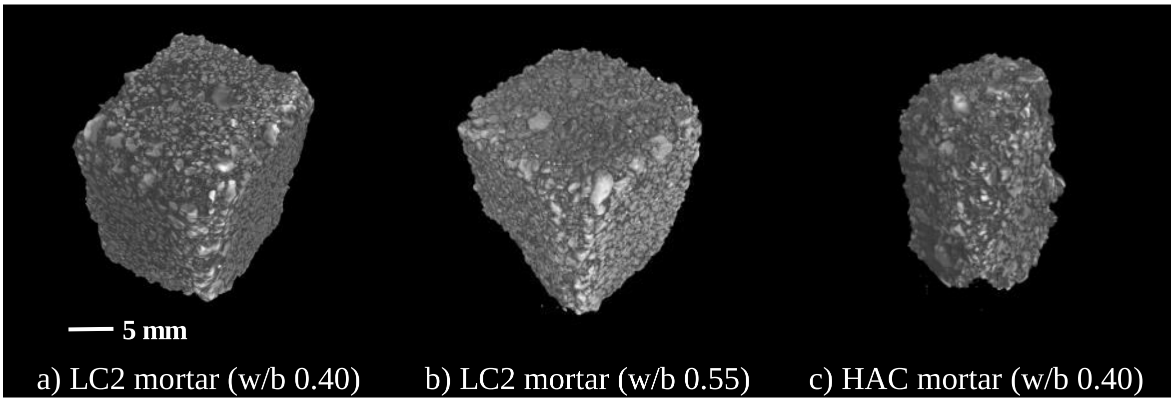

a) LC2 mortar (w/b 0.40) b) LC2 mortar (w/b 0.55) c) HAC mortar (w/b 0.40)

Figure 7.70 3D rendered CT images of LC2 and HAC mortar on exposure to 0.25M acetic acid

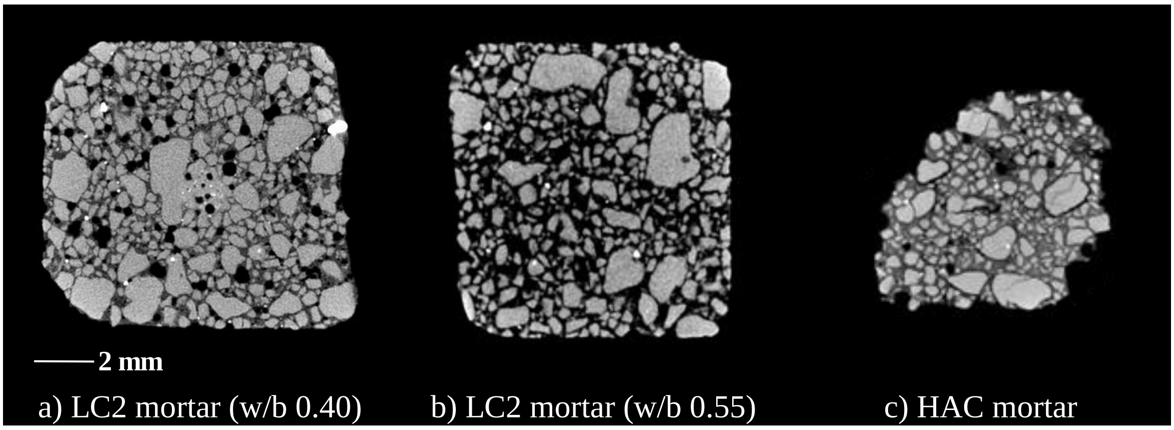

a) LC2 mortar (w/b 0.40) b) LC2 mortar (w/b 0.55) c) HAC mortar

Figure 7.71 CT images of LC2 and HAC mortar on exposure to 0.5M acetic acid

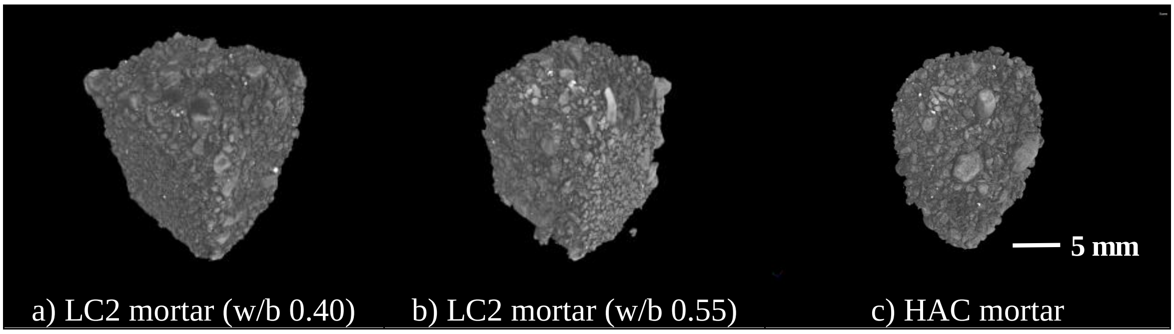

a) LC2 mortar (w/b 0.40) b) LC2 mortar (w/b 0.55) c) HAC mortar

Figure 7.72 3D rendered CT images of LC2 and HAC mortar on exposure to 0.5M acetic acid

7.5.2 Thermo-gravimetric analysis

The consumption of Portlandite due to acid attack was estimated using TGA analysis. The TGA/DTG curves of the mortar samples before and after exposure are provided in Appendix C (Figures C-47 to C-49) and the results are summarised in Table 7.8. On exposure to 1% sulphuric acid, the reduction in Portlandite was calculated to be 58.3%, 73.4%, 42.6% and 62.9% for OPC, FA30, BFS50 and SF10 respectively. A small reduction in the quantity of calcium carbonate is also noted as part of it in the degraded layer might have undergone dissolution in acid. These observations are consistent with the XRD patterns observed explained in the later sections. The dehydroxylation peaks for the transformation of Portlandite were not evident in the TGA/DTG curves of mortar exposed to 0.25M acetic acid (Refer Appendix C, Figure C-49). This indicates that the whole Portlandite in the system has been consumed. In the case of SCM systems, this also implies that there is direct attack on CSH gel due to the non-availability of Portlandite.

Table 7.8 Estimation of Portlandite and calcite contents in mortar (w/b 0.40) before and after acid exposure

Mix	Solution	$Ca(OH)_2$ (%)	$CaCO_3$ (%)
OPC	Saturated lime water	10.21	10.63
FA30	Saturated lime water	7.49	14.69
BFS50	Saturated lime water	2.98	5.03
SF10	Saturated lime water	6.17	10.79
OPC	1% sulphuric acid	4.26	7.24
FA30	1% sulphuric acid	1.99	4.51
BFS50	1% sulphuric acid	1.71	2.89
SF10	1% sulphuric acid	2.29	5.27
OPC	0.25M acetic acid	0.00	8.91
FA30	0.25M acetic acid	0.00	3.62
BFS50	0.25M acetic acid	0.00	4.19
SF10	0.25M acetic acid	0.00	4.56

7.5.3 Scanning electron microscopy

Secondary electron imaging of acid exposed mortar specimens was done primarily to understand the microstructure of degraded products in the outer layer and in the ITZ. The micrograph of OPC mortar (w/b 0.40) exposed to 1% sulphuric acid (Figure 7.73(a)) showed ITZ filled with prismatic deposits of gypsum having varied sizes. This indicates that the ITZ area is severely affected due to the attack even at 1% concentration of sulphuric acid. Figure 7.73(b) shows a depression region wherein fine aggregates could have been present. The area was found to be filled completely with gypsum. This might have been formed due to the reaction of Portlandite present in the ITZ with the acid ions penetrating towards inside. Figure 7.74 shows the morphology of the outer degraded layer of OPC mortar exposed to 1% sulphuric acid. The image showed large deposits of fine sized gypsum near to the ITZ region. This precipitation might have blocked the porosity left behind the decalcification of hydrates leading to a protective effect in limiting the penetration of acids to the inside at early ages of exposure and the associated mass gain observed in the study of alteration kinetics. Ettringite was seen in the middle layer as the pH of the pore solution is higher compared to the outer layer (Figure 7.75). Portlandite crystals were found to be stable in the innermost core layer which is not yet attacked by the acid (Figure 7.76). The BFS50 mortar also showed similar morphology on exposure to 1% sulphuric acid. The ITZ in the degraded layer was found to be filled with fine sized gypsum which might be the reaction product of CSH gel and the acid (Figure 7.77). A magnified image of the gypsum deposits (Figure 7.78) shows that the layer is less porous and this could have contributed in limiting the kinetics in the case of 1% sulphuric acid. Figure 7.79 shows a depression region in the outer degraded layer of BFS50 mortar exposed to 1% sulphuric acid showing gypsum, ettringite and silica gel.

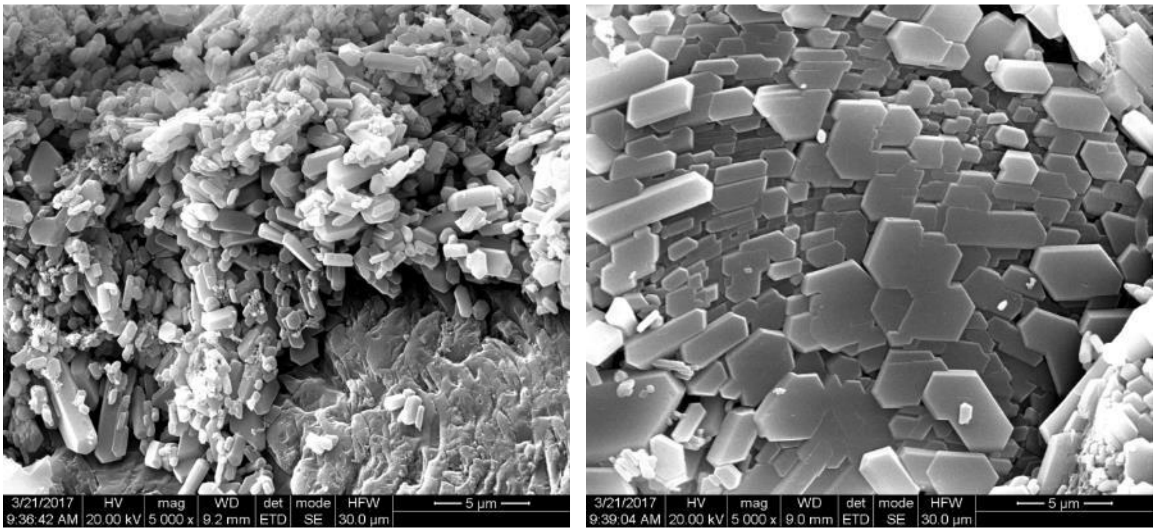

a) ITZ showing gypsum deposits b) ITZ showing gypsum

Figure 7.73 OPC mortar exposed to 1% sulphuric acid showing gypsum in ITZ

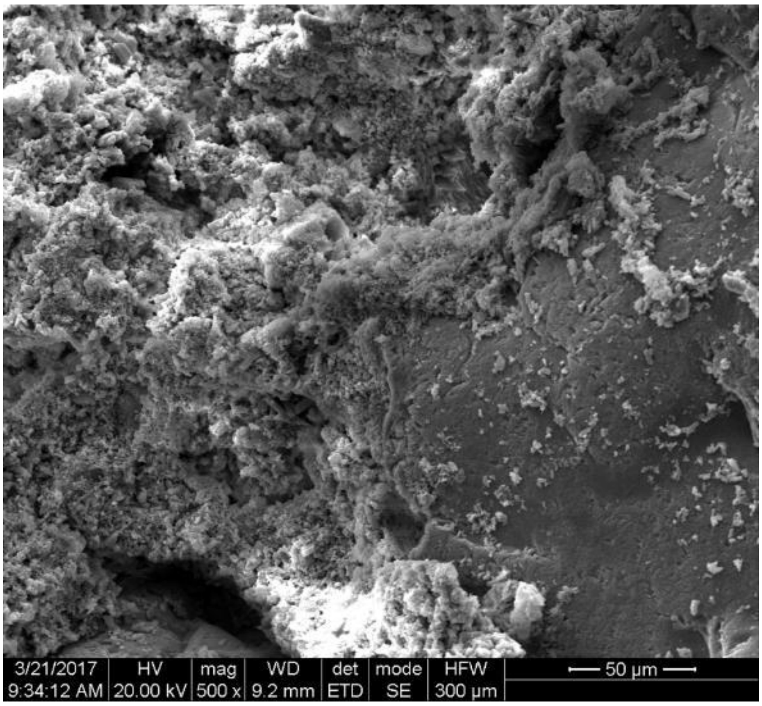

Figure 7.74 Morphology of the outer degraded layer of OPC mortar exposed to 1% sulphuric acid showing finer sized gypsum deposits near to ITZ

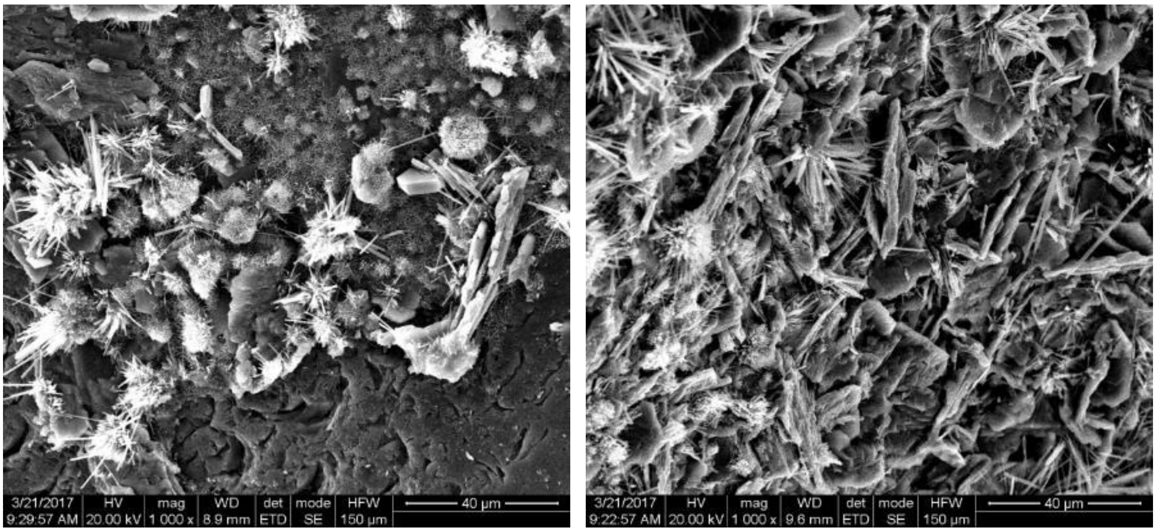

Figure 7.75 Morphology of the inner middle layer of OPC mortar exposed to 1% sulphuric acid showing ettringite formation

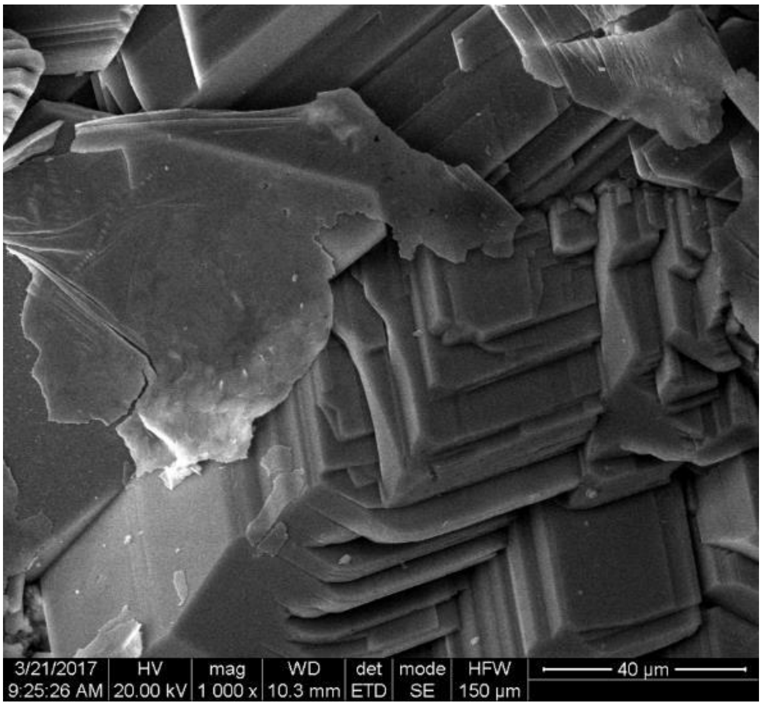

Figure 7.76 The inner layer of OPC mortar exposed to 1% sulphuric acid showing the presence of Portlandite crystals

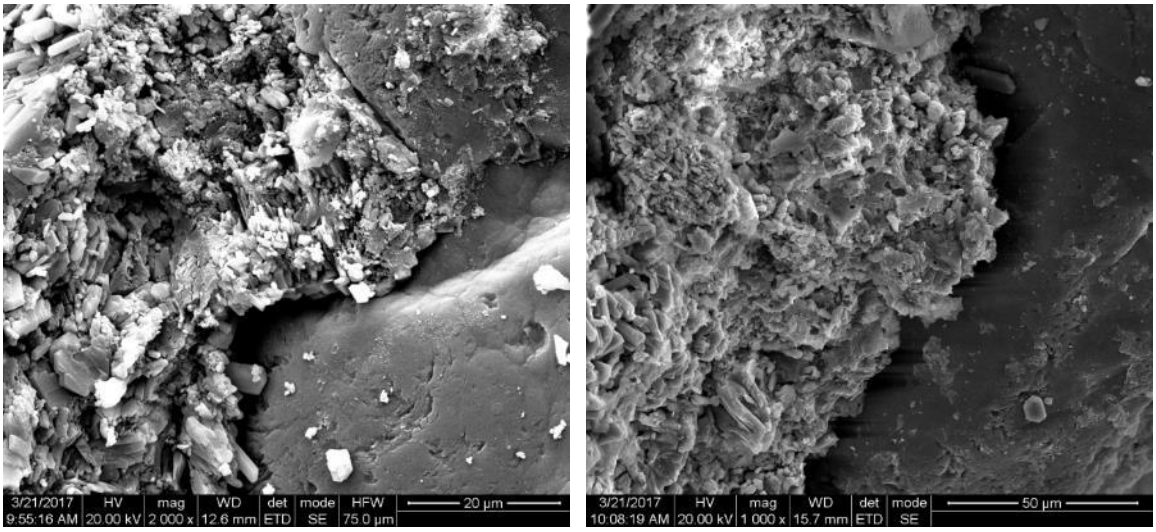

Figure 7.77 Morphology of the outer degraded layer of BFS50 mortar exposed to 1% sulphuric acid showing finer sized gypsum deposits near to ITZ

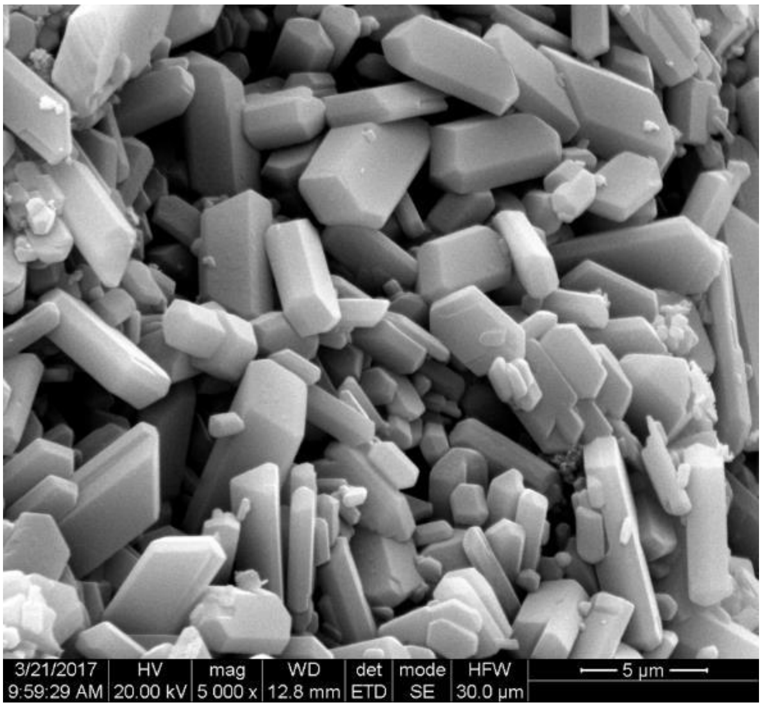

Figure 7.78 Morphology of finer gypsum formed in the outer layer of BFS50 mortar exposed to 1% sulphuric acid

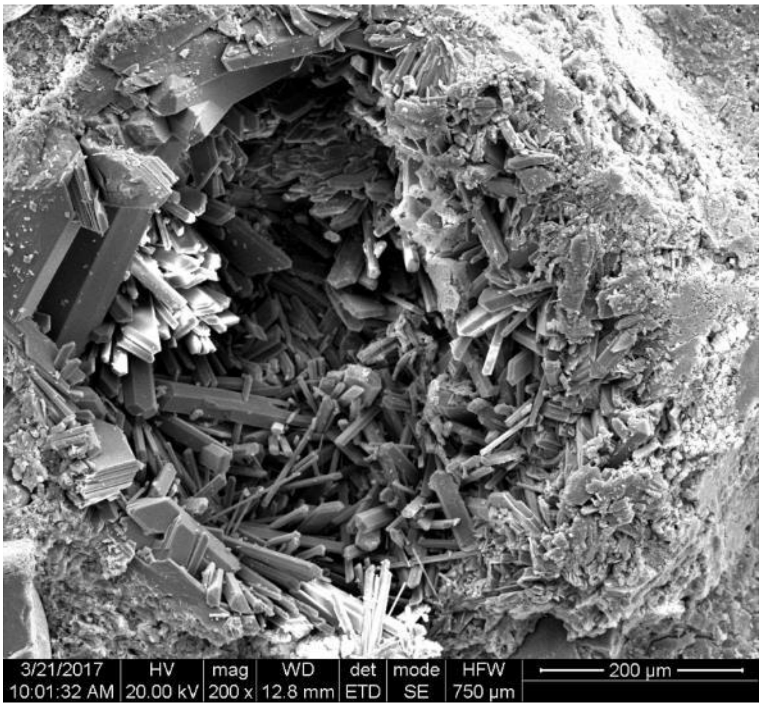

Figure 7.79 A depression region in the outer degraded layer of BFS50 mortar exposed to 1% sulphuric acid showing gypsum, ettringite and silica gel

On exposure to 3% sulphuric acid, thick deposits of gypsum were noted in the degraded layer, which were comparatively larger in size to the gypsum observed in the case of 1% sulphuric acid (Figure 7.80). The size of gypsum being higher, might have led to more expansive pressure leading to loss of mass and delamination of the outer degraded layer.

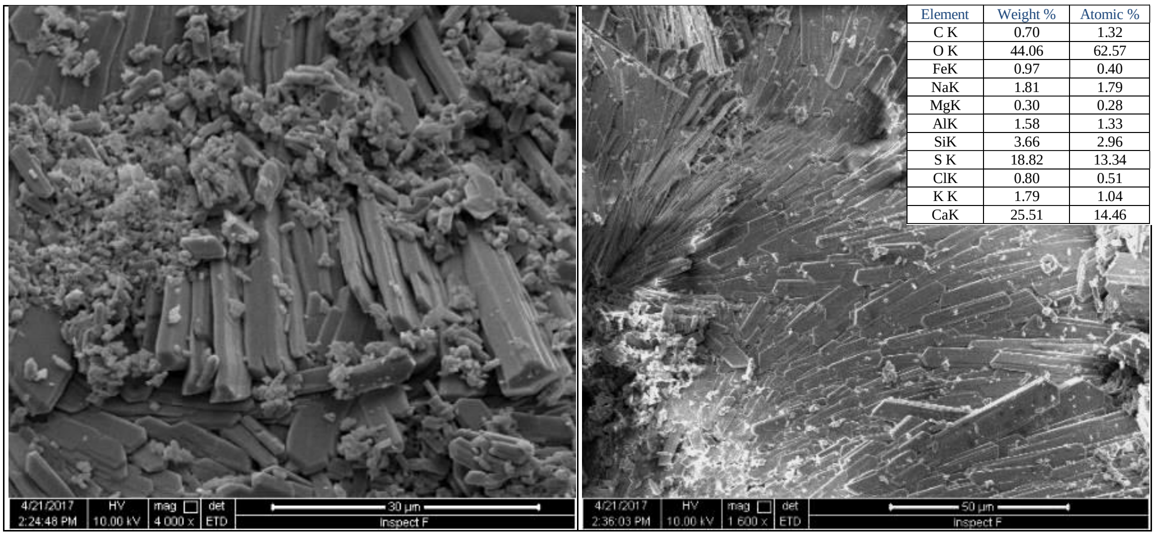

Element	Weight %	Atomic %
C K	0.70	1.32
O K	44.06	62.57
FeK	0.97	0.40
NaK	1.81	1.79
MgK	0.30	0.28
AlK	1.58	1.33
SiK	3.66	2.96
S K	18.82	13.34
ClK	0.80	0.51
K K	1.79	1.04
CaK	25.51	14.46

Figure 7.80 Morphology of the outer degraded layer of BFS50 mortar exposed to 3% sulphuric acid showing columnar deposits of gypsum

The morphology of mortar exposed to 0.25M acetic acid showed granularity and complete deterioration of the outer layer. The microstructure of outer layer of OPC mortar appeared highly porous and disintegrated owing to the formation of silica gel on exposure to 0.25M acetic acid (Figure 7.81). The ITZ in the degraded layer was found to be weak and permeable, filled with loose deposits of silica gel as shown in Figure 7.82. Similar observations were noted in the case of BFS50 mortar also wherein the degraded layer showed granular disintegration. The EDS spectrum (Figure 7.83) revealed the reaction product to be silica gel rich in aluminium and iron. The ITZ was found to be filled with the silica gel which is porous by itself as shown in Figure 7.84. The core layer which is not attacked by the acid showed no granular deterioration and the layer was found to be rich in calcium hydrates (Figure 7.85).

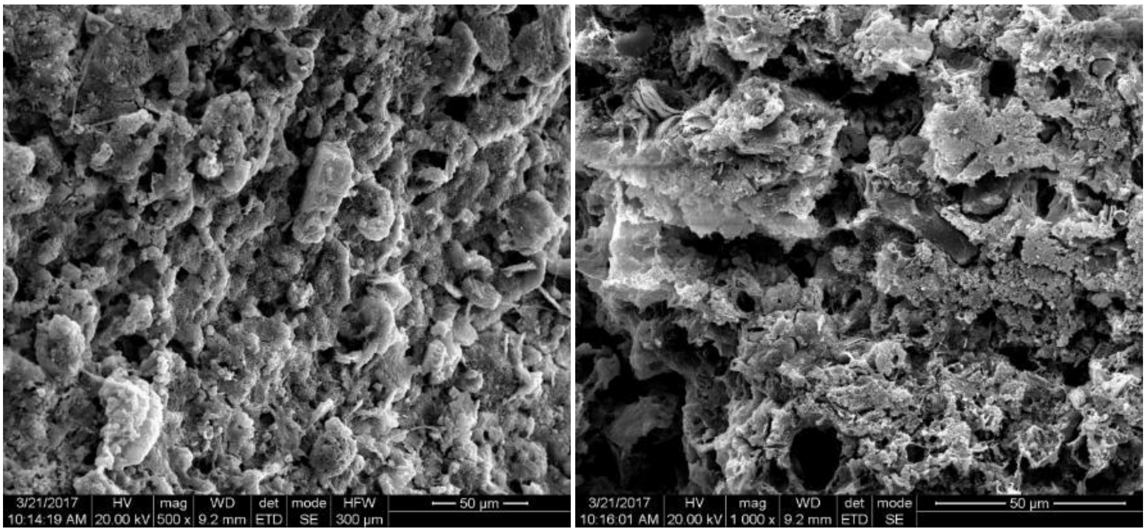

Figure 7.81 Outer degraded layer of OPC mortar exposed to 0.25M acetic acid showing deterioration and porous microstructure

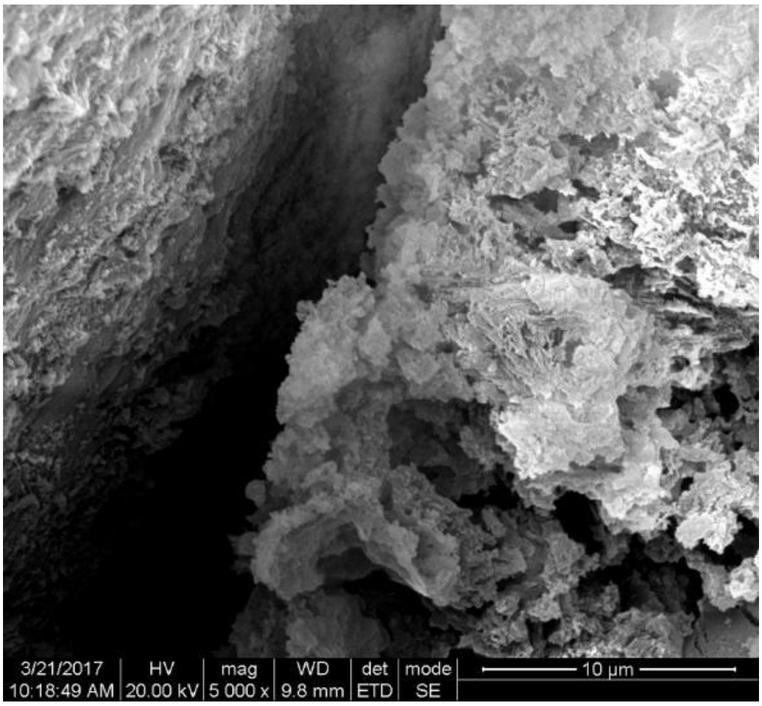

Figure 7.82 A micrograph showing permeable ITZ enriched with silica gel of OPC mortar exposed to 0.25M acetic acid

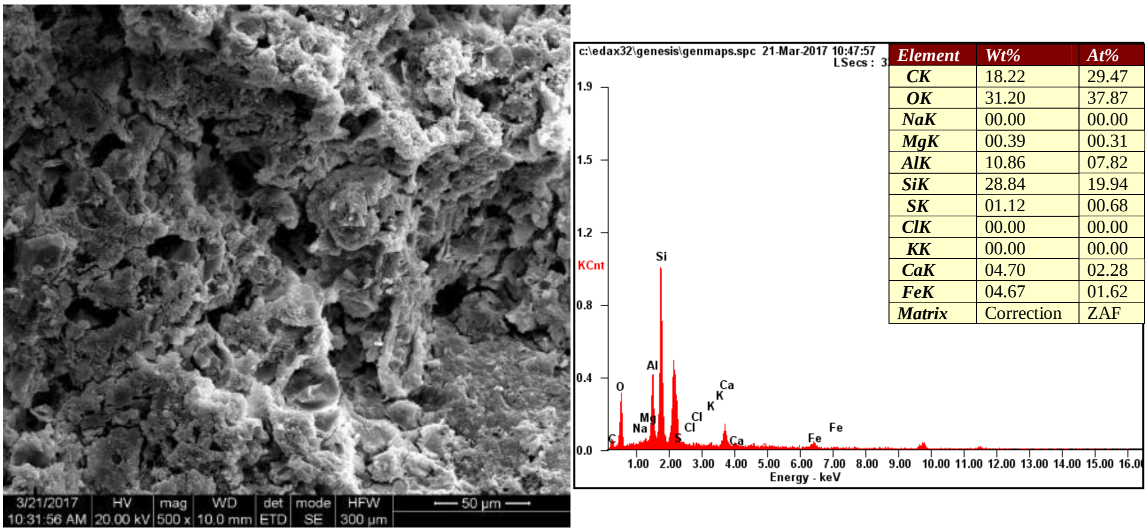

Element	*Wt%*	*At%*
CK	18.22	29.47
OK	31.20	37.87
NaK	00.00	00.00
MgK	00.39	00.31
AlK	10.86	07.82
SiK	28.84	19.94
SK	01.12	00.68
ClK	00.00	00.00
KK	00.00	00.00
CaK	04.70	02.28
FeK	04.67	01.62
Matrix	Correction	ZAF

Figure 7.83 Morphology and EDS spectrum of the outer degraded layer of BFS50 mortar exposed to 0.25M acetic acid

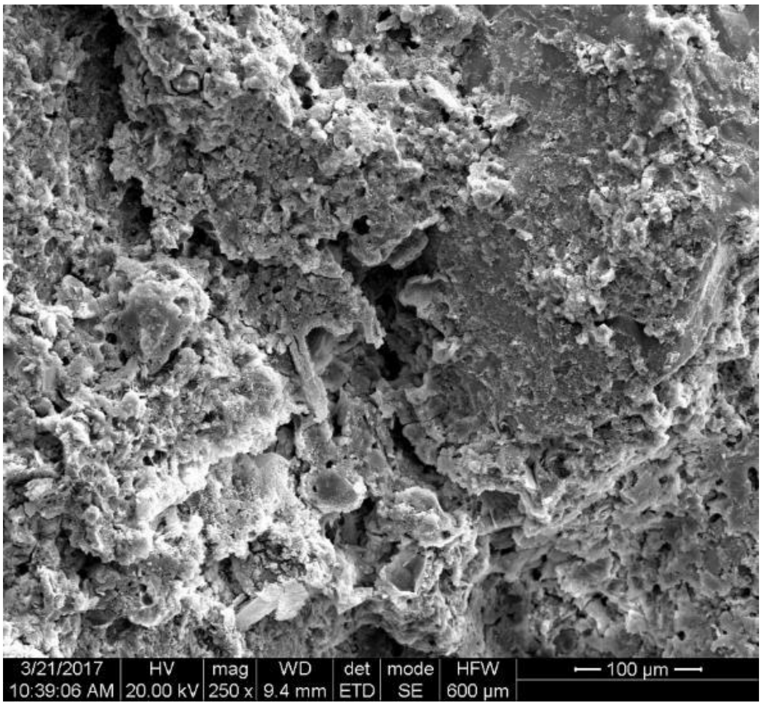

Figure 7.84 Morphology of the outer degraded layer of BFS50 mortar exposed to 0.25M acetic acid showing ITZ filled with silica gel

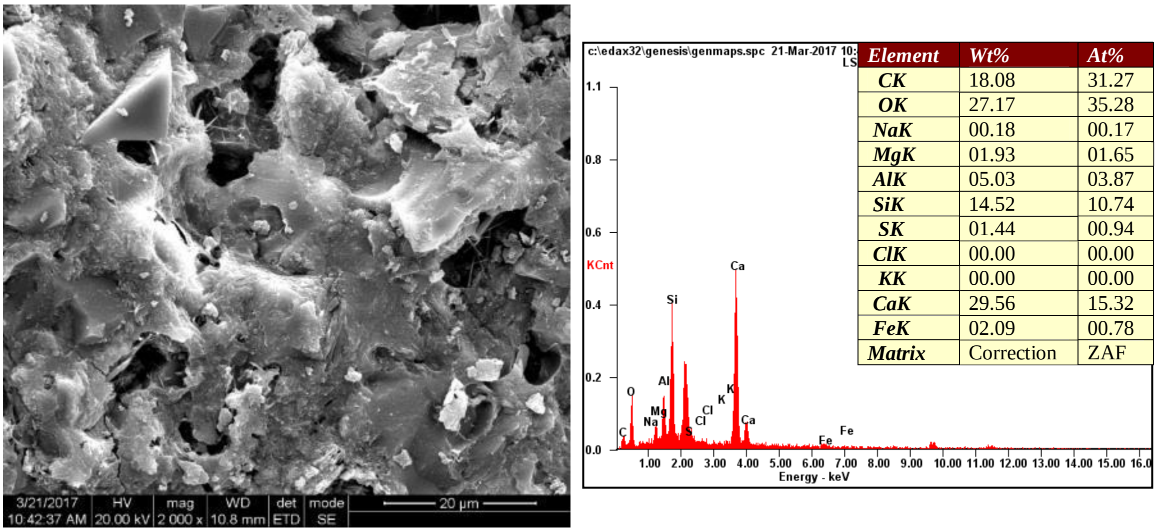

Element	*Wt%*	*At%*
CK	18.08	31.27
OK	27.17	35.28
NaK	00.18	00.17
MgK	01.93	01.65
AlK	05.03	03.87
SiK	14.52	10.74
SK	01.44	00.94
ClK	00.00	00.00
KK	00.00	00.00
CaK	29.56	15.32
FeK	02.09	00.78
Matrix	Correction	ZAF

Figure 7.85 Morphology and EDS spectrum of the inner core layer of BFS50 mortar exposed to 0.25M acetic acid showing presence of calcium rich hydrates

7.5.4 X-ray diffraction

The powdered mortar samples were tested using X-ray diffraction to understand the changes in the mineralogy due to acid attack. The terms L, S and A in the X-ray diffractograms (Figures 7.86 to 7.90) represent saturated lime water, sulphuric acid and acetic acid respectively. The mortar samples before the attack showed the presence of hydrates such as Portlandite (Figure 7.86). The presence of quartz in the fine aggregate resulted in tall peaks due to which other small peaks were not identifiable in the XRD pattern. Other crystalline phases identified in the samples before the exposure include quartz (from fine aggregate), calcite, C_2S, and C_3S. The presence of ettringite and brownmillerite peaks was also noted, but not visible on the diffractogram when compared to the peak intensity of quartz. The mineralogical changes in the OPC mortar exposed to various concentrations of sulphuric acid are shown in Figure 7.87. On exposure to 0.5% sulphuric acid, gypsum was formed in small quantities. Portlandite and anyhydrous phases were still present in the inner layer of the specimen. In the case of 1% sulphuric acid, consumption of Portlandite was evident and increased gypsum formation was noted. The diffractograms for the other SCM mixes were found to be similar to OPC (Figure 7.88). However, no gypsum formation was observed on exposure to pH2 sulphuric acid as no peaks corresponding to gypsum were identified in the X-ray diffractogram. The XRD pattern was similar to the diffractogram before the exposure which explains the less deterioration observed in the CT images and in the kinetics study.

The mineralogical changes in the OPC mortar exposed to various concentrations of acetic acid are shown in Figure 7.89. A substantial reduction in Portlandite was observed for OPC mortar exposed to 0.125M acetic acid. This indicates that Portlandite is highly unstable in acidic environment and the increased consumption could be due to the effect of ITZ. The ITZ is attacked and the Portlandite in the ITZ is decalcified to form the salt which leaches away to the solution. The whole Portlandite present in the system was found to be consumed on exposure to 0.25M and 0.5M acetic acid. Traces of anhydrous phases were still present in the samples exposed to 0.25M acetic acid. However, the sample had turned out to be completely amorphous on exposure to 0.5M acetic acid, with only peaks of quartz and traces of calcite (in the inner layers) present in the XRD pattern. The diffractograms of other SCM mixes also showed similar pattern (Figure 7.90), with an amorphous hump at 20-30° 2θ along with quartz and calcite. These observations are consistent with the deterioration observed in the CT images (Figure 7.58). In the case of pH4 acetic acid, the XRD pattern was similar to 0.125M acetic acid, as the depth of decalcification was limited due to lower concentration of acid at pH4. Similar analysis was carried out for other binder systems exposed to various concentrations of sulphuric and acetic acid and these results are presented in Appendix C (Figures C-50 to C-54).

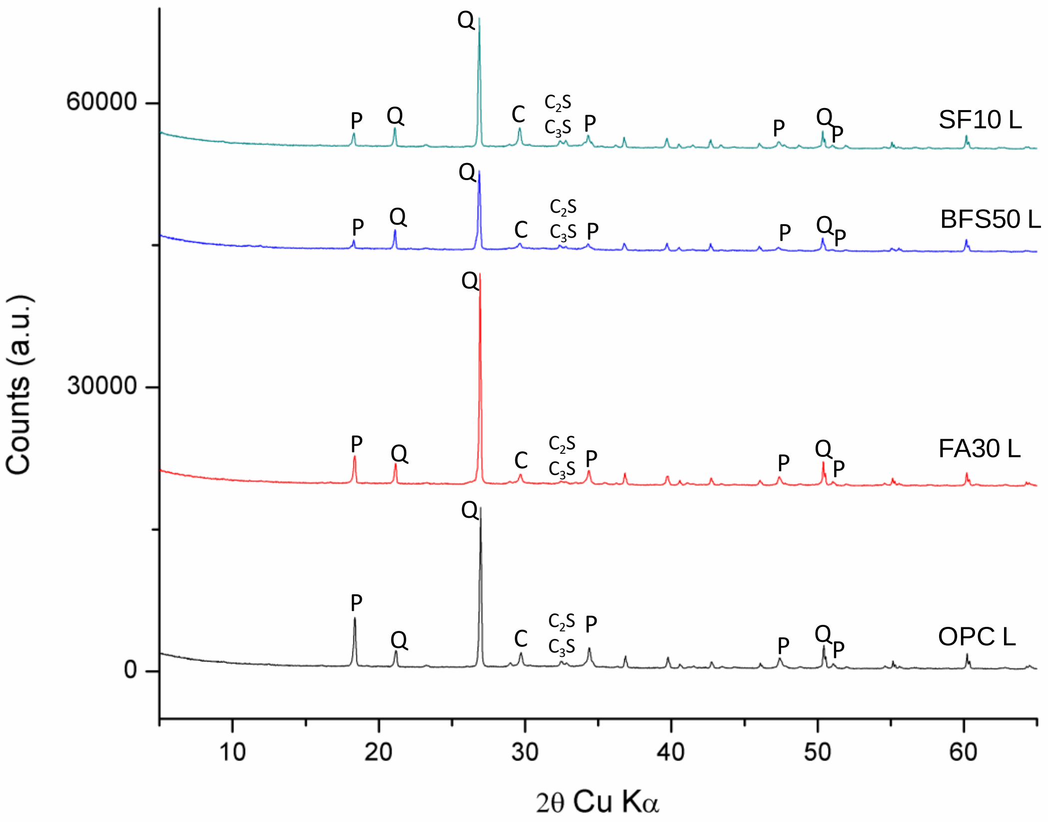

Figure 7.86 X-ray diffractograms of mortar (w/b 0.40) before the acid exposure

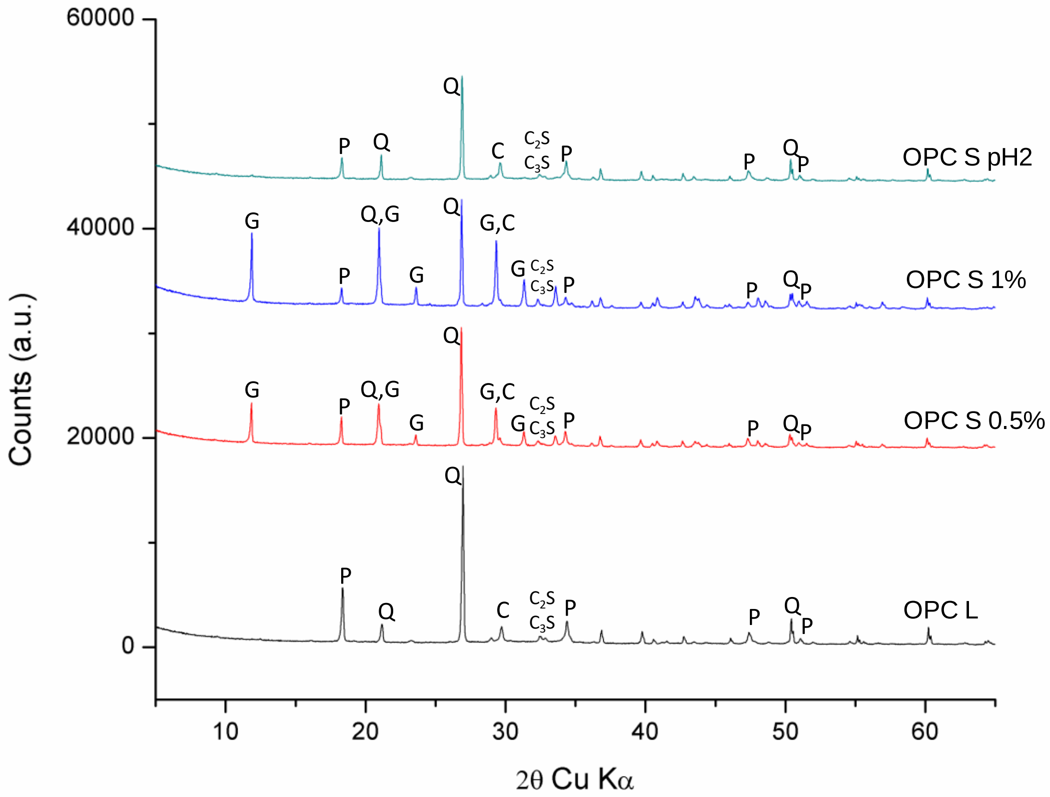

Figure 7.87 X-ray diffractograms of OPC mortar (w/b 0.40) exposed to sulphuric acid

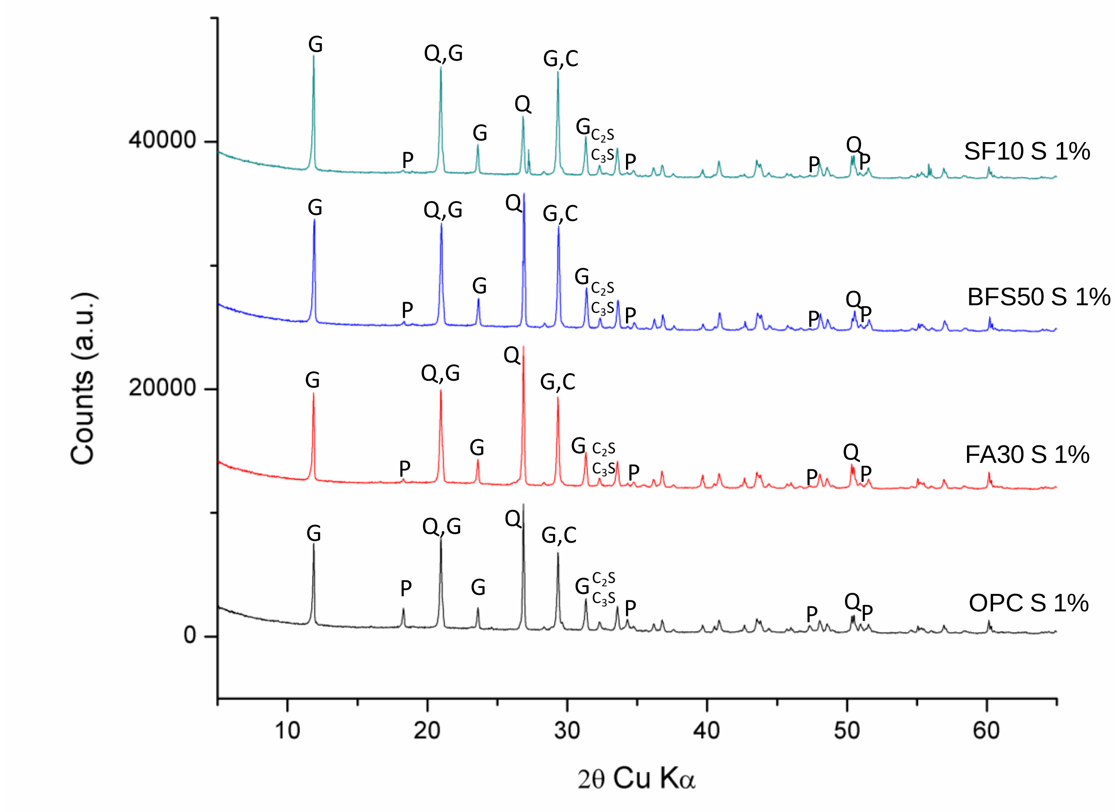

Figure 7.88 X-ray diffractograms of mortar (w/b 0.40) exposed to 1% sulphuric acid

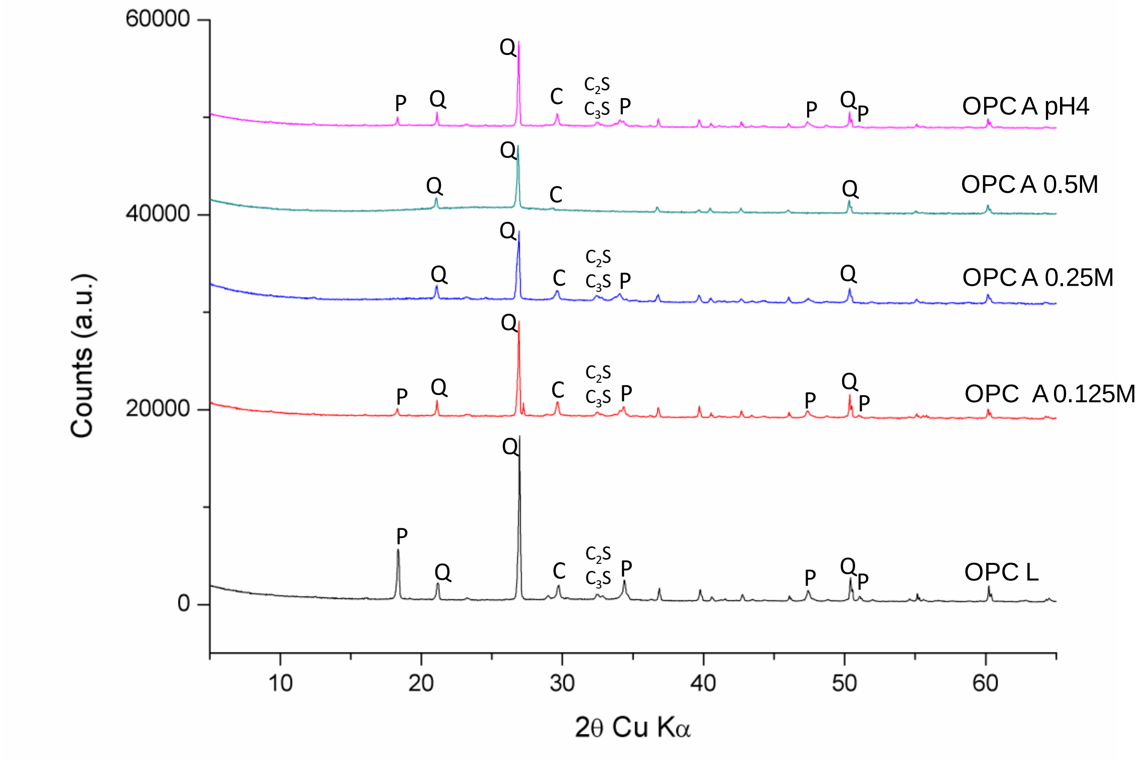

Figure 7.89 X-ray diffractograms of OPC mortar (w/b 0.40) exposed to acetic acid

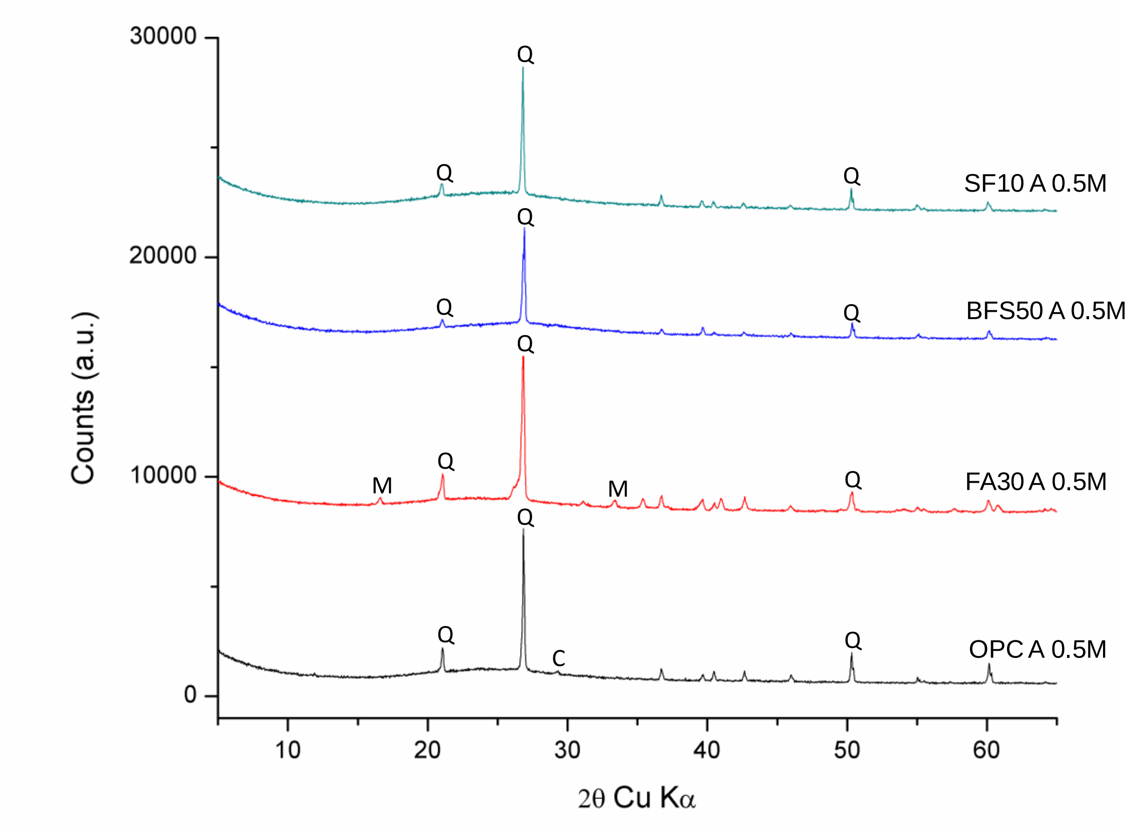

Figure 7.90 X-ray diffractograms of mortar (w/b 0.40) exposed to 0.5M acetic acid

7.6 SUMMARY

The immersion test done for the paste was extended to mortar in order to study the role of binders in mortar and the specific role of ITZ in influencing acid attack. Based on the kinetics study, it is inferred that although mass losses are less for SCMs exposed to lower concentrations of acids, the alteration depths are higher. This indicates the necessity of using multitude of parameters for the performance evaluation of binders. A parameter known as relative dynamic modulus of elasticity was introduced as an additional measure of changes in the physico-mechanical properties due to acid attack.

The study indicated that the use of lower w/b results in higher mass loss in the case of exposure to sulphuric acid. However, lowering the w/b proved to be better on exposure to acetic acid as the mass losses were less when compared to higher w/b. In the case of special binder systems, LC2 mortar showed better performance on exposure to lower concentration of sulphuric acid and acetic acid while HAC mortar showed improved performance on exposure to higher concentration of sulphuric acid. The ITZ present in the mortar was found to accelerate the degradation kinetics. On exposure to sulphuric acid, the ITZ was found to be filled with gypsum deposits and the decalcification of paste resulted in the debonding of aggregates from the matrix resulting in mass loss. However, in the case of acetic acid, no aggregates were lost from the matrix. The ITZ was found to be permeable, filled with silica gel. Thus, for both the acids studied, the presence of ITZ accelerated the degradation kinetics in mortar.

CHAPTER 8

EFFECT OF AGGREGATE TYPE ON ACID ATTACK

8.1 INTRODUCTION

The response of any cementitious material to acid attack clearly depends on architecture of tests as well as various other parameters influencing it, such as acid related, binder related and aggregate related factors. Among the aggregate related factors, the mineralogical nature of the aggregate (calcareous or siliceous) affects the kinetics of degradation. Calcareous (e.g. Limestone) and siliceous aggregates could behave differently when they come into contact with an acidic environment (Alexander and Fourie, 2011). Hence, this chapter aims to investigate the influence of mineralogical nature of fine aggregate on the degradation due to sulphuric and acetic acid. The first section of the chapter discusses on the comparative influence of limestone aggregates on the degradation kinetics when compared to the siliceous aggregates. This is followed by a discussion on the effect of aggregates on altering the physico-mechanical properties of mortar exposed to acids. The last section gives a brief insight into the microstructural changes by imaging using X-ray micro-tomography.

8.2 VISUAL OBSERVATIONS

Immersion test method explained in the section 3.6.3 was used in the study. The aspect of mortar specimens made using river sand (siliceous aggregates, designated as RS) and limestone aggregates (calcareous, designated as LS) before and after the acid exposure is shown in Figure 8.1 and 8.2 respectively. The calcium bearing phases in the cementitious system react with the sulphuric acid to form gypsum salts of low solubility (as shown earlier in Table 2.3). Hence, the salts precipitate as white soft deposits on the specimen. In the case of RS specimens, the aggregates being inert were seen to be exposed. Also, considerable loss of thickness was evident from the visual observations on exposure to high concentration of sulphuric acid (3%). The loss in thickness is attributed to the expansive pressure exerted by the formation of gypsum crystals. However, in the case of

LS specimens, the aggregates were seen to be less protruded compared to the RS specimens. More precipitate formation was seen on the periphery of the specimens on exposure to sulphuric acid. This could be due to the incongruent dissolution of calcium bearing phases from the limestone aggregate acting as sacrificial protection to the dissolution of cement hydrates. Both RS and LS specimens appeared orange brown in colour on exposure to acetic acid. The surface appeared smoother compared to sulphuric acid as the calcium salts formed were highly soluble in the case of acetic acid (as shown in Table 2.3). Hence, thickness changes were found to be less. However, LS specimens appeared to be more porous and degraded when compared to RS specimens.

Before exposure	Without brushing		With brushing		Without brushing	
	1% Sulphuric	3% Sulphuric	1% Sulphuric	3% Sulphuric	0.25M Acetic	0.5 M Acetic

Figure 8.1 Aspect of mortar specimens made with river sand

Before exposure	Without brushing		With brushing		Without brushing	
	1% Sulphuric	3% Sulphuric	1% Sulphuric	3% Sulphuric	0.25M Acetic	0.5 M Acetic

Figure 8.2 Aspect of mortar specimens made with limestone sand

8.3 EFFECT OF AGGREGATE ON DEGRADATION KINETICS

The degradation kinetics was evaluated on mortar specimens of size 10 × 10 × 60 mm by performing a continuous immersion test. In the case of sulphuric acid, the tests were done with and without abrasive action to understand the changes in the kinetics in two different test conditions. However, no abrasive action was used for mortar exposed to acetic acid. The parameters used for understanding the degradation kinetics include mass changes, thickness changes and changes in the pH of the acid solution and the results are discussed below.

8.3.1 Mass changes

The mass changes of specimens are calculated based on the initial mass (mass of the specimen before the acid exposure). The RS mix suffered mass loss on exposure to sulphuric acid due to direct attack on cement hydrates forming gypsum and silica gel. This renders the matrix weak and the binding ability is affected leading to mass loss. However, the LS mix had mass gain for 1% sulphuric acid (Figure 8.3). This could be ascribed to the increased precipitation of gypsum due to increased calcium content of the system. Also, there could be sacrificial protection effect by the limestone aggregates, protecting the hydrates of the cementitious system. This trend is observed for both test cases (with and without brushing). The mass loss of LS mix exposed to 3% sulphuric acid was significantly less than RS mix (Figure 8.4). Periodic abrasive action in the form of brushing accelerated the process of degradation due to the removal of corroded layer of gypsum, which is soft.

Both RS and LS mixes had mass loss on exposure to acetic acid, as leaching was the driving process (Figure 8.5). As the calcium salts are soluble, they leach out to the acid solution making the matrix porous. It was observed that the mass losses of LS mixes were higher compared to RS mixes in acetic acid. This increased mass loss may be attributed to the increased calcium content of the mix and the higher solubility of salts. The protective effect of gypsum clogging the pores in sulphuric acid attack was not present in acetic acid. Also, it is noted that the variation of mass loss is linear with the acid exposure period and is almost directly proportional to the concentration of acetic acid.

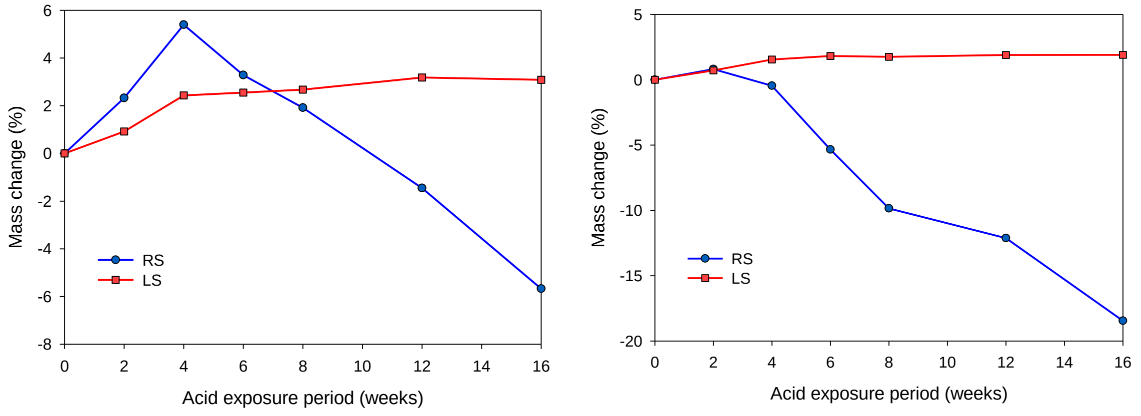

a) without brushing b) with brushing

Figure 8.3 Mass changes of limestone sand mortar and river sand mortar on exposure to 1% sulphuric acid

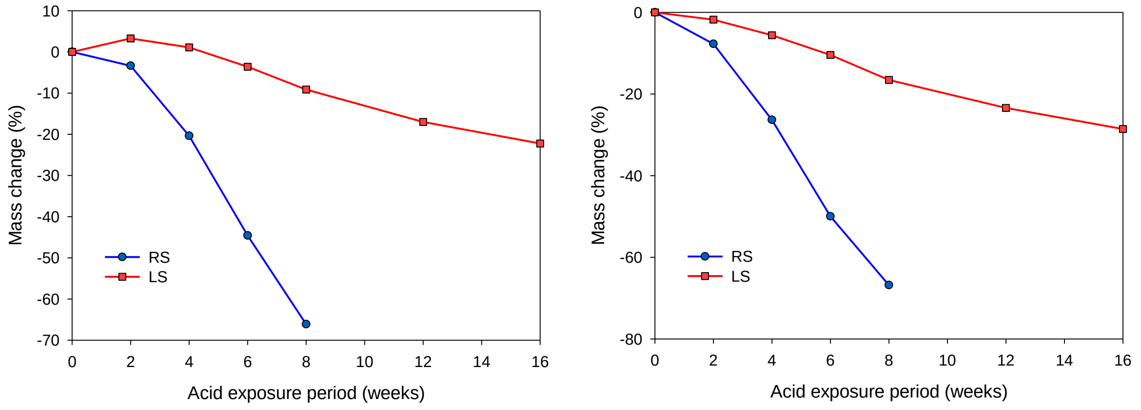

a) without brushing b) with brushing

Figure 8.4 Mass changes of limestone sand mortar and river sand mortar on exposure to 3% sulphuric acid

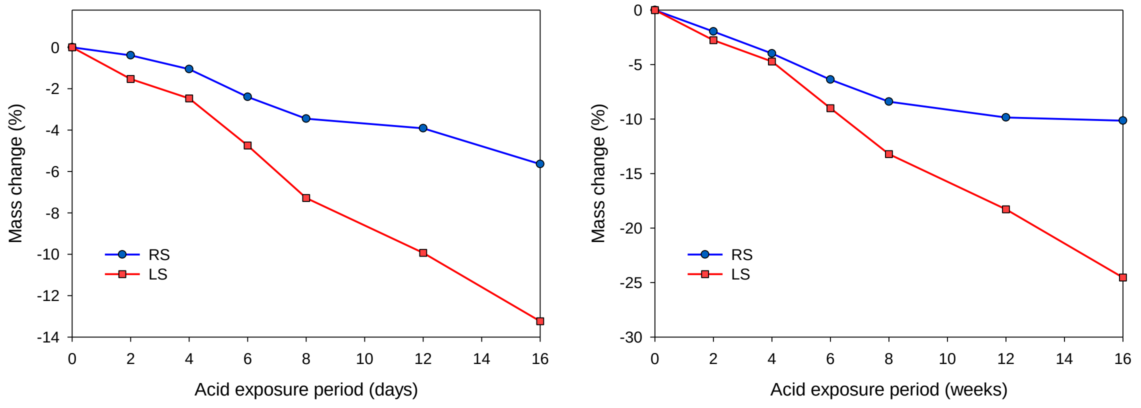

a) 0.25M acetic acid b) 0.5M acetic acid

Figure 8.5 Mass changes of limestone sand mortar and river sand mortar on exposure to acetic acid (without brushing)

8.3.2 Changes in pH of the acid solution

Figures 8.6 to 8.8 show the average pH of the sulphuric and acetic acid solutions measured just before each acid renewal. As strong acids are completely dissociative, their chemical properties are reflected also in the evolution of pH of the solution. Also, the lower pH of sulphuric acid solution compared to acetic acid may be linked with the solubility of calcium salts. The more the solubility of calcium salts, the higher will be the pH of the acid solution on exposure. It was noted that, despite the higher neutralisation capacity of the LS mix (due to acid soluble calcite), there was no significant difference in the pH of the acid solutions between the RS and LS mixes on exposure to lower concentrations of sulphuric (1%) and acetic acid (0.25M). However, the neutralisation effect of LS mix was prominent in higher concentrations of sulphuric (3%) and acetic acid (0.5M). The higher pH of the solutions for LS mix implies that the acid solution is less aggressive and hence leads to lower mass changes and associated degradation.

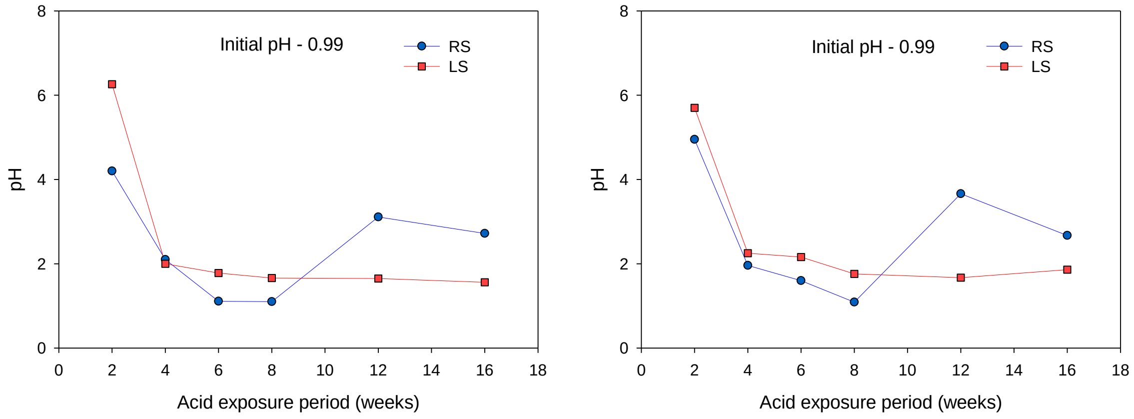

a) without brushing b) with brushing

Figure 8.6 Changes in pH of the acid solution for limestone sand mortar and river sand mortar on exposure to 1% sulphuric acid

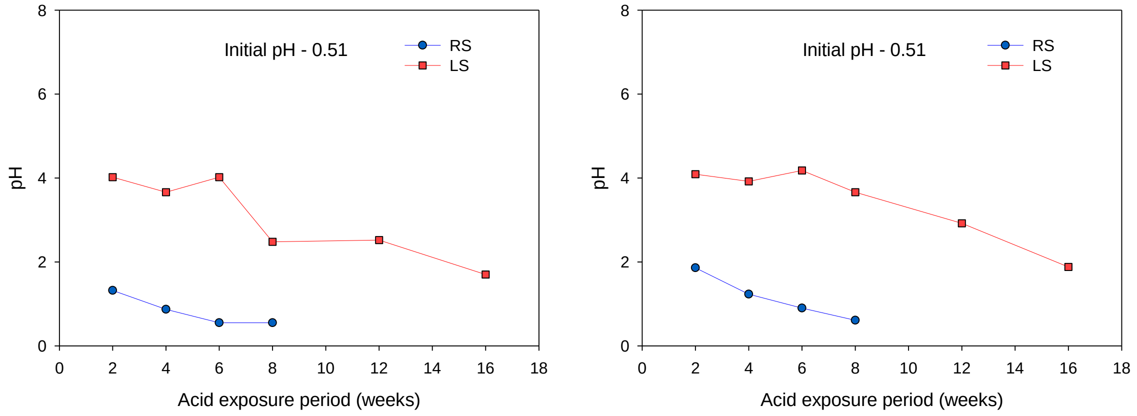

a) without brushing b) with brushing

Figure 8.7 Changes in pH of the acid solution for limestone sand mortar and river sand mortar on exposure to 3% sulphuric acid

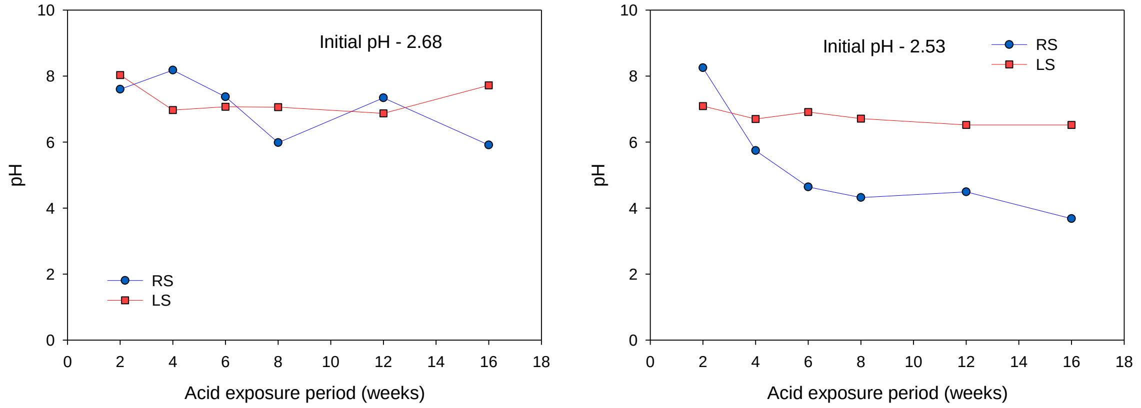

a) 0.25M acetic acid b) 0.50M acetic acid

Figure 8.8 Changes in pH of the acid solution for limestone sand mortar and river sand mortar on exposure to acetic acid

8.3.3 Thickness changes

Similar to mass changes, the thickness changes are calculated based on the initial thickness of the specimens. The thickness changes were found to be in alignment with the mass measurements. Based on the thickness measurements, it is observed that the LS mix performed better on exposure to 1% and 3% sulphuric acid. The residual thickness after the sulphuric acid exposure for the LS mix was higher compared to the RS mix (Figure 8.9). The less thickness change for LS mix may be ascribed to the sacrificial protection and the additional calcium buffer provided by the limestone aggregates. Gypsum was precipitated in large quantities covering the surface of the specimens rendering a protective effect, limiting the kinetics. However, on exposure to acetic acid, LS mix incurred considerably higher loss of thickness when compared to RS mix as evident from Figure 8.10. The additional calcium buffer in the LS mortar leads to the formation of salt in greater quantities (salt is formed from the calcium present in paste and limestone aggregate). But, as the salts are soluble, they leach into the solution, leaving the matrix porous. Additionally, the removal of calcium from the aggregate could affect its stability within the matrix. The paste aggregate bond is affected and all these factors could have possibly led to increased thickness loss in the case of exposure to acetic acid. It was also observed that the change in thickness is directly proportional to the concentration of acetic acid.

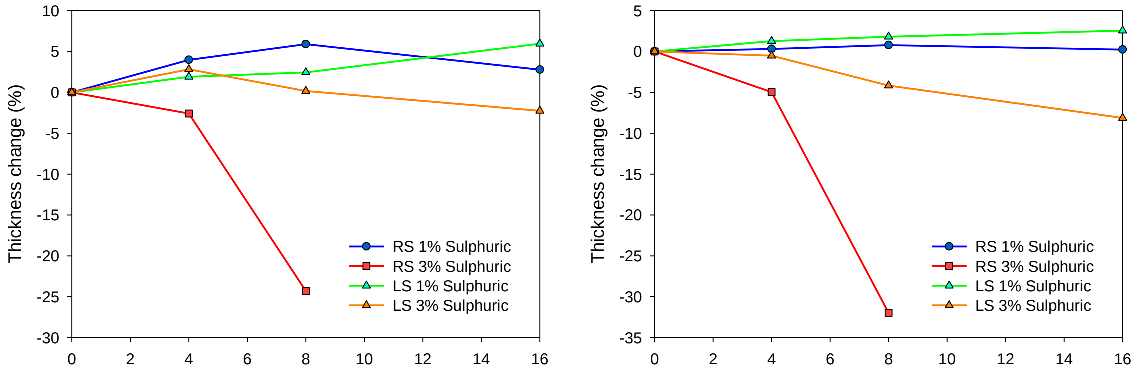

a) without brushing

b) with brushing

Figure 8.9 Changes in thickness of limestone sand mortar and river sand mortar on exposure to sulphuric acid

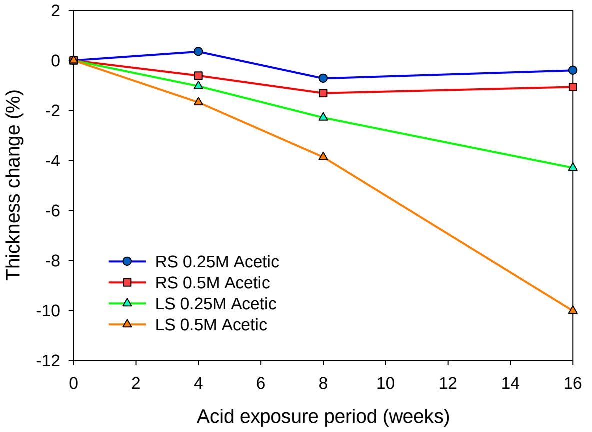

Figure 8.10 Changes in thickness of limestone sand mortar and river sand mortar on exposure to acetic acid (without brushing)

8.4 EFFECT OF AGGREGATE ON ALTERATIONS IN PHYSICO-MECHANICAL PROPERTIES

The cylindrical mortar specimens of size 25 mm diameter and 50 mm height at specific intervals of acid exposure were tested to evaluate the changes in physico-mechanical properties such as compressive strength, bulk density (in saturated state), ultrasonic pulse velocity (UPV) and dynamic modulus of elasticity. The tests were done without any abrasive action to preserve the corroded zones. These results are summarised in Appendix D (Table D-1) and discussed below.

8.4.1 Strength changes

The aspect of cylindrical mortar specimens after the acid exposure is shown in Appendix D (Figure D-1). The compressive strength of specimens was found to reduce on acid exposure due to degradation. Figures 8.11 and 8.12 show the variation of compressive strength of mortar specimens on acid exposure. The drop in the strength values was more pronounced in the case of specimens exposed to acetic acid. This may be ascribed to the high porosity and altered depth of the degraded layers due to the higher aggressiveness of acetic acid and higher solubility of calcium salts. It was observed that the residual strength after exposure was higher for LS mix compared to RS mix for 1% sulphuric acid (Figure 8.11(a)). This could be due to the combined effect of gypsum clogging the pores created by the decalcification of calcium bearing phases and the sacrificial protection offered by the limestone aggregates. However, the residual strengths were comparable at higher concentrations of sulphuric acid (3%), which is evident from Figure 8.11(b).

On exposure to acetic acid, it was noted that OPC mixes with RS suffered higher degradation of strength on prolonged exposure. Despite the higher mass loss of LS mixes, the residual strength of LS mix at 16 weeks of exposure was found to be marginally higher when compared to RS mixes (Figure 8.12). It is hypothesised that this effect is due to neutralisation of limestone aggregates. The sacrificial loss of calcium from aggregates means that there is less dissolution of hydrates especially CSH gel, thus resulting in higher mass loss but increased strength at prolonged ages of exposure.

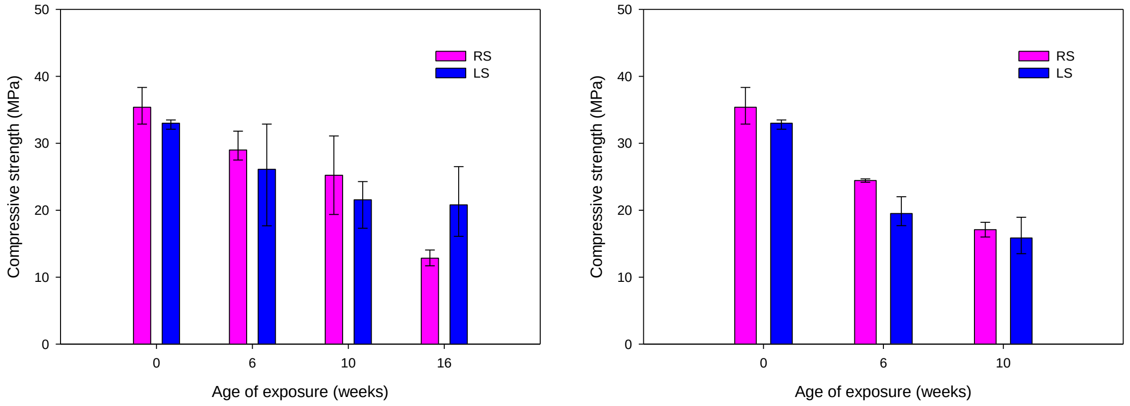

a) 1% sulphuric acid b) 3% sulphuric acid

Figure 8.11 Strength changes of limestone sand mortar and river sand mortar on exposure to sulphuric acid

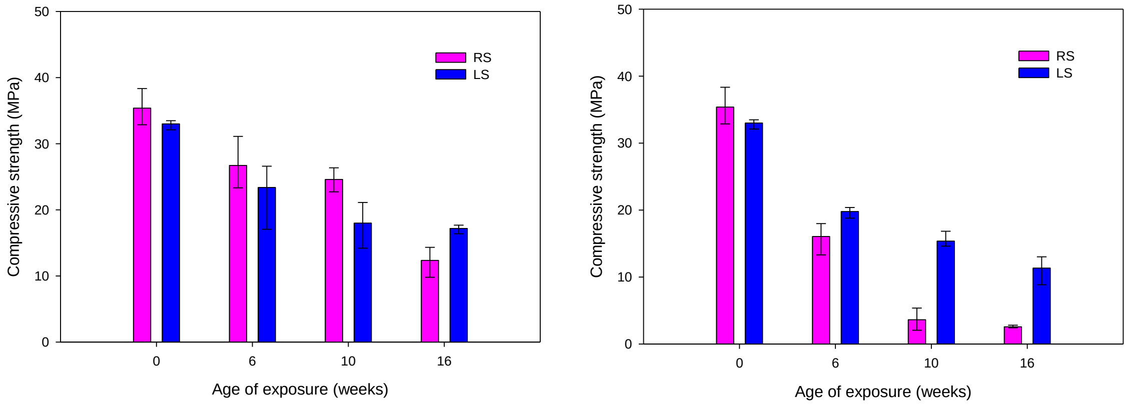

a) 0.25M acetic acid b) 0.5M acetic acid

Figure 8.12 Strength changes of limestone sand mortar and river sand mortar on exposure to acetic acid

8.4.2 Changes in ultrasonic pulse velocity

The variation in UPV with the acid exposure is presented in Table 8.1. The UPV measurements indicate that the LS mixes always show higher velocity values compared to RS mixes. This behaviour may be attributed to increased density of limestone compared to river sand aggregates (higher specific gravity). The loss in UPV due to deterioration was evident for all mixes. However, the loss was significantly higher for acetic acid, indicating serious deterioration of microstructure compared to sulphuric acid. The trend observed in strength measurements was evident in UPV measurements also. The residual UPV (after the acid exposure) was higher for LS mixes for all concentrations of both the acids investigated.

Table 8.1 Changes in UPV of limestone sand mortar and river sand mortar specimens on acid exposure

Acid	1% sulphuric		0.25M acetic		0.5M acetic	
Mix / Age (weeks)	RS	LS	RS	LS	RS	LS
0	4739	5038	4739	5038	4739	5038
6	4612	4980	4431	4794	4059	4432
10	3881	4817	4374	4558	3929	4167
16	3423	4824	3634	4076	2305	3873

Note: UPV is presented in m/s

8.4.3 Changes in bulk density

The bulk density of specimens in saturated condition was noted by measuring the average diameter and height of cylinders just before testing the specimens for the compressive strength. In general, it was noticed that bulk density of specimens reduces with acid attack as shown in Table 8.2. The reduction in density was marginal for both the mixes on exposure to 1% sulphuric acid, while it was considerable for 3% sulphuric acid. It is observed that the bulk density at the end of exposure period for the LS mix was slightly less than RS mix for 0.5M acetic acid. This is in alignment with the mass and thickness measurements. The loss of more calcium from the LS aggregates led to mass loss and hence the reduction in bulk density. This increased porosity of LS mix on exposure to 0.5M acetic acid was also evident on visual observation.

Table 8.2 Changes in bulk density of limestone sand mortar and river sand mortar specimens on acid exposure

Acid	Sulphuric		Acetic		Sulphuric		Acetic	
Concentration	1%	3%	0.25M	0.5M	1%	3%	0.25M	0.5M
Mix / Age (weeks)	RS	RS	RS	RS	LS	LS	LS	LS
0	2.15	2.15	2.15	2.15	2.24	2.24	2.24	2.24
6	2.15	2.02	2.17	2.08	2.19	2.17	2.22	2.14
10	2.12	1.92	2.15	2.02	2.19	2.09	2.16	2.06
16	2.11	-	2.07	2.00	2.21	-	2.17	1.90

Note: Bulk density is presented in g/cm^3

8.4.4 Changes in dynamic modulus of elasticity

The changes in dynamic modulus of elasticity 'E' were evaluated based on the UPV and bulk density measurements. Figures 8.13 to 8.15 show the variation of E value of specimens on exposure to 1% sulphuric, 0.25M acetic and 0.5M acetic acid respectively. The drop in E value was evident with acid exposure period due to reduction in bulk density and reduction in UPV values. It is noted that E value for LS mix was higher for all the acids at all ages of exposure compared to RS mix. As the smoothness of the specimen surface was affected on exposure to 3% sulphuric acid, UPV measurements were not possible and hence E values could not be obtained for 3% sulphuric acid.

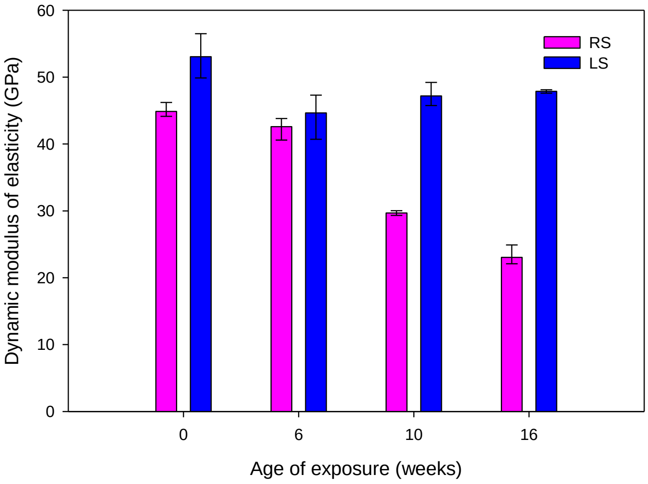

Figure 8.13 Changes in E value of limestone sand mortar and river sand mortar specimens on exposure to 1% sulphuric acid

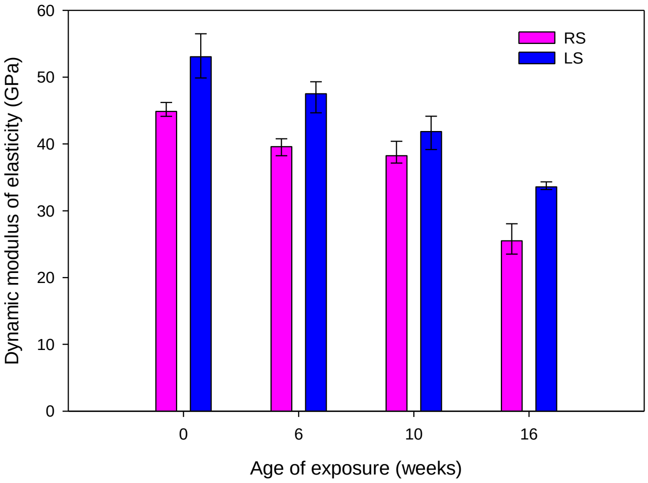

Figure 8.14 Changes in E value of specimens on limestone sand mortar and river sand mortar specimens on exposure to 0.25M acetic acid

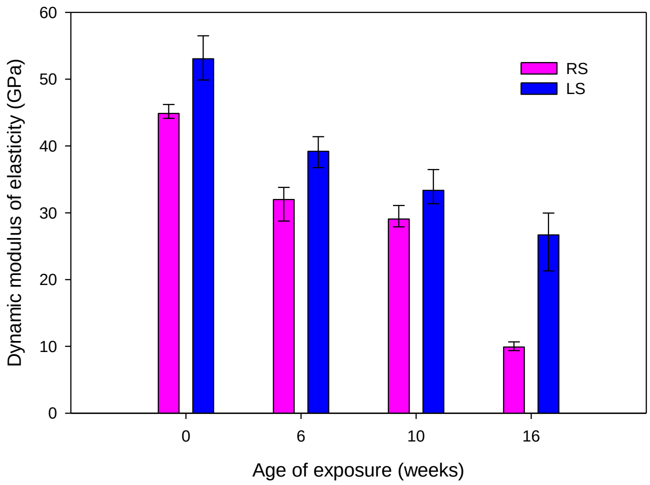

Figure 8.15 Changes in E value of limestone sand mortar and river sand mortar specimens on exposure to 0.5M acetic acid

8.5 MICROSTRUCTURE STUDY

The changes in the microstructure of limestone sand mortar and river sand mortar specimens were studied using X-ray computed micro-tomography and the observations are discussed below.

8.5.1 X-ray micro-tomography

The microstructural deterioration due to acid attack was evident from the CT slice images shown in Figure 8.16. On exposure to 1% sulphuric acid, RS mix undergoes deterioration. The removal of soft gypsum on prolonged exposure led to popping out of aggregates. Severe cracking around the interfacial transition zone of the aggregate was evident. The cracking is because of the expansive pressure generated due to the precipitation of gypsum, which has higher molar volume compared to the cement hydrates (Portlandite and CSH). However, minimal deterioration was observed in the LS mix, as evident also from the 3D rendered CT image (Figure 8.17). An extremely thin layer of gypsum was observed around the periphery of the specimen. This behaviour may be due to the sacrificial protection offered by LS, already explained in the previous discussions.

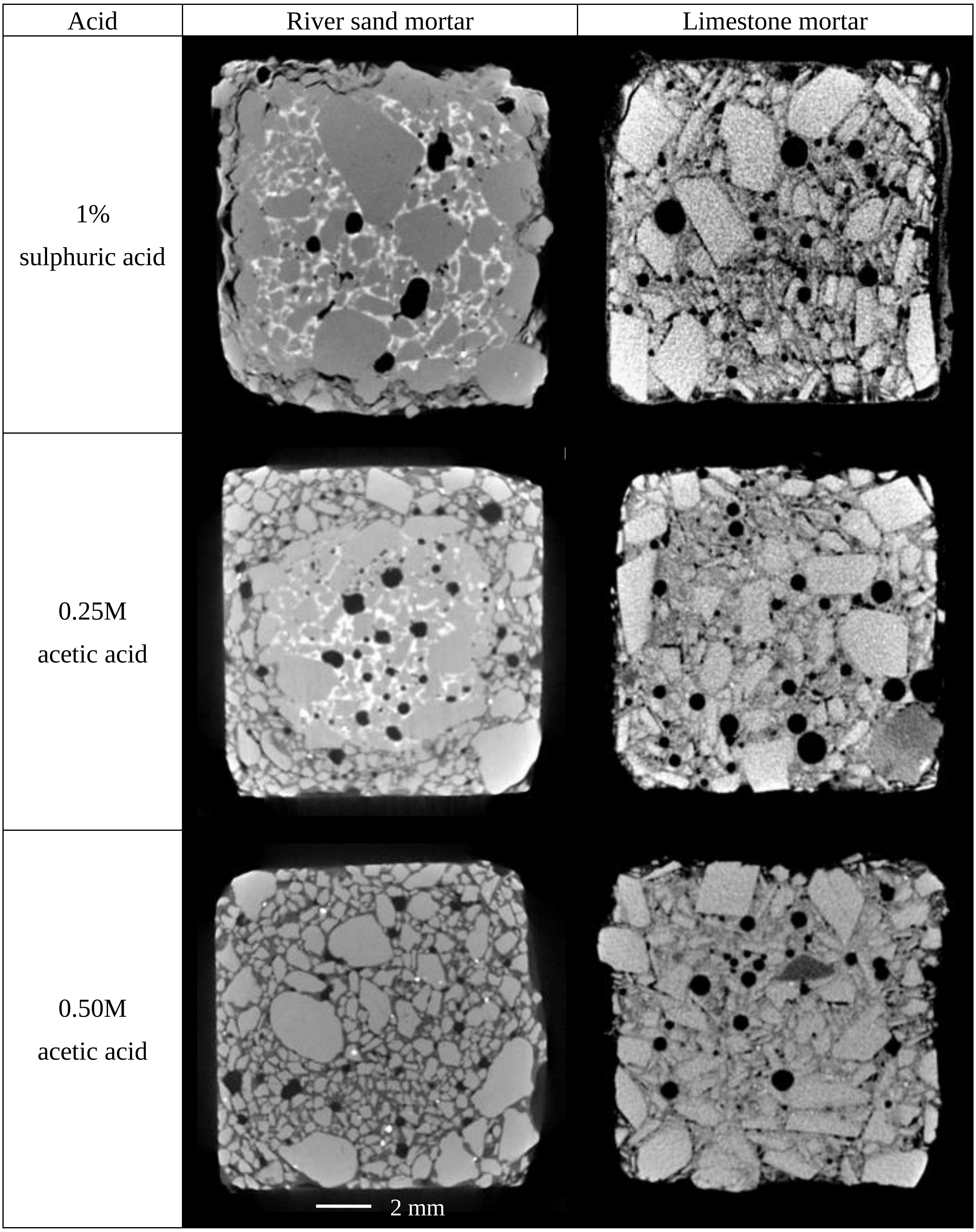

Figure 8.16 X-ray tomography images of limestone sand mortar and river sand mortar specimens after 16 weeks of acid exposure

The altered depth of RS mix on exposure to 0.25M acetic acid was found to be higher. The increased penetration of acid may be due to factors such as higher solubility of calcium salt, and buffer action capacity exhibited by acetic acid. However, it is interesting to note that the altered depth could not be measured from the CT images of LS mix. There was no clear mineralogical zonation and hence depths could not be measured. The entire cross-section of RS mix was deteriorated on exposure to 0.5M acetic acid. However, the altered depth was not much traceable from the CT images of LS mix. It appears, however, that the paste has been decalcified (as the paste appeared dark; less grayscale value of pixels may be attributed to the formation of silica gel from the decalcification of CSH gel).

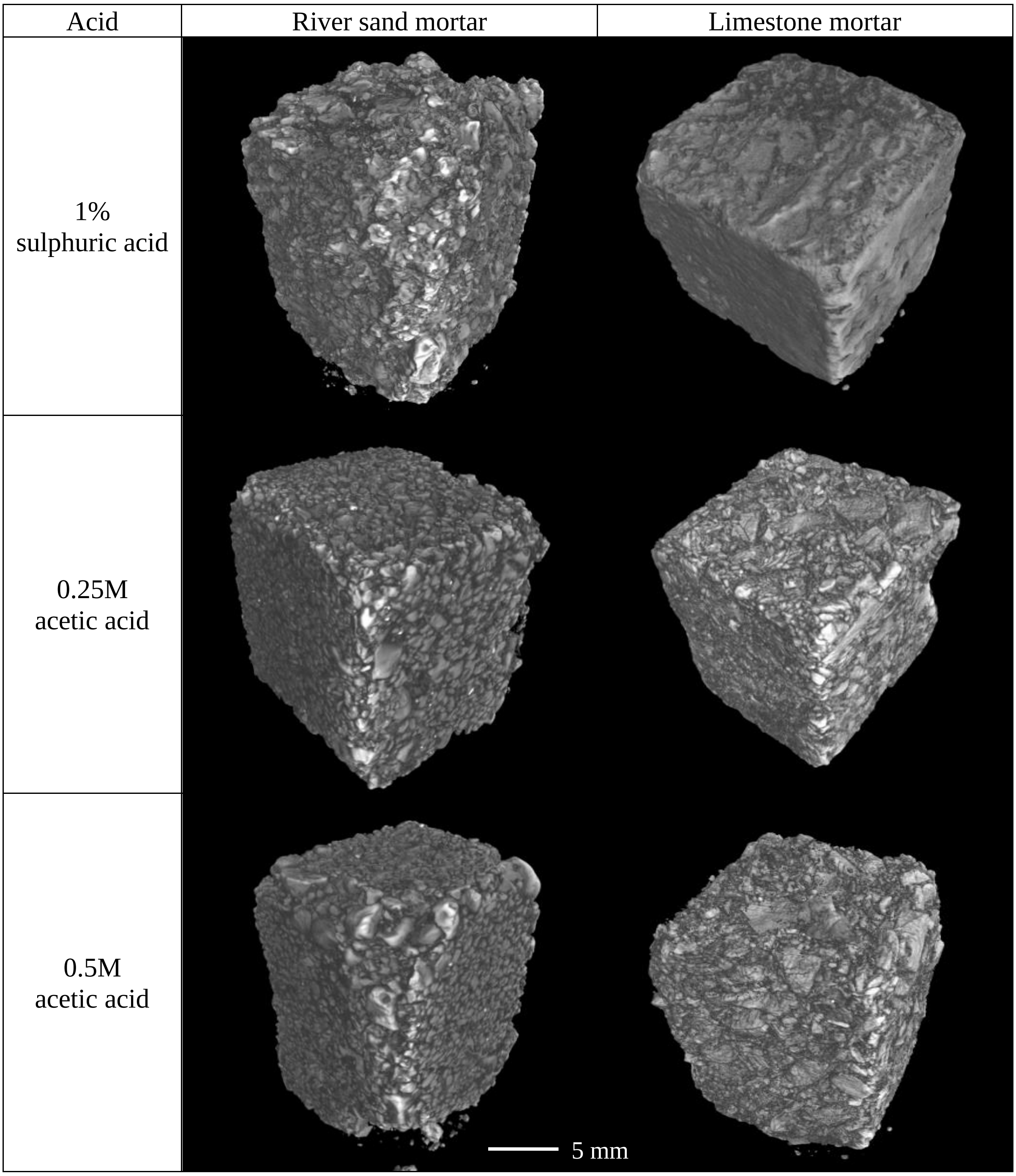

Figure 8.17 3D rendered CT images of limestone sand mortar and river sand mortar specimens exposed to sulphuric and acetic acid

The 3D rendered CT images of limestone sand mortar and river sand mortar specimens exposed to sulphuric and acetic acid are shown in Figure 8.17. It can be noted that the surface of the LS mortar specimens appeared smoother while the RS mortar specimens had a rough appearance. The smooth surface of LS mortar is due to the sacrificial protection and additional buffer provided by the limestone aggregates. In the case of RS mortar, paste is directly attacked which affects the bond between aggregate and paste, causing the aggregates to be protruded.

8.6 SUMMARY

The kinetics of degradation is affected by a multitude of factors related to acid, binders, aggregate and the architecture of the test method. The influence of mineralogical nature of aggregates on acid attack has been investigated in the current chapter by studying the alteration kinetics of cement mortar based on the mass change, change in pH of the acid solution, and thickness change. The alterations in the physico-mechanical properties were studied using parameters such as changes in compressive strength, bulk density, ultrasonic pulse velocity and dynamic modulus of elasticity. The imaging using X-ray micro-tomography was done to understand the changes in microstructure.

It was found that the aggregate type had an effect on the degradation kinetics. The mortar with limestone aggregates showed a less degradation depth than did the mortar with inert (siliceous river sand) aggregates. The limestone aggregates locally created a buffering environment due to acid soluble calcium, thus rendering a sacrificial protective effect, protecting the cement paste from the acid dissolution. However, this more pronounced neutralisation was not noticed in the pH change of the acid solution, especially on exposure to lower concentrations of sulphuric and acetic acid. Based on the parameters investigated, it was found that the limestone aggregates perform better on exposure to sulphuric acid environment when compared to siliceous aggregates. However, mass loss for limestone aggregates on exposure to acetic acid was found to be significantly higher when compared to siliceous aggregates owing to the solubility of calcium salts. Despite higher mass loss, the residual properties measured by compressive strength and dynamic modulus of elasticity were found to be marginally higher for limestone aggregates. It may be concluded that limestone aggregates could be a better option on exposure to those acids which form less soluble salt as in the case of sulphuric acid. Limestone aggregates may not be a better option for exposure to those acids which form highly soluble salts as in the case of acetic acid.

CHAPTER 9

ANALYSIS AND RECOMMENDATIONS

9.1 INTRODUCTION

This chapter deals with a detailed analysis of the various key findings and the recommendations based on the study. The salient findings from the study on degradation kinetics are discussed first, including the qualitative observations made, role of aggregate in influencing the alteration kinetics, and modelling the degradation kinetics of paste and mortar. The subsequent section deals with a brief analysis of the effect of various factors that influence the degradation kinetics. This is followed by a section on the discussion on findings of the micro-analytical characterisation studies done in order to understand the mechanism of degradation. The next section provides a detailed account on the considerations to be followed in the development of a test method to assess acid attack, which includes the considerations with respect to the choice of test parameters used to evaluate the degradation kinetics and the test recommendations based on the study.

9.2 DEGRADATION KINETICS DUE TO ACID ATTACK

9.2.1 Qualitative observations

The study on degradation kinetics using accelerated immersion test on paste and mortar shows that the acid attack is primarily influenced by the solubility of calcium salt and its properties such as molar volume, and its affinity with the inner cement matrix. At first, accelerated immersion tests were done on paste specimens. In the paste study, specimens made with common and advanced binders were exposed to various acids which differ in their dissociation capacity and solubility of the salts they produce. Strong acids such as sulphuric and hydrochloric acid and weak acids such as acetic and citric acids were studied. Among the acids tested, 0.5M citric acid was the most aggressive which resulted in severe mass and thickness loss in specimens. The paste specimens on exposure to 1%

hydrochloric acid and acetic acid (0.25M and 0.5M) showed considerable mass loss as leaching was the primary process driving the deterioration.

On exposure to 1% sulphuric acid, the kinetics was found to be different from the other acids. The specimens had an initial mass gain, followed by a mass loss on prolonged exposure. The gypsum (reaction product) formed had a protective effect limiting the alteration kinetics by plugging the pores left behind by the decalcification of hydrates in the case of paste exposed to 1% sulphuric acid. Moreover, this protective effect was more pronounced in the case of paste with SCMs. In the case of SCM binder systems and LC2 binder system, Portlandite being already consumed, CSH gel was decalcified resulting in finer sized gypsum (which could block the capillary pores) and silica gel and thus, the protective effect was found to be more in the case of SCM based binder systems. The protective effect observed in 1% sulphuric acid was not observed in the case of 3% sulphuric acid. In the case of 3% sulphuric acid, the high concentration of acid led to a rapid increase in the kinetics. Gypsum was formed in large quantities, causing expansion and cracking, and got destabilised in the highly concentrated acid solution on exposure.

Among the common binders tested, the slag paste showed better performance against sulphuric, hydrochloric and acetic acids, based on the mass changes, while OPC and SF10 mix showed less mass loss on exposure to citric acid. The alteration depths for SCM paste were found to be higher compared to OPC which is indicative of direct attack of CSH gel caused by the limited availability of Portlandite in the system. Special composites such as high alumina cement and limestone calcined clay binder performed well only in the case of exposure to lower concentrations of sulphuric and acetic acids. The performance of commonly used SCMs and special binders were ordinary when exposed to higher concentrations of sulphuric and acetic acids.

The paste study using smaller sized specimens revealed that accelerated testing should be performed with higher concentration of acid than the realistic concentration of the acid expected in the real structure, in order to clearly distinguish the performance of various binder systems.

9.2.2 Role of aggregate

The degradation kinetics observed in the mortar was different from the paste. The presence of ITZ in mortar was found to accelerate the penetration of acids when compared to the paste. Notably, the mortar specimens showed higher mass changes when compared to the paste specimens on exposure to sulphuric acid. The increased mass loss observed in mortar may be due to the dislodging of aggregates from the matrix affected by the decalcification (due to the formation of expansive gypsum). However, the mass loss of mortar exposed to acetic acid was found to be less when compared to the paste at the same age of exposure. In this case, siliceous aggregates were inert, and no aggregates were lost from the matrix. It was found the CT images that only the paste phase was decalcified to form silica gel. The cracks seen along the ITZ in the case of sulphuric acid were not seen in the case of acetic acid.

If mass losses of mortar and paste are compared, it appears as if mortar has less degradation kinetics in the case of acetic acid. However, it is worth to consider the paste fraction present in the mortar (31.8% in the case of 1:3 mortar made with w/b of 0.40). Assuming that no mass is lost from the aggregates, the mass loss of mortar has to be converted to the mass loss encountered by the paste fraction in the mortar. When this value of mass loss is compared against the mass loss observed in the paste study, it is inferred that more paste was decalcified in mortar when compared to the paste. This could also explain the relatively higher alteration depths found in mortar when compared to the paste. Thus, it can be concluded that the ITZ in the mortar accelerates the kinetics due to the acid attack. Similar behaviour is expected in the concrete, although there could be additional scale effects owing to changes in the size of the specimen.

Figure 9.1 shows the relationship between the experimental values of mass changes obtained for OPC paste and OPC mortar (w/b 0.40) exposed to acetic acid. It can be observed that there is a strong relationship between the mass change of paste and mass change of mortar for both the 0.25M and 0.50M acetic acids investigated in the study (R^2 of 0.967 and 0.957 for 0.25M and 0.50M acetic acid respectively). Also, the relationship between paste and mortar appears to be a function of concentration of acetic acid.

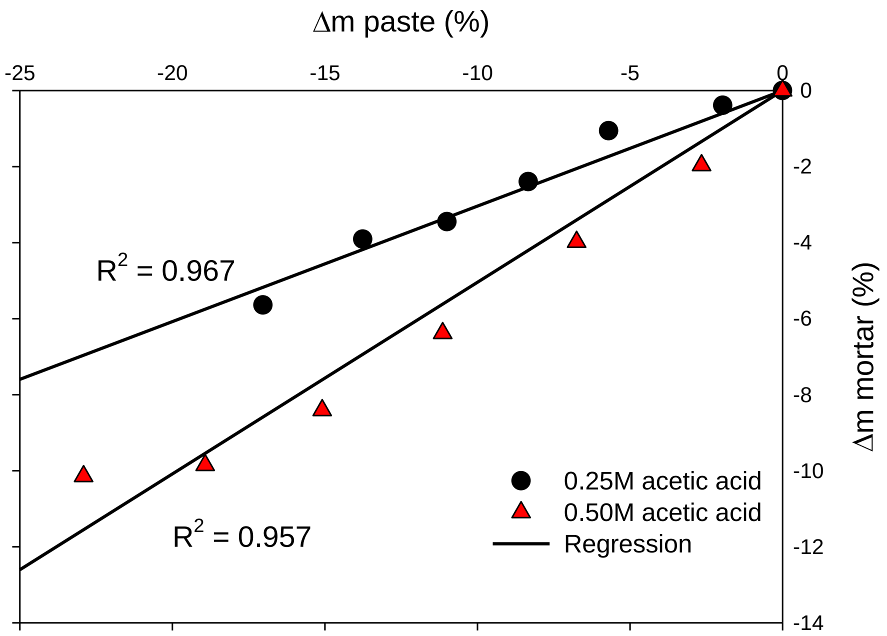

Figure 9.1 Relationship between the mass changes of OPC paste and mortar (w/b 0.40) exposed to acetic acid (without brushing)

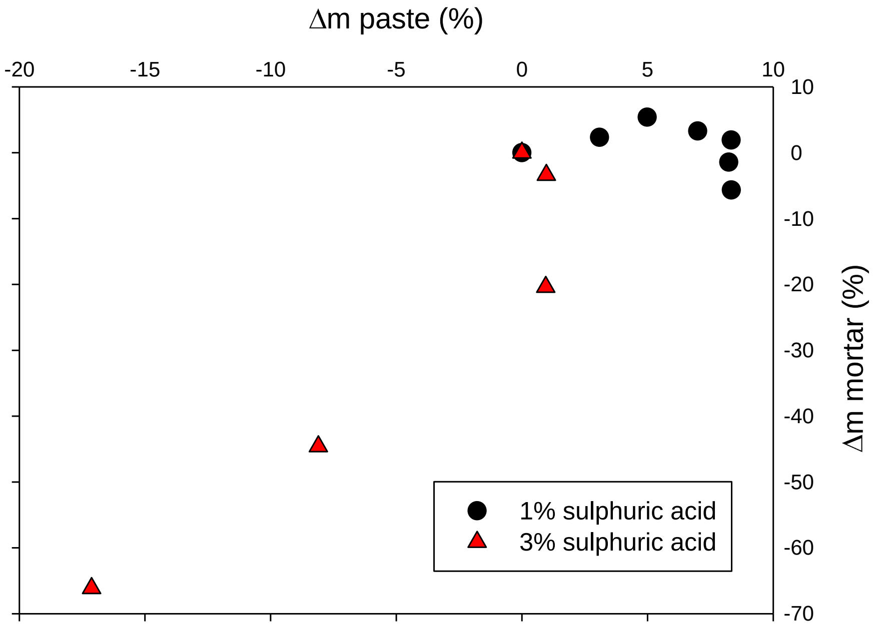

Figure 9.2 Relationship between the mass changes of OPC paste and mortar (w/b 0.40) exposed to sulphuric acid (without brushing)

Figure 9.2 shows the relationship between the experimental values of mass changes (Δm in %) obtained for OPC paste and OPC mortar (w/b 0.40) exposed to sulphuric acid. It can be observed that there exists no well defined relationship between the paste and mortar. This could be due to difference in the behaviour and kinetics of paste and mortar. The paste and mortar specimens may experience precipitation of gypsum and removal of degraded layer at different time periods. Also, in the case of sulphuric acid, the aggregates could be dislodged from the matrix on gypsum formation (due to the expansive pressure). This also makes the creation of a model for predicting mass changes difficult in the case of sulphuric acid when compared to acetic acid.

Figure 9.3 shows the behaviour of OPC paste and mortar (w/b 0.40) exposed to various acids. It can be inferred that the mass changes of mortar are higher compared to paste on exposure to high concentrations of sulphuric acid (3% sulphuric acid with and without brushing) and for 1% sulphuric acid (with brushing). This indicates that the ITZ helps in accelerating the attack in the case of OPC mix.

In the case of acetic acid, as expansive precipitates were not formed, there was no loss of aggregates from the matrix. The mass changes observed in mortar are normalised with respect to the paste fraction in the mortar in the case of acetic acid (paste fraction of 31.82% for 1:3 mortar with w/b of 0.40). The role of ITZ can be assessed from the Figures 9.3(d) and 9.3(e). At low concentrations of acetic acid (0.25M), the mass change curve of mortar (normalised) is above the curve for paste, which points out that the ITZ is less affected at lower concentrations. However, in the case of 0.5M acetic acid, the mass change of mortar (after normalisation) was found to be matching with the paste curve. It must be remembered that the acid renewal frequency used for the paste and mortar study were different. Despite a longer interval between the successive replenishments in the case of mortar, the kinetics was found to be higher, which indicates that the presence of the ITZ accelerated the attack at higher concentrations of acetic acid.

In the case of sulphuric acid, the mass changes of mortar could not be normalised with respect to paste fraction, as aggregates were lost from the matrix (due to expansive stresses exerted by gypsum). Instead of the age of exposure, alternatively, if the behaviour of paste and mortar are assessed based on the number of acid replenishments (almost same pH regime observed for paste and mortar), the strengthening/accelerating effect could be more pronounced. The behaviour of paste and mortar (w/b 0.40) for the FA30, BFS50, SF10, LC2 and HAC mixes is given in Appendix E (Figures E-1 to E-5).

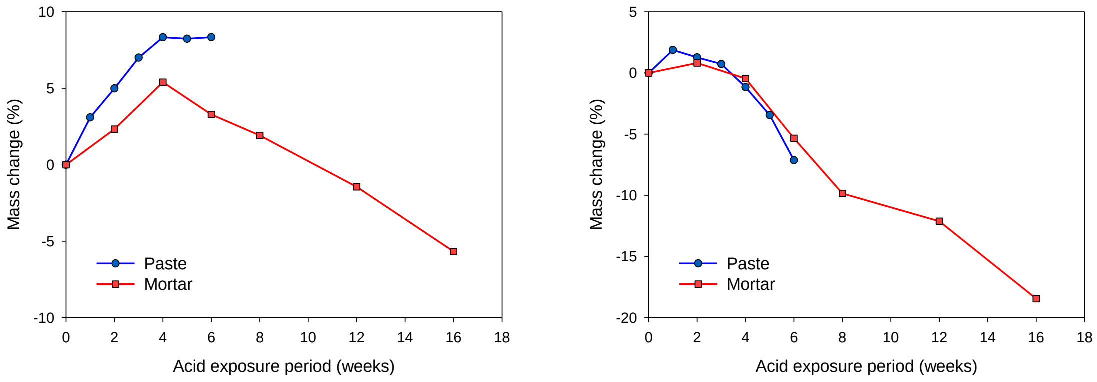

a) 1% sulphuric acid (without brushing) b) 1% sulphuric acid (with brushing)

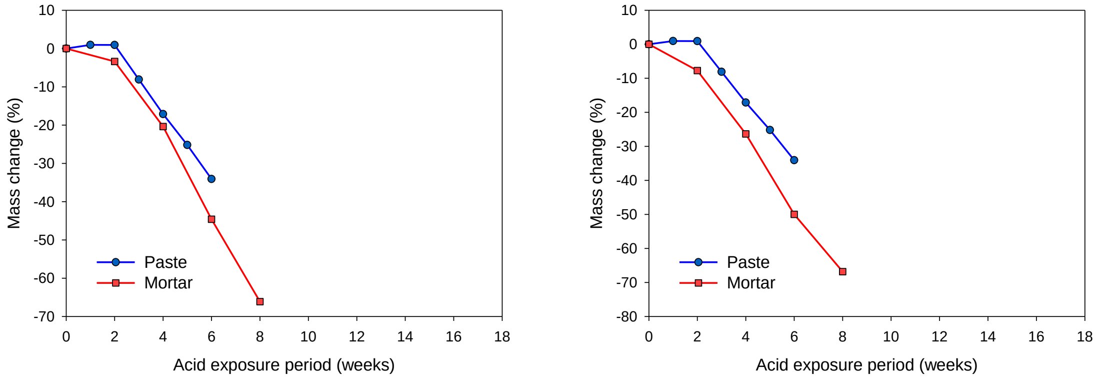

c) 3% sulphuric acid (without brushing) d) 3% sulphuric acid (with brushing)

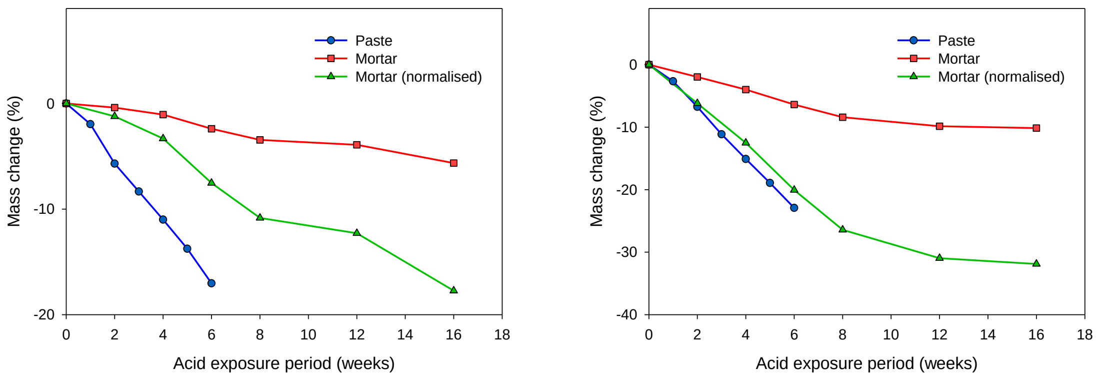

e) 0.25M acetic acid f) 0.50M acetic acid

Figure 9.3 Behaviour of OPC paste and mortar on exposure to acids

In the case of SCM based binder systems, the kinetics of mortar was less compared to paste at early ages of exposure to lower concentrations of sulphuric and acetic acid. However, on further exposure, ITZ could have been affected as the mass change curves of mortar are close to the paste. At higher concentrations of sulphuric and acetic acid, ITZ was found to accelerate the attack at all ages of acid exposure. Based on these analyses, it can be concluded that the ITZ in mortar influences the kinetics of degradation. The strengthening of ITZ in the SCM binder systems could play a role in limiting the kinetics marginally in the case of exposure to lower concentrations of sulphuric and acetic acid at early ages, while it clearly accelerates the kinetics on prolonged exposure to lower concentrations of acids and exposure to higher concentrations of sulphuric and acetic acid for all ages of exposure. These observations are consistent with the mass changes observed during the kinetics study. The SCM mixes showed marginally better performance on exposure to lower concentration of acids when compared to OPC and this may be attributed partially to the strengthening of ITZ in mortar.

9.2.3 Modelling the degradation kinetics

Modelling of cementitious materials exposed to acid solutions has received only limited attention (Le Bescop et al., 2013). Many studies have reported that the rate of mass loss and the thickness of the degraded layer are proportional to the square root of the exposure time (Pavlik, 1994a). Segura et al. (2013) modelled kinetics of degradation as a function of open porosity and CaO concentration of the cementitious system. Further, the authors developed equations to predict degraded depth based on the values of ultrasonic pulse velocity test results. In this study, degradation kinetics in terms of mass changes was modelled as a non-linear function of concentration of acid and age of acid exposure. As the degradation in sulphuric acid was controlled by the precipitation of reaction products at early ages and destabilisation of these products in the long term (i.e. mass gain followed by mass loss), a reliable non-linear model could not be built for sulphuric acid attack. However, the degradation in the case of acetic acid was controlled by leaching of soluble salts, the rate of which can be modelled. The Excel solver add-in was used to create a non-linear model with minimum error.

The model developed for predicting the mass change of OPC paste on exposure to acetic acid (without brushing) is given in Eq. 9.1. The mass change data of OPC paste exposed to 0.25M and 0.5M acetic acid was used to create the model. The negative sign in the equation indicates mass loss. The conventional approach in modelling is to use a coefficient for age of exposure as 0.5, as the phenomenon is controlled by the process of diffusion. But, based on the paste study exposed to acetic acid, it was observed that the mass loss variation of the paste specimens is almost linear with the age of exposure, irrespective of the binder systems. Hence, a non-linear model (shown in Eq. 9.1) was developed by assigning a value of 1 for the coefficient of age of exposure 't'. A good fit was obtained with R^2 of 0.993. In the case of paste specimens, the degradation was limited to a certain depth from the external surface, and continued at a constant rate, and hence, the kinetics was found to vary linearly with the age of acid exposure.

$$\Delta m = -\ 0.94\ c^{0.81}\ t^{1} \qquad (9.1)$$

Where,

Δm = mass change of OPC paste without brushing (in %)

c = concentration of acetic acid (in molarity)

t = age of acid exposure (in days)

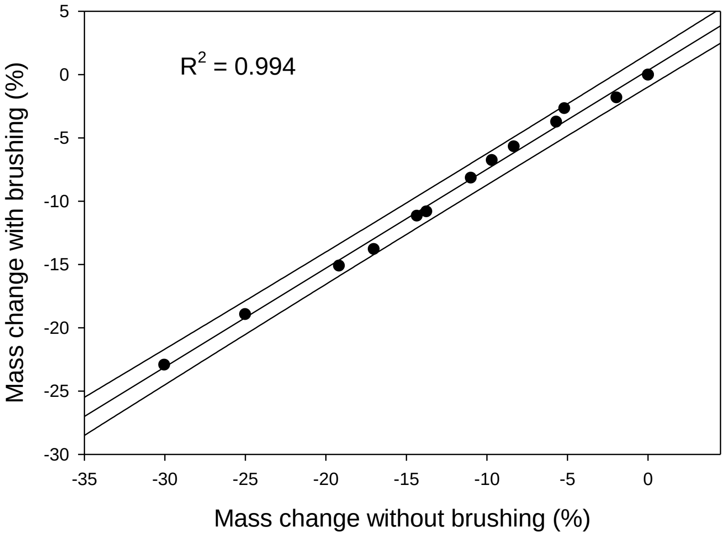

Figure 9.4 Correlation between the mass changes of OPC paste tested with and without brushing

The mass changes of OPC paste tested with and without brushing were compared. It was found that there exists a strong linear relationship between mass changes with and without brushing for both 0.25M and 0.5M acetic acid. Further, a term known as brushing factor 'B' was computed by finding the slope of the plot between the mass changes (experimental values) with brushing on Y axis and mass changes (experimental values) without brushing on X axis (Figure 9.4). A plot with good correlation was obtained ($R^2 = 0.994$). The slope of the plot (brushing factor) was obtained as 1.30. The mass changes of OPC paste with brushing (Δm_B) can now be predicted by multiplying this brushing factor 'B' with the equation developed for predicting the mass loss without brushing and the expression is given in Eq. 9.2. Also, it was inferred that the brushing factor is independent of the concentration of acetic acid.

$$\Delta m_B = -\ 1.22\ c^{0.81}\ t^1 \tag{9.2}$$

In order to ascertain the performance of various binders, the mass loss data points of various binder systems obtained from the paste study (exposed to acetic acid and tested with brushing) were plotted along with the model equation (Eq. 9.2) developed for OPC paste. Separate plots were made for 0.25M and 0.5M acetic acid (Figures 9.5 and 9.6).

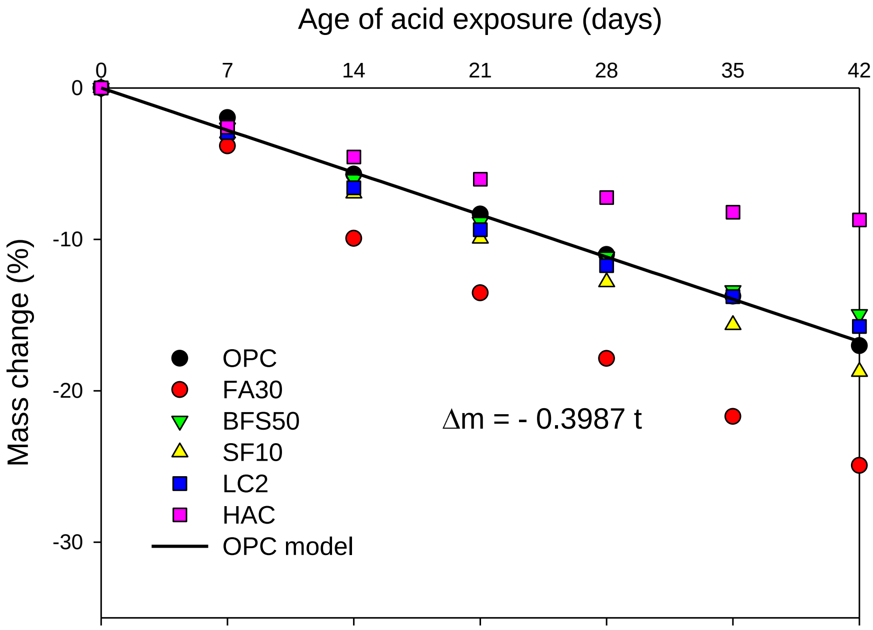

Figure 9.5 Comparison of mass change of paste mixes with predicted model for OPC paste on exposure to 0.25M acetic acid

It can be noted that the performance of paste mixes such as HAC and BFS50 were better compared to the model curve predicted for OPC in the case of 0.25M acetic acid. This could be due to limited availability of Portlandite in BFS50 system, and change in the composition of hydration products in the case of HAC system. These alumina rich binder systems were found to have less mass loss which leads to a conclusion that the presence of alumina adds stability to the corroded layer, which further improves its resistance against abrasion, resulting in lower mass loss when tested with brushing. The data points of the LC2 system were very close to the OPC model. On the other hand, the performance of paste mixes such as SF10 and FA30 were found to be inferior, as the data points were below the model curve for OPC paste. At high concentration of acetic acid (0.5M), the improved performance of SCM binder systems was evident, especially for slag, as the data points were well above the predicted curve for OPC paste. The analysis further reinstates the fact that reducing the Portlandite content and increasing the alumina content in the system reduces the mass loss due to deterioration.

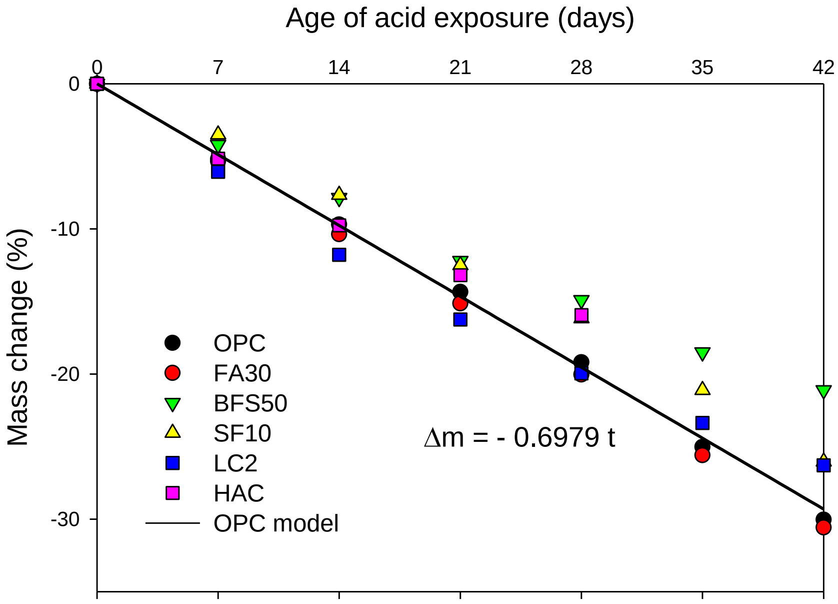

Figure 9.6 Comparison of mass change of paste mixes with predicted model for OPC paste on exposure to 0.5M acetic acid

Similar to paste, the degradation kinetics for mortar in terms of mass change was modelled as a function of concentration of acid and age of acid exposure. Figures 9.7 and 9.8 show the variations in mass change for mortars with different binder systems, exposed to 0.25M and 0.50M acetic acid respectively. A generic model equation was obtained by constructing a non-linear model using Excel solver, combining the two data sets (for 0.25M acetic acid and 0.5M acetic acid) of the various binder systems. As the mass loss curve for mortar starts flattening on prolonged exposure, it was assumed that the phenomenon is controlled by diffusion of acid ions and salts through the degraded layer. Hence the coefficient of t was fixed as 0.50, as suggested by the literature. The generic model thus obtained for the minimum error condition is given in Eq. 9.3.

$$\Delta m = - 2.15\, c^{1.27}\, t^{\,0.50} \qquad (9.3)$$

Where,

Δm = mass change of mortar without brushing (in %)

c = concentration of acetic acid (in molarity)

t = age of acid exposure (in days)

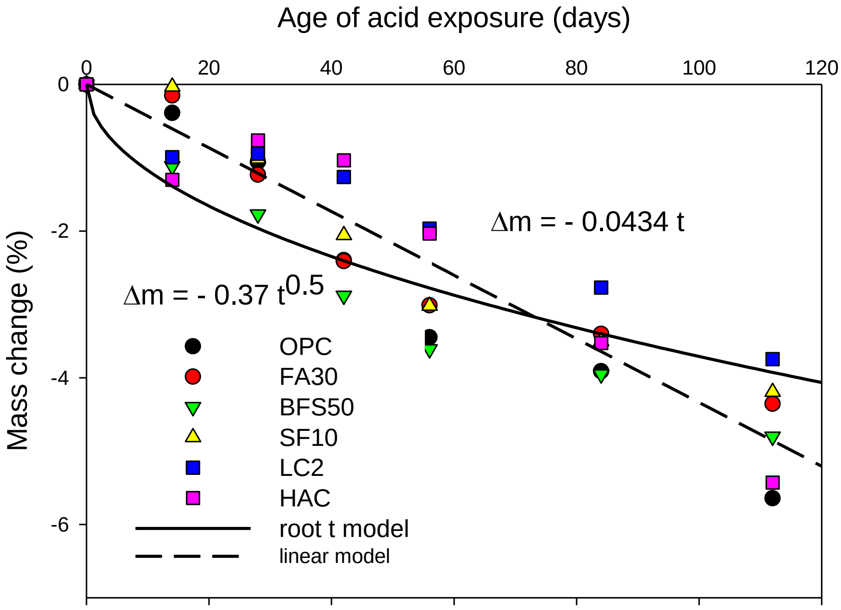

Figure 9.7 Comparison of mass change of mortar mixes with predicted model for mortar on exposure to 0.25M acetic acid

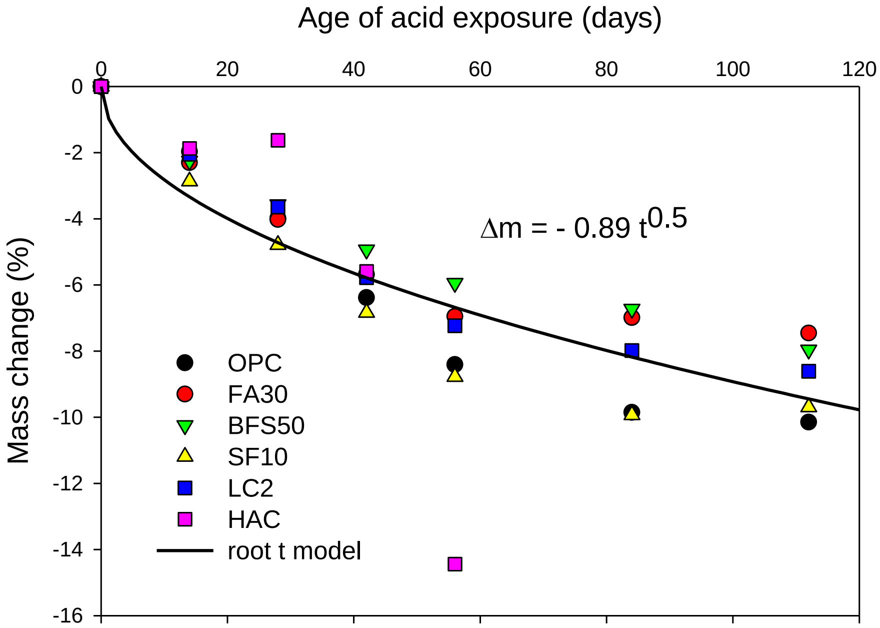

Figure 9.8 Comparison of mass change of mortar mixes with predicted model for mortar on exposure to 0.5M acetic acid

The data points of all the binders were found to fit reasonably well with the $t^{0.5}$ model. Although, in the case of 0.25M acetic acid (Figure 9.7), it appears that a linear model fits better (model made with coefficient of age of exposure as unity – shown as the dashed line in Figure 9.7) when compared to $t^{0.5}$ model. This is because the entire cross-section of the specimen was not attacked in the case of 0.25M acetic acid at the end of 4 months of exposure. However, the $t^{0.5}$ model was found to be more suitable for mortar exposed to high concentration of acetic acid (0.5M). In this case, it was observed from the CT images that the entire cross-section of the specimen was nearly decalcified. Due to this reason, the rate of mass change reduced on prolonged exposure to 0.5M acetic acid. The corroded layer was thick and the kinetics was more controlled by the diffusion of ions through the corroded layer in the case of high concentrations of acetic acid. This justifies the use of 0.50 as the coefficient for the age of acid exposure. On exposure to 0.25M acetic acid, the mortar mixes such as LC2 and HAC perform better when compared to the other mixes. The improved performance of BFS50 at 0.5M acetic acid exposure is evident from Figure 9.8 as the data points of slag are above the line predicted by the generic model.

Thus, based on the study, it is recommended to use t models (i.e. models where the power coefficient of the time variable t is 1) for predicting the deterioration of paste, especially on exposure to lower concentrations of acetic acid. On the other hand, $t^{0.5}$ model should be used for predicting the deterioration of mortar, especially on exposure to higher concentrations of acetic acid.

9.3 FACTORS INFLUENCING DEGRADATION KINETICS

The effect of various acid and material related factors on degradation kinetics of paste and mortar were evaluated in the study. The factors include the type of binder, type of acid, concentration of acid, initial pH of the acid solution, type of aggregate, and water to binder ratio of mortar. The results show that the performance of SCMs is better only on exposure to relatively lower concentrations of sulphuric and acetic acid. At high concentrations of sulphuric acid, the performance of SCM based mixes, except for slag, was ordinary when compared to OPC. It is also inferred that the alteration depths of SCM paste/mortar were higher when compared to OPC. This may be due to the direct attack in the CSH gel because of the limited availability of Portlandite in the SCM systems. Thus, the selection of the binder should be made specific to the aggressive environment. For example, in the case of effluents predominantly having citric acid, either OPC or silica fume should be chosen to resist the attack. In the case of acetic acid environment, slag should be chosen as the binder to resist the attack.

The degradation kinetics was found to primarily depend on the solubility of the salt, which in turn depends on the type of acid. It is seen that the kinetics, to a large extent, depends also on the concentration of the acid solution. As the concentration of acid is increased, the relative performance of binders is also changed. The immersion tests in mortar exposed to pH2 sulphuric acid and pH4 acetic acid indicate that the kinetics are lowered to a significant extent as the pH of the solution is increased by adding caustic soda to the acid solution. This again reinstates the need for adopting suitable accelerated test methods.

The kinetics also was influenced by the mineralogy of the aggregate. The limestone aggregates showed better performance on exposure to sulphuric acid as the mass loss was less when compared to mortar with siliceous aggregates. However, severe precipitation of gypsum was noted despite the lower mass loss. As the calcium carbonates are soluble in acetic acid, the limestone aggregates showed higher mass loss compared to siliceous aggregates.

The mortar study indicated that a higher w/b ratio is preferable on exposure to sulphuric acid to minimise the damage. The use of lower w/b creates more expansive pressure within the porosity leading to more damage compared to a higher w/b. At the same time, the use of lower w/b is recommended in the case of exposure to acetic acid. These observations have implications in the formulation of the mix design of concrete to resist aggressive acidic environments.

9.4 MECHANISM OF DEGRADATION

The test results show that the attack by weak organic acids such as acetic acid is comparable to that of strong inorganic acids such as hydrochloric acid. There is almost no difference between weak and strong acids with soluble salts in terms of deterioration mechanisms. The degradation mechanism was also found to be similar across the common binder systems for a particular type of acid.

The degradation in the case of exposure to sulphuric acid was due to the formation of expansive gypsum. Although ettringite formation was noted, it was restricted to the inner layers. The gypsum was found to be embedded in silica gel rich in alumina. A layer of iron hydroxides adjacent to gypsum layer was also evident.

The deterioration in the case of acids that form soluble salts was primarily due to leaching. The salts being soluble leach out, leaving only silica gel in the outer degraded layer. However, the SCMs containing reactive alumina (slag system) were found to have lower mass losses, which may be due to the enhanced stability of the corroded layer owing to the enrichment of alumina. The severe damage observed due to citric acid was attributed to the expansive non-protective salt that is formed along with silica gel.

9.5 DEVELOPMENT OF TEST METHODS FOR ACID ATTACK

Currently, there are no codes or standards available for evaluating resistance of materials to acid attack. The absence of standardised test method hinders the adequate evaluation of the performance of cementitious materials in acid environments. Moreover, this absence is also a major obstacle to the evaluation of alternative binders in terms of performance and deterioration mechanisms and thus to their commercial development. The general considerations to be given in the development of a test method to evaluate the acid resistance are discussed in the subsequent sections.

9.5.1 Considerations with respect to the choice of test parameters

The choice of the degradation measure may lead to different conclusions while ranking the performance of various binder systems (Bertron et al., 2006, De Belie et al., 1996). In the current study, several parameters were used to measure the degradation kinetics; mass changes, altered depth, thickness changes, and changes in the pH of the acid solution. The alterations in the microstructure manifest in the form of mass changes and could be considered as one of the key indicators of the degradation kinetics. However, there are instances found in the study when mass loss observed is less but altered depth is high (in

SCM binder systems). Thus, mass changes alone cannot be considered as a reliable lonely indicator of degradation. Instead of adopting one single measure, a multitude of parameters should be used to ascertain the performance of various binder systems exposed to acids.

Based on the study, a new Performance Ranking Factor (PRF) is proposed by combining various test parameters related to the degradation kinetics. The proposed formula for the PRF is given in Eq. 9.4 and 9.5. PRF is defined as one third of the sum of area ratio, mass ratio and relative dynamic E value of specimens at specific age of acid exposure. Area ratio reflects the microstructural changes due to decalcification on acid exposure whereas mass ratio is derived based on mass change calculated. The term relative dynamic E value reflects the alterations in the physico-mechanical properties on acid exposure. In this way, a single test parameter is formulated which combines the parameters related to changes in mass, alterations in microstructure and physico-mechanical properties. The mass ratio can be obtained based on the mass change as per Eq. 9.6.

$$\mathrm{PRF} = \frac{1}{3}\,(\text{area ratio} + \text{mass ratio} + \text{relative dynamic E value}) \tag{9.4}$$

$$\mathrm{PRF} = \frac{1}{3}\left(\frac{A_c}{A_i} + \frac{M_t}{M_0} + \frac{E_t}{E_0}\right) \tag{9.5}$$

$$\frac{M_t}{M_0} = \left(\frac{\Delta m}{100} + 1\right) \tag{9.6}$$

Where,

M_t = mass of the specimen after acid exposure for a period ‘t’ (g)

M_0 = mass of the specimen before the acid exposure (g)

Δm = mass change (%)

A_c = core unattacked area of the specimen after the acid exposure measured from CT image analysis (mm^2)

A_0 = initial area of the specimen (mm^2)

E_t = dynamic modulus of elasticity of the specimen after the acid exposure for a period ‘t’ (GPa)

E_0 = dynamic modulus of elasticity of the specimen before the acid exposure (GPa)

Table 9.1 shows the ranking of performance of various binders exposed to acids (without brushing), based on the proposed test parameter called PRF. The colour codes used for the ranking of performance are: red – poor; orange – moderate; yellow – good and green – excellent category. It can be seen that the ranking of binders vary depending on the choice of the degradation measure. On exposure to 0.25M acetic acid, slag mortar was found to be ranked one (excellent) followed by OPC, SF10 and FA30 mortars. Also, fly ash, even though ranked one based on lower mass loss, was ranked four (poor performance) based on PRF. This could be due to the reduced area ratio and relative dynamic modulus of elasticity of fly ash mortar on exposure to 0.25M acetic acid. On exposure to 0.5M acetic acid, it is noted that the acid penetrated the full cross-sections for all the mixes (as evident from the CT slice images). Hence area ratio is taken as zero (as core area, $A_c = 0$). Based on the values of PRF, the performance of slag was found to be excellent while SF10 mortar was ranked the worst.

On exposure to 1% sulphuric acid, although OPC was ranked the worst based on mass changes (higher mass loss), the area ratio and the relative E value were found to be higher. Based on the values of PRF, the performance of OPC was found to be excellent while slag was found to be inferior (due to relatively lower area ratio and relative dynamic E value). However, in this case, the PRF values were close to each other and the PRF value of BFS50 mortar was only marginally lower when compared to FA30 and SF10 mortars. Similar analysis was done for the specimens tested with brushing wherein the mass ratio was calculated based on the specimens tested with brushing (Table 9.2). In this case, area ratio could not be calculated because CT imaging was not done for these specimens. Hence, PRF is calculated as one half of the sum of area ratio and relative E value of mortar specimens after the acid exposure. Based on the values of PRF, the SF10 mortar was ranked better followed by fly ash, slag and OPC. Thus, it can be seen that SCM binder systems may resist flowing effluents containing sulphuric acid better compared to OPC. However, it has to be noted that the above ranking for the tests with brushing was without considering the area ratio. In the case of effluents containing acetic acid, the performance of slag blended system was found to be better.

Alternatively, if area ratio could not be measured owing to lack of testing facilities like X-ray CT, it can be computed based on the altered depth measurements (estimated using a suitable technique such as microscopy or phenolphthalein indication). The formulas for calculating the area ratios for the square prismatic specimens are given in Eq. 9.7 and 9.8.

$$A_c = (T_0 - 2D)^2 \tag{9.7}$$

$$\frac{A_c}{A_i} = \left(\frac{(T_0 - 2D)^2}{{T_0}^2}\right) \tag{9.8}$$

Where,

D = total altered depth of the specimen (in mm) = DD + DM + DR

T_0 = initial thickness of the specimen before the acid exposure (in mm)

For cylindrical specimens, the following equations (Eq. 9.9 and 9.10) may be used in estimating the area ratio. In the absence of sophisticated testing facilities, phenolphthalein depth could be measured by spraying on fresh cut surface. This phenolphthalein depth may be approximately considered as equal to the depth of alteration (i.e. DD + DM). The terms DD, DM and DR are explained earlier in the section 3.7.4.

$$A_c = \frac{\pi}{4}(T_0 - 2D)^2 \tag{9.9}$$

$$A_i = \frac{\pi}{4}{T_0}^2 \tag{9.10}$$

Table 9.1 Performance ranking factor for mortars (w/b 0.40) exposed to acids (without brushing)

Mix	Acid solution and concentration	Mass ratio	Ranking based on mass ratio	Area ratio	Ranking based on area ratio	Relative E value	Ranking based on relative E value	PRF	Ranking based on PRF
OPC	Acetic 0.25M	0.9436	**4**	0.419	**1**	0.57	**2**	0.644	**2**
FA30	Acetic 0.25M	0.9564	**2**	0.223	**4**	0.52	**4**	0.566	**4**
BFS50	Acetic 0.25M	0.9520	**3**	0.321	**3**	0.67	**1**	0.648	**1**
SF10	Acetic 0.25M	0.9581	**1**	0.325	**2**	0.52	**3**	0.601	**3**
OPC	Acetic 0.50M	0.8986	**4**	-	-	0.22	**2**	0.373	**2**
FA30	Acetic 0.50M	0.9255	**1**	-	-	0.17	**3**	0.365	**3**
BFS50	Acetic 0.50M	0.9204	**2**	-	-	0.47	**1**	0.463	**1**
SF10	Acetic 0.50M	0.9030	**3**	-	-	0.09	**4**	0.331	**4**
OPC	Sulphuric 1%	0.9432	**4**	0.747	**1**	0.51	**1**	0.733	**1**
FA30	Sulphuric 1%	1.0545	**3**	0.536	**2**	0.49	**2**	0.693	**2**
BFS50	Sulphuric 1%	1.0634	**2**	0.480	**4**	0.47	**4**	0.671	**4**
SF10	Sulphuric 1%	1.0791	**1**	0.489	**3**	0.48	**3**	0.683	**3**

Table 9.2 Performance ranking factor for mortars (w/b 0.40) exposed to acids (with brushing)

Mix	Acid solution and concentration	Mass ratio	Ranking based on mass ratio	Area ratio	Ranking based on area ratio	Relative E value	Ranking based on relative E value	PRF	Ranking based on PRF
OPC	Sulphuric 1%	0.8154	4	*	*	0.51	1	0.663	4
FA30	Sulphuric 1%	0.8950	3	*	*	0.49	2	0.692	2
BFS50	Sulphuric 1%	0.9027	2	*	*	0.47	4	0.686	3
SF10	Sulphuric 1%	0.9269	1	*	*	0.48	3	0.703	1

* area ratio was not calculated as CT imaging was not done for these specimens

9.5.2 Recommendations based on the study

In the current study, accelerated continuous immersion tests were carried out on paste and mortar specimens. These immersion tests may be more suitable to simulate the environment wherein the concrete could be attacked by acids present in large quantities (storage tanks, treatment plants etc.) and it is easy to perform in the laboratories. The use of smaller sized specimens with large surface area to volume ratio is recommended in order to achieve accelerated test results. The test recommendations proposed based on the study with respect to the type and concentration of acid, use of abrasive action and the nature of specimen are summarised in Table 9.3 and discussed in the subsequent sections.

Table 9.3 Summary of recommendations based on the study

Exposure environment	Concrete sewers, sewage treatment plant, other wastewater applications			Agricultural and agro-food effluents		
Objective of the study	Degradation kinetics	Degradation mechanism	Role of ITZ	Degradation kinetics	Degradation mechanism	Role of ITZ
Nature of specimen	Mortar	Paste	Paste and mortar	Mortar	Paste	Paste and mortar
Use of abrasive action	Yes	No	Yes	Yes	No	Yes
Type of acid	Sulphuric acid			Acetic acid		
Concentration of acid	1%			0.5M		

Note: The above recommendations are based on the laboratory investigations on paste and mortar specimens. The interaction of microbes with cementitious matrix in the case of sewers is critical, but excluded from the current study.

9.5.2.1 Type of acid

The kinetics and the mechanism of attack differ significantly depending upon the characteristics of the salt formed during the reactions, which in turn depend on the anions of the acid. Also, based on the study, it is found that a binder which performs well in one acid environment may not perform well in another acid. Hence, the type of acid to be chosen for the test should be specific to the environment in which the concrete is likely to be exposed.

Sulphuric acid should be used if the concrete is to be tested for its suitability for concrete sewers, sewage treatment plants or similar waste water applications, whereas acetic acid should be used for testing if the concrete is likely to be exposed in agricultural and agro-food environments, which predominantly contain acetic acid. If a new binder has to be tested for its acid resistance, it is recommended to conduct the testing with both sulphuric and acetic acid so as to capture the effect of solubility of salt on the kinetics of acid attack in the new binder system.

Also, care has to be taken for the frequent renewal of acid solutions to maintain the aggressiveness. This is especially important when the specimens are exposed to acids that form soluble salts. It is observed from the study that the pH of the acid solution rises within a shorter period of time when exposed to acids like HCl and acetic acid. Hence, it is recommended to renew the solutions on a regular basis, at least once in a week.

9.5.2.2 Concentration of acid

Based on the study, it is recommended to use higher concentration of acids (when compared to the realistic concentration of the aggressive solution) while investigating the kinetics. However, as pointed out by Bertron (2013), it must be ensured that the degradation mechanism is unaltered even on testing with the concentration of acid selected. Immersion tests with very low concentrations of acids are not recommended, as it is found from the study that the kinetics are so low that the performance of various binder systems could not be distinguished properly on exposure to lower concentrations of acids (0.5% sulphuric acid, pH2 sulphuric acid, 0.125M acetic acid, 0.25M acetic acid and pH4 acetic acid).

It is recommended to use 1% sulphuric acid (pH = 0.99) for assessing the material resistance in environments such as concrete sewers, waste water treatment plants etc. Testing very high concentrations of sulphuric acid may be avoided as there is a risk of under-predicting the performance of SCMs. When the concrete is likely to come into contact with agricultural and agro-food effluents which predominantly contain acetic acid, it is recommended to do the testing with 0.5M acetic acid to assess the material resistance.

9.5.2.3 Use of abrasive action

It was found from the study that the use of abrasive action accelerated the kinetics of paste and mortar specimens exposed to acids. The abraded OPC paste had a mass loss of 7.1% against a mass gain of 8.3% when tested without abrasive action. Abrasive action in the form of manual (or automated) brushing on the specimen surface should be used to accelerate the attack kinetics. This is especially important when the acids form insoluble salts with lower molar volume (such as in the case of sulphuric acid) which will then seal the porosity of the outer degraded layer rendering a protective effect in limiting the alteration kinetics. In such cases, where the salts are precipitated, plugging the pores in the matrix hindering the kinetics, it is advisable to accelerate the kinetics by using periodic abrasive action. The abrasive action could remove the loosely held precipitates that are attached to the matrix, exposing relatively fresh areas for attack. Moreover, the abrasive action will simulate the action of flowing effluents on the cementitious surfaces such as in the case of concrete sewers and sewage treatment plants.

The effect of abrasive action will be more predominant only in the cases of acids forming less soluble and protective salts. The effect of abrasive action in the acceleration of kinetics will be marginally less though, on exposure to acids that form soluble salts such as hydrochloric and acetic acid, and in the case of acids that form expansive non-protective salts such as in the case of citric acid. Since the use of abrasive action removes at least part of the corroded layer, the method may not be suitable for micro-analytical studies to understand the mechanism of degradation. Thus, if the objective is to characterise the degradation mechanism, the tests should be conducted without any abrasive action so as to preserve the corroded layers for the micro-analytical characterisation tests. Also, testing without any abrasive action is helpful in understanding the behaviour of material in static acidic conditions, such as in effluent storage tanks.

9.5.2.4 Nature of specimen

The choice of test specimen is an important question to be answered while developing a test method. The current study indicates that mortar specimens may be an ideal choice for testing; testing mortar would not only give accelerated results but also provide an insight into the role of binders and ITZ. Hence, it is recommended to use mortar specimens for evaluating the degradation kinetics due to acid attack.

Testing concrete is not recommended due to the long term testing needed to get the salient results which are distinguishable across the binder systems. Also, the specimen size being larger decreases the kinetics, making it a long term durability test. Hence, it is recommended to use smaller sized mortar specimens with higher surface area to volume ratio for evaluating the degradation kinetics.

However, if the primary objective is to study the mechanism of degradation, the studies may be restricted to the paste exposure. Paste is preferred for characterising degradation as the presence of aggregates in mortar/concrete interferes with the characterisation testing. It also makes the preparation of samples and mineralogical analysis difficult and complicated.

If the specific objective is to investigate the role of ITZ, it is recommended to conduct the kinetics studies on both paste and mortar specimens, with similar testing conditions (i.e. similarity in specimen size, in volume ratio, frequency of acid replenishment, age of exposure etc.). The effect of ITZ can then be ascertained by comparing the behaviour of mortar with respect to the paste.

9.6 SUMMARY

The role of ITZ in influencing the degradation kinetics and the paste-mortar behaviour on exposure to acids was discussed in this chapter. Based on the mass data collected from the study, an attempt was made to model the degradation kinetics of paste and mortar exposed to acetic acid. It was found that the t (linear function of age of exposure) model was best suitable to explain the kinetics in paste whereas non-linear model ($t^{0.5}$ model was found to be more suitable to explain the kinetics in mortar) on exposure to acetic acid.

The general considerations to be given in the development of a test method to evaluate the acid resistance of materials are discussed in two sub-sections; considerations with respect to choice of test measures and the recommendations made based on the study. A new test parameter named performance ranking factor was formulated, which combines the parameters related to changes in mass, alterations in microstructure and physico-mechanical properties related to degradation kinetics. The performance of various binder systems were ranked based on the PRF. Based on the study, specific recommendations were made with respect to the type and concentration of acid solution to be used, the use of abrasive action and the nature of specimen to be used for testing acid attack.

CHAPTER 10

CONCLUSIONS

10.1 CONCLUDING REMARKS

Concrete structures are vulnerable to the deterioration by aggressive acidic solutions present in the industrial effluents. Cement hydrates are unstable in such low pH environments; these leach out to the solution and form salts, and this process results in the rapid deterioration of microstructure, affecting the concrete durability. This phenomenon is influenced by multitude of factors and there are hardly any codes or standards available, which holistically address the durability testing of cement-based materials exposed to acids. Moreover, the results depicting the performance of SCMs in aggressive acidic environments are, in general, inconclusive. In this context, the current study deals with a comprehensive investigation of acid attack phenomenon by testing cementitious paste and mortar specimens made with common and advanced binder systems exposed to various acids that are present in the industrial effluents. The study is one of its first kind in Indian context addressing the performance evaluation of various binder systems exposed to different acids.

To achieve these objectives, field investigations were conducted in order to understand the severity and macro-nature of the problem. Further, micro-analytical characterisation tests were conducted on the samples collected to understand the nature of degradation. This was followed by laboratory investigations on paste and mortar. Accelerated immersion tests exposed to various acids were done on paste and mortar specimens made with commonly used and special binders, with and without the abrasive action, to investigate the degradation kinetics. The degradation kinetics was studied using parameters such as mass change, change in pH of the acid solution, altered depth and thickness change. In the case of mortar, the alterations in the physico-mechanical properties were studied based on change in strength and dynamic modulus of elasticity. Additionally, the effect of factors such as concentration of acid, pH of acid solution and water to binder ratio on the degradation kinetics of mortar was also investigated. Micro-analytical studies including X-ray diffraction (XRD), X-ray tomography (CT), scanning electron microscopy (SEM), mercury intrusion porosimetry (MIP), and thermogravimetric analysis (TGA) were done on the attacked paste and mortar samples to understand the mechanism of degradation and the role of interfacial transition zone (ITZ) in mortar. Further, the effect of mineralogical nature of aggregate on the kinetics of degradation in mortar was also investigated.

In addition to the regular choice of test parameters such as changes in mass and strength, new test parameters such as altered area/depth and relative dynamic modulus of elasticity are proposed as additional measures of degradation, which are related to the alterations in the microstructure. A test parameter combining the above-said test measures is proposed to assess the material resistance to acid attack. An attempt was also made to develop models for predicting the deterioration due to acid attack. Additionally, recommendations for the development of a sound test method to assess the material resistance to acid attack were formulated.

The study on degradation kinetics in paste showed that the acid attack is profoundly influenced by the solubility of salt and its properties such as molar volume. Organic acids such as acetic and citric acid were found to be aggressive to the cementitious matrix. It is found that the performance of slag was better on exposure to sulphuric, hydrochloric and acetic acids based on the mass changes. A general notion that blended cements will be more durable than a plain cement was found to be inappropriate in the case of acidic environments as the performance of binder system differs based on the acid type. The aggregate type and the presence of ITZ were found to influence the kinetics of degradation. The ITZ in mortar was found to accelerate the degradation. In general, it can be noted that additional calcium buffer in the system could lead to enhanced resistance on exposure to sulphuric acid whereas reduced calcium content in the binder system is found to enhance the acid resistance on exposure to acids that form soluble salts such as acetic acid. The degradation kinetics and the mechanism of degradation due to acid attack were comprehensively investigated through a set of experiments and the use of characterisation techniques. X-ray tomography was used as a novel technique to shed more light on the deterioration of cement-based materials exposed to various acids. The specific conclusions drawn from the study are discussed in the subsequent section.

10.2 SPECIFIC CONCLUSIONS

10.2.1 Field Investigations

- The micro-analytical characterisation on samples collected from sewage treatment plant and molasses based distillery plant indicated intense decalcification of the hydrated phases, exhibiting porous microstructure. The presence of gypsum was noted in both the cases and it could be inferred that the attack is possibly due to sulphuric and other organic acids produced by microbes thriving in these effluents.

- The SEM images with EDS show gypsum bound with amorphous silica gel enriched in aluminium for the samples collected from the sewage treatment plant, which is a characteristic microstructure of attack by sulphuric acid.

- The micro-analytical studies done on the samples collected from the sewage treatment plant reveal that the deterioration was more pronounced in the screen and grit chamber when compared to locations such as primary and secondary clarifier. This reinstates that the continuous flow of sewage and the eroding action on the cementitious surfaces plays a major role in accelerating the attack, in addition to the aggressiveness of the acid solutions.

- The case study investigation done on the sugar molasses based distillery plant revealed severe premature deterioration of concrete tank that is used to store spent wash. The micro-analytical studies indicate that the attack is primarily due to the attack by various acids (sulphuric acid and organic acids) that are present in the spent wash. The microstructure of the sample revealed decalcification of hydrates exhibiting porous microstructure with mineralogical zonation.

- The XRD analysis of the outer layer of the deteriorated sample collected from the distillery plant was found to be amorphous, with a prominent amorphous silica band centered at 2θ of about 27° indicating the formation of silica gel due to the attack.

- Sulphuric acid present in the spent wash reacts with cement hydrates to form gypsum, which is found to be embedded in a gel skeleton rich in silica and alumina. Some organic acids present in the spent wash also react with hydrates to form mostly soluble salts on reaction that get leached away to the spent wash solution, increasing the porosity of the samples in the process.

10.2.2 Evaluation of degradation kinetics in paste

General observations

- The study on degradation kinetics using accelerated immersion test on paste shows that the acid attack is primarily influenced by the solubility of calcium salt and its properties such as molar volume, and its affinity with the inner cement matrix.
- The specimens exposed to sulphuric acid and citric acid formed precipitates on the surface of the matrix, as the salts were very less soluble. However, no precipitation was observed in the case of acetic and hydrochloric acid because of the high solubility of the calcium salts, and the deterioration was less evident on the visual observations.
- Among the acids tested, citric acid was the most aggressive which resulted in severe mass and thickness loss in specimens. In the case of OPC paste exposed to 0.5M citric acid (with brushing), the mass loss was 74.5% when compared against 7.1%, 34%, 34.4%, 17% and 30% in the case of exposure to 1% sulphuric, 3% sulphuric, 1% HCl, 0.25M acetic and 0.5M acetic acid respectively.
- In the case of testing without brushing, the OPC paste exposed to 1% sulphuric acid had a mass gain of 8.33% (due to buildup of gypsum), while the OPC paste exposed to 3% sulphuric acid had a considerable mass loss of 32.03%. On exposure to 1% HCl, 0.25M acetic, 0.5M acetic and 0.5M citric acids, the mass losses of OPC paste were 14.85%, 13.77%, 22.91% and 83.70% respectively.
- The gypsum formed had a protective effect limiting the alteration kinetics by plugging the pores created by the decalcification in the case of paste exposed to 1% sulphuric acid (79% less mass loss compared to 3% sulphuric acid) tested with brushing. This protective effect was more pronounced in the case of paste with SCMs like slag and fly ash.

- The use of abrasive action accelerated the kinetics in the case of sulphuric acid attack. The abraded OPC paste had a mass loss of 7.1% against a mass gain of 8.3% in the case without abrasive action. It is recommended that the abrasive action may be used to evaluate the kinetics exposed to those acids which form less soluble salts like sulphuric acid. The role of abrasive action in accelerating the kinetics was found to be less pronounced in the case of paste exposed to acids that form soluble salts such as HCl and acetic acid.

- As the concentration of acid increased, the kinetics of degradation increased significantly. In the case of acetic acid, the variation in mass loss of paste was found to be linearly proportional to the age of acid exposure.

- Among the common binders, the slag paste showed better performance against sulphuric, hydrochloric and acetic acids based on the mass changes. The OPC and silica fume paste mixes showed less mass losses on exposure to citric acid.

- The alteration depths for the paste made with SCMs were found to be higher compared to OPC, which is indicative of direct attack of CSH gel caused by the limited availability of Portlandite in the SCM binder systems.

- Special composites such as high alumina cement and limestone calcined clay binder performed better only in the case of exposure to lower concentrations of sulphuric and acetic acids.

- The paste study revealed that accelerated testing should be performed with high concentration of acid to clearly demarcate the performance of each binder.

- The increase in the pH of acid solution was higher for the pastes exposed to acids forming soluble salts, which demands the use of higher volume ratio or frequent renewal of acid under such cases, to maintain the aggressiveness of the solution. However, the increase in the pH for the acids which form sparingly soluble salts such as sulphuric and citric acid was found to be marginal.

Degradation kinetics specific to acid

Sulphuric acid

- The paste specimens exposed to lower concentration of sulphuric acid (1%) experienced an initial mass gain due to gypsum formation and mass loss on prolonged exposure due to delamination of the corroded layer. The slag paste (BFS50) showed better performance based on mass changes on exposure to 1% sulphuric acid followed by FA30, SF10 and OPC (tested with abrasive action).

- The performance in terms of mass changes of common binders such as FA30, SF10 was found to be ordinary and comparable to OPC in the case of paste exposed to 3% sulphuric acid. Only the slag mix showed improved resistance as the gypsum layer was found to be adherent to the matrix.

Hydrochloric acid

- All the paste specimens exposed to HCl showed mass loss at all ages, as leaching was the driving process of deterioration. The mass loss was found to increase at a constant rate with the acid exposure period. The abrasive action increased the kinetics, but at a lower rate compared to 1% sulphuric acid.

- In both the cases, with and without brushing, the performance of slag paste exposed to 1% HCl was found to be better, as the mass loss was less when compared to the other mixes.

Acetic acid

- Acetic acid, although considered as a weak organic acid, was found to be aggressive to the cementitious medium leading to strong calcium leaching as the degradation led to considerable mass losses and alteration depths. The performance of slag paste was found to be better irrespective of the concentration of acetic acid and the test method (with and without brushing) when compared with the other common binder systems.

- It is observed that the kinetics of OPC, fly ash and silica fume paste were close to each other at lower concentration of acetic acid (0.25M). This necessitates the need to develop tests using higher concentrations to distinguish the performance of mixes.

- Despite the lower initial Ca content in the mix, the performance of the fly ash paste (FA30) was found to be the worst on exposure to 0.25M and 0.5M acetic acid. The attack resulted in the highest alteration depth among the binder systems evaluated.

Citric acid

- On exposure to 0.5M citric acid, the performance of silica fume (SF10) was found to be better followed by OPC paste. Notably, the performance of paste such as FA30 and BFS50 was found unsatisfactory as the mass losses were considerably higher. The role of abrasion was found to be minimal as the salt precipitated defragmented by itself, and only a thin layer of it could be seen attached on the surface of the specimen.

Performance of special binders

- The test results with brushing indicate that the performance of LC2 paste is better than OPC and HAC on exposure to 1% sulphuric acid. Instead of mass gain, mass loss was observed for HAC paste on exposure to 1% sulphuric acid at all ages of acid exposure. On exposure to 3% sulphuric acid, the HAC paste performed poorly as the mass loss was found to be higher compared to the OPC and LC2 paste.

- On exposure to acetic acid, the HAC mix showed better performance as mass loss was found to be less when compared to the OPC and LC2 pastes. Even though the HAC paste had less mass loss in 0.5M acetic acid, the specimens became weak and brittle on prolonged exposure to 0.5M acetic acid.

- The pH rise of the acid solution was higher for HAC paste on exposure to sulphuric acid, when compared to LC2 and OPC. On exposure to acetic acid, the OPC paste showed higher pH of the solution followed by LC2 and HAC.

10.2.3 Study on degradation mechanism in paste

- The mineralogical zonation due to the attack was captured by imaging using X-ray tomography. In the case of sulphuric and citric acids, it was evident from the images that the deterioration of the paste mixes was due to the formation of expansive salts with higher molar volume. In the case of acetic and hydrochloric acid, decalcification shrinkage was observed on the corroded surfaces and the darker regions of the paste in the images indicated decalcification of phases.

- Further, image analysis was done based on the slice images obtained from tomography in order to estimate the altered depth to understand the kinetics. The altered depth was estimated as the sum of depths of degraded outer layer and the middle decalcified layer, added to the depth lost due to reactions and/or brushing.

- A considerable increase in cumulative intruded volume due to acid attack was evident from MIP results. The increase in porosity due to decalcification could then affect the transport properties, leading to further ingression of acids and deterioration.

- The increase in capillary porosity was found to be higher for the paste exposed to 0.5M acetic acid. The altered depth comprising of porous silica gel was greater for acetic acid and this resulted in considerable increase in capillary porosity.

- The MIP results reveal that the intrusion porosity in OPC paste is higher in the case of 0.5M acetic acid (porosity of 57% when compared to 15.6%, 32% and 25.2% in the case of 1% sulphuric, 1% hydrochloric, 0.5M citric acid respectively). A substantial increase in the capillary porosity was evident after the acid exposure, enhancing the rate of diffusion of acid further.

- The MIP results showed substantial reduction in the bulk density and increase in the intrusion porosity of paste on exposure to acetic and hydrochloric acids that form soluble salts. The fly ash (FA30) mix had greater reduction in the bulk density and increase in the porosity and this resulted in highest alteration depth in the case of 0.5M acetic acid. Among the mixes, the attacked slag paste (BFS50) had the minimum porosity and the altered depth on exposure to 1% hydrochloric and 0.5M acetic acid.

- Based on SEM and XRD analysis, the major reaction products identified in sulphuric acid attack were gypsum, ettringite and silica gel, whereas Friedel’s salt, ettringite and silica gel were formed on exposure to hydrochloric acid. In the case of acetic acid, the products formed were soluble salt of calcium along with silica gel, whereas calcium citrate tetra hydrate salt was precipitated in enormous quantities on exposure to citric acid along with formation of silica gel. In the case of high alumina cement, C_3AH_6 was found to be unstable in sulphuric and acetic acids, forming the products gypsum, ettringite and amorphous AH_3 in the case of sulphuric acid, and soluble calcium acetate and amorphous AH_3 in the case of acetic acid.

- The SEM images revealed gypsum deposits embedded in silica gel in the case of all pastes exposed to sulphuric acid. The crystallisation of ettringite was seen only in the inner layers. On exposure to hydrochloric acid and acetic acid, the degraded layer showed porous and fragmented microstructure comprising of silica gel. In the case of citric acid, severe precipitation of expansive salts was evident along with the formation of silica gel.

- TGA results show that the reduction in Portlandite content is more pronounced in the case of acetic and hydrochloric acid. The reduction in Portlandite content was found to be less in the case of exposure to 1% sulphuric acid and 0.5M citric acid.

10.2.4 Evaluation of degradation kinetics in mortar

Performance of common binders

- The kinetics study in mortar revealed the improved performance of silica fume (SF10) when compared to the ordinary behaviour exhibited in paste, possibly due to the influence of strengthening of ITZ and better de-densification of silica fume in mortar.

- Slag and mortar showed best performance in both sulphuric and acetic acid compared to the other common binders, based on the mass changes.

- The fly ash mortar (FA30) and slag mortar (BFS50) showed less mass loss on exposure to 0.5M acetic acid (26% and 21.5% less compared to OPC mortar), however with higher alteration depths (94.3% and 37.4% higher alteration depths compared to OPC mortar for a w/b of 0.40).

- All the binder systems except slag showed poor performance in terms of mass changes on exposure to higher concentration of sulphuric acid (3%).

- The degradation of mortar exposed to pH2 sulphuric and pH4 acetic acids was limited when compared to the kinetics in 1% sulphuric and 0.25M acetic acid. This again reinstates the need to test higher concentrations for the performance evaluation of binders.

- Similar to paste study, the use of abrasive action accelerated the kinetics in mortar in the case of exposure to sulphuric acid, predominantly at lower concentrations of sulphuric acid (1%).

- The size effect (i.e. surface area to volume ratio) of the specimens in influencing the degradation kinetics was studied on prismatic specimens. It was found that the kinetics got accelerated as the surface area to volume ratio of the specimen is increased. However, the effect was more pronounced only in the case of exposure to high concentration of acetic acid and found to be marginal on exposure to sulphuric acid.

- Similar to the observations in the paste study, the mortar mixes made using SCM had higher altered depths compared to the OPC. Among the SCM mixes, the fly ash mix showed the highest altered depth due to the attack.

- A progressive reduction in the compressive strength was observed for all the mortar specimens on exposure to sulphuric and acetic acid. The drop in compressive strength was found to be higher on exposure to acetic acid because of the relatively higher depth of decalcification.

- The dynamic modulus of elasticity estimated based on the ultrasonic pulse velocity and the bulk density of the mortar specimens showed a good declining trend with the age of acid exposure. Unlike the strength results which showed larger variability, the variability in the dynamic modulus of elasticity was found to be less and this could be used as a choice of degradation measure in studying the alterations in physico-mechanical properties of mortar.

- The study indicated that a lower w/b ratio of 0.40 resulted in higher mass changes when compared to a higher w/b of 0.55 for all the mixes exposed to sulphuric acid (104% higher mass loss for w/b of 0.40 compared to w/b of 0.55 in the case of OPC mortar exposed to 1% sulphuric acid, tested with brushing). In the case of acetic acid, the use of lower w/b of 0.40 resulted in lower mass loss compared to w/b of 0.55 (15.4% and 13.6% less mass loss for 0.40 compared to w/b of 0.55 for OPC mortar exposed to 0.25M and 0.5M acetic acid respectively). This is also reflected in the relative dynamic modulus of elasticity (14% higher E value for 0.4 w/b compared to w/b of 0.55 for OPC mortar exposed to 0.25M acetic acid).
- The ITZ in mortar was found to accelerate the kinetics in acid attack. The OPC mortar (with w/b of 0.40) on exposure to 0.5M acetic acid showed a mass loss of 10.1% only when compared to 22.9% mass loss in paste after 5 cycles of acid renewal. Considering the fact that siliceous aggregates are inert and no aggregates are lost from the matrix during exposure, it is the paste phase which undergoes decalcification. The paste content in the 1:3 mortar with a w/b of 0.40 being 31.8% (by mass), it can be inferred that 10.1% mass loss is from 31.8% paste in the mortar, i.e. 31% mass loss due to decalcification of paste in mortar, which is higher than the 22.9% mass loss observed in paste, indicating the role of ITZ in acid attack.
- A single test parameter called Performance Ranking factor (PRF) is formulated as a performance indicator which combines the kinetics parameters related to changes in mass, alterations in microstructure and physico-mechanical properties.

Performance of special binders

- As observed in the paste, the performance of LC2 mortar was better on exposure to 1% sulphuric acid. In the case of HAC mortar, the dissolution of C_3AH_6 resulted in the mass loss higher than the mass loss observed in the paste. The performance of these special binders was ordinary on exposure to 3% sulphuric acid compared to OPC mortar.

- On exposure to 0.25M acetic acid, the LC2 mortar made with a lower w/b of 0.40 was found to be better compared to HAC and OPC mortar. However, the use of higher w/b of 0.55 was observed to reduce the mass loss for LC2 mortar on exposure to 1% sulphuric acid. In the case of 0.5M acetic acid, LC2 mortar performed better compared to HAC and OPC mortar.

10.2.5 Study on degradation mechanism in mortar

- The mortar on exposure to sulphuric acid showed deterioration due to the formation of gypsum and silica gel. The expansion due to gypsum resulted in the loss of binding property causing the aggregates to separate from the matrix. Severe cracks along the ITZ of mortar were seen in the tomography images.
- In the case of acetic acid, the deterioration was due to increase in the porosity due to the formation of soluble salts and silica gel. The paste phase was decalcified causing dark appearance in tomography images. However, as expansive precipitates were not formed, aggregates were not removed from the matrix.
- In the case of 3% sulphuric acid, the improved performance of slag mortar was evident in the tomography image. The thick degraded layer comprising of gypsum was seen to adhere with the matrix, resulting in lower mass loss compared to the other mixes.
- TGA results indicate that the whole Portlandite in the mortar specimens was consumed for the reaction on exposure to 0.5M acetic acid.
- The SEM micrographs show that the ITZ in the mortar is filled with finer sized gypsum deposits on exposure to 1% sulphuric acid. Ettringite being unstable at low pH was seen only in the inner layers of the specimen. In the case of 3% sulphuric acid, long needle shaped gypsum deposits were noted in the degraded layer; expansion and delamination of the gypsum layer occurred on prolonged exposure. The presence of ettringite was limited to the inner layers.

- The morphology of the degraded layer of mortar exposed to acetic acid showed severe degradation. The microstructure appeared granulated and highly porous comprising of silica gel. The ITZ was also seen to be porous with loose deposits of silica gel.

- The presence of ITZ in mortar influenced the kinetics. The ITZ accelerated the kinetics, especially at higher concentrations of acid. Hence, the use of mortar specimens is recommended, if the primary objective is to investigate the alteration kinetics.

- Accelerated testing with smaller specimen size and increased concentration of acid (when compared to the realistic concentration) with frequent replenishment of acid solutions is recommended to enable a better performance evaluation of various mixture formulations. However, laboratory testing with very high concentration of acid can underestimate the better performance of SCMs evident on exposure to lower concentrations of sulphuric and acetic acid.

10.2.6 Effect of mineralogy of aggregate

- It was found that the aggregate type had an effect on the degradation kinetics. The mortar with limestone (calcareous) aggregates showed a less degradation depth than did the mortar with inert (siliceous river sand) aggregates.

- The limestone aggregates locally created a buffering environment due to acid soluble calcium thus rendering a sacrificial protective effect, protecting the cement paste from the acid dissolution. Based on the parameters investigated in terms of alteration kinetics and physico-mechanical properties, it was found that the mortar with limestone aggregates performed better on exposure to sulphuric acid environment when compared to mortar with siliceous aggregates. However, the mass loss for limestone aggregate mortar on exposure to acetic acid was found to be significantly higher when compared to mortar with siliceous aggregates owing to the solubility of calcium salts.

10.3 SCOPE FOR FUTURE WORK

- From the present study, it was observed that the presence of alumina in the binder system enhances the resistance against acid attack by increasing the stability of the corroded layer. More detailed study can be carried out addressing this aspect further. The various binder systems rich in alumina such as metakaolin, limestone calcined clay systems may be tested to ascertain their performance in various acids.
- From the present study, it was noted that the fly ash paste and mortar specimens performed poorly on exposure to organic acids. More in-depth studies should be done to understand the influence of particle size and reactivity of SCMs such as fly ash on the degradation due to acid attack.
- In most of the cases such as concrete sewers, biogas reactors etc., the sulphuric acid is produced by microbes thriving in these effluents. New test methods should be developed based on the action of microbes that simulates the real environment.
- The design of mortar specimen in developing a sound accelerated test method needs further study. The effect of particle packing, composition of binders and aggregates, binder to aggregate ratio, size and shape of the specimen need to be explored in this regard.
- The size effect in acid attack has to be investigated further for developing a model to predict the response of large specimens against acid attack.
- The various parameters influencing the aggressiveness of organic acids needs further study.
- The influence of kinetics of salt formation and its stability in acid solution, morphology and mesoscopic shape of the salts formed and their affinity to the cement matrix has to be explored further.
- The role of geopolymer paste and mortar in resisting acids should be explored.
- More clarification is needed on the mechanism of acids whose salts are slightly soluble to insoluble and in the role of various SCMs.
- The performance ranking factor proposed in the study shall be further developed and modified as a reliable indicator of acid attack.

REFERENCES

ACI 201.2R-16 (2016) Guide to durable concrete (Reported by ACI Committee 201), *American Concrete Institute*, Farmington Hills, USA, 1-84.

ACI 210.1R-94 (1994) Compendium of case histories on repair of erosion-damaged concrete in hydraulic structures (Reapproved 1999), ACI Committee 210, *American Concrete Institute,* Farmington Hills, USA, 1-33.

Aiken, T. A., Sha, W., Kwasny, J., and M. N. Soutsos (2017) Resistance of geopolymer and Portland cement based systems to silage effluent attack, *Cement and Concrete Research*, **92 (2)**, 56-65.

Alexander, M. G. and H. Beushausen (2009) Deformation and volume change of hardened concrete, pp. 111-154. In Owens, G., (Ed.) *Fulton's Concrete Technology*, Chapter 8, Cement & Concrete Institute, Ninth edition, Midrand, South Africa.

Alexander, M. G. and C. Fourie (2011) Performance of sewer pipe concrete mixtures with Portland and calcium aluminate cements subject to mineral and biogenic acid attack, *Materials and Structures*, **44**, 313-330.

Alexander, M. G. and S. Mindess (2005) *Aggregates in Concrete***,** Taylor and Francis, London.

Alexander, M. G., and N. De Belie (2013) Testing for degradation by inorganic acids, pp. 289-303, In: Alexander, M. G., Bertron, A., De Belie, N. (Eds.) RILEM TC 211 - PAE State-of-the-Art Report: Performance of Cement-Based Materials in Aggressive Aqueous Environments.

Aligizaki, K. K. (2005) *Pore Structure of Cement-Based Materials: Testing, Interpretation and Requirements,* Taylor & Francis Group, CRC Press, Boca Raton.

Allahverdi, A. and F. Skvara (2000a) Acidic corrosion of hydrated cement based materials: Part 2: Kinetics of the phenomenon and mathematical models, *Ceramics-Silikáty*, **44**, 152-160.

Allahverdi, A. and F. Škvára (2000b) Acidic corrosion of hydrated cement-based materials: Part 1. Mechanisms of the phenomenon. *Ceramics-Silikáty*, **44**, 114-120.

Amin, M. and M. T. Bassuoni (2018) Response of concrete with blended binders and nanoparticles to sulfuric acid attack, *Magazine of Concrete Research*, **70(12)**, 617-632.

Antoni, M. (2013) Investigation of cement substitution by blends of calcined clays and limestone, Ph.D. dissertation, École Polytechnique Fédérale de Lausanne, Lausanne.

Antoni, M., Rossen, J., Martirena, F., and K. Scrivener (2012) Cement substitution by a combination of metakaolin and limestone, *Cement and Concrete Research*, **42**, 1579-1589.

ASTM D4644 – 16 (2016) Standard test method for slake durability of shales and other similar weak rocks, *ASTM International*, West Conshohocken, Pennsylvania.

ASTM E632-82 (1988), Practice for developing accelerated tests to aid prediction of the service life of building components and materials**,** *American Society for Testing and Materials*, Philadelphia.

Attiogbe, K. A. and S. H. Rizkalla (1988) Response of concrete to sulphuric acid attack, *ACI Material Journal*, **84**, 481-488.

Ballim, Y., Alexander, M. G., and H. Beushausen (2009) Durability of Concrete, In: *Fulton's concrete technology*, Gill Owens (Ed.), Cement and Concrete Institute, Midrand, South Africa.

Balonis, M. and F. P. Glasser (2009) The density of cement phases, *Cement and Concrete Research*, **39**, 733-739.

Beddoe, R. E. and H. W. Dorner (2005) Modelling acid attack on concrete: Part 1. The essential mechanism, *Cement and Concrete Research*, **35**, 2333-2339.

Bentz, D. P., Sato, T., de la Varga, I. and W. J. Weiss (2012) Fine limestone additions to regulate setting in high volume fly ash mixtures, *Cement and Concrete Composites*, **34**, 11-17.

Berodier, E. and K. Scrivener (2014) Understanding the filler effect on the nucleation and growth of C-S-H, *Journal of the American Ceramic Society*, **97(12)**, 3764-3773.

Bertron, A. (2013) Methods for testing cementitious materials exposed to organic acids, pp. 355-387, In: Alexander, M. G., Bertron, A., De Belie, N. (Eds.) RILEM TC 211 - PAE State-of-the-Art Report: Performance of Cement-Based Materials in Aggressive Aqueous Environments.

Bertron, A. (2014) Understanding interactions between cementitious materials and microorganisms: A key to sustainable and safe concrete structures in various contexts, *Materials and Structures*, **47(11)**, 1787-1806.

Bertron, A. and J. Duchesne (2013) Attack of cementitious materials by organic acids in agricultural and agrofood effluents, pp. 131-173, In: Alexander, M. G., Bertron, A., De Belie, N. (Eds.) RILEM TC 211 - PAE State-of-the-Art Report: Performance of Cement-Based Materials in Aggressive Aqueous Environments.

Bertron, A., Duchesne, J., and G. Escadeillas (2005) Attack of cement pastes exposed to organic acids in manure, *Cement and Concrete Composites*, **27**, 898-909.

Bertron, A., Duchesne, J., and G. Escadeillas (2007) Degradation of cement pastes by organic acids, *Materials and Structures*, **40(3)**, 341-354.

Bertron, A., Escadeillas, G., and J. Duchesne (2004) Cement pastes alteration by liquid manure organic acids: Chemical and mineralogical characterization, *Cement and Concrete Research*, **34(10)**, 1823-1835.

Bertron, A., Escadeillas, G., and J. Duchesne (2006) Durability of various binders exposed to organic acids in liquid manure. In: Malhotra, V. M. (Ed.) Proceeding of the 7th CANMET/ACI International Conference on Durability of Concrete, Montreal.

Bertron, A., Larreur-Cayol, S., and G. Escadeillas (2011) Organic acids' attack on cementitious materials: aggressiveness and degradation mechanisms, In: Instituto de Ciencias de la Construccio´n "Eduardo Torroja". CSIC. Palomo, A., Zaragoza, A., Lopez Aguii, J.C. (Eds.) Proceedings of the XIIIth International Conference on the Chemistry of Cement, Madrid.

Bertron, A., Larreur-Cayol, S., Le, T., and G. Escadeillas (2009) Degradation of cementitious materials by some organic acids found in agroindustrial effluents, pp. 96-107, In: Alexander, M. G., Bertron, A. (Ed.) Proceedings of the RILEM TC 211-PAE Final Conference, Toulouse.

Bertron, A., Lavigne, M. P., Patapy, C. and B. Erable (2017) Biodeterioration of concrete in agricultural, agro-food and biogas plants: state of the art and challenges. *RILEM Technical Letters*, **2**, 83-89.

Boel, V., Cnudde, V., De Schutter, G., and B. Van Meel (2008) X-ray computed microtomography on cementitious materials: Possibilities and limitations, International RILEM Symposium on Concrete Modeling - CONMOD'08, 487-494.

Bossa, N., Chaurand, P., Vicente, J., Borschneck, D., Levard, C., and O. Aguerre-Chariol (2015) Micro- and nano-X-ray computed-tomography : A step forward in the characterization of the pore network of a leached cement paste, *Cement and Concrete Research*, **67**, 138-147.

Brouwer, P. N. (2010) *Theory of XRF*, ISBN 90-9016758-7 (Third edition), PANalytical B. V., The Netherlands.

BS 8500-1 (2015) Concrete – complementary British standard to BS EN 206: Part 1 - Method of specifying and guidance of the specifier, *British Standards Institution*, London, 1-68.

BS EN 206 (2013) Concrete specification, performance, production, and conformity, *British Standards Institution*, London, 1-98.

Burlion, N., Bernard, D., and D. Chen (2006) X-ray microtomography: Application to microstructure analysis of a cementitious material during leaching process, *Cement and Concrete Research*, **36**, 346-357.

Cerny R. and P. Rovnanikova (2002) *Transport processes in concrete*, Spon Press, London.

Cesen, A., Korat, L., Mauko, A., and A. Legat (2013) Microtomography in building materials, *Materials and Technology*, **47(5)**, 661-664.

Chang, Z. T., Song, X. J., Munn, R., and M. Marosszeky (2005) Using limestone aggregates and different cements for enhancing resistance of concrete to sulphuric acid attack, *Cement and Concrete Research*, **35**, 1486-1494.

Chatterjee, A. and A. Goyns (2013) Cementitious materials performance in aggressive aqueous environments – Engineering perspectives, pp. 391-449, In: Alexander, M. G., Bertron, A., De Belie, N. (Eds.) RILEM TC 211 - PAE State-of-the-Art Report: Performance of Cement-Based Materials in Aggressive Aqueous Environments.

Chenn, J. J., Thomas, J. J., and H. M. Jennings (2006) Decalcification shrinkage of cement paste, *Cement and Concrete Research*, **36(5)**, 801-809.

Chotard, T. J. and A. Smith (2003) Application of X-ray computed tomography to characterise the early hydration of calcium aluminate cement, *Cement and Concrete Composites*, **25(1)**, 145-152.

Chotard, T. J., Smith, A., Boncoeur, M., Fargeot, D., and C. Gault (2003) Characterisation of early stage calcium aluminate cement hydration by combination of non-destructive techniques: acoustic emission and X-ray tomography, *Journal of the European Ceramic Society*, **23(13)**, 2211-2223.

Comité Euro-International du Béton (1989) Durable concrete structures bulletin d'information No. 182, Paris.

Cong, X., Gong, S., Darwin, D., and S. L. McCabe (1992) Role of silica fume in compressive strength of cement paste, mortar and concrete. *ACI Material Journal*, **89(4)**, 375–387.

De Belie, N. (2008) Evaluation of methods for testing concrete degradation in aggressive solution, Workshop on Performance of Cement based Materials in Aggressive Aqueous Environments—Characterisation, Modelling, Test Methods and Engineering Aspects, RILEM Publications SARL, 79-90.

De Belie, N. (2013) General considerations: Methods for testing concrete degradation in aggressive aqueous environments, pp. 219-234, In: Alexander, M. G., Bertron, A., De Belie, N. (Eds.) RILEM TC 211 - PAE State-of-the-Art Report: Performance of Cement-Based Materials in Aggressive Aqueous Environments.

De Belie, N., Monteny, J., and L. Taerwe (2002) Apparatus for accelerated degradation testing of concrete specimens, *Materials and Structures*, **35**, 427-433.

De Belie, N., Monteny, J., Beeldens, A., Vincke, E., Van Gemert, D., and W. Verstraete (2004) Experimental research and prediction of the effect of chemical and biogenic sulfuric acid on different types of commercially produced concrete sewer pipes, *Cement and Concrete Research*, **34**, 2223-2236.

De Belie, N., Verselder, H. J., De Blaere, B., Van Nieuwenburg, D., and R. Verschoore (1996) Influence of the cement type on the resistance of concrete to feed acids, *Cement and Concrete Research*, **26(11)**, 1717-1725.

De Graef, B., Cnudde, V., Dick, J. De Belie, N., Jacobs, P., and W. Verstraete (2005) A sensitivity study for the visualisation of bacterial weathering of concrete and stone with computerised X-ray microtomography, *Science of the Total Environment*, **341**, 173-183.

De Muynck, W., De Belie, N., and W. Verstraete (2009) Effectiveness of admixtures, surface treatments and antimicrobial compounds against biogenic sulfuric acid corrosion of concrete, *Cement and Concrete Composites*, **31**, 163-170.

De Schutter, G. (1999) Hydration and temperature development of concrete made with blast-furnace slag cement, *Cement and Concrete Research*, **29(1)**, 143-149.

De Windt, L., Bertron, A., Larreur-Cayol, S., and G. Escadeillas (2015) Interactions between hydrated cement paste and organic acids: Thermodynamic data and speciation modeling, *Cement and Concrete Research*, **69**, 25-36.

Dhandapani, Y. and M. Santhanam (2017) Assessment of pore structure evolution in the limestone calcined clay cementitious system and its implications for performance, *Cement and Concrete Composites*, **84**, 36-47.

Dhandapani, Y., Sakthivel, T., Santhanam, M., Gettu, R., and R. G. Pillai (2018) Mechanical properties and durability performance of concretes with Limestone Calcined Clay Cement (LC^3), *Cement and Concrete Research*, **107**, 136-151.

Dhanya, B. S. (2015) Study of the influence of supplementary cementitious materials on selected durability parameters of concrete, Ph.D. Thesis, IIT Madras.

Dhir, R. K., El-Mohr, M. A. K., and T.D. Dyer (1996) Chloride binding in GGBS concrete, *Cement and Concrete Research*, **26(12)**, 1767-1773.

Diamond, S. and E. N. Landis (2007) Microstructural features of a mortar as seen by computed microtomography, *Materials and Structures*, **40(9)**, 989-993.

Duchesne, J. and A. Bertron (2013) Leaching of cementitious materials by pure water and strong acids (HCl and HNO_3), pp. 91-112, In: Alexander, M. G., Bertron, A., De Belie, N. (Eds.) RILEM TC 211 - PAE State-of-the-Art Report: Performance of Cement-Based Materials in Aggressive Aqueous Environments.

Dyer, T. (2014) *Concrete Durability*, CRC Press, Taylor & Francis Group, 1-420.

Dyer, T. (2016) Influence of cement type on resistance to organic acids, *Magazine of Concrete Research*, **69(4)**, 175-200.

Dyer, T. (2017) Influence of cement type on resistance to attack from two carboxylic acids. *Cement and Concrete Composites*, **83**, 20-35.

Eštokova, A., Harbuľáková, V. O., Luptáková, A., and N. Števulová (2012) Study of the deterioration of concrete influenced by biogenic sulphate attack, *Procedia Engineering*, **42**, 1731-1738.

Fattuhi, N. I. and B. P. Hughes (1988) SRPC and modified concretes subject to severe sulphuric acid, *Magazine of Concrete Research*, **40**, 159-166.

Fernandes, I., Pericao, M., Hagelia, P., Noronha, F., Ribeiro, M. A., and J. Maia (2012) Identification of acid attack on concrete of a sewage system, *Materials and Structures*, **45**, 337-350.

Fryda, H., Scrivener, K. L., Chanvillard, G. and Féron, C. (2001) Relevance of laboratory tests to field applications of calcium aluminate cement concretes, pp. 227-246, In: Mangabhai, R.J. and Glasser, F.P. (Eds.), Calcium Aluminate Cements. IOM Communications, London.

Gallucci, E., Scrivener, K., Groso, A., Stampanoni, M., and G. Margaritondo (2007) 3D experimental investigation of the microstructure of cement pastes using synchrotron X-ray microtomography (μCT), *Cement and Concrete Research*, **37(3)**, 360-368.

Gjrov, O. E. (1993) Durability of concrete containing condensed silica fume, *ACI Special Publications SP-79*, 695-708.

Gosselin, C. (2009) Microstructural development of calcium aluminate cement based systems with and without supplementary cementitious materials, Ph.D. dissertation. École Polytechnique Fédérale de Lausanne, Lausanne.

Grengg, C., Mittermayr, F., Baldermann, A., Bottcher, M. E., Leis, A., Koraimann, G., Grunert, P. and M. Dietzel (2015) Microbiologically induced concrete corrosion: A case study from a combined sewer network, *Cement and Concrete Research*, **77**, 16-25.

Grengg, C., Mittermayr, F., Koraimann, G., Konrad, F., Szabo, M., Demeny, A. and M. Dietzel (2017) The decisive role of acidophilic bacteria in concrete sewer networks: A new model for fast progressing microbial concrete corrosion, *Cement and Concrete Research*, **101**, 93-101.

Gu, J. D., Ford, T. E., Berke, N. S., and R. Mitchell (1998) Biodeterioration of concrete by the fungus Fusarium, *International Biodeterioration & Biodegradation*, **4**, 101-109.

Gutberlet, T., Hilbig, H., and R. E. Beddoe (2015) Acid attack on hydrated cement – Effect of mineral acids on the degradation process, *Cement and Concrete Research*, **74**, 35-43.

Gutiérrez-Padilla, M. G. D., Bielefeldt, A., Ovtchinnikov, S., Hernandez, M., and J. Silverstein (2010) Biogenic sulfuric acid attack on different types of commercially produced concrete sewer pipes, *Cement and Concrete Research*, **40**, 293-301.

Haneefa, M. K. (2014) Performance characterisation of concrete for elevated temperature and hot sodium exposure applications in nuclear industry, Ph.D. Thesis, IIT Madras.

Harbulakova, V. O., Estokova, A., Stevulova , N., and A. Luptakova (2014) Different aggressive media influence related to selected characteristics of concrete composites investigation, *International Journal of Energy and Environmental Engineering*, **5**, 1-6.

Harrison, W. H. (1987) Durability of concrete in acidic soils and waters, *Concrete*, **2**, 18-24.

Herisson, J., Van Hullebusch, E. D., Moletta-Denat, M., Taquet, P., and T. Chaussadent (2013) Toward an accelerated biodeterioration test to understand the behavior of Portland and calcium aluminate cementitious materials in sewer networks, *International Biodeterioration & Biodegradation*, **84**, 236-243.

Hewayde, E., Nehdi, M., Allouche, E., and G. Nakhla (2007) Effect of mixture design parameters and wetting-drying cycles on resistance of concrete to sulfuric acid attack, *ASCE Journal of Materials in Civil Engineering*, **19**, 155-163.

Hormann, K., Hofmann, F., and M. Schmidt (1997) Stability of concrete against biogenic sulfuric acid corrosion, a new method for determination. In: Proceedings of the 10th International Congress on the Chemistry of Cement, Gothenberg.

http://www.perkinelmer.com, access verified on May 2018 (site hosted by Perkin Elmer).

https://www.bruker.com/products/x-ray-diffraction-and-elemental-analysis/x-ray-fluorescence.html, access verified on May 2018 (site hosted by Bruker).

https://www.microtrac.com, access verified on May 2018 (site hosted by Microtrac).

Huber, B., Hilbig, H., Drewes, J. E. and E. Muller (2017) Evaluation of concrete corrosion after short- and long-term exposure to chemically and microbially generated sulfuric acid, *Cement and Concrete Research*, **94**, 36-48.

Hudon E., Mirza S. and D. Frigon (2011) Biodeterioration of concrete sewer pipes: State of the art and research needs, *ASCE Journal of Pipeline Systems Engineering and Practice*, **2(2)**, 42-52.

Hughes, B. P., and J. E. Guest (1978) Limestone and siliceous aggregate concretes subjected to sulphuric acid attack, *Magazine of Concrete Research*, **30**, 11-18.

IS 10050: 1981 (1996) Indian Standard method for determination of slake durability index of rocks, *Bureau of Indian Standards*, New Delhi, India (Reaffirmed 1996).

IS 12269: 2013 (2013): Ordinary Portland cement, 53 grade – specification, *Bureau of Indian Standards*, New Delhi, India.

IS 13311 (Part 1): 1992 (2004) Indian Standard non-destructive testing of concrete – methods of test Part 1: ultrasonic pulse velocity, *Bureau of Indian Standards*, New Delhi, India (Reaffirmed 2004).

IS 1727: 1967 (2004) Indian Standard method of test for pozzolanic materials, *Bureau of Indian Standards*, New Delhi, India (Reaffirmed 2004).

IS 4031 (Part 6): 1988 (2005) Indian Standard methods of physical tests for hydraulic cement, *Bureau of Indian Standards*, New Delhi, India (Reaffirmed 2005).

IS 4032: 1985 (2005) Indian Standard method of chemical analysis of hydraulic cement, *Bureau of Indian Standards*, New Delhi, India (Reaffirmed 2005).

IS 650: 1991 (2008) Indian Standard: Standard sand for testing cement – Specification, *Bureau of Indian Standards*, New Delhi, India (Reaffirmed 2008).

IS 9103: 1999 (2004) Indian Standard concrete admixtures – Specification, *Bureau of Indian Standards*, New Delhi, India (Reaffirmed 2004).

IS: 15895 – 2011 (2011) Indian standard high alumina refractory cement – specification, *Bureau of Indian Standards*, New Delhi.

IS: 3812 (Part 1) – 2013 (2013) Indian standard pulverized fuel ash – specification Part 1 for use as pozzolana in cement, cement mortar and concrete, *Bureau of Indian Standards*, New Delhi.

Jacobs, P., Sevensa, E., and M. Kunnenb (1995) Principles of computerised X-ray tomography and applications to building materials, *The Science of the Total Environment*, **167**, 161-170.

Jain, J. and N. Neithalath (2009) Analysis of calcium leaching behavior of plain and modified cement pastes in pure water, *Cement and Concrete Composites*, **31**, 176-185.

Kiliswa, M. W. (2016) Composition and microstructure of concrete mixtures subjected to biogenic acid corrosion and their role in corrosion prediction of concrete outfall sewers, Ph.D. Thesis, University of Cape Town.

Kim, K. Y., Yun, T. S., and K. P. Park (2013) Evaluation of pore structures and cracking in cement paste exposed to elevated temperatures by X-ray computed tomography, *Cement and Concrete Research*, **50**, 34-40.

Kim, K. Y., Yun, T. S., Choo, J., Kang, D. H., and H. S. Shin (2012) Determination of air-void parameters of hardened cement-based materials using X-ray computed tomography, *Construction and Building Materials*, **37**, 93-101.

Koenig, A. and F. Dehn (2016) Main considerations for the determination and evaluation of the acid resistance of cementitious materials, *Materials and Structures*, **49(5)**, 1693-1703.

Landis, E. N. and D. T. Keane (2010) X-ray microtomography, *Materials Characterization*, **61(12)**, 1305-1316.

Lane, R. O. and J. F. Best (1982) Properties and use of fly ash in Portland cement concrete, *Concrete International*, **4(7)**, 81-92.

Larreur-Cayol, S., Bertron, A., and G. Escadeillas (2011a) Degradation of cement-based materials by various organic acids in agro-industrial waste-waters, *Cement and Concrete Research*, **41(8)**, 882-892.

Larreur-Cayol, S., Bertron, A., San Nicolas, R., and G. Escadeillas (2011c) Durability of different binders in synthetic agricultural effluents, pp. 56-66, In: Godbout, S., Potvin, L. (Eds.) Proceedings of 7th International Symposium on Cement Based Materials for a Sustainable Agriculture, Quebec.

Larreur-Cayol, S., De Windt, L., Bertron, A., and G. Escadeillas (2011b) Biodeterioration of cementitious matrices by organic acid in agricultural effluents: experiments and modeling, pp. 38-45, In: Godbout, S. Potvin, L. (Eds.) Proceedings of 7th International Symposium on Cement Based Materials for a Sustainable Agriculture, Quebec.

Lavigne, M. P., Bertron, A., Botanch, C., Auer, L., Hernandez, G., Cockx, A., Foussard, J., Escadeillas, G., and E. Paul (2016) Innovative approach to simulating the biodeterioration of industrial cementitious products in sewer environment Part II: Validation on CAC and BFSC linings, *Cement and Concrete Research*, **79**, 409-418.

Lavigne, M. P., Bertron, A., Botanch, C., Auer, L., Hernandez, G., Cockx, A., Foussard, J., Escadeillas, G., and E. Paul (2015) An innovative approach to reproduce the biodeterioration of industrial cementitious products in a sewer environment Part I: Test design, *Cement and Concrete Research*, **73**, 246-256.

Le Bescop, P., Lothenbach, B., Samson, E., and K. A. Snyder (2013) Modeling degradation of cementitious materials in aggressive aqueous environments, pp. 177-218, In: Alexander, M. G., Bertron, A., De Belie, N. (Eds.) RILEM TC 211 - PAE State-of-the-Art Report: Performance of Cement-Based Materials in Aggressive Aqueous Environments.

Lewis, R., Sear, L., Wainwright, P., and Ryle, R. (2003) Cementitious additions, In: Newmann, J., and Choo, B. S. (Eds.) *Advanced Concrete Technology – Constituent Materials*, Butterworth-Heinemann, Oxford.

Lopez, R. F. (2009) Calcined Clayey Soils as a Potential Replacement for Cement in Developing Countries, Ph.D. Thesis, EPFL, Lausanne.

Lu, S., Landis, E. N., and D. T. Keane (2006) X-ray microtomographic studies of pore structure and permeability in Portland cement concrete, *Materials and Structures*, **39(6)**, 611-620.

Lydzba, D., Rajczakowska, M., Stefaniuk, D., and A. Kmita (2014) Identification of the carbonation zone in concrete using X-ray microtomography, *Studia Geotechnica et Mechanica*, **36(1)**, 47-54.

Magniont, C., Coutand, M., Bertron, A., Cameleyre, X., Lafforgue, C., Beaufort, S., and G. Escadeillas (2011) A new test method to assess the bacterial deterioration of cementitious materials, *Cement and Concrete Research*, **41(4)**, 429-438.

Mehta, P. K. and P. J. M. Monteiro (2006) *Concrete Microstructure, Properties, and Materials*, 3rd Edition, McGraw-Hill, New York.

Mehta, P. K. and P. J. M. Monteiro (2013) *Concrete: Microstructure, Properties, and Materials*, 3rd edition, McGraw-Hill, New Delhi.

Menendez, E., Matschei, T., and F. P. Glasser (2013) Sulfate attack of concrete, pp. 7-74, In: Alexander, M. G., Bertron, A., De Belie, N. (Eds.) RILEM TC 211 - PAE State-of-the-Art Report: Performance of Cement-Based Materials in Aggressive Aqueous Environments.

Mohana, S., Acharya, B. K., and D. Madamwar (2009) Distillery spent wash: Treatment technologies and potential applications, *Journal of Hazardous Materials*, **163**, 12-25.

Monteny, J., De Belie, N., and L. Taerwe (2003) Resistance of different types of concrete mixtures to sulfuric acid, *Materials and Structures*, **36**, 242-249.

Monteny, J., De Belie, N., Vincke, E., Verstraete, W., and L. Taerwe (2001) Chemical and microbiological tests to simulate sulfuric acid corrosion of polymer-modified concrete, *Cement and Concrete Research*, **31**, 1359-1365.

Monteny, J., Vincke, E., Beeldens, A., De Belie, N., Taerwe, L., Van Gemert, D., and W. Verstraete (2000) Chemical, microbiological, and in situ test methods for biogenic sulfuric acid corrosion of concrete, *Cement and Concrete Research*, **30**, 623-634.

Moradian, M., Shekarchi, M., Pargar, F., Bonakdar, A., and M. Valipour (2012) Deterioration of concrete caused by complex attack in sewage treatment plant environment, *Journal of Performance of Constructed Facilities*, **26(1)**, 124-134.

Murugan, M. (2017) Performance of concrete based water filtration system: Influence of reduced grapheme oxide and accelerated carbonation, Ph.D. Thesis, IIT Madras.

Murugan, M., and M. Santhanam (2018) Effect of reduced graphene oxide, alumina and silica nanoparticles on the deterioration characteristics of portland cement paste exposed to acidic environment, *Cement and Concrete Composites*, **91**, 118-137.

Naik, N. N., Jupe, A. C., Stock, S. R., Wilkinson, A. P., Lee, P. L., and K. E. Kurtis, K. (2006) Sulphate attack monitored by microCT and EDXRD: Influence of cement type, water-to-cement ratio and aggregate, *Cement and Concrete Research*, **36(1)**, 144-159.

Newmann, J. and Choo, B. S. (2003) *Advanced Concrete Technology – Constituent Materials*, Butterworth-Heinemann.

O'Connell, M., McNally, C., and M. G. Richardson (2010) Biochemical attack on concrete in wastewater applications: A state of the art review, *Cement and Concrete Composites*, **32**, 479-485.

O'Connell, M., McNally, C., and M. G. Richardson (2012) Performance of concrete incorporating GGBS in aggressive wastewater environments, *Construction and Building Materials*, **27**, 368-374.

Okabe, S., Odagiri, M., Ito, T., and H. Satoh (2006) Succession of sulfur oxidizing bacteria in the microbial community on corroding concrete in sewer systems, *Journal of Applied & Environmental Microbiology*, **73**, 971-980.

Oueslati, O. and J. Duchesne (2011a) Acetic acid attack of cement matrix: Evaluation of durability parameters, In: Instituto de Ciencias de la Construccio´n "Eduardo Torroja". CSIC. Palomo, A., Zaragoza, A., Lopez Aguii, J. C. (Eds.) Proceedings of the XIIIth International Conference on the Chemistry of Cement, Madrid.

Oueslati, O. and J. Duchesne (2012) The effect of SCMs and curing time on resistance of mortars subjected to organic acids, *Cement and Concrete Research*, **42(1)**, 205-214.

Oueslati, O., and J. Duchesne (2011b) Impact of acetic acid attack on the chemical, physical and mineralogical evolution of cement pastes, pp. 28-37, In: Godbout, S. Potvin, L. (Eds.) Proceedings of 7th International Symposium on Cement Based Materials for a Sustainable Agriculture, Quebec.

Pant, D. and A. Adholeya (2007) Biological approaches for treatment of distillery wastewater: A review, *Bioresource Technology*, **98**, 2321-2334.

Papadakis, V. G. (2000) Effect of supplementary cementing materials on concrete resistance against carbonation and chloride ingress, *Cement and Concrete Research*, **30**, 291-299.

Pavlik, V. (1994a) Corrosion of hardened cement paste by acetic and nitric acids; Part I: Calculation of corrosion depth, *Cement and Concrete Research*, **24**, 551-562.

Pavlik, V. (1994b) Corrosion of hardened cement paste by acetic and nitric acids; Part II: Formation and the chemical composition of the corrosion products layer, *Cement and Concrete Research*, **24(8)**, 1495-1508.

Pavlik, V. (1996) Corrosion of hardened cement paste by acetic and nitric acids Part III: influence of water/cement ratio, *Cement and Concrete Research*, **26(3)**, 475-490.

Perraton, D., Aitcin, P. C., and D. Vezina (1988) Permeabilities of silica fume concretes, *ACI Special Publications SP-108*, 63-84.

Ponikiewski, T., Katzer, J., Bugdol, M., and M. Rudzki (2014) Determination of 3D porosity in steel fibre reinforced SCC beams using X-ray computed tomography, *Construction and Building Materials*, **68**, 333-340.

Promentilla, M. A. B. (2011) Characterizing the microstructure of deteriorated cementitious materials with X-ray Microtomography, Invited Paper, 12-21.

Promentilla, M. A. B., Sugiyam, T., Hitomi, T., and N. Takeda (2009) Quantification of tortuosity in hardened cement pastes using synchrotron-based X-ray computed microtomography, *Cement and Concrete Research*, **39(6)**, 548-557.

Provis, J. L., Myers, R. J., White, C. E., Rose, V., and J. S. J. Van Deventer (2012) X-ray microtomography shows pore structure and tortuosity in alkali activated binders, *Cement and Concrete Research*, **42(6)**, 855-864.

Puerta-Falla, G., Balonis, M., Le Saout, G., Falzone, G., Zhang, C., Neithalath, N., and G. Sant (2015) Elucidating the role of the aluminous source on limestone reactivity in cementitious materials, *Journal of the American Ceramic Society*, **98**, 1-14.

Ramachandran, V. S. and J. J. Beaudoin (Eds.) (2001) *Handbook of analytical techniques in concrete science and technology: Principles, Techniques, and Applications*, Noyes Publications, Park Ridge, New Jersey, USA.

Ramaswamy, K. P. and M. Santhanam (2016) Degradation kinetics of cement-based materials in citric acid, Proceedings of 10th Structural Engineering Convention, Chennai, 1690-1695.

Ramaswamy, K. P. and M. Santhanam (2017) Durability of cementitious materials in acidic environments: evaluation of degradation kinetics, 14th International Conference on Durability of Building Materials and Components, University of Ghent, Belgium.

Ramaswamy, K. P., Bertron, A., and M. Santhanam (2017b) Additional insights on the influencing factors and mechanism of degradation due to acid attack: Special case of acids forming soluble salts, Vol. 4, pp. 279-290, In: Santhanam, M., Gettu, R., Pillai, R. G., and Nayar, S. K. (Eds.) Proceedings of International Conference on Advances in Construction Materials and Systems, Chennai.

Ramaswamy, K., P., Sivakumar, R., Santhanam, M., and R. Gettu (2017a) Micro-analytical characterisation of concrete deterioration due to acid attack in a sewage treatment plant, Vol. 2, pp. 647-656, In: Santhanam, M., Gettu, R., Pillai, R. G., and Nayar, S. K. (Eds.) Proceedings of International Conference on Advances in Construction Materials and Systems, Chennai.

Richardson, M. G. (2002) *Fundamentals of durable concrete*, Spon Press, London.

Roberts, D. J., Nica, D., Zuo, G., and J. L. Davis (2002) Quantifying microbially-induced deterioration of concrete: Initial studies, *International Biodeterioration & Biodegradation*, **49**, 227-234.

Rodhe, H., Dentener, F., M. Schulz (2002) The global distribution of acidifying wet deposition, *Environmental Science and Technology*, **36**, 4382-4388

Rougelot, T, Burlion, N, Bernard, D, and F. Skoczylas (2010) About microcracking due to leaching in cementitious composites: X-ray microtomography description and numerical approach, *Cement and Concrete Research*, **40**, 271-283

Roy, D. M., Arjunan, P., and M. R. Silsbee (2001) Effect of silica fume, metakaolin, and low-calcium fly ash on chemical resistance of concrete, *Cement and Concrete Research*, **31**, 1809-1813.

Saha, N. K., Balakrishnan, M., and V. S. Batra (2005) Improving industrial water use: Case study for an Indian distillery, *Resources, Conservation and Recycling*, **43**, 163-174.

Sand, W., Dumas, T., and S. Marcdargent (1992) Tests for biogenic sulfuric acid corrosion in a simulation chamber confirming the on-site performance of calcium aluminate based concretes in sewages, International Symposium on Microbiologically Influenced Corrosion (MIC) Testing, Miami, Florida.

Santhanam, M., Cohen, M. D., and J. Olek (2003) Mechanism of sulfate attack: a fresh look Part 2. Proposed mechanisms, *Cement and Concrete Research*, **33**, 341-346.

Saricimen, H., Shameem, M., Barry, M. S., Ibrahim, M., and T. A. Abbasi (2003) Durability of proprietary cementitious materials for use in wastewater transport systems, *Cement and Concrete Composites*, **25**, 421-427.

Schmidt, M., Hormann, K., Hofmann, F., and E. Wagner (1997) Concrete with greater resistance to acid and to corrosion by biogenous sulfuric acid, *Concrete Precasting and Technology*, **4**, 64-69.

Scrivener, K. L. (2014) Options for the future of cements, *Indian Concrete Journal*, **88**, 11-21.

Scrivener, K., and N. De Belie (2013) Bacteriogenic sulfuric acid attack of cementitious materials in sewage systems, pp. 305-318, In: Alexander, M. G., Bertron, A., De Belie, N. (Eds.) RILEM TC 211 - PAE State-of-the-Art Report: Performance of Cement-Based Materials in Aggressive Aqueous Environments.

Scrivener, K., Martirena, F., Bishnoi, S., and S. Maity (2017) Calcined clay limestone cements (LC^3), *Cement and Concrete Research* (Available online).

Scrivener, K., Snellings, R., and B. Lothenbach (2016) *A Practical Guide to Microstructural Analysis of Cementitious Materials*, CRC Press, Taylor and Francis Group, Boca Raton, Florida.

Segura, I., Molero, M., Aparicio, S., Anaya, J. J., and A. Moagues (2013) Decalcification of cement mortars: Characterisation and modelling, *Cement and Concrete Composites*, **35**, 136-150.

Sersale, S., Frigione, G., and L. Bonavita (1998) Acid depositions and concrete attack: Main influences, *Cement and Concrete Research*, **28**, 19-24.

Siddique, R. and M. I. Khan (2011) *Supplementary cementing materials*, Springer, Berlin.

Sivakumar, R. (2017) Study of effect of acid attack on concrete, M.Tech Thesis, IIT Madras, 1-88.

Stock, S. R. (2008) Recent advances in X-ray microtomography applied to materials, *International Materials Reviews,* **53(3)**, 129-181.

Stock, S. R., Naik, N. N., Wilkinson, A. P., and K. E. Kurtis (2002) X-ray microtomography (microCT) of the progression of sulfate attack of cement paste, *Cement and Concrete Research*, **32(10)**, 1673-1675.

Stutzman, P. (2004) Scanning electron microscopy imaging of hydraulic cement microstructure, *Cement and Concrete Composites*, **26(8)**, 957-966.

Stutzman, P. E. and J. R. Clifton (1999) Specimen preparation for scanning electron microscopy, pp. 10-22, In: Jany, L. and A. Nisperos (Eds.) Proceedings from the Twenty-First International Conference on Cement Microscopy, Las Vegas, Nevada, USA.

Sugiyama, T., Promentilla, M. A. B., Hitomi, T., and N. Takeda (2010) Application of synchrotron microtomography for pore structure characterization of deteriorated cementitious materials due to leaching, *Cement and Concrete Research*, **40**, 1265-1270.

Taylor, H. F. W. (1997) *Cement Chemistry*, Thomas Telford, London.

Tewari, P. K., Batra, V. S., and M. Balakrishnan (2007) Water management initiatives in sugarcane molasses based distilleries in India, *Resources, Conservation and Recycling*, **52**, 351-367.

Thomas, M. D. A. (2013) *Supplementary Cementing Materials in concrete*, CRC Press, Francis & Taylor Group, Florida, USA.

Torii, K. and M. Kawamura (1994) Effects of fly ash and silica fume on the resistance of mortar to sulfuric acid and sulfate attack, *Cement and Concrete Research*, **24(2)**, 361-370.

Vipulanandan, C. and J. Liu (2002) Glass-fiber mat-reinforced epoxy coating for concrete in sulfuric acid environment, *Cement and Concrete Research*, **32**, 205-210.

Vipulanandan, C. and J. Liu (2005) Performance of polyurethane-coated concrete in sewer environment, *Cement and Concrete Research*, **35**, 1754-1763.

Voegel, C., Bertron, A., and B. Erable (2016) Mechanisms of cementitious material deterioration in biogas digester, *Science of the Total Environment*, **571**, 892-901.

Wan, K., Xu, Q., Li, L., and W. Sun (2013) 3D porosity distribution of partly calcium leached cement paste, *Construction and Building Materials*, **48**, 11-15.

Wan, K., Xu, Q., Wang, Y., and G. Pan (2014) 3D spatial distribution of the calcium carbonate caused by carbonation of cement paste, *Cement and Concrete Composites*, **45(1)**, 255-263.

Wang, J., Dewanckele, J., Cnudde, V., Vlierberghe, S. V., Verstraete, W., and N. De Belie (2014) X-ray computed tomography proof of bacterial-based self-healing in concrete, *Cement and Concrete Composites*, **53**, 289-304.

Wei, S., Yiqiang, C., Yunsheng, Z., and M. R. Jones (2013) Characterization and simulation of microstructure and thermal properties of foamed concrete, *Construction and Building Materials*, **47**, 1278-1291.

Wells, T. and R. E. Melchers (2014) An observation-based model for corrosion of concrete sewers under aggressive conditions, *Cement and Concrete Research*, **61-62**, 1-10.

Wong, R. C. K. and K. T. Chau (2005) Estimation of air void and aggregate spatial distributions in concrete under uniaxial compression using computer tomography scanning, *Cement and Concrete Research*, **35(8)**, 1566-1576.

Young, J. F., Mindess, S., Bentur, A., and R. J. Gray (1998) *The science and technology of civil engineering materials*, Prentice Hall, Upper Saddle River, N.J., U.S.A.

Zhang, M. (2017) Pore-scale modelling of relative permeability of cementitious materials using X-ray computed microtomography images, *Cement and Concrete Research*, **95**, 18-29.

Zhang, M. and A. P. Jivkov (2016) Micromechanical modelling of deformation and fracture of hydrating cement paste using X-ray computed tomography characterisation, *Composites Part B: Engineering*, **88**, 64-72.

Zivica V. and A. Bajza (2001) Acidic attack of cement based materials - A review (Part 1): Principle of acidic attack, *Construction and Building Materials*, **15**, 331-340.

APPENDICES

APPENDIX A

STUDY ON DEGRADATION KINETICS IN PASTE EXPOSED TO ACIDS

Before acid exposure	After acid exposure					
	1% Sulphuric	3% Sulphuric	1% HCl	0.25M Acetic	0.5M Acetic	0.5M Citric
						

Figure A-1 Aspect of FA30 specimens before and after the acid exposure (B28)

Before acid exposure	After acid exposure					
	1% Sulphuric	3% Sulphuric	1% HCl	0.25M Acetic	0.5M Acetic	0.5M Citric
						

Figure A-2 Aspect of FA30 specimens before and after the acid exposure (WB28)

Before acid exposure	After acid exposure					
	1% Sulphuric	3% Sulphuric	1% HCl	0.25M Acetic	0.5M Acetic	0.5M Citric
						

Figure A-3 Aspect of BFS50 specimens before and after the acid exposure (B28)

Before acid exposure	After acid exposure					
	1% Sulphuric	3% Sulphuric	1% HCl	0.25M Acetic	0.5M Acetic	0.5M Citric
						

Figure A-4 Aspect of BFS50 specimens before and after the acid exposure (WB28)

Before acid exposure	After acid exposure					
	1% Sulphuric	3% Sulphuric	1% HCl	0.25M Acetic	0.5M Acetic	0.5M Citric
						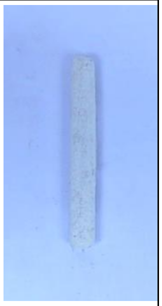

Figure A-5 Aspect of SF10 specimens before and after the acid exposure (B28)

Before acid exposure	After acid exposure					
	1% Sulphuric	3% Sulphuric	1% HCl	0.25M Acetic	0.5M Acetic	0.5M Citric
						

Figure A-6 Aspect of SF10 specimens before and after the acid exposure (WB28)

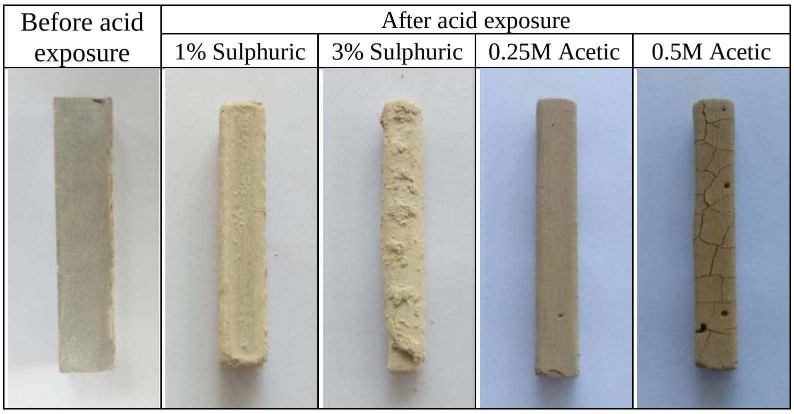

Figure A-7 LC2 paste before and after acid exposure (with brushing)

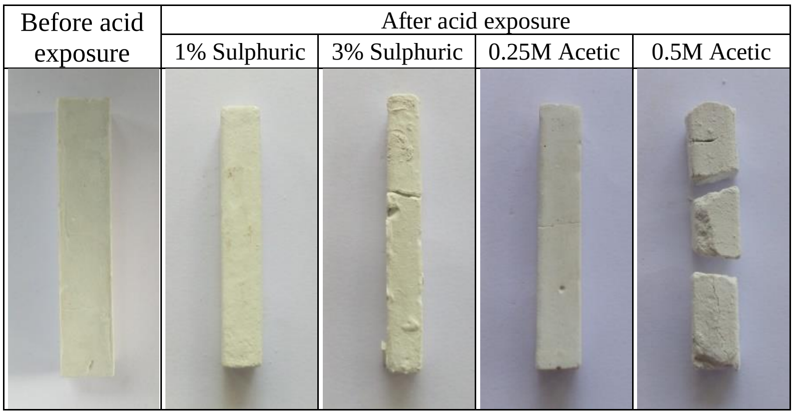

Figure A-8 HAC paste before and after acid exposure (with brushing)

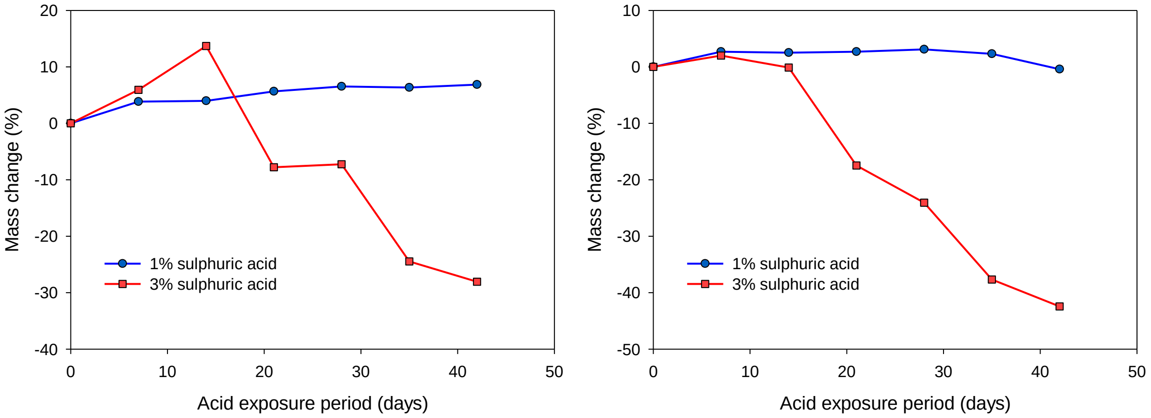

a) without brushing (WB28)　　b) with brushing (B28)

Figure A-9 Effect of concentration of sulphuric acid on mass changes of FA30 paste

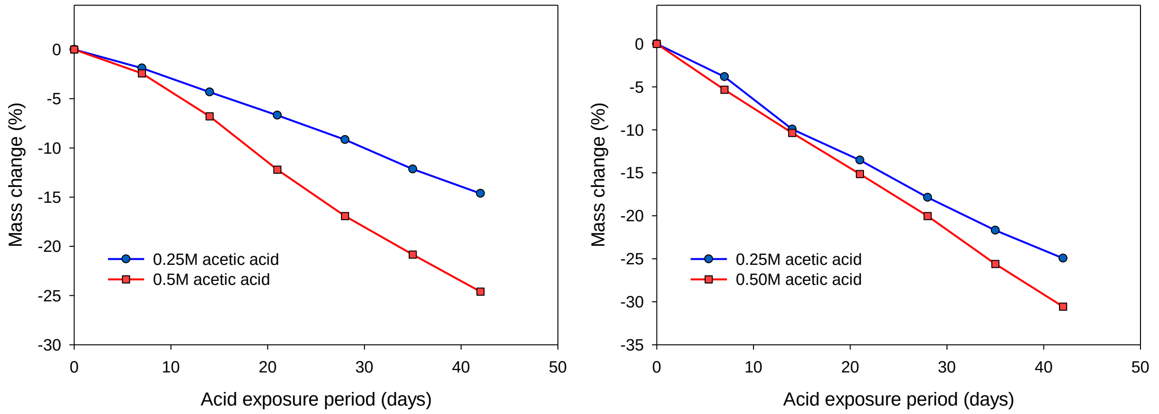

a) without brushing (WB28)   b) with brushing (B28)

Figure A-10 Effect of concentration of acetic acid on mass changes of FA30 paste

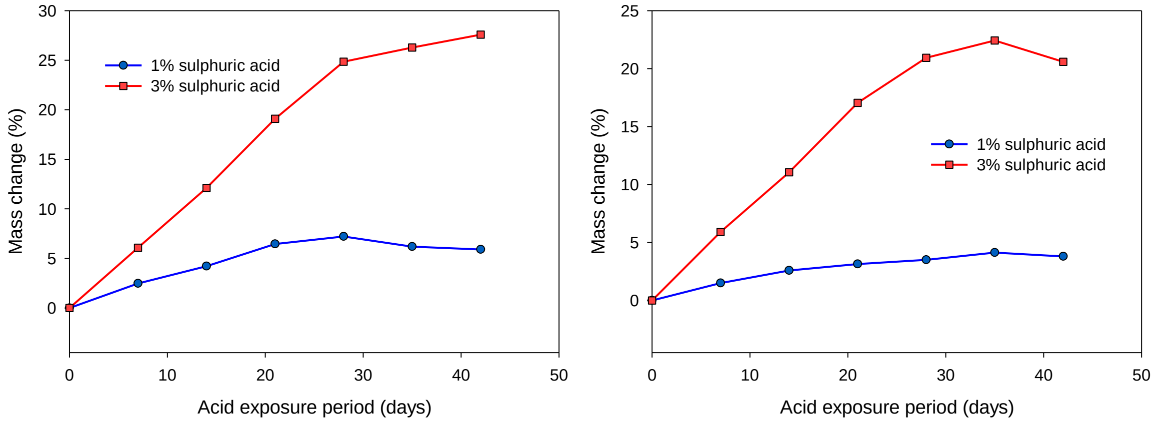

a) without brushing (WB28)   b) with brushing (B28)

Figure A-11 Effect of concentration of sulphuric acid on mass changes of BFS50 paste

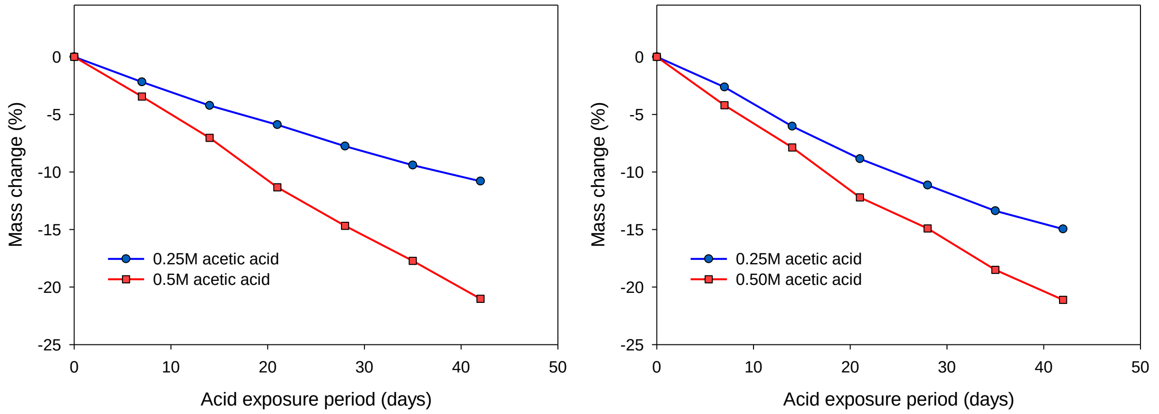

a) without brushing (WB28)   b) with brushing (B28)

Figure A-12 Effect of concentration of acetic acid on mass changes of BFS50 paste

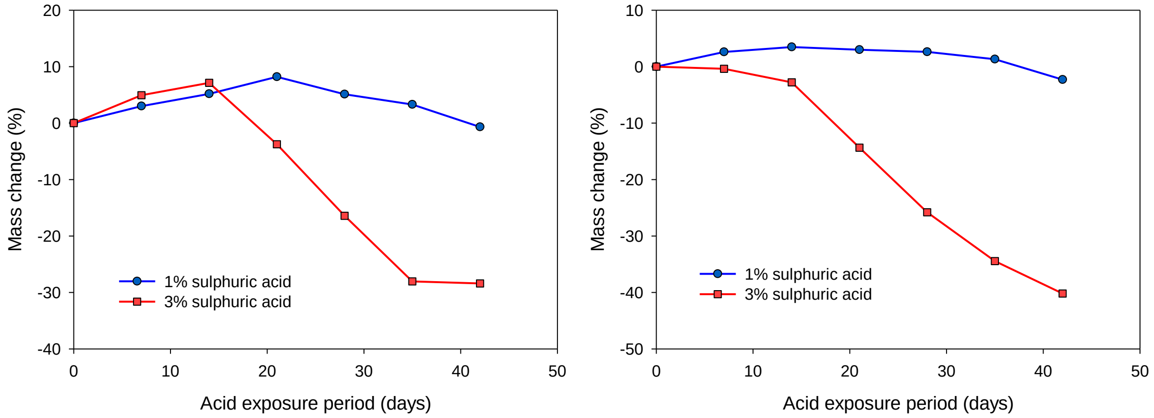

a) without brushing (WB28) b) with brushing (B28)

Figure A-13 Effect of concentration of sulphuric acid on mass changes of SF10 paste

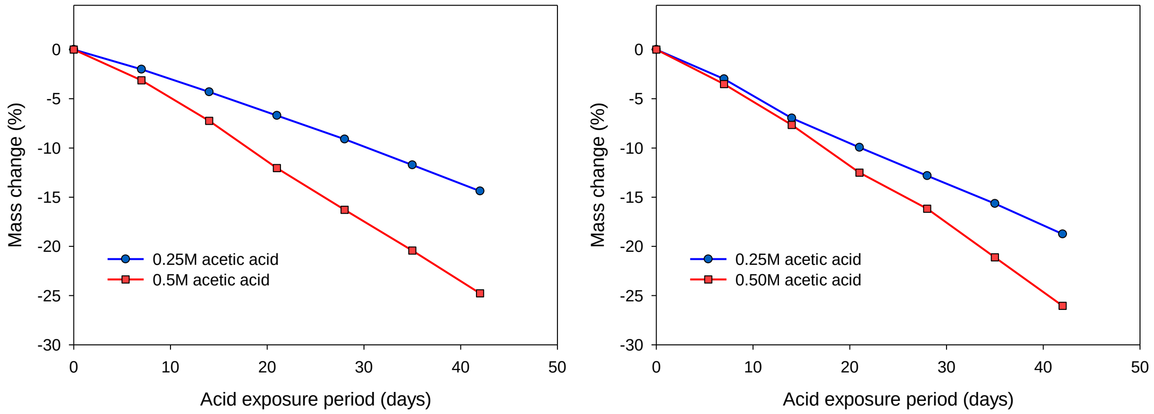

a) without brushing (WB28) b) with brushing (B28)

Figure A-14 Effect of concentration of acetic acid on mass changes of SF10 paste

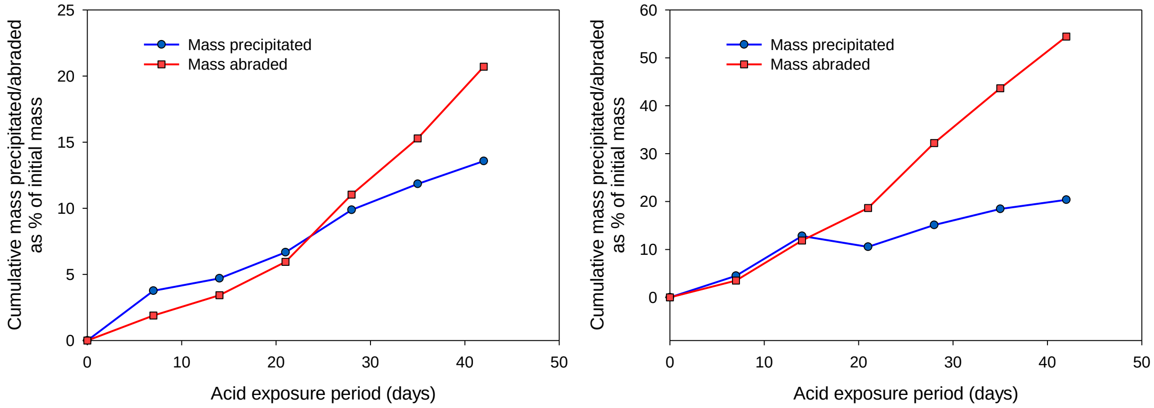

a) 1% sulphuric acid b) 3% sulphuric acid

Figure A-15 Kinetics of precipitated and abraded mass of OPC paste on exposure to 1% and 3% sulphuric acid

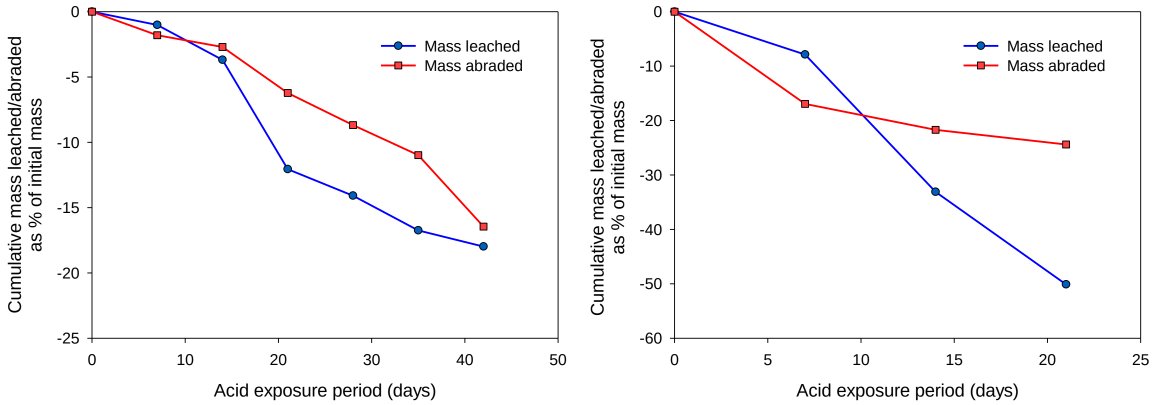

a) 1% hydrochloric acid b) 0.5M citric acid

Figure A-16 Kinetics of leached and abraded mass of OPC paste on exposure to 1% hydrochloric and 0.5M citric acid

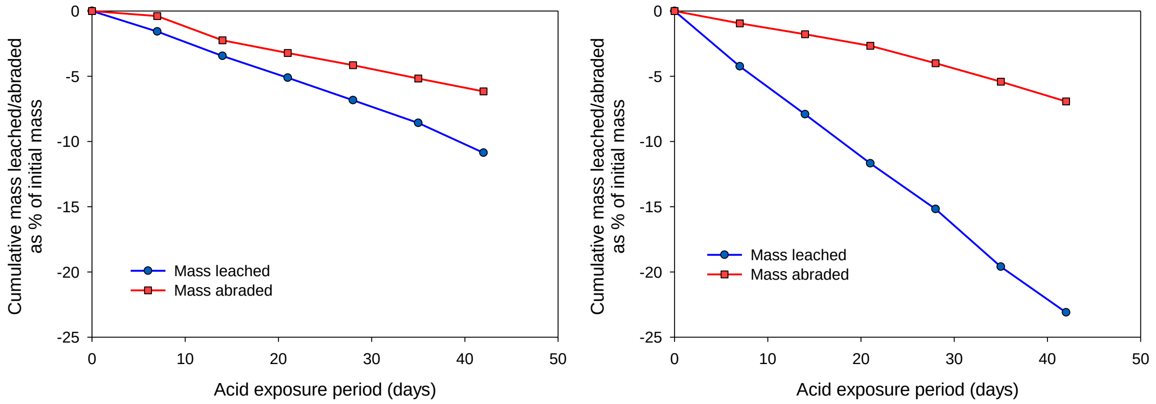

a) 0.25M acetic acid b) 0.5M acetic acid

Figure A-17 Kinetics of leached and abraded mass of OPC paste on exposure to 0.25M and 0.5M acetic acid

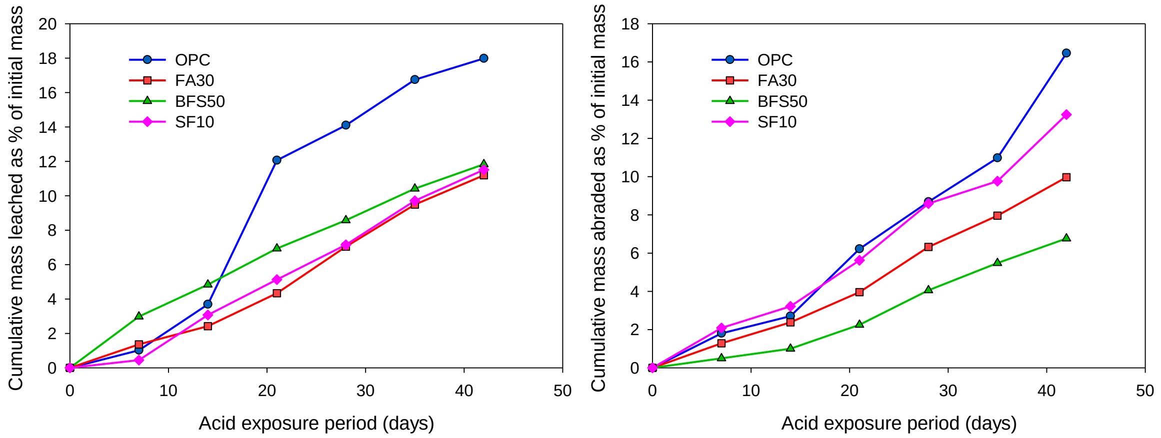

a) Cumulative mass leached b) Cumulative mass abraded

Figure A-18 Variation of cumulative mass leached and abraded of paste mixes on exposure to 1% hydrochloric acid

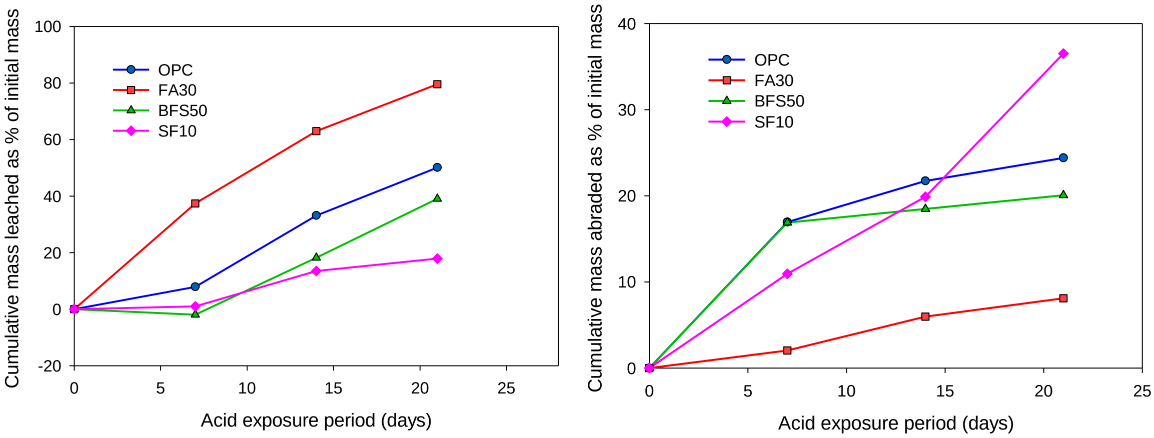

a) Cumulative mass leached b) Cumulative mass abraded

Figure A-19 Variation of cumulative mass leached and abraded of paste mixes on exposure to 0.5M citric acid

Table A-1 Results of dynamic test for accelerated degradation of paste specimens on exposure to 1% sulphuric acid

Mix	Revolutions	1% sulphuric acid			Saturated lime water		Net mass loss (%)
		pH	Mass (g)	Mass loss (%)	Mass (g)	Mass loss (%)	
OPC	0	0.99	288.820	0.00	286.195	0.00	0.00
OPC	5000	1.90	279.990	-3.06	278.592	-2.66	-0.40
OPC	10000	5.63	267.220	-7.48	274.360	-4.14	-3.34
OPC	15000	1.24	256.300	-11.26	271.324	-5.20	-6.06
OPC	20000	4.33	247.763	-14.22	267.850	-6.41	-7.81
FA30	0	0.99	256.100	0.00	256.518	0.00	0.00
FA30	5000	2.12	240.120	-6.24	246.868	-3.76	-2.48
FA30	10000	5.66	221.930	-13.34	243.240	-5.18	-8.17
FA30	15000	1.28	203.180	-20.66	239.250	-6.73	-13.93
FA30	20000	3.97	191.786	-25.11	235.906	-8.04	-17.08
BFS50	0	0.99	279.910	0.00	285.691	0.00	0.00
BFS50	5000	1.81	264.300	-5.58	277.840	-2.75	-2.83
BFS50	10000	5.30	251.150	-10.27	271.796	-4.86	-5.41
BFS50	15000	1.39	238.050	-14.95	268.430	-6.04	-8.91
BFS50	20000	3.65	229.880	-17.87	263.096	-7.91	-9.96
SF10	0	0.99	281.340	0.00	287.425	0.00	0.00
SF10	5000	1.80	269.900	-4.07	277.278	-3.53	-0.54
SF10	10000	5.54	256.420	-8.86	274.286	-4.57	-4.29
SF10	15000	1.19	244.870	-12.96	269.524	-6.23	-6.73
SF10	20000	3.92	233.636	-16.96	265.030	-7.79	-9.16

Note: the acid solution is renewed after 10000 revolutions

Table A-2 Altered area measurements based on CT image analysis (B28)

Mix	Acid	Concentration	Area as % of the initial area of the specimen				
			Area of outer layer	Area of middle layer	Area of specimen decalcified	Area of core layer	Area expanded/lost
OPC	Sulphuric	1%	9.68	5.20	14.88	92.59	7.46
FA30	Sulphuric	1%	4.58	18.63	23.21	68.31	-8.48
BFS50	Sulphuric	1%	3.57	21.64	25.21	74.82	0.03
SF10	Sulphuric	1%	7.92	11.94	19.86	73.90	-6.24
OPC	HCl	1%	25.67	4.26	29.92	50.48	-19.60
FA30	HCl	1%	18.14	23.08	41.22	29.45	-29.34
BFS50	HCl	1%	22.93	5.34	28.28	54.19	-17.53
SF10	HCl	1%	19.57	0.00	19.57	56.26	-24.18
OPC	Acetic	0.25M	26.88	2.98	29.86	42.83	-27.32
FA30	Acetic	0.25M	24.09	17.30	41.39	37.06	-21.55
BFS50	Acetic	0.25M	13.23	23.57	36.81	60.94	-2.25
SF10	Acetic	0.25M	15.57	15.70	31.27	47.13	-21.59
OPC	Acetic	0.5M	53.01	26.35	79.36	5.52	-15.12
FA30	Acetic	0.5M	81.75	0.00	81.75	0.00	-18.25
BFS50	Acetic	0.5M	61.46	4.46	65.92	23.46	-10.62
SF10	Acetic	0.5M	58.90	22.75	81.65	7.05	-11.29
OPC	Citric	0.5M	2.23	0.00	2.23	20.56	-77.21
FA30	Citric	0.5M	4.79	3.84	8.63	11.85	-79.52
BFS50	Citric	0.5M	9.80	3.97	13.77	32.78	-53.45
SF10	Citric	0.5M	4.57	0.00	4.57	39.06	-56.37

Table A-3 Altered depth measurements based on CT image analysis (B28)

Mix	Acid	Concentration	DD (µm)	DM (µm)	DA (µm)	DR (µm)
OPC	Sulphuric	1%	180.25	256.75	437.00	183.65
FA30	Sulphuric	1%	190.00	1296.50	1486.50	-220.46
BFS50	Sulphuric	1%	177.50	1029.75	1207.25	0.77
SF10	Sulphuric	1%	270.75	848.75	1119.50	-164.24
OPC	HCl	1%	869.25	107.50	976.75	-508.05
FA30	HCl	1%	714.25	861.50	1575.75	-804.35
BFS50	HCl	1%	719.00	169.75	888.75	-462.50
SF10	HCl	1%	689.75	0.00	689.75	-659.37
OPC	Acetic	0.25M	1002.50	70.00	1072.50	-782.46
FA30	Acetic	0.25M	844.00	737.00	1581.00	-590.33
BFS50	Acetic	0.25M	501.75	700.50	1202.25	-56.26
SF10	Acetic	0.25M	537.50	525.50	1063.00	-583.92
OPC	Acetic	0.5M	1825.25	1549.75	3375.00	-389.36
FA30	Acetic	0.5M	4730.75	0.00	4730.75	-486.38
BFS50	Acetic	0.5M	2063.00	183.75	2246.75	-272.64
SF10	Acetic	0.5M	2010.75	1303.50	3314.25	-294.47
OPC	Citric	0.5M	255.75	0.00	255.75	-2633.45
FA30	Citric	0.5M	344.75	269.75	614.50	-2765.73
BFS50	Citric	0.5M	418.50	162.75	581.25	-1557.11
SF10	Citric	0.5M	194.50	0.00	194.50	-1728.56

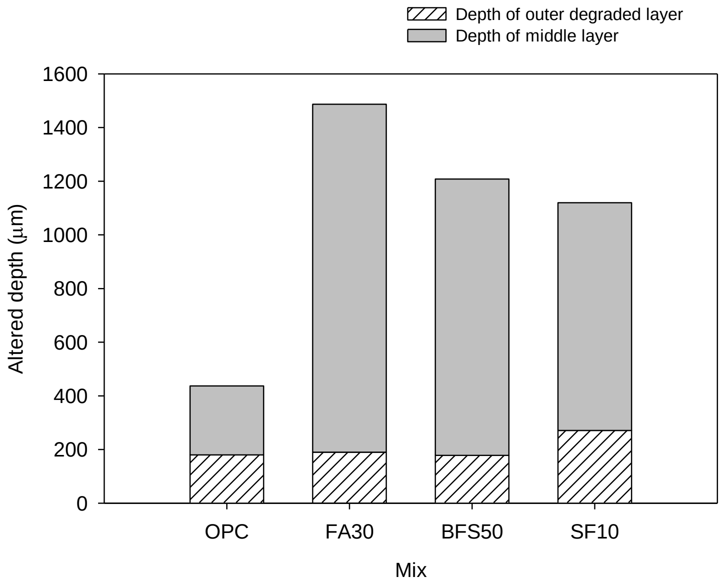

Figure A-20 Altered depth of paste exposed to 1% sulphuric acid (with brushing)

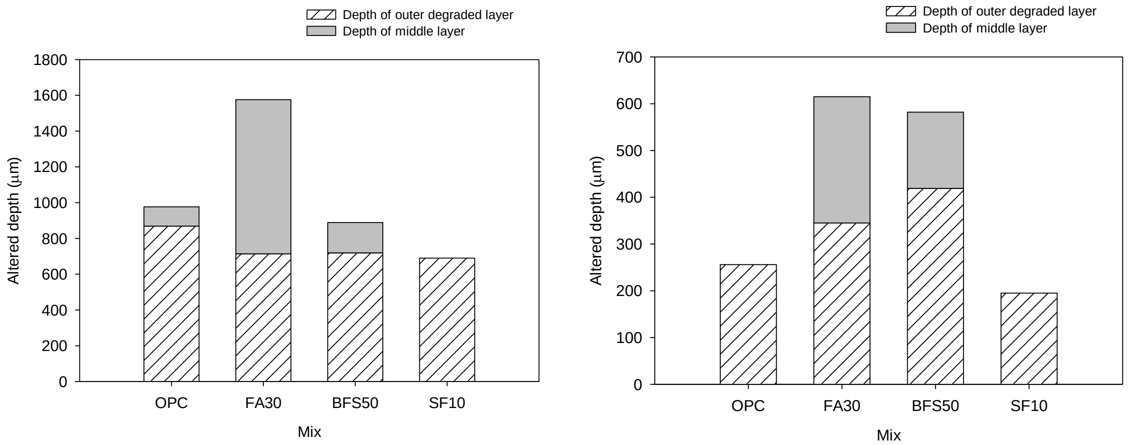

a) 1% hydrochloric acid

b) 0.5M citric acid

Figure A-21 Altered depth of paste exposed to hydrochloric and citric acid (with brushing)

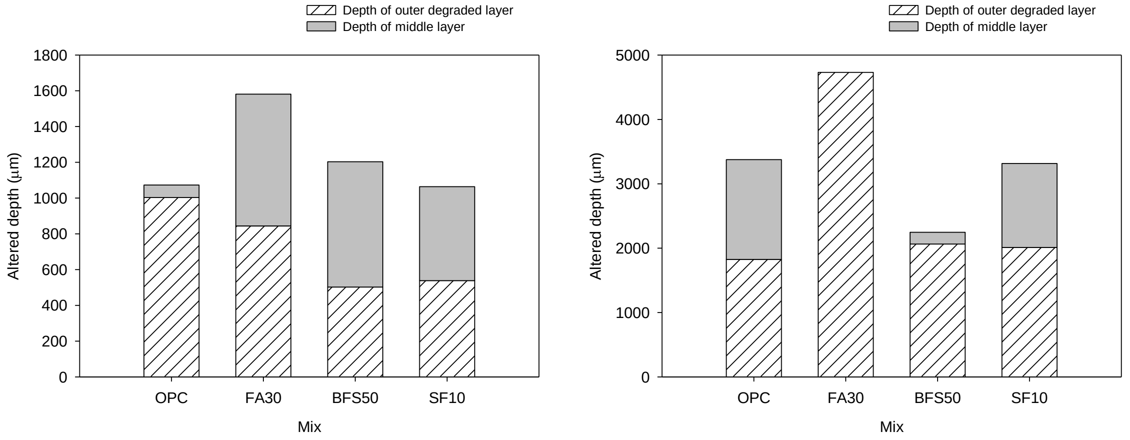

a) 0.25M acetic acid

b) 0.5M acetic acid

Figure A-22 Altered depth of paste exposed to acetic acid (with brushing)

APPENDIX B

MICRO-ANALYTICAL INVESTIGATION OF PASTE EXPOSED TO ACIDS

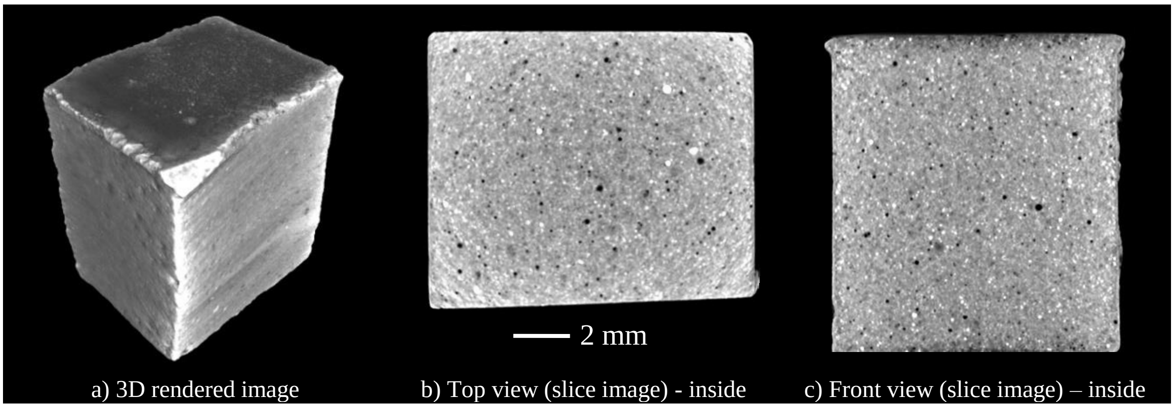

a) 3D rendered image b) Top view (slice image) - inside c) Front view (slice image) – inside

Figure B-1 CT images of FA30 paste specimen before acid exposure

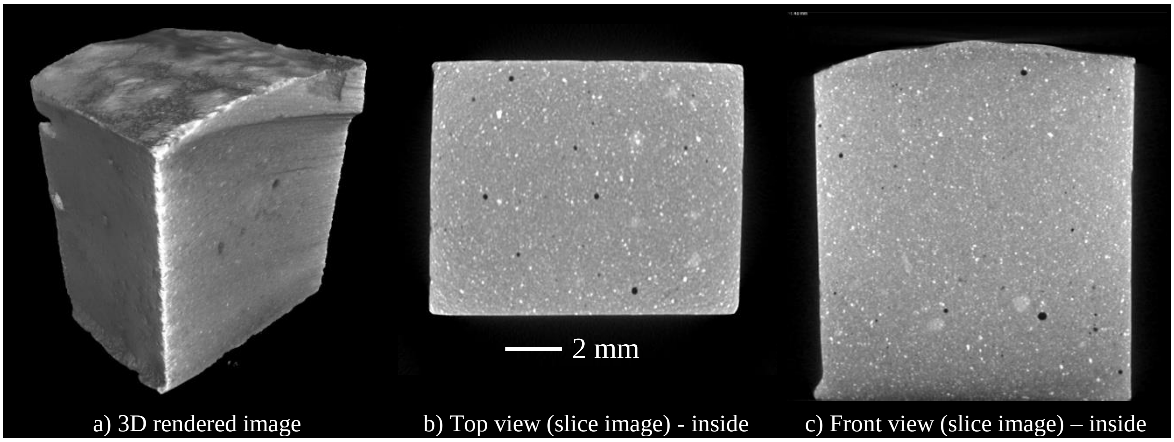

a) 3D rendered image b) Top view (slice image) - inside c) Front view (slice image) – inside

Figure B-2 CT images of BFS50 paste specimen before acid exposure

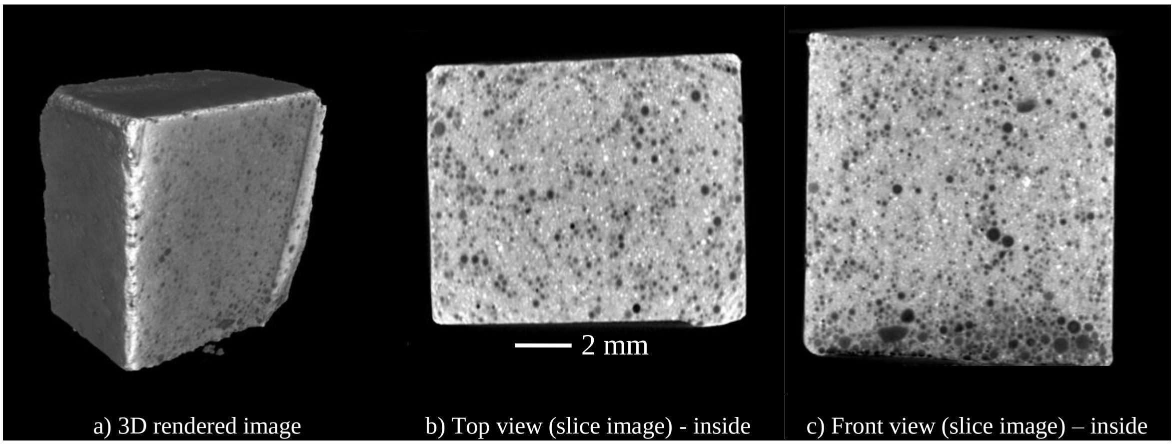

a) 3D rendered image b) Top view (slice image) - inside c) Front view (slice image) – inside

Figure B-3 CT images of SF10 paste specimen before acid exposure

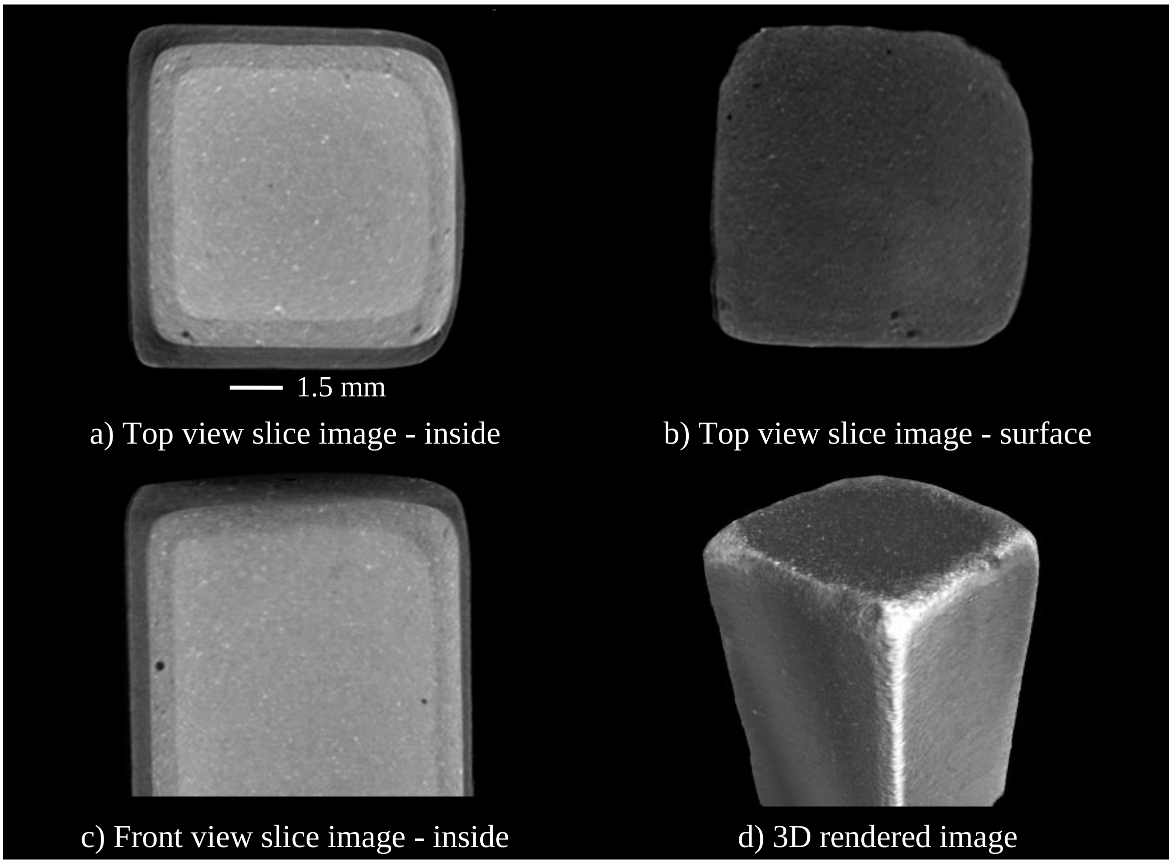

a) Top view slice image - inside b) Top view slice image - surface

c) Front view slice image - inside d) 3D rendered image

Figure B-4 CT images of OPC paste exposed to 0.25M acetic acid (without brushing)

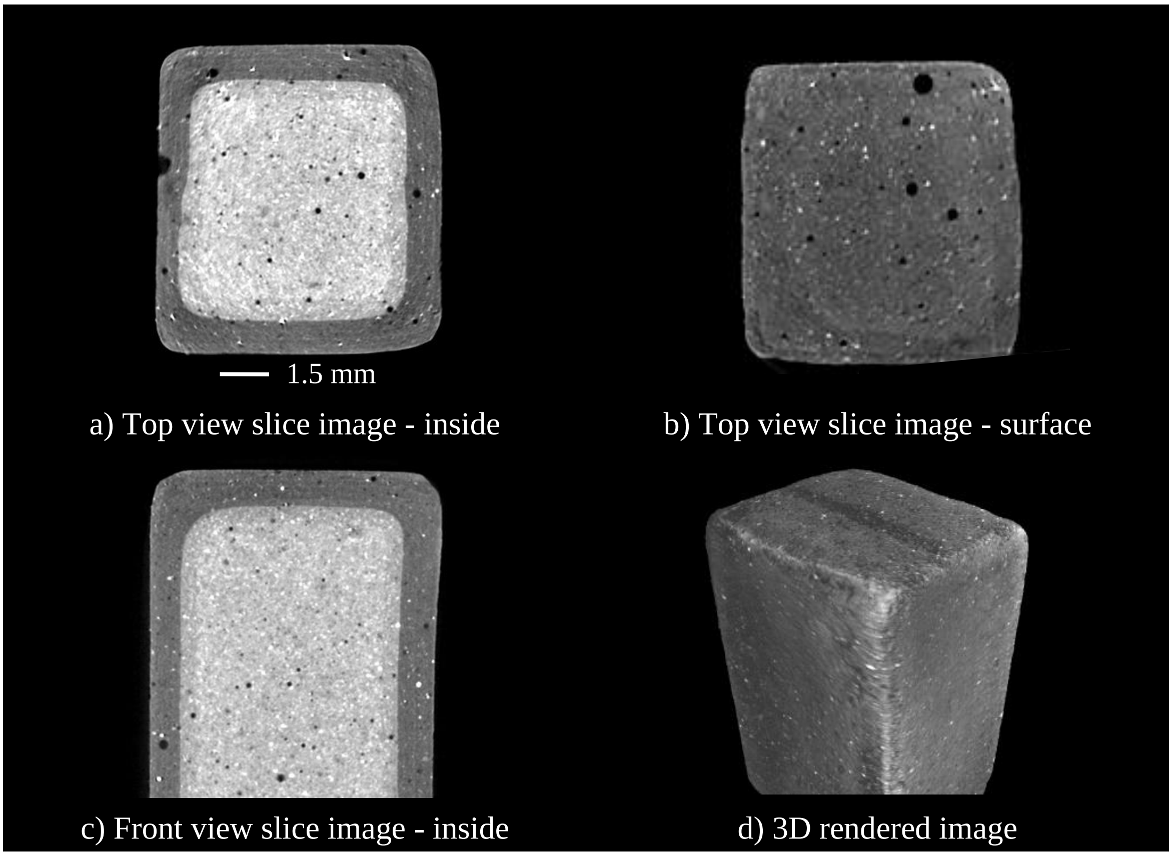

a) Top view slice image - inside b) Top view slice image - surface

c) Front view slice image - inside d) 3D rendered image

Figure B-5 CT images of FA30 paste exposed to 0.25M acetic acid (without brushing)

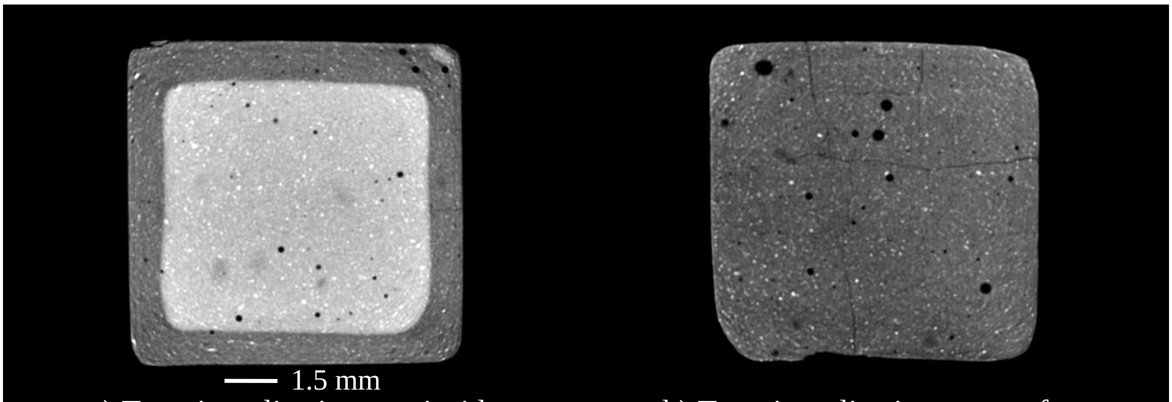

a) Top view slice image - inside

b) Top view slice image - surface

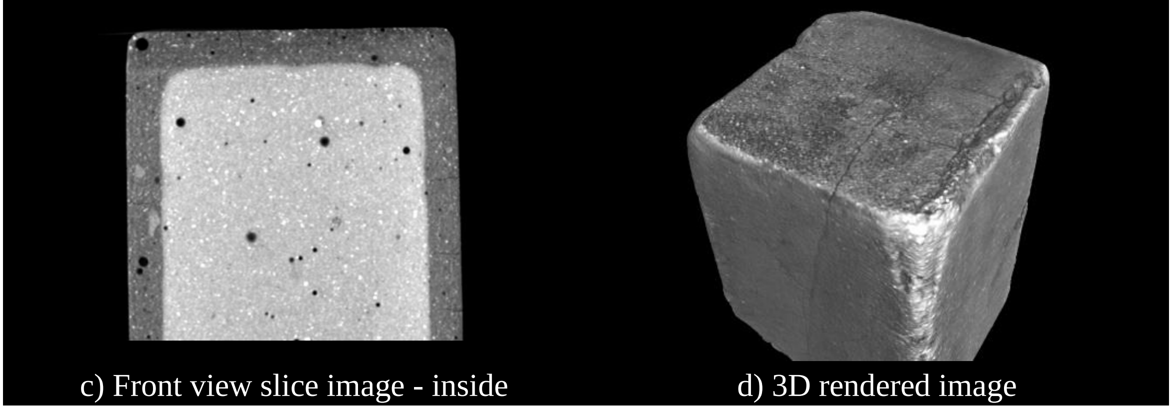

c) Front view slice image - inside

d) 3D rendered image

Figure B-6 CT images of BFS50 paste exposed to 0.25M acetic acid (without brushing)

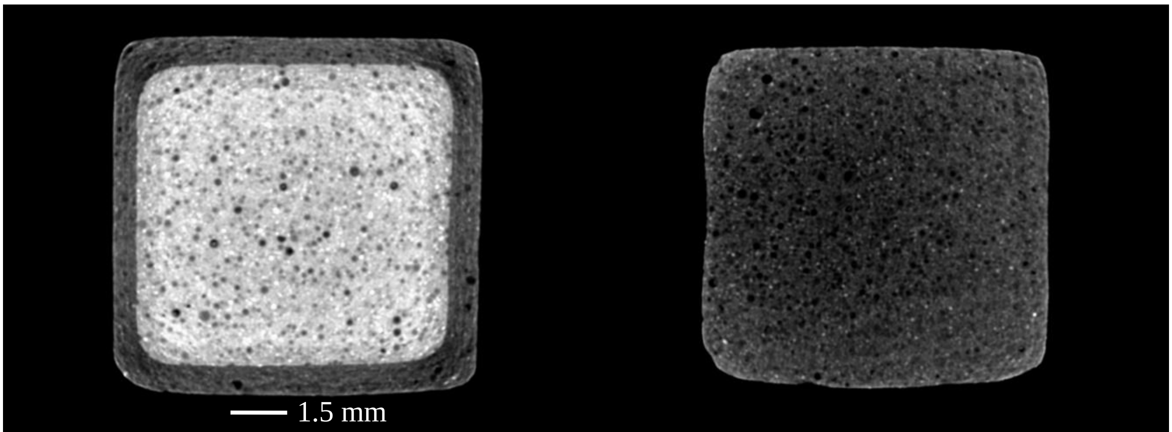

a) Top view slice image - inside

b) Top view slice image - surface

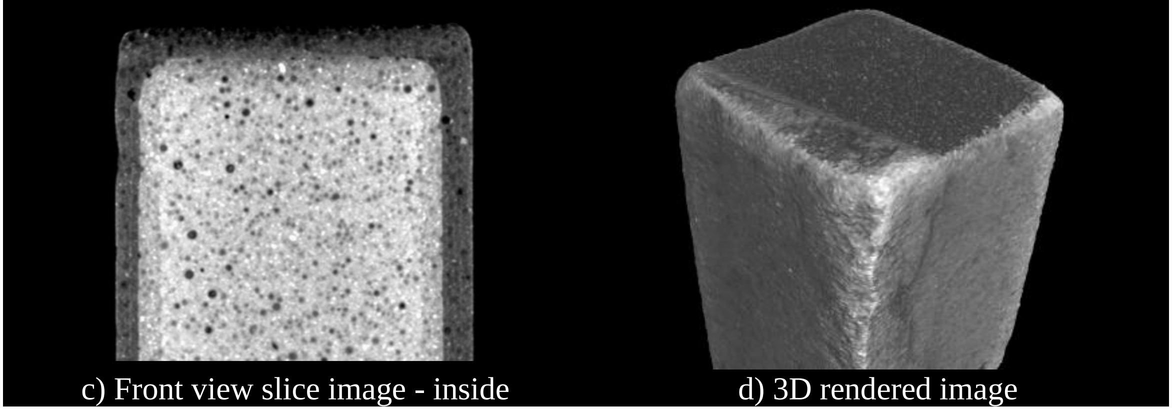

c) Front view slice image - inside

d) 3D rendered image

Figure B-7 CT images of SF10 paste exposed to 0.25M acetic acid (without brushing)

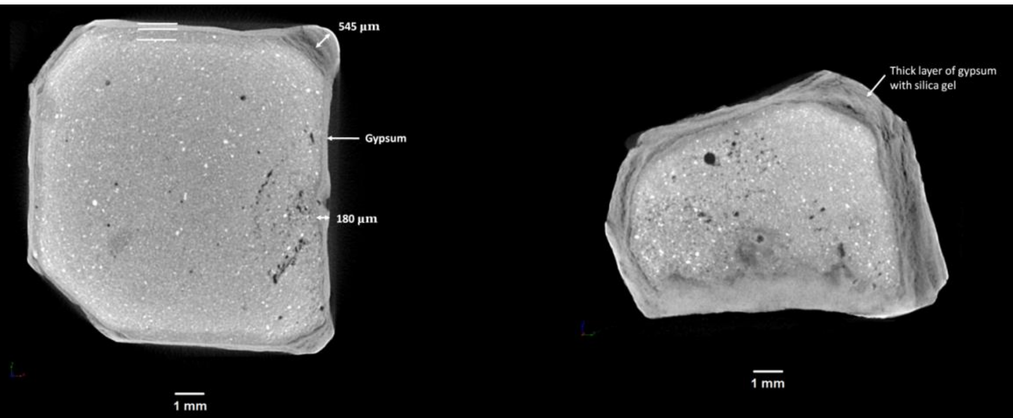

a) Top view (slice image) - inside b) Top view (slice image) - surface

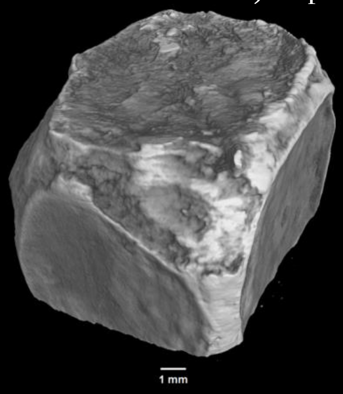

c) 3D rendered image

Figure B-8 CT images of OPC paste exposed to 1% sulphuric acid (with brushing)

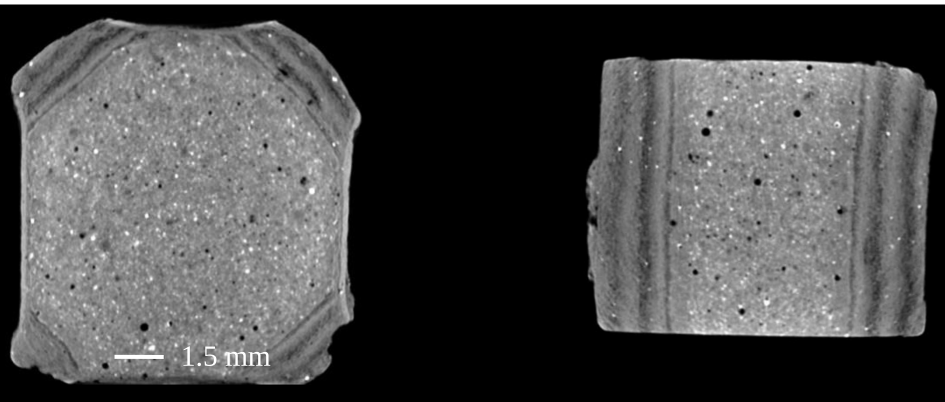

a) Top view (slice image) - inside b) Front view (slice image) - inside

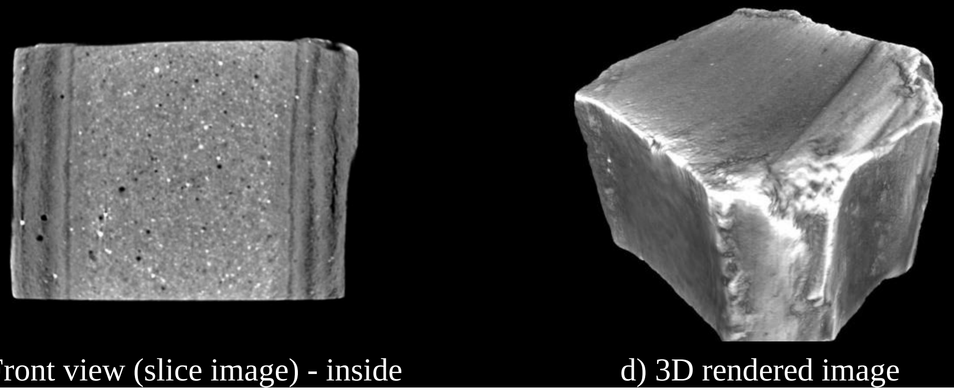

c) Front view (slice image) - inside d) 3D rendered image

Figure B-9 CT images of FA30 paste exposed to 1% sulphuric acid (with brushing)

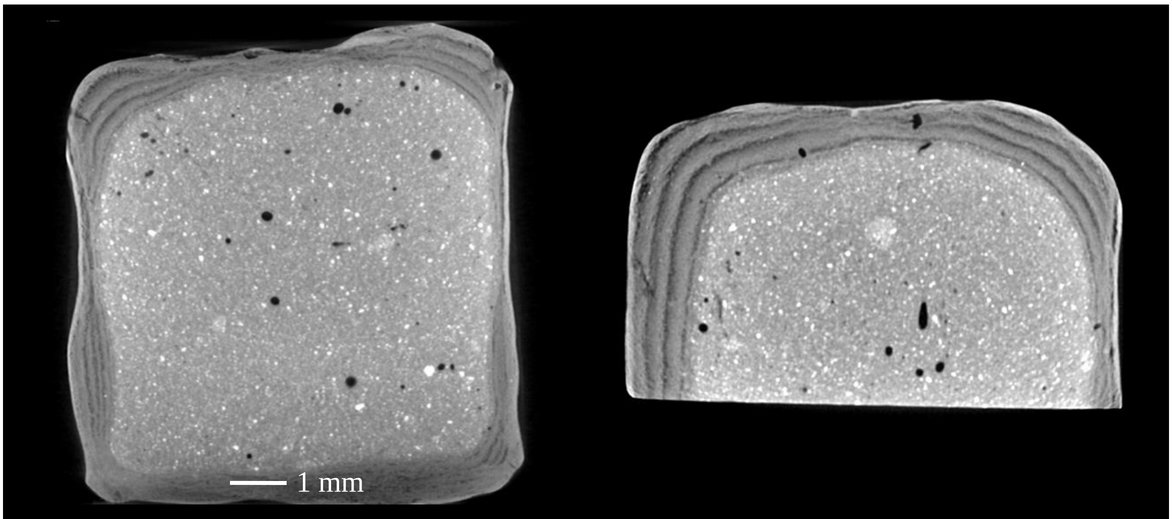

a) Top view (slice image) - inside b) Front view (slice image) - inside

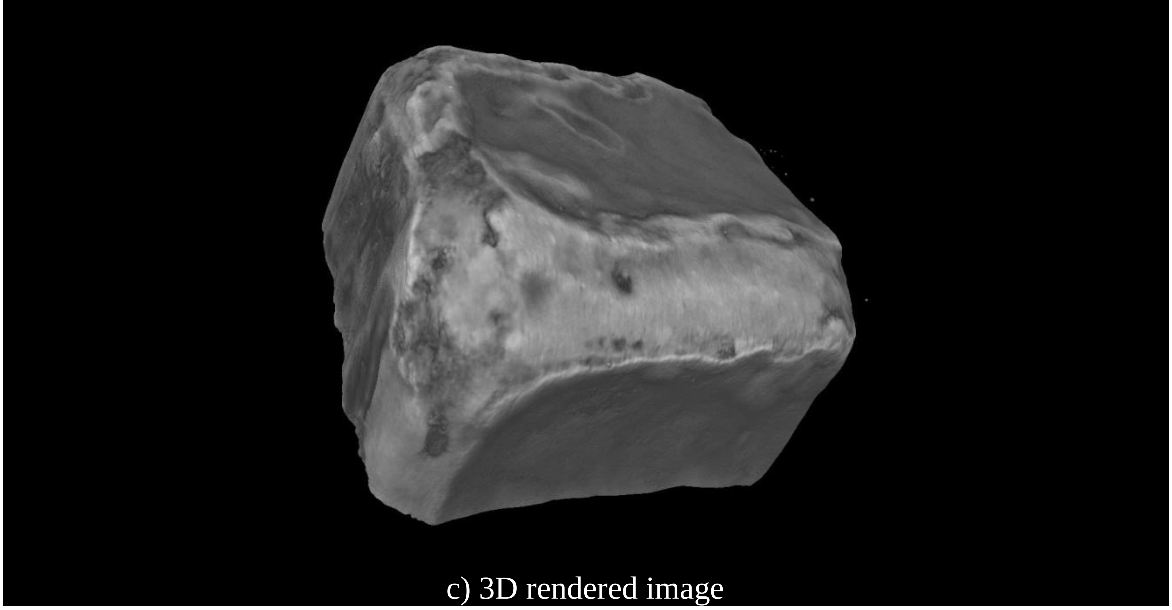

c) 3D rendered image

Figure B-10 CT images of BFS50 paste exposed to 1% sulphuric acid (with brushing)

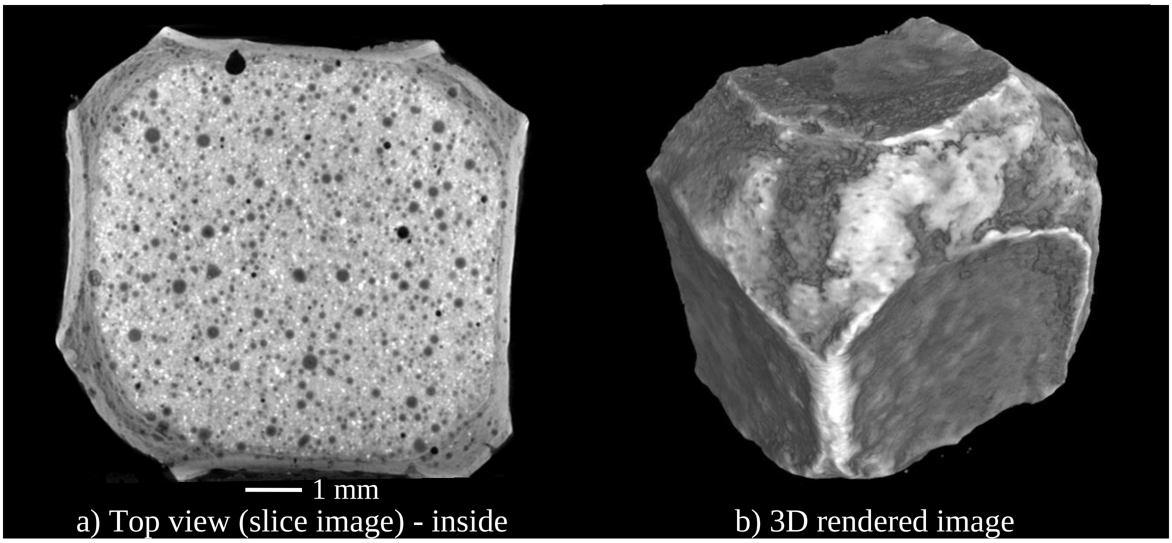

a) Top view (slice image) - inside b) 3D rendered image

Figure B-11 CT images of SF10 paste exposed to 1% sulphuric acid (with brushing)

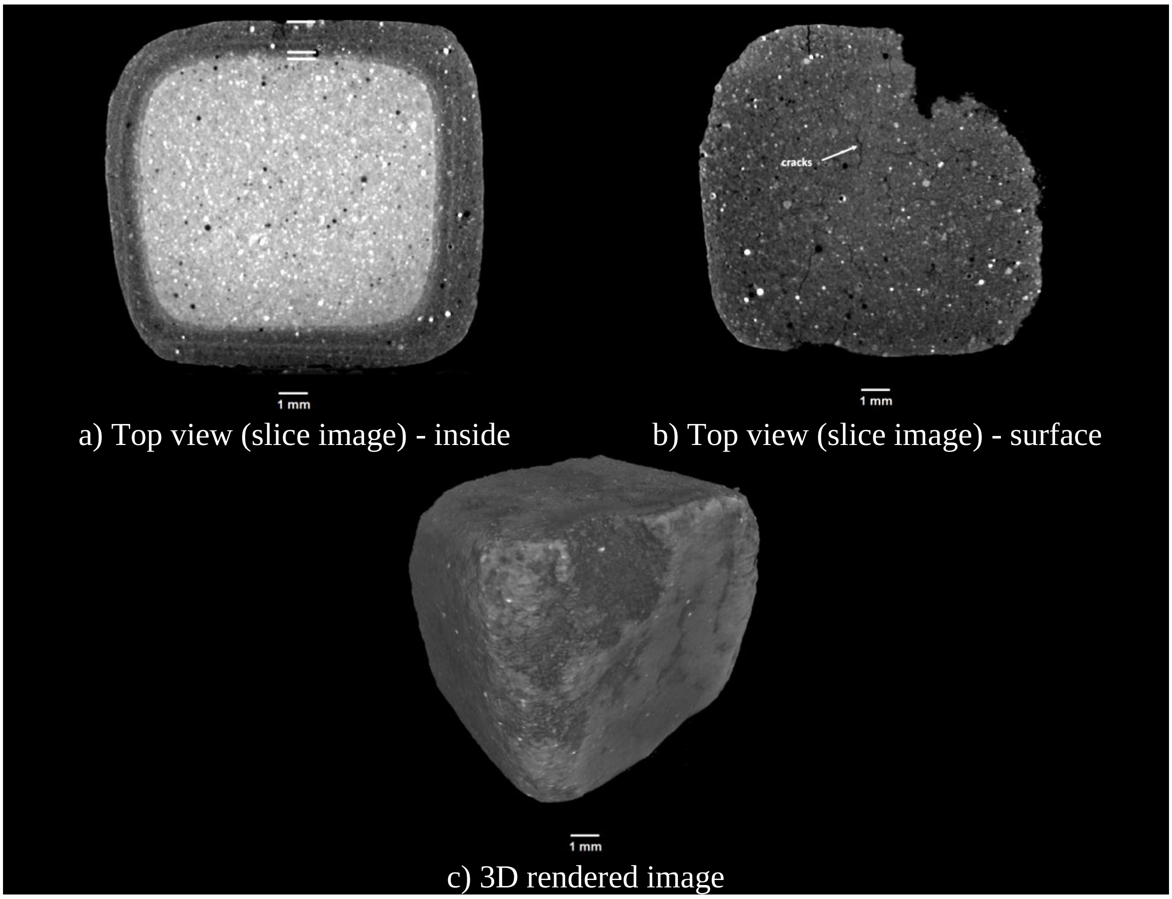

a) Top view (slice image) - inside

b) Top view (slice image) - surface

c) 3D rendered image

Figure B-12 CT images of OPC paste exposed to 1% hydrochloric acid (with brushing)

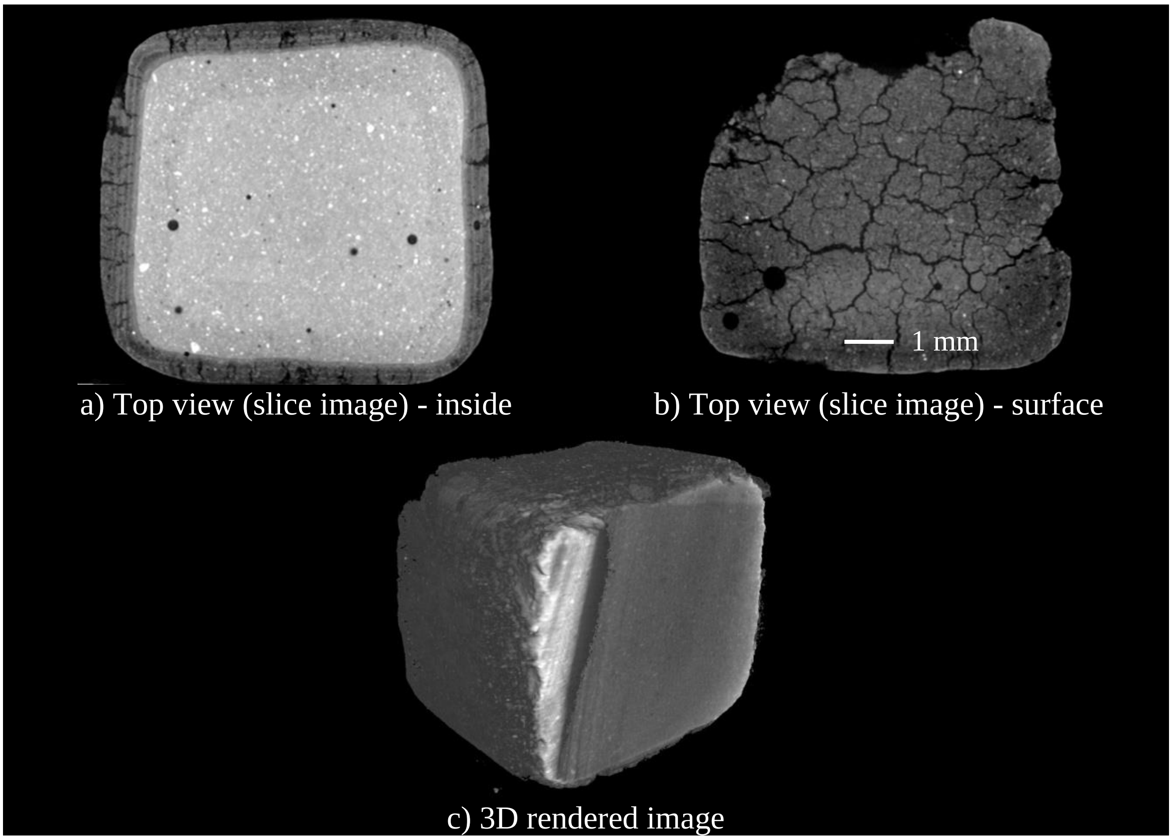

a) Top view (slice image) - inside

b) Top view (slice image) - surface

c) 3D rendered image

Figure B-13 CT images of FA30 paste exposed to 1% hydrochloric acid (with brushing)

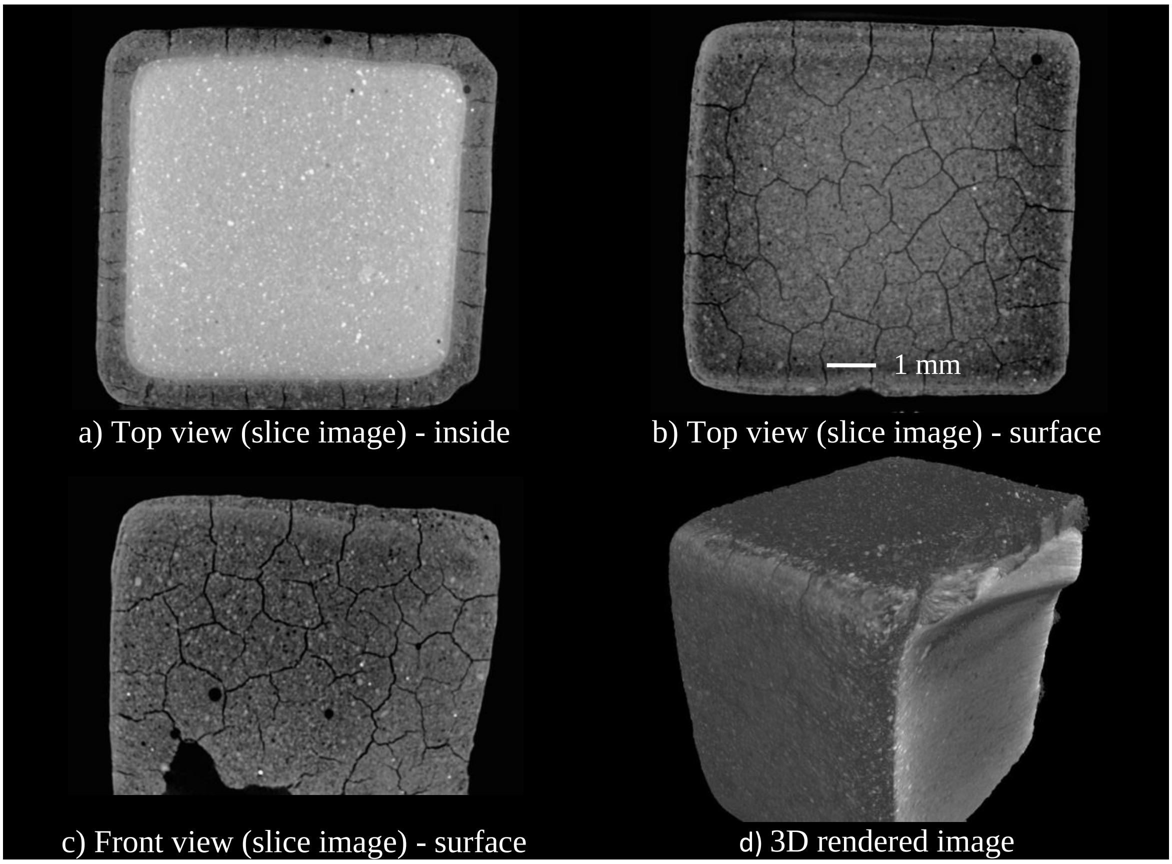

Figure B-14 CT images of BFS50 paste exposed to 1% hydrochloric acid (with brushing)

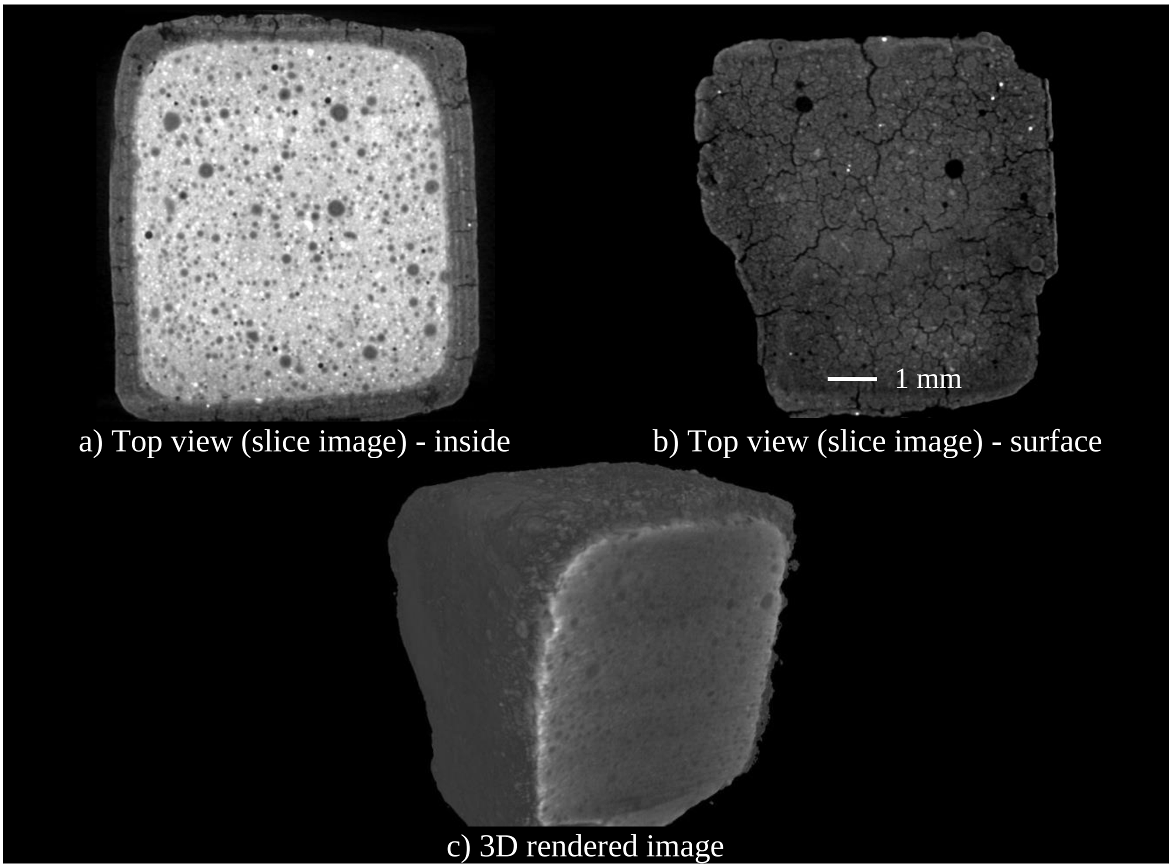

Figure B-15 CT images of SF10 paste exposed to 1% hydrochloric acid (with brushing)

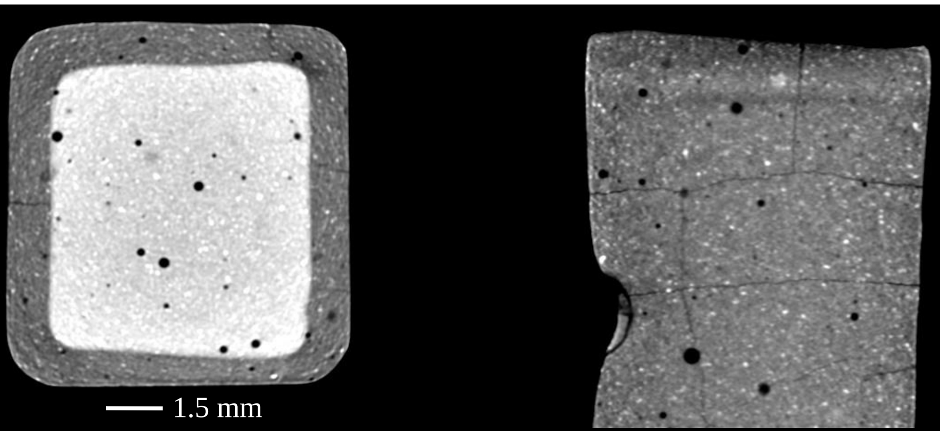

a) Top view (slice image) - inside b) Front view (slice image) - surface

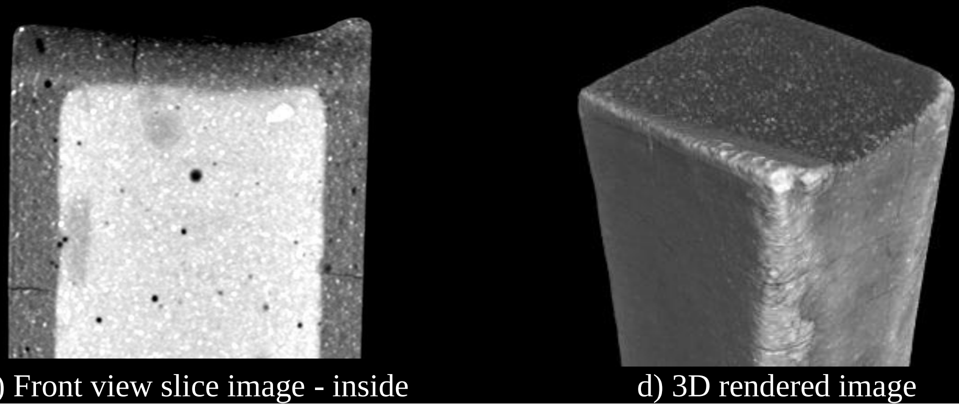

c) Front view slice image - inside d) 3D rendered image

Figure B-16 CT images of OPC paste exposed to 0.25M acetic acid (with brushing)

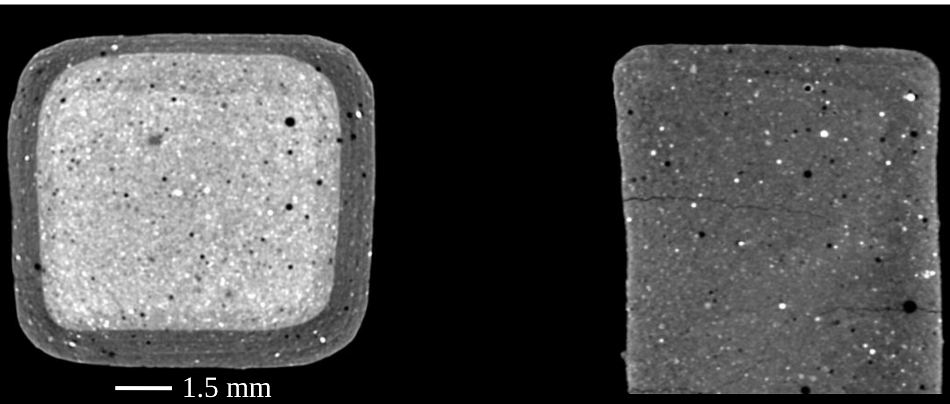

a) Top view (slice image) - inside b) Front view (slice image) - surface

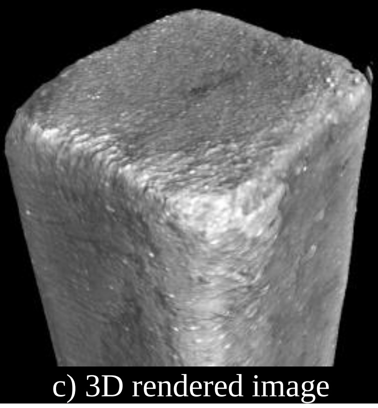

c) 3D rendered image

Figure B-17 CT images of FA30 paste exposed to 0.25M acetic acid (with brushing)

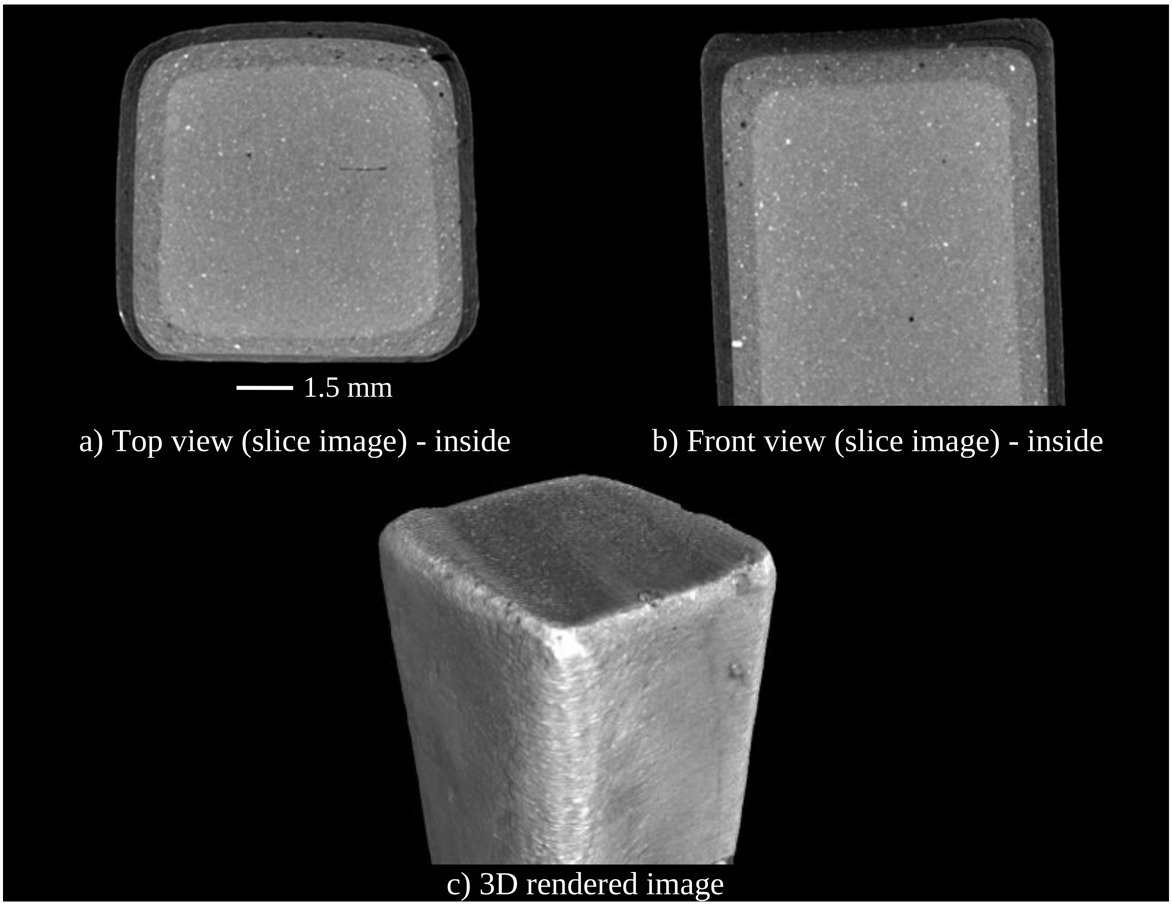

a) Top view (slice image) - inside

b) Front view (slice image) - inside

c) 3D rendered image

Figure B-18 CT images of BFS50 paste exposed to 0.25M acetic acid (with brushing)

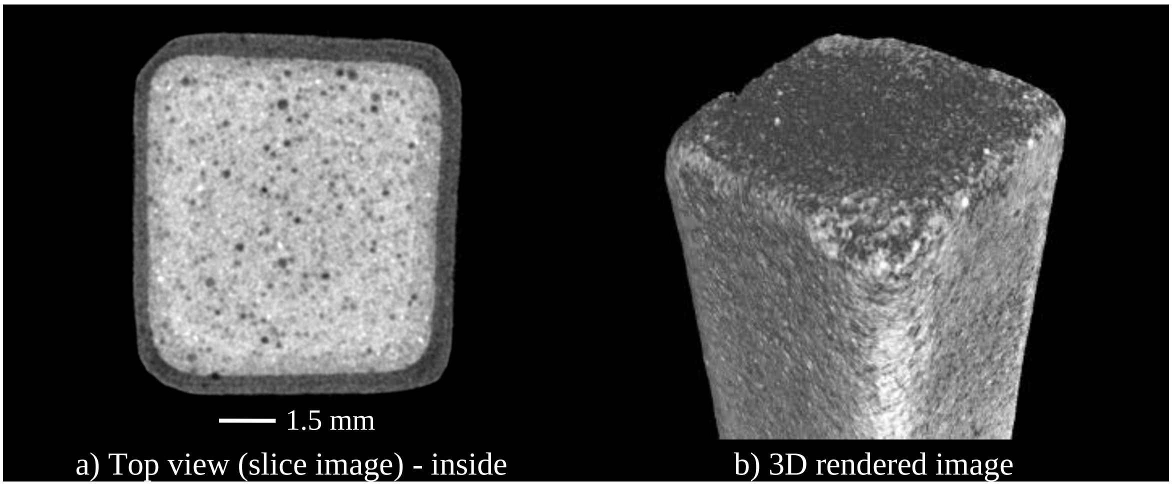

a) Top view (slice image) - inside

b) 3D rendered image

Figure B-19 CT images of SF10 paste exposed to 0.25M acetic acid (with brushing)

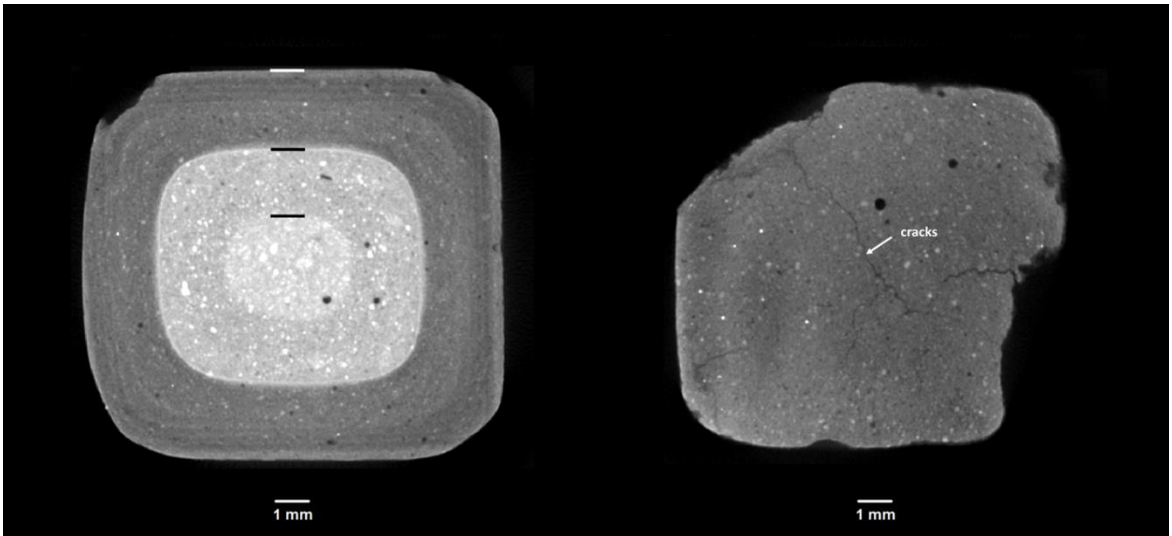

a) Top view (slice image) - inside

b) Top view (slice image) - surface

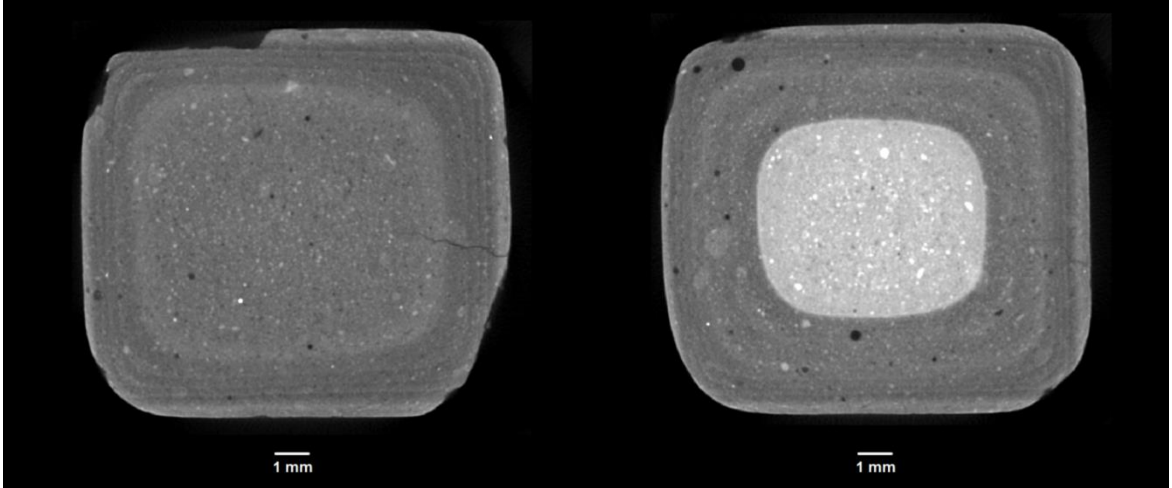

c) Top view (slice image) - surface

d) Top view (slice image) - surface

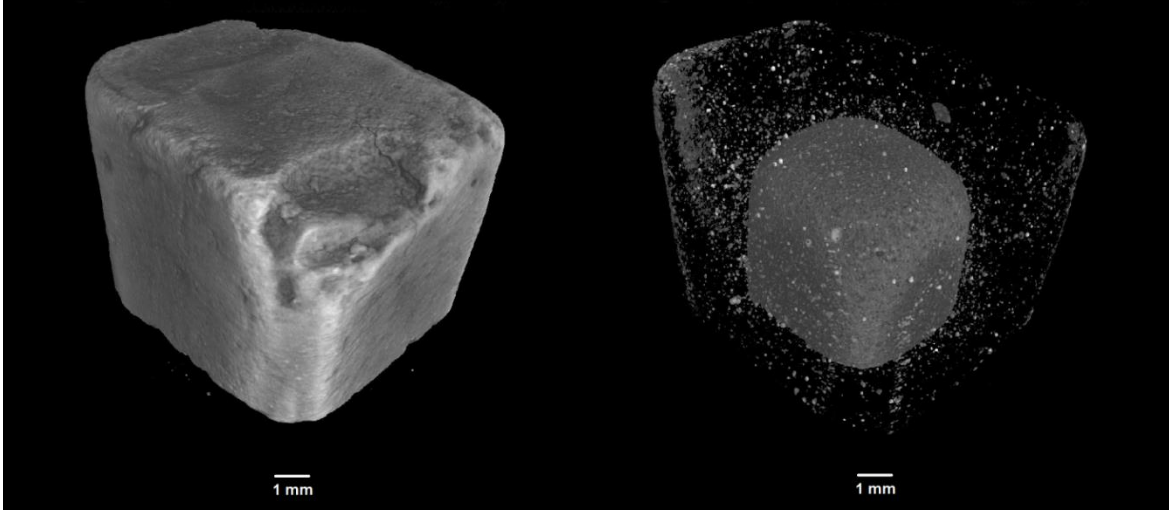

e) 3D rendered image

f) 3D image showing core volume

Figure B-20 CT images of OPC paste exposed to 0.5M acetic acid (with brushing)

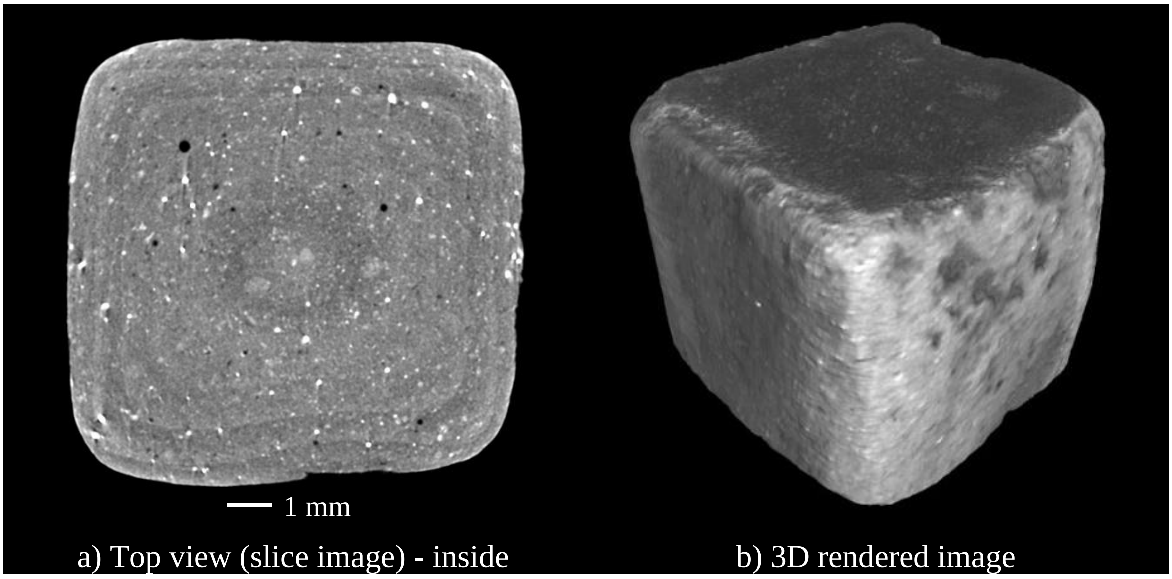

a) Top view (slice image) - inside b) 3D rendered image

Figure B-21 CT images of FA30 paste exposed to 0.5M acetic acid (with brushing)

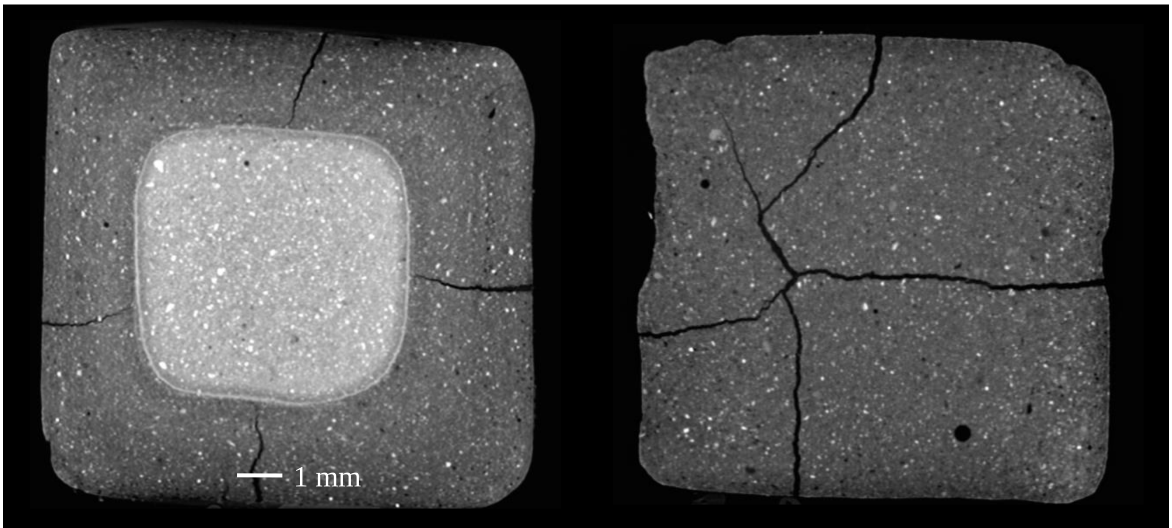

a) Top view (slice image) - inside b) Top view (slice image) - surface

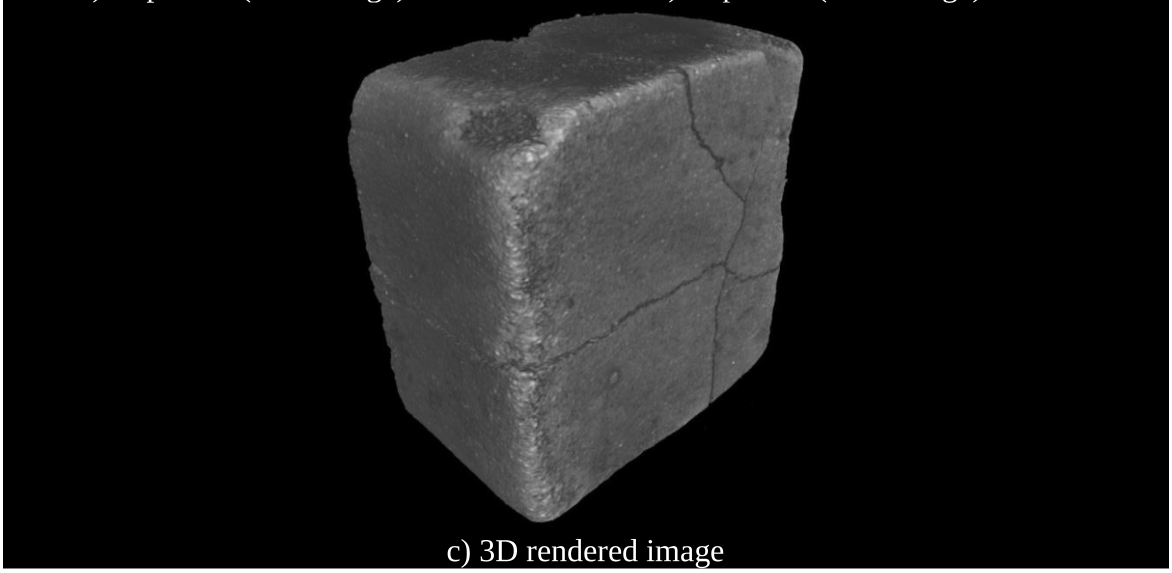

c) 3D rendered image

Figure B-22 CT images of BFS50 paste exposed to 0.5M acetic acid (with brushing)

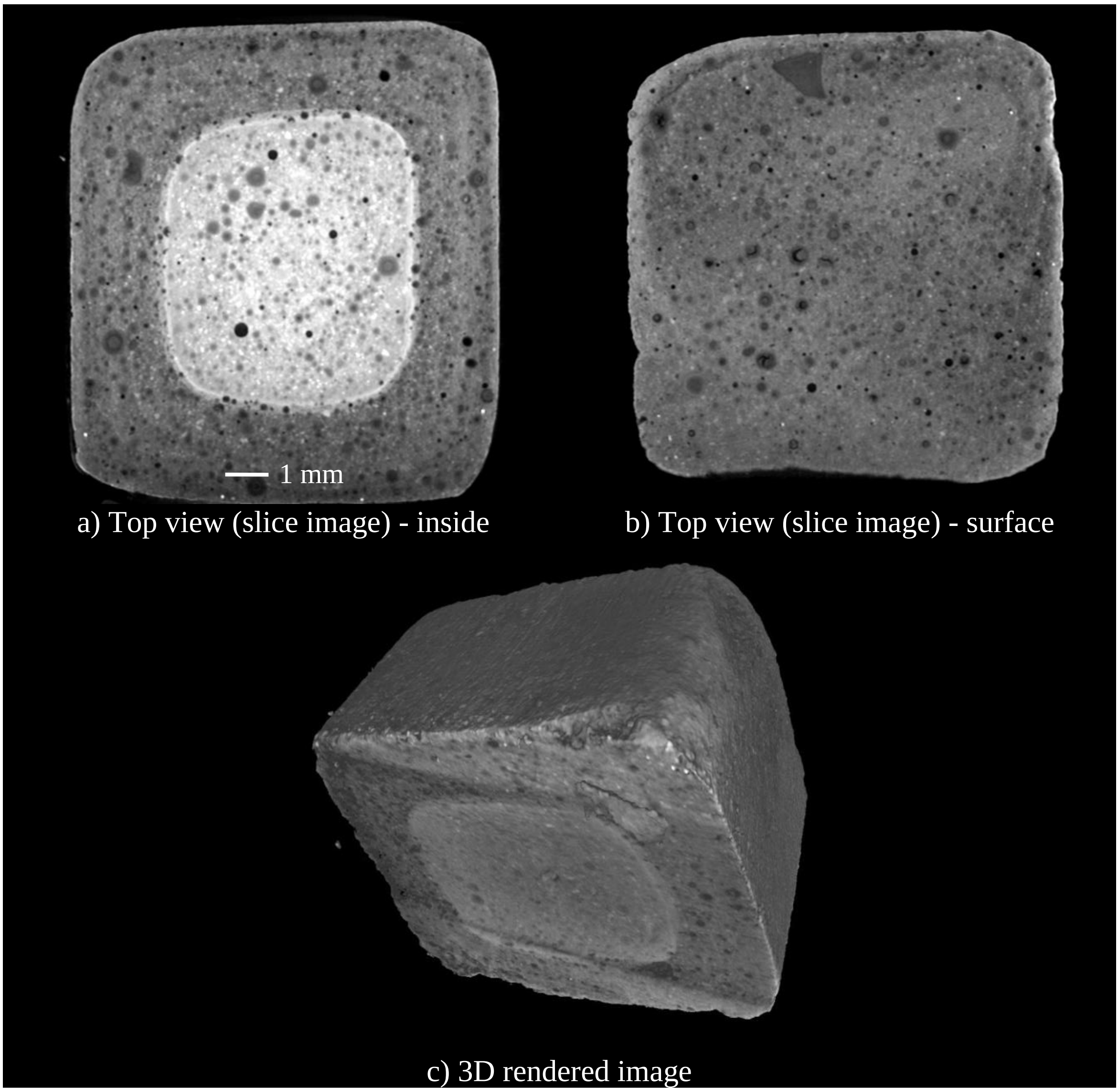

a) Top view (slice image) - inside

b) Top view (slice image) - surface

c) 3D rendered image

Figure B-23 CT images of SF10 paste exposed to 0.5M acetic acid (with brushing)

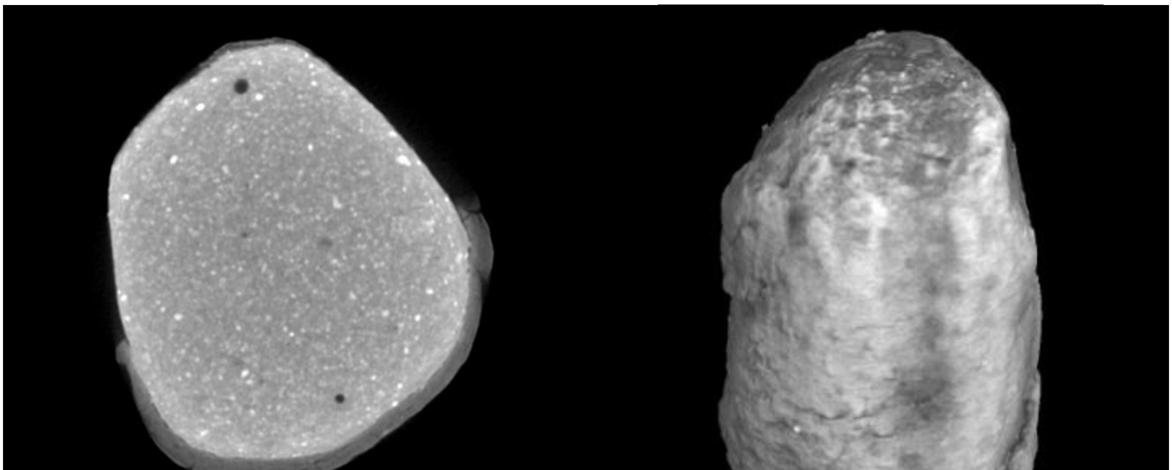

a) Top view (slice image) - inside

b) 3D rendered image

Figure B-24 CT images of OPC paste exposed to 0.5M citric acid (with brushing)

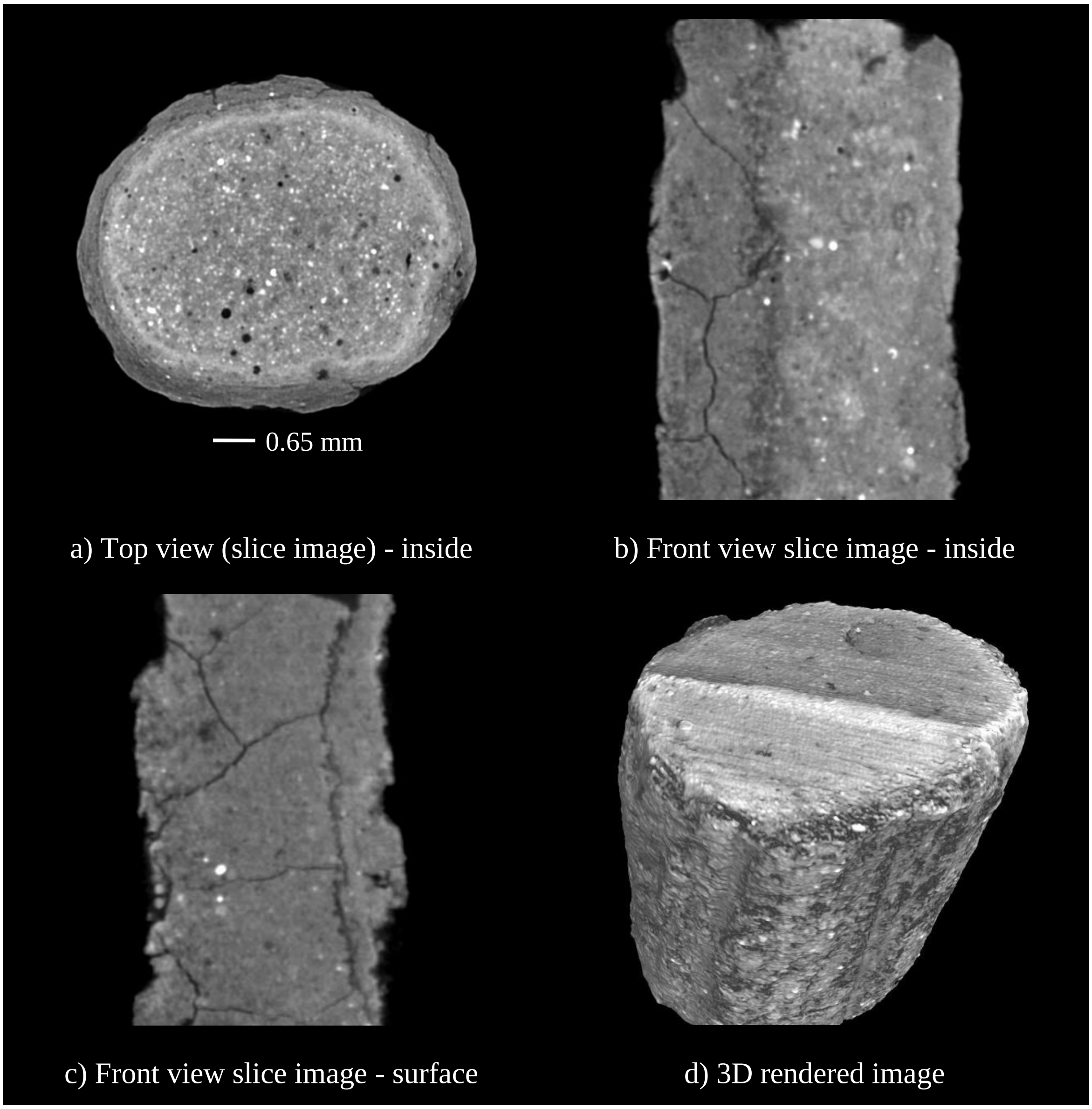

a) Top view (slice image) - inside

b) Front view slice image - inside

c) Front view slice image - surface

d) 3D rendered image

Figure B-25 CT images of FA30 paste exposed to 0.5M citric acid (with brushing)

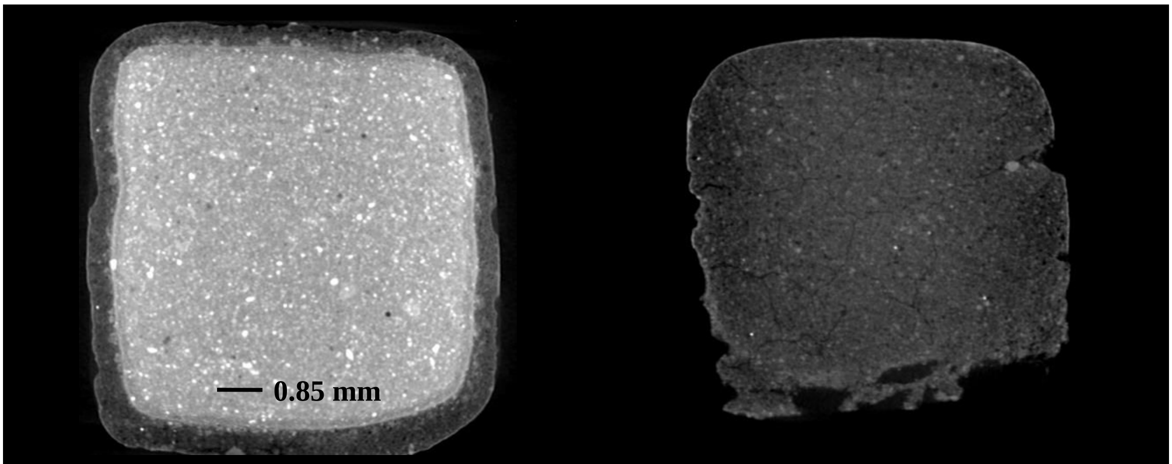

a) Top view (slice image) - inside b) Top view (slice image) - surface

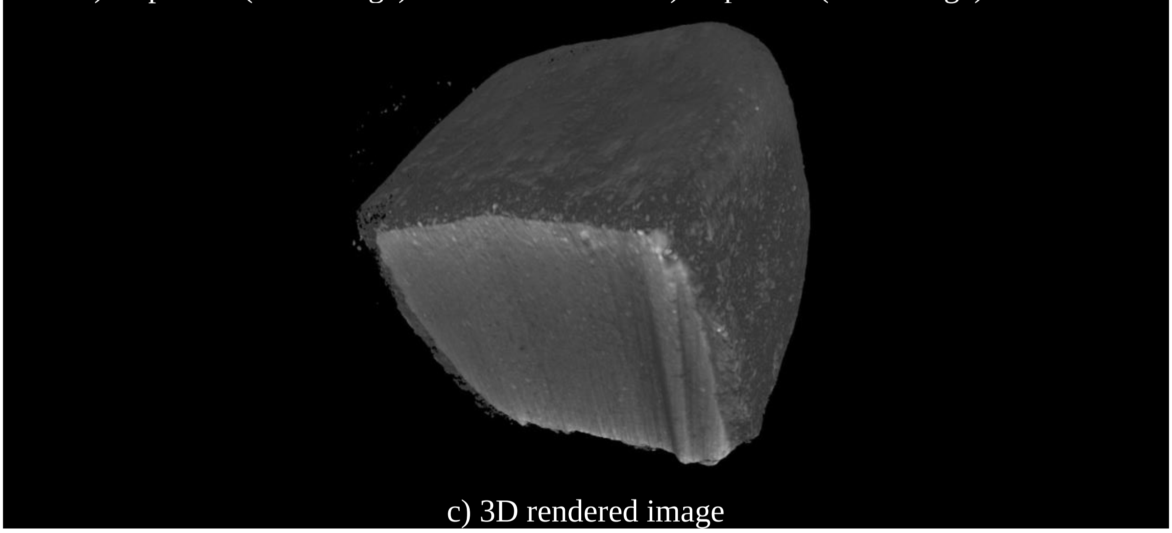

c) 3D rendered image

Figure B-26 CT images of BFS50 paste exposed to 0.5M citric acid (with brushing)

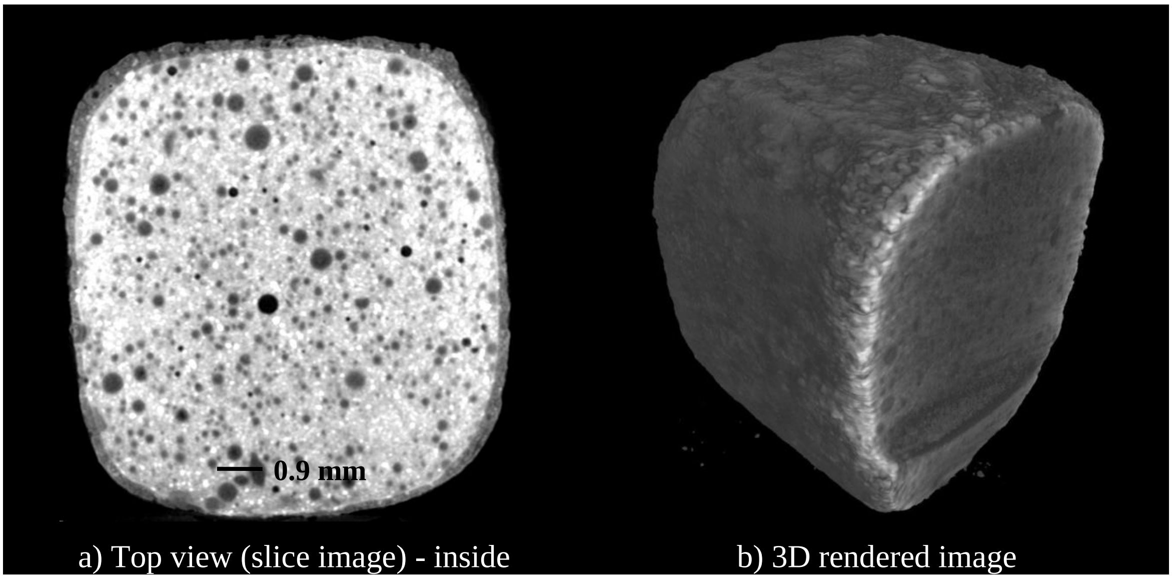

a) Top view (slice image) - inside b) 3D rendered image

Figure B-27 CT images of SF10 paste exposed to 0.5M citric acid (with brushing)

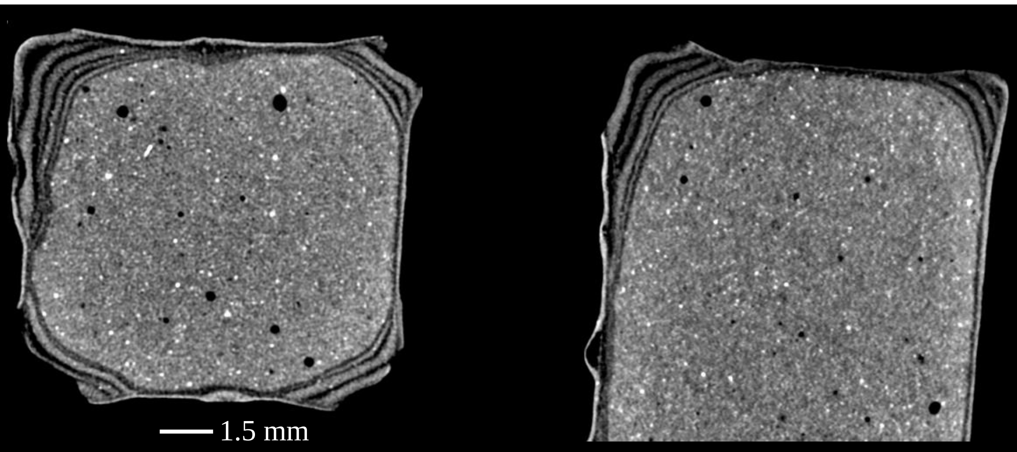

a) Top view slice image - inside

b) Front view slice image - inside

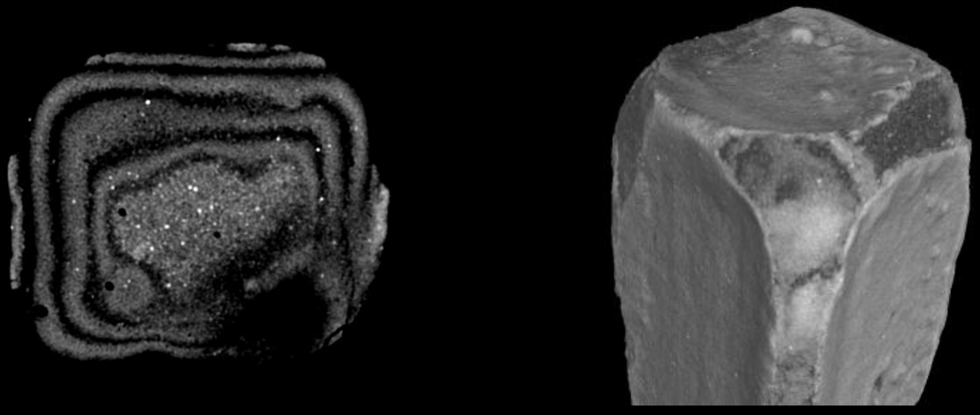

c) Top view slice image - surface

d) 3D rendered image

Figure B-28 CT images of LC2 paste exposed to 1% sulphuric acid (with brushing)

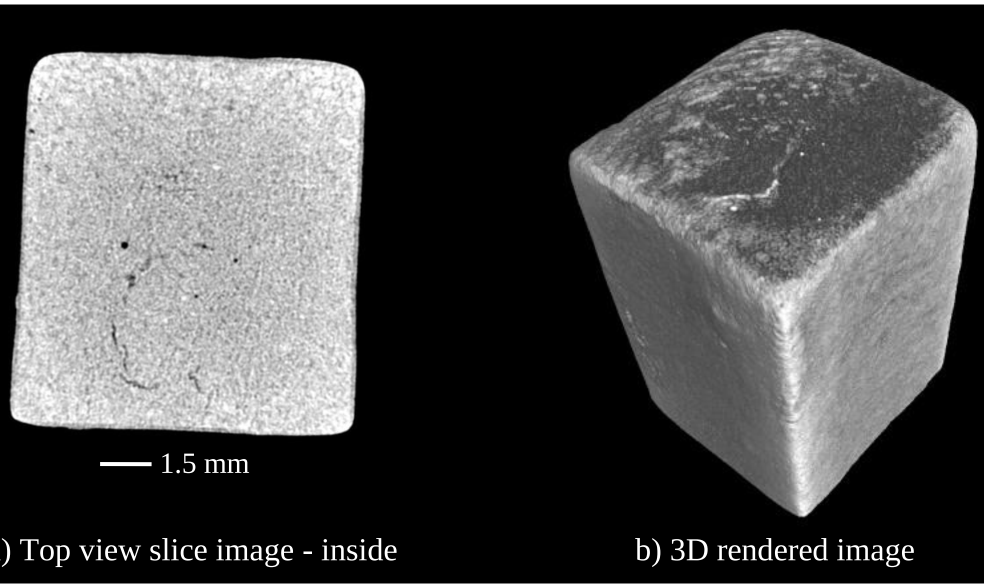

a) Top view slice image - inside

b) 3D rendered image

Figure B-29 CT images of HAC paste exposed to 1% sulphuric acid (with brushing)

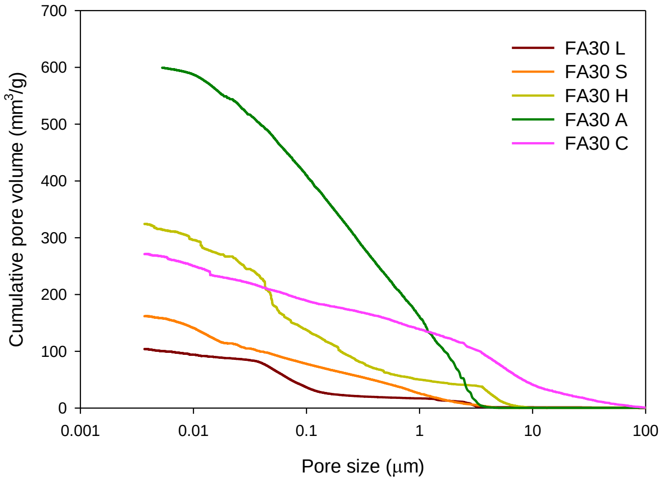

Figure B-30 Cumulative pore volume curve of FA30 paste exposed to acids

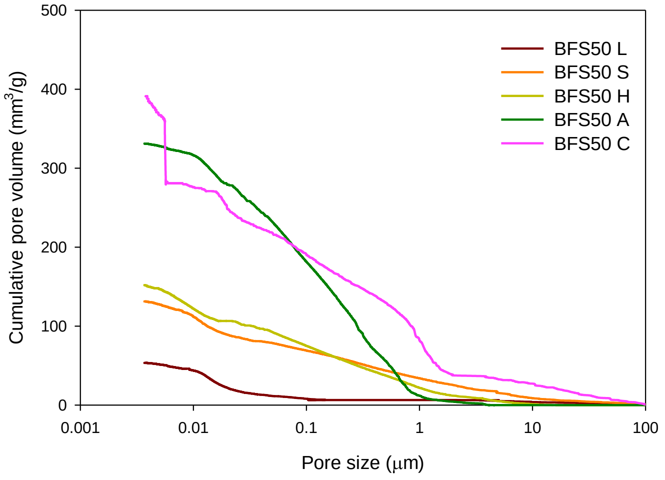

Figure B-31 Cumulative pore volume curve of BFS50 paste exposed to acids

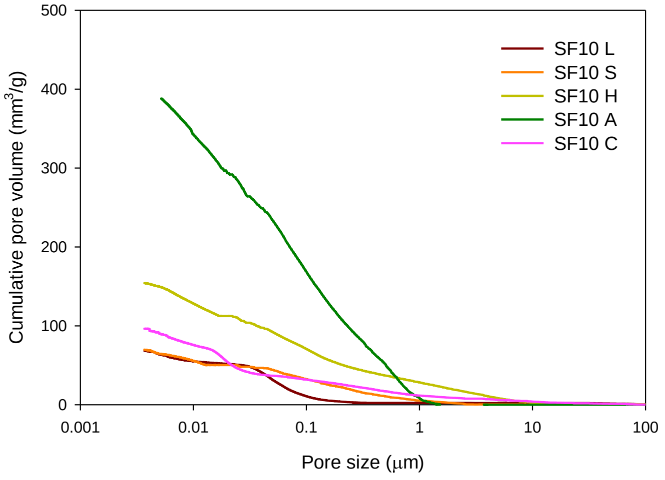

Figure B-32 Cumulative pore volume curve of SF10 paste exposed to acids

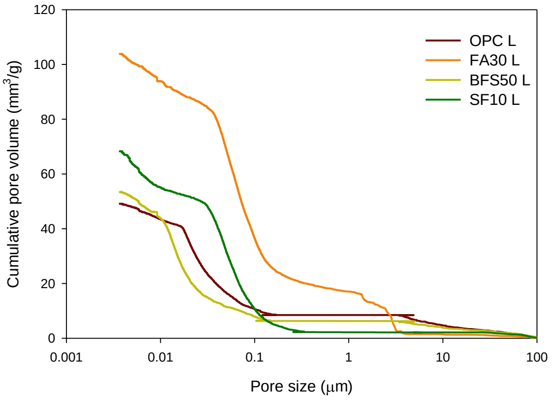

a) control mixes in saturated lime water

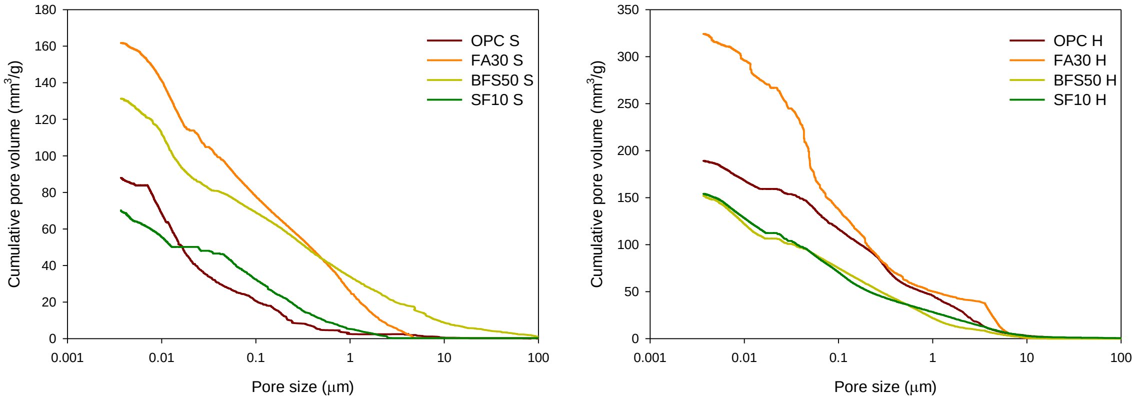

b) 1% sulphuric acid

c) 1% hydrochloric acid

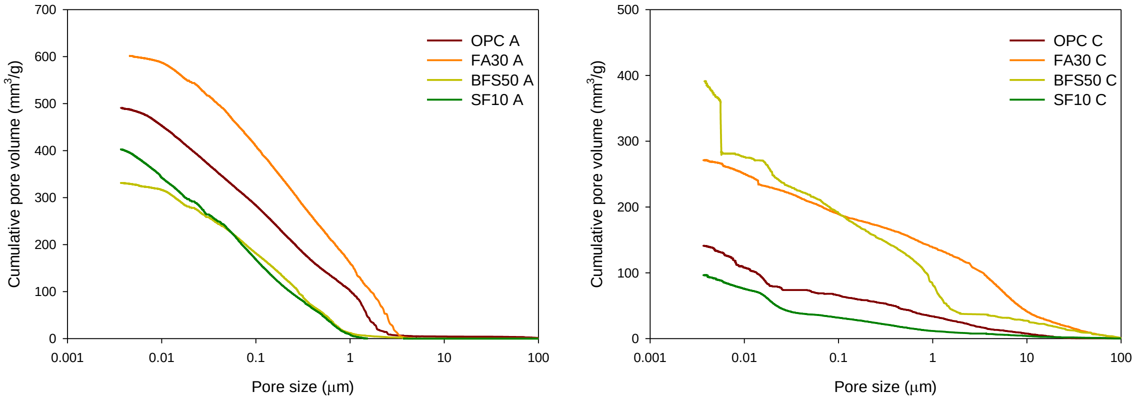

d) 0.5M acetic acid

e) 0.5M citric acid

Figure B-33 Cumulative pore volume curve of paste mixes after the exposure period

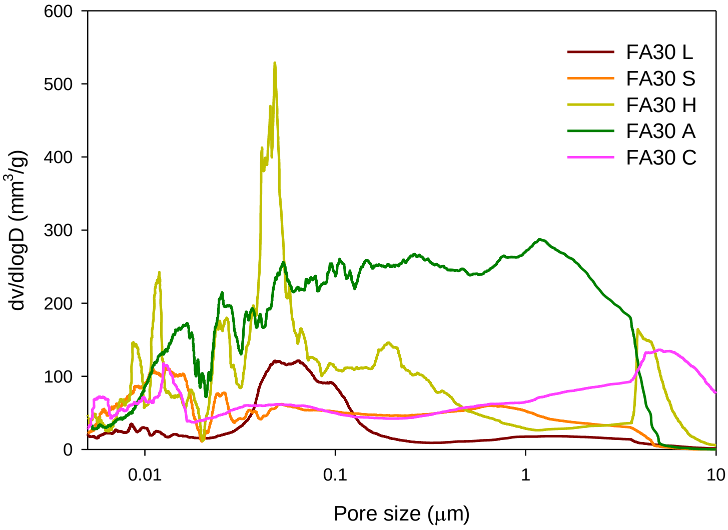

Figure B-34 Differential intruded volume curve of FA30 paste exposed to acids

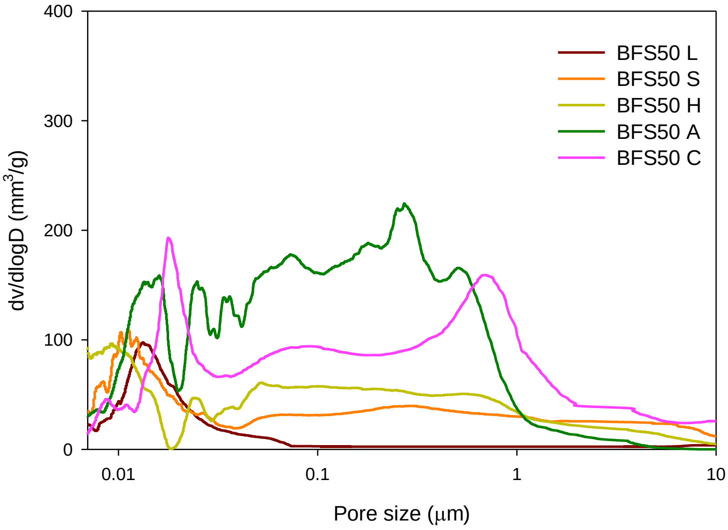

Figure B-35 Differential intruded volume curve of BFS50 paste exposed to acids

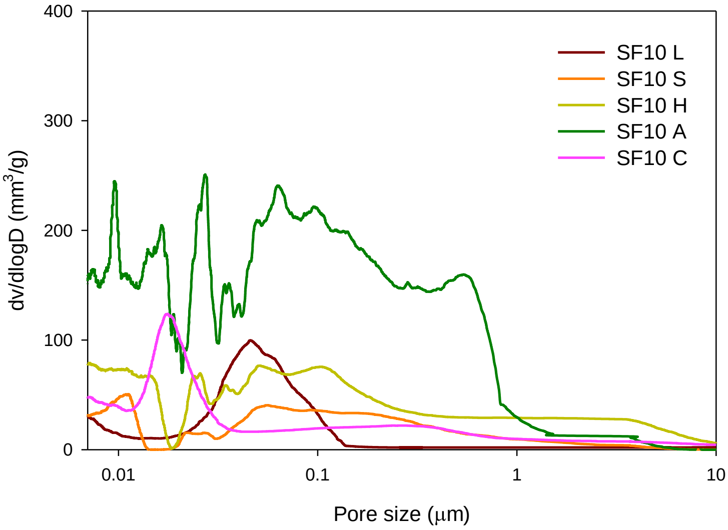

Figure B-36 Differential intruded volume curve of SF10 paste exposed to acids

Table B-1 TGA analysis results of paste before and after the acid exposure

Mix/ solution	Residual mass as % of initial mass					Bound water (%)	Peak temp for dehydroxylation of $Ca(OH)_2$ (˚C)	$Ca(OH)_2$ (%)	Peak temp for decarbonation of $CaCO_3$ (˚C)	$CaCO_3$ (%)
	Res. mass 105˚C	Res. mass 400˚C	Res. mass 500˚C	Res. mass 750˚C	Res. mass 860˚C					
OPC L	95.5	87.9	85.2	78.6	78.3	17.21	434.7	10.98	684.9	13.85
OPC S	92.0	81.3	78.8	74.8	74.4	17.60	429.9	8.02	694.3	8.06
OPC H	91.8	81.2	79.6	74.6	74.1	17.64	432.2	5.56	688.7	11.77
OPC A	90.6	79.3	77.9	74.2	73.6	16.99	431.8	2.13	696.6	8.90
OPC C	94.6	86.0	83.6	77.1	76.5	18.05	432.5	8.97	709.0	15.48
FA30 L	96.7	90.1	87.7	80.1	79.3	17.44	435.7	8.46	704.0	18.45
FA30 S	94.9	85.3	84.1	80.4	79.9	14.96	429.1	4.00	707.4	8.63
FA30 H	93.8	85.1	83.9	80.4	79.8	14.02	-	0.00	657.1	7.76
FA30 A	89.5	81.7	80.5	79.2	79.1	10.41	-	0.00	647.2	2.02
FA30 C	96.6	90.5	89.6	84.2	83.5	13.10	433.6	2.63	688.7	12.19
BFS50 L	91.9	84.7	83.5	79.8	79.5	12.49	436.6	5.20	707.8	6.58
BFS50 S	92.1	81.8	80.0	77.3	77.0	15.08	437.9	5.04	691.9	6.40
BFS50 H	93.8	83.3	81.8	78.2	77.7	16.07	437.7	3.18	663.0	8.50
BFS50 A	90.6	78.8	77.1	75.0	74.6	15.99	-	0.00	664.2	2.67
BFS50 C	94.8	85.0	82.8	77.7	77.2	17.61	438.7	3.92	681.5	11.11
SF10 L	97.1	91.7	89.7	83.2	81.3	15.82	432.5	9.35	680.9	11.38
SF10 S	94.3	83.5	80.9	76.9	76.3	17.94	432.4	9.11	702.5	9.94
SF10 H	93.5	83.4	81.9	76.8	76.4	17.10	432.8	4.28	682.6	12.34
SF10 A	91.1	80.1	78.8	75.6	75.2	15.92	-	0.00	690.1	4.50
SF10 C	93.9	84.7	82.3	74.2	73.7	20.29	449.6	7.28	711.4	19.00

L – saturated lime water, S – 1% sulphuric acid, H – 1% hydrochloric acid, A – 0.5M acetic acid, C – 0.5M citric acid

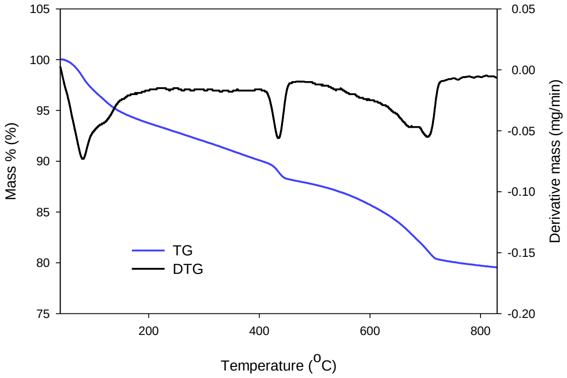

a) before the acid exposure

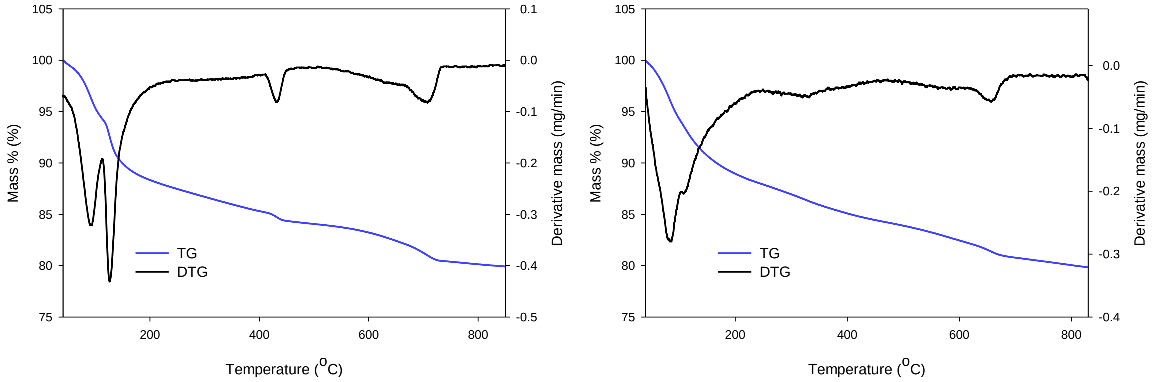

b) 1% sulphuric acid

c) 1% hydrochloric acid

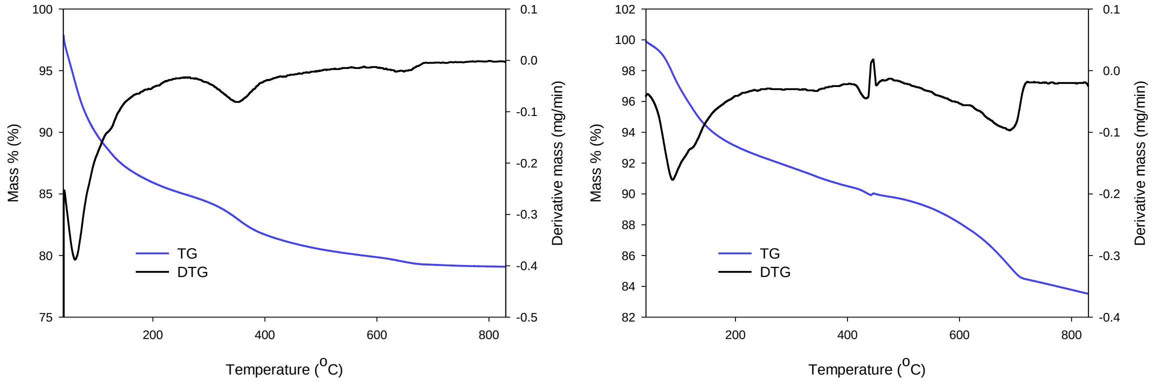

d) 0.5M acetic acid

e) 0.5M citric acid

Figure B-37 TGA/DTG curve of FA30 paste before and after the acid exposure

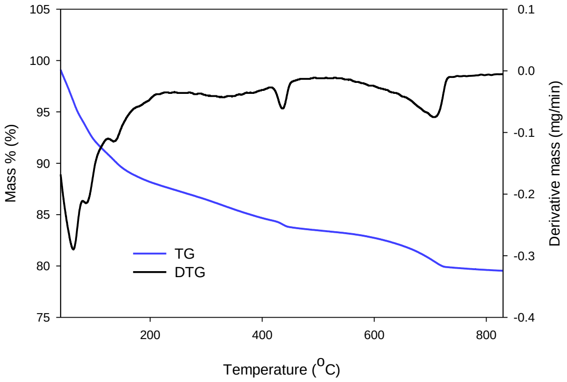

a) before the acid exposure

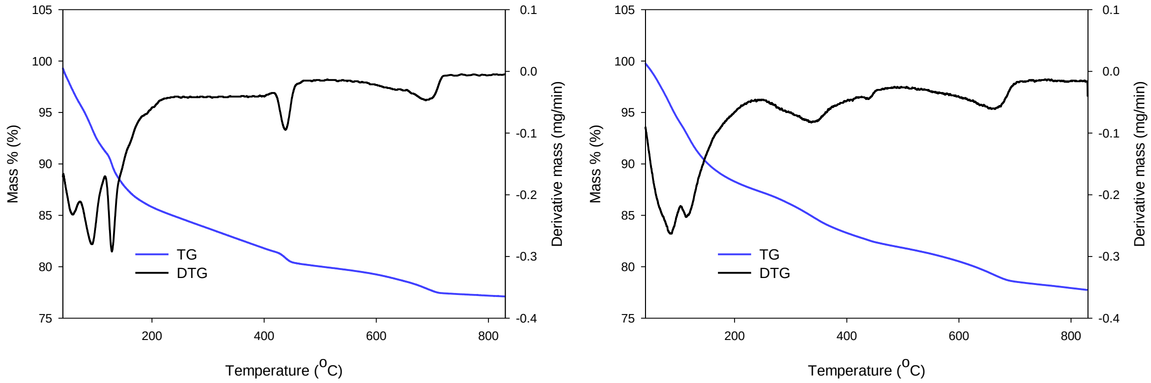

b) 1% sulphuric acid

c) 1% hydrochloric acid

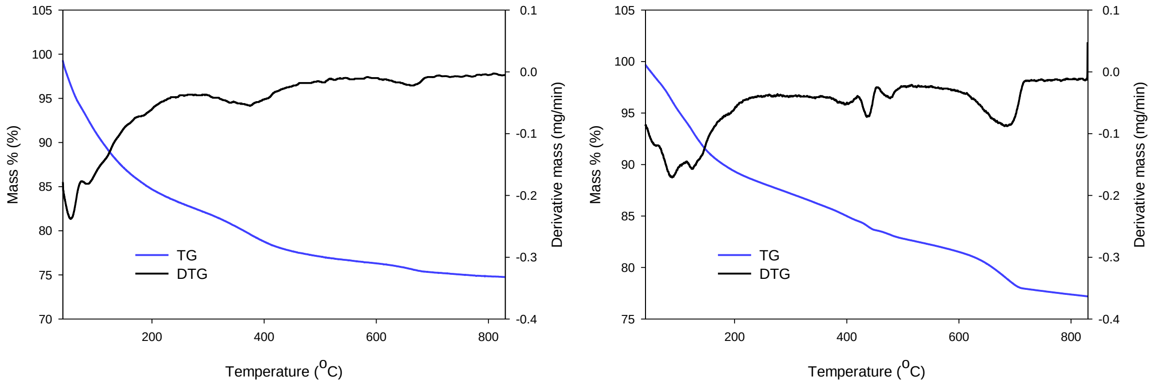

d) 0.5M acetic acid

e) 0.5M citric acid

Figure B-38 TGA/DTG curve of BFS50 paste before and after the acid exposure

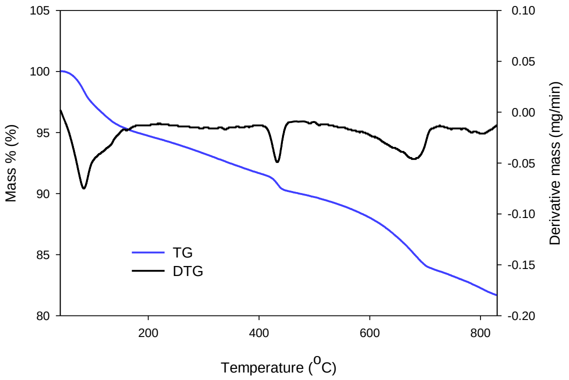

a) before the acid exposure

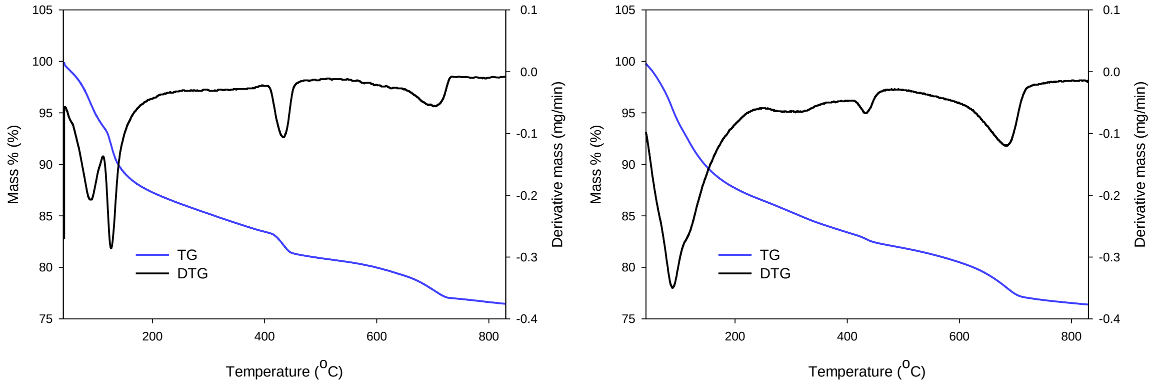

b) 1% sulphuric acid

c) 1% hydrochloric acid

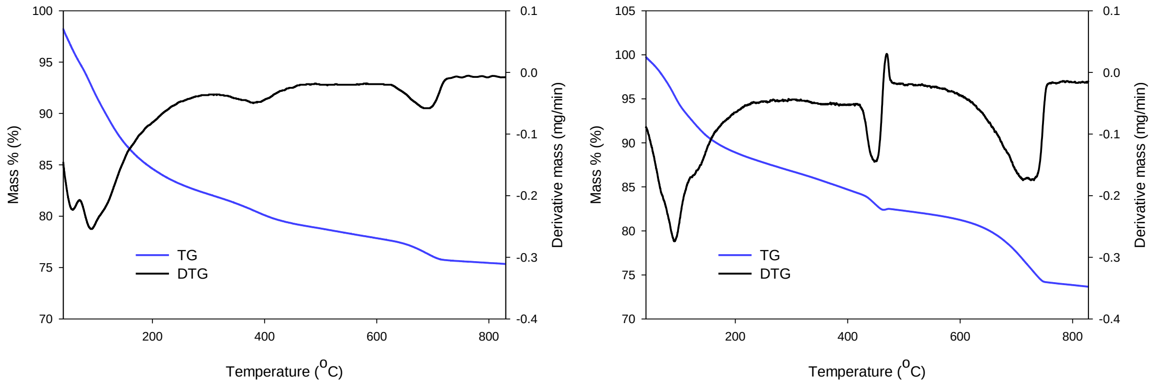

d) 0.5M acetic acid

e) 0.5M citric acid

Figure B-39 TGA/DTG curve of SF10 paste before and after the acid exposure

APPENDIX C

INVESTIGATIONS ON MORTAR EXPOSED TO ACIDS

Before acid exposure	After acid exposure					
	0.5% Sulphuric	1% Sulphuric	3% Sulphuric	0.12M Acetic	0.25M Acetic	0.5M Acetic
			*			

* showed 100% mass loss due to severe degradation

Figure C-1 FA30 mortar (w/b 0.40) specimens before and after the acid exposure

Before acid exposure	After acid exposure					
	0.5% Sulphuric	1% Sulphuric	3% Sulphuric	0.12M Acetic	0.25M Acetic	0.5M Acetic
						

Figure C-2 BFS50 mortar (w/b 0.40) specimens before and after the acid exposure

Before acid exposure	After acid exposure					
	0.5% Sulphuric	1% Sulphuric	3% Sulphuric	0.12M Acetic	0.25M Acetic	0.5M Acetic
						

Figure C-3 SF10 mortar (w/b 0.40) specimens before and after the acid exposure

Acid solution	OPC	FA30	BFS50	SF10
Sulphuric 0.5%				
Sulphuric 1%				
Sulphuric 3%	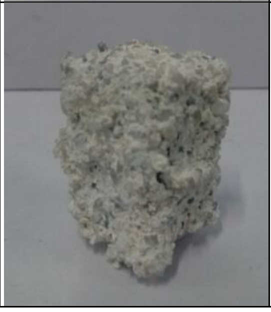			

Figure C-4 Mortar specimens (25 × 25 × 35 mm) exposed to sulphuric acid (w/b 0.55)

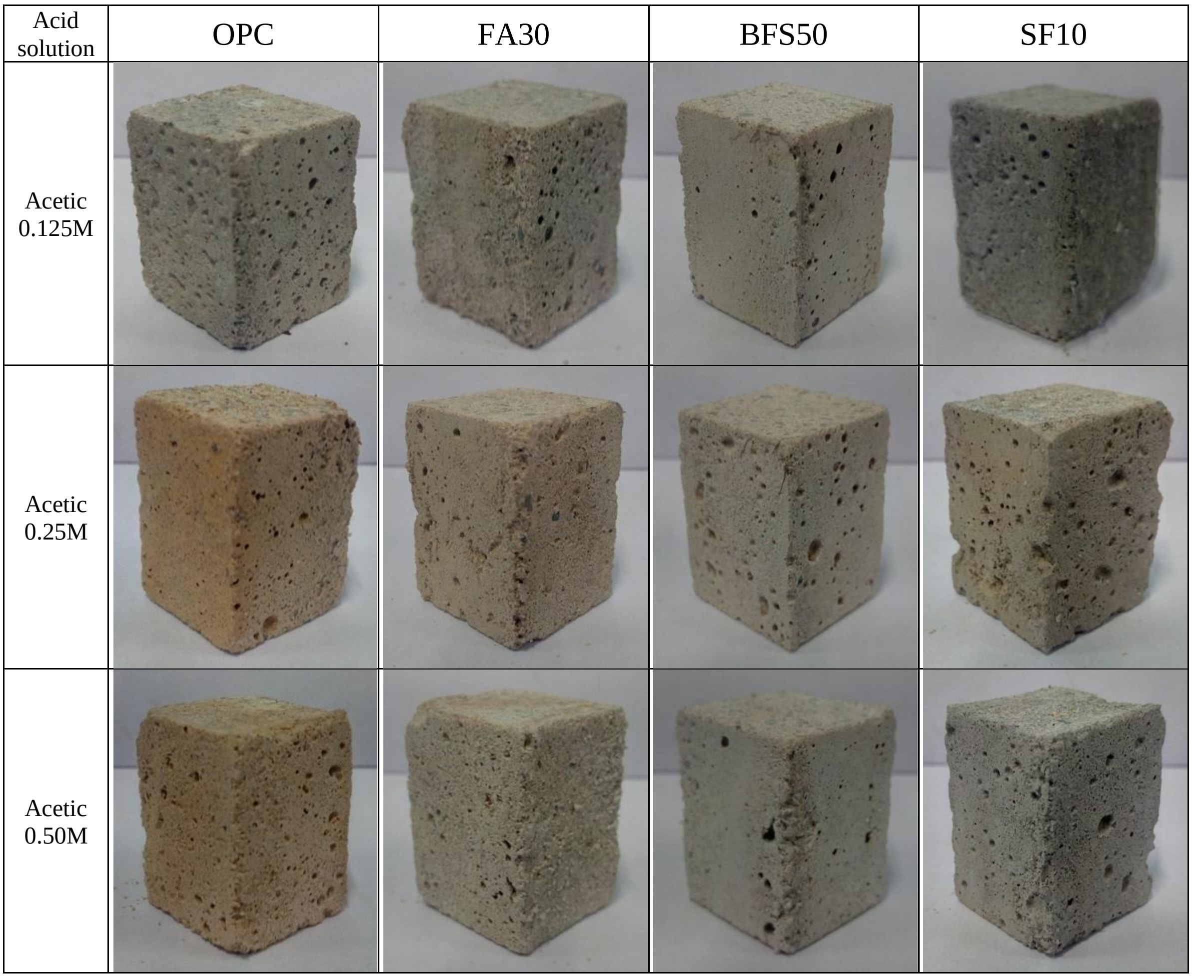

Figure C-5 Mortar specimens (25 × 25 × 35 mm) exposed to acetic acid (w/b 0.55)

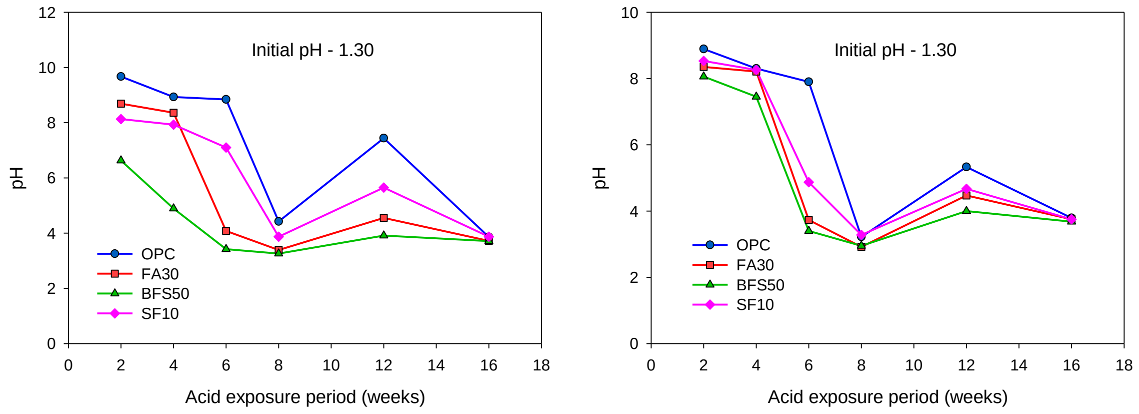

a) without brushing b) with brushing

Figure C-6 Changes in pH of acid solution exposed to 0.5% sulphuric acid (mortar w/b 0.55)

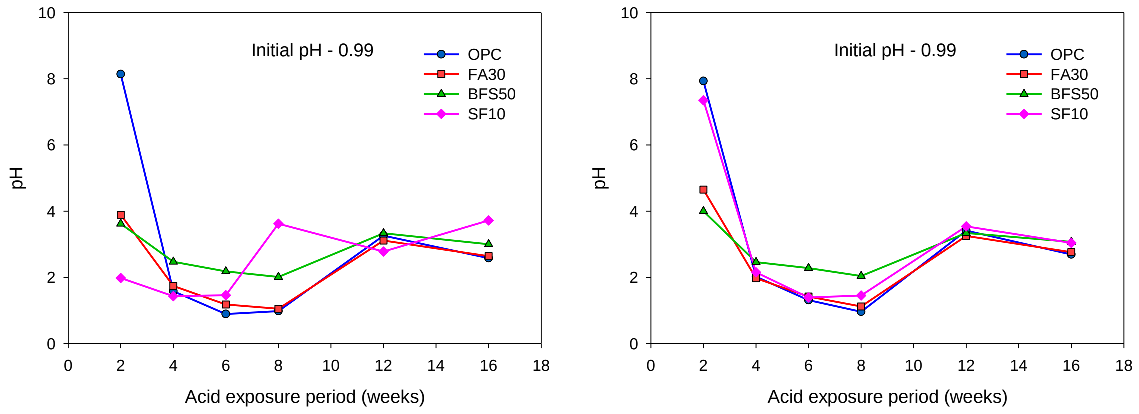

a) without brushing b) with brushing

Figure C-7 Changes in pH of acid solution exposed to 1% sulphuric acid (mortar w/b 0.55)

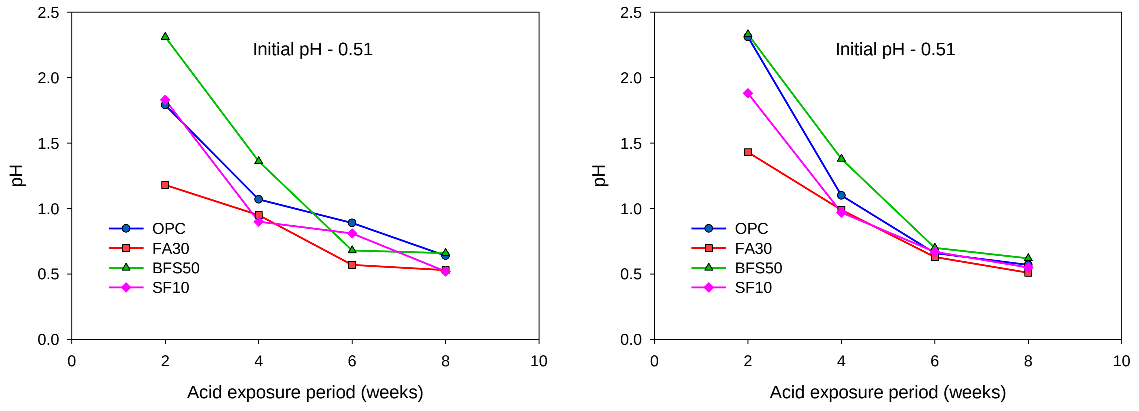

a) without brushing b) with brushing

Figure C-8 Changes in pH of acid solution exposed to 3% sulphuric acid (mortar w/b 0.55)

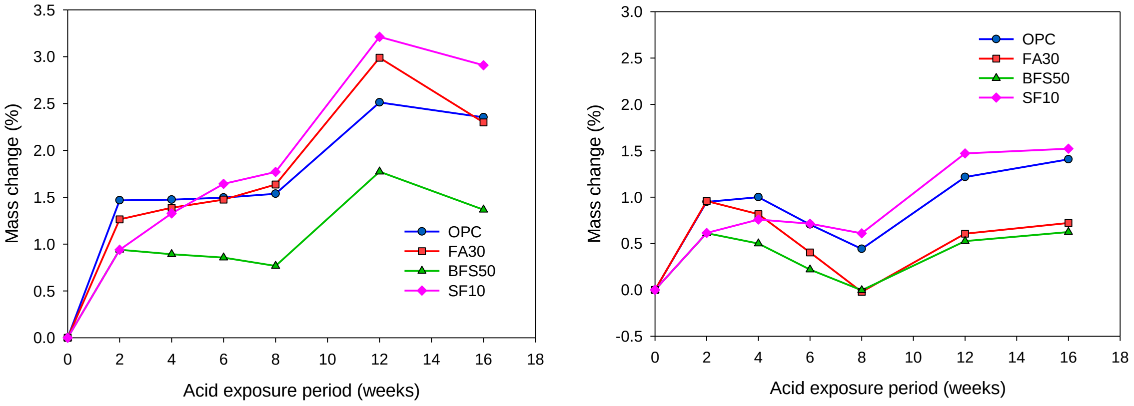

a) without brushing b) with brushing

Figure C-9 Mass changes of mortar (25 × 25 × 35 mm) exposed to 0.5% sulphuric acid (w/b 0.55)

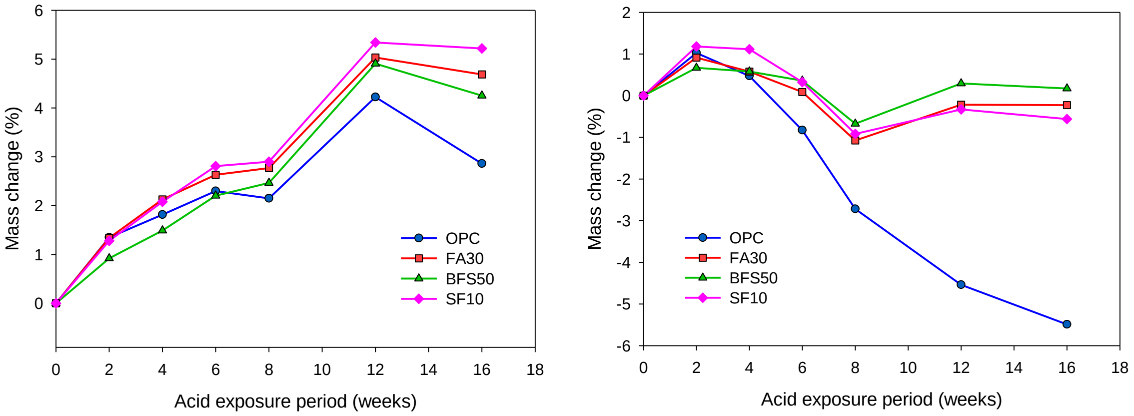

a) without brushing b) with brushing

Figure C-10 Mass changes of mortar (25 × 25 × 35 mm) exposed to 1% sulphuric acid (w/b 0.55)

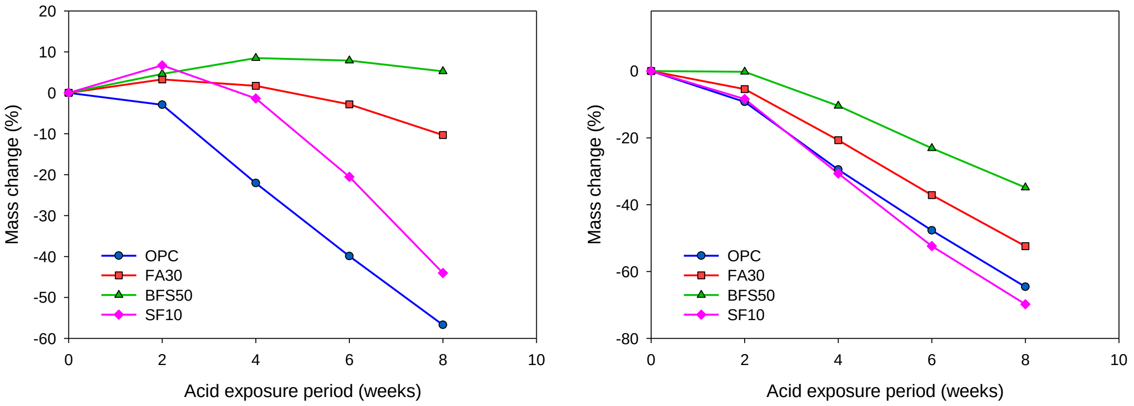

a) without brushing b) with brushing

Figure C-11 Mass changes of mortar (25 × 25 × 35 mm) exposed to 3% sulphuric acid (w/b 0.55)

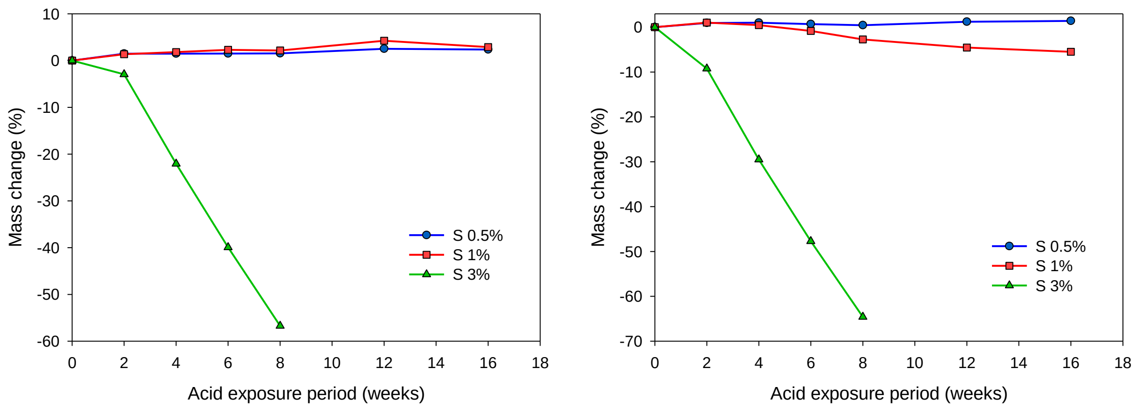

a) without brushing b) with brushing

Figure C-12 Mass changes of OPC mortar (25 × 25 × 35 mm) exposed to sulphuric acid (w/b 0.55)

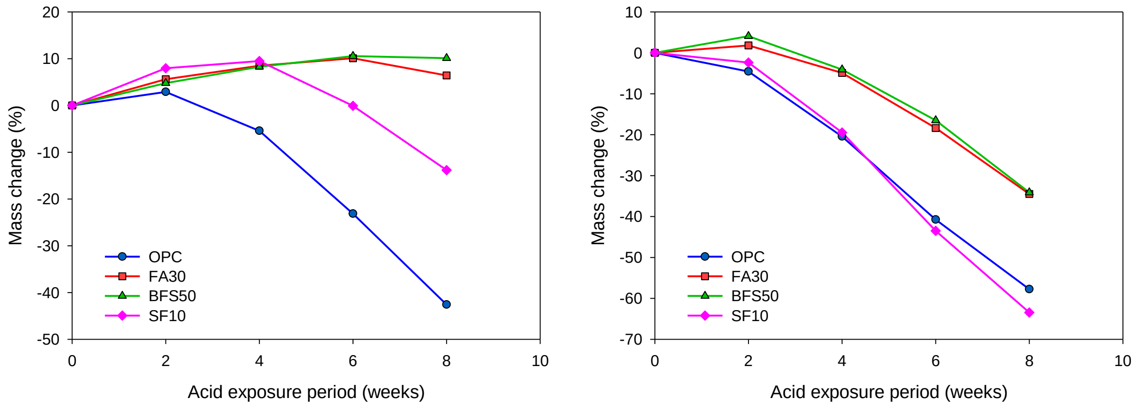

a) without brushing b) with brushing

Figure C-13 Mass changes of mortar cylinder (ϕ 25 × 50 mm) exposed to 3% sulphuric acid (w/b 0.55)

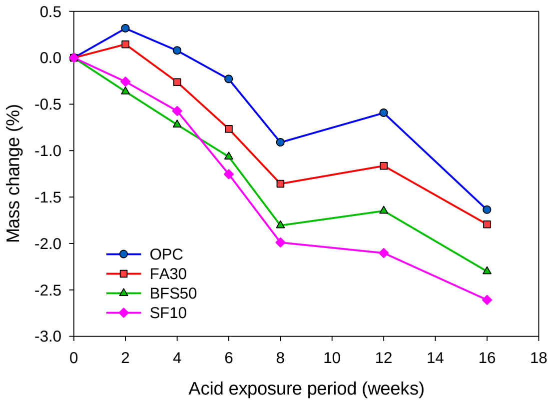

Figure C-14 Mass changes of mortar (25 × 25 × 35 mm) exposed to 0.125M acetic acid (w/b 0.55)

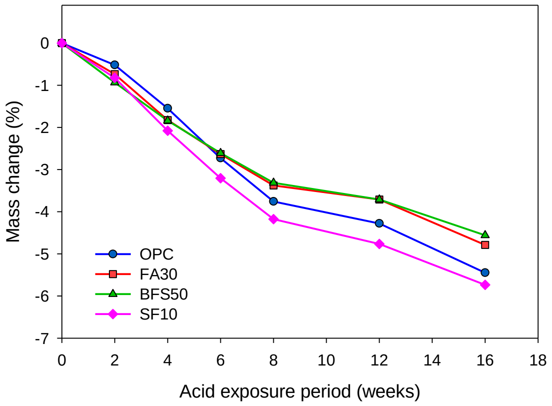

Figure C-15 Mass changes of mortar (25 × 25 × 35 mm) exposed to 0.25M acetic acid (w/b 0.55)

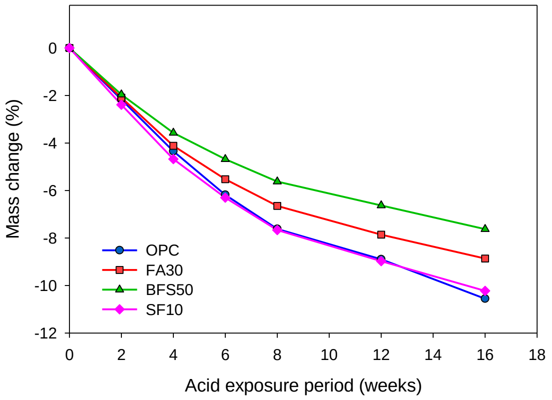

Figure C-16 Mass changes of mortar (25 × 25 × 35 mm) exposed to 0.50M acetic acid (w/b 0.55)

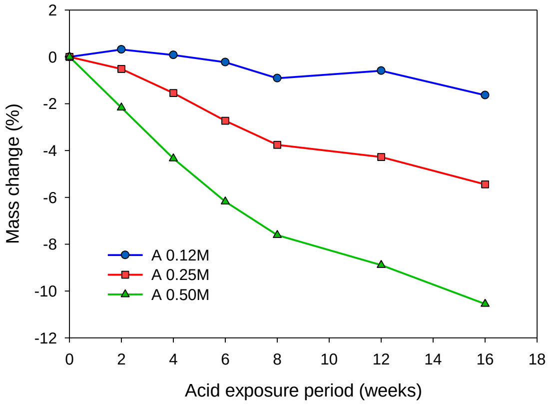

Figure C-17 Mass changes of OPC mortar (25 × 25 × 35 mm) exposed to acetic acid (w/b 0.55)

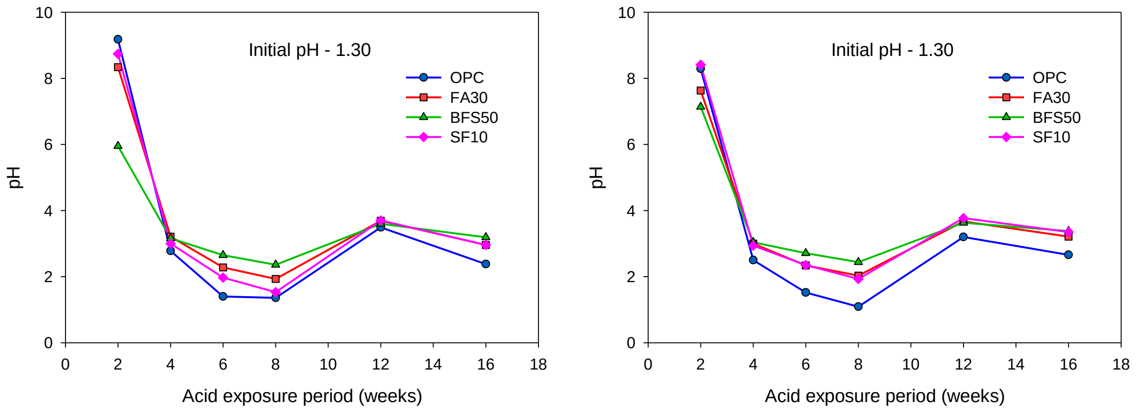

a) without brushing b) with brushing

Figure C-18 Changes in pH of acid solution for mortar (25 × 25 × 35 mm) exposed to 0.5% sulphuric acid (mortar w/b 0.55)

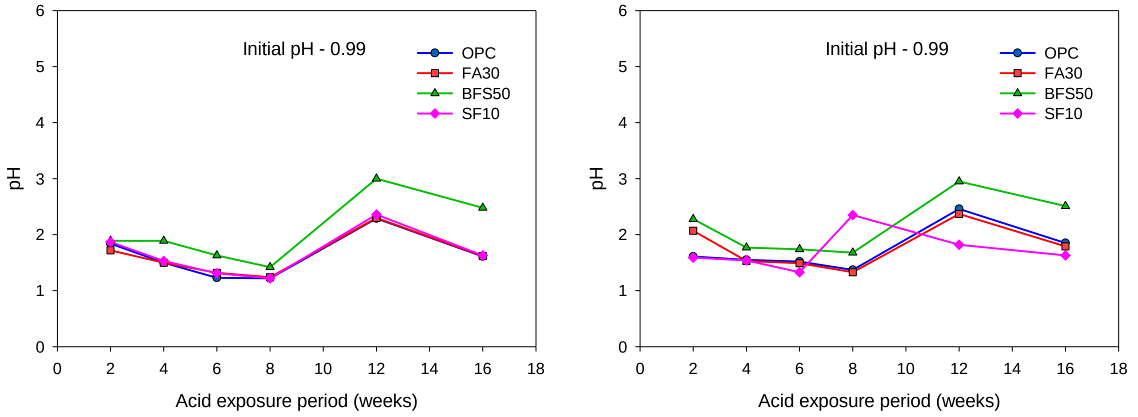

a) without brushing b) with brushing

Figure C-19 Changes in pH of acid solution for mortar (25 × 25 × 35 mm) exposed to 1% sulphuric acid (mortar w/b 0.55)

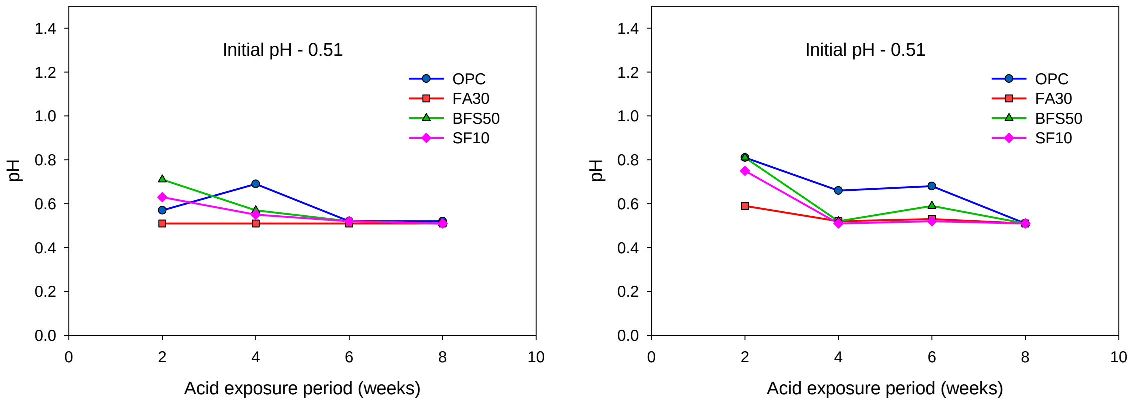

a) without brushing b) with brushing

Figure C-20 Changes in pH of acid solution for mortar (25 × 25 × 35 mm) exposed to 3% sulphuric acid (mortar w/b 0.55)

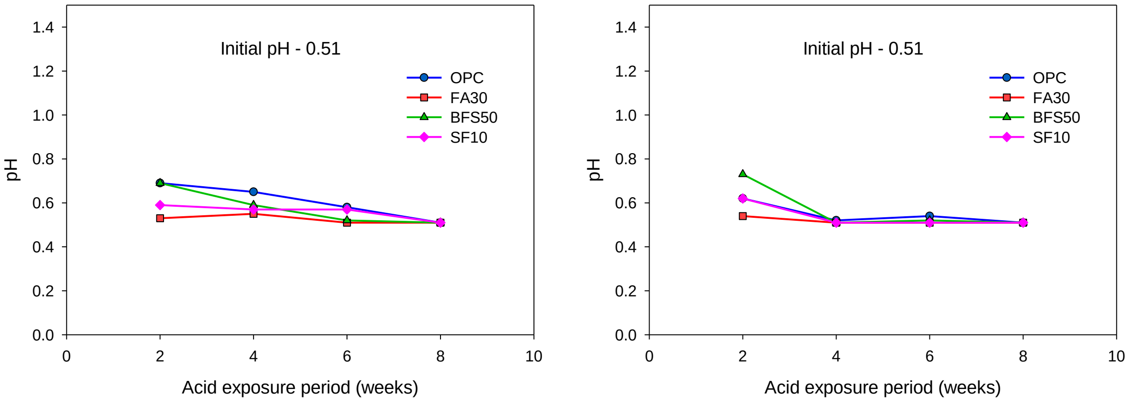

a) without brushing b) with brushing

Figure C-21 Changes in pH of acid solution for mortar cylinder (ϕ 25 × 50 mm) exposed to 3% sulphuric acid (mortar w/b 0.55)

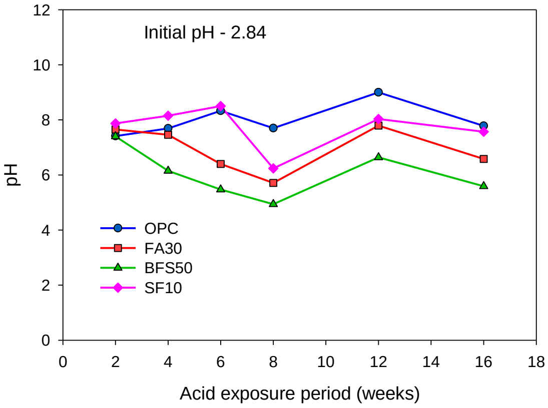

Figure C-22 Changes in pH of acid solution for mortar (25 × 25 × 35 mm) exposed to 0.125M acetic acid (mortar w/b 0.55)

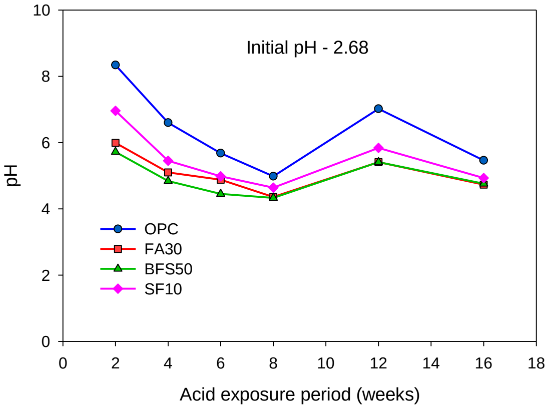

Figure C-23 Changes in pH of acid solution for mortar (25 × 25 × 35 mm) exposed to 0.25M acetic acid (mortar w/b 0.55)

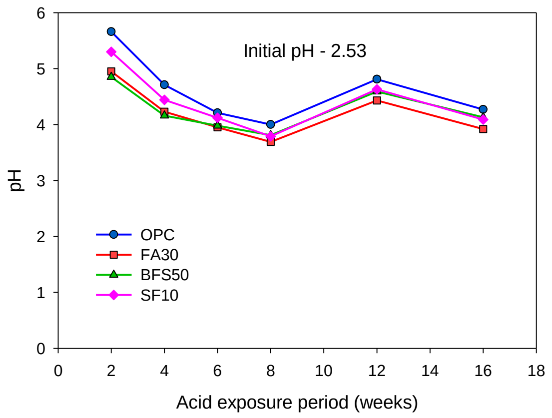

Figure C-24 Changes in pH of acid solution for mortar (25 × 25 × 35 mm) exposed to 0.50M acetic acid (mortar w/b 0.55)

Table C-1 Thickness changes of mortar (10 × 10 × 60 mm) after acid exposure (w/b 0.55)

	Without brushing (WB28)						With brushing (B28)		
Mix	0.5% Sulphuric	1% Sulphuric	3% Sulphuric	0.125M Acetic	0.25M Acetic	0.5M Acetic	0.5% Sulphuric	1% Sulphuric	3% Sulphuric
OPC	+1.59	+5.83	-31.12	-0.27	-0.20	-0.40	+1.36	+1.99	-32.43
FA30	+3.01	+7.68	-64.49	-0.16	-1.12	-1.63	+0.81	+4.15	-100.00
BFS50	+2.67	+9.53	+35.08	-1.14	-0.91	-1.26	+1.82	+7.42	-25.88
SF10	+3.43	+9.72	+10.08	-0.85	-2.17	-2.27	+0.80	+6.94	-36.83

Table C-2 Thickness changes of mortar (25 × 25 × 35 mm) after acid exposure (w/b 0.55)

	Without brushing (WB28)						With brushing (B28)		
Mix	0.5% Sulphuric	1% Sulphuric	3% Sulphuric	0.125M Acetic	0.25M Acetic	0.5M Acetic	0.5% Sulphuric	1% Sulphuric	3% Sulphuric
OPC	+1.44	+5.08	-25.18	+0.49	-0.22	-0.30	+1.00	+1.71	-29.02
FA30	+1.66	+3.96	+12.10	-0.26	-1.26	-0.60	+0.91	+2.34	-11.94
BFS50	+1.24	+6.59	+13.41	+0.38	+0.22	-0.43	+0.58	+4.75	-1.52
SF10	+2.32	+4.41	-12.69	-0.35	-0.16	-0.27	+0.63	+3.01	-29.03

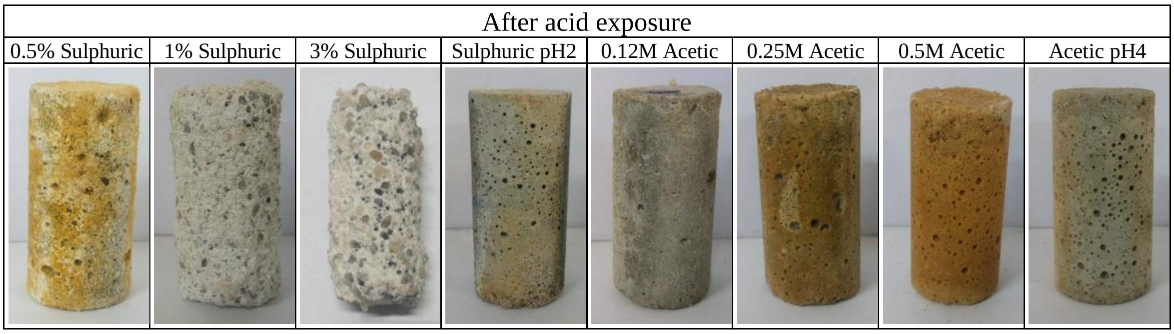

Figure C-25 OPC mortar (w/b 0.40) cylindrical specimens after the acid exposure

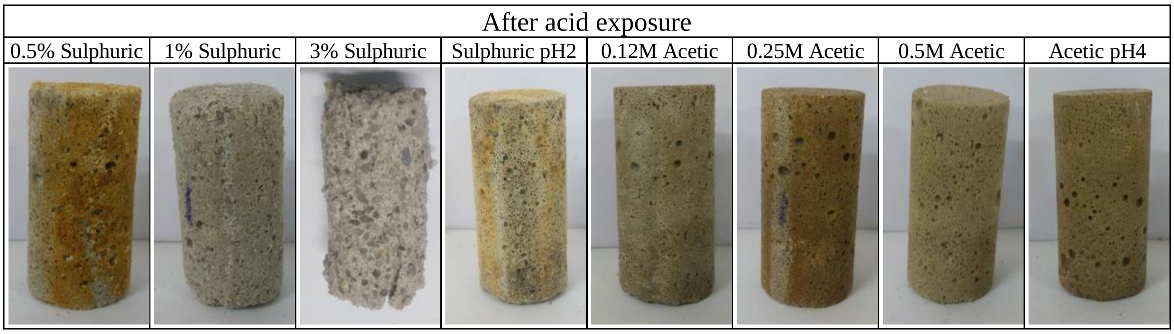

Figure C-26 FA30 mortar (w/b 0.40) cylindrical mortar specimens after the acid exposure

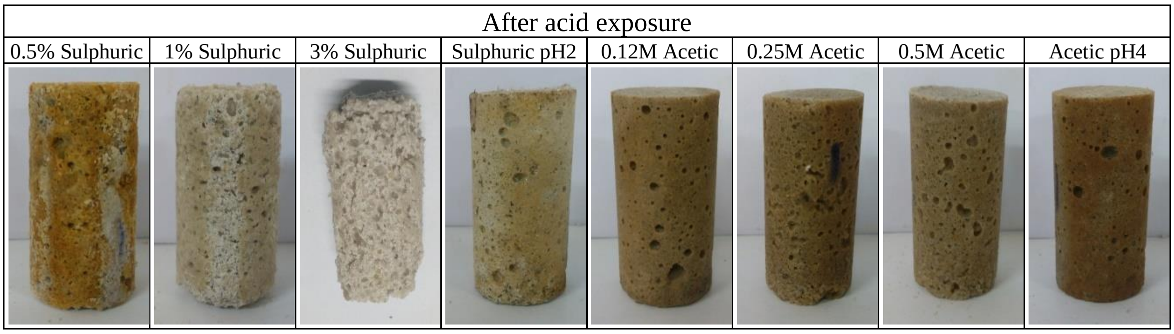

Figure C-27 BFS50 mortar (w/b 0.40) cylindrical specimens after the acid exposure

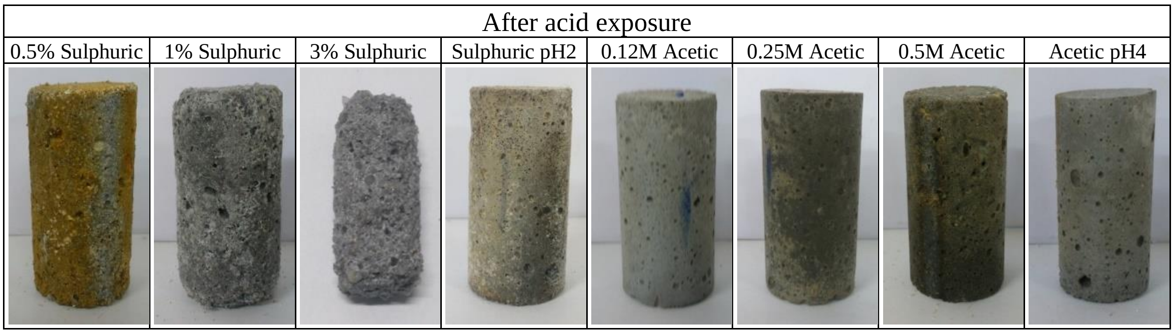

Figure C-28 SF10 mortar (w/b 0.40) cylindrical specimens after the acid exposure

Before exposure	After acid exposure			
	1% Sulphuric	3% Sulphuric	0.25M Acetic	0.5M Acetic

Figure C-29 LC2 mortar before and after acid exposure (w/b 0.40)

Before exposure	After acid exposure			
	1% Sulphuric	3% Sulphuric	0.25M Acetic	0.5M Acetic

Figure C-30 HAC mortar before and after acid exposure (w/b 0.40)

Before exposure	After acid exposure			
	1% Sulphuric	3% Sulphuric	0.25M Acetic	0.5M Acetic

Figure C-31 LC2 mortar before and after acid exposure (w/b 0.55)

Table C-3 Physico-mechanical properties of OPC mortar (w/b 0.40) exposed to acids

Solution	Concentration	Age (weeks)	Strength (MPa)	Bulk density (g/cm^3)	UPV (m/s)	E value (GPa)	Relative E
Lime water	0.20%	0	35.4	2.15	4739	44.9	1.00
Sulphuric	0.50%	6	36.8	2.18	4801	46.7	1.04
Sulphuric	0.50%	10	36.9	2.16	4411	39.0	0.87
Sulphuric	0.50%	16	31.0	2.18	4105	34.2	0.76
Sulphuric	1.00%	6	29.0	2.15	4612	42.6	0.95
Sulphuric	1.00%	10	25.2	2.12	3881	29.7	0.66
Sulphuric	1.00%	16	12.8	2.11	3423	23.1	0.51
Sulphuric	3.00%	6	24.4	2.02	4285	23.3	0.52
Sulphuric	3.00%	10	17.1	1.92	-	-	-
Sulphuric	3.00%	16	-	-	-	-	-
Sulphuric	pH2	6	33.0	2.16	4845	47.1	1.05
Sulphuric	pH2	10	33.2	2.21	4393	39.6	0.88
Sulphuric	pH2	16	33.3	2.18	4437	39.9	0.89
Acetic	0.12M	6	32.2	2.18	4458	40.5	0.90
Acetic	0.12M	10	28.5	2.18	4440	40.0	0.89
Acetic	0.12M	16	24.0	2.17	4103	34.0	0.76
Acetic	0.25M	6	26.7	2.17	4431	39.6	0.88
Acetic	0.25M	10	24.6	2.15	4374	38.2	0.85
Acetic	0.25M	16	12.3	2.07	3634	25.5	0.57
Acetic	0.50M	6	16.0	2.08	4059	32.0	0.71
Acetic	0.50M	10	3.6	2.02	3929	29.1	0.65
Acetic	0.50M	16	2.6	2.00	2305	9.9	0.22
Acetic	pH4	6	32.4	2.14	4703	44.1	0.98
Acetic	pH4	10	24.9	2.13	4442	39.2	0.87
Acetic	pH4	16	23.4	2.16	4059	33.1	0.74

Table C-4 Physico-mechanical properties of FA30 mortar (w/b 0.40) exposed to acids

Solution	Concentration	Age (weeks)	Strength (MPa)	Bulk density (g/cm^3)	UPV (m/s)	E value (GPa)	Relative E
Lime water	0.20%	0	37.9	2.14	4766	45.3	1.00
Sulphuric	0.50%	6	33.5	2.10	4782	44.7	0.99
Sulphuric	0.50%	10	37.4	2.13	4425	38.9	0.86
Sulphuric	0.50%	16	36.2	2.15	4002	32.0	0.71
Sulphuric	1.00%	6	28.7	2.10	4431	38.4	0.85
Sulphuric	1.00%	10	21.8	2.08	3950	30.2	0.67
Sulphuric	1.00%	16	10.4	2.05	3418	22.3	0.49
Sulphuric	3.00%	6	16.1	1.77	4593	23.7	0.52
Sulphuric	3.00%	10	5.7	1.63	-	-	-
Sulphuric	3.00%	16	-	-	-	-	-
Sulphuric	pH2	6	36.2	2.15	4804	46.1	1.02
Sulphuric	pH2	10	34.2	2.16	4258	36.5	0.81
Sulphuric	pH2	16	33.6	2.14	4365	38.0	0.84
Acetic	0.12M	6	28.6	2.10	4361	37.2	0.82
Acetic	0.12M	10	28.8	2.13	4443	39.1	0.86
Acetic	0.12M	16	24.4	2.15	4010	32.1	0.71
Acetic	0.25M	6	24.7	2.12	4267	36.0	0.79
Acetic	0.25M	10	15.8	2.11	4171	34.3	0.76
Acetic	0.25M	16	6.6	2.06	3507	23.6	0.52
Acetic	0.50M	6	14.6	2.06	4103	32.3	0.71
Acetic	0.50M	10	6.6	2.04	3768	26.9	0.59
Acetic	0.50M	16	4.2	1.99	2054	7.8	0.17
Acetic	pH4	6	29.8	2.07	4356	36.7	0.81
Acetic	pH4	10	22.9	2.13	4342	37.4	0.83
Acetic	pH4	16	15.8	2.13	3721	27.5	0.61

Table C-5 Physico-mechanical properties of BFS50 mortar (w/b 0.40) exposed to acids

Solution	Concentration	Age (weeks)	Strength (MPa)	Bulk density (g/cm^3)	UPV (m/s)	E value (GPa)	Relative E
Lime water	0.20%	0	43.7	2.20	4821	47.6	1.00
Sulphuric	0.50%	6	42.2	2.16	4846	47.3	0.99
Sulphuric	0.50%	10	37.1	2.18	4380	39.0	0.82
Sulphuric	0.50%	16	35.6	2.14	4270	36.3	0.76
Sulphuric	1.00%	6	31.7	2.15	4610	42.5	0.89
Sulphuric	1.00%	10	28.7	2.10	4051	32.0	0.67
Sulphuric	1.00%	16	13.9	2.01	3474	22.5	0.47
Sulphuric	3.00%	6	33.5	1.90	4328	22.7	0.48
Sulphuric	3.00%	10	19.0	1.84	-	-	-
Sulphuric	3.00%	16	-	-	-	-	-
Sulphuric	pH2	6	48.1	2.20	4832	47.7	1.00
Sulphuric	pH2	10	39.9	2.17	4265	36.9	0.77
Sulphuric	pH2	16	42.6	2.21	4429	40.4	0.85
Acetic	0.12M	6	37.5	2.16	4847	47.1	0.99
Acetic	0.12M	10	34.2	2.15	4755	45.1	0.95
Acetic	0.12M	16	37.1	2.18	4344	38.4	0.81
Acetic	0.25M	6	28.3	2.08	4752	43.6	0.92
Acetic	0.25M	10	26.9	2.15	4524	41.1	0.86
Acetic	0.25M	16	20.2	2.09	4034	31.7	0.67
Acetic	0.50M	6	25.8	2.09	4507	39.5	0.83
Acetic	0.50M	10	16.7	2.13	4330	37.1	0.78
Acetic	0.50M	16	7.7	2.07	3411	22.5	0.47
Acetic	pH4	6	42.3	2.18	4692	44.6	0.94
Acetic	pH4	10	32.1	2.17	4762	45.9	0.96
Acetic	pH4	16	30.9	2.18	4178	35.4	0.74

Table C-6 Physico-mechanical properties of SF10 mortar (w/b 0.40) exposed to acids

Solution	Concentration	Age (weeks)	Strength (MPa)	Bulk density (g/cm^3)	UPV (m/s)	E value (GPa)	Relative E
Lime water	0.20%	0	35.5	2.14	4745	44.7	1.00
Sulphuric	0.50%	6	37.0	2.10	4669	42.5	0.95
Sulphuric	0.50%	10	36.3	2.13	4258	36.0	0.80
Sulphuric	0.50%	16	29.9	2.10	4065	32.3	0.72
Sulphuric	1.00%	6	28.3	2.08	4412	37.7	0.84
Sulphuric	1.00%	10	16.2	1.98	4048	30.2	0.67
Sulphuric	1.00%	16	14.3	1.98	3419	21.6	0.48
Sulphuric	3.00%	6	22.8	1.87	4180	20.6	0.46
Sulphuric	3.00%	10	15.2	1.93	-	-	0.00
Sulphuric	3.00%	16	-	-	-	-	0.00
Sulphuric	pH2	6	36.9	2.10	4587	41.1	0.92
Sulphuric	pH2	10	29.5	2.16	4333	37.7	0.84
Sulphuric	pH2	16	29.5	2.10	4223	34.9	0.78
Acetic	0.12M	6	34.4	2.13	4625	42.4	0.95
Acetic	0.12M	10	30.8	2.09	4485	39.2	0.88
Acetic	0.12M	16	28.2	2.13	4044	32.4	0.72
Acetic	0.25M	6	24.1	2.11	4323	36.6	0.82
Acetic	0.25M	10	16.3	2.09	4143	33.4	0.75
Acetic	0.25M	16	12.8	2.08	3468	23.3	0.52
Acetic	0.50M	6	10.3	2.02	4147	32.3	0.72
Acetic	0.50M	10	5.4	2.05	3751	26.8	0.60
Acetic	0.50M	16	2.5	1.96	1509	4.1	0.09
Acetic	pH4	6	32.5	2.07	4497	38.9	0.87
Acetic	pH4	10	29.0	2.11	4398	37.9	0.85
Acetic	pH4	16	21.1	2.09	3851	28.8	0.64

Table C-7 Physico-mechanical properties of OPC mortar (w/b 0.55) exposed to acids

Solution	Concentration	Age (weeks)	Strength (MPa)	Bulk density (g/cm^3)	UPV (m/s)	E value (GPa)	Relative E
Lime water	0.20%	0	29.3	2.16	4419	39.2	1.00
Sulphuric	0.50%	6	24.1	2.15	4293	36.8	0.94
Sulphuric	0.50%	10	30.5	2.19	4225	36.4	0.93
Sulphuric	0.50%	16	22.1	2.16	4032	32.6	0.83
Sulphuric	1.00%	6	23.4	2.13	4340	37.4	0.95
Sulphuric	1.00%	10	17.8	2.04	3766	27.0	0.69
Sulphuric	1.00%	16	14.4	2.07	3447	23.0	0.59
Sulphuric	3.00%	6	19.7	2.08	3954	19.9	0.51
Sulphuric	3.00%	10	10.1	2.06	-	-	-
Sulphuric	3.00%	16	-	-	-	-	-
Sulphuric	pH2	6	31.4	2.17	4330	37.8	0.96
Sulphuric	pH2	10	28.6	2.21	4097	34.5	0.88
Sulphuric	pH2	16	24.2	2.17	4174	35.2	0.90
Acetic	0.12M	6	24.7	2.13	4408	38.5	0.98
Acetic	0.12M	10	17.9	2.14	4268	36.3	0.93
Acetic	0.12M	16	15.5	2.13	3714	27.3	0.70
Acetic	0.25M	6	22.0	2.12	4041	32.3	0.82
Acetic	0.25M	10	14.1	2.09	3957	30.5	0.78
Acetic	0.25M	16	7.1	2.11	3164	19.6	0.50
Acetic	0.50M	6	11.9	2.10	3975	30.8	0.79
Acetic	0.50M	10	5.4	2.01	3480	22.7	0.58
Acetic	0.50M	16	1.5	1.96	1200	2.6	0.07
Acetic	pH4	6	23.4	2.12	4185	34.5	0.88
Acetic	pH4	10	16.6	2.16	4165	34.9	0.89
Acetic	pH4	16	11.1	2.13	3671	26.7	0.68

Table C-8 Physico-mechanical properties of FA30 mortar (w/b 0.55) exposed to acids

Solution	Concentration	Age (weeks)	Strength (MPa)	Bulk density (g/cm^3)	UPV (m/s)	E value (GPa)	Relative E
Lime water	0.20%	0	26.8	2.08	4386	37.3	1.00
Sulphuric	0.50%	6	24.0	2.16	4349	38.0	1.02
Sulphuric	0.50%	10	23.2	2.10	4143	33.5	0.90
Sulphuric	0.50%	16	24.2	2.15	3993	31.8	0.85
Sulphuric	1.00%	6	21.8	2.13	4299	36.6	0.98
Sulphuric	1.00%	10	20.9	2.09	3851	28.8	0.77
Sulphuric	1.00%	16	13.6	2.12	3472	23.8	0.64
Sulphuric	3.00%	6	14.7	1.85	4393	22.5	0.60
Sulphuric	3.00%	10	6.5	1.84	-	-	-
Sulphuric	3.00%	16	-	-	-	-	-
Sulphuric	pH2	6	27.7	2.12	4279	36.1	0.97
Sulphuric	pH2	10	28.8	2.12	4177	34.5	0.93
Sulphuric	pH2	16	31.4	2.15	4010	32.2	0.86
Acetic	0.12M	6	21.9	2.13	4249	35.8	0.96
Acetic	0.12M	10	20.9	2.14	4053	32.7	0.88
Acetic	0.12M	16	20.3	2.13	3681	26.8	0.72
Acetic	0.25M	6	17.7	2.07	4201	33.9	0.91
Acetic	0.25M	10	13.1	2.08	3934	29.9	0.80
Acetic	0.25M	16	4.5	2.06	3094	18.3	0.49
Acetic	0.50M	0	26.8	2.08	4386	37.3	1.00
Acetic	0.50M	6	8.4	2.06	3834	28.2	0.76
Acetic	0.50M	10	4.0	1.97	3194	18.7	0.50
Acetic	pH4	6	21.3	2.10	4162	33.9	0.91
Acetic	pH4	10	17.6	2.10	3942	30.4	0.82
Acetic	pH4	16	14.7	2.12	3254	20.8	0.56

Table C-9 Physico-mechanical properties of BFS50 mortar (w/b 0.55) exposed to acids

Solution	Concentration	Age (weeks)	Strength (MPa)	Bulk density (g/cm^3)	UPV (m/s)	E value (GPa)	Relative E
Lime water	0.20%	0	32.5	2.17	4777	46.1	1.00
Sulphuric	0.50%	6	31.9	2.16	4541	41.4	0.90
Sulphuric	0.50%	10	32.0	2.16	4378	38.5	0.84
Sulphuric	0.50%	16	32.3	2.15	4269	36.5	0.79
Sulphuric	1.00%	6	24.8	2.16	4420	39.2	0.85
Sulphuric	1.00%	10	25.0	2.10	4046	32.0	0.69
Sulphuric	1.00%	16	15.4	2.09	3401	22.4	0.49
Sulphuric	3.00%	6	12.1	1.89	4223	20.8	0.45
Sulphuric	3.00%	10	12.4	1.94	-	-	-
Sulphuric	3.00%	16	-	-	-	-	-
Sulphuric	pH2	6	39.0	2.19	4704	45.0	0.98
Sulphuric	pH2	10	39.0	2.19	4341	38.3	0.83
Sulphuric	pH2	16	35.3	2.21	4174	35.8	0.78
Acetic	0.12M	6	29.6	2.19	4274	37.2	0.81
Acetic	0.12M	10	26.8	2.16	4449	39.8	0.86
Acetic	0.12M	16	22.2	2.17	3939	31.3	0.68
Acetic	0.25M	6	25.0	2.15	4172	34.8	0.76
Acetic	0.25M	10	17.5	2.12	4267	35.8	0.78
Acetic	0.25M	16	13.4	2.11	3592	25.3	0.55
Acetic	0.50M	6	17.3	2.12	4184	34.5	0.75
Acetic	0.50M	10	10.4	2.05	3823	27.8	0.60
Acetic	0.50M	16	4.6	2.05	2553	12.4	0.27
Acetic	pH4	6	32.7	2.15	4254	36.3	0.79
Acetic	pH4	10	27.8	2.13	4303	36.6	0.79
Acetic	pH4	16	18.3	2.13	3712	27.4	0.59

Table C-10 Physico-mechanical properties of SF10 mortar (w/b 0.55) exposed to acids

Solution	Concentration	Age (weeks)	Strength (MPa)	Bulk density (g/cm^3)	UPV (m/s)	E value (GPa)	Relative E
Lime water	0.20%	0	28.7	2.10	4475	39.2	1.00
Sulphuric	0.50%	6	26.4	2.07	4289	35.4	0.90
Sulphuric	0.50%	10	28.9	2.10	4241	35.2	0.90
Sulphuric	0.50%	16	28.5	2.07	3956	30.2	0.77
Sulphuric	1.00%	6	25.0	2.09	4276	35.6	0.91
Sulphuric	1.00%	10	25.8	2.08	3853	28.7	0.73
Sulphuric	1.00%	16	14.0	2.02	3544	23.6	0.60
Sulphuric	3.00%	6	13.5	1.75	4083	18.1	0.46
Sulphuric	3.00%	10	6.7	1.70	-	-	-
Sulphuric	3.00%	16	-	-	-	-	-
Sulphuric	pH2	6	31.2	2.09	4302	36.1	0.92
Sulphuric	pH2	10	31.5	2.07	4117	32.6	0.83
Sulphuric	pH2	16	32.9	2.12	3899	30.0	0.77
Acetic	0.12M	6	30.1	2.08	4217	34.4	0.88
Acetic	0.12M	10	28.5	2.07	4270	35.1	0.90
Acetic	0.12M	16	23.7	2.12	3797	28.5	0.73
Acetic	0.25M	6	25.2	2.13	3883	29.9	0.76
Acetic	0.25M	10	19.8	2.04	3920	29.2	0.75
Acetic	0.25M	16	7.2	2.03	3008	17.1	0.44
Acetic	0.50M	6	12.0	1.99	3895	28.2	0.72
Acetic	0.50M	10	4.4	1.96	3362	20.6	0.53
Acetic	0.50M	16	2.4	1.94	1406	3.6	0.09
Acetic	pH4	6	27.2	2.07	4163	33.3	0.85
Acetic	pH4	10	24.2	2.09	4116	33.0	0.84
Acetic	pH4	16	17.7	2.09	3484	23.6	0.60

Table C-11 Average altered depth of mortar cylinder (ϕ 25 × 50 mm) after the acid exposure (10th and 16th weeks) based on vernier measurements

Mix	w/b	S 0.5%		S 1%		S 3%	A 0.125M		A 0.25M		A 0.5M	
		10	16	10	16	10	10	16	10	16	10	16
OPC	0.40	0.725	0.838	0.682	2.687	4.960	2.858	4.779	2.957	4.657	3.471	12.710
FA30	0.40	1.227	1.671	2.910	4.418	7.307	2.673	3.669	3.304	5.842	4.917	12.631
BFS50	0.40	0.803	1.281	1.746	4.144	5.023	1.166	1.794	2.661	3.895	5.000	12.639
SF10	0.40	1.092	1.527	2.323	3.720	5.033	2.204	2.515	2.459	4.716	6.655	12.653
OPC	0.55	1.073	1.300	1.398	2.869	3.890	3.143	4.992	3.746	5.865	7.269	12.650
FA30	0.55	0.796	1.855	2.765	4.940	7.607	3.488	4.405	3.640	6.387	6.238	12.761
BFS50	0.55	1.007	1.567	2.325	4.391	6.045	1.358	3.067	2.447	4.794	5.617	12.673
SF10	0.55	1.072	1.861	1.820	4.142	6.253	2.640	3.900	2.602	4.939	5.313	12.675

Note: S – sulphuric acid, A – acetic acid, Altered depth reported in mm

Table C-12 Physico-mechanical properties of LC2 mortar (w/b 0.40) exposed to acids

Solution	Concentration	Age (weeks)	Strength (MPa)	Bulk density (g/cm^3)	UPV (m/s)	E value (GPa)	Relative E
Lime water	0.20%	0	26.85	2.10	4581	41.07	1.00
Sulphuric	1%	6	24.89	2.07	4218	34.30	0.84
Sulphuric	1%	10	22.48	2.04	3991	30.29	0.74
Sulphuric	1%	16	15.77	2.00	4085	31.04	0.76
Sulphuric	3%	6	6.50	1.93	-	-	-
Sulphuric	3%	10	1.22	1.69	-	-	-
Acetic	0.25M	6	19.23	2.05	4252	34.46	0.84
Acetic	0.25M	10	17.88	2.03	3947	29.44	0.72
Acetic	0.25M	16	12.64	2.02	3837	27.67	0.67
Acetic	0.5M	6	12.92	2.02	3910	28.82	0.70
Acetic	0.5M	10	5.89	1.97	3555	23.20	0.56
Acetic	0.5M	16	4.02	1.97	3526	22.79	0.55

Table C-13 Physico-mechanical properties of HAC mortar (w/b 0.40) exposed to acids

Solution	Concentration	Age (weeks)	Strength (MPa)	Bulk density (g/cm^3)	UPV (m/s)	E value (GPa)	Relative E
Lime water	0.20%	0	25.71	2.07	4416	37.55	1.00
Sulphuric	1%	6	25.71	2.14	4710	44.13	1.18
Sulphuric	1%	10	20.59	2.03	4701	41.84	1.11
Sulphuric	1%	16	17.67	2.00	4307	34.55	0.92
Sulphuric	3%	6	15.28	2.07	-	-	-
Sulphuric	3%	10	13.22	2.06	-	-	-
Acetic	0.25M	6	27.74	2.19	4467	40.67	1.08
Acetic	0.25M	10	17.40	2.16	4252	36.43	0.97
Acetic	0.25M	16	13.18	2.17	4276	36.89	0.98
Acetic	0.5M	6	9.91	2.10	4096	32.71	0.87
Acetic	0.5M	10	5.49	2.01	3540	23.46	0.62
Acetic	0.5M	16	2.06	1.91	3412	20.21	0.54

Table C-14 Physico-mechanical properties of LC2 mortar (w/b 0.55) exposed to acids

Solution	Concentration	Age (weeks)	Strength (MPa)	Bulk density (g/cm^3)	UPV (m/s)	E value (GPa)	Relative E
Lime water	0.20%	0	22.22	2.09	4359	36.95	1.00
Sulphuric	1%	6	19.38	2.11	4085	32.75	0.89
Sulphuric	1%	10	13.31	2.07	3733	26.85	0.73
Sulphuric	1%	16	10.62	2.03	3771	26.92	0.73
Sulphuric	3%	6	5.65	2.03	-	-	-
Sulphuric	3%	10	1.18	1.71	-	-	-
Acetic	0.25M	6	16.63	2.09	3929	30.03	0.81
Acetic	0.25M	10	10.95	2.06	3640	25.40	0.69
Acetic	0.25M	16	8.12	2.05	3529	23.71	0.64
Acetic	0.5M	6	10.00	2.06	3550	24.16	0.65
Acetic	0.5M	10	3.24	2.03	3128	18.45	0.50
Acetic	0.5M	16	1.35	2.00	2888	15.59	0.42

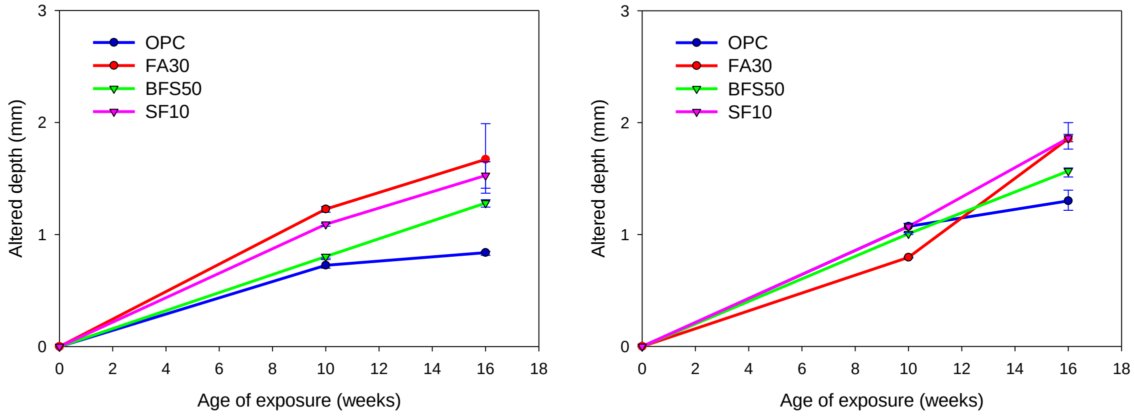

a) w/b 0.40 b) w/b 0.55

Figure C-32 Altered depth of mortar cylinder (ϕ 25 × 50 mm) exposed to 0.5% sulphuric acid

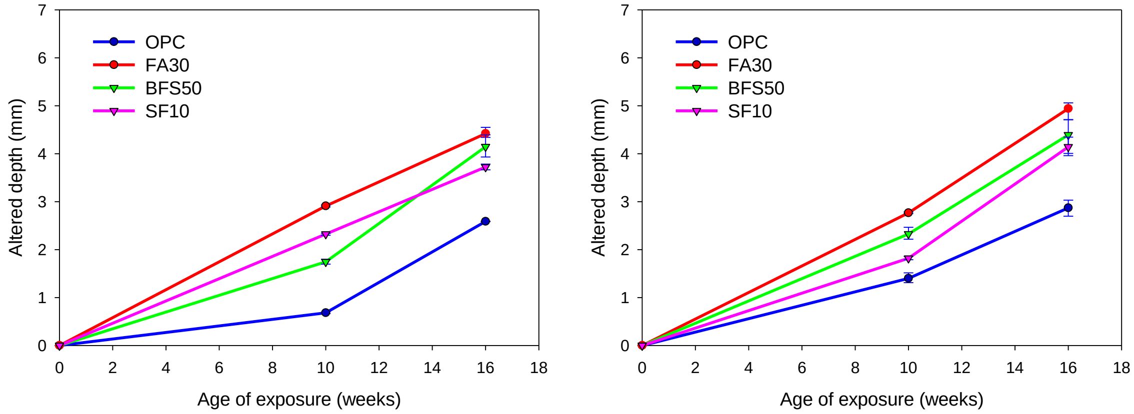

a) w/b 0.40 b) w/b 0.55

Figure C-33 Altered depth of mortar cylinder (ϕ 25 × 50 mm) exposed to 1% sulphuric acid

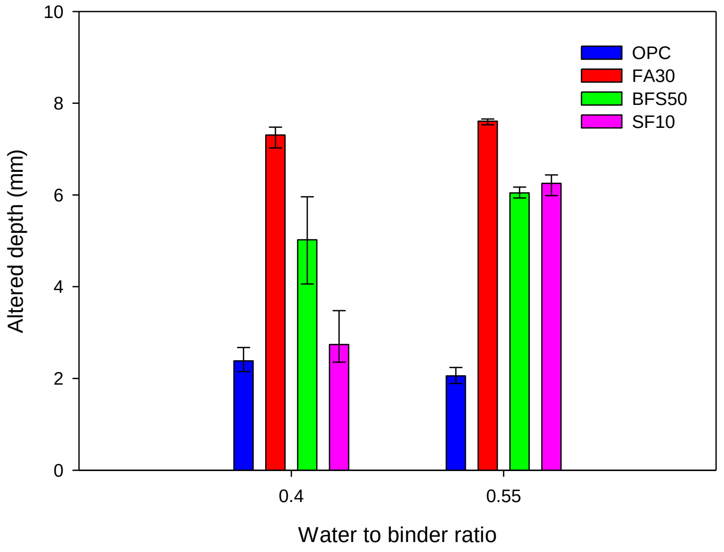

Figure C-34 Altered depth of mortar cylinder (ϕ 25 × 50 mm) exposed to 3% sulphuric acid

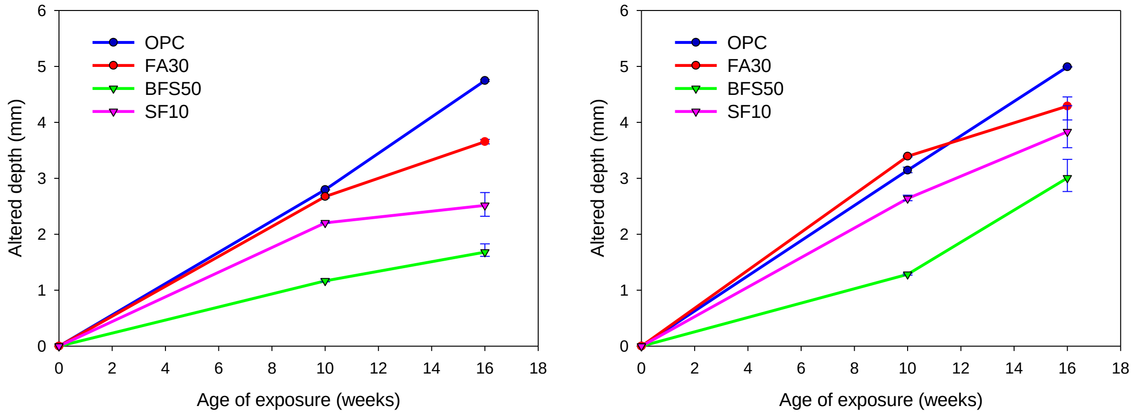

a) w/b 0.40 b) w/b 0.55

Figure C-35 Altered depth of mortar cylinder (ϕ 25 × 50 mm) exposed to 0.125M acetic acid

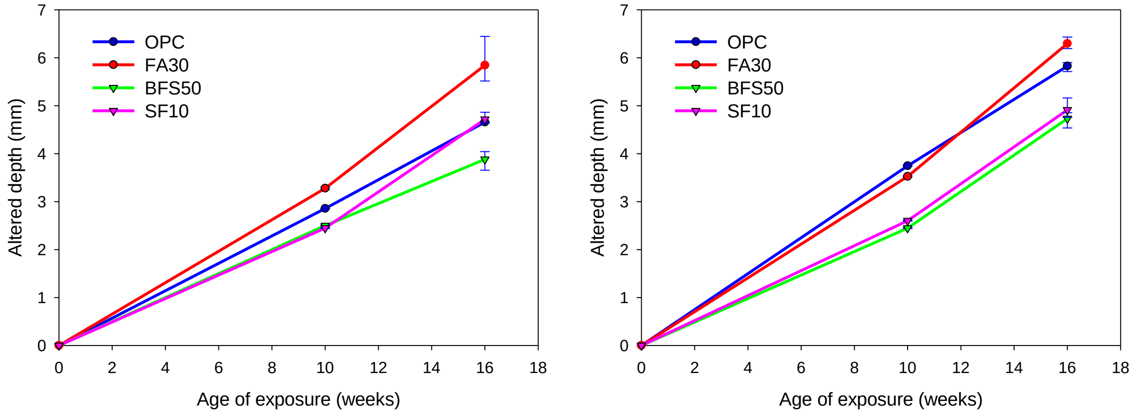

a) w/b 0.40 b) w/b 0.55

Figure C-36 Altered depth of mortar cylinder (ϕ 25 × 50 mm) exposed to 0.25M acetic acid

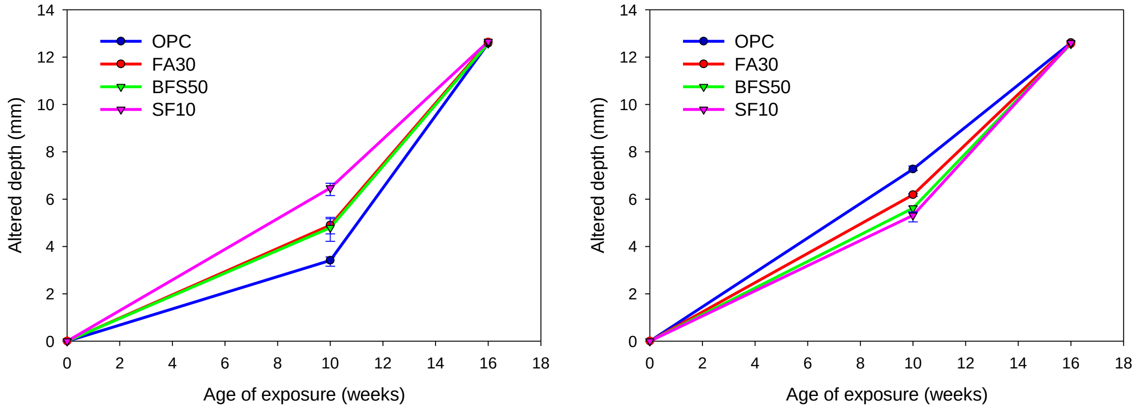

a) w/b 0.40 b) w/b 0.55

Figure C-37 Altered depth of mortar cylinder (ϕ 25 × 50 mm) exposed to 0.5M acetic acid

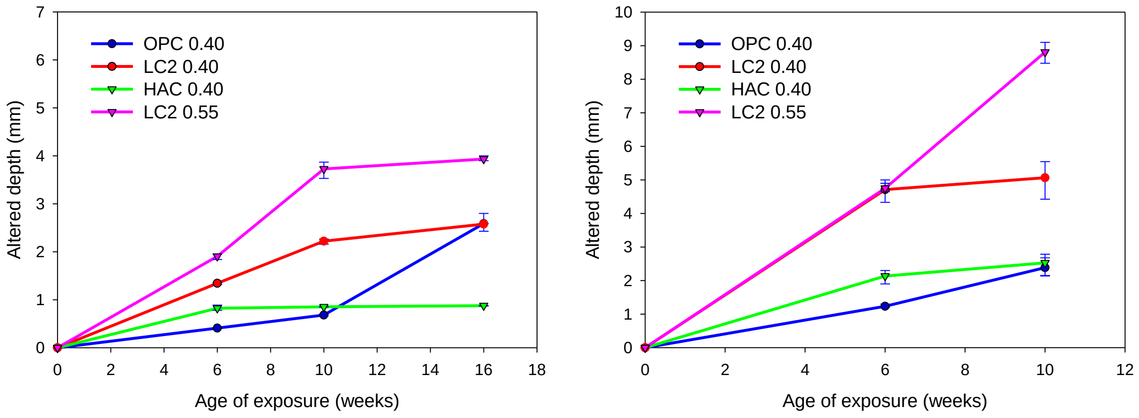

a) 1% sulphuric acid b) 3% sulphuric acid

Figure C-38 Altered depth of LC2 and HAC mortar cylinder (ϕ 25 × 50 mm) exposed to sulphuric acid

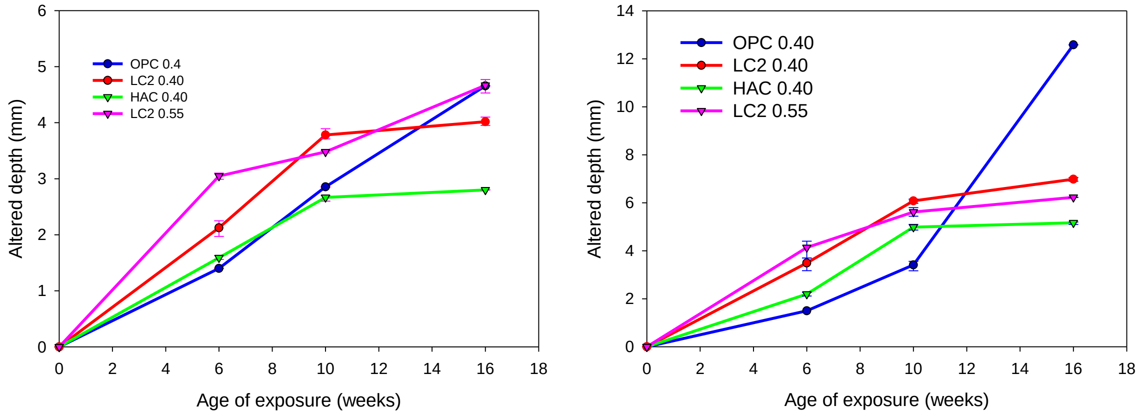

a) 0.25M acetic acid b) 0.5M acetic acid

Figure C-39 Altered depth of LC2 and HAC mortar cylinder (ϕ 25 × 50 mm) exposed to acetic acid

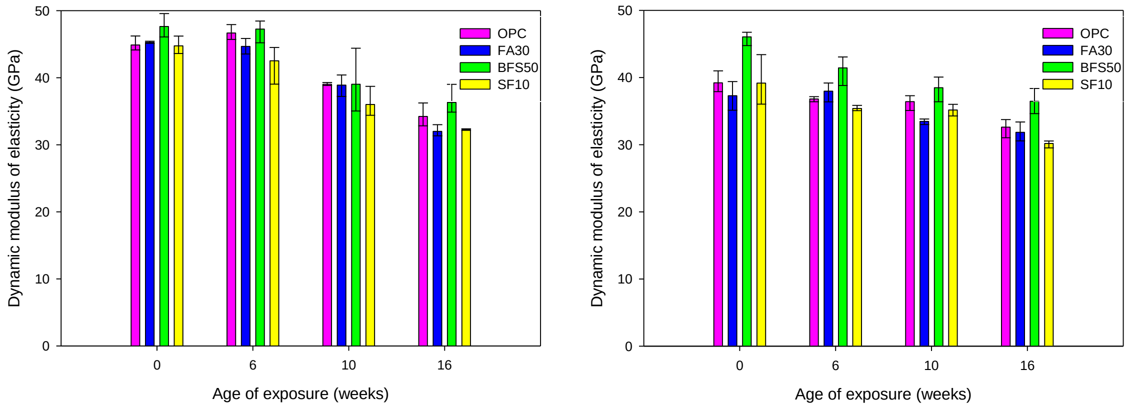

a) w/b 0.40 b) w/b 0.55

Figure C-40 Changes in dynamic modulus of elasticity of mortar exposed to 0.5% sulphuric acid

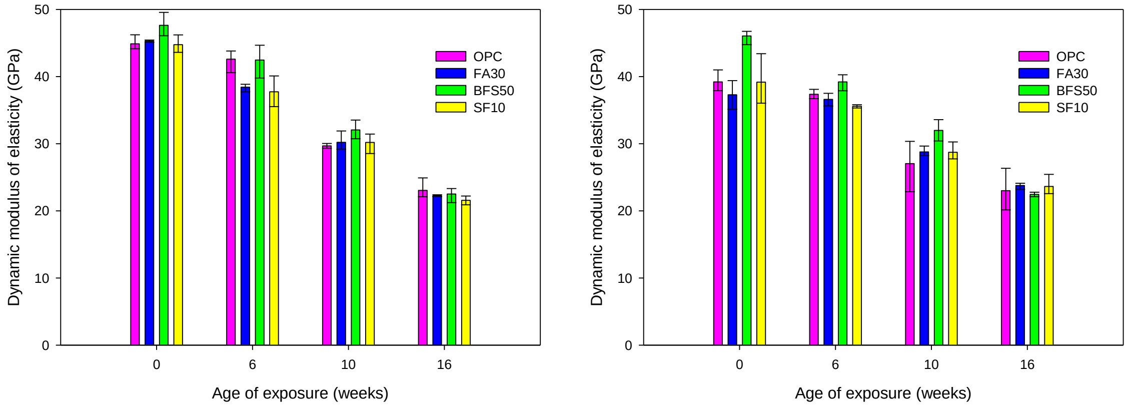

a) w/b 0.40 b) w/b 0.55

Figure C-41 Changes in dynamic modulus of elasticity of mortar exposed to 1% sulphuric acid

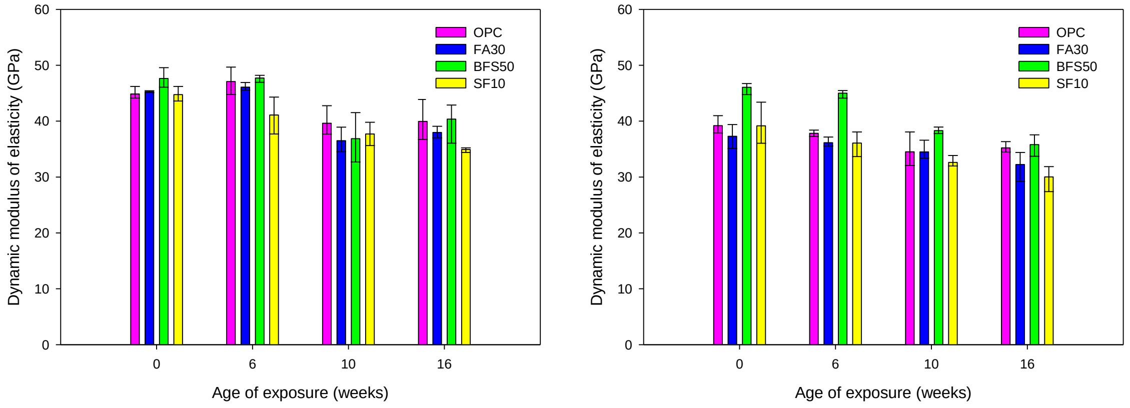

a) w/b 0.40 b) w/b 0.55

Figure C-42 Changes in dynamic modulus of elasticity of mortar exposed to pH2 sulphuric acid

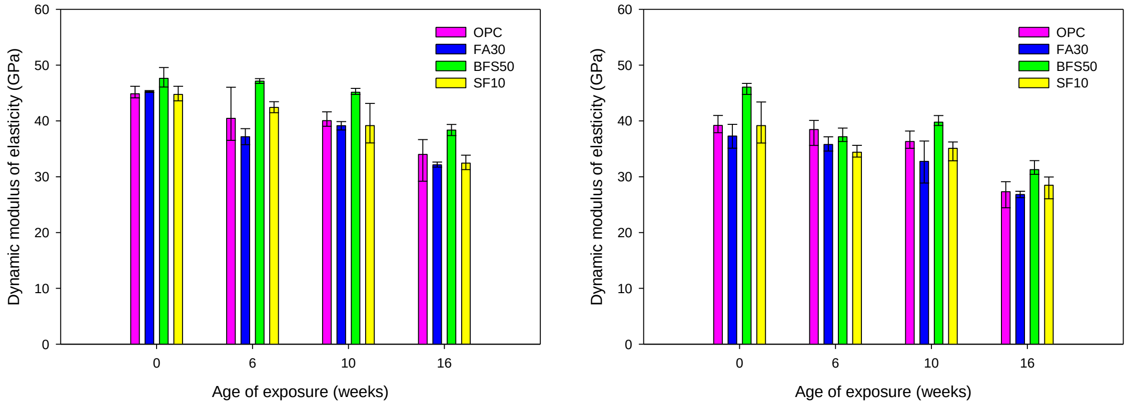

a) w/b 0.40 b) w/b 0.55

Figure C-43 Changes in dynamic modulus of elasticity of mortar exposed to 0.125M acetic acid

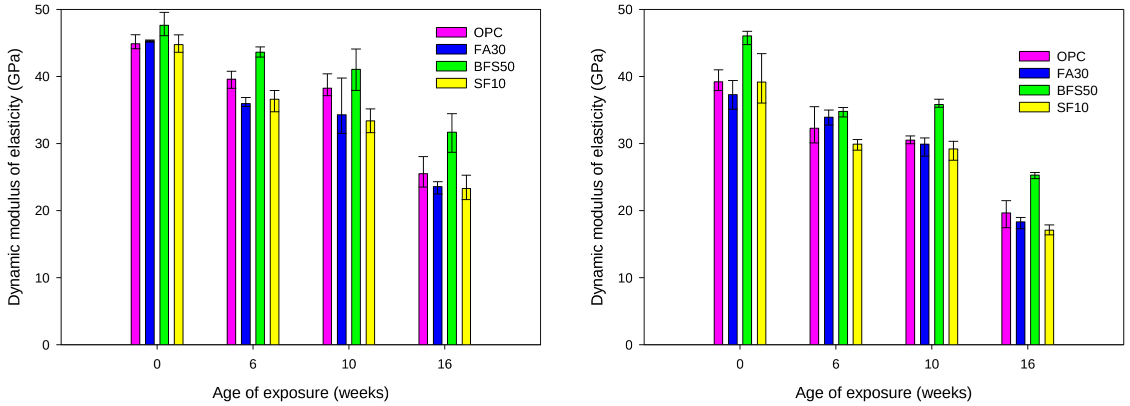

a) w/b 0.40 b) w/b 0.55

Figure C-44 Changes in dynamic modulus of elasticity of mortar exposed to 0.25M acetic acid

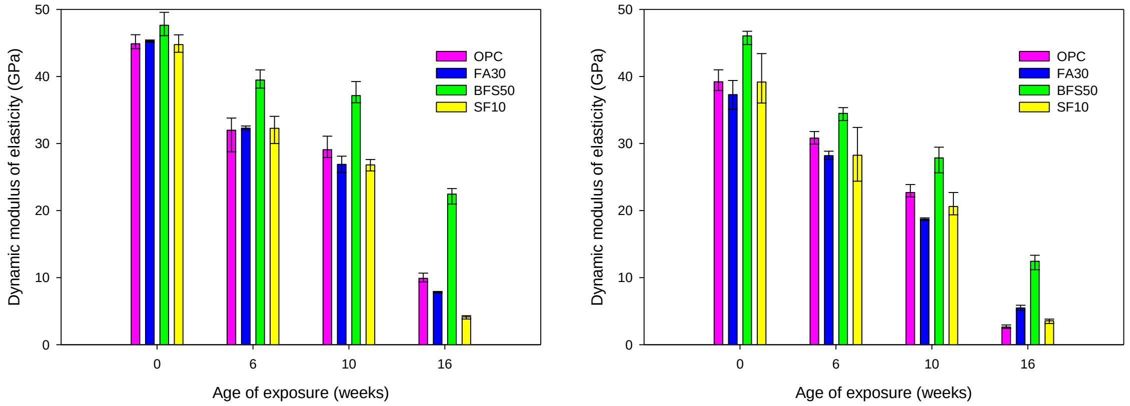

a) w/b 0.40 b) w/b 0.55

Figure C-45 Changes in dynamic modulus of elasticity of mortar exposed to 0.50M acetic acid

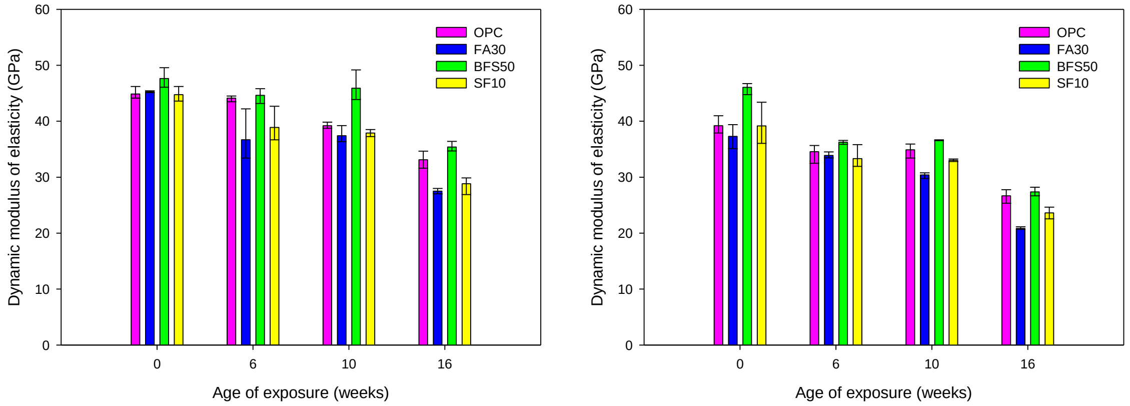

a) w/b 0.40 b) w/b 0.55

Figure C-46 Changes in dynamic modulus of elasticity of mortar exposed to pH4 acetic acid

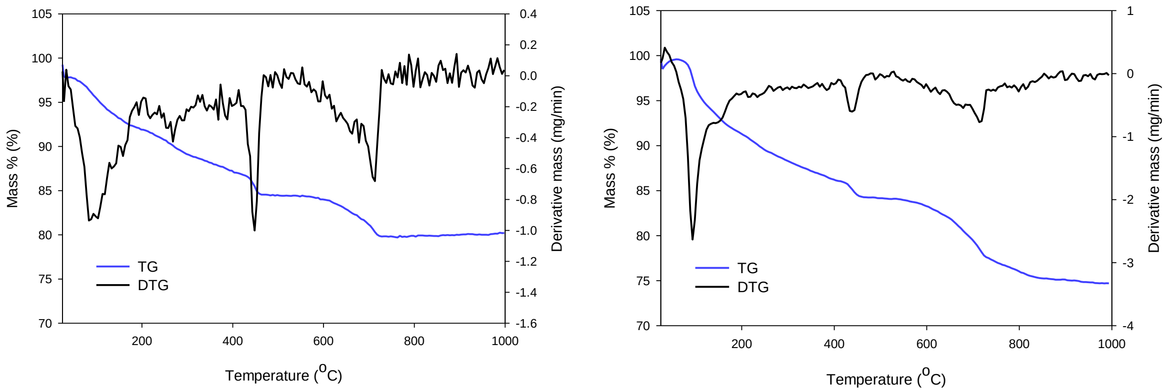

a) OPC b) FA30

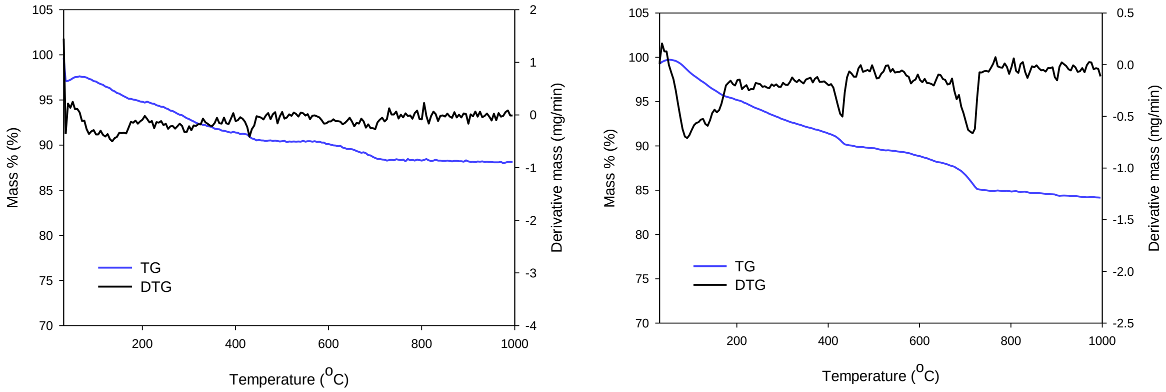

c) BFS50 d) SF10

Figure C-47 TGA/DTG curve of mortar (w/b 0.40) before the acid exposure

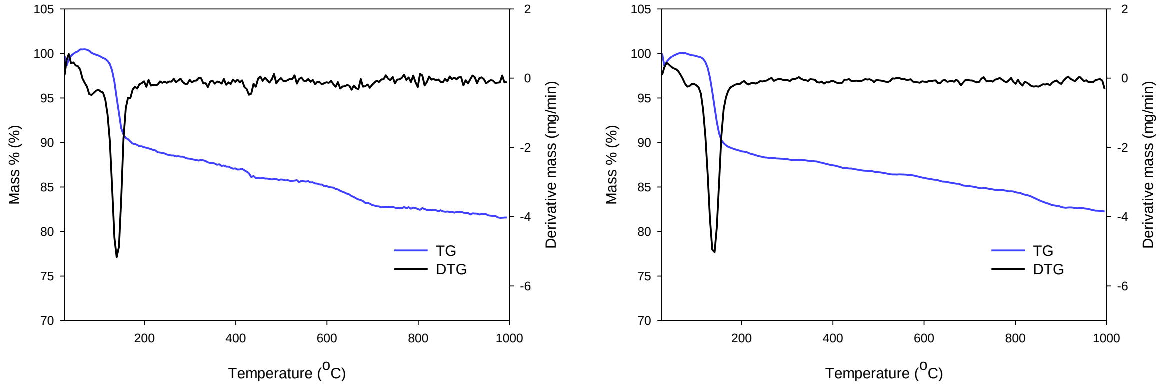

a) OPC b) FA30

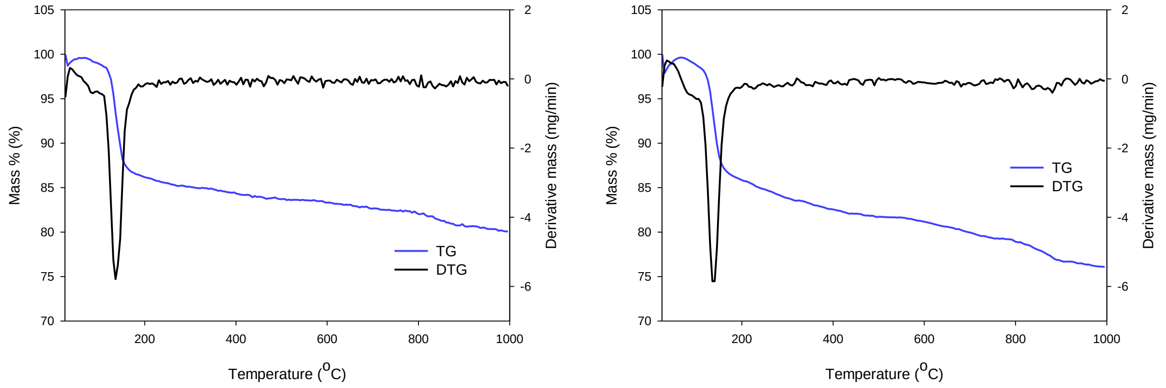

c) BFS50 d) SF10

Figure C-48 TGA/DTG curve of mortar (w/b 0.40) exposed to 1% sulphuric acid

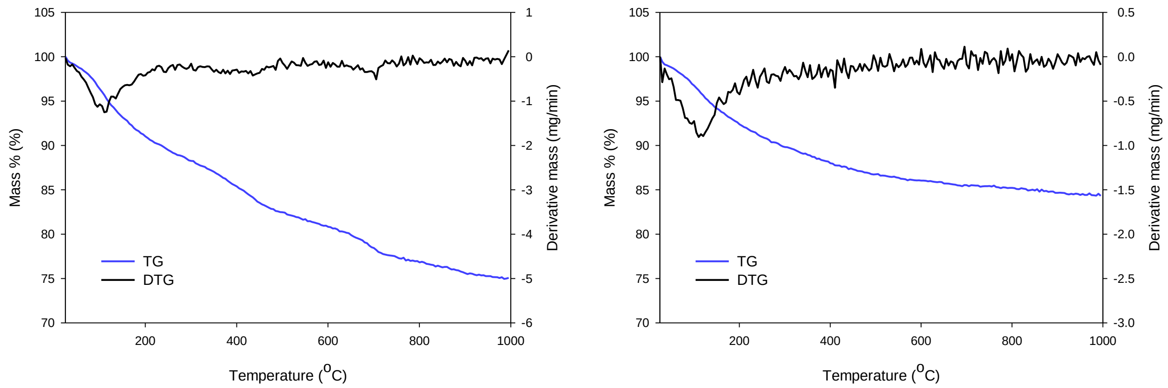

a) OPC b) FA30

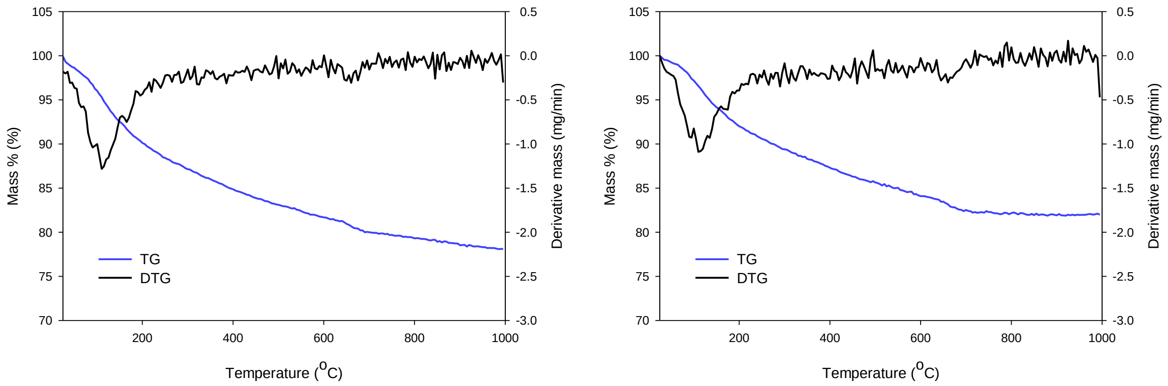

c) BFS50 d) SF10

Figure C-49 TGA/DTG curve of mortar (w/b 0.40) exposed to 0.25M acetic acid

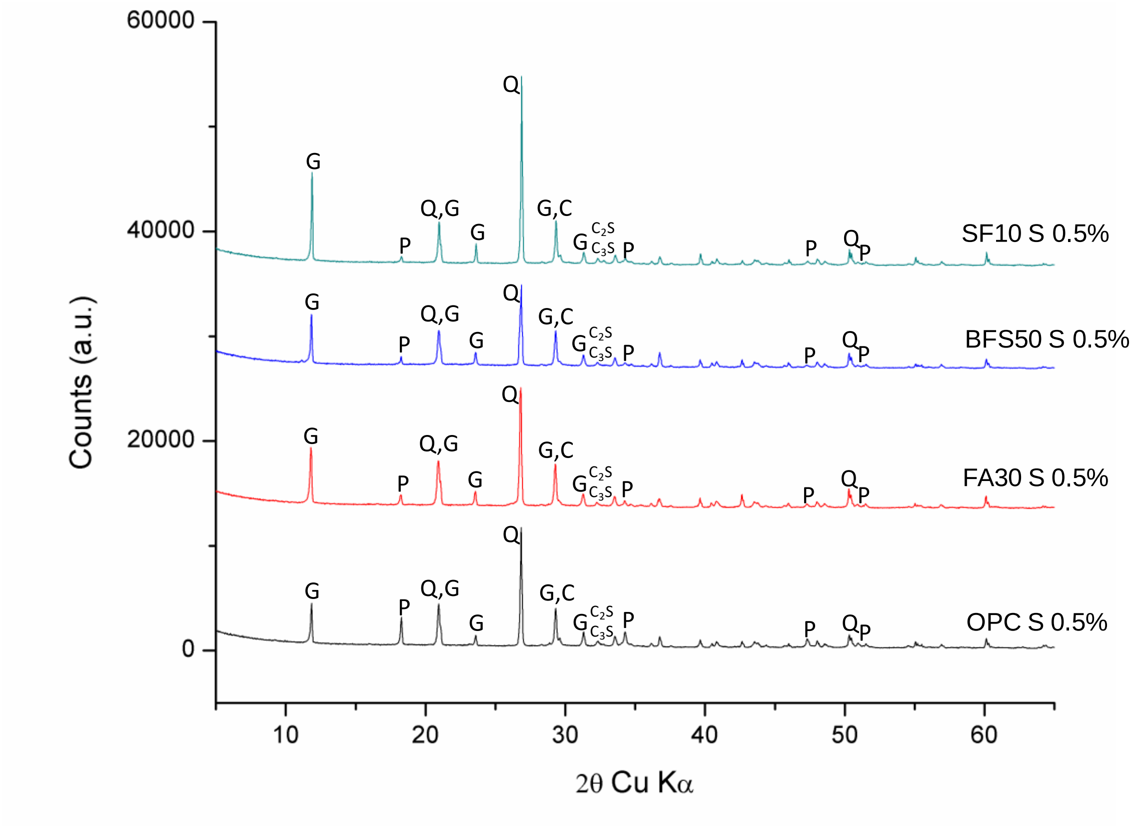

Figure C-50 X-ray diffractograms of mortar (w/b 0.40) exposed to 0.5% sulphuric acid

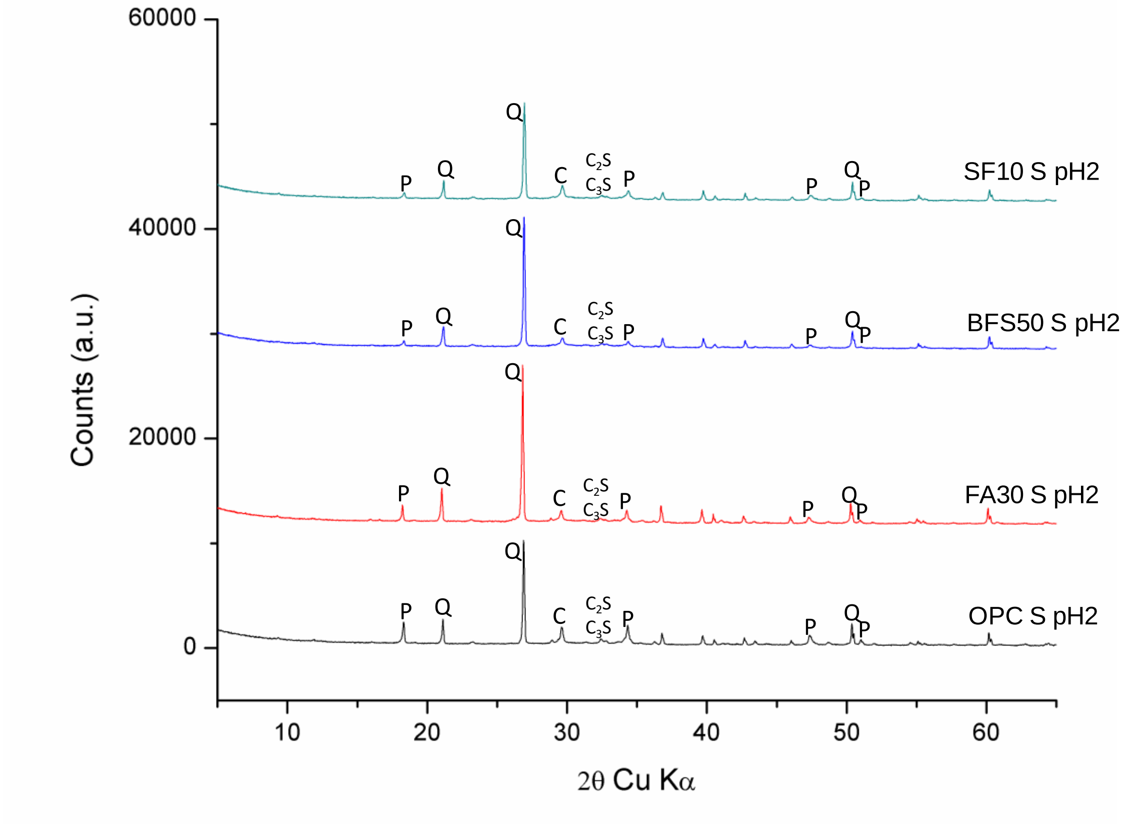

Figure C-51 X-ray diffractograms of mortar (w/b 0.40) exposed to pH2 sulphuric acid

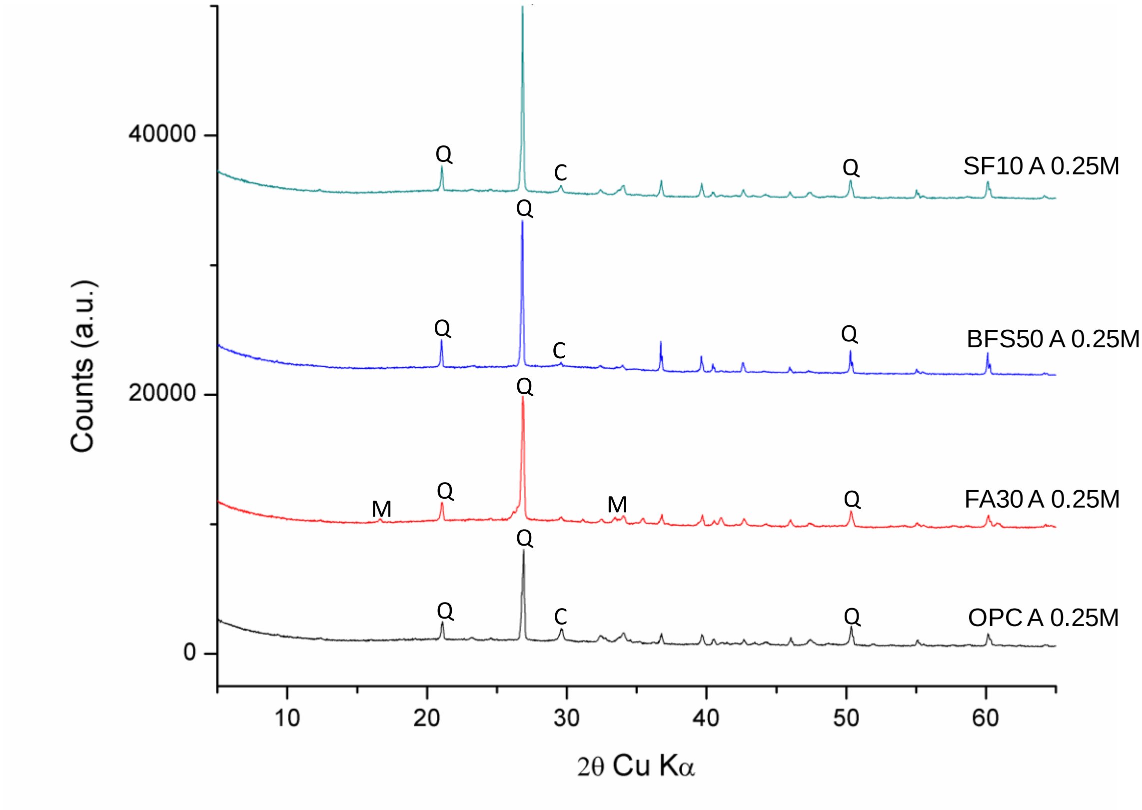

Figure C-52 X-ray diffractograms of mortar (w/b 0.40) exposed to 0.25M acetic acid

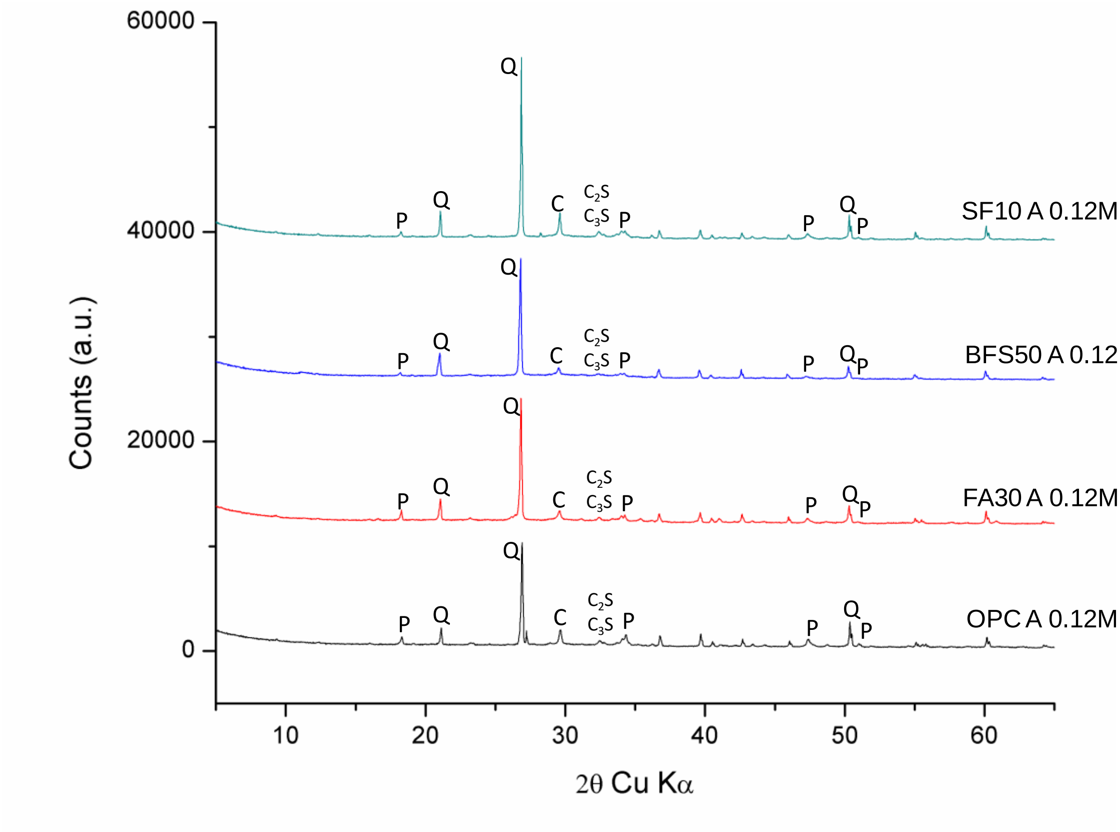

Figure C-53 X-ray diffractograms of mortar (w/b 0.40) exposed to 0.125M acetic acid

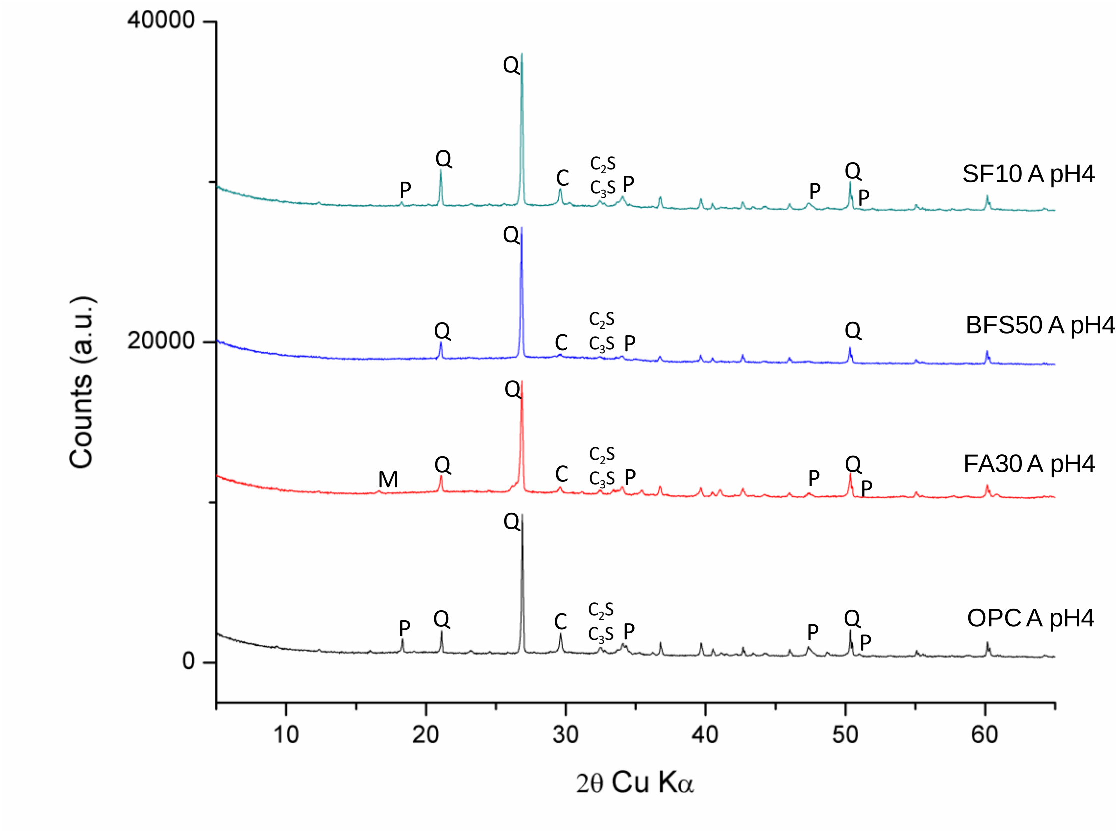

Figure C-54 X-ray diffractograms of mortar (w/b 0.40) exposed to pH4 acetic acid

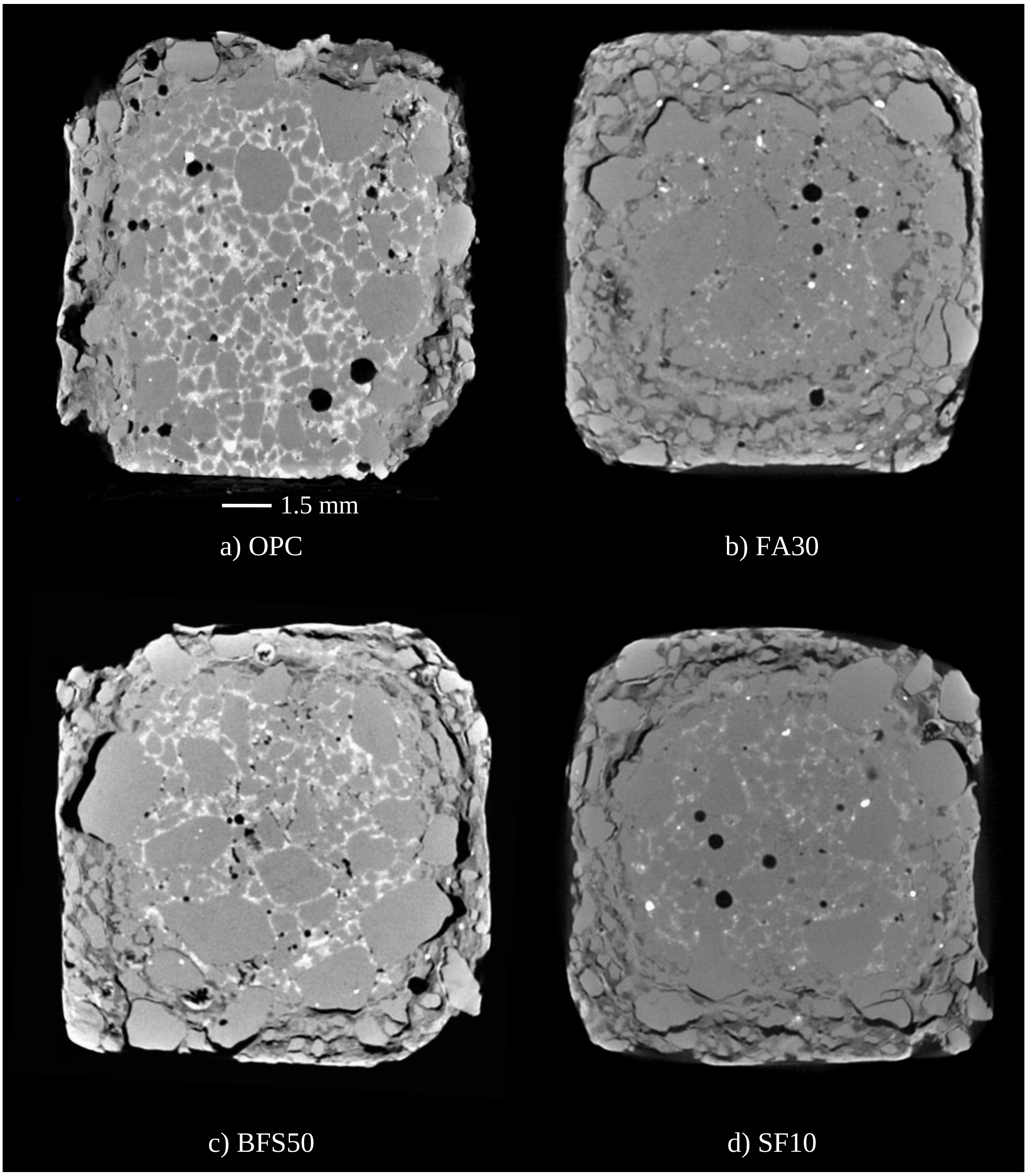

a) OPC

b) FA30

c) BFS50

d) SF10

Figure C-55 Top view CT slice images of mortar (w/b 0.55) after exposure to 1% sulphuric acid

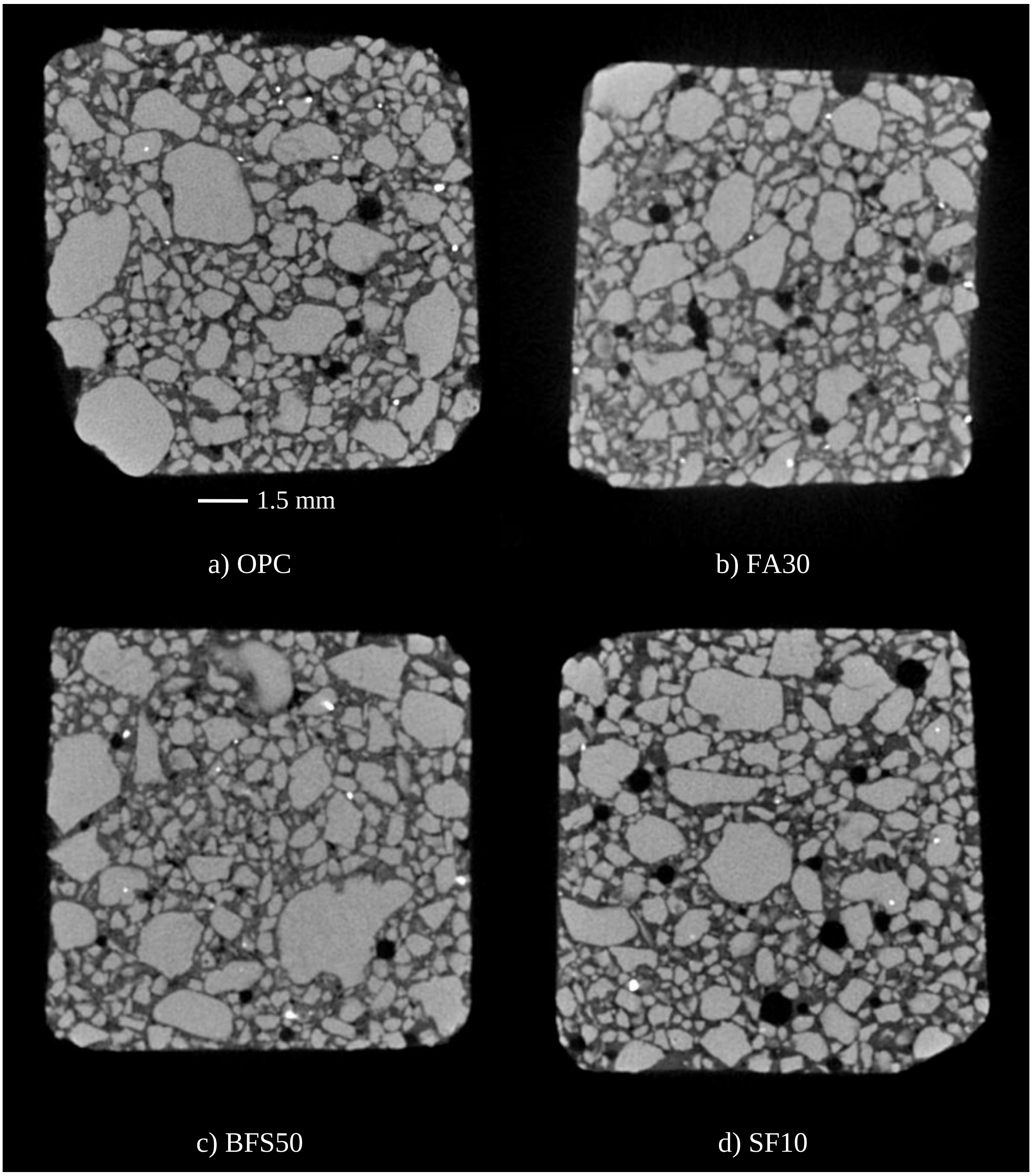

a) OPC

b) FA30

c) BFS50

d) SF10

Figure C-56 Top view CT slice images of mortar (w/b 0.55) after exposure to 0.5M acetic acid

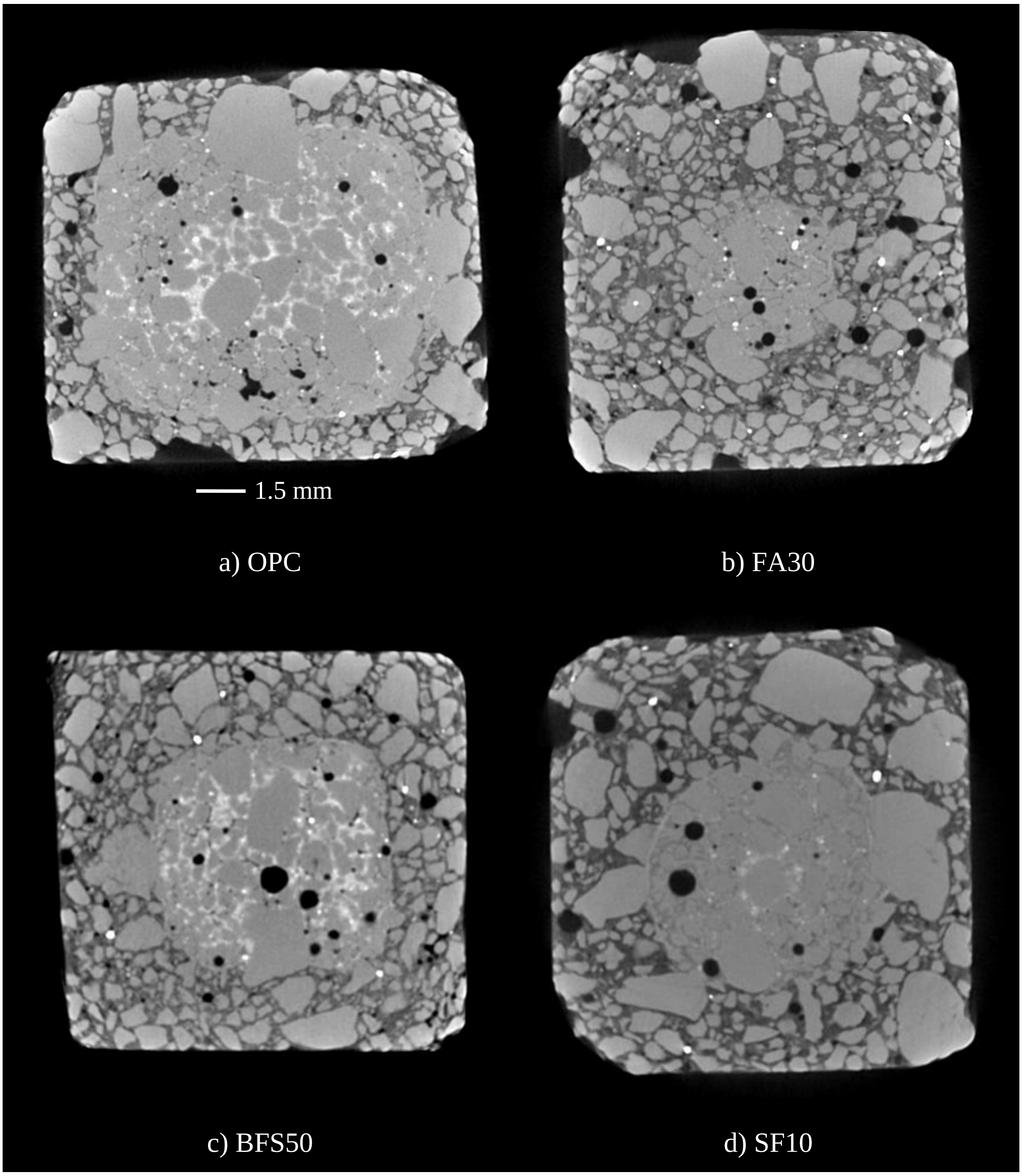

a) OPC

b) FA30

c) BFS50

d) SF10

Figure C-57 Top view CT slice images of mortar (w/b 0.55) after exposure to 0.25M acetic acid

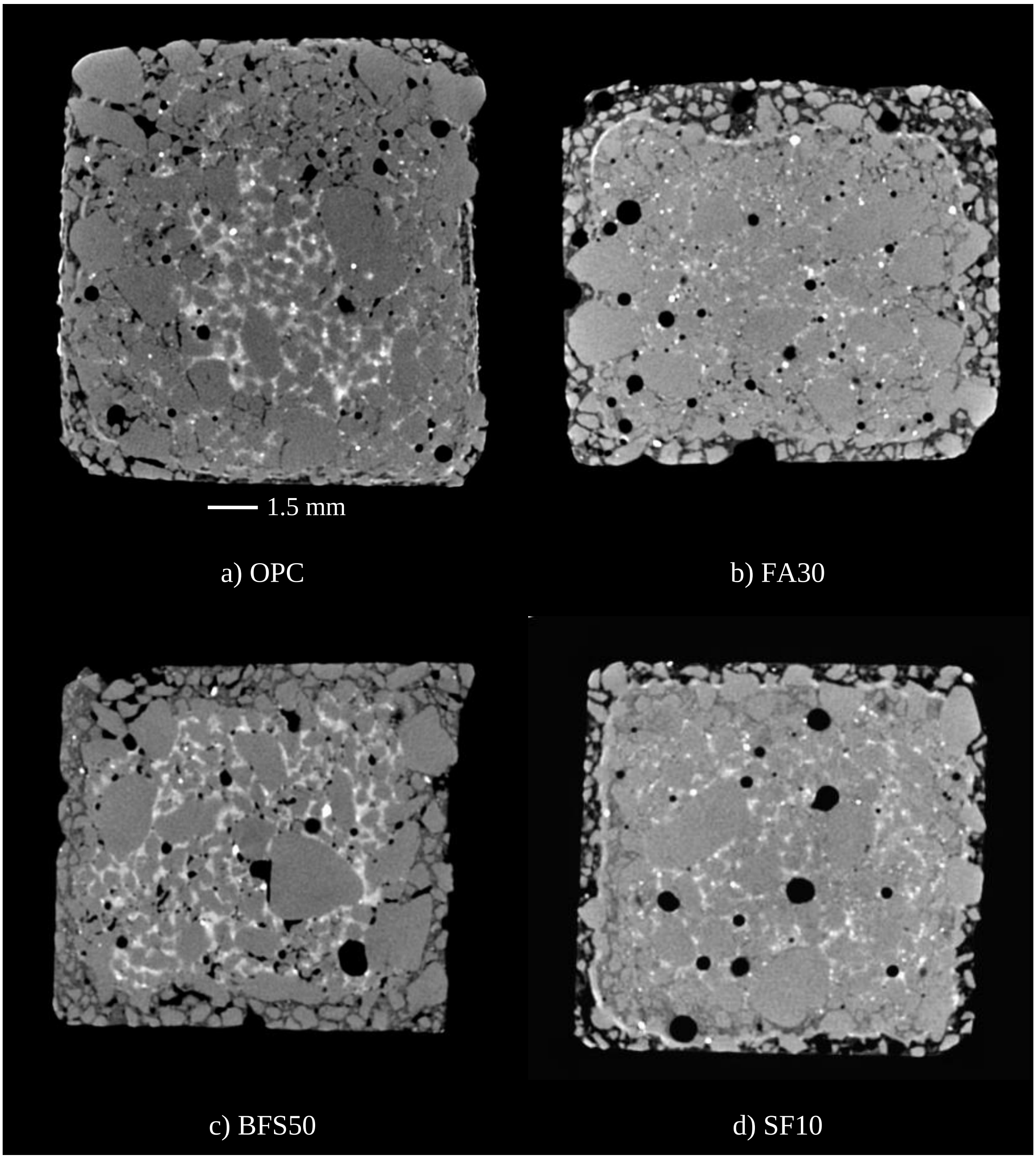

a) OPC

b) FA30

c) BFS50

d) SF10

Figure C-58 Top view CT slice images of mortar (w/b 0.55) after exposure to 0.125M acetic acid

APPENDIX D

EFFECT OF AGGREGATE TYPE ON ACID ATTACK

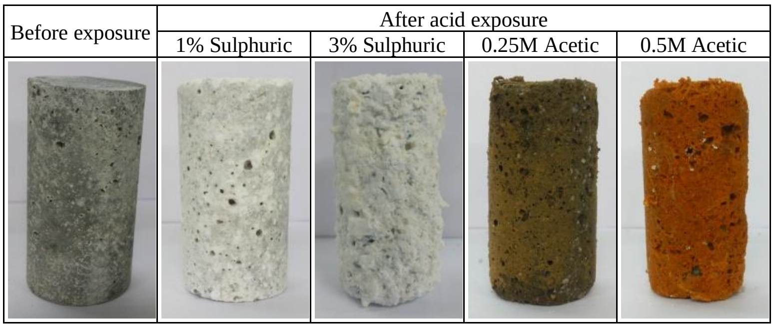

Figure D-1 Limestone sand (LS) mortar before and after acid exposure (w/b 0.40)

Table D-1 Physico-mechanical properties of limestone sand mortar (w/b 0.40) exposed to acids

Solution	Concentration	Age (weeks)	Strength (MPa)	Bulk density (g/cm^3)	UPV (m/s)	E value (GPa)	Relative E
Lime water	0.20%	0	25.20	2.07	4454	38.30	1.00
Sulphuric	1%	6	26.11	2.19	4680	44.65	1.17
Sulphuric	1%	10	21.55	2.19	4817	47.19	1.23
Sulphuric	1%	16	20.80	2.21	4824	47.88	1.25
Sulphuric	3%	6	19.51	2.17	-	-	-
Sulphuric	3%	10	15.85	2.09	-	-	-
Acetic	0.25M	6	23.38	2.22	4794	47.52	1.24
Acetic	0.25M	10	17.99	2.16	4558	41.86	1.09
Acetic	0.25M	16	17.18	2.17	4076	33.58	0.88
Acetic	0.5M	6	19.78	2.14	4432	39.19	1.02
Acetic	0.5M	10	15.36	2.06	4167	33.35	0.87
Acetic	0.5M	16	11.34	1.90	3873	26.69	0.70

APPENDIX E

PASTE – MORTAR BEHAVIOUR EXPOSED TO ACIDS

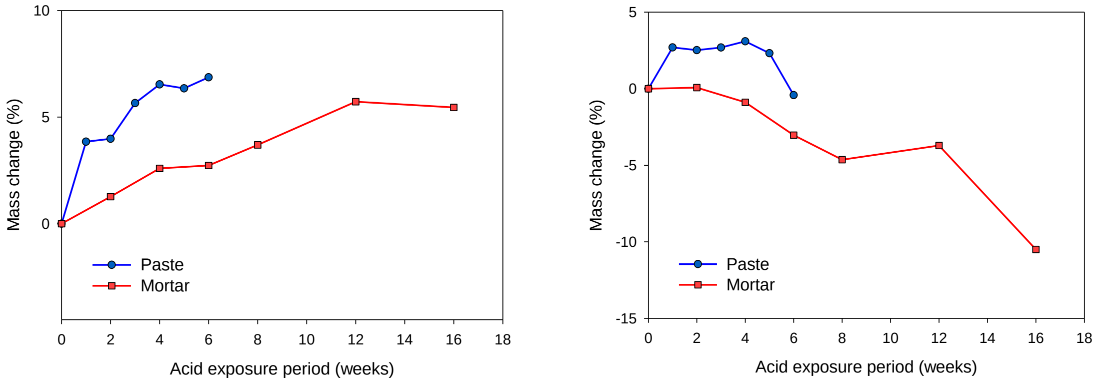

a) 1% sulphuric acid (without brushing)   b) 1% sulphuric acid (with brushing)

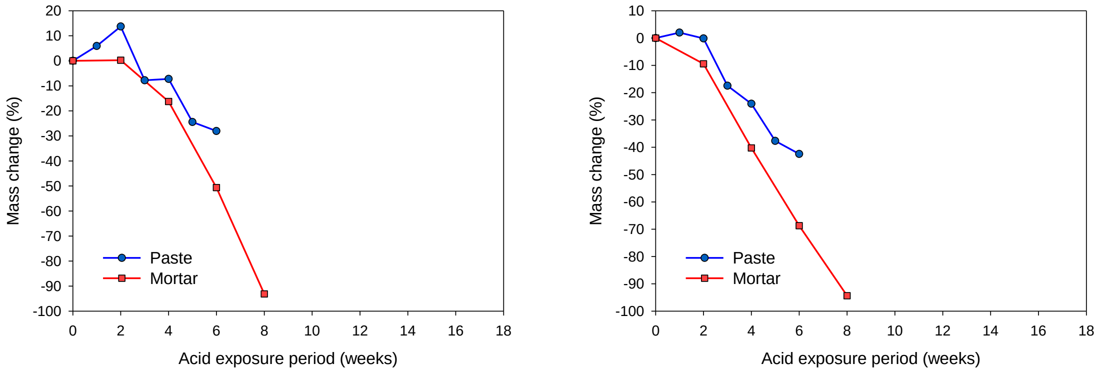

c) 3% sulphuric acid (without brushing)   d) 3% sulphuric acid (with brushing)

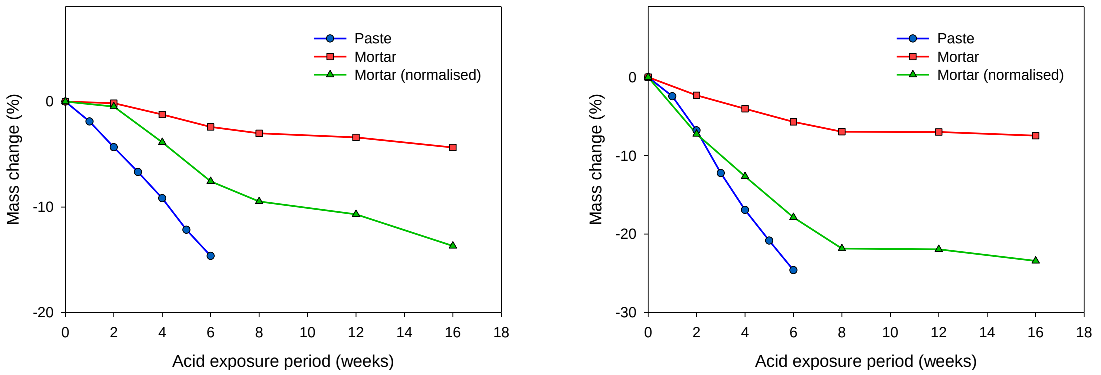

e) 0.25M acetic acid   f) 0.50M acetic acid

Figure E-1 Behaviour of FA30 paste and mortar on exposure to acids

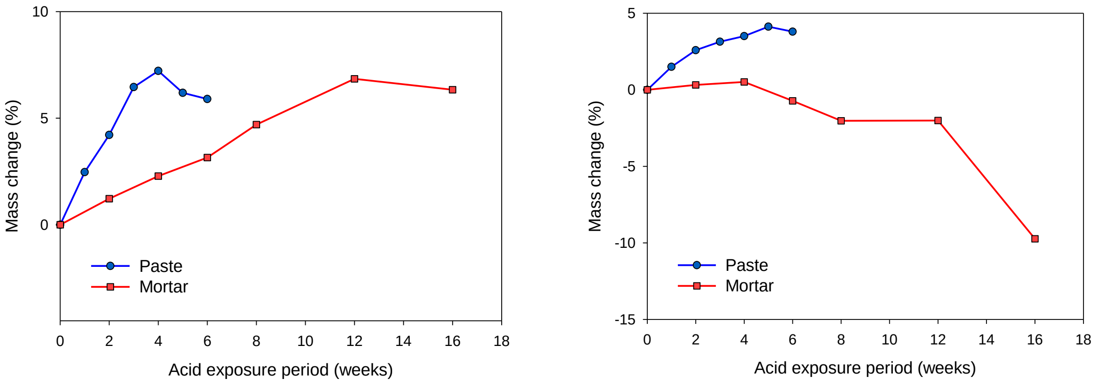

a) 1% sulphuric acid (without brushing)

b) 1% sulphuric acid (with brushing)

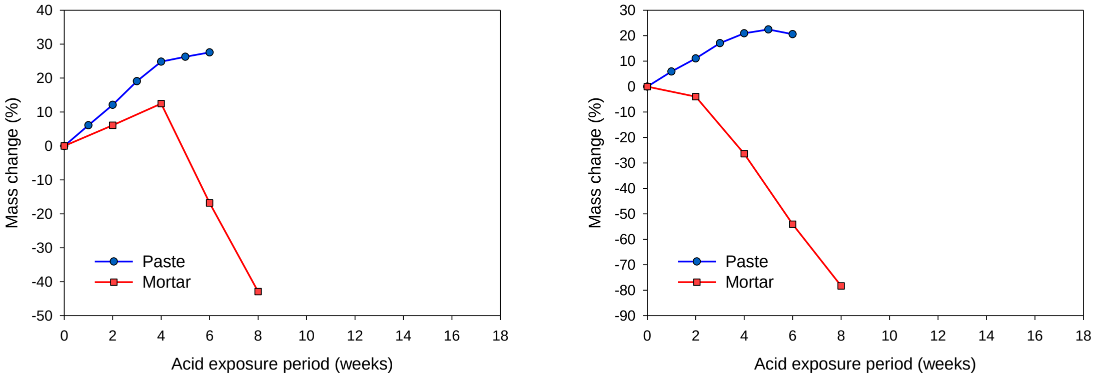

c) 3% sulphuric acid (without brushing)

d) 3% sulphuric acid (with brushing)

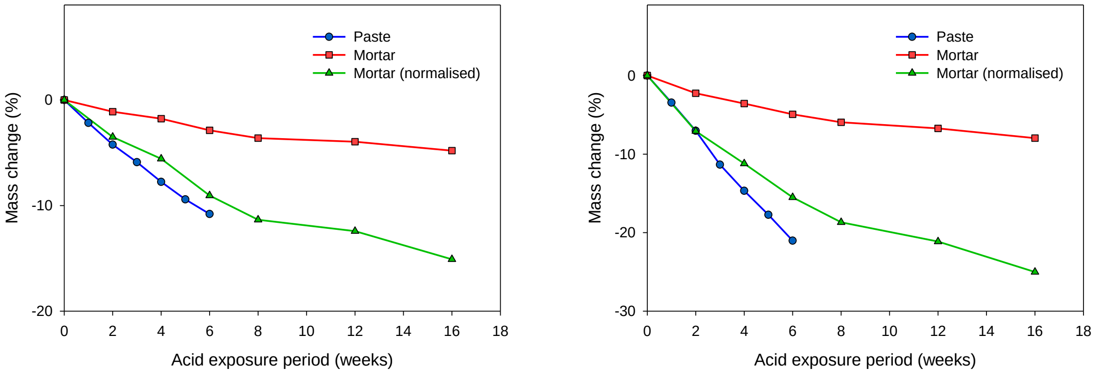

e) 0.25M acetic acid

f) 0.50M acetic acid

Figure E-2 Behaviour of BFS50 paste and mortar on exposure to acids

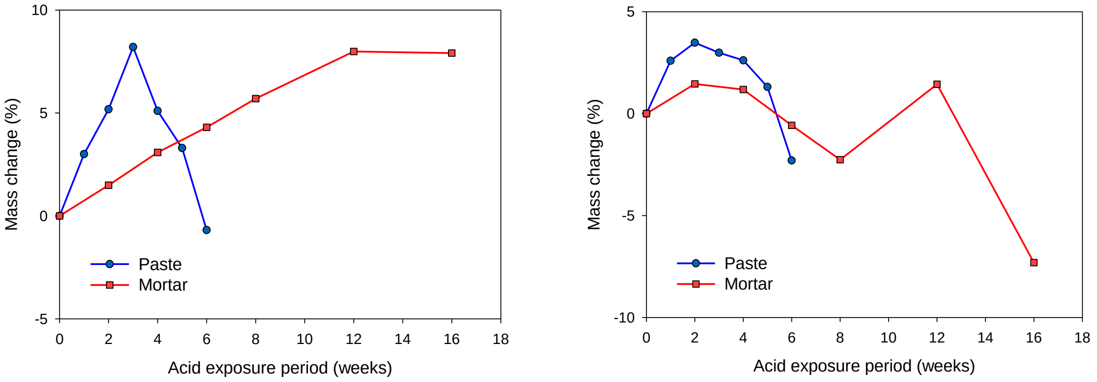

a) 1% sulphuric acid (without brushing)

b) 1% sulphuric acid (with brushing)

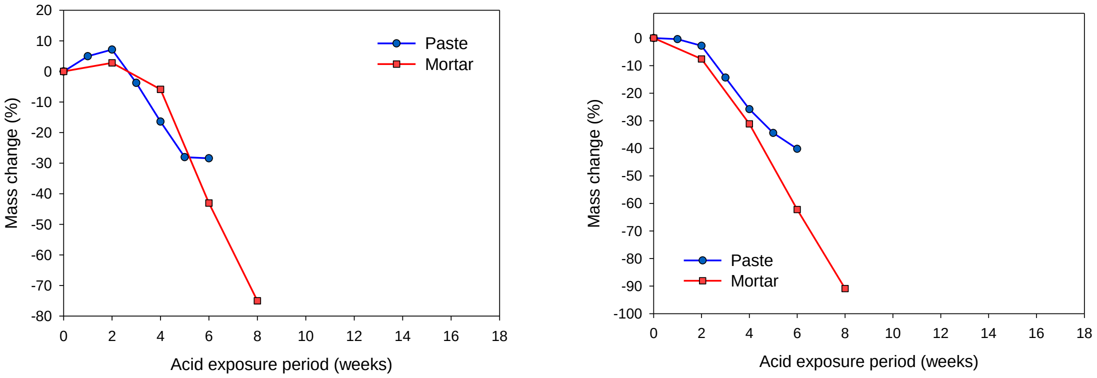

c) 3% sulphuric acid (without brushing)

d) 3% sulphuric acid (with brushing)

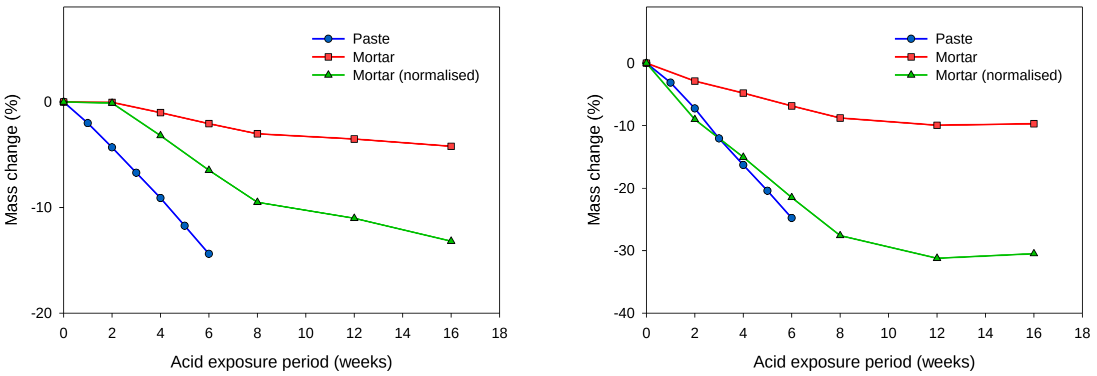

e) 0.25M acetic acid

f) 0.50M acetic acid

Figure E-3 Behaviour of SF10 paste and mortar on exposure to acids

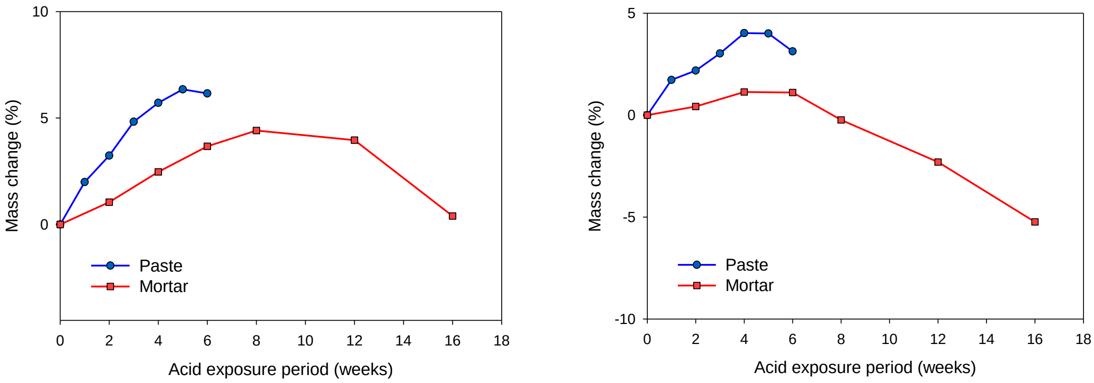

a) 1% sulphuric acid (without brushing)

b) 1% sulphuric acid (with brushing)

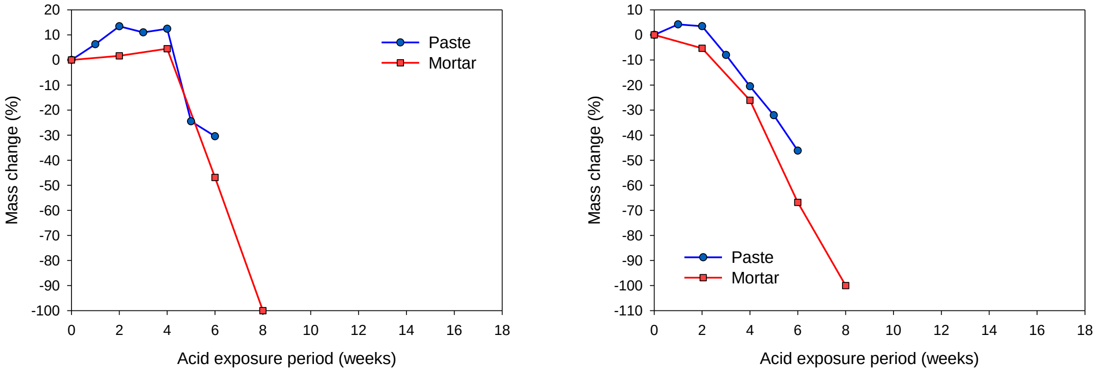

c) 3% sulphuric acid (without brushing)

d) 3% sulphuric acid (with brushing)

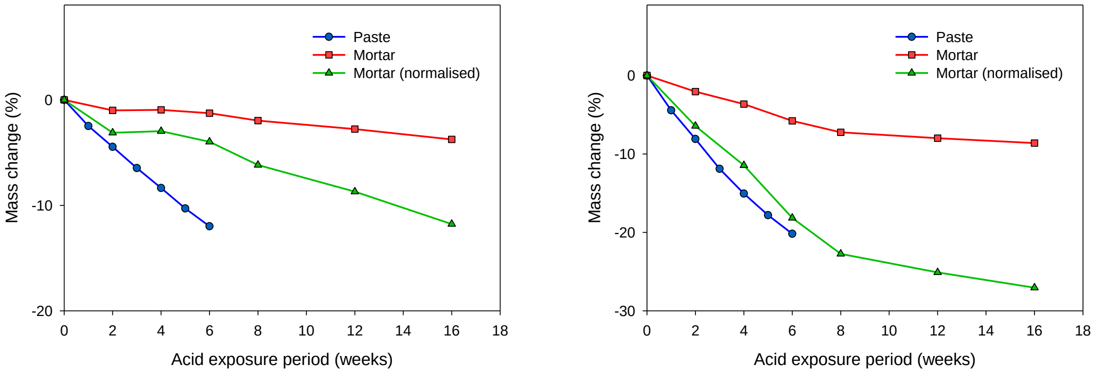

e) 0.25M acetic acid

f) 0.50M acetic acid

Figure E-4 Behaviour of LC2 paste and mortar on exposure to acids

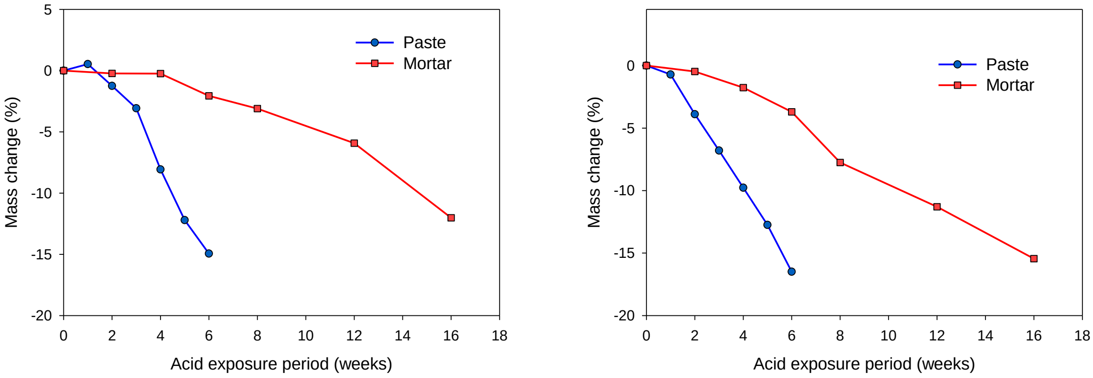

a) 1% sulphuric acid (without brushing)

b) 1% sulphuric acid (with brushing)

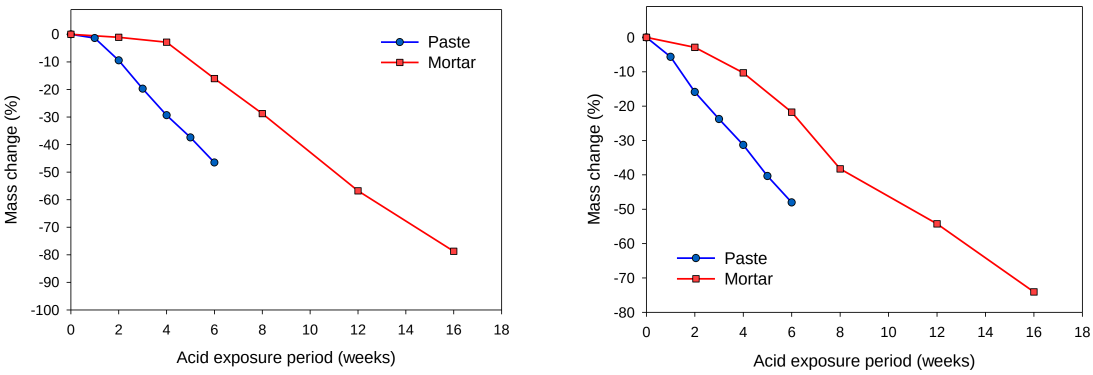

c) 3% sulphuric acid (without brushing)

d) 3% sulphuric acid (with brushing)

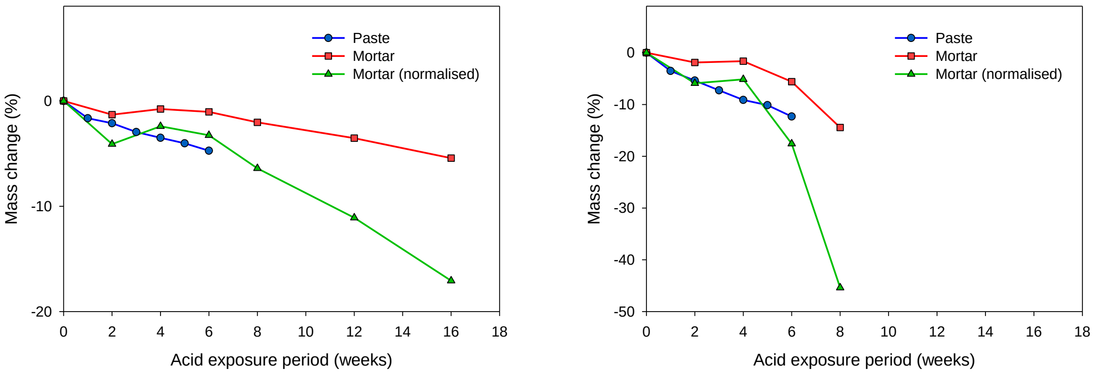

e) 0.25M acetic acid

f) 0.50M acetic acid

Figure E-5 Behaviour of HAC paste and mortar on exposure to acids

LIST OF PAPERS ON THE BASIS OF THIS THESIS

REFEREED JOURNALS

1. **Ramaswamy, K. P., and M. Santhanam** (2018) A study of deterioration of cement paste due to acid attack using X-ray computed micro-tomography, *Advances in Cement Research*, **30(3)**, 123–138.

PRESENTATIONS IN INTERNATIONAL CONFERENCES

1. **Ramaswamy, K. P., and M. Santhanam** (2018) Influence of mineralogical nature of aggregates on acid resistance of mortar, Sixth International Conference on Durability of Concrete Structures, University of Leeds, Leeds, UK.
2. **Ramaswamy, K. P., Bertron, A., Santhanam, M., and Raisa Shabeer** (2017) Acid-related factors affecting the degradation kinetics of cement-based materials, 4th International Conference on Modeling and Simulation in Civil Engineering, TKM College of Engineering, Kollam (Published as Special Issue in International Journal of Engineering and Advanced Technology, Vol. 7, 202–211).
3. **Ramaswamy, K. P., and M. Santhanam** (2017) Durability of cementitious materials in acidic environments, (Keynote Paper) 15th NCB International Seminar on Cement, Concrete and Building Materials, National Council for Cement and Building Materials, New Delhi.
4. **Ramaswamy, K. P., Satyanarayana Rao, N., and M. Santhanam** (2017) Durability of bagasse-ash based cementitious systems in acidic environment, Vol. 4, pp. 243–252, In: Santhanam, M., Gettu, R., Pillai, R. G., and S. K. Nayar (Eds.), RILEM Proceedings PRO 118 (Proceedings of International Conference on Advances in Construction Materials and Systems, Chennai), RILEM Publications S. A. R. L., Paris, France.
5. **Ramaswamy, K. P., Sivakumar, R., Santhanam, M., and R. Gettu** (2017) Micro-analytical characterisation of concrete deterioration due to acid attack in a sewage treatment plant, Vol. 2, pp. 647–656, In: Santhanam, M., Gettu, R., Pillai, R. G., and S. K. Nayar (Eds.), RILEM Proceedings PRO 118 (Proceedings of International Conference on Advances in Construction Materials and Systems, Chennai), RILEM Publications S. A. R. L., Paris, France.

6. **Ramaswamy, K. P., Padmanabhan, K., and M. Santhanam** (2017) A study of concrete deterioration faced by distillery industry, Vol. 2, pp. 485–494, In: Santhanam, M., Gettu, R., Pillai, R. G., and S. K. Nayar (Eds.), RILEM Proceedings PRO 118 (Proceedings of International Conference on Advances in Construction Materials and Systems, Chennai), RILEM Publications S. A. R. L., Paris, France.
7. **Ramaswamy, K. P., Bertron, A., and M. Santhanam** (2017) Additional insights on the influencing factors and mechanism of degradation due to acid attack: Special case of acids forming soluble salts, Vol. 4, pp. 279–290, In: Santhanam, M., Gettu, R., Pillai, R. G., and S. K. Nayar (Eds.), RILEM Proceedings PRO 118 (Proceedings of International Conference on Advances in Construction Materials and Systems, Chennai), RILEM Publications S. A. R. L., Paris, France.
8. **Ramaswamy, K. P. and M. Santhanam** (2017) Durability of cementitious materials in acidic environments: Evaluation of degradation kinetics, In: De Schutter, G., De Belie, N., Janssens, A., and N. V. D. Bossche (Eds.), RILEM Proceedings PRO 107 (14th International Conference on Durability of Building Materials and Components, Ghent University, Belgium), RILEM Publications S. A. R. L., Paris, France.
9. **Ramaswamy, K. P., Murugan, M., and M. Santhanam** (2015) Characterization of cement paste modified with nano-materials using X-ray computed microtomography, pp. 131–138, In: Bindu, S. and Anu V. Thomas (Eds.), Proceedings of 3rd International Conference on Modeling and Simulation in Civil Engineering, TKM College of Engineering, Kollam.

PRESENTATIONS IN NATIONAL CONFERENCES

1. **Ramaswamy, K. P., and M. Santhanam** (2016) Degradation kinetics of cement-based materials in citric acid, pp. 1690-1695, In: Rao, A. R. M. and K. Ramanjaneyulu (Eds.), Proceedings of 10th Structural Engineering Convention, Chennai. (In: Rao, A. R. M. and K. Ramanjaneyulu (Eds.), Chapter 71, Recent Advances in Structural Engineering, Volume 1, *Lecture Notes in Civil Engineering*, Series Volume 11, Springer Publishers (In Press)).

DOCTORAL COMMITTEE

CHAIR PERSON	Dr. Ramamurthy K. Professor and Head Department of Civil Engineering
GUIDE	Dr. Manu Santhanam Professor Department of Civil Engineering
MEMBERS	Dr. Amlan K. Sengupta Professor Department of Civil Engineering
	Dr. Murty B. S. Professor Department of Metallurgical and Materials Engineering
	Dr. Radhakrishna G. Pillai Associate Professor Department of Civil Engineering

CURRICULUM VITAE

Name : Ramaswamy K. P.

Date of Birth : 02 - 09 - 1985

Education qualification

2007 : **Bachelor of Technology (B. Tech)**
Institution : NSS College of Engineering, Palakkad, Kerala
University : University of Calicut
Specialisation : Civil Engineering

2009 : **Master of Technology (M. Tech)**
Institution : Indian Institute of Technology Madras, Chennai, India
University : Indian Institute of Technology Madras, Chennai, India
Specialisation : Construction Technology and Management

2018 : **Doctor of Philosophy (Ph.D.)**
Institution : Indian Institute of Technology Madras, Chennai, India
Specialisation : Building Technology and Construction Management
Registration date : 14 July 2014

Career details
2009 – Till date : Assistant Professor in Civil Engineering
TKM College of Engineering, Kollam, Kerala
(Department of Technical Education, Government of Kerala)
2014 – 2017 : Deputation under QIP

(To do Ph.D. at Indian Institute of Technology Madras, Chennai)